A Genetic and Functional Investigation of Inherited Neuropathies: Charcot-Marie Tooth Disease and Brown-Vialetto-Van Laere Syndrome

Amelie Pandraud

Department of Molecular Neuroscience, UCL Institute of Neurology
& MRC Centre for Neuromuscular Diseases

PhD Supervisors: Professor Mary Reilly, Professor Henry Houlden &
Dr Matilde Laurá

A Thesis submitted for the degree of
Doctor of Philosophy
University College London
June 2014

Declaration

I, Amelie Pandraud, confirm that the work presented in this Thesis is my own. Where information has been derived from other sources, I confirm that this has been indicated in the Thesis.

Date: 30.05.14

Abstract

Charcot-Marie-Tooth (CMT) disease and Brown-Vialetto-Van Laere syndrome (BVVL) are two inherited neuropathies. Although most CMT type 1A patients carry the same sized duplication containing the *peripheral myelin protein 22* (*PMP22*) gene, they present with a wide range of severities both within and between families. Some CMT1A patients exhibit chronic inflammatory demyelinating polyneuropathy (CIDP)-like features. An association study was performed in a CMT1A and a CIDP cohort to identify the genetic factors modifying the CMT1A phenotype. Variants associated with CIDP and/or with autoimmune/inflammatory diseases were determined to be unlikely to modulate disease severity in CMT1A, or to contribute to CMT1A pathogenesis. A susceptibility locus for CIDP was identified in the *PXK* gene. CMT1 genes were screened in CMT1 patients from the UK, Greece and Russia, thereby establishing mutation frequencies and expanding phenotype-genotype correlations. Some cases of CMT1 remain without a genetic diagnosis; two potential CMT1 candidate genes were identified by exome sequencing in two families. The genetic causes of selected canine neuropathies were investigated and several CMT genes were ruled out.

BVVL is a rare, recessive motor neurone disease (MND) with early onset; a severe sensory-motor neuropathy is part of the phenotype. Mutations have been found in genes encoding riboflavin transporters, leading to flavin deficiency. To characterise the disease and facilitate early access to therapy, the riboflavin transporter genes were screened in patients with BVVL-like phenotypes; *SLC52A2* mutations were most common. A candidate gene for complex axonal neuropathy resembling BVVL was uncovered by exome sequencing. Riboflavin and its active metabolites play a role in energy metabolism. Three cell models were used to investigate BVVL in vitro: patient fibroblasts, as well as a neuroblastoma cell line and mouse motor neurones in which one of the riboflavin transporters was knocked down. Mitochondrial dysfunction was suggested as a potential pathway leading to neuronal damage in BVVL.

Acknowledgments

I wish to express my sincere gratitude to my supervisors, Professor Mary Reilly, Professor Henry Houlden, and Dr Matilde Laurá, for their invaluable support, insight and guidance throughout my PhD, and for being such wonderful teachers. I am deeply indebted to the patients and their families for their support in my research. I would also like to thank the current and past members of my lab group, the faculty members in the ION Department of Molecular Neuroscience especially Dr Helene Plun-Favreau, Dr Andrey Abramov and Dr Alan Pittman, Dr Bernadett Kalmar and other members of Professor Linda Greensmith's lab at the ION, the Neurogenetics Unit especially Dr James Polke, as well as the Neurometabolic Unit at the NHNN, particularly Dr Iain Hargreaves and Marcus Oppenheim, for their help, advice, and valuable suggestions during my PhD. I also thank all our collaborators for their essential contribution to my research.

This Thesis is dedicated to Pierre-Jean, to my parents Annick and Jean-Marc, and to my sisters Charlotte and Alice, for their continued encouragement, patience, efforts, and love over the past four years. Thank you for giving me confidence and believing in me. I am forever grateful to all of you, and I could not have completed this PhD without you. I also thank all my friends who provided moral support and motivation.

The experiments in this Thesis were funded by the CMTUK patient support group, the MRC Centre for Neuromuscular diseases, and the Muscular Dystrophy Campaign.

Table of Contents

Supplementary material: Full text of published papers on attached disc (references for published/in press papers are in Appendix IX).

List of Figures

List of Tables

List of Abbreviations

AARS	Alanyl-tRNA synthetase
AAAS	Achalasia-Addisonianism-Alacrima Syndrome
AAE	Age at examination
Acetyl-CoA	Acetyl-Coenzyme A
ACTBL2	Actin, beta-like 2
Acyl-CoA	Acyl-Coenzyme A
AD	Autosomal dominant
ALS	Amyotrophic Lateral Sclerosis
ANOVA	Analysis of variance
AR	Autosomal recessive
ARHGEF10	Rho guanine nucleotide exchange factor 10
ARHGEF11	Rho guanine nucleotide exchange factor 11
ATP	Adenosine 5'-triphosphate
ATP5β	ATP-synthase β (subunit)
BED	Binary PED
Bp	Base pair
BSA	Bovine serum albumin
BVVL	Brown-Vialetto-Van Laere syndrome
C20orf54	Chromosome 20 open reading frame 54
cAMP	Cyclic adenosine monophosphate
CCD	Charge-coupled device
cDNA	Complementary deoxyribonucleic acid
CG69	Complete Genomics 69
CHN	Congenital hypomyelinating neuropathy
Chr17	Chromosome 17
CI	Confidence interval
CIDP	Chronic inflammatory demyelinating polyneuropathy
CMAP	Compound muscle action potential
CMT	Charcot-Marie-Tooth disease
CMT1A-REP	Charcot-Marie-Tooth disease Type 1A repeat sequences
CMTES	CMT examination score

CMTNS	CMT neuropathy score
CNB	Complete Neurobasal (medium)
CNS	Central nervous system
CoQ	Coenzyme Q
CoQ_1	Coenzyme Q_1
CoQ_{10}	Coenzyme Q_{10}
COX10	Cytochrome c oxidase assembly homolog 10
CS	Citrate synthase
CSF	Cerebrospinal fluid
C_t	Threshold cycle
CTDP1	CTD (carboxy-terminal domain, RNA polymerase II, polypeptide A) phosphatase, subunit 1
DAPI	4',6-Diamidino-2-phenylindole
dbSNP	Single nucleotide polymorphism database
DCPIP	2,6-Dichlorophenol-indophenol
ddNTP	Dideoxynucleotides
dH_2O	Deionised water
dHMN	Distal hereditary motor neuropathy
DIV	Days in vitro
DMEM	Dulbecco's modified eagle medium
DMSO	Dimethyl sulfoxide
DNA	Deoxyribonucleic acid
DNM2	Dynamin 2
DNMT1	DNA (cytosine-5-)-methyltransferase 1
DNP	2,4-Dinitrophenol
dNTP	Deoxyribonucleotide triphosphate
DPBS	Dulbecco's phosphate buffered saline
Dpm	Disintegrations per minute
DSD	Dejerine-Sottas disease
DTT	Dithiothreitol
DYNC1H1	Dynein, cytoplasmic 1, heavy chain 1
ECL	Electrochemiluminescence
EDTA	Ethylenediaminetetraacetic acid

EEG	Electroencephalogram
EGR	Erythrocyte glutathione reductase
EGR2	Early growth response 2
EMG	Electromyogram
ER	Endoplasmic reticulum
Ero1	ER oxidoreductin 1
ETF	Electron transfer flavoprotein
ETFDH	Electron transfer flavoprotein dehydrogenase
ETF:QO	Electron transfer flavoprotein-ubiquinone oxidoreductase
EVS	Exome Variant Server
FAD	Flavin adenine dinucleotide
$FADH_2$	Flavin adenine dinucleotide (reduced)
FBS	Foetal bovine serum
FCCP	Carbonyl cyanide-4-(trifluoromethoxy)phenylhydrazone
FCS	Foetal calf serum
FGD4	FYVE, RhoGEF and PH domain containing 4
FIG4	SAC1 lipid phosphatase domain containing
FL	Fazio-Londe
FMN	Flavin mononucleotide
FNAD	Foetal-onset neuroaxonal dystrophy
FosTes	Fork stalling and template switching
GAPDH	Glyceraldehyde-3-phosphate dehydrogenase
GARS	Glycyl-tRNA synthetase
GATK	Genome Analysis Tool Kit
GDAP1	Ganglioside induced differentiation associated protein 1
gDNA	Genomic DNA
GERP	Genomic evolutionary rate profiling
GFP	Green fluorescent protein
GJB1	Gap junction protein, beta 1
GOSH	Great Ormond Street Hospital
GPR172B	G protein-coupled receptor 172B
GSH	Glutathione (reduced)
GSSG	Glutathione (oxidised dimeric form)

GSTZ1	Glutathione-5-transferase zeta-1
GWAS	Genome-wide association study
HBSS	Hank’s balanced salt solution
HCl	Hydrochloric acid
HEK293T	Human embryonic kidney 293T
HEPES	4-(2-Hydroxyethyl)-1-piperazineethanesulfonic acid
HLA	Human leukocyte antigen
HMSN	Hereditary motor and sensory neuropathy
HNPP	Hereditary neuropathy with liability to pressure palsies
HPLC	High-performance liquid chromatography
hRFT1	Human riboflavin transporter 1
hRFT2	Human riboflavin transporter 2
hRFT3	Human riboflavin transporter 3
HRP	Horseradish peroxidase
HSAN	Hereditary sensory and autonomic neuropathy
HSP	Hereditary spastic paraplegia
HSPB1	Heat shock 27kDa protein 1
HSPB8	Heat shock 22kDa protein 8
HWE	Hardy-Weinberg equilibrium
ICH	Institute of Child Health
ICMT	Intermediate Charcot-Marie-Tooth disease
IF1	Initiation factor 1
IGHMBP2	Immunoglobulin mu binding protein 2
Indel	Insertion/deletion
ION	Institute of Neurology
IPS (cell)	Induced pluripotent stem (cell)
IS	Internal standard
IVIG	Intravenous immunoglobulin
Kb	Kilobase
KCN	Potassium cyanide
KD	Knockdown
KIF1A	Kinesin family member 1A
KIF1B	Kinesin family member 1B

LAMP1	Lysosomal-associated membrane protein 1
LB	Luria-Bertani (broth)
LD	Linkage disequilibrium
LITAF	Lipopolysaccharide-induced TNF factor
LMN	Lower motor neurone
LMNA	Lamin A/C
LRSAM1	Leucine rich repeat and sterile alpha motif containing 1
MAAI	Maleylacetoacetate isomerase
MADD	Multiple acyl-CoA dehydrogenase deficiency
MAF	Minor allele frequency
MARS	Methionyl-tRNA synthetase
Mb	Megabase
MEF	Mouse embryonic fibroblast
MFF	Mitochondrial fission factor
MFN2	Mitofusin 2
MFT	Mitochondrial folate transporter
MHC	Major histocompatibility complex
MLPA	Multiplex ligation-dependent probe amplification
MNCV	Motor nerve conduction velocity
MND	Motor neurone disease
MPZ	Myelin protein zero
MRC	Mitochondrial respiratory chain
MRC (Centre)	Medical Research Council (Centre)
MRI	Magnetic resonance imaging
mRNA	Messenger ribonucleic acid
MTMR2	Myotubularin related protein 2
MTMR13	Myotubularin related protein 13
MUC6	Mucin 6
NaCN	Sodium cyanide
NAD^+	Nicotinamide adenine dinucleotide (oxidised)
NAD-CA	Neuroaxonal dystrophy and cerebellar abiotrophy
NADH	Nicotinamide adenine dinucleotide (reduced)
NAHR	Non-allelic homologous recombination

NaOH	Sodium hydroxide
NCBI	National Centre for Biotechnology Information
NCS	Nerve conduction study
NCV	Nerve conduction velocity
NDRG1	N-myc downstream regulated 1
NEB	New England Biolabs
NEFH	Neurofilament heavy polypeptide
NEFL	Neurofilament, light polypeptide
NGS	Next-generation sequencing
NHEJ	Non-homologous end joining
NHNN	National Hospital for Neurology and Neurosurgery
NMD	Nonsense-mediated decay
Nrf2	Nuclear respiratory factor 2
OR	Odds ratio
OR4C45	Olfactory receptor, family 4, subfamily C, member 45
P/S	Penicillin/streptomycin
PBS	Phosphate buffered saline
PCR	Polymerase chain reaction
PDK3	Pyruvate dehydrogenase kinase, isozyme 3
PEO1	Progressive external ophthalmoplegia 1
PFA	Paraformaldehyde
PKA	Protein kinase A
PLA2G6	Phospholipase A2, group VI
PMP22	Peripheral myelin protein 22
PNS	Peripheral nervous system
POLG	Polymerase (DNA directed), gamma
PRX	Periaxin
PXK	PX domain containing serine/threonine kinase
QQ (plot)	Quantile-quantile (plot)
qPCR	Quantitative polymerase chain reaction
RAB7	Rab7 member RAS oncogene family
RFVT1	Riboflavin transporter 1 (human)
RFVT2	Riboflavin transporter 2 (human)

RFVT3	Riboflavin transporter 3 (human)
RM	Recording medium
RNA	Ribonucleic acid
ROS	Reactive oxygen species
Rpm	Revolutions per minute
RQ	Relative quantification value
RR-MADD	Riboflavin-responsive multiple acyl-CoA dehydrogenase deficiency
RT	Reverse transcription
RT-qPCR	Real-time reverse transcription polymerase chain reaction
SDH	Succinate dehydrogenase
SDS	Sodium dodecyl sulphate
SEM	Standard error of the mean
SEPT9	Septin 9
SH3TC2	SH3 domain and tetratricopeptide repeats 2
shRNA	Short hairpin ribonucleic acid
shRNAmir	MicroRNA-adapted short hairpin ribonucleic acid
SIFT	Sorting Intolerant From Tolerant
SLC52A1	Solute carrier family 52, riboflavin transporter member 1
SLC52A2	Solute carrier family 52, riboflavin transporter member 2
SLC52A3	Solute carrier family 52, riboflavin transporter member 3
SLE	Systemic lupus erythematosus
SMA	Spinal muscular atrophy
SMARD	Spinal muscular atrophy with respiratory distress
SMARD1	Spinal muscular atrophy with respiratory distress type 1
SMN1	Survival motor neuron 1
SNAP	Sensory nerve action potential
SNP	Single nucleotide polymorphism
SOD1	Superoxide dismutase 1
SOX10	SRY (sex determining region Y)-box 10
SPTLC1	Serine palmitoyltransferase, long chain base subunit 1
SPTLC2	Serine palmitoyltransferase, long chain base subunit 2
TBCE	Tubulin-specific chaperone cofactor E
TBCEL	Tubulin-specific chaperone cofactor E-like protein

TBE	Tris/borate/EDTA
TMRM	Tetramethylrhodamine methyl ester
TRAK2	Trafficking protein kinesin binding 2
TRPV4	Transient receptor potential cation channel, subfamily V, member 4
TTFA	2-Thenoyltrifluoroacetone
TU	Transducing units
UCL	University College London
UCLH	University College London Hospital
UCSC	University of California Santa Cruz (genome browser)
UMN	Upper motor neurone
UTR	Untranslated region
UV	Ultraviolet
VCP	Valosin-containing protein
VSV-G	Vesicular stomatitis virus
WT	Wild-type
WTCCC	Wellcome Trust Case Control Consortium
YARS	Tyrosyl-tRNA synthetase
$\Delta\Psi_m$	Mitochondrial membrane potential

This list only includes abbreviations used more than once in the text.

Chapter 1 Introduction

1.1 Motor and sensory pathways of the peripheral nervous system

The nervous system is divided into the central nervous system (CNS) and the peripheral nervous system (PNS). The CNS is made up of the brain and spinal cord. Nerves in the PNS connect the CNS to the rest of the body by relaying information from the brain and spinal cord to the limbs, and then back to the CNS. The basic unit of the nervous system is the nerve cell or neurone. Peripheral nerves consist of bundles of nerve fibres ensheathed in connective tissue. The PNS is comprised of 12 pairs of cranial nerves, connecting the brain to the head and neck muscles via skull openings, and 31 pairs of spinal nerves, connecting the spinal cord to the trunk and limbs. The motor cranial nerves start in the brainstem and end on the muscle, while sensory cranial nerves start in the sensory organs and end in the brainstem. Near the spinal cord, the spinal nerves separate into dorsal and ventral roots which carry sensory and motor fibres, respectively. Sensory pathways include the spinothalamic tract (touch, pain, temperature) and the dorsal column-medial lemniscus pathway (proprioception, fine touch). Upper motor neurones (UMNs) originate in the motor cortex and brainstem, and control the activity of lower motor neurones (LMNs). Motor pathways formed by the UMNs include the corticobulbar tract, which controls the motor neurones in the cranial nerve nuclei, and the corticospinal tract, which regulates the activity of spinal cord motor neurones. LMNs originate in the ventral horn of the spinal cord and in the motor cranial nerve nuclei of the brainstem, and innervate skeletal muscle (Crossman & Neary, 2010).

Nerve fibres may or may not be ensheathed with myelin. Early on in the development of the PNS, axons larger than 1 μm in diameter become wrapped by myelin, which consists of layers of Schwann cell plasma membrane. Schwann cells are the glial cells of the PNS. Myelin nourishes the axon and allows for fast saltatory conduction of the action potentials at the nodes of Ranvier, which mark the separation of individual Schwann cells (Jessen & Mirsky, 1998). In the PNS, the myelin membrane is mainly comprised of compact myelin, which is made up of cholesterol and other lipids in addition to proteins like myelin protein zero (MPZ) and peripheral myelin protein 22 (PMP22). The functions of PMP22 include cell

cycle control, proliferation and differentiation of Schwann cells, axonal maintenance, and regulation of myelin stability and thickness (Adlkofer et al., 1995; Giambonini-Brugnoli et al., 2005). Proteins such as connexin-32 and myelin-associated glycoprotein are located in the non-compact portion. Mutations in genes encoding these and other structural proteins can cause neuropathy of peripheral nerves (Patzkó & Shy, 2011).

1.2 Peripheral neuropathies

Damage to sensory, motor and/or autonomic nerves may cause peripheral neuropathy; the defect may principally involve the axon (axonopathy), cell body (neuronopathy), or myelin sheath/Schwann cells (myelinopathy). Demyelinating neuropathies, or myelinopathies, result from defects in the development and functioning of Schwann cells and the myelin sheath they produce, leading to secondary axonal degeneration (Hughes, 2008).

Single nerves or multiple nerves may be affected in peripheral neuropathies. Carpal tunnel syndrome, an acquired cause of neuropathy usually caused by nerve compression, is an example of a mononeuropathy as a single peripheral nerve is damaged. Rheumatoid arthritis and certain infectious diseases may result in a multiple mononeuropathy, which affects two or more nerves in several parts of the body. The term polyneuropathy is used to refer to conditions where multiple nerves in all limbs are involved; examples include Charcot-Marie-Tooth (CMT) disease and chronic inflammatory demyelinating polyneuropathy (CIDP) (Hughes, 2008).

Approximately 2.4% of the population suffers from symmetrical polyneuropathy; elderly individuals are more likely to be affected (Hughes, 2008). A common cause of polyneuropathy is diabetic polyneuropathy, which is believed to affect 50% of patients with long-standing diabetes (Shakher & Stevens, 2011).

Peripheral neuropathy is often length-dependent and therefore affects the longest nerves first. In humans, this translates to symptoms starting in the feet and progressing to the hands and more proximal areas later on in the disease course. Interestingly, the laryngeal nerve is the first to suffer damage in horses with

peripheral neuropathy, as this is the longest nerve in this animal. Symptoms vary depending on the type of nerve which is damaged: sensory loss, neuropathic pain and tingling, burning, or numbness sensations result from damage to sensory nerves; fasciculations and muscle weakness are caused by impairment to motor nerves; autonomic nerve damage involves changes in blood pressure, bladder function and sexual function (Asbury & Thomas, 1995). Interestingly, mutations in certain CMT-associated genes render particular sets of neurones more vulnerable to damage; for example, hereditary motor neuropathy due to mutations in *glycyl-tRNA synthetase* (*GARS*) is characterised by upper limb predominance of symptoms, while *heat shock 27kDa protein 1* (*HSPB1*) and *heat shock 22kDa protein 8* (*HSPB8*) mutations cause length-dependent neuropathy, where the legs are more affected than the arms (Reilly & Shy, 2009).

Severity of disease varies greatly; the range of phenotypes associated with peripheral neuropathies will be discussed in detail later on in this Chapter. Indeed, patients with peripheral neuropathy may be asymptomatic and disease may be evident only from electrophysiological tests. At the other end of the spectrum, some patients may require wheelchairs for mobility and ventilatory support, ultimately leading to susceptibility to infections such as chest infections that can be fatal. In neuropathies such as CIDP, Guillain–Barré Syndrome, hereditary neuropathy with liability to pressure palsies (HNPP), porphyria and Refsum's disease, patients may experience periods of disease exacerbation characterised by intermittent relapses. Disease may be acute, sub-acute or chronic. A slowly progressive course is usually typical of most polyneuropathies (Asbury & Thomas, 1995).

There is currently no effective treatment to reverse the damage in most peripheral neuropathies. Patients suffering from an acquired neuropathy are advised to avoid the cause of their neuropathy, such as alcohol, toxins or drugs, and to control their diabetes, if appropriate. Corticosteroids, plasmapheresis and/or intravenous immunoglobulins (IVIG) may be helpful in CIDP patients and in some CMT cases presenting with an overlapping inflammatory neuropathy (Ginsberg et al., 2004). Treatment is palliative for most inherited neuropathies; patients may benefit from

physical therapy, use of orthotics, orthopaedic interventions, pain management and genetic counselling (Reilly et al., 2011).

Peripheral neuropathy may be the principal manifestation of disease, such as in CMT and CIDP, or part of a more generalized disorder as in Brown-Vialetto-Van Laere syndrome (BVVL), hereditary spastic paraplegia (HSP), hereditary ataxia, neuroaxonal dystrophy (NAD), the genetic forms of porphyrias, metachromatic leukodystrophy, Krabbe disease, Tangier disease, Fabry disease, Refsum's disease and others (Reilly & Shy, 2009). Neuropathy may be acquired or inherited.

1.2.1 Acquired peripheral neuropathies

Diabetes remains the most common cause of acquired neuropathy in the Western world, whilst in developing countries leprosy is responsible for the majority of cases. Chronic alcoholism is also frequently associated with acquired neuropathies. Other diseases also cause peripheral neuropathy, for example viral or bacterial infections such as Lyme disease, Hepatitis B and C, HIV/AIDS and varicella-zoster, and some autoimmune diseases including vasculitis due to rheumatoid arthritis, celiac disease, CIDP, multifocal motor neuropathy and paraproteinaemia, amongst others (Martyn & Hughes, 1997). Other causes include tumours, which may apply excessive pressure on a nerve, or traumatic injury to a nerve due to an accident or compression. Being exposed to toxic chemicals and heavy metals or taking drugs such as vincristine may also lead to neuropathy (Martyn & Hughes, 1997). Nutritional deficiencies in vitamin B_1, B_2, B_6, B_{12} and E, as well as disease of the kidney or liver can cause neuropathy (Hughes, 2008).

1.2.2 Inherited peripheral neuropathies

Examples of genetic diseases where peripheral neuropathy is part of the phenotype include CMT, BVVL, neuroaxonal dystrophy, HSP, hereditary ataxia, Fabry disease, Refsum's disease and others (Reilly & Shy, 2009). This thesis will begin by an exploration of CMT disease genetics, a pure neuropathy which may be a myelinopathy and/or an axonopathy, and will be followed by a genetic and functional investigation of BVVL, a neuronopathy which often presents with a CMT-like sensory-motor neuropathy as part of a more widespread disorder.

1.3 Charcot-Marie-Tooth (CMT) disease: an inherited peripheral neuropathy

1.3.1 CMT: phenotypes and classification

Three physicians first described CMT in 1886: Jean-Marie Charcot, Pierre Marie and Howard Henry Tooth (Charcot & Marie, 1886; Tooth, 1886). CMT, also known as hereditary motor and sensory neuropathy (HMSN), is the most common inherited neuromuscular disorder, with a prevalence of 5-40 per 100,000 depending on the population studied (Foley et al., 2012; Martyn & Hughes, 1997; Skre, 1974). Neurologists recognise it as one of the most phenotypically and genetically heterogeneous diseases in neurology. The most common symptoms include distal muscle weakness and wasting which is generally symmetrical and becomes proximal with disease progression, sensory loss, decreased reflexes and foot deformities (pes cavus and hammer toes) (Pareyson & Marchesi, 2009). Inherited neuropathies consisting mainly of sensory and autonomic abnormalities are referred to as hereditary sensory and autonomic neuropathies (HSAN), and those with only motor involvement are termed distal hereditary motor neuropathies (dHMN). There is significant phenotypic and genotypic overlap between HSAN, dHMN and CMT (Reilly & Shy, 2009). CMT is generally not fatal, and wheelchair use remains rare. However, early-onset generally predicts a more severe disease (Reilly et al., 2011).

The CMT neuropathy score (CMTNS) is used to quantify disability in CMT and is divided into mild (CMTNS $\leq$ 10), moderate (CMTNS 11 to 20) and severe (CMTNS $\geq$ 21). The parameters used to calculate the CMTNS include sensory and motor symptoms (legs and arms), pin sensibility, vibration, leg and arm strength, compound muscle action potentials (CMAPs) and sensory nerve action potentials (SNAPs) (Shy et al., 2005). The sensitivity of the CMTNS was recently improved; the second version is known as CMTNS2 (Murphy, Herrmann, et al., 2011).

Before the first genetic cause of CMT was identified, CMT was mainly described by neurophysiology and peripheral nerve pathology. CMT was classified using the upper limb motor nerve conduction velocity (MNCV), where patients with the demyelinating form (CMT1) have MNCVs less than 38 m/s and those with the axonal form (CMT2) have MNCVs above 38 m/s (Dyck & Lambert, 1968a; Dyck &

Lambert, 1968b; Harding & Thomas, 1980). An intermediate form of CMT (ICMT) refers to patients with MNCVs between 25 and 45 m/s (Reilly et al., 2011).

The demyelinating and axonal forms of CMT may show autosomal dominant (AD), recessive (AR), or X-linked inheritance. CMT3, also known as congenital hypomyelinating neuropathy (CHN) or Dejerine-Sottas disease (DSD), refers to early-onset severe demyelinating or hypomyelinating CMT. CMT4 refers to AR demyelinating CMT (Reilly et al., 2011).

1.3.2 The genetic maze: diagnosis of CMT

Advances in sequencing technology have allowed for over 60 genes or loci to be linked to CMT (Pandraud et al., 2012; Rossor et al., 2013), which have been classified according to their axonal or demyelinating nature and inheritance pattern (Appendix I Table I-1). Defects in the same gene may be associated with multiple phenotypes, while the same phenotype may result from mutations in different genes.

The significant number of genes known to be associated with CMT as well as the phenotypic overlap between CMT subtypes makes diagnosis a challenging task for clinicians. In addition to the neurological examination, the diagnosis of CMT is made using a combination of family history, neurophysiological studies to assess nerve conduction velocities (NCVs), genetic testing, and a nerve biopsy if appropriate, although the latter are performed more rarely than they used to be (Pareyson & Marchesi, 2009). Mode of inheritance may be difficult to establish due to intrafamilial phenotypic variability; additionally, de novo mutations account for a non-negligible percentage of patients (Pareyson & Marchesi, 2009). Disease severity, age at onset, and the presence of certain rare features such as vocal cord palsy, optic atrophy or cranial nerve involvement may help point to the responsible gene. As will be discussed further in Chapter 3, the ethnic background of the patient also helps to target the genetic tests according to the frequency of CMT subtypes in the population of interest (Reilly et al., 2011).

1.3.3 Animal models of CMT

Rodent models of CMT have been instrumental in gaining a deeper understanding of the pathomechanisms associated with particular CMT subtypes, as well as for identifying drug targets and assessing their therapeutic value (Fledrich, Stassart, et al., 2012). Whether naturally occurring or generated in the laboratory, rodent models are available for several CMT subtypes such as CMT associated with mutations and/or gene dosage alterations in *PMP22, MPZ, gap junction protein, beta 1* (*GJB1*), *early growth response 2* (*EGR2*), *mitofusin 2* (*MFN2*), *periaxin* (*PRX*), *myotubularin related protein 2* (*MTMR2*), *myotubularin related protein 13* (*MTMR13*), *neurofilament, light polypeptide* (*NEFL*), *HSPB1, leucine rich repeat and sterile alpha motif containing 1* (*LRSAM1*), *GARS* and *lamin A/C* (*LMNA*) (Bouhy & Timmerman, 2013; Cartoni et al., 2010; Fledrich, Stassart, et al., 2012; Meyer Zu Hörste & Nave, 2006; Seo et al., 2014).

Naturally occurring animal models of peripheral neuropathies have been described in many species, including canines, which are of particular interest in this study. Peripheral neuropathies in canines may be part of a generalised disorder involving both the CNS and PNS, or may be "non-syndromic" and involve a peripheral neuropathy alone (Granger, 2011). Similar to CMT in humans, non-syndromic canine peripheral neuropathies may be motor, sensory and/or autonomic, and may be demyelinating or axonal with early or late-onset; in contrast to humans, only AR inheritance has been described in dogs, however sporadic forms exist as well (Granger, 2011). Axonal neuropathies tend to be more common than the demyelinating form in canines (Coates & O'Brien, 2004; Granger, 2011; Vanhaesebrouck et al., 2008). Animals affected by peripheral neuropathies resembling CMT or canines with mutations in known CMT genes may serve as disease models (Matiasek & Drögemüller, 2011); this topic will be investigated in Chapter 3. Determining the genetic cause of disease in canines may lead to a greater understanding of disease pathogenesis in humans, as well as to the identification of new candidate genes (Vanhaesebrouck et al., 2008).

1.4 CMT type 1A as an example of phenotypic heterogeneity in CMT

1.4.1 The CMT1A phenotype

CMT1A patients with the chromosome 17 (Chr17) p11.2 duplication usually have disease onset in childhood and a classic phenotype of progressive muscle weakness and atrophy with predominance in the lower limbs, sensory loss, walking difficulties, loss of reflexes, and foot deformities. Breathing difficulties may also be present; cerebellar or bulbar involvement is rare (Birouk et al., 1997; Thomas et al., 1997). CMT1A is very slowly progressive (Marques et al., 2005; Shy et al., 2008). Motor and sensory nerve conduction studies (NCS) usually show a uniform slowing with velocities of 15-30 m/s and onion bulb formations on nerve biopsy (Birouk et al., 1997; Marques et al., 2005; Thomas et al., 1997). Disease severity may be mild or moderate, and is not influenced by gender or pregnancy (Birouk et al., 1997; Swan et al., 2007). Motor nerve conduction slowing does not correlate with muscle wasting and extent of sensory involvement; however, severity is correlated with CMAP and SNAP decrease, since disease symptoms are due to axonal damage rather than damage to the myelin sheath in CMT1A (Kim et al., 2012; Shy et al., 2008). CMAPs correlate with disease duration but not age at onset, although an earlier age of onset had previously been found to predict a more severe disease course (Birouk et al., 1997; Kim et al., 2012). NCVs are a marker of disease but not of severity because they do not show significant change over time after the conduction velocities are established at three to five years of age (Kaku et al., 1993).

1.4.2 Coexistent inflammatory neuropathy in CMT

CIDP is a chronic acquired autoimmune inflammatory neuropathy associated with multifocal demyelination in the spinal root, plexuses and proximal nerve trunks. There are multiple forms of CIDP: motor and sensory, solely motor, solely sensory, or entirely distal. The neurophysiological profile includes decreased NCV, conduction block with features such as dispersion, and evidence of loss of axons and denervation (Dalakas, 2011). Compared to CMT1, CIDP is later onset, acquired, asymmetric, has a relapsing or subacute disease course, does not cause skeletal deformities, and leads to multi-focal demyelination (Latov, 2011).

Various cases of CMT (including CMT1A) with coexistent inflammatory features such as those seen in CIDP have been documented. CIDP-like features which have been found in some CMT patients include acute worsening of symptoms, asymmetrical symptoms, positive sensory symptoms, neuropathic pain, increased cerebrospinal fluid (CSF) protein, atypical NCS findings, positive response to IVIG, corticosteroids or plasma exchange, evidence of macrophage-associated demyelination, and inflammatory infiltrates on biopsy (Ben Youssef-Turki et al., 2011; Carvalho et al., 2005; Desurkar et al., 2009; Dyck et al., 1982; Gabriel et al., 2000; Ginsberg et al., 2004; Houlden et al., 2009; Latov, 2011; Malandrini et al., 1999; Mazzeo et al., 2012; Miki et al., 2013; Pál et al., 2009; Thomas et al., 1997; Vital et al., 1992; Vital et al., 2003; Williams & Penn, 1979). It should be noted that some of these features may be seen exclusively in CMT without overlap of an inflammatory neuropathy (Ginsberg et al., 2004). Of note, a superimposed acquired neuropathy associated with anti-myelin associated glycoprotein activity was documented in a CMT1A patient (Piscosquito et al., 2013). CMT patients were also found to be more likely than controls to have IgA deficiency (Williams & Penn, 1979).

This association of CMT with CIDP is thought to occur more often than expected by chance; as calculated by Ginsberg et al. (2004), we would expect about 1 in 250 cases of CMT to have coexistent inflammation, while the prevalence of CIDP in the general population is approximately 1 in 100,000. In fact, it has been proposed that CMT may increase the chances of developing CIDP (Ginsberg et al., 2004). Numerous animal models of CMT1 have noted an implication of immune cells in disease pathogenesis and an amelioration of disease in immune-deficient conditions, suggesting that the immune system may participate in the demyelination process (Carenini et al., 2001; Ip et al., 2006; Kobsar et al., 2005; Kohl et al., 2010; Mäurer et al., 2002; Schmid et al., 2000; Stoll et al., 1998; Williams et al., 1993). It is possible that an inflammatory component is always part of the pathogenic mechanism in CMT1, but is subclinical in most patients, although this is less likely as most patients do not respond to immunosuppressant therapy (Ginsberg et al., 2004; Martini & Toyka, 2004). Nevertheless, it remains unclear whether autoimmune involvement occurs in most CMT1 patients, or a subset of patients who

develop a secondary acquired autoimmune-mediated neuropathy (Martini & Toyka, 2004). Immune-mediated components of CMT disease pathogenesis and their possible involvement in modifying the CMT1A phenotype will be discussed in more detail in Chapter 4.

1.4.3 The chromosome 17 (Chr17) duplication in CMT1A

The genetic cause of disease in several CMT1 kindreds was linked to Chr17 in 1989 (Raeymaekers et al., 1989; Vance et al., 1989). A 1.5 megabase (Mb) duplication was subsequently found in the Chr17p11.2 region (Lupski et al., 1991; Raeymaekers et al., 1991). CMT1A is the most common type of CMT, accounting for approximately 55% of CMT and 66.8% of CMT1 cases (Saporta et al., 2011). About 10% of CMT1A cases are sporadic (Blair et al., 1996; Reilly et al., 2011). The duplication is usually of paternal origin (Blair et al., 1996; Lopes et al., 1997; Palau et al., 1993). The discovery of the CMT1A-linked duplication is still the most significant event in the history of CMT genetics. The duplication results from non-allelic homologous recombination (NAHR) between two highly homologous 24 kilobase (Kb) low-copy repeat sequences called Charcot-Marie-Tooth disease Type 1A repeat sequences (CMT1A-REPs) located at either end of the duplicated region (Chance et al., 1994; Pentao et al., 1992; Reiter et al., 1996). The duplication of the CMT1A–REP sequence arose during speciation from the gorilla to the chimpanzee (Boerkoel et al., 1999; Kiyosawa & Chance, 1996). The proximal copy of the CMT1A-REP misaligns and pairs with the distal copy from the other chromosome homologue during meiosis (Chance et al., 1994; Palau et al., 1993; Pentao et al., 1992). A reciprocal deletion of the same segment of deoxyribonucleic acid (DNA) was linked to HNPP, an AD condition of focal motor sensory neuropathy with recurrent pressure palsies (Chance et al., 1993). Shortly thereafter, the *PMP22* gene was mapped within the duplication and the encoded protein was found to be highly expressed in Schwann cells (Matsunami et al., 1992; Patel et al., 1992; Timmerman et al., 1992; Valentijn, Bolhuis, et al., 1992). The unequal crossing over results in three copies of *PMP22* instead of two (Figure 1-1) (Valentijn, Bolhuis, et al., 1992).

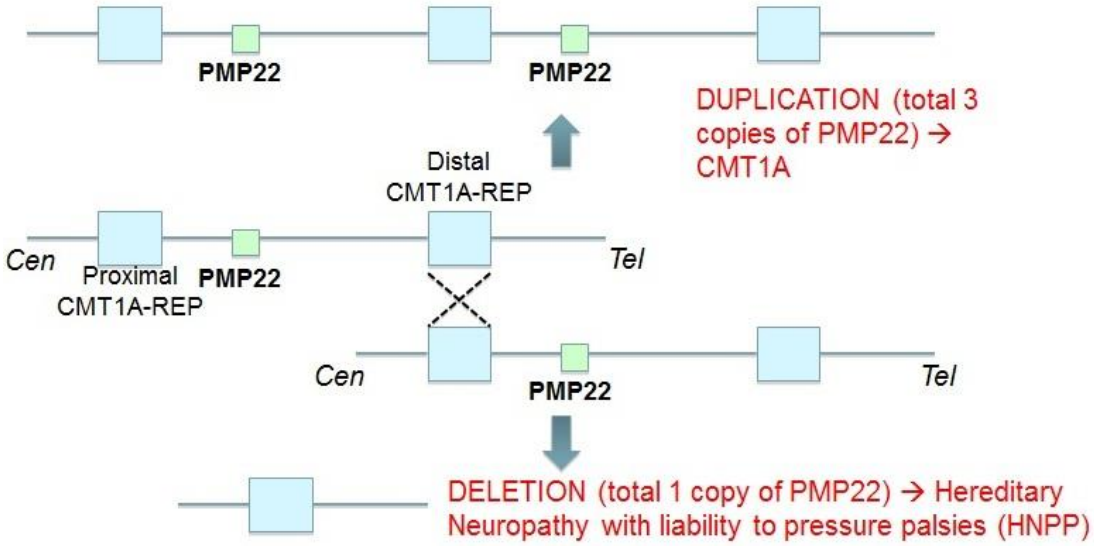

Figure 1-1 CMT1A and HNPP duplication/deletion mechanisms; Cen: centromere; Tel: telomere (adapted from Reiter et al., 1997).

The CMT1A-like demyelinating pathology found in the *Trembler* (p.Gly150Asp) and *Trembler-J* (p.Leu16Pro) mice carrying spontaneous *Pmp22* point mutations provided further evidence for the involvement of this gene in disease pathogenesis (Suter, Moskow, et al., 1992; Suter, Welcher, et al., 1992). *PMP22* point mutations, including the same point mutations as those found in the *Trembler-J* and *Trembler* mice were subsequently found in CMT1 and DSD patients not carrying the duplication, providing additional proof that this is the causative gene within the duplicated region (Ionasescu, Searby, Ionasescu, Chatkupt, et al., 1997; Ionasescu, Searby, Ionasescu, Reisin, et al., 1997; Roa, Garcia, Pentao, et al., 1993; Roa, Garcia, Suter, et al., 1993; Suter, Moskow, et al., 1992; Valentijn, Baas, et al., 1992). Point mutations in *PMP22* usually cause a rare, more severe form of CMT (Reilly et al., 2011; Valentijn, Baas, et al., 1992). In addition, when smaller duplications (Huang et al., 2010; Ionasescu et al., 1993; Palau et al., 1993; Valentijn et al., 1993) or deletions (Chapon et al., 1996) were discovered, *PMP22* was always found within the affected segment of DNA. Similarly, patients with a partial trisomy of Chr17p encompassing *PMP22* have a demyelinating neuropathy (Lupski et al., 1992; Roa et al., 1996). These findings, in addition to the observation that messenger ribonucleic acid (mRNA) levels of *PMP22* are increased in CMT1A patient nerve biopsies suggest that disease occurs via an increased gene dosage mechanism rather than by

gene disruption or mutation in another gene within the duplication (Boerkoel et al., 1999; Lupski et al., 1992; Yoshikawa et al., 1994). Recently, shorter duplications upstream of and not including *PMP22* were found to be associated with CMT1A. It is postulated that these smaller duplications affect *PMP22* expression via an as-of-yet undetermined mechanism (Weterman et al., 2010, Zhang et al., 2010).

1.4.4 Phenotypic variability in CMT1A: a role for genetic modifiers?

CMT1A patients with the same size duplication display high intra- and interfamilial phenotypic variability in terms of age of onset, extent of weakness and wasting, sensory signs and NCVs, even between monozygotic twins (Birouk et al., 1997; Garcia et al., 1995; Kaku et al., 1993; Thomas et al., 1997). While some patients may have serious skeletal deformities with severe proximal weakness and may be wheelchair-bound, others may remain asymptomatic and unaware they are affected (Pareyson & Marchesi 2009). A mildly affected father of a CMT1A patient was found to be a mosaic for the duplication therefore mosaicism may be a rare source of phenotypic variability in CMT1A (Sorour et al., 1995). In a study of 119 CMT1A patients, 25% were found to be asymptomatic, however patients will always have decreased NCV if they carry the duplication (Kaku et al., 1993; Birouk et al., 1997). A CMT1A patient was asymptomatic late in life with a mild phenotype on examination, while his son was severely affected (Berciano et al., 2012). Anticipation, or increase in disease severity over generations, has been described in CMT1A, with significantly earlier age of onset and more severe phenotype in some children of affected parents (Steiner et al., 2008).

Consistent with the predicted dosage effect mechanism of CMT1A, some rare CMT1A cases with four copies of *PMP22* have a more severe phenotype, although this is not always the case. In fact, levels of *PMP22* mRNA or protein were not found to correlate with disease severity. It follows that the expression level of *PMP22* does not completely determine the phenotype (Boerkoel et al., 1999; Hanemann et al., 1994; Huang et al., 2010; Kaku et al., 1993; Katona et al., 2009; LeGuern et al., 1997, Lupski et al., 1991).

A phenotype modifier effect of the environment as well as stochastic or epigenetic

effects would be predicted on the basis that identical twins show variable disease severity (Boerkoel et al., 1999; Fraga et al., 2005; Garcia et al. 1995). Hypothyroidism, obesity and exposure to toxins have been found to cause a mild increase in CMTNS scores and decrease in ambulation ability of CMT1A patients (Ursino et al., 2013). Diabetes is also usually associated with more severe sensory and motor impairment in patients with CMT1A. Diabetes may lead to deficient action potential propagation in motor nerve terminals, impaired axonal transport or mitochondrial function; therefore, the compound effect of CMT and diabetes pathologies would be expected to worsen the phenotype (Sheth et al., 2008; Ursino et al., 2013). However, it is unlikely that environmental factors and co-morbidities account for all of the disease variability. Therefore, epigenetics and genetic modifiers probably also play a role in influencing disease severity (Pareyson & Marchesi, 2009). As discussed in Section 1.4.2, it is possible that some of the phenotypic variability may be explained by immunological mechanisms in CMT1A (Ginsberg et al., 2004).

1.5 Novel disease genes in undiagnosed CMT patients

Despite the large number of genes already known to cause CMT, a genetic diagnosis is only reached in 70% of patients, therefore many patients remain undiagnosed, especially in CMT2 (Saporta et al., 2011). Obtaining a genetic diagnosis is crucial as it enables patients to receive more accurate counselling for family planning and rules out potentially treatable, acquired causes of neuropathy (Reilly et al., 2011). Identifying novel CMT-causing genes expands the list of pathomechanisms involved in CMT, allowing a better understanding of disease and the discovery of novel possible drug targets. Exome sequencing, or targeted sequencing of the protein-coding portion of the genome, has already been used successfully numerous times to identify new CMT genes or novel mutations in known CMT genes (Lupski et al., 2010; Montenegro et al., 2011; Weedon et al., 2011). This method is particularly time and cost-effective in genetically heterogeneous diseases such as CMT (Montenegro et al., 2011).

The many pathways involved in peripheral nerve degeneration render it difficult to identify the causative variant within the exome sequencing data. CMT genes encode

proteins with a variety of functions, including myelin structural components (*PMP22*, *MPZ*, *GJB1*, *PRX*), mitochondrial fusion and fission (*MFN2*, *ganglioside induced differentiation associated protein 1* (*GDAP1*)), endocytosis, intracellular protein sorting and quality control (*HSPB1*, *HSPB8*, *SH3 domain and tetratricopeptide repeats 2* (*SH3TC2*), *dynamin 2* (*DNM2*), *LRSAM1*, *MTMR2*, *MTMR13*, *SAC1 lipid phosphatase domain containing* (*FIG4*), *rab7 member RAS oncogene family* (*RAB7*), *lipopolysaccharide-induced TNF factor* (*LITAF*)), transcription factors and regulation of gene expression (*EGR2*, *LMNA*, *mediator complex subunit 25* (*MED25*), *CTD (carboxy-terminal domain, RNA polymerase II, polypeptide A) phosphatase, subunit 1* (*CTDP1*)), ion channels (*transient receptor potential cation channel, subfamily V, member 4* (*TRPV4*)), protein synthesis (*GARS*, *tyrosyl-tRNA synthetase* (*YARS*), *alanyl-tRNA synthetase* (*AARS*), *lysyl-tRNA synthetase* (*KARS*), *methionyl-tRNA synthetase* (*MARS*)), as well as cytoskeletal dynamics, axonal transport, and vesicular motility (*NEFL*, *inverted formin, FH2 and WH2 domain containing* (*INF2*), *FYVE, RhoGEF and PH domain containing 4* (*FGD4*), *kinesin family member 1B* (*KIF1B*), *dynein, cytoplasmic 1, heavy chain 1* (*DYNC1H1*)) (Pandraud, in press*;* Patzkó & Shy, 2011). The protein functions of the CMT-associated genes are summarized in Appendix I Table I-2. It remains unknown whether mutations in all CMT genes act via a small number of shared pathomechanisms, or if the mechanism of neurodegeneration is unique for each mutation; elucidating this issue will be important for the development of treatment strategies in CMT (Roberts, 2012).

The genes causing demyelinating neuropathy are all expressed in Schwann cells. However, many of these genes such as *LITAF*, *GJB1*, *MTMR2*, *SH3TC2*, *FGD4* and *FIG4* are also expressed in other cell types (Scherer & Wrabetz, 2008). While it is fascinating that mutations in ubiquitously-expressed genes may exclusively cause a peripheral neuropathy, and that proteins involved in CMT have many different cell functions, it renders novel gene finding very complicated. The intricacies of exome sequencing in CMT will be highlighted in Chapter 5.

Exome sequencing was recently successfully used to identify a mutation in a novel gene causing another related neuropathy, BVVL (Green et al., 2010; Johnson, Gibbs,

et al., 2010). A severe sensory-motor neuropathy is present in BVVL as part of a more complex disorder. This discovery has identified a new pathway leading to neuropathy along with a potential treatment.

1.6 Brown-Vialetto-Van Laere (BVVL) syndrome: a severe neuronopathy

1.6.1 The BVVL phenotype

BVVL, a rare condition characterised by progressive pontobulbar palsy with deafness is named after the physicians who described it initially. Charles Brown first defined this condition as an Amyotrophic Lateral Sclerosis (ALS)-like disease with infantile-onset and hearing loss (Brown, 1894). The index case was a 15-year old German boy with severe deafness, respiratory insufficiency and bulbar weakness with labio-glosso laryngeal paralysis and atrophy of the hand and arm muscles (Brown, 1894). According to Brown (1894), five such cases of progressive bulbar paralysis had been described since 1889. In 1936, Vialetto reported three siblings with hearing loss and pontobulbar palsy; a similar phenotype was described in four sisters by M. J. Van Laere in 1966 (Van Laere, 1966; Vialetto, 1936).

Disease onset ranges from infancy to early on in the third decade of life, however the age of onset may be variable, even within families (Dipti et al., 2005; Gallai et al., 1981; Johnson, Gibbs, et al., 2010; Sathasivam, 2008). The disease is most frequently diagnosed in the second decade. Patients may present with pontobulbar palsy, bilateral sensorineural hearing loss (usually the presenting symptom), diaphragmatic paralysis, LMN signs in the limbs and severe sensory-motor neuropathy (Sathasivam, 2008). There is often upper and lower limb wasting and weakness (Dipti et al., 2005; Gallai et al., 1981; Mégarbané et al., 2000; Sathasivam, 2008). Some patients may have less bulbar involvement but these patients often have significant weakness of the trunk and limbs. UMNs are less frequently affected (Dipti et al., 2005; Sathasivam, 2008). Two main phenotypes have been described. The type with onset in infancy is more severe and includes hypotonia, respiratory insufficiency, rapid progression and early death. An early-onset BVVL phenotype may also involve ptosis, stridor caused by vocal cord paresis, and facial and upper limb weakness. Later onset cases display deafness, cranial nerve palsies and neuronopathy. Hearing loss may not always be clinically obvious, and may need to

be confirmed with brainstem auditory evoked potentials, especially in younger cases (Voudris et al., 2002).

In a recent review of 74 patients described in a total of 35 reports in the literature, the mean age of presentation was 8.2 years. The most common symptoms for all age groups were: bulbar palsy (92%), hearing loss (81%), facial weakness (77%) and respiratory compromise (64%) (Bosch et al., 2012). Features such as retinitis pigmentosa, epilepsy, optic atrophy, autonomic dysfunction, cerebellar ataxia and cognitive impairment may also be present, albeit these remain rare (Bosch et al., 2012; Sathasivam et al., 2008).

The course of disease is variable (Sathasivam et al., 2008). It may be fatal with a short disease course; infants with BVVL become dependent on ventilation early on in the disease, with most dying before the age of 10 years old. Alternatively, BVVL patients may stay stable or improve over time, but events such as viral infection, fever, surgery, or pregnancy during which riboflavin is in higher demand may trigger the onset of disease or cause a worsening of symptoms (Bandettini Di Poggio et al., 2014; De Grandis et al., 2005; Dipti et al., 2005; Francis et al., 1993; Gallai et al., 1981; Heller et al., 1974; Powers, 2003; Vialetto, 1936). Cardiac complications have been reported in BVVL patients (Descatha et al., 2006), including one patient who developed cor pulmonale likely due to hypoventilation (Da Silva-Júnior et al., 2011). Sleep-disordered breathing due to central sleep apnoea has also been reported (Miao et al., 2007).

Approximately half of cases are sporadic; inheritance is mostly AR although some rare cases with AD or X-linked inheritance have been reported (De Grandis et al., 2005; Hawkins et al., 1990; Sathasivam, 2008). Incomplete penetrance and variable phenotypes among affected family members have been described (Hawkins et al., 1990; Lombaert et al., 1976). Males are more severely affected and die at a younger age, which may explain the female to male ratio of 3:1 (Gallai et al., 1981; Sathasivam, 2008).

CMAPs may be reduced (De Grandis et al., 2005) but NCVs are often normal (Sathasivam, 2008; Yiu & Ryan, 2012). Magnetic resonance imaging (MRI) is

usually normal in BVVL, although brainstem and cerebellar atrophy, and/or hyperintensity of basal ganglia, brainstem nuclei, cerebellar peduncles or subcortical white matter have been described in some cases (Ciccolella et al., 2012; Dakhil et al., 2010; Francis et al., 1993; Koul et al., 2006; Koy et al., 2012; Malheiros et al., 2007; Sathasivam, 2008). BVVL often results in degeneration of the cranial nerve nuclei of the brainstem with chromatolysis and gliosis (Sathasivam, 2008; Spagnoli & De Sousa, 2011). The cranial nerves VII to XII are most commonly affected; it is less common for the II to VI cranial nerves to become involved as the disease progresses (Bosch et al., 2012; Gallai et al., 1981; Koul et al., 2006; Sathasivam, 2008). Reports have also described anterior horn cell degeneration and loss of myelinated fibres in the ventral roots of the spinal cord, as well as axon loss in the peripheral nerve (Francis et al., 1993; Gallai et al., 1981; McShane et al., 1992; Spagnoli & De Sousa, 2011). Muscle biopsies are either normal or show myopathic changes or grouped atrophic fibres (Sathasivam, 2008). Signs of reinnervation in the limbs and facial muscles have been reported (De Grandis et al., 2005).

BVVL is therefore an early-onset motor neurone disease (MND), with bulbar and corticospinal tract involvement (De Grandis et al., 2005; Dipti et al., 2005). However, given the presence of a CMT-like sensory or sensory-motor polyneuropathy in many BVVL cases, with damage to primary sensory neurones and many times absence of sensory responses, it has been suggested to consider BVVL a severe sensory-motor neuropathy and not just a pure anterior horn disease or motor neuronopathy (Gallai et al., 1981; Mégarbané et al., 2000; Sathasivam et al., 2000). In contrast to demyelinating neuropathies, there is usually more CNS involvement in early-onset motor neuronopathies and early-onset axonal neuropathies. Axonal sensory-motor neuropathies with early-onset are not always easy to distinguish from motor neuronopathies, both clinically and on NCS (Yiu & Ryan, 2012).

Fazio-Londe (FL) syndrome is now considered to be an allelic condition and part of a clinical spectrum with BVVL; it has the same clinical presentation but without the deafness (Dipti et al., 2005; Fazio, 1892; Londe, 1893; Londe, 1894; McShane et al., 1992). Other diseases closely resembling BVVL include Madras MND, Boltshauser syndrome and Nathalie Syndrome. Madras MND is predominantly seen in India;

patients exhibit muscle weakness and wasting in the limbs, deafness, and palsies of the VII, IX and XII cranial nerves. Most cases are sporadic. Boltshauser syndrome has AD inheritance and is characterized by deafness, distal muscular atrophy and vocal cord paralysis without LMN limb signs. Patients with Nathalie syndrome have no lower cranial nerve signs but have deafness and weakness in addition to spinal muscular atrophy (SMA), cataracts, hypogonadism and cardiac conduction defects (Sathasivam, 2008).

The phenotypes of both ALS and SMA may overlap with the complex BVVL phenotype (Horvath, 2012; Sathasivam, 2008). Although spinal muscular atrophy type 1 mostly involves motor neurones of the anterior horns, patients with homozygous gene defects in *survival motor neuron 1* (*SMN1*) may have peripheral motor and sensory nerve involvement (Yiu & Ryan, 2012). Spinal muscular atrophy with respiratory distress type 1 (SMARD1) is an "SMA plus" syndrome caused by AR mutations in *immunoglobulin mu binding protein 2* (*IGHMBP2*), usually leading to early-onset severe axonal polyneuropathy with distal muscle and lower limb weakness and respiratory failure due to diaphragmatic paralysis. Infantile-onset is most common. There may also be autonomic involvement, pneumonia and hypotonia but no deafness has been described (Yiu & Ryan, 2012). ALS is characterised by adult-onset degeneration of motor neurones in the corticospinal tract, brainstem and anterior horn cells of the spinal cord. Patients have UMN and LMN limb signs with progressive muscle weakness and wasting, fasciculations and spasticity. Patients often die of respiratory paralysis (Hardiman et al., 2011). BVVL has been described as an AR juvenile form of ALS since both BVVL and ALS have bulbar and LMN involvement (Brown, 1894; De Grandis et al., 2005; Gallai et al., 1981; Sathasivam, 2008). BVVL differs from ALS in that BVVL patients have deafness, an earlier age of onset, a more irregular disease course, and UMN limb signs are not invariably present (De Grandis et al., 2005; Gallai et al., 1981; Sathasivam, 2008). Of note, *ubiquilin 2* (*UBQLN2*) mutations have been identified as a rare cause of ALS; a recent study has identified a heterozygous mutation in a related gene previously linked to neurodegeneration, *ubiquilin 1* (*UBQLN1*), in a BVVL patient with atypical early-onset ALS with bulbar palsy and hearing loss. Although the pathogenicity of

this mutation remains uncertain, this finding highlights the overlap of BVVL and ALS phenotypes (González-Pérez et al., 2012).

1.6.2 Biochemical profile of BVVL: clue to new mechanism of neuropathy

The first clue into the genetic cause of BVVL came from results of fatty acid β-oxidation analyses. In the matrix of mitochondria, fatty acid β-oxidation breaks down long chains of acyl-Coenzyme A (acyl-CoA) fatty acids into acetyl-Coenzyme A (acetyl-CoA) molecules, which are needed for adenosine 5'-triphosphate (ATP) production via the Krebs cycle. During the first step of fatty acid metabolism, the fatty acid moiety of acyl-CoA esters is oxidised by either short-chain, medium-chain or long-chain acyl-CoA dehydrogenases. The next two enzymes involved, electron transfer flavoprotein (ETF) and electron transfer flavoprotein ubiquinone oxidoreductase (ETF:QO) carry reducing equivalents to Coenzyme Q (CoQ) in the mitochondrial electron transport chain. CoQ transfers these electrons to oxygen in an ATP-producing process (Henriques et al., 2010).

Metabolic studies of BVVL patients reveal accumulating acyl-CoA and carnitine esters in the plasma, as well as a urine organic acid profile which both mimic the fatty acid β-oxidation defect seen in patients with mild multiple acyl-CoA dehydrogenase deficiency (MADD). BVVL patients showed evidence of elevated short and medium-chain acylcarnitines. Long-chain acylcarnitines were elevated in only one of the patients (Anand et al., 2012; Bosch et al., 2011; Haack et al., 2012; Johnson et al., 2012).

MADD may be early-onset with a severe, often fatal disease course and hypoketotic hypoglycaemia, or late-onset with a mild phenotype of lipid storage myopathy. MADD results in impaired flavin adenine dinucleotide (FAD)-dependent dehydrogenation reactions during mitochondrial fatty acid β-oxidation and amino acid metabolism as a result of mutations in *electron transfer flavoprotein alpha/beta subunit* (*ETFA/ETFB*), which encodes ETF, or *electron transfer flavoprotein dehydrogenase* (*ETFDH*), which encodes ETF:QO, leading to accumulation of metabolic intermediates (Bosch et al., 2011; Gregersen et al., 2008; Olsen et al., 2007; Powers, 2003). FAD, one of the active co-enzyme forms of riboflavin, is an

essential cofactor for acyl-CoA dehydrogenases, as well as ETF and EFT:QO, functioning as an electron carrier in fatty acid β-oxidation (Depeint et al., 2006; Gregersen, 1985; Henriques et al., 2009; Massey, 2000). Interestingly, studies of riboflavin-deficient rats have shown that moderate riboflavin deficiency results in an MADD-like metabolic profile (Brady & Hoppel, 1985; Goodman, 1981). In fact, as will be discussed in Chapter 7, some forms of MADD are responsive to riboflavin treatment.

Another important insight into the genetic basis of BVVL was that BVVL patients had decreased plasma levels of riboflavin and its active coenzyme forms, FAD and flavin mononucleotide (FMN), which were not due to nutritional riboflavin deficiency (Bosch et al., 2011).

1.6.3 Riboflavin transporter mutations: a novel cause of motor and sensory neuropathy

As of 2008, 58 cases of BVVL with no known genetic cause had been described in the literature since the first report in 1894 (Sathasivam, 2008). Since then, the genetic cause of over 20 BVVL cases has been found. The decrease in plasma flavin levels and MADD-like profile suggested that riboflavin transporters may play a role in BVVL disease pathogenesis (Bosch et al., 2011). Indeed, Green et al. (2010) were the first to report mutations in *solute carrier family 52, riboflavin transporter, member 3* (*SLC52A3*) (previously *chromosome 20 open reading frame 54* (*C20orf54*)) as the cause of disease in a consanguineous family with BVVL, and later in other unrelated families (Green et al., 2010). *SLC52A3* was found to produce the intestinal human riboflavin transporter 3 (RFVT3) (previously human riboflavin transporter 2 (hRFT2)), a protein necessary for riboflavin absorption. As described by Bosch et al. (2011) a block in the riboflavin transport due to a mutation in *SLC52A3* leads to decreased availability of riboflavin, FAD and FMN (as evidenced by reduced plasma levels of all three); this causes metabolic dysfunction via an increase in the levels of acylcarnitines resulting from impaired dehydrogenation reactions in fatty acid β-oxidation, thus explaining the MADD-like biochemical profile. Almost simultaneously, Johnson, Gibbs, and colleagues (2010) described additional families with mutations in *SLC52A3*. Bosch et al. (2011) also found a defect in the same gene in a BVVL patient and two siblings with FL syndrome with

early-onset progressive muscle weakness, respiratory insufficiency, cranial nerve palsies and diaphragmatic paralysis (Bosch et al., 2011). Additional reports confirmed the association of *SLC52A3* mutations and the BVVL phenotype (Anand et al., 2012; Bandettini Di Poggio et al., 2013; Ciccolella et al., 2012; Dezfouli et al., 2012; Johnson et al., 2012; Koy et al., 2012).

Solute carrier family 52, riboflavin transporter member 1 (*SLC52A1*) (previously *G protein-coupled receptor 172B* (*GPR172B*)) encodes another human riboflavin transporter, human riboflavin transporter 1 (RFVT1) (previously human riboflavin transporter 1 (hRFT1)) (Yonezawa et al., 2008). Haploinsufficiency in *SLC52A1* caused by a heterozygous deletion of exons 2 and 3 can cause mild maternal riboflavin deficiency (Chiong et al., 2007; Ho et al., 2010). While the haploinsufficient mother showed no symptoms, she had an MADD-like biochemical profile and plasma flavin deficiency. In her infant however, the heterozygous deletion of two exons in the mother in addition to the nutritional riboflavin deficiency during pregnancy resulted in a transient riboflavin-responsive disorder with an MADD-like clinical and biochemical profile at birth (Ho et al., 2010). As only one patient with a genetic defect in *SLC52A1* has been reported and the clinical picture was MADD-like, it remains unclear if mutations in *SLC52A1* may be associated with BVVL. Interestingly, a report has previously described a pregnant mother with MADD with an unknown defect in riboflavin metabolism; the mother had several floppy or stillborn babies, but the syndrome could be prevented in further pregnancies by supplementation with riboflavin. A defect in FAD transport or synthesis was suggested to cause the disease (Harpey et al., 1983).

Johnson et al. (2012) performed exome sequencing in a cohort of BVVL patients negative for *SLC52A3* mutations and found a homozygous mutation in *solute carrier family 52, riboflavin transporter member 2* (*SLC52A2*) in a Lebanese kindred with childhood MND and BVVL features (Johnson et al., 2012). *SLC52A2* (previously *G protein-coupled receptor 172A* (*GPR172A*)) encodes a third riboflavin transporter, human riboflavin transporter 2 (RFVT2) (previously human riboflavin transporter 3 (hRFT3)) (Yao et al., 2010). The same mutation was found in another family on a different haplotype; BVVL patients in both families shared a similar phenotype as

well as an MADD-like biochemical profile (Johnson et al., 2012). Additional patients with compound heterozygous or homozygous *SLC52A2* mutations were soon described (Ciccolella et al. 2013; Haack et al., 2012). In contrast to patients with *SLC52A3* mutations, plasma flavin levels are often normal in patients with *SLC52A2* mutations, most likely because the *SLC52A3* encoded-transporter RFVT3 is responsible for riboflavin uptake from food while the *SLC52A2*-encoded transporter RFVT2 transports riboflavin from the blood into target cells (Haack et al., 2012). It should be noted that the metabolic profile may also be normal in both *SLC52A2* and *SLC52A3* mutated patients (Bosch et al., 2012; Ciccolella et al., 2012; Ciccolella et al., 2013; Koy et al., 2012). Furthermore, acylcarnitines profiles of the newborn bloodspots of BVVL patients were normal and patients did not show a phenotype at birth, likely due to the riboflavin available from the baby's mother (Bosch et al., 2011). Therefore, acylcarnitine profiles cannot be used as a diagnostic tool at birth (Bosch et al., 2012).

Although there have been significant advances in the genetic diagnosis of BVVL in the past few years, many cases remain unresolved, suggesting genetic heterogeneity in this disease. Chapter 6 will investigate the genetics of BVVL by performing a genetic screening of *SLC52A1, SLC52A2* and *SLC52A3* in BVVL and BVVL-like patients, and by searching for novel causative genes in BVVL and related neuropathies using exome sequencing.

1.6.4 Phenotype of nutritional riboflavin deficiency

Riboflavin deficiency (ariboflavinosis) is common in many parts of the world, especially amongst individuals whose diets lack meat and dairy products. The recommended daily intake is 1.1 mg and 1.3 mg for adult females and males, respectively (Lienhart et al., 2013; Powers, 2003). In developed countries, riboflavin deficiency usually remains subclinical and its effects are usually only seen at the biochemical level (Foraker et al., 2003). In contrast to the phenotype of BVVL, the symptoms associated with riboflavin deficiency are usually dermatological in nature and usually include anaemia, inflammation of the tongue and mouth, cracked and red lips, mouth ulcers, cheilosis, sore throat but also neuropathy (Depeint et al., 2006; Powers, 2003; Spagnoli & De Sousa, 2011). In animals, riboflavin deficiency can be

associated with foetal development abnormalities (Powers, 2003). Biochemical indications of deficiency generally appear after a few days of following a riboflavin-free diet (Powers, 2003). A rare case of neurodegeneration with progressive deafness, vision loss, anaemia, gait ataxia and sensory-motor polyneuropathy has been described in a patient with moderate riboflavin deficiency; most of the symptoms resolved upon riboflavin treatment (Leshner et al., 1981). A demyelinating peripheral neuropathy characterized by hypertrophic Schwann cells, tomaculae and onion bulb formation was also observed in young chickens with riboflavin deficiency, with remyelination taking place when riboflavin levels were restored (Cai et al., 2009). Demyelination has also been noted in pigeons and rats fed a riboflavin-deficient diet (Powers, 2003). Riboflavin deficiency may increase the risk of certain cancers, although this is a matter of debate (Powers, 2003). Riboflavin is also necessary for the proper functioning of the endocrine, cardiovascular and immune systems, and deficiency may therefore negatively impact these systems as well (Mazur-Bialy et al., 2013; Powers, 2003).

1.6.5 Response to high-dose riboflavin treatment in BVVL patients

Before the identification of riboflavin transporter mutations in BVVL patients, treatment was palliative and involved gastrostomy and assisted ventilation; patients usually died of respiratory failure (Sathasivam, 2008). Treatment with steroids and immunoglobulins was usually not successful or allowed only temporary stabilization or improvement of only some of the symptoms (Ciccolella et al., 2012; Dakhil et al., 2010; Gallai et al., 1981; Hawkins et al., 1990; Koy et al., 2012; Sathasivam, 2008).

Given the role of the causative genes in riboflavin transport, a treatment of intravenous or oral riboflavin at 10 mg/kg body weight/day was initiated in some patients. In a review of BVVL patients treated with riboflavin, the mean age at the start of treatment was 6.9 years, with the first improvements seen within days for some and gradually over a few months for other patients (Bosch et al., 2012). Eight patients among the 13 treated showed very good clinical improvement (Bosch et al., 2012). Indeed, most BVVL and FL patients carrying *SLC52A3* mutations improved from a clinical and biochemical point of view when administered high-dose riboflavin therapy early on in the disease course (Anand et al., 2012; Bosch et al.,

2011). In the *SLC52A3* patients described in the Ciccolella et al. (2012) study, one patient with a severe phenotype showed a halt in disease progression after eight months of treatment, but there was no improvement in the other patient. Another case with a normal metabolic profile and *SLC52A3* mutations did not improve on high-dose riboflavin (Koy et al., 2012). In *SLC52A2* mutated patients, there was either moderate improvement of symptoms (Haack et al., 2012) or good clinical improvement with normalization of the biochemical profile (Johnson et al., 2012).

Overall, most BVVL patients treated with riboflavin had less need for ventilation, and some showed full recovery. In all cases, riboflavin restored acylcarnitine profiles and plasma flavin levels to normal. Importantly, improvements were also seen in patients with normal plasma acylcarnitine profiles and flavin levels. Symptoms often came back if supplementation was stopped and in the long-term, the effect of the riboflavin treatment sometimes decreased (Bosch et al., 2012). The patients who did not respond to riboflavin were either not treated for very long, or received prolonged treatment but remained stable with no improvement; three out of the five unresponsive patients did not have mutations in *SLC52A1*, *SLC52A2* or *SLC52A3*. In the untreated patients that died, the mean age of death was 11.6 years with a mean time span between presentation and death of five years. The most common cause of death was respiratory insufficiency (Bosch et al., 2012). Given the promising results of riboflavin therapy, Bosch and colleagues (2012) suggest not to wait for results of genetic tests to start treatment. This treatment needs to be administered early on in the disease course because diaphragmatic paralysis is probably not reversible (Bosch et al., 2012; Spagnoli & De Sousa, 2011). Riboflavin supplementation may only delay disease progression and may be ineffective if too much damage has already occurred in the early disease stages (Bosch et al., 2012; Spagnoli & De Sousa, 2011).

The identification of riboflavin transporter mutations as a novel genetic cause of neuropathy has uncovered yet another new disease pathway leading to damage of peripheral nerves. Importantly, this exciting discovery has made BVVL the first treatable inherited neuropathy. Riboflavin may also be a potential therapy in other MNDs.

1.6.6 Biological functions of riboflavin, flavin adenine dinucleotide (FAD) and flavin mononucleotide (FMN)

An understanding of the biological functions of riboflavin and its cofactors is essential for elucidating the disease mechanisms leading to the BVVL phenotype, which is the principal aim of Chapter 7. Riboflavin (7,8-dimethyl-10-ribityl-isoalloxazine, $C_{17}H_{20}N_4O_6$, vitamin B_2), one of the eight B vitamins, is a yellow fluorescent water-soluble vitamin which was first observed in 1872 and recognized to be riboflavin in the early 1930s when it was still known as the "old yellow enzyme" (Massey, 2000; McCormick, 1989; Northrop-Clewes & Thurnham, 2012). Riboflavin is sensitive to sunlight and ultraviolet (UV) rays. Unlike prokaryotes, humans cannot synthesize riboflavin and therefore need to obtain it from food via intestinal absorption as it is continually excreted through the urine (Depeint et al., 2006; Northrop-Clewes & Thurnham, 2012). Riboflavin is necessary for normal cellular function, growth and development. In our diet, riboflavin is found in the highest quantities in eggs, milk, cheese, leafy green vegetables, meat, almonds and yeast (Depeint et al., 2006; Powers, 2003). A small amount of riboflavin is also obtained from a bacterial source as it is synthesized by the microflora of the large intestine in humans (Powers, 2003).

Riboflavin is a precursor of FAD (riboflavin 5' adenosine diphosphate) and FMN (riboflavin-5′-phosphate), its biologically active forms (Depeint et al., 2006; Northrop-Clewes & Thurnham, 2012). In addition to the isoalloxazine tricyclic ring and ribityl side chain of riboflavin, FMN contains an additional phosphate group at the 5' hydroxyl side chain terminus of riboflavin, and FAD contains the FMN structure with an added AMP moiety (Figure 1-2). Riboflavin is converted to FMN by riboflavin kinase and FAD synthetase converts FMN to FAD (Henriques et al., 2010; McCormick, 1989).

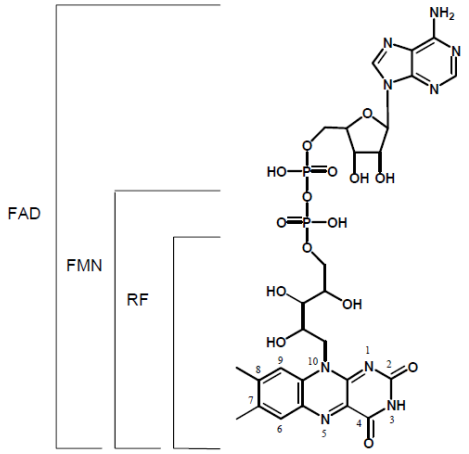

Figure 1-2 Structure of riboflavin and its cofactor forms, FAD and FMN (reproduced from Johnson et al., 2012).

FMN and FAD are prosthetic groups of flavoenzymes, which may be flavin oxidases, flavin reductases, or flavin dehydrogenases (Depeint et al., 2006; Massey, 2000). Due to the aromatic ring structure of the FAD and FMN cofactors, flavins are able to donate or accept one or two electrons in oxidation, reduction and dehydrogenation reactions. Most flavoenzymes (84%) use FAD as a prosthetic group and most are non-covalently bound to either FAD or FMN (Henriques et al., 2010; Lienhart et al., 2013; Powers, 2003). Over 90 genes encode flavin-dependent proteins, and mutations in about 60% of them are involved in causing human disease, many of which are mitochondrial since most flavins in the cell are located in the mitochondria (Lienhart et al., 2013; Rhead et al., 1993).

Flavoenzymes and flavoproteins are involved in a large number of biochemical reactions therefore riboflavin, FAD and FMN are extremely important for a wide range of cellular functions. In the case of a riboflavin deficiency or error in riboflavin metabolism or transport, activity of many of these enzymes and proteins is affected (Henriques et al., 2010; Massey, 2000). Some functions of flavoenzymes include but are not limited to: metabolism of lipids, proteins and carbohydrates, iron metabolism, conversion of vitamin A to retinoic acid, conversion of tryptophan to vitamin B_3, activation of vitamin B_6 and folate, choline metabolism, biosynthesis of Coenzyme A, CoQ, steroid and thyroxine, phospholipid metabolism, neurotransmitter

metabolism, synthesis of sphingosine, production of superoxide, reduction of hydroperoxides and light production in bioluminescent bacteria (Lienhart et al., 2013; Massey, 2000). Flavoproteins have signal transduction roles in DNA repair (Schuman Jorns et al., 1987) and apoptosis (Susin et al., 1999). Riboflavin has also been found to have anti-inflammatory and anti-nociceptive properties (Mazur-Bialy et al., 2013).

As mentioned in Section 1.6.2, riboflavin and its cofactors are important for energy metabolism due to the role of FAD as a coenzyme for acyl-CoA dehydrogenase, ETF and ETF:QO during fatty acid β-oxidation. However, FMN and FAD are also needed for cellular respiration in the mitochondrial respiratory chain (MRC). Complexes I and II are two flavin-dependent complexes of the MRC. FMN is the primary electron acceptor for complex I. FAD is the initial electron acceptor in complex II, a second point of entry into the MRC. Mitochondrial diseases, which may include neuropathies, are associated with suboptimal oxidative phosphorylation and ATP production (Marriage et al., 2003). Interestingly and as will be discussed further in Chapter 7, riboflavin has proven an effective therapy in patients with mitochondrial diseases associated with complex I and/or complex II deficiencies (Bernsen et al., 1993; Bugiani et al., 2006; Gerards et al., 2011; Gianazza et al., 2006; Marriage et al., 2003; Olsen et al., 2007; Scholte et al., 1995; Vergani et al., 1999). The functions of FAD and FMN in energy metabolism, as well as their possible involvement in the pathogenesis of BVVL will be discussed extensively in Chapter 7.

In addition to its role in energy metabolism, riboflavin also acts indirectly as an antioxidant: FAD is needed for the recycling of glutathione as it is a cofactor for glutathione reductase. Glutathione reductase converts oxidised glutathione (GSSG) to reduced glutathione (GSH). Therefore, FAD is indirectly necessary for protection against oxygen-derived free radicals since GSH is a scavenger of free radical and reactive oxygen species (ROS) (Depeint et al., 2006; Henriques et al., 2010). In fact, the erythrocyte glutathione reductase (EGR) test, which assesses the activity of EGR with and without FAD, is commonly performed to test for riboflavin nutritional status (Northrop-Clewes & Thurnham, 2012).

1.7 Thesis aims

This Thesis focuses on several aspects of two inherited peripheral neuropathies, CMT and BVVL, and utilises both genetic and molecular biology-based methods with the following aims:

- **Chapter 3:** To provide frequency data of mutations in CMT1 genes in selected populations (United Kingdom, Greece and Russia), and to expand phenotype-genotype correlations in CMT1. It is hoped that this work will help clinicians target genetic tests in CMT. Canines with peripheral neuropathies will also be screened for CMT genes in the hope that they may serve as animal models of CMT.

- **Chapter 4:** To elucidate the pathogenesis of CMT1A by identifying the genetic factors modulating the disease phenotype. This work may lead to the identification of targets for drug treatment, and allow for more accurate prediction of the phenotype in patient counselling.

- **Chapter 5:** To identify novel causes of CMT in undiagnosed families using exome sequencing.

- **Chapter 6:** To detect unrecognized cases of BVVL and allow for early treatment by screening cases with a BVVL-like phenotype for mutations in riboflavin transporter genes, a novel genetic cause of severe but treatable infantile neuropathy. This Chapter also aims to identify the genetic cause of disease in patients with BVVL-like phenotypes and in patients with AR polyneuropathy with a predominant motor component.

- **Chapter 7:** To elucidate the pathogenesis of riboflavin transporter mutations in BVVL, a novel neuropathy-associated disease pathway.

Chapter 2 Materials and methods

2.1 Genetic studies

2.1.1 Ethics approval and consent

This study has been granted ethical approval by the National Research Ethics Service Committee of the National Hospital for Neurology and Neurosurgery (NHNN) in Queen Square, London, UK. The University College London Hospital (UCLH) REC numbers are 09/H0716/61 for the CMT genetic study and 99/N103 for the BVVL genetic study and any disorder of the peripheral nerve and spinal cord. Written informed consent was obtained from all patients, parental guardians and/or included family members.

2.1.2 Control deoxyribonucleic acid (DNA) samples

DNA of British controls for CMT sequencing studies was obtained from the Wellcome Trust Case Control Consortium (WTCCC) 1958 British Birth Cohort (http://www.wtccc.org.uk). DNA of controls of Northern European origin for the CMT Immunochip association study was obtained from the WTCCC2 (http://www.wtccc.org.uk/ccc2/). The WTCCC is a collaborative study composed of over 50 research groups from the UK designed to look at genetic variation in the human population and its role in disease.

2.1.3 DNA extraction from blood, snap-frozen muscle and saliva

The QIAamp DNA blood Midi kit (spin protocol; Qiagen, Germany) was used to extract total DNA from 700 µl ethylenediaminetetraacetic acid (EDTA) blood of some canines with peripheral neuropathies according to the manufacturer's instructions. The DNeasy Blood & Tissue kit (Qiagen) was used to extract total DNA from snap-frozen muscle of additional canines. Briefly, for both DNA extraction kits, the lysate was added to the spin column following enzymatic lysis. DNA remained bound to the silica membrane column, and impurities were washed away. Finally, DNA was eluted in autoclaved deionised water (dH_2O).

The Oragene kit (OraSure technologies, USA) was used to extract total DNA from human saliva of one BVVL patient following the manufacturer's instructions (details of standard protocol in Appendix II).

2.1.4 Whole-genome DNA amplification

Due to the low amount of DNA available for Sanger sequencing, a whole-genome amplification of genomic DNA (gDNA) samples (10 ng) from the Russian CMT cohort was performed using the GenomePlex Complete Whole-Genome Amplification kit according to the manufacturer's instructions (Sigma, USA). This kit enables 500-fold amplification of gDNA. It is based upon 1) random fragmentation of gDNA 2) library preparation by converting the resulting small fragments to polymerase chain reaction (PCR)-amplifiable OmniPlex Library molecules flanked by universal priming sites, and 3) PCR amplification of library using universal oligonucleotide primers. Following this procedure, the whole-genome amplification product was purified using Millipore Multiscreen HTS filter plates (Merck-Millipore, Germany). For quality control, products were run on a 1.3% w/v agarose (Roche, Switzerland) gel. DNA concentration and purity were assessed using the NanoDrop ND-1000 spectrophotometer (NanoDrop Technologies, USA) (Section 2.1.5).

2.1.5 DNA concentration and purity

DNA concentration and purity were assessed using the NanoDrop ND-1000 spectrophotometer as per the manufacturer's instructions (NanoDrop Technologies). The DNA concentration was assayed at 260 nm. Nucleic acids and proteins have absorbance maxima at 260 and 280 nm, respectively. Absorbance at 230 nm reflects the presence of other contaminants. The 260/280 and 260/230 absorbance ratios are used to evaluate contamination with protein, phenol or other compounds. For DNA, a 260/280 absorbance ratio of approximately 1.8 and a 260/230 absorbance ratio of 1.8-2.2 are considered acceptable.

2.1.6 Quantitative polymerase chain reaction for confirmation of the Chr17p11.2 duplication

Quantitative polymerase chain reaction (qPCR) for confirmation of the Chr17p11.2 duplication in selected CMT1A cases was carried out by assessing gene dosage of *PMP22* exon 4 using SYBR Green I chemistry (Applied Biosystems, USA). The SYBR Green dye binds to all double-stranded DNA non-specifically therefore the fluorescence signal represents the amount of double-stranded DNA product generated during the PCR reaction. Primer sequences for *PMP22* exon 4 (obtained from Kim et al., 2003) and the housekeeping gene *actin, beta-like 2* (*ACTBL2*) are found in Appendix IV Table IV-1. qPCR was performed according to the standard SYBR Green I protocol (see Appendix II). The comparative delta-delta threshold cycle (C_t) method was used for relative quantification of *PMP22* gene dosage since both the target and housekeeping genes amplified at similar efficiencies. The C_t, or threshold cycle in the log phase of PCR, is the number of cycles needed for the fluorescent signal to exceed background signal; it is inversely proportional to the amount of DNA in the sample (Livak & Schmittgen, 2001). Samples with relative quantification values (RQ) between 0.8 and 1.2 did not carry the duplication and those with RQ between 1.3 and 1.7 were considered to carry the *PMP22* duplication.

2.1.7 Transcriptional analysis of a small duplication and deletion in the Greek CMT cohort

For the transcriptional analysis of the small duplication and deletion in the Greek CMT cohort, ribonucleic acid (RNA) was obtained from peripheral blood using the PreAnalytiX PAXgene blood RNA system as per the manufacturer's instructions (Qiagen). Complementary DNA (cDNA) was synthesized using the High capacity cDNA reverse transcription (RT) kit following the manufacturer's instructions (Applied Biosystems). This work was carried out entirely by Dr George Koutsis from Eginitio Hospital, Athens, Greece.

2.1.8 Fragment analysis of a small duplication and deletion in the Greek CMT cohort

The small duplication and deletion in the Greek CMT cohort were further analysed by fluorescent PCR amplification and subsequent capillary electrophoresis using a Hi-Di Formamide mix (Life Technologies, USA). Fragment analysis was analysed

with GeneMapper software (Applied Biosystems) after running fragments on the 3730XL capillary sequencer (Applied Biosystems) with a GeneScan 500 LIZ dye size standard (Applied Biosystems). This work was carried out entirely by Dr George Koutsis.

2.1.9 Polymerase chain reaction (PCR)

The PCR technique to select and amplify specific DNA fragments was originally developed by Kary Mullis in the 1980s (Mullis et al., 1986). PCR uses a DNA polymerase to synthesize DNA strands complementary to the template strands using primers, a DNA template, and nucleotides or deoxyribonucleotide triphosphates (dNTPs).

For PCR amplification prior to DNA sequencing, primers were designed using Primer3Plus software (www.bioinformatics.nl/primer3plus/; Rozen & Skaletsky, 2000) to cover coding exons and at least 20 base pairs (bp) of flanking intronic sequences. Gene sequences were retrieved from Ensembl (www.ensembl.org). Primers were checked for specificity using the basic local alignment search tool (BLAST) feature in Ensembl (http://www.ensembl.org/Multi/blastview). Primers were purchased from Sigma. Optimal annealing temperatures were determined using a gradient block, ranging from 50°C to 65°C or, for touchdown PCRs, by testing multiple touchdown temperatures on individual thermalcyclers. Touchdown PCR, where the annealing temperature is decreased in increments over subsequent cycles, allows for increased binding specificity at the higher annealing temperatures. These specific fragments are amplified at lower annealing temperatures as well, but will be present in a higher proportion compared to the nonspecific sequences which may arise from low annealing temperatures (Don et al., 1991).

For the PCR reaction, DNA was used at 50-100 ng/µl. The PCR reactions included 0.75 µl of both forward and reverse primers (each at 10 µM), 12.5 µl of 2X PCR Master Mix (Roche), 10 µl of autoclaved dH_2O and 1 µl DNA. When required for particular primer pairs, the following PCR reaction mix was used: 2.5 µl of 10X TopTaq PCR buffer (Qiagen), 0.5 µl of dNTP mix (10 nM of each) (Qiagen), 5 µl of 5X Q-Solution (Qiagen), 1 µl of both forward and reverse primers (each at 10 µM),

0.25 µl of TopTaq DNA Polymerase (Qiagen), 13.75 µl of autoclaved dH_2O and 1 µl of DNA. One well per plate served as a negative control, where autoclaved dH_2O was used instead of DNA. Plates were sealed with heat-resistant covers, centrifuged, and run on a GeneAmp PCR System PerkinElmer 9700 Thermalcycler (PerkinElmer, USA). PCR thermalcycling conditions were as follows: 15 min at 95°C (initialization stage), followed by 35 cycles of 30 s at 95°C (denaturation stage), 30 s at specified annealing temperature (annealing stage), and 45 s at 72°C (elongation stage) before a final 10 min elongation stage at 72°C. For touchdown PCR, the starting annealing temperature is decreased in 0.4°C increments to a final annealing temperature for every successive set of cycles. Transcript references used for primer design, gene-specific primers sequences, and fragment-specific PCR cycling conditions are detailed in Appendix III Tables III-1 to III-3, Appendix IV Table IV-2, Appendix V Table V-1, Appendix VI Tables VI-3, VI-4, and VI-5, and Appendix VII Tables VII-4, VII-6, VII-9, and VII-10.

2.1.10 Agarose gel electrophoresis of PCR products

After PCR amplification, the length of PCR products was verified by agarose gel electrophoresis, in which 5 µl of the PCR product was mixed with 3 µl Orange G loading dye (Sigma) and run on a 1.3% w/v agarose gel with a 1 Kb DNA ladder (Promega, USA). Samples were electrophoresed for 25 min at 60 V and visualized under a UV transilluminator. Digital photographs were obtained using the Syngene GeneGenius image acquisition system and GeneSnap software (Synoptics, UK). The recipes for the Orange G loading dye, agarose gel, and 10X Tris/borate/EDTA (TBE) are provided in Appendix II.

2.1.11 PCR product purification

The PCR products were purified using either of two methods. For the first method, 80 µl of autoclaved dH_2O was added to each PCR product. The diluted PCR products were transferred to a Multiscreen HTS filter plate (Merck-Millipore) and vacuumed at 25 inches Hg for 5 min until dry. 80 µl of autoclaved dH_2O was once again added to the filter plate, and placed on the vacuum at 25 inches Hg for 5 min. 50 µl of autoclaved dH_2O was added to each well and placed on a shaker for 30 min. The 50

µl of resuspended PCR product was added to a storage plate to serve as a template for future sequencing.

For the second method, 5 µl of PCR product was transferred to a fresh PCR plate. Exo-Fast mix was prepared by combining 50 µl Exonuclease I (Thermo Fisher Scientific, USA), 200 µl of FastAP alkaline phosphatase (Thermo Fisher Scientific) and 750 µl autoclaved dH_2O. FastAP and Exonuclease I remove unincorporated dNTPs and single-stranded DNA from PCR products. 2 µl of Exo-Fast mix was added to each well and was pipette-mixed with the PCR product. The PCR plate was sealed with a heat-resistant cover, centrifuged, and run on a PerkinElmer 9700 thermalcycler at 37°C for 30 min and 80°C for 15 min.

2.1.12 Sanger sequencing

The Sanger (or dideoxy-chain-termination) method of sequencing was developed in the 1970s by Frederick Sanger (Sanger & Coulson, 1975). The Sanger method consists in synthesising DNA complementary to the PCR product using dNTPs and fluorescently labelled dideoxynucleotides (ddNTPs), DNA polymerase, primers and a template. When a ddNTP is incorporated in place of a normal nucleotide (a dNTP), this terminates DNA synthesis. This results in a series of fragments terminating with a ddNTP at different positions along the DNA sequence. In automated sequencing, the fluorescence of each fragment depends on which ddNTP is incorporated.

Sanger sequencing was carried out bi-directionally using BigDye Terminator v3.1 Cycle Sequencing kit (Life Technologies). Primers used were the same as those used for PCR. Each sequencing reaction contained 1 µl forward or reverse primer at 3.2 µM, 3.5 µl of purified PCR product, 2 µl of 5X BigDye Terminator v3.1 sequencing buffer (Life Technologies), 3.25 µl of autoclaved dH_2O and 0.25 µl BigDye Terminator v3.1 reaction mix (Life Technologies). The plates were sealed with a heat-resistant cover, centrifuged briefly and placed on the PerkinElmer 9700 Thermalcycler. Thermalcycling conditions were as follows: 10 s at 96°C, 5 s at 50°C, and 4 min at 60°C for a total of 25 cycles.

Dye removal was carried out to remove excess fluorescently labelled ddNTPs and salts from the sequencing reactions. Dye removal was performed by one of three methods. The first method utilised the Dye Terminator Removal kit (Thermo Fisher Scientific) as per the manufacturer's instructions. Briefly, the Dye Terminator Removal plate was centrifuged at 2,150 revolutions per minute (rpm) for 3 min, and then placed over a fresh PCR plate. 10 µl of autoclaved dH_2O was added to each sequencing reaction, and the diluted sequencing reaction was added to the Dye Terminator Removal plate. Both the Dye Terminator Removal plate and the PCR plate were centrifuged at 2,150 rpm for 3 min. The second method utilised the Multiscreen HTS filter plates (Merck-Millipore). The same protocol as for PCR product purification was followed, except that sequencing reactions were resuspended in 20 µl of autoclaved dH_2O. The third method utilised the Sephadex G-50 BioReagent (Sigma). To prepare the Sephadex mix for each sequencing plate, 2.9 g of Sephadex was diluted in 40 ml of autoclaved dH_2O. The mix was left to hydrate for 30 min at room temperature. The purification plate was prepared by adding 350 µl of Sephadex mix to each well of a Corning FiltrEX filter plate (Corning, USA). The filter plate was placed on an empty collection plate and centrifuged at 700 g for 3 min. The filter plate was placed on a fresh sequencing plate and the entire volume of the sequencing reaction was pipetted onto the Sephadex purification column. The plate was centrifuged at 910 g for 5 min. Following dye removal, plates were resolved on a 3730XL capillary sequencer (Applied Biosystems). Sequences were aligned and analysed using the Sequencher v4.10 software (Gene Codes, USA). PCR and sequencing were repeated at least twice to reconfirm variants.

2.1.13 HumanCytoSNP-12 v.2.1 BeadChip analysis

The HumanCytoSNP-12 v.2.1 BeadChip (Illumina, USA) is a whole-genome scanning panel allowing detection of duplications and deletions with better resolution than comparative genomic hybridisation arrays. The BeadChip contains 220,000 genome-wide tag single nucleotide polymorphisms (SNPs). In a BVVL patient with a homozygous *SLC52A2* mutation, the BeadChip was used to exclude a large deletion on the other allele and to establish the likelihood of the mutation actually being homozygous by evaluating the frequency of homozygous genotypes in the surrounding genomic region. The BeadChip was run by Kerra Pearce at University

College London (UCL) Genomics as per the manufacturer's instructions. The genotyping module within GenomeStudio (v. 2010.1, Illumina) was used to visualise the array data. Each allele is labelled with a different fluorophore; the genotypes are assigned based on the intensities of the A and B alleles. The B allele frequency is the proportion of the hybridized sample which carries the B allele as opposed to the A allele, therefore the genotypes BB, BA and AA have B allele frequencies of 1, 0.5, and 0, respectively, where B allele is the less frequent allele. The plot of B allele frequencies can therefore be used to detect regions of homozygosity. The log R ratio is the log of the ratio of observed probe intensity to expected probe intensity, and reflects copy number changes when it deviates from zero; deletions are represented by a decrease in intensity (i.e. decrease in the log R ratio). The Illumina Genome Viewer was used to examine the plots of B allele frequencies and log R ratio at SNPs surrounding *SLC52A2*.

2.1.14 Human Immuno BeadChip genotyping

The genotyping on the Illumina Infinium HD Human Immuno BeadChip (Illumina) was performed entirely by Kerra Pearce using the Infinium HD Ultra Assay according to the manufacturer's protocol (Rev B, 2010, Illumina) (details of standard protocol in Appendix II).

2.1.15 Exome sequencing

Briefly, exome capture involves randomly shearing gDNA into short fragments of a few hundred bp, ligating DNA to sequencing adapters, enriching for exons by hybridising the library to baits specific for the exome via immobilisation on a solid support, washing off non-targeted fragments, eluting selected fragments to create a library composed mainly of protein-coding regions, and PCR amplification of the library. Exome capture is followed by massively parallel sequencing of the library. Data processing involves alignment to a reference sequence, quality control, variant calling, and data filtering (Bamshad et al., 2011). In this PhD, the steps prior to data filtering were performed by several exome sequencing facilities, and I performed the data filtering. The commercial platforms for exome capture and sequencing used by each facility are specified in the appropriate Chapters. Details of the data processing are available in Appendix II.

2.1.16 Exome sequencing: gene coverage and read depth

Some genes, exons or genomic areas with certain characteristics may not be covered by the hybridization probe design as the efficiency of capture probes varies greatly. Furthermore, read depth, which is defined as the number of independent reads at a particular base pair, is often quite variable from gene to gene and may not always be sufficient to ensure accuracy of data (Bamshad et al., 2011). Therefore, gene coverage and read depths of known disease-associated genes and candidates genes were determined by exploring BAM files using the GenomeBrowse software (Golden Helix, USA). A base was considered poorly covered if it had less than 15-20X coverage. The values for overall mean target coverage and total number of reads were obtained from the data processing. The mean target coverage is defined as "the mean coverage of targets that received at least coverage depth=2 at one base" (http://picard.sourceforge.net).

2.1.17 Exome sequencing: variant filtering

All genes known to be involved in CMT/BVVL or related diseases were checked for variants, as were genes which were considered potential candidates. Variants were filtered so as to fit with the predicted inheritance pattern. All synonymous variants were removed as these do not alter the amino acid sequence and are less likely to be deleterious. Variants found in the general population were excluded (see Section 2.6 for control databases used). The cut-off point of the minor allele frequency (MAF) was adapted to the predicted mode of inheritance, as will be described in the appropriate Chapters. Any remaining variants with a low quality score (below 20) were excluded. Any variant within a segmental duplication region with identity ≥96% was removed; variants within these regions are frequently false positive calls (Bamshad et al., 2011). The coverage depth of all variants of interest was also verified, as described in Section 2.1.16. In-silico predictions of pathogenicity and conservation between species were assessed for all variants of interest as described in Section 2.6. Details of gene expression in various tissues and location of the mutated amino acid within the protein were obtained as described in Section 2.6. The GEM.app (https://genomics.med.miami.edu), described in Section 2.6, was used for CMT exome data.

2.2 Cellular model: *solute carrier family 52, riboflavin transporter member 2* (*SLC52A2*) patient fibroblasts

2.2.1 Ethics approval and consent

This study has been granted ethical approval by the National Research Ethics Service Committee of the NHNN (UCLH REC number 99/N103). Written informed consent to perform a skin biopsy and obtain fibroblasts was obtained from all patients and/or parental guardians.

2.2.2 Generation of human fibroblast cultures and details of control fibroblast lines

The 6 mm punch skin biopsies were taken under local anaesthetic at the NHNN/Great Ormond Street Hospital (GOSH). Fibroblasts of BVVL patients with *SLC52A2* mutations were generated at the Medical Research Council (MRC) Centre for Neuromuscular Diseases Biobank, Dubowitz Centre, UCL Institute of Child Health (ICH) by Dr Diana Johnson, or were sent to us in culture by our collaborators. Three age-matched controls were obtained from the ICH Biobank: control-1 (age at biopsy: 14 years; female); control-2 (age at biopsy: nine years; male); control-3 (age at biopsy: five years; male). A neuromuscular cause of disease was excluded for all control fibroblast lines.

2.2.3 Cell culture

Fibroblasts were grown at 37°C in 95% air and 5% CO_2. Unless otherwise specified, cells were maintained in Dulbecco's modified eagle medium (DMEM)-GlutaMAX (high glucose and pyruvate; Life Technologies) with 10% v/v foetal bovine serum (FBS; heat-inactivated, non-USA origin; Life Technologies) and 1% v/v Penicillin/Streptomycin (P/S; 5000 U/5000 μg per ml; Gibco, UK) in 75 cm^2 tissue culture flasks. This fibroblast cell medium is referred to as "regular DMEM" throughout the Thesis. The medium was changed every four days. Cultures were passaged when cells reached 70-80% confluence. To split or freeze cells, the medium was removed from the flask. Cells were washed in 7 ml of 1X Dulbecco's phosphate buffered saline (DPBS; Life Technologies). 1.5 ml of 0.05% 1X trypsin-EDTA (Life Technologies) was added and cells were placed back in the incubator at 37°C for 5 min. The flask was swirled and tapped to detach the fibroblasts. 5 ml of medium was

added to the flask to quench the trypsin, and cells were collected and centrifuged at 1,200 rpm for 5 min. The supernatant was discarded. To split cells, the cell pellet was resuspended in medium and split into new flasks as appropriate. To freeze cells, the cell pellet was resuspended in ½ final volume FBS and ½ final volume freezing medium (recipe in Appendix II) and placed in labelled cryovials (1 ml per cryovial; two cryovials per 80% confluent 75 cm^2 flask). Cells were first frozen at -80°C for 24 h in a tightly sealed Polystyrene box, and then were transferred to liquid nitrogen for long-term storage. Cells were defrosted quickly in a 37°C water bath and seeded at a density of 5 x 10^3 cells/cm^2 into 75 cm^2 tissue culture flasks. To obtain reproducible results, only fibroblasts of passage number 2 to 12 were used in experiments.

2.2.4 Cell counting

To establish the number of fibroblast cells in 1 ml of cell suspension prior to cell seeding, a 10 µl sample of suspension was added to 10 µl of 0.4% trypan blue (Sigma). The solution was pipetted onto a haemocytometer and the number of live cells (colourless and bright) in 4 sets of 16 corner squares of the grid was counted under a light microscope. The total count was divided by four and multiplied by two to adjust for the 1:2 dilution in trypan blue. The resulting value x 10^4 is equivalent to the number of cells per ml of suspension.

2.2.5 Cell harvesting for biochemical analysis

For the FMN/FAD assay, the measurement of activities of MRC complexes I and II and citrate synthase (CS), and for the Coenzyme Q_{10} (CoQ_{10}) assay, fibroblasts were harvested from confluent 75 cm^2 flasks. The medium was removed, and cells were washed once with DPBS and then detached with trypsin-EDTA as described in Section 2.2.3. Cell medium was added to the flask and cells were collected and centrifuged at 1,200 rpm for 5 min. The cell pellet was washed in DPBS. Cells were centrifuged again at 1200 rpm for 5 min. The cell pellet was resuspended in DPBS, aliquoted into Eppendorfs and stored at -80°C. For the FMN/FAD assay, the pellet was resuspended in 150 µl DPBS (25 µl for protein determination, 125 µl for the FMN/ FAD assay). For the MRC complex activities, the pellet was resuspended in 160 µl DPBS (10 µl for protein determination, 60 µl for complex I, 60 µl for complex

II, and 30 µl for CS measurements). For the CoQ_{10} assay, the pellet was resuspended in 175 µl DPBS (25 µl for protein determination, 50 µl for CoQ_{10} assay).

2.2.6 Cell harvesting for Western blot

For Western blot analysis, fibroblasts were harvested from confluent 75 cm^2 flasks. The medium was removed, and cells were washed once with DPBS and then detached with trypsin-EDTA as described in Section 2.2.3. Cell medium was added to the flask and cells were collected and centrifuged at 1,200 rpm for 5 min. The resulting cell pellet was washed in DPBS. Cells were centrifuged again at 1,200 rpm for 5 min. The cell pellet was resuspended in 50 µl of cold lysis buffer (recipe in Appendix II) and the sample was transferred to a new, cold Eppendorf and stored at -80°C.

2.2.7 Total protein determination

For all biochemical and Western blot experiments, the Bio-Rad DC protein assay (Bio-Rad Laboratories, USA) was used to normalise for protein concentration. The assay was performed as per the manufacturer's instructions with all samples and bovine serum albumin (BSA) standards plated in triplicate on a 96-well plate. Briefly, a 6-point standard line was prepared with BSA in DPBS from 0 to 1 mg/ml. All samples were diluted in DPBS as necessary for the sample concentrations to fall within the standard curve. 2 µl of each sample was added per well. 25 µl of "S+A" reagent mix (30 µl reagent "S" + 970 µl reagent "A") and 200 µl of reagent "B" were then added to each well. The plate was incubated for 15 min in the dark at room temperature. The relative absorbance at an excitatory wavelength of 750 nm was obtained using a FLUOstar omega plate reader (BMG Labtech Ltd, Germany). The relative concentration of each sample was determined relative to the absorbance of the BSA standards.

2.2.8 Optimisation of riboflavin concentration in cell medium

As discussed in Sections 7.1.5 and 7.3.4, studies using fibroblasts of patients with riboflavin-responsive diseases have indicated that high concentrations of the vitamin in cell medium may mask metabolic defects in vitro. As many BVVL patients improve clinically and biochemically as a result of riboflavin therapy (Section 1.6.5),

and as DMEM typically contains supra-physiological concentrations of riboflavin (1.06 M), the minimum amount of riboflavin required in the medium which would support a healthy metabolism in controls (see Section 7.1.5 for effects of riboflavin deprivation in vitro) but expose any metabolic defects in the BVVL patient fibroblasts was determined. Custom-made DMEM without riboflavin was purchased from Merck-Millipore. As regular FBS contains high levels of riboflavin, it was replaced with dialysed FBS (heat-inactivated, non-USA origin; Life Technologies) which was determined to contain 6.6 nM riboflavin by high-performance liquid chromatography (HPLC) (Section 2.2.14) by Marcus Oppenheim in the Neurometabolic Unit, NHNN. FMN and FAD were below limits of detection. The remaining riboflavin in the dialysed FBS is likely bound to larger molecular weight proteins which escaped the process of dialysis. As dialysed FBS was used at 10% in the medium, it contributed 0.66 nM riboflavin. 1% P/S was added to the medium as before. (-)-Riboflavin in powder form (≥98%; Sigma) was diluted to 0.1 g/L in sterile H_2O (riboflavin solubility: 1 g per 3-15 L H_2O), sterile-filtered, and kept frozen in small light-protected aliquots. All tissue culture work involving added riboflavin was performed in the dark as riboflavin is sensitive to light (Depeint et al., 2006; Rhead et al., 1993).

MRC complex I and II activities (Sections 2.2.15-2.2.17) were used as a measure in controls to establish the lower threshold at which function became compromised. Riboflavin was added to the medium to obtain the following final concentrations (including the dialysed FBS): 0.85 nM (0.32 μg/L; severely deficient), 3.1 nM (1.17 μg/L; moderately deficient or "low riboflavin"), 12.6 nM (4.7 μg/L; physiologic), and 300.6 nM (113 μg/L; pharmacological or "riboflavin-supplemented"). The concentration of riboflavin was reduced until complex I and II activities in controls were determined to be at the lower limit of normal (controls grown in riboflavin-supplemented medium). These concentrations were chosen based on this logic: 300.6 nM is the riboflavin concentration in plasma of riboflavin-supplemented adults; 12.6 nM is the concentration in normal human plasma; 3.1 nM is the concentration in plasma of moderately deficient pregnant women; 0.85 nM is the concentration in plasma of severely deficient patients with cystic fibrosis or in pre-term infants treated with phototherapy (Camporeale & Zempleni, 2003).

For the first trial, control fibroblasts were first grown for four days in medium with physiological (12.6 nM) concentrations of riboflavin to adjust the cells to this medium (Camporeale & Zempleni, 2003). For the subsequent four days, one half of the cells was grown in severely deficient medium (0.85 nM) and the other in riboflavin-supplemented medium (300.6 nM) (see Appendix VII Table VII-1 for complex I and II activity data; n=1). MRC complex I and II activities were severely reduced in controls grown in 0.85 nM riboflavin. Complex I and II activities for the severely riboflavin-deficient (0.85 nM) control fibroblasts were on average 24% and 38% of those grown in riboflavin-supplemented medium. In the second trial, control fibroblasts were again grown for four days in physiological concentrations, and were then grown for an additional four days in 3.1 nM, 12.6 nM or 300.6 nM riboflavin (see Appendix VII Table VII-2 for complex I and II activity data; n=1). Although complex activities had a mild tendency to decrease as riboflavin concentration was reduced from 300.6 nM to 3.1 nM, the reduction was much less drastic than that seen with 0.85 nM riboflavin. Therefore, the minimum amount of riboflavin required by control human fibroblasts (as determined by a single parameter, i.e. MRC complex I and II activities) when grown under these conditions lies between 0.85 nM and 3.1 nM. The latter concentration was therefore trialled in BVVL patient fibroblasts.

Unless otherwise specified, for all experiments, patient and control fibroblasts were grown for four days in medium containing physiological (12.6 nM) concentrations of riboflavin. After this time, cells were 60-70% confluent and cultures were split 1:2: half was transferred to riboflavin-supplemented (300.6 nM) medium, and the other was transferred to low riboflavin (3.1 nM) medium. Cells were cultured in these media for an additional four days before harvesting or using in experiments. Fibroblasts were not kept in the low riboflavin medium longer as a previous study had shown that culturing control fibroblasts in medium with <3.72 nM riboflavin for two weeks caused a reduction of more than 85% in the cellular FAD content (Rhead et al., 1993). Cells grown in low riboflavin medium were never exposed to medium containing higher concentrations of riboflavin throughout the tissue culture procedures.

Fibroblasts for RNA extraction and subsequent real-time reverse transcription polymerase chain reaction (RT-qPCR) analysis were grown in regular DMEM to minimize the potential confounding effect of riboflavin deprivation on *SLC52A2* transcript levels. Fibroblasts for immunocytochemistry were also cultured in regular DMEM. Fibroblasts for HPLC (FMN and FAD), spectrophotometry (complex I, complex II and CS activities), mitochondrial membrane potential ($\Delta\Psi_m$), reduced nicotinamide adenine dinucleotide (NADH) assay, lactate/pyruvate assay, and CoQ_{10} assay were cultured in low riboflavin and riboflavin-supplemented medium as described above. All Western blot experiments were performed using physiological medium followed by low riboflavin medium only.

2.2.9 Ribonucleic acid (RNA) extraction

Prior to RNA extraction, fibroblasts were grown to confluence in 6-well plates. Total RNA was isolated from fibroblasts using the MiRNeasy Mini kit (Qiagen) following the manufacturer's instructions. The RNase-Free DNase Set (Qiagen) was also used during the RNA extraction procedure to ensure complete DNA removal. RNA concentration and purity were assessed using the NanoDrop ND-1000 spectrophotometer as per the manufacturer's instructions (NanoDrop Technologies). A 260/280 absorbance ratio of approximately 2.0 is generally acceptable for RNA (Section 2.1.5).

2.2.10 Complementary deoxyribonucleic acid (cDNA) synthesis

Following RNA extraction, cDNA was synthesized from total RNA using the First-Strand cDNA SuperScript II Reverse Transcriptase kit (Life Technologies) as per the manufacturer's instructions (details in Appendix II). To assess the efficiency of cDNA synthesis and to test for DNA contamination, a PCR (60°C annealing temperature) and agarose gel electrophoresis were performed (Sections 2.1.9 and 2.1.10) with cDNA primers and exon/intron boundary-spanning gDNA primers, respectively. A PCR reaction using *SLC52A2* primers and subsequent agarose gel electrophoresis also served to confirm that *SLC52A2* is expressed in human fibroblasts as seen by a strong, single band on the gel.

2.2.11 Real-time reverse transcription polymerase chain reaction (RT-qPCR)

RT-qPCR was carried out using a Taqman probe-based gene expression assay (Applied Biosystems) to assess levels of *SLC52A2* mRNA in the fibroblasts. In Taqman-based qPCR assays, a Taq DNA polymerase cleaves a labelled Taqman probe during hybridization to the target complimentary sequence, and the resulting fluorescence signal allows for quantitative measurements of the PCR product accumulated during the exponential stage. The Taqman gene expression assay is a 20X mix of forward primer, reverse primer, and a FAM or VIC dye-labelled probe. Taqman probes for *SLC52A2* (Assay ID: Hs04194586_s1; FAM-labelled) and the housekeeping gene *actin, beta* (*ACTB*) (Reference sequence: NM_001101.2; VIC-labelled) were purchased from Applied Biosystems. Each RT-qPCR reaction contained 1 µl of template cDNA diluted 1:10 v/v with nuclease-free H_2O, 0.5 µl of 20X Taqman *SLC52A2* gene expression assay, 0.5 µl of 20X Taqman *ACTB* gene expression assay, 5 µl of 2X Rotor-Gene Multiplex PCR Master Mix (Qiagen) and 3 µl nuclease-free H_2O. A 6–point standard curve with serial fivefold dilutions of a cDNA sample from a control fibroblast line was constructed; the same control fibroblast line was used to construct the standard curve for all replicate experiments. Samples and standards were run in triplicates in a 100-well circular plate. A "no template" control was used to assess possible well-to-well contamination; a "no RT" control was used to control for DNA contamination in the RNA samples. Cycling conditions were as follows: 95°C for 5 min, followed by 45 cycles of 95°C for 15 s and 60°C for 15 s with fluorescence acquisition in the green and yellow channels (Figure 2-1).

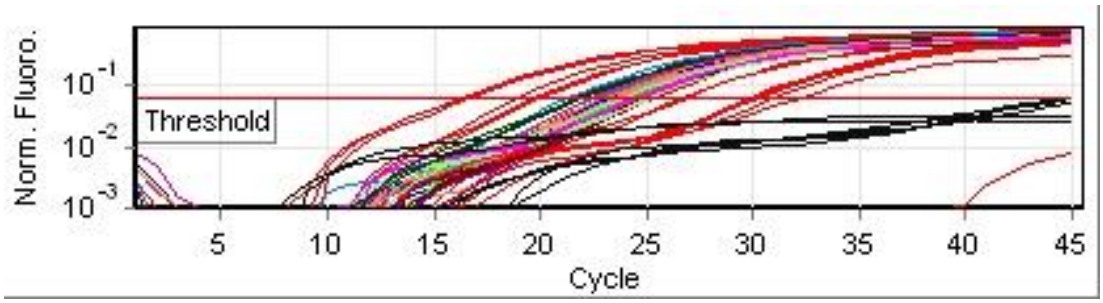

Figure 2-1 Sample plot of amplification curves of an RT-qPCR experiment in fibroblasts. The black-coloured curves not reaching the threshold of detection represent the "no template" controls.

As the amplification efficiencies of *SLC52A2* and *ACTB* were not comparable, standard curves for both the target and housekeeping genes were constructed by plotting the C_t values (Section 2.1.6) (y-axis) against the log of template amount (x-axis). The amount of target and reference in the samples were calculated using the C_t values and the corresponding standard curve. To calculate the normalised amount of target, the amount of target was divided by the amount of reference. The relative expression level of the target gene in the patient and carrier fibroblasts was determined by dividing the normalised target amounts by the average value of the calibrators (i.e. average of the normalised target amounts in the three control fibroblast lines).

2.2.12 [^{3}H]-Riboflavin uptake assay

For the [^{3}H]-Riboflavin uptake trial assays, control fibroblasts were seeded in 12-well plates and cultured for four days in either riboflavin-supplemented (300.6 nM) or low riboflavin (3.1 nM) medium (Section 2.2.8). In another trial, control fibroblasts were grown in 12-well plates for 48 h; 24 h before the experiment, the medium was changed to either riboflavin-supplemented (300.6 nM) or medium with 0.4 nM riboflavin. Fibroblasts reached 80-90% confluence and were used for experiments immediately following these time periods.

The [^{3}H]-Riboflavin uptake assay protocol was based on the method used by Ciccolella et al. (2013). The protocol and various modifications trialled are detailed in Appendix II. Overall, the disintegrations per minute (dpm) values (measure of the

intensity of the radioactivity) were not sufficiently higher than basal levels to allow for accurate determination of [^{3}H]-Riboflavin uptake; the experiment could not be optimised.

2.2.13 Immunocytochemistry

To determine the subcellular localisation of endogenous RFVT2 in the fibroblasts, 2 x 10^{4} fibroblast cells were seeded per well of a 24-well plate and grown overnight on 13 mm glass round coverslips (VWR, USA) previously coated with Poly-D-lysine hydrobromide (0.025 mg/ml) (Sigma). Cells were washed in 1X phosphate buffered saline (PBS), fixed in 4% w/v paraformaldehyde (PFA) for 20 min, washed and permeabilised in PBS-0.05% Triton X-100 for 10 min. Cells were then washed three times with 1X PBS and blocked with 10% FBS in 1X PBS (Life Technologies) for 1.5 h. Coverslips were incubated with 40 µl of primary antibody for 60 min, washed three times with 1X PBS, and incubated with secondary antibody for 60 min. Coverslips were washed three times with 1X PBS, mounted on microscope slides (VWR) with ProLong Gold Antifade reagent with 4',6-diamidino-2-phenylindole (DAPI) (Life Technologies), and imaged using a Zeiss LSM 710 confocal microscope (Carl Zeiss AG, Germany) and 40X and 63X oil immersion objectives. For all experiments, a negative control (incubated overnight in blocking solution only, with no primary antibody) was included to assess the specificity of the secondary antibody. The primary antibody used was rabbit polyclonal anti-human *SLC52A2* (1:200 and 1:500; Sigma). The secondary antibody used was Alexa Fluor 488 Goat Anti-Rabbit IgG (1:2,000 in 10% FBS or 1% w/v BSA in PBS-Tween; Life Technologies).

Despite extensive optimisation of the immunocytochemistry protocol (including modifications of antibody concentration/incubation time, blocking agent and blocking time, and number of PBS washes), the endogenous RFVT2 staining in both the control and patient fibroblasts showed very diffuse staining which was not specific for the plasma membrane. No conclusions could be drawn from the RFVT2 localization experiments in the fibroblasts given the poor quality of the commercial antibodies. Yonezawa et al. (2008) had previously reported on the difficulty of producing an antibody against RFVT1 as it is a multi-membrane spanning protein

and its amino acid sequence is similar to that of a G protein-coupled receptor family member.

2.2.14 Intracellular levels of FMN and FAD by high-performance liquid chromatography (HPLC)

HPLC is a technique to separate and identify compounds in a sample by chromatography, and to quantify the amount of each compound in the mixture. As riboflavin is naturally fluorescent, fluorescent tags are not necessary. During reverse-phase HPLC, a high-pressure pump generates a flow rate of polar mobile phase. The sample is introduced into the mobile phase by an injector and is driven through the HPLC column for compound separation. The column is made of hydrophobic, non-polar silica-based chromatographic packing material (the stationary phase). A detector records the electrical signal as the compound passes through the detector flow cell, and generates a chromatogram (Figure 2-2). Each compound passing through the column has to "choose" between interacting with the mobile phase and the column. Hydrophilic, polar compounds move faster through the hydrophobic column, and generate a peak earlier on the chromatogram. In this case, the retention time, or time taken for a compound to travel through the column, is shorter. Reverse-phase HPLC with fluorescence detection was used to determine the total intracellular FMN and FAD levels in the fibroblasts using the Whole Blood Chromsystems vitamins B_1/B_2 kit (Chromsystems, Germany) as per the manufacturer's protocol. The levels of riboflavin were not reported as the levels frequently fell below the threshold of detection for cells grown in the low riboflavin medium (riboflavin threshold of detection: 5.31-664.25 nM).

Cell aliquots for the FMN and FAD assay were obtained as described in Section 2.2.5. Briefly, test samples were kept frozen and protected from light until needed. The calibration standard was reconstituted in 1 ml ultra-pure H_2O, and two quality control samples were reconstituted in 2 ml ultra-pure H_2O. Samples were thawed and 50 µl of standard, two quality controls samples, and all test samples were aliquoted into labelled, light-protected Eppendorf tubes. 50 µl of extraction buffer was added and tubes were incubated for 5 min at room temperature. 100 µl of cooled precipitation reagent was added to each tube. Tubes were mixed and incubated for 10 min at 4°C. 100 µl of stabilisation buffer was added to each tube. Samples were

mixed and centrifuged at 14,000 rpm for 10 min. 100 µl of the supernatant was aliquoted into capped, labelled autosampler vials. The reverse-phase HPLC components included a Jasco AS-950 intelligent autosampler (SpectraLab Scientific, Canada), a Jasco PU-980 intelligent pump (SpectraLab Scientific), a Chromsystems HPLC column for vitamin B_2 analysis (Chromsystems), and a Jasco FP-920 intelligent fluorescence detector (SpectraLab Scientific). The autosampler was programmed to inject 50 µl of each sample onto the column, allowing a run time of 14 min with five flushes between each injection. Riboflavin, FMN and FAD were detected using the fluorimetric detector (excitation 465 nm, emission 525 nm). Peak integration and data analysis on the HPLC were performed by Marcus Oppenheim. The height of the peak is proportional to the amount of a particular compound which has passed through the detector. Peaks were integrated and peaks of interest were identified and quantified using the Azur data capture system (Kromatek, UK) as per the manufacturer's instructions. The concentration of each analyte expressed in nmol/L was calculated by relating the height of the peak in the chromatogram of the sample to the height of the peak in the chromatogram of the standard (Figure 2-2):

$$[\text{analyte}] = \frac{\text{peak height in sample}}{\text{peak height in standard}} \times [\text{standard}]\ \text{nmol/L}$$

The concentration in nmol/L was converted to nmol/g using the protein concentration of the original sample (Section 2.2.7). All FMN and FAD levels were compared to the mean levels in controls separately for each experimental day and each medium condition (low versus high riboflavin).

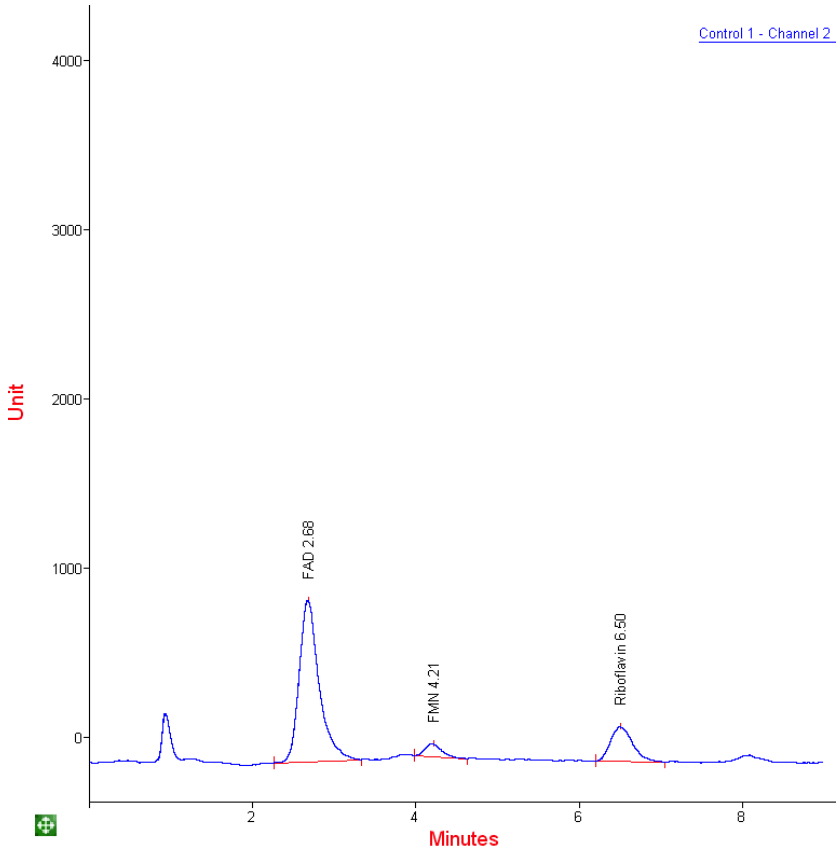

Figure 2-2 Sample chromatogram of HPLC retention time (x-axis) and fluorescence (y-axis) for FAD, FMN and riboflavin resulting from chromatographic separation by the HPLC system and detection of the analyte by the detector flow cell, with each peak corresponding to a different compound. FAD moves at a speed closer to the mobile phase than to the stationary phase; it moves fastest through the chromatographic packing material particles and elutes first from the column, followed by FMN and lastly riboflavin, reflecting the relative polarity of these compounds (FAD>FMN>riboflavin).

2.2.15 Mitochondrial respiratory chain (MRC) complex I assay

NADH: ubiquinone oxidoreductase (complex I) activity was measured spectrophotometrically by measuring the decrease of UV absorbance at 340 nm associated with the oxidation of NADH by electron transfer to ubiquinone in the MRC. This assay was performed according to the method of Reed and Ragan (1987). Rotenone, a complex I inhibitor, was used to assess the level of complex I-independent NADH oxidation. Prior to the assay, cell aliquots obtained as described

in Section 2.2.5 were thawed on ice, vortexed, and refrozen in liquid nitrogen three times before being thawed and used in the assay. This procedure helps to rupture the cell and mitochondrial membranes so the substrates in the assay may reach the active sites.

20 µl of each sample (diluted 1:2 or 1:5 as necessary) was added to two microcuvettes (Sigma) in parallel containing at final concentration: 2.5 mg/ml BSA (≥96%; Sigma), 0.2 mM β-NADH disodium salt hydrate (≥97%; Sigma), 1 mM potassium cyanide (KCN) (VWR) in a 20 mM potassium phosphate (VWR) buffer with 8 mM magnesium chloride (VWR) (pH 7.2). The final volume in each cuvette was 1 ml. Samples were mixed by double inversion and loaded onto the Uvikon 941 spectrophotometer (Northstar Scientific, UK). Duplicate cuvettes were placed into the reference or sample compartment. The reaction was primed by adding 10 µl of 5 mM Coenzyme Q_1 (CoQ_1) (~95%; Sigma) into the sample cuvette and subsequent mixing. The reaction was monitored at an absorbance of 340 nm at 30 s intervals for 6 min at 30˚C. 20 µl of 1 mM rotenone (≥95%; Sigma) was added to each sample cuvette and measurement was continued for an additional 5 min. Rotenone-insensitive complex I activities (activities after addition of rotenone) were subtracted from total complex I activities thus providing a value for rotenone-sensitive complex I NADH oxidation. The Beer-Lambert law was used to convert absorbance to molar concentration:

$$\frac{\Delta A \times l = c}{\varepsilon}$$

where ΔA is the specific change in absorbance, ε is the extinction coefficient (6.81 x 10^3 M^{-1} cm^{-1}), l is the path length (1 cm) and c is the concentration in mole/min/ml. Results were expressed both as nmol/min/mg of protein (as determined in Section 2.2.7) and as a ratio to activity of CS, a mitochondrial marker enzyme, to normalise for mitochondrial enrichment (Hargreaves et al., 1999) (see Section 2.2.17 for description of CS activity assay). All complex I activities were compared to the mean activity in controls for each experimental day and each medium condition (low versus high riboflavin) separately.

2.2.16 MRC complex II assay

Succinate: ubiquinone oxidoreductase (complex II) activity was measured spectrophotometrically by measuring the decrease of UV absorbance at 600 nm associated with the secondary 2-thenoyltrifluoroacetone (TTFA)-sensitive reduction of the 2,6-dichlorophenol-indophenol (DCPIP; Sigma) dye by the ubiquinol formed during the oxidation of succinate in complex II. This assay was performed according to the method of Birch-Machin et al. (1994). Prior to the assay, cell aliquots obtained as described in Section 2.2.5 were thawed on ice, vortexed, and refrozen in liquid nitrogen three times before being thawed and used in the assay.

20 µl of each sample (diluted 1:2 or 1:5 as necessary) was added to two microcuvettes (Sigma) in parallel containing at final concentration: 0.1 mM EDTA (VWR), 0.12 mM DCPIP, 20 mM succinate (Sigma), 1 mM KCN (Sigma), 0.01 mM rotenone (≥95%; Sigma), in a 50 mM potassium phosphate (VWR) buffer (pH 7.4). 1 mM final concentration of TTFA (VWR) was added to the reference sample. The final volume in each cuvette was 1 ml. Samples were mixed by double inversion and loaded onto the Uvikon 941 spectrophotometer (Northstar Scientific). Duplicate cuvettes were placed into the reference or sample compartment. The reaction was initiated by the addition of 10 µl 5 mM CoQ_1 (Sigma) into the sample cuvette and subsequent mixing. The reaction was monitored at an absorbance of 600 nm at 30 s intervals for 6 min at 30˚C. 20 µl 1 mM TTFA was added to each sample cuvette to block complex II activity and measurement was continued for an additional 7 min. Subtraction of the decrease before and after TTFA addition produced a specific value for complex II reduction of DCPIP. The Beer-Lambert law was used to convert absorbance to molar concentration as described in Section 2.2.15 (extinction coefficient=9.1 x 10^3 M^{-1} cm^{-1}). Results were expressed both as nmol/min/mg of protein (as determined in Section 2.2.7) and as a ratio to CS activity. All complex II activities were compared to the mean activity in controls for each experimental day and each medium condition (low versus high riboflavin) separately.

2.2.17 Citrate synthase (CS) assay

CS, an enzyme in the Krebs cycle, catalyses the condensation of oxaloacetate and acetyl-CoA to citric acid and Coenzyme A. CS activities provide an estimate of

mitochondrial content and were therefore used to normalise complex I and II activities for mitochondrial enrichment (Hargreaves et al., 1999). The CS activity is quantified by measuring the reaction of free Coenzyme A with 5,5'-dithio-bis(2-nitrobenzoic acid) (DTNB; ≥98%; Sigma). This assay was performed according to the method of Shepherd and Garland (1969). Prior to the assay, cell aliquots obtained as described in Section 2.2.5 were thawed on ice, vortexed, and refrozen in liquid nitrogen three times before being thawed and used in the assay.

10 µl of each sample (diluted 1:2 or 1:5 as necessary) was added to two microcuvettes (Sigma) in parallel containing at final concentration 0.1 mM acetyl-CoA (≥ 93%; Sigma), 0.2 mM DNTB (Sigma) in 100 mM Tris (Sigma) and 0.1% v/v Triton X-100 (≥99.5%; Sigma) buffer (pH 8.0). The final volume in each cuvette was 1 ml. Samples were mixed by double inversion and loaded onto the Uvikon 941 spectrophotometer (Northstar Scientific). Duplicate cuvettes were placed into the reference or sample compartment. The reaction was initiated by the addition of 10 µl 20 mM oxaloacetate (≥97%; Sigma) into the sample cuvette and subsequent mixing. The reaction was monitored at an absorbance of 412 nm at 30 s intervals for 6 min at 30˚C. The Beer-Lambert law was used to convert absorbance to molar concentration as described in Section 2.2.15 (extinction coefficient=13.6 x 10^3 M^{-1} cm^{-1}). In addition to using CS activities to normalize for mitochondrial enrichment, results were also expressed as nmol/min/mg of protein (as determined in Section 2.2.7). After correcting CS activity for protein content, it was important to check that the CS activity per se was not affected by the *SLC52A2* mutations as it was used as a marker enzyme in our assay. An increase or decrease in CS activity may indicate an increase or decrease in mitochondrial number; the former may suggest a compensation effect whereby the cell attempts to increase its energy-making capacity. CS activity was not affected by *SLC52A2* status or by concentration of riboflavin in the culture medium.

2.2.18 Confocal microscopy: mitochondrial membrane potential ($\Delta\Psi_m$)

For live-cell confocal microscopy, fibroblasts needed to be alive and adherent to 25 mm glass coverslips. Autoclaved coverslips were placed into 6-well plates and sterilized under the UV light for 60 min. After growing the fibroblasts for four days in physiological concentrations of riboflavin (Section 2.2.8), fibroblasts were seeded

into 6-well plates containing low riboflavin or riboflavin-supplemented medium and were cultured for another four days at which point they reached 70-80% confluence. The experiment was performed immediately following this time period.

The $\Delta\Psi_m$, the difference in electrochemical potential between the cytoplasm and the matrix generated by the MRC during cellular respiration, is the driving force for ATP synthesis and is a key function of mitochondria. Thus, the ΔΨm is an indicator of mitochondrial health and cellular metabolism (Brand & Nicholls, 2011; Cecchini, 2003). The tetramethylrhodamine methyl ester (TMRM) dye used in this experiment is a membrane-permeable cationic dye with a single delocalized positive charge, which is sequestered in the mitochondria due to the electrochemical potential gradient between the mitochondria and the cytosol; the resulting fluorescence intensity is representative of the ΔΨm. The dye is released into the cytosol upon depolarization of the mitochondria, leading to a decrease in signal intensity in the mitochondria, and an increase in signal in the cytosol (Brand & Nicholls, 2011; Burchell et al., 2010; Duchen, 2004).

The cell medium was removed and cells were loaded with 25 nM TMRM (Life Technologies) in 500 µl 1X Hank's balanced salt solution (HBSS) (with Ca^{2+} and Mg^{2+}, without phenol red; Gibco) or glucose-free HBSS where glucose is replaced with 2-deoxy-D-glucose (recipe in Appendix II) to block glycolysis and increase dependence on oxidative phosphorylation for energy production, as described in Section 7.8.4. Cells were incubated in the dark at room temperature for 40 min-1 h for the cells to reach equilibrium. The dye was present in the chamber throughout the experiment for use in redistribution mode (Abramov et al., 2010).

Images were obtained using a Zeiss LSM 710 confocal microscope (Carl Zeiss AG), 40X oil immersion objective, and fixed laser power and detector sensitivity (Figure 2-3). TMRM was excited using the 560 nm laser line and the emission fluorescence was measured above 580 nm. The pinhole was set to 1 airy unit for optimal resolution and laser intensity was kept as low as possible to minimize phototoxicity. For the basal ΔΨm measurements, three to four "z-stack" scans were obtained per coverslip.

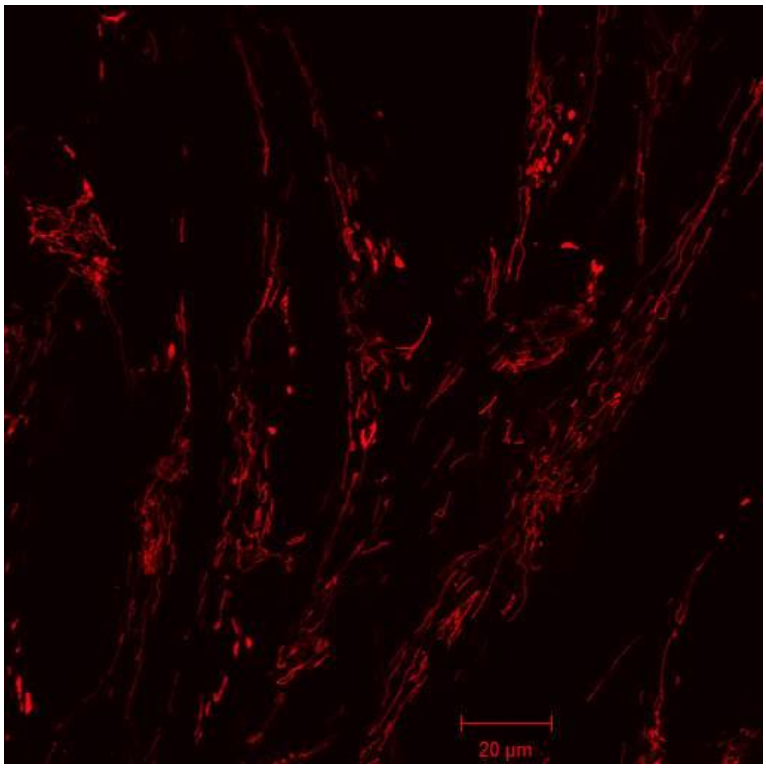

Figure 2-3 Fibroblasts incubated with 25 nM TMRM.

For assessing the response of the ΔΨm to the mitochondrial toxins oligomycin, rotenone, and carbonyl cyanide-4-(trifluoromethoxy)phenylhydrazone (FCCP) (described in Chapter 7 and in Gandhi et al., 2009), images were obtained at 10 s intervals from a single focal plane. After measuring baseline TMRM intensity for 2-3 min, oligomycin from *Streptomyces diastatochromogenes* (2 μg/ml; Sigma) was added to the chamber and fluorescence measured for another 4-5 min (until a plateau was reached), following which rotenone (10 μM; Sigma) was added. After 4-5 min, 1 μM FCCP (≥98%; Sigma) was added and recordings were stopped after 2-3 min when the mitochondria had fully depolarised. One such time-series experiment was performed per coverslip.

Basal ΔΨm measurements were analysed using the Volocity image analysis software (PerkinElmer). To control for mitochondrial mass, TMRM fluorescence intensity from background signals (below a defined threshold) was removed for the analysis, and the mean TMRM fluorescence intensity across the pixels containing mitochondria was measured. All measurements were compared to the mean intensity

in controls for each experimental day and each medium condition (low versus high riboflavin) separately.

Time-series data were analysed using the Zeiss Zen software (Carl Zeiss AG). A total of 10-20 areas were selected for analysis and the average dye intensity across these areas was plotted on the y-axis against time on the x-axis. The change in TMRM intensity after addition of each toxin was expressed as a percentage of basal intensity (basal=baseline $\Delta\psi m$ - $\Delta\psi m$ after FCCP). Because mitochondrial movement may affect measurement accuracy, it was sometimes necessary to express the dye intensity in the mitochondria as a ratio of that in the cytosol to establish the extent of dye redistribution (Figure 2-4). The top graph in Figure 2-4 shows that in this instance, measuring the change in dye intensity in the mitochondria alone does not adequately reflect the extent of depolarization following oligomycin addition. This depolarization is more accurately represented when the increase in dye intensity within the cytosol is accounted for (bottom graph).

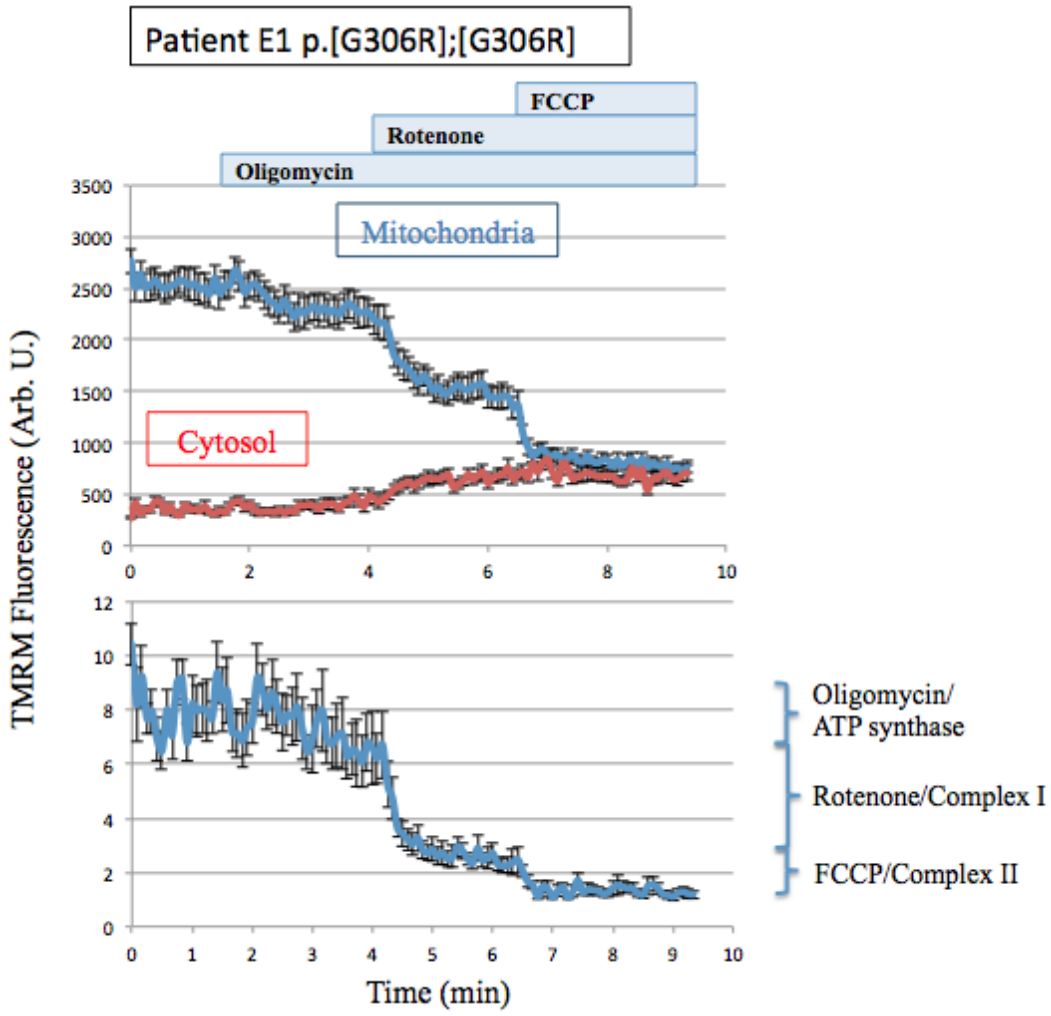

Figure 2-4 TMRM time-series experiment requiring the dye intensity in the mitochondria to be expressed as a ratio of the intensity in the cytosol.

2.2.19 Charge-coupled device (CCD) camera: reduced nicotinamide adenine dinucleotide (NADH)

For the NADH assay, fibroblasts needed to be alive and adherent to 25 mm glass coverslips in 6-well plates. Coverslips were sterilised as described in Section 2.2.18. Fibroblasts were cultured for four days in physiological concentrations of riboflavin (Section 2.2.8), seeded into 6-well plates containing low riboflavin or riboflavin-supplemented medium, and cultured for an additional four days at the end of which they reached 70-80% confluence. The experiment was performed immediately following this time period.

The cell medium was removed and cells were washed once in HBSS (with Ca^{2+} and Mg^{2+}, without phenol red; Life Technologies) at room temperature. The coverslip

was placed in a chamber with 500 µl of HBSS. NADH is intrinsically autofluorescent therefore no indicators need to be artificially introduced to measure NADH levels. The oxidised nicotinamide adenine dinucleotide (NAD^+) is not fluorescent (Duchen, 2004). The resting level of NADH autofluorescence was measured in fibroblasts using an epifluorescence inverted microscope with a X20 fluorite objective as described in Bartolome et al. (2013). Excitation light at 350 nm from a Xenon arc lamp passed through a monochromator (Cairn Research, UK). Emitted fluorescence light passed through a 455 nm long-pass filter to a cooled charge-coupled device (CCD) camera (Retiga, QImaging, Canada). Illumination intensity was minimised to prevent phototoxicity. The pinhole was set to produce a ~2 µm optical slice. The NADH redox index was determined by calibration of the NADH fluorescence signal with the mitochondrial inhibitors sodium cyanide (NaCN) and FCCP. After acquiring the basal NADH autofluorescence for 2 min, 2 µM final concentration of FCCP (Sigma) was added, and 3-4 min later, 2 mM final concentration of NaCN (Sigma) was added to the chamber.

The Andor IQ software (Andor, UK) was used to collect and analyse imaging data. For data analysis, 30-50 regions were selected within the field (one per coverslip). The average autofluorescence intensity across these areas was plotted on the y-axis against time on the x-axis. The redox index was calculated by expressing the basal NADH levels as a percentage of the range, i.e. the difference between the maximally oxidised (response to the uncoupler FCCP, which maximises respiration (0% NADH)) and maximally reduced signals (response to NaCN, a complex IV inhibitor which fully inhibits respiration (100% NADH)) (Duchen, 2004; Gandhi et al., 2009). The NADH pool was calculated by subtracting the NADH autofluorescence after addition of FCCP from the fluorescence after addition of NaCN. All measurements were compared to the mean intensity in controls for each experimental day and each medium condition (low versus high riboflavin) separately.

2.2.20 Lactate/pyruvate ratio

For the lactate/pyruvate ratio assessment, cells were grown to confluence in 75 cm^2 flasks. The flasks were gently shaken and a 400 µl aliquot of the medium was collected. The cell medium was mixed with 400 µl of 0.8 M perchloric acid (VWR)

and immediately stored at -80°C. Perchloric acid is used to stabilise pyruvate. The pyruvate concentration was determined according to the method described by Harrison et al. (1988) by monitoring the decrease in NADH fluorometrically in the presence of excess lactate dehydrogenase. The lactate concentration was assessed as described by Gutman & Wahlefeld (1974) by monitoring the increase in NADH fluorometrically in the presence of excess lactate dehydrogenase at pH 9. The background level of lactate and pyruvate in fresh, unused medium was subtracted from the concentration of lactate and pyruvate in the samples. This assay was performed by the Neurometabolic Unit at the NHNN. All lactate/pyruvate ratios were compared to the ratios in controls for each experimental day and each medium condition (low versus high riboflavin) separately.

2.2.21 Coenzyme Q_{10} (CoQ_{10}) status

Cell lysates for the CoQ_{10} assays were prepared as described in Section 2.2.5. CoQ_{10} status was assessed by both reversed-phase HPLC with UV detection and tandem mass spectrometry. Briefly, after addition of an internal standard (IS) to samples, samples were freeze-thawed three times and CoQ_{10} was extracted using a 5:2 v/v hexane/ethanol solution. Samples were centrifuged at 15,000 rpm for 3 min at room temperature, and the top layer (hexane) was collected and stored on ice. The bottom layer was re-extracted two more times. Samples were evaporated using a rotary evaporator, resuspended in 300 µl ethanol and filtered.

The HPLC method was based on that described by Boitier et al. (1998) and was carried out using the following equipment: PU-980 intelligent pump (SpectraLab Scientific), AS-950 intelligent autosampler (SpectraLab Scientific), Techsphere ODS 5 µm 150 x 4.6 mm column, TSPChromojet SP4400 series integrator, and PG-975-50 UV/VIS detector (SpectraLab Scientific). 50 µl of sample was injected and the absorbance of CoQ_{10} was measured at 275 nm. The CoQ_{10} concentration in pmol/ml was quantified by relating the sample peak height to the IS peak height, and was divided by the protein concentration (Section 2.2.7) to obtain the concentration in pmol/mg. CoQ_{10} quantification by tandem mass spectrometry was carried out as described in Duberley et al. (2013). This work was entirely carried out by Dr Kate

Duberley at the Institute of Neurology (ION), although I assisted with the extraction of CoQ_{10}.

2.2.22 Western blot

Cell lysates for Western blot prepared as described in Section 2.2.6 were thawed on ice and centrifuged at 4°C at 13.2 rpm for 10 min. The supernatant was transferred to a cold Eppendorf on ice. The protein concentration of the supernatant was assayed as described in Section 2.2.7. Samples were prepared using 25 µl 4X sodium dodecyl sulphate (SDS) buffer (Life Technologies), 1 µl 1 M dithiothreitol (DTT) (Sigma), sample at 2 mg/ml, made up to 100 µl with lysis buffer (recipe in Appendix II). Samples were mixed, heated at 70°C for 10 min, and spun down briefly. 40 µg of each sample was loaded per well along with one well containing 3 µl pre-stained protein standard molecular weight marker (Life Technologies). Samples were electrophoresed on a NuPAGE Novex 4-12% Bis-Tris Gel (Life Technologies) in SDS running buffer (recipe in Appendix II) at 180 V for 1 h or until the samples had run to the bottom of the gel. Proteins were transferred to an Amersham Hybond electrochemiluminescence (ECL) nitrocellulose membrane (GE Healthcare, UK) in a cassette containing sponge and blotting paper at 35 V for 2 h in Tris transfer buffer (recipe in Appendix II). The membranes were removed and soaked in Ponceau solution (Sigma) for 2 min to confirm the protein transfer. The membranes were washed in PBS-Tween and blocked in 5% milk in PBS-Tween or in 5% w/v BSA in PBS-Tween for 1 h at room temperature with gentle agitation. Membranes were washed once with PBS-Tween, and incubated in primary antibody overnight at 4°C. The following morning, membranes were washed three times with PBS-Tween and incubated with secondary antibody for 1 h. Membranes were washed three times with PBS-Tween. The primary antibodies used were horseradish peroxidase (HRP)-conjugated rabbit polyclonal anti-glyceraldehyde-3-phosphate dehydrogenase (GAPDH) (1:1,000 in 1% BSA; Abcam, UK), mouse monoclonal anti-ATP-synthase β subunit (ATP5β) (1:1,000; Abcam), and mouse monoclonal anti-β-Actin (1:10,000; Sigma). The secondary antibodies used were goat anti-mouse IgG-HRP (1:5,000; Santa Cruz Biotechnology, USA) and goat anti-rabbit IgG-HRP (1:5,000; Santa Cruz Biotechnology). Primary and secondary antibodies were diluted in 1% milk in PBS-Tween unless stated otherwise. β-Actin was used as the loading control. Antibody

binding was detected in a dark room on Super Rx X-ray film (Fujifilm, Japan) in an Amersham autoradiography cassette (GE Healthcare) using an ECL kit with each ECL reagent at a 1:1 ratio (Thermo Fisher Scientific).

Optimisation of the Western blot protocol for measurement of expression levels of endogenous RFVT2 is found in Appendix II. This experiment could not be successfully optimised due to the poor quality of the commercially available antibodies.

2.3 Cellular model: *SLC52A2*-short hairpin ribonucleic acid (shRNA) knockdown (KD) SH-SY5Y neuroblastoma cells

2.3.1 Cell line

Human neuroblastoma (SH-SY5Y) cells were kindly provided by Dr Kate Duberley; these cells were originally acquired from the European Collection of Cell Cultures (Health Protection Agency, Salisbury, UK). The SK-N-SH cell line had initially been grown from a bone-marrow biopsy of a female patient with a chest neuroblastoma (Biedler et al., 1973). The neuroblast-like cells from this biopsy were sub-cloned three times as SH-SY, SHSY5 and SH-SY5Y (Biedler et al., 1978). The SK-N-SH cell line had been determined to have dopaminergic, acetylcholinergic and adenosinergic neurotransmitter activity (Biedler et al., 1978).

2.3.2 Cell culture

SH-SY5Y cells were grown at 37°C in 95% air and 5% CO_2. Unless otherwise specified, cells were maintained in DMEM (high glucose and pyruvate; Life Technologies) with 10% v/v FBS (heat-inactivated, non-USA origin; Life Technologies) and 1% v/v P/S (5,000 U/5,000 μg per ml; Gibco) in 75 cm^2 tissue culture flasks. The medium was changed every four days. Cultures were passaged when cells reached 70-80% confluence. To split or freeze cells, the medium was removed from the flask. Cells were washed in 7 ml of 1X DPBS (Life Technologies). 1.5 ml of 0.25% 1X trypsin-EDTA (Life Technologies) was added and cells were placed back in the incubator at 37°C for 3 min. The flask was swirled and tapped to detach the cells. 5 ml of medium was added to the flask to quench the trypsin, and cells were collected and centrifuged at 1,200 rpm for 5 min. The supernatant was

discarded. To split cells, the cell pellet was resuspended in medium and split into new flasks as appropriate. To freeze cells, the cell pellet was resuspended in 40% FBS, 10% dimethyl sulfoxide (DMSO) (Sigma) and 50% cell medium and placed in labelled cryovials (1 ml per cryovial) at a density of 1 x 10^6 cells/ml. Cells were first frozen at -80°C for 24 h in a tightly sealed Polystyrene box, and then transferred to liquid nitrogen for long-term storage. Cells were defrosted quickly in a 37°C water bath and seeded at a density of 4 x 10^4 cells/cm^2 into 75 cm^2 tissue culture flasks. To obtain reproducible results, only SH-SY5Y cells of passage number 19-25 were used in experiments.

2.3.3 Cell counting

Cell counting was performed as described in Section 2.2.4.

2.3.4 pGIPZ lentiviral *SLC52A2* shRNAmir vectors: description

Two human pGIPZ lentiviral microRNA-adapted short hairpin ribonucleic acid (shRNAmir) vectors containing hairpin sequences uniquely targeting *SLC52A2* (*SLC52A2*-short hairpin ribonucleic acid (shRNA) 1 and *SLC52A2*-shRNA2) were purchased as bacterial agar stab cultures from Open Biosystems (Thermo Fisher Scientific) (see Appendix VII Table VII-3 for clone IDs and hairpin sequences). The pGIPZ lentiviral shRNAmir empty vector (no shRNAmir insert) and non-targeting (non-silencing) shRNAmir vector (referred to as scrambled shRNA herein) were used as controls and were kindly provided by Dr Klaus Wanisch at the ION. The pGIPZ lentiviral vector contains a microRNA-adapted shRNA insert for RNA interference via Drosha and Dicer processing of the expressed hairpin. Some other features of the pGIPZ lentiviral vector include a CMV promoter, Turbo-green fluorescent protein (GFP) reporter, and ampicillin and puromycin antibiotic resistance markers. The 5' LTR is a hybrid promoter required for high expression of viral transcripts in the target cells. The pUC origin is required for high-copy replication in *Escherichia coli* cells (Figure 2-5).

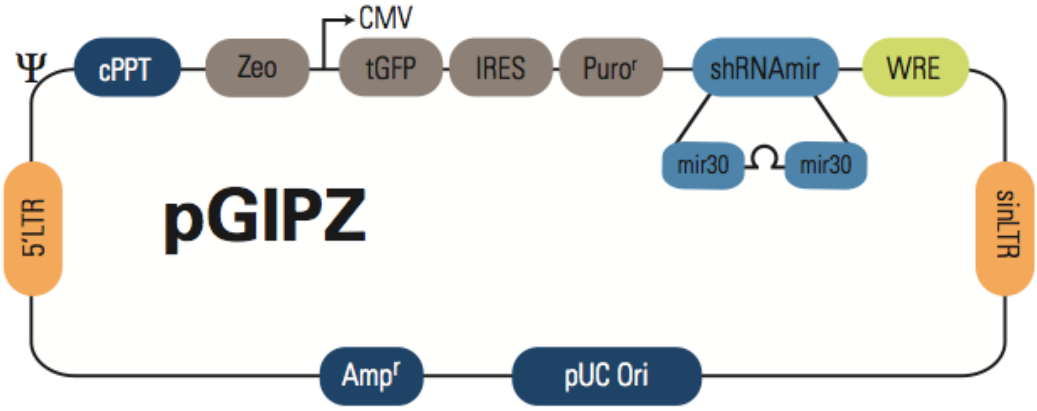

Figure 2-5 Map of the pGIPZ lentiviral shRNAmir vector (reproduced from Thermo Fisher Scientific website).

2.3.5 Transformation of chemically competent cells

Bacteria from the surface of the agar stab cultures corresponding to each of two *SLC52A2* pGIPZ shRNAmir vectors (*SLC52A2*-shRNA1 and *SLC52A2*-shRNA2) were streaked on pre-warmed Luria-Bertani (LB) agar plates (recipe in Appendix II) containing 50 µg/ml ampicillin and incubated upside down overnight at 37°C. The following day, single colonies were picked aseptically and inoculated into a tube containing 2 ml of LB broth (recipe in Appendix II) with 50 µg/ml ampicillin. These starter cultures were grown for 7 h on a shaking (225 rpm) incubator at 37°C. 300 µl of starter culture was aseptically added to a 500 ml flask containing 150 ml of LB broth (1:500 dilution) with 50 µg/ml ampicillin and grown overnight at 37°C in a shaking (225 rpm) incubator. Glycerol stocks of all clones were prepared by mixing 500 µl of the overnight culture with 500 µl glycerol at 50% v/v and freezing at -80°C. Overnight cultures were harvested by centrifugation at 4°C at 3,000 rpm for 20 min; the pellet was frozen at -80°C.

2.3.6 Maxiprep isolation of plasmid DNA and quality control

To obtain high-quality plasmid DNA for mammalian cell transfection, plasmid DNA for human pGIPZ lentiviral shRNAmir clones with empty control, scrambled control, and *SLC52A2*-targeting (*SLC52A2*-shRNA1 and *SLC52A2*-shRNA2) hairpin sequences was purified from the cell pellets obtained from overnight bacterial cultures (Section 2.3.5) using the Qiafilter Maxiprep kit (Qiagen) as per the

manufacturer's instructions. Plasmid DNA purity and concentration were determined as described in Section 2.1.5.

All pGIPZ vectors were sequenced by the UCL DNA sequencing service to confirm that the hairpin sequences were correct (see Appendix VII Table VII-4 for sequence of pGIPZ vector sequencing primer). A restriction digest was performed on all clones to ensure no recombination had occurred. The digest reaction contained: 2 µl 10X restriction enzyme buffer 4 (New England Biolabs (NEB), USA), 0.5 µl restriction enzyme SacII (20 U; NEB), 300 ng plasmid DNA, made up to 20 µl final volume with dH_2O. The reaction was mixed and incubated at 37°C for 2 h. 10 µl of the digested samples were loaded with 2 µl 5X loading dye (Qiagen) onto a 1% w/v agarose gel with 1 Kb DNA ladder (NEB). Uncut samples were run alongside the digested samples for comparison. Three bands of the expected size were obtained, confirming that no recombination had occurred.

2.3.7 Stable transfection

The night before transfection, cells were plated at approximately 50% confluence in 6-well plates and incubated under normal conditions. The following morning, SH-SY5Y cells were transfected with empty control, scrambled control, and *SLC52A2*-shRNA using the Effectene transfection reagent following the manufacturer's protocol with minor modifications (Qiagen). A control well of untransfected cells was also prepared. For each well, 2 µg of DNA was diluted with 100 µl DNA-condensation buffer in an Eppendorf tube, followed by gentle mixing. DNA for the two *SLC52A2*-shRNAs were either pooled or transfected as individual shRNAs. 3.2 µl of enhancer was added and the tube was mixed briefly. 10 µl of Effectene transfection reagent was added to the DNA-enhancer mixture, followed by brief mixing. Tubes were incubated for 20 min at room temperature. In the meantime, the growth medium was replaced with fresh medium. The entire content of each tube was added drop-wise to the appropriate well, following by gentle swirling. Cells were placed back into the incubator. The day after transfection, transfection efficiency was assessed microscopically by visualising Turbo-GFP expression. For stable knockdown (KD) of *SLC52A2*, the polyclonal SH-SY5Y cells were maintained in selective medium containing 2 µg/ml puromycin dihydrochloride from

Streptomyces alboniger (Sigma) from 48 h after transfection to eliminate cells not expressing Turbo-GFP. The well of non-transfected cells was also treated with puromycin; when all cells in this well were dead, it could be presumed that the cells which did not take up the vector in the transfected wells would also be dead. The puromycin concentration was reduced to 1 μg/ml after two weeks.

2.3.8 RNA extraction

Prior to RNA extraction, SH-SY5Y cells were grown to confluence in 6-well plates. To assess KD efficiency of *SLC52A2*-shRNA, total RNA was extracted from purely transfected cells using the MiRNeasy Mini kit (Qiagen) and the RNase-free DNase set (Qiagen) as described in Section 2.2.9.

2.3.9 cDNA synthesis

Following RNA extraction, cDNA was synthesized from total RNA using the First-Strand cDNA SuperScript II Reverse Transcriptase kit (Life Technologies) as described in Section 2.2.10. The efficiency of cDNA synthesis and the possibility of DNA contamination were assessed as described in Section 2.2.10. A PCR reaction using *SLC52A2* primers and subsequent agarose gel electrophoresis also served to confirm that *SLC52A2* is expressed in SH-SY5Y cells as evidenced by a strong, single band on the gel.

2.3.10 RT-qPCR

To assess KD efficiency of the *SLC52A2* shRNAs in the SH-SY5Y cells, RT-qPCR was performed as described in Section 2.2.11 with minor modifications. The standard curve was constructed using a cDNA sample corresponding to the scrambled shRNA. For relative quantification, the scrambled shRNA was used as the calibrator.

2.3.11 Optimisation of riboflavin concentration in SH-SY5Y cell medium

As was done for the fibroblast medium, the riboflavin concentration in the SH-SY5Y cell medium was optimised, as an effect of high riboflavin levels in the medium on the parameters of interest could not be discarded. It is expected that the threshold of riboflavin concentration for demonstrating biochemical defects would vary between

cell lines (S. Olpin, personal communication). Complex I and II activities (see Sections 2.3.12-2.3.16 for methods) were again used as a measure of cell health for medium optimisation in the empty control, scrambled control, and *SLC52A2*-KD shRNA (clones 1, 2 and 1+2 combined) SH-SY5Y cells. Five independent optimisation trials were carried out using a total of seven different concentrations of riboflavin ranging from 0.66 nM to 300.6 nM, leaving cells to grow in the medium from one to eight days, and using either dialysed or regular FBS. Unfortunately, no condition revealed a specific defect in *SLC52A2*-KD shRNA cells compared to empty and scrambled control shRNA cells. Details and results of all optimisation trials are available in Appendix VII Table VII-5 and in Section 7.9.

2.3.12 Cell harvesting for biochemical analysis

For the MRC complex I and II activities assay, SH-SY5Y cells were grown in variable concentrations of riboflavin for varying lengths of time (see Appendix VII Table VII-5), and were harvested from confluent 75 cm^2 flasks. The medium was removed, and cells were washed once with DPBS and then detached with trypsin-EDTA as described in Section 2.3.2. Cell medium was added to the flask and cells were collected and centrifuged at 1,200 rpm for 5 min. The cell pellet was washed in DPBS. Cells were centrifuged again at 1,200 rpm for 5 min. The pellet was resuspended in 160 µl DPBS in aliquots (10 µl for protein determination, 60 µl for complex I, 60 µl for complex II, and 30 µl for CS measurements). Samples were stored at -80°C.

2.3.13 Total protein determination

The total protein content of the SH-SY5Y cell lysates was determined using the Bio-Rad DC protein assay (Bio-Rad Laboratories) as described in Section 2.2.7.

2.3.14 MRC complex I assay

The MRC complex I assay was performed as described in Section 2.2.15.

2.3.15 MRC complex II assay

The MRC complex II assay was performed as described in Section 2.2.16.

2.3.16 CS assay

The CS assay was performed as described in Section 2.2.17.

2.4 Cellular model: embryonic mouse mixed ventral horn cultures

2.4.1 Ethics approval

BL6/SJL hybrid wild-type (WT) female mice (Harlan Laboratories, UK) were examined in the experiments performed in this Thesis. All procedures and experiments using mice were performed under License from the UK Home Office in accordance with the Animals (Scientific Procedures) Act of 1986 and following ethical approval from the Ethical Review Panel of the ION. All work involving mice prior to culturing was performed entirely by Dr Bernadett Kalmar at the ION.

2.4.2 Cell culture of mixed ventral horn cultures

6-well plates, 12-well plates, 35 mm glass-bottomed microscope MatTek dishes (MatTek Corporation, USA), or previously autoclaved 13 mm round glass coverslips in 24-well plates (Beckton Dickinson, USA) were coated with 1.5 mg/ml polyornithine (Sigma) diluted 1:1,000 in sterile H_2O (Baxter Healthcare, USA) and left overnight at 37°C. In the morning, the polyornithine was aspirated and dishes were coated with 1 mg/ml laminin (Sigma) at 1:200 in L-15 medium (Sigma) for 2 h at 37°C. Laminin was removed prior to cell seeding.

Following euthanisation by cervical dissection, day 12-13 (E12-E13) embryos were harvested from pregnant WT female mice by hysterectomy and placed in a petri dish with chilled HBSS (Ca^{2+}, Mg^{2+} free, without phenol red; Sigma) with 2% v/v P/S (Gibco). Single embryos were placed in a 2 cm petri dish with HBSS and 2% P/S under a dissecting light microscope and the yolk sack was removed. The ventral horn of the spinal cord was dissected and mixed ventral horn cultures were prepared as described in Camu & Henderson (1994). Using this technique, on average 30-50% of mixed ventral horn cultures are primary motor neurones, the remaining cells being fibroblasts and astroglia. Purifying cultures to increase the proportion of motor neurones results in decreased viability as glia and fibroblasts promote motor neurone survival.

First, the head, liver, intestines and stomach of the embryos were removed and the embryo was laid down flat with the spinal cord on top. The skin covering the neural tube was carefully removed using forceps and the spinal cord was teased away from the body. The meninges were peeled off and the dorsal column removed with a scalpel. Ventral columns were placed in fresh chilled HBSS with 2% P/S for subsequent dissociation and seeding.

At most four dissected spinal cords were pooled (all WT genotype) and placed in 1 ml HBSS (Ca^{2+}, Mg^{2+} free; Sigma) with 10 µl of 2.5% w/v trypsin in PBS (final concentration 0.025%; Sigma) at 37°C for 9 min. The resultant clump of tissue was transferred to a tube containing 800 µl L-15 medium, 100 µl BSA (4% w/v in L-15; Sigma) and 100 µl DNAse (1 mg/ml in L-15) and gently triturated twice with a 1 ml pipette. After allowing the cord to settle, the supernatant (containing the motor neurones) was transferred to a new 15 ml tube. 900 µl L-15, 100 µl BSA and 20 µl DNAse were added to the remaining pellet and the solution was gently triturated six times. After allowing the solution to settle again, the supernatant was collected and pooled with the first supernatant. 1 ml of BSA was layered at the bottom of the tube containing the supernatants, and the tube was centrifuged at 380 g for 5 min at room temperature. The supernatant was discarded and the pellet was resuspended in 1 ml complete Neurobasal (CNB) medium (see Appendix II for recipe). Cells were counted as described in Section 2.2.4 and plated at the appropriate density depending on the experiment. For biochemical measurements (complex I, complex II and CS activities), cells were plated on 6-well plates at a density of 2-2.5 x 10^5 cells per well. For RNA extraction, cells were plated on 12-well plates at a density of 1.5 x 10^5 cells per well. For confocal microscopy experiments, 1 x 10^5 cells were plated per MatTek. For determination of viral titre by immunocytochemistry, cells were seeded in 24-well plates at a density of 2.5-5 x 10^4 cells per well on glass coverslips. Cells were maintained in a 37°C incubator with 5% CO_2 and were examined daily. This work was performed with the help of Dr Bernadett Kalmar.

For riboflavin deprivation experiments in the mixed ventral horn cultures, the concentration of riboflavin in the CNB medium was first determined. The horse serum (non-USA origin; Life Technologies) contained 49 nM (18.4 µg/L) riboflavin

as determined by HPLC performed by Marcus Oppenheim; therefore the serum contributes 0.98 nM (0.369 μg/L) riboflavin to the medium as it represents 2% of the CNB medium. The 1X Neurobasal medium (Life Technologies) contains 1,060 nM (400 μg/L) riboflavin (according to the Life Technologies specifications) and contributes approximately 1,004 nM (378.9 μg/L) riboflavin to the CNB medium. All other components of the CNB medium are riboflavin-free (according to company specifications) therefore the total concentration of riboflavin in prepared CNB medium (termed "regular CNB medium") is approximately 1,005 nM (379.3 μg/L). To prepare the medium for riboflavin deprivation experiments, the Neurobasal medium in the regular CNB medium was replaced with an equivalent volume of custom-made DMEM without riboflavin (Merck-Millipore); no other components were changed therefore the riboflavin concentration was 0.98 nM riboflavin (from the horse serum) in this "modified DMEM". Riboflavin was diluted and prepared as described in Section 2.2.8. For the riboflavin-supplemented modified DMEM (no deprivation), riboflavin was added to match the concentration in the regular CNB medium (1,005 nM). For the 50% riboflavin-deficient modified DMEM, the final concentration of riboflavin was 502.5 nM (189.7 μg/L). For the modified DMEM with 99% deprivation (0.98 nM), no riboflavin was added to the medium. For the biochemical and confocal microscopy experiments, the day following seeding, the medium was changed from regular CNB medium to one of the riboflavin-defined media described above; the mixed ventral horn cultures were maintained for a further nine days in vitro (DIV) in riboflavin-defined medium.

2.4.3 Cell counting

Cell counting was performed as described in Section 2.2.4.

2.4.4 pGIPZ lentiviral *Slc52a2* and *solute carrier family 52, riboflavin transporter member 3* (*Slc52a3*) microRNA-adapted short hairpin RNA (shRNAmir) vectors

Two pGIPZ lentiviral shRNAmir vectors containing hairpin sequences uniquely targeting the mouse *Slc52a2* (*Slc52a2*-1) or *Slc52a3* (*Slc52a3*-1 and *Slc52a3*-2) genes were purchased as bacterial agar stab cultures from Open Biosystems (Thermo Fisher Scientific) (see Appendix VII Table VII-8 for clone IDs and hairpin sequences). The pGIPZ lentiviral shRNAmir empty vector (no shRNAmir insert) and

non-targeting (non-silencing) shRNAmir vector (referred to as scrambled shRNA) were used as controls and were kindly provided by Dr Klaus Wanisch. The pGIPZ lentiviral vector was previously described in Section 2.3.4. This vector is also suitable for transductions using the replication-incompetent HIV-based lentivirus.

2.4.5 Transformation of chemically competent cells

Transformation of chemically competent cells from bacterial agar stab cultures of the pGIPZ lentiviral *Slc52a2* and *Slc52a3* shRNAmir vectors as well as the empty and scrambled control vectors was performed as described in Section 2.3.5.

2.4.6 Maxiprep isolation of plasmid DNA and quality control

To obtain high-quality plasmid DNA for transduction, DNA for the empty control, scrambled control, *Slc52a2*-targeting (*Slc52a2*-1) and *Slc52a3*-targeting (*Slc52a3*-1 and *Slc52a3*-2) hairpin sequences was purified from the cell pellets obtained from overnight bacterial cultures (Section 2.4.5) using the Qiagen HiSpeed Maxi kit (Qiagen) or EndoFree Plasmid Maxi kit (Qiagen) as per the manufacturer's instructions. Plasmid DNA purity and concentration were determined as described in Section 2.1.5. All pGIPZ vectors were sequenced by the UCL DNA sequencing service to confirm that the hairpin sequences were correct (see Appendix VII Table VII-4 for sequence of pGIPZ vector sequencing primer).

2.4.7 Second generation lentivirus preparation

Second generation lentiviral particles for empty control, scrambled control, *Slc52a2*-targeting (*Slc52a2*-1) and *Slc52a3*-targeting (*Slc52a3*-1 and *Slc52a3*-2) hairpin sequences were prepared by packaging in human embryonic kidney 293T (HEK293T) cells. Three components are required to produce a 2nd generation lentivirus: a packaging plasmid, an envelope plasmid, and the shRNA (or cDNA)-containing transfer plasmid (Figure 2-6). The pGIPZ transfer plasmid was described in Section 2.3.4. The envelope plasmid used here is the pMD2.g plasmid coding for the *vesicular stomatitis virus* (*VSV-G*) envelope gene (Figure 2-7; Addgene, USA). The packaging plasmid used here, p8.91 (Addgene), encodes the HIV *gag*, *pol*, *rev* and *tat* genes.

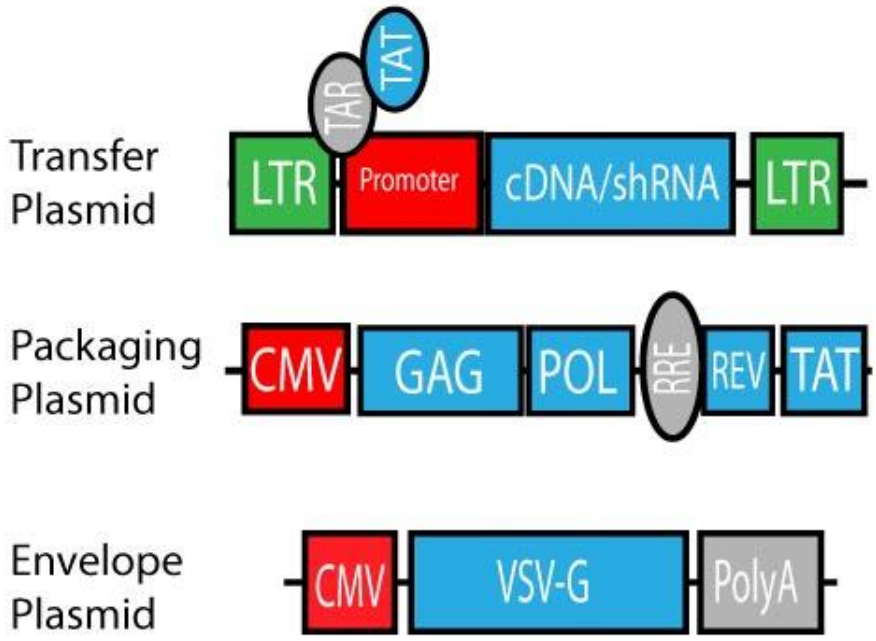

Figure 2-6 Components required for 2nd generation virus: a transfer plasmid, a packaging plasmid, and an envelope plasmid (image obtained from http://www.addgene.org/ lentiviral/packaging/).

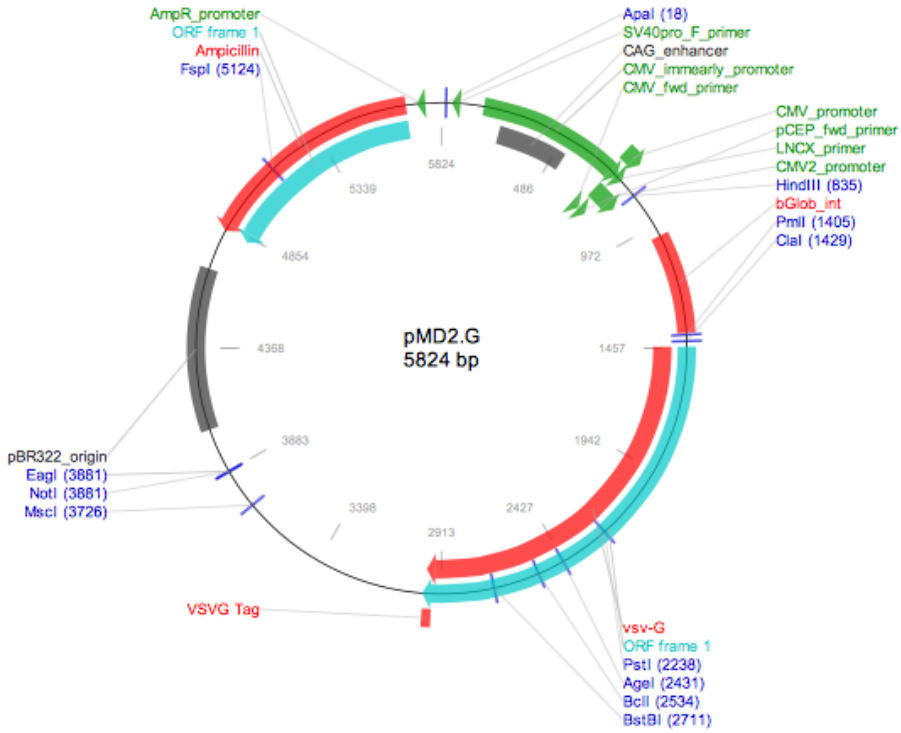

Figure 2-7 Vector map of the envelope plasmid pMD2.g coding for the *VSV-G* gene (image obtained from http://www.addgene.org/12259/).

HEK293T cells required for 2nd generation lentivirus preparation and viral titre determination were kindly provided by Dr Klaus Wanisch. On day 0, 1 x 10^6 HEK293T cells were seeded on 100 mm round dishes (Corning) with 15 ml HEK cell medium (DMEM High glucose (Gibco) + 10% foetal calf serum (FCS) (Gibco) + 1% P/S (Gibco)). Four dishes were used per virus. On day 3, the medium was replaced with 10 ml of Optimem-I (without serum and P/S; Gibco). The Lipofectamine mix "A" was prepared by mixing 2 ml Optimem-I with 60 µl Lipofectamine 2000 (Life Technologies) per dish. The DNA mix "B" was prepared by mixing (per dish) 12 µg p8.91 packaging plasmid, 7 µg ENV envelope plasmid, 25 µg of transfer plasmid (lentiviral vector containing shRNA), made up to 2 ml with Optimem-I. Mix "A" and "B" were incubated separately for 5 min and then combined and incubated for 20 min with several inversions during incubation. The mixture was added to the dish of HEK293T cells in Optimem-I medium. The morning of day 4, the medium was changed to HEK cell medium and transfection

efficiency was assessed by visualising GFP fluorescence. On day 5, the virus was collected by removing the cell medium (lentiviral particle-containing supernatant), placing it in a 50 ml tube, spinning at 4,500 rpm for 15 min, passing the supernatant through a 0.4 μm filter, and storing at 4˚C. The dish with the HEK293T cells was replenished with 15 ml fresh HEK cell medium. On day 6, the virus was again collected as before and combined with the supernatant from day 5 into a 50 ml Oakridge top ultracentrifuge tube (Nalgene- Thermo Fisher Scientific). The combined supernatants were spun in a refrigerated ultracentrifuge at 47,000 g for 2.5 h. The supernatant was removed and the viral pellet resuspended in 200 μl PBS (Sigma). 20 μl aliquots were prepared and stored at -80˚C. Empty control, scrambled control, *Slc52a2*-KD (*Slc52a2*-1) and *Slc52a3*-KD (*Slc52a3*-1 and *Slc52a3*-2) shRNA mixed ventral horn cultures, mouse embryonic fibroblasts (MEFs), and HEK293T cells were generated by lentiviral infection with variable concentrations of these viruses.

2.4.8 Immunocytochemistry for viral titre determination in human embryonic kidney 293T (HEK293T) cells and mixed ventral horn cultures

Immunocytochemistry was used to determine the viral titres (number of transducing units (TU) per ml) for the empty control, scrambled control, *Slc52a2*-KD (*Slc52a2*-1) and *Slc52a3*-KD (*Slc52a3*-1 and *Slc52a3*-2) shRNAs transduced into HEK293T cells and mixed ventral horn cultures.

On day 0, HEK293T cells were seeded on 13 mm glass coverslips in a 24-well plate with 500 μl/well HEK cell medium at a density of 5 x 10^3 cells per well. On day 1, the HEK293T cells were infected with 5 μl (1:100), 1 μl (1:500) or 0.5 μl (1:1,000) of empty control, scrambled control, *Slc52a2*-KD (*Slc52a2*-1) or *Slc52a3*-KD (*Slc52a3*-1 or *Slc52a3*-2) lentivirus. Un-transduced control wells were also used to assess the effect of the virus on cell death. After 48 h, immunocytochemistry was performed. The medium was removed and cells were washed once in 1X PBS (Life Technologies). All PBS washes lasted 5 min. Cells were fixed for 20 min in 4% w/v PFA (10% Ultra pure EM grade; Polysciences Inc., USA) diluted in 1X PBS, followed by two washes with 1X PBS. The coverslips were mounted on polylysine slides (VWR) using fluorescent mounting medium (Dako, UK).

Mixed ventral horn cultures were seeded on day 0 on glass coverslips in a 24-well plate with 300 µl CNB medium per well as described in Section 2.4.2. On day 1, mixed ventral horn cultures were infected with 3 µl (1:100) or 0.6 µl (1:500) of empty control, scrambled control, *Slc52a2*-KD (*Slc52a2*-1) or *Slc52a3*-KD (*Slc52a3*-1 or *Slc52a3*-2) lentivirus. Un-transduced control wells were also used. After 18 h, the virus was replaced with fresh CNB medium. On day 5, the medium was removed and cells were washed once in 1X PBS (Life Technologies). Cells were fixed for 20 min in 4% w/v PFA diluted in 1X PBS, followed by two washes with 1X PBS. Cells were blocked at room temperature in PBS-0.1% Triton X-100 (Sigma) with 5% goat serum for 40 min. The blocking solution was aspirated and a mouse monoclonal primary antibody for the neuronal marker β-III tubulin (1:500; Covance, USA) diluted in blocking solution was applied for 2 h. Cells were washed three times in 1X PBS. Cells were incubated with a goat anti-mouse Alexa Fluor 568 secondary antibody (1:1,000; Life Technologies) diluted in blocking solution for 1.5 h in the dark. The secondary antibody was removed and cells were washed once with nuclear stain DAPI (1:1,000 in 1X PBS; Sigma) for 10 min in the dark. Cells were washed twice with 1X PBS before mounting the coverslips on polylysine slides (VWR) using fluorescent mounting medium (Dako).

Coverslips were imaged using a Leica DFC420C fluorescence microscope (Leica Microsystems- Danaher, USA), the Leica Application Suite software (Leica Microsystems- Danaher), and a 20X objective lens. The coverslip with the infection ratio giving approximately 10% GFP-positive cells was selected. Three to four fields were randomly selected so that a total of 300-400 DAPI-positive cells were counted. For the titre determination in HEK293T cells, the total number of GFP-positive cells and total number of DAPI-stained cells were counted. For the motor neurones, the total number of GFP-positive motor neurones and the total number of DAPI-positive cells (which includes other cell types besides motor neurones) were counted. Motor neurones were identified according to their morphology (Section 2.4.17) and positive staining for β-III tubulin and DAPI. The data was analysed using the Image J web-based software (http://rsb.info.nih.gov/ij/). As an example of titre calculation, let us presume that 40 GFP and DAPI-positive HEK293T cells were counted out of a total of 400 DAPI-positive HEK293T cells for all fields counted on a single coverslip.

The number of TU (40 GFP and DAPI-positive cells) was then calculated to the original number of cells seeded (500 TU for 5000 cells seeded). If the coverslip corresponding to the 1:500 dilution (1 µl virus per 500 µl medium) was used for counting, the viral titre would be 5 x 10^5 TU/ml (=500 TU x 1,000). The viral titres in HEK293T cells and mixed ventral horn cultures are provided in Section 7.11.1.

2.4.9 RNA extraction

To establish the mRNA expression levels of *Slc52a2* and *Slc52a3* in WT mixed ventral horn cultures, cells were seeded in 12-well plates as described in Section 2.4.2 and were grown for five DIV in regular CNB medium. To assess KD efficiency of *Slc52a2* and *Slc52a3* shRNAs in purely transduced MEFs, on day 0, one vial of passage 0 WT MEFs was thawed and seeded into a 100 mm petri dish in 15 ml of DMEM High glucose (Gibco) with 10% FCS (Gibco) and 1% P/S (Gibco). On day 1, cells were split 1:3 into 6-well plates. On day 2, cells were transduced with empty control, scrambled control, *Slc52a2*-KD (*Slc52a2*-1) or *Slc52a3*-KD (*Slc52a3*-1 or *Slc52a3*-2) lentivirus at a 1:100 ratio. On day 3, the virus was removed and the medium replaced. On day 4, puromycin was added at 4 µg/ml for selection of transduced cells. Cells were split 1:2 on day 5 and on day 6, cells were harvested for RNA. Control (untransduced) wells of WT MEFs were also used to measure the mRNA expression levels of *Slc52a2* and *Slc52a3* in WT MEFs. Total RNA was extracted using the MiRNeasy Mini Kit (Qiagen) and the RNase-free DNase set (Qiagen) as described in Section 2.2.9.

2.4.10 cDNA synthesis

cDNA was synthesized from total RNA using the First-Strand cDNA SuperScript II Reverse Transcriptase kit (Life Technologies) as described in Section 2.2.10. The efficiency of cDNA synthesis and the possibility of DNA contamination were assessed as described in Section 2.2.10 (see Appendix VII Tables VII-9 and VII-10 for DNA and cDNA primer sequences).

2.4.11 RT-qPCR

To assess KD efficiency of the *Slc52a2* and *Slc52a3* shRNAs in the MEFs, as well as the relative mRNA expression levels of *Slc52a2* and *Slc52a3* in mixed ventral horn

cultures and WT MEFs, RT-qPCR was performed as described in Section 2.2.11 with minor modifications. The Taqman gene expression assay (Applied Biosystems) IDs were the following: Mm01205717_g1 (*Slc52a2*); Mm00510191 (*Slc52a3*); Mm00607939 (*Actb*). As the three probes were all FAM-labelled, separate reactions had to be prepared for each assay. Each RT-qPCR reaction contained 2 µl of template cDNA diluted 1:10 v/v with nuclease-free H_2O, 0.5 µl 20X Taqman gene expression assay (Applied Biosystems), 5 µl 2X Rotor-Gene Multiplex PCR Master Mix (Qiagen) and 2.5 µl RNase-free H_2O. The standard curve was constructed using a cDNA sample corresponding to the scrambled shRNA. For relative quantification, the scrambled shRNA was used as the calibrator.

2.4.12 Cell harvesting for biochemical analysis

For the MRC complex I and II activities assay, cells were seeded into 6-well plates as described in Section 2.4.2 and grown in 99% riboflavin-deficient, riboflavin-supplemented modified DMEM, or regular CNB medium. After nine DIV, the medium was removed, and cells were washed once with 1X DPBS (Life Technologies) and detached with trypsin-EDTA. Cell medium was added to each well to quench the trypsin; for each sample, cells from three replicate wells were collected, combined, and centrifuged at 380 g for 5 min. The cell pellet was resuspended in DPBS to wash. Cells were centrifuged again at 380 g for 5 min. The pellet was resuspended in 160 µl DPBS in aliquots (10 µl for protein determination, 60 µl for complex I, 60 µl for complex II, and 30 µl for CS measurements). Samples were stored at -80°C.

2.4.13 Total protein determination

The total protein content of the cell lysates was determined using the Bio-Rad DC protein assay (Bio-Rad Laboratories) as described in Section 2.2.7.

2.4.14 MRC complex I assay

The MRC complex I assay was performed as described in Section 2.2.15.

2.4.15 MRC complex II assay

The MRC complex II assay was performed as described in Section 2.2.16.

2.4.16 CS assay

The CS assay was performed as described in Section 2.2.17.

2.4.17 Confocal microscopy: $\Delta\Psi_m$

For live-cell confocal microscopy, mixed ventral horn cultures were seeded on MatTeks as described in Section 2.4.2. For studies in WT mixed ventral horn cultures, the day after seeding, cells were placed in riboflavin-defined medium (99% riboflavin-deficient, riboflavin-supplemented modified DMEM, or regular CNB medium) and cultured for an additional eight to nine DIV. For studies of *Slc52a2* and *Slc52a3*-KD mixed ventral horn cultures, the day after seeding, cells were infected with empty control, scrambled control, *Slc52a2*-KD (*Slc52a2*-1) or *Slc52a3*-KD (*Slc52a3*-1 or *Slc52a3*-2) lentivirus at 1:50 ratio. The virus was removed after 24 h, and the medium was changed to 99% riboflavin-deficient modified DMEM to prevent masking a possible metabolic defect in KD cells by riboflavin supplementation. Cells were grown for a further eight to nine DIV.

The cell medium was removed and cells were washed twice with warm recording medium (RM) at pH 7.35 (see Appendix II for recipe). Cells were incubated in 1 ml RM containing 20 nM TMRM for 30 min in the dark. The basal TMRM and response to mitochondrial toxins were measured as described in Section 2.2.18 with minor modifications. The final concentrations of toxins used were the following: 2 μg/ml oligomycin, 5 μM rotenone, and 1 μM FCCP. Motor neurones were selected using the following criteria: triangular appearance of the cell body, more than two neuritic processes (to differentiate them from interneurons), smaller size than fibroblasts and astroglia, and usually growing on the upper focal plane (above the layer of fibroblasts and astroglia) (Bilsland et al., 2008) (Figure 2-8).

A. 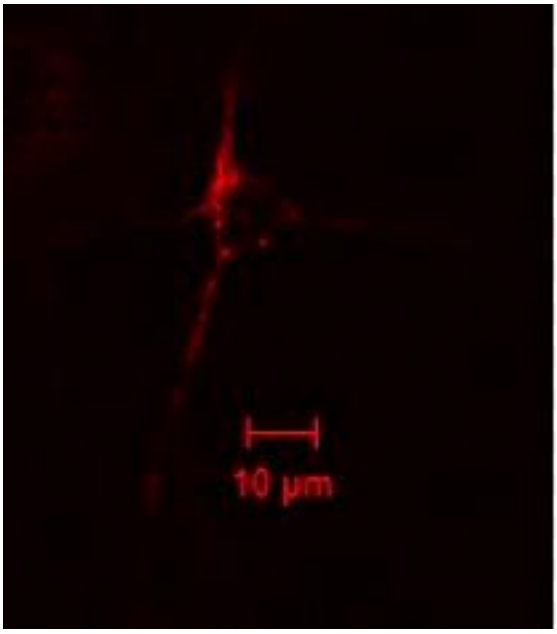

B. 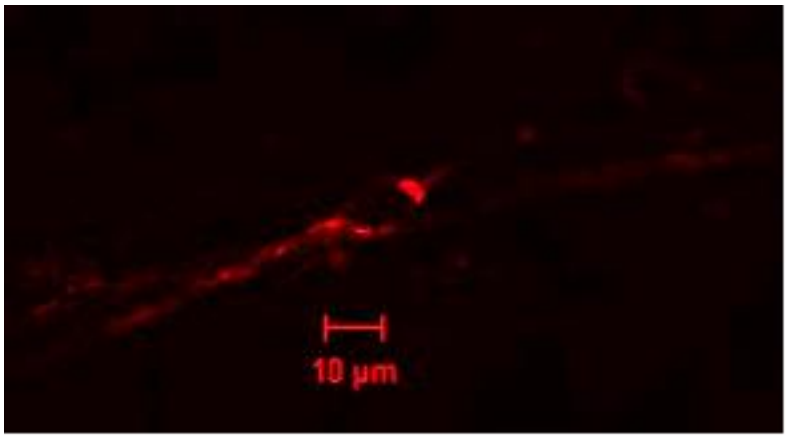

Figure 2-8 Example of a cell representing a motor neurone (A) and a cell which is not a motor neurone (B) according to specific criteria (Bilsland et al., 2008). Both cells are of a similar size, but the motor neurone has three neuritic processes while cell B has only two.

Basal ΔΨm measurements were analysed using the Zeiss Zen software (Carl Zeiss AG). For each z-stack, the focal plane corresponding to the highest TMRM intensity was selected and the mean TMRM fluorescence intensity across the pixels containing mitochondria was measured for each coverslip, each representing a minimum of three cells. In the WT mixed ventral horn cultures, for each experimental day all measurements were compared to the mean intensity in cells grown in riboflavin-supplemented modified DMEM. For studies of *Slc52a2* and

Slc52a3-KD mixed ventral horn cultures, all measurements for each experimental day were compared to the mean intensity in the scrambled control.

Time-series experiments were only performed in the study of *Slc52a2* and *Slc52a3*-KD mixed ventral horn cultures. Time-series data was analysed using the Zeiss Zen software (Carl Zeiss AG) as described in Section 2.2.18, except that only areas within GFP-expressing cells were selected. Due to poor transduction efficiency, only one GFP-positive cell was usually present within the chosen field for each coverslip (Figure 2-9).

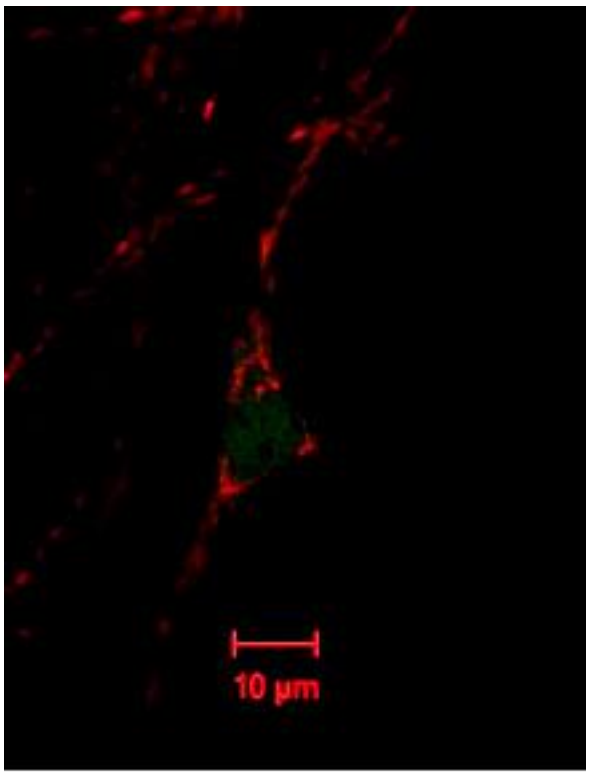

Figure 2-9 A GFP-positive (green) motor neurone incubated with 20 nM TMRM (red).

2.5 Statistical analysis

All statistical analyses were performed using the R software package (http://www.R-project.org/; R Development Core Team, 2008). For comparison of means of >2 groups, a Tukey's two-tailed post-hoc test or Dunnett's post-hoc test was performed after a one-way analysis of variance (ANOVA). For fibroblast experiments (which

involved more than one control), a one-way ANOVA was initially performed to determine if the controls were significantly different from one another. If the results of the ANOVA showed that the controls were not significantly different from each other at the $p<0.05$ level, the data from the three controls was pooled and considered as a whole. In this case, a Dunnett's two-tailed post-hoc test was performed for pairwise comparison of the control group to each patient and carrier. If the ANOVA suggested that the controls differed significantly from each other ($p<0.05$), a Tukey's two-tailed post-hoc test was performed for pairwise comparison between each control and patient/carrier individually. In this case, the highest p-value resulting from each of the three control-patient or control-carrier comparisons was used to assess significance. Additional details of statistical analysis for fibroblast experiments are provided in Section 7.3.16. For experiments with a single control sample (e.g. scrambled control shRNA) where data had to be normalised to this control for each experimental day, it is mathematically incorrect to test for statistical significance as the control sample has zero variance (control is set at 100% on all experimental days).

2.6 Additional Web resources and software

The functional impact of variants detected in the Sanger sequencing and exome sequencing studies was assessed using in-silico prediction programmes including PolyPhen-2 (http://genetics.bwh.harvard.edu/pph2/; Adzhubei et al., 2010), which uses sequence, structural and phylogenetic information, Sorting Intolerant From Tolerant (SIFT) (http://sift.jcvi.org; Ng & Henikoff, 2001) which uses sequence homology and biochemical properties, and Mutation Taster (www.mutationtaster.org/; Schwarz et al., 2010), which takes into account evolutionary, biochemical and structural features to classify variants. SpliceView, a splicing signal prediction programme (http://zeus2.itb.cnr.it/~webgene/wwwspliceview_help.html; Rogozin & Milanesi, 1997), was used to assess the functional impact of splicing variants. The TMHMM Server v.2 was used for membrane protein topology prediction in the transmembrane riboflavin transporters (http://www.cbs.dtu.dk/services/TMHMM-2.0/; Krogh et al., 2001). Details of gene expression in various tissues were obtained from the Human Protein Atlas (http://www.proteinatlas.org). Location of the mutated amino acid with respect to

protein domains and other features was assessed using UniProtKB (http://www.uniprot.org).

Conservation amongst species is powerful for assessing the pathogenicity of variants as purifying selection usually removes deleterious variants (Cooper & Shendure, 2011). To assess conservation among species of the mutated amino acid residues, Ensembl was used to retrieve the orthologous sequences and the Clustal Omega software (http://www.ebi.ac.uk/Tools/msa/clustalo/; Thompson et al., 1994) was used for multiple sequence alignment. The genomic evolutionary rate profiling (GERP) score was also used to estimate the degree of sequence conservation (mendel.stanford.edu/SidowLab/downloads/gerp/; Cooper & Shendure, 2011). This program compares the observed rate of evolutionary change at the nucleotide level with that expected for a neutral position; higher scores refer to nucleotides with fewer substitutions, and therefore higher evolutionary constraint (Cooper & Shendure, 2011).

The following websites or browsers were used to search for SNP and gene information: Ensembl, National Centre for Biotechnology Information (NCBI) (http://www.ncbi.nlm.nih.gov/gene/), and University of California Santa Cruz (UCSC) genome browser (http://genome.ucsc.edu). The NCBI Single Nucleotide Polymorphism database (dbSNP) (http://www.ncbi.nlm.nih.gov/projects/SNP/), the 1000 Genomes Project database (http://browser.1000genomes.org/index.html; v.2011) the UCL HEX database of control human brain sequences (http://hex.ion.ucl.ac.uk), the Complete Genomics 69 database (CG69; http://www.completegenomics.com/public-data/), and the National Heart, Lung, and Blood Institute Exome Variant Server (NHLBI EVS) database (http://evs.gs.washington.edu/EVS/) were used to filter against polymorphisms. The GEM.app, provided by University of Miami's Miller School of Medicine, was used during exome sequencing analysis to search for variants in the candidate genes in families with similar phenotypes. This tool allows for the storage, annotation and analysis of variants in the genome (Gonzalez et al., 2013). The Cyrillic software was used to draw pedigrees (www.cyrillicsoftware.com). The DOG2.0 software (Ren et al., 2009) was used to prepare figures of protein domain structures.

The R software package was used for statistical analysis and graphics using the ggplot2 plotting system. This software was also used to construct quantile-quantile (QQ) plots in the CMT1A association study (see Appendix IV for command lines), and to assess intra- and interfamilial variability in CMT1A, as described in Chapter 4.

The gPLINK software package (pngu.mgh.harvard.edu/~purcell/plink/gplink.shtml; Purcell et al., 2007) was used for Immunochip data quality control and association analyses in the CMT1A study. gPLINK is an open-source Java-based C/C++ tool set commonly used for whole-genome association analysis. It is run from the command line and was used for large-scale data management, summary statistics for quality control and basic association testing. Command lines used in gPLINK are found in Appendix IV.

Chapter 3 CMT gene screening

3.1 Introduction

3.1.1 Frequency of genetic subtypes

Following the finding of the Chr17p11.2 duplication as the genetic cause of CMT1A, more than 60 additional genes or loci have been shown to cause CMT (Pandraud et al., 2012; Reilly et al., 2011; Rossor et al., 2013). Although these discoveries have uncovered an array of proteins involved in Schwann cell myelination and axonal function, the high phenotypic and genotypic heterogeneity found in CMT has made the diagnosis of this condition a much more complex endeavour (Patzkó & Shy, 2011). Screening known disease-causing genes in diverse populations provides invaluable information for clinicians by helping them target genetic tests according to the frequency of genetic subtypes in a particular population.

Although CMT is said to affect 5-40 per 100,000 people, the prevalence of CMT as a whole and the frequency of the genetic subtypes vary in different populations (Braathen et al., 2011; Foley et al., 2012; Skre, 1974). CMT is found in people of all ethnicities. Approximately 90% of CMT cases are inherited in an AD or X-linked manner in European/UK and USA populations. However, in geographical areas where the practice of consanguineous marriage is frequent such as the Mediterranean basin, 40% of CMT cases display AR inheritance (Reilly et al., 2011).

The most common genetic subtypes of CMT overall are as follows: CMT1A (55% of CMT and 66.8% of CMT1); CMT1X (15.2% of CMT and 18.4% of CMT1); HNPP (9.1% of CMT), CMT1B (8.5% of CMT and 10.4% of CMT1); CMT2A (4% of CMT and 21.9% of CMT2) (Saporta et al., 2011); most other subtypes make up fewer than 1% of all CMT cases (Boerkoel et al., 2002; Foley et al., 2012; Nelis et al., 1996; Pareyson & Marchesi, 2009; Saporta et al., 2011; Shy & Patzkó, 2011). Importantly for genetic testing targeting strategies, 92% of the CMT patients who received a genetic diagnosis in the Saporta et al. (2011) study carried either the Chr17p11.2 duplication/deletion, *MPZ*, *GJB1*, or *MFN2* mutations (Amato & Reilly, 2011). *LITAF* mutations accounted for 0.6% of patients with AD CMT1 (Latour et al., 2006). Studies of CMT patients in other populations such as Norway and

Germany resulted in a similar frequency distribution of genetic subtypes, with the most frequent subtypes being CMT1A, and then CMT1X, CMT2A and CMT1B (Braathen et al., 2011; Gess et al., 2013). *SH3TC2* mutations are the most common cause of AR cases of CMT (42.9% of CMT4) (Murphy, Laura, et al., 2012; Saporta et al., 2011). Some AR CMT subtypes are present at higher rates in certain genetically isolated populations, such as *n-myc downstream regulated 1* (*NDRG1*), *SH3TC2* and *hexokinase 1* (*HK1*)-linked CMT subtypes, which are especially frequent in the Gypsy population (Reilly et al., 2011).

Frequency studies of CMT subtypes in the UK, Greek and Russian populations are described below as these populations were studied in the context of this Chapter. In a recent large UK study, a genetic diagnosis was obtained in 62.6% of patients seen at the inherited neuropathy clinic in Queen Square, London (in 80.4% of CMT1 patients and 25.2% of CMT2 patients); a diagnosis was made in 37.7% of CMT patients not attending this clinic (Murphy, Laura, et al., 2012). In agreement with previous studies (Foley et al., 2012; Saporta et al., 2011) the Chr17p11.2 duplication, *GJB1*, *MPZ* and *MFN2* mutations were most common, accounting for more than 90% of genetic diagnoses (Murphy, Laura, et al., 2012). I was involved in the determination of *EGR2* mutation frequencies in this UK cohort, the results of which are presented in this Chapter.

A study by Karadima et al. (2011) uncovered the genetic cause of disease in 30% of Greek CMT1 cases; 26% had the Chr17p11.2 duplication, 5% had mutations in *GJB1* and 1% in *MPZ.* The frequency of CMT1A due to the Chr17p11.2 duplication in the Greek population is relatively low compared to most populations in Europe and the USA, but is similar to that found in certain populations such as Japan and Norway (Braathen et al., 2011; Karadima et al., 2011; Mostacciuolo et al., 2001; Nelis, et al., 1996; Nicolaou et al., 2010; Numakura et al., 2002; Silander et al., 1998). In Greece, only approximately 35% of CMT1 patients have a mutation in the genes associated with AD demyelinating CMT (Karadima et al., 2011). This frequency contrasts with the 80.4% of UK CMT1 patients attending an inherited neuropathy clinic who received a genetic diagnosis in the Murphy, Laura, et al. (2012) study.

In a study of 174 CMT patients of Russian origin, 53.7%, 7.4%, 4.6% and 1.9% of CMT1 patients had the Chr17p11.2 duplication, *GJB1*, *MPZ*, and *PMP22* mutations, respectively. Amongst CMT2 patients, 3.1% had a *GJB1* mutation. In cases with unspecified CMT, 2.9%, 17.6% and 2.9% had the Chr17p11.2 duplication, *GJB1* and *MPZ* mutations, respectively (Mersiyanova et al., 2000).

Taking into consideration the frequencies of CMT subtypes above, the Chr17p11.2 duplication should be tested first in patients with demyelinating sporadic or AD CMT followed by *GJB1* if there is no male-to-male transmission. If there is male-to-male inheritance, screening of *MPZ* and *PMP22* should follow, ending with the less common genes, *EGR2*, *LITAF* and *NEFL* (Pandraud et al., 2012; Pareyson & Marchesi, 2009; Reilly et al., 2011; Saporta et al., 2011; Siskind & Shy, 2011). *MFN2* and *GJB1* should be prioritized in AD cases of classic, axonal CMT with no male-to-male transmission, followed by *MPZ*, *NEFL*, *AARS*, *GDAP1* and *TRPV4*. Testing *MFN2* is generally more appropriate for severe early-onset cases, while *MPZ* is usually associated with later-onset AD axonal CMT (Pandraud et al., 2012; Reilly et al., 2011; Saporta et al., 2011). In certain cases, CMT, HSAN and HMN may be difficult to distinguish from one another. Screening of *serine palmitoyltransferase, long chain base subunit 1* (*SPTLC1*) and *RAB7* is warranted in patients with CMT2 and AD inheritance with significant sensory symptoms and signs. If motor symptoms predominate, *GARS (*patients with prominent upper-limb involvement), *HSPB1*, *HSPB8*, *BSCL2* and *TRPV4* should be sequentially screened (Pandraud et al., 2012; Reilly et al., 2011; Shy & Patzkó, 2011). ICMT cases should be screened for *GJB1*, followed by *MPZ*, *NEFL*, *DNM2* and *YARS* (Pareyson & Marchesi, 2009). A consideration for specific clinical features as well as the patient's ethnic background is especially valuable for AR CMT cases (Reilly et al., 2011); *GDAP1* should generally be tested first when the inheritance pattern is AR (Pareyson & Marchesi, 2009).

Diagnostic algorithms which take into account frequencies of CMT subtypes are particularly useful in highly genetically and phenotypically heterogeneous diseases such as CMT and especially for AD CMT1. Algorithms have allowed for a genetic

diagnosis to be obtained in 70% of CMT patients (Pareyson & Marchesi, 2009; Reilly et al., 2011; Saporta et al., 2011).

Following diagnostic guidelines adapted for the patient's ethnicity avoids the unwarranted and costly use of large gene panels (Amato & Reilly, 2011). However, as is evident from the above reports, rates of CMT subtypes have not been extensively studied in certain populations, and in most populations, the frequency of the less common CMT genes remains unknown as these genes are not available for routine diagnostic testing. Although no treatments are available at this time for CMT, receiving a genetic diagnosis is essential for patients as it allows the physician to provide a more accurate prognosis, to give appropriate counselling for family planning, and it provides the patient with the possibility of predictive, pre-natal or pre-implantation diagnosis (Pandraud et al., 2012; Pareyson & Marchesi, 2009; Reilly et al., 2011). As Amato & Reilly (2011) acknowledge, assigning a genetic diagnosis to a patient will admittedly not affect the way a single patient is managed and will not predict exactly how that patient's condition is going to progress. However, a genetic diagnosis allows the physician to exclude inflammatory causes of neuropathy such as CIDP which may be treatable, and also helps to limit the number of unnecessary medical interventions and treatment trials (Amato & Reilly, 2011; Reilly et al., 2011). Eventually, therapies will be developed which will likely target specific genetic subtypes of disease, providing further incentive for finding the causative gene in patients (Reilly & Shy, 2009; Reilly et al., 2011).

3.1.2 Phenotypes associated with selected CMT subtypes

The range of phenotypes resulting from *PMP22*, *MPZ*, *EGR2*, *NEFL*, *LITAF* and *GJB1* mutations are described below as these were screened in cohorts of CMT1 patients and canines with neuropathies as part of our study. Point mutations in *PMP22* may cause DSD, CHN or HNPP. The phenotype is usually more severe with earlier onset than in CMT1A, but it may also be classical CMT1A. Patients with *MPZ* mutations generally fall into two groups: the severe, early-onset demyelinating form or the less severe axonal form with later onset. Mutations in *MPZ* may sometimes lead to typical CMT1. The phenotype associated with *LITAF* mutations is generally similar to that seen in CMT1A. *EGR2* mutations generally cause severe

disease with early-onset and possible cranial nerve involvement, but may also cause CMT1. Both AD and AR inheritance have been described for *PMP22*, *MPZ* and *EGR2* mutations (Reilly et al., 2011; Siskind & Shy, 2011). Mutations in *NEFL* may cause either axonal or demyelinating NCVs with either a classical CMT phenotype or early-onset severe disease. *MFN2* mutations often lead to severe disease with early-onset, which may involve the CNS; the phenotype may also be classical CMT. Finally, the X-linked form of CMT caused by mutations in *GJB1* causes a severe phenotype with earlier onset and slower NCVs in males compared to females. Females are usually mildly affected although the phenotype is variable most likely due to X-inactivation (Murphy, Ovens, et al., 2012; Patzkó & Shy, 2011; Reilly et al., 2011; Siskind & Shy, 2011).

3.1.3 Genotype-phenotype studies in CMT

Correlating clinical manifestations with genetic mutations as is done in genotype-phenotype studies and carrying out large natural history studies will be important for predicting disease progression in individual patients in the future (Amato & Reilly, 2011). From a biological perspective, determining the mutation leading to a particular phenotype helps to elucidate protein function and disease mechanisms (Reilly & Shy, 2009; Reilly et al., 2011). However, as is apparent in Section 3.1.2, variable phenotypes can result from genetic defects in one particular gene, and sometimes from identical mutations in the same gene.

Studies using animal models of CMT are also invaluable for assessing the effect of selected CMT gene mutations on protein function and phenotype. As discussed in Section 1.3.3, these studies have shed light on some of the possible disease mechanisms in certain CMT subtypes, and are a useful tool for identifying potential therapeutic targets (Fledrich, Stassart, et al., 2012). Interestingly, naturally occurring peripheral neuropathies have been reported in several species, including canines. Canine axonal and demyelinating peripheral neuropathies were introduced in Section 1.3.3, and will now be discussed in detail as they are of particular interest in this study.

3.1.4 CMT genes in canines with peripheral neuropathies or neuroaxonal dystrophy

CMT-like neuropathies have been described in several dog breeds, which are reviewed in Granger (2011). Leonberger dogs with inherited CMT-like axonal neuropathy and vocal cord paresis have been described; these dogs had high-steppage gait, weakness and wasting of distal limb muscles as well as decreased tendon reflexes. Electrophysiological studies showed changes characteristic of polyneuropathy with denervation, and nerve biopsies displayed loss of myelinated fibres (Shelton et al., 2003). A sensory ataxic neuropathy due to a mutation in the mitochondrial *tRNA^{Tyr}* gene was described in Golden Retriever dogs (Baranowska et al., 2009). A deletion in *NDRG1*, a gene mutated in human CMT, was found in a family of Greyhounds with predominantly axonal polyneuropathy, thus representing the first canine CMT model (Drögemüller et al., 2010). A missense mutation in *NDRG1* was recently identified in Alaskan Malamute dogs with early-onset progressive polyneuropathy (Bruun et al., 2013).

The first demyelinating polyneuropathy with focally folded myelin sheaths was recently described in a family of highly inbred Miniature Schnauzer dogs (Vanhaesebrouck et al., 2008). In humans, such tomaculae resulting from excessive myelin folding is associated with HNPP, demyelinating forms of CMT, as well as CIDP. Affected dogs in this family of Schnauzer dogs presented with respiratory dysfunction with no generalised weakness. They had decreased motor and sensory nerve conduction velocities and segmental demyelination. The histopathological changes seen in these dogs are similar to that seen in demyelinating CMT with tomaculae. The genes mutated in demyelinating forms of CMT in humans are candidate genes for the neuropathy in these Schnauzer dogs (Vanhaesebrouck et al., 2008). These Schnauzers dogs were screened as part of our study in this Chapter.

Investigating canines with mutations in genes known to cause CMT in humans may help clarify the function of the mutant protein and elucidate disease pathways in the human disease, even if not associated with CMT in canines. A small deletion in *MFN2*, associated with axonal CMT in humans, has recently been found in a family of dogs with AR foetal-onset neuroaxonal dystrophy (FNAD) mimicking the human phenotype (Fyfe et al., 2011). NAD is a neurodegenerative pathology in the CNS

and/or PNS distinguished by spheroids, or swellings, and axonal atrophy. In humans, AR infantile NAD has been associated with *phospholipase A2, group VI* (*PLA2G6*) mutations and may cause hypotonia, amyotrophy, areflexia and psychomotor problems, as well as a sensorimotor axonal neuropathy (Yiu & Ryan, 2012). As suggested in the Fyfe et al. (2011) study, *MFN2* may be a candidate gene for human cases of FNAD. The association of known CMT genes with non-CMT diseases is interesting to study as it may uncover novel functions for these genes and expands the phenotypes associated with CMT genes (Fyfe et al., 2011). A silent polymorphism in *MFN2* leading to a splicing defect has also been found in cattle with degenerative axonopathy in the CNS (Drögemüller et al., 2011).

Canines are particularly suited for genetic studies as they benefit from close examination by veterinary experts and a well-characterised genome (Matiasek & Drögemüller, 2011). Dogs have developed in the same environment as humans and their genome is highly similar to ours, therefore disease pathways are likely to be comparable (Karlsson et al., 2007).

3.2 Aims of this study

CMT is a disease with particularly high phenotypic and genotypic heterogeneity. This study had three primary aims. The first aim was to assist clinicians in targeting genetic tests for patients with CMT by determining frequencies of genetic subtypes in different ethnicities. The second aim was to expand the phenotypes associated with particular CMT genetic subtypes and mutations. To fulfil these two aims, we screened CMT1 genes including *PMP22*, *EGR2*, *LITAF*, *NEFL* and/or *GJB1* in three cohorts of CMT1 patients from different geographical areas, namely the UK, Greece, and the Yakutsk province in Russia. We were particularly interested in screening genes not available for routine diagnostic testing to determine their frequency. The third aim of this study was to screen known CMT genes, specifically *PMP22* and *MPZ* in canines with peripheral neuropathy and *MFN2* in a canine with neuroaxonal dystrophy and cerebellar abiotrophy (NAD-CA) in the hope that they may serve as potential animal models of human peripheral nerve disease and provide clues into pathogenic mechanisms of disease in peripheral neuropathies.

3.3 Methods

3.3.1 CMT1 patient cohorts

Patients from the UK, Greece, and the Yakutsk province in Russia who have demyelinating CMT disease according to NCS and neurological examination but lacked a genetic diagnosis were screened for mutations in selected CMT1-associated genes. Details of ethics approval and patient consent are found in Section 2.1.1.

The UK cohort consisted of 135 CMT1 patients negative for the Chr17p11.2 duplication/deletion with or without a family history. Patients were assessed by consultant neurologists Professor Mary Reilly and Dr Matilde Laurá at the inherited neuropathy clinic at the NHNN or by consultant neurologists in other UK CMT clinics. DNA was obtained from the Neurogenetics diagnostic laboratory at the NHNN or was sent to our centre from throughout the UK for research genetic testing. Patients in the UK cohort were tested for Chr17p11.2 rearrangements by semi-quantitative fluorescent PCR or multiplex ligation-dependent probe amplification (MLPA) in diagnostic laboratories, including the Neurogenetics diagnostic laboratory at the NHNN. The UK cohort was screened as part of a larger study published in Murphy, Laura, et al. (2012). DNA of UK controls was obtained from the 1958 British Birth Cohort of the WTCCC.

The Greek cohort was comprised of 86 Greek CMT1 patients (64 familial, 22 sporadic) who had previously tested negative for the Chr17p11.2 duplication/deletion and *MPZ* and *GJB1* mutations, as described in Karadima et al., 2011. The Chr17p11.2 duplication/deletion was tested by the long PCR method. DNA of Greek CMT1 patients was obtained from our collaborator Dr George Koutsis at Eginitio Hospital, Athens, Greece. The average median NCV of the patients in this cohort was 23.7 m/s. DNA of Greek controls was provided by Dr George Koutsis.

Dr Polina Innokentyevna from Yakutsk in Russia (Figure 3-1) kindly provided the DNA samples for the Russian CMT1 patients. The Yakutsk cohort consisted of 54 patients who were negative for the Chr17p11.2 duplication/deletion.

Where available, clinical information for the CMT1 patients in whom variants were found is discussed in Sections 3.4.1, 3.4.2 and 3.4.3.

Figure 3-1 Yakutsk province in Russia. Obtained from http://en.wikipedia.org/wiki/Yakutsk.

3.3.2 Cohort of canines with peripheral neuropathies or neuroaxonal dystrophy and cerebellar abiotrophy (NAD-CA)

Samples were obtained from Dr Nicolas Granger at the Queen's Veterinary School Hospital at the University of Cambridge, UK. Our cohort was comprised of eight affected dogs with peripheral neuropathies. Among these were two Miniature Schnauzers with AR demyelinating CMT-like polyneuropathy with focally folded myelin sheaths resembling HNPP as well as *MTMR2* and *MTMR13*-linked CMT (Vanhaesebrouck et al., 2008; Matiasek & Drögemüller, 2011); these dogs correspond to the two affected males in the family of dogs with multiple consanguineous loops described in the report by Vanhaesebrouck and colleagues (2008) and in the review by Granger (2011), as well as in Section 3.1.4. We also had samples for one Labrador Retriever with sporadic unspecified peripheral nerve disease, one Leonberger with unspecified familial peripheral neuropathy, and one Cocker Spaniel with sporadic, late-onset demyelinating neuropathy with onion bulb formation. Other canines in our cohort included two Black Russian Terriers with familial juvenile axonal neuropathy with one specific type of fibre loss. Finally, the

last member of our cohort was a Golden Retriever with late-onset generalised peripheral nerve disease; a number of large breed dogs are reportedly affected by a similar disease (N. Granger, personal communication). Inheritance is likely to be AR or X-linked in most of these canines. Samples were obtained as DNA, EDTA blood or snap-frozen muscle.

DNA for the Papillon dog with NAD-CA was provided by Dr Urs Giger at the School of Veterinary Medicine at the University of Pennsylvania, USA. The Papillon dog was negative for *PLA2G6* mutations.

3.3.3 DNA extraction from canine blood and tissue

For the cohort of canines with peripheral neuropathies, DNA was extracted from canine EDTA blood and snap-frozen muscle as described in Section 2.1.3.

3.3.4 Whole-genome DNA amplification

gDNA from the Yakutsk cohort was whole-genome amplified as described in Section 2.1.4 prior to Sanger sequencing, as an insufficient amount of DNA was available for sequencing in this cohort.

3.3.5 Gene screening in CMT1 patient and canine cohorts

Purity and concentration of DNA samples were assessed as described in Section 2.1.5. PCR, agarose gel electrophoresis, purification of PCR products, Sanger sequencing, dye removal and sequencing analysis were performed using standard conditions as described in Sections 2.1.9-2.1.12. Coding exons and flanking intronic sequences were sequenced for human *PMP22*, *EGR2*, *GJB1*, *LITAF* and *NEFL*, and for canine *PMP22*, *MPZ* and *MFN2* using species-appropriate reference sequences. Transcript references used for primer design, as well as sequences of gene-specific primers and PCR cycling conditions can be found in Appendix III Tables III-1 and III-2. SNP chromosomal locations are based on Genome Build 37.3.

At the time of this study, neuropathy gene panels were not available and genetic testing was done on a gene-by-gene basis. In the UK cohort, *EGR2* was screened in 135 CMT1 patients as this gene is not available for routine diagnostic testing due to

its low frequency. Patients in the Greek CMT1 cohort (n=86) who remained without a genetic diagnosis after the gene screening described in Karadima et al. (2011) were tested for mutations in *PMP22*, *EGR2*, *LITAF* and *NEFL*. This sequencing was done both by Dr George Koutsis and myself. CMT1 patients in the Yakutsk cohort were selectively screened for mutations in *PMP22*, *GJB1*, and/or *EGR2* depending on inheritance pattern and phenotype. *PMP22* and *GJB1* were screened in 10 patients and *EGR2* in 54 patients. This sequencing was done both by Dr Polina Innokentyevna and myself.

All eight canines in the peripheral neuropathy cohort were screened for mutations in canine *PMP22* and *MPZ.* The affected Papillon dog with NAD-CA was screened for mutations in canine *MFN2*.

Both canine *PMP22* and human *PMP22* have four coding exons and encode a protein 160 amino acids long. Canine *MPZ* and human *MPZ* have six coding exons but the canine gene is 258 amino acids long while the human gene is 10 amino acids shorter. Both human and canine *MFN2* have 17 coding exons and are 757 amino acids long. Canine *PMP22*, *MPZ* and *MFN2* have 93%, 92%, and 97% of the sequence matching with the human *PMP22*, *MPZ* and *MFN2*, respectively (corresponding values are 86%, 94% and 95% between the mouse and human *PMP22*, *MPZ* and *MFN2*, respectively). Although the percentage alignment match between human/canine and human/mouse CMT genes like *PMP22, MPZ* and *MFN2* are similar, canines represent a better model for human CMT than rodent models given their larger size and similar body structure to humans (Drögemüller et al., 2010).

In-silico analyses were performed as described in Section 2.6. Variants were searched in the dbSNP, 1000 Genomes and/or EVS databases. Segregation analysis of variants in family members was performed where DNA was obtainable. Potentially pathogenic variants were screened in controls of matching ethnicity where available.

3.3.6 Fragment analysis of small duplication and deletion

Fluorescent PCR amplification and subsequent capillary electrophoresis were performed as described in Section 2.1.8. Primers used for fluorescent PCR amplification were the same as those used for PCR and Sanger sequencing of *PMP22* exons 4 and 5, with the addition of a fluorescent tag. The fragment analysis as well as the transcriptional analysis described below were carried out entirely by Dr George Koutsis.

3.3.7 Transcriptional analysis of small duplication and deletion

RNA was extracted from peripheral blood and cDNA was synthesized as described in Section 2.1.7. Sequences of primers used to amplify the 391 bp-long cDNA region of interest in *PMP22* for the small duplication and deletion identified in the Greek cohort are found in Appendix III Table III-3. cDNA was sequenced according to the DNA sequencing protocol as described in Section 2.1.12.

3.4 Results

3.4.1 UK CMT1 cohort: *Early growth response 2* (*EGR2*) sequencing

As mentioned previously, the screening of *EGR2* in the UK CMT1 cohort was part of a larger study aiming to determine the frequency of genetic subtypes in CMT to provide a guideline for genetic testing (Murphy, Laura, et al., 2012).

Sequencing of *EGR2* in the UK cohort of 135 patients with demyelinating CMT revealed a total of seven unique heterozygous variants, three of which are likely to be pathogenic: p.Arg359Trp (c.1075C>T) in one patient (0.74%); p.Arg381Cys (c.1141C>T) in two patients (1.48%); p.Arg426Gln (c.1277G>A) in one patient (0.74%) (see Appendix III Table III-4 for complete list of mutations and pathogenicity predictions). The other four mutations (p.Pro209Pro (c.627A>G); p.Thr215Met (c.644C>T); p.Arg362Arg (c.1086A>C); p.Gly451Val (c.1352G>T)) are likely to be polymorphisms as they are either synonymous variants, found in our UK control cohort and/or were present in dbSNP, 1000 Genomes or EVS databases. The p.Arg362Arg variant has been reported as a polymorphism in several studies (Choi et al., 2004; Timmerman et al., 1999). The p.Gly451Val mutation was previously found in the heterozygous state in a patient with unspecified CMT

(Takashima et al., 2001). However, it was also present in 1/185 (0.54%) of our UK control cohort and therefore it is likely to be a non-pathogenic, albeit rare, variant.

All three likely pathogenic mutations were located in exon 2 of *EGR2*, were found in the heterozygous state, were predicted damaging by Polyphen-2 and SIFT and were located at amino acids partially (p.Arg426Gln) or highly (p.Arg359Trp; p.Arg381Cys) conserved across species. p.Arg426Gln has not been previously described in the literature. The p.Arg381Cys and the p.Arg426Gln mutations were not found in 257 and 264 UK controls, respectively. p.Arg359Trp was not screened in controls as its pathogenicity is well established in the literature (Boerkoel et al., 2001; Choi et al., 2004; Chung et al., 2005; Taroni et al., 1999; Timmerman et al., 1999; Warner et al., 1999). No family members were available for segregation analysis for any of the variants identified in the UK cohort.

Our patient with the p.Arg359Trp mutation had facial weakness, ophtalmoplegia, difficulty swallowing, kyphoscoliosis, deformity of fingers and feet, and sensory loss. The patient's MNCV was 11 m/s. This mutation was discovered previously in patients with generally sporadic DSD and cranial nerve involvement (Boerkoel et al., 2001; Taroni et al., 1999; Timmerman et al., 1999) although it has also been found to cause a classic CMT1 phenotype with severe loss of myelinated fibres and onion bulb formation (Choi et al., 2004; Chung et al., 2005). It is located in the alpha-helix domain of the first zinc-finger of *EGR2* and is predicted to act in a dominant-negative manner (Szigeti et al., 2007).

The p.Arg381Cys mutation was found in two patients. The first patient had a two-year history of peripheral sensory loss and weakness, as well as deafness. There was severe MNCV slowing on NCS. The second patient had a MNCV of 46 m/s with dispersion. In the literature, it is associated with late-onset, mild cases of CMT1 and the phenotype is less severe than that associated with the p.Arg381His mutation (Briani et al., 2010; Pareyson et al., 2000; Taroni et al., 1999; Vandenberghe et al., 2002; Yoshihara et al., 2001). In one study, a patient with the p.Arg381Cys mutation had a mild phenotype with late-onset of disease, severe loss of myelinated fibres and onion bulb formation (Yoshihara et al., 2001). Another patient carrying the p.Arg381Cys mutation had sporadic CMT1 with MNCV of 22 m/s and CMTNS of 9

(Briani et al., 2010). This mutation is located in the second zinc-finger domain. As with other *EGR2* zinc-finger mutations like p.Arg359Trp, this mutation is predicted to act in a dominant-negative manner and interfere with DNA binding. Disease severity has been found to correlate with the amount of residual binding for *EGR2* zinc-finger mutations (Warner et al., 1999).

No clinical details were available for the patient carrying the p.Arg426Gln mutation. Unlike most *EGR2* mutations associated with CMT, this variant is not located within a zinc-finger domain (Szigeti et al., 2007; Warner et al., 1999). Its pathogenicity remains uncertain.

The prevalence of *EGR2* mutations in our selected cohort of CMT1 patients from the UK negative for the Chr17p11.2 duplication was 2.96% (4/135).

3.4.2 Greek CMT1 cohort

The mutational screening of CMT genes in Greek patients was part of a collaborative study and resulted in two publications (Koutsis et al., 2012; Koutsis et al., 2013). A complete list of mutations with pathogenicity prediction and patient phenotypes is available in Appendix III Table III-5.

Three heterozygous variants were found in *PMP22*; all are likely to be pathogenic and none have been previously reported in the literature. All three variants were found in 1/86 patients (1.2%), were not found in 225 Greek controls and were absent from dbSNP, 1000 Genomes and EVS databases. As described below, one of the variants was in fact associated with an HNPP rather than a CMT1 phenotype due to misdiagnosis.

The first mutation, p.(Gln27_Asn59 del_Glu60AsnfsX10) (c.79-2A>G), is located at a splice site in the 3' region of the intronic sequence between exons 2 and 3, and is expected to disrupt the acceptor site by SpliceView (Figure 3-2). It is predicted to cause skipping of exon 3 and frameshift, leading to a premature stop codon. The transcript is likely to undergo nonsense-mediated decay (NMD) as the stop codon is predicted to occur further than 55 bp from a downstream intron/exon boundary (Nagy & Maquat, 1998). Unfortunately, transcriptional analysis could not be

performed as RNA was not available. Nonsense mutations usually cause an HNPP phenotype (Reilly et al., 2011). In fact, our patient (family 3) had been diagnosed as CMT1, but was found to have an HNPP phenotype upon further investigation (Koutsis et al., 2012). She was mildly affected and had an ulnar sensory neuropathy starting in adolescence with transient positional sensory symptoms. Her median and peroneal MNCVs were 45.4 m/s and 28 m/s respectively. Her right ulnar MNCV above the elbow was 37 m/s, and 42 m/s below the elbow. She had pes cavus and reduced tendon reflexes. There were no other affected family members (Koutsis et al., 2012). Interestingly, frameshift mutations leading to a truncated PMP22 protein have been known to lead to an HNPP phenotype clinically and electrophysiologically, but with additional neuropathic characteristics resembling CMT1 such as pes cavus, areflexia, greater NCV slowing and onion bulb formation on nerve biopsy; it is therefore not surprising that our patient was initially misdiagnosed as CMT1. It has been proposed that the disease mechanism in this case may be haploinsufficiency coupled with additional impairment of Schwann cell function (Lenssen et al., 1998).

The second mutation is an in-frame 6 bp deletion in exon 4, p.Thr99_Gly100del (c.296_301delCTGGAA). Upon PCR amplification, two fragments of 388 bp (size of WT PCR amplicon) and 382 bp (amplicon with deletion) were seen as two bands on agarose gel electrophoresis with hetero-duplex formation (Figure 3-2). Although the two fragments were not resolved well on the agarose gel, fragment analysis and cDNA sequencing confirmed the presence of the two fragments. The proband (family 2, II-6) was 22 years old and his phenotype was severe CMT1/DSD. Onset of disease was in infancy, when he was unsteady and fell frequently. He was never able to walk independently and required orthotics and bilateral support. He also had scoliosis, absent reflexes and weakness, atrophy and sensory signs in the upper and lower limbs. Nerve biopsy showed evidence of hypomyelinating neuropathy and MNCV was 2.3 m/s. This is likely to be a *de novo* mutation in the family (Koutsis et al., 2012).

The third mutation is p.Val110_Ile116dup (c.328_348dup21), an in-frame 21 bp duplication in exon 5 of *PMP22*. Two fragments of 406 bp (WT amplicon) and 427

bp (amplicon with duplication) were distinguishable upon PCR amplification, although three bands were seen on agarose gel electrophoresis due to hetero-duplex formation (Figure 3-2). The presence of the two fragments was confirmed by fragment analysis. cDNA analysis and sequencing confirmed that two fragments of different lengths were present; formation of a hetero-duplex was once again seen on the agarose gel. The proband in this family (III-1 in family 1), a 14 year-old male, had disease onset at 18 months with frequent falls and unsteadiness of gait. He had difficulty walking and needed assistance for climbing stairs. Lack of reflexes, lower and peripheral upper limb atrophy and weakness, pes cavus, scoliosis, and upper and lower limb sensory signs were noted on neurological examination. His MNCV was severely slowed, at 14.3 m/s. The proband's mother (II-4 in family 1) was found to carry the same mutation upon segregation analysis. Although she had severe MNCV slowing (7.1 m/s), she was more mildly affected with disease onset in adolescence. Her gait was unstable; she had problems with fast walking and could not wear high-heeled shoes. Neurological examination showed pes cavus, sensory signs in the lower limbs, absent reflexes and peripheral lower limb weakness. The unaffected sister of patient III-1 did not carry the mutation. Although no additional DNA samples were available for analysis, no other family members suffered from the same condition therefore the mutation likely arose *de novo* in the proband's mother. To our knowledge, this variant is the first small duplication of a few bps in *PMP22* to be associated with CMT1 (Koutsis et al., 2012).

As with other CMT1-associated *PMP22* mutations located in the third transmembrane domain, it is likely that p.Thr99_Gly100del and p.Val110_Ile116dup act via a dominant-negative or toxic gain-of-function mechanism by causing protein aggregation and disturbed trafficking of mutant PMP22 to the plasma membrane (Koutsis et al. 2012).

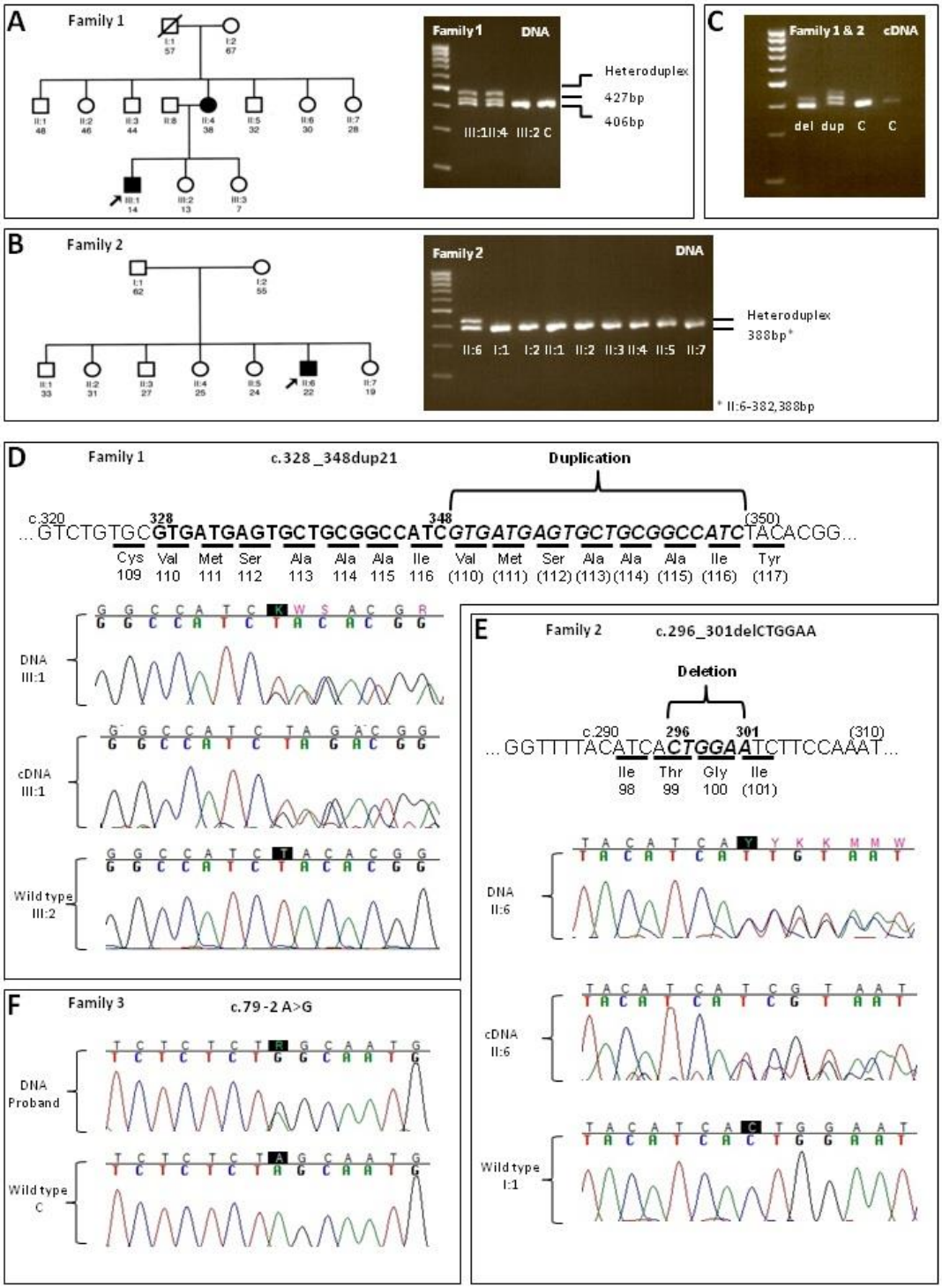

Figure 3-2 Pedigrees, agarose gel electrophoresis and sequencing results of families with *PMP22* micromutations. (A) Pedigree and DNA agarose gel electrophoresis of family 1 with the c.328_348dup21 mutation; a third band visible in affected members is due to hetero-duplex formation. (B) Pedigree and DNA agarose gel electrophoresis of family 2 with the c.296_301delCTGGAA mutation; a second band

visible in the proband is due to hetero-duplex formation. (C) cDNA agarose gel electrophoresis of probands from families 1 and 2, as well as two controls; probands have extra bands due to hetero-duplex formation. (D) Graphic representation of the c.328_348dup21 (p.Val110_Ile116dup) mutation; DNA and cDNA sequencing results of the proband compared with the WT sequence. (E) Graphical representation of the c.296_301delCTGGAA (p.Thr99_Gly100del) mutation; DNA and cDNA sequencing results of the proband compared with the WT sequence. (F) DNA sequencing results of the c.79-2A> G splice site mutation; proband compared with WT sequence. del=deletion; dup=duplication (reproduced from Koutsis et al., 2012).

Four heterozygous variants were detected in *EGR2*: p.Arg362Arg (c.1086A>C), p.Arg381His (c.1142A>G), p.Gly451Val (c.1352G>T), p.Gly451Asp (c.1352G>A). Only the p.Arg381His is predicted to be pathogenic. Although the p.Gly451Val was not found in 225 Greek controls, it has been detected in our UK control cohort, as mentioned in Section 3.4.1, and was found in the unaffected mother of the proband. The other mutation at the same amino acid, p.Gly451Asp, was detected in 1/224 (0.45%) Greek controls and was found in the unaffected father of the proband. Neither is likely to be pathogenic although it remains possible that they are rare variants with decreased penetrance (Koutsis et al., 2013).

The p.Arg381His mutation was found in 1/86 (1.2%) patients. This mutation was previously described in a severe CMT1 patient with cranial nerve involvement (Pareyson et al., 2000) and a case of congenital hypomyelination (Vandenberghe et al., 2002). The p.Arg381His *EGR2* mutation was associated with a case of early-onset severe CMT1 in our cohort. Inheritance was likely AD but this could not be confirmed. At three years old, the patient had weak legs, was unsteady, and fell frequently. At 12 years old, she walked with assistance. She had no cranial nerve involvement but had atrophy, weakness and sensory signs in the lower and peripheral upper limbs, pes cavus, scoliosis and absent reflexes in the lower limbs. Her NCV was 27.5 m/s and nerve biopsy showed onion bulb formation and loss of myelinated fibres (Koutsis et al., 2013). This mutation is located at the same amino acid as the p.Arg381Cys variant identified in our UK cohort.

The three variants identified in *LITAF* (p.Thr78Thr (c.234G>A); p.Ile92Val (c.274A>G); p.Ala111Ala (c.333C>T)) and the three found in *NEFL* (p.Leu223Leu (c.667C>T), p.Asp468Asn (c.1402G>A), p.Glu527del (c.1579_1581 delGAG)) are not predicted to be pathogenic as they are either synonymous variants and/or found in dbSNP, 1000 Genomes or EVS databases (Koutsis et al., 2013). The p.Glu527del variant in *NEFL* had been previously labelled as pathogenic (Jordanova et al., 2003), but was later found in controls (Abe et al., 2009; Yamamoto et al., 2004; Yoshihara et al., 2002), albeit not in our Greek control cohort (Koutsis et al., 2013).

3.4.3 CMT1 cohort from the Yakutsk province, Russia

No variants were identified in *PMP22* in the cohort of Yakutsk CMT1 patients (n=10). Two synonymous variants were identified in *EGR2*; both have been found in our UK cohort and are unlikely to be pathogenic: p.Pro209Pro (c.627A>G) in 2/54 (3.7%) patients and p.Arg362Arg (c.1086A>C) in 8/54 patients (seven heterozygous (13%) and one homozygous (1.85%)). One hemizygous variant, p.Cys280Ser (c.839G>C), was identified in exon 2 of *GJB1* in 1/10 patients (10%). The list of variants identified in the Yakutsk CMT1 patients along with pathogenicity predictions can be found in Appendix III Table III-6.

The p.Cys280Ser mutation is novel and is located at an amino acid partially conserved across species. It is predicted benign by Polyphen-2 but damaging by SIFT. No Yakutsk controls were available to screen for the mutation in healthy individuals. Over 400 mutations have been described in *GJB1* to date and only one is thought to be a polymorphism (Kleopa et al., 2012). The patient is male and had demyelinating CMT with onset at 35 years and weakness in the feet and foot deformities. Both parents were unaffected. No further clinical details were available. Another mutation, p.Cys280Gly, has been previously reported at this amino acid in a Hungarian family (Castro et al., 1999). The proband in this Hungarian family was a 30-year-old male with CMT; his mother was reportedly healthy and carried the mutation, however she had decreased NCV. Three other unaffected family members did not carry the mutation and the variant was not present in 100 controls (Castro et al., 1999). The same group studied the effects of this mutation on the formation of hemichannels, which are the precursors of gap junction channels, and on the gap

junction channels themselves. The p.Cys280Gly mutant expressed in *Xenopus* oocytes had near normal hemijunctional conductance and voltage-gating properties were similar to WT hemichannels. This mutant had a negligible effect on the ability to form gap junction channels (Castro et al., 1999). The mutation affects an evolutionarily conserved prenylation motif which is usually necessary for the attachment of cytosolic proteins (rather than intrinsic membrane proteins like connexin-32) to the cell membrane. The p.Cys280Gly mutants did not display altered trafficking in myelinating Schwann cells and were able to rescue demyelination in *GJB1*-null mice. Although a milder phenotype might be predicted for this mutation and nearby mutations, it was not the case for a patient with a p.Ser281Stop mutation (Huang et al., 2005; Kleopa et al., 2012). The pathogenicity of the p.Cys280Gly mutation, as well as the variant identified in our study remains uncertain.

3.4.4 Canines with peripheral neuropathies cohort

No variants were identified in canine *PMP22* in the cohort of dogs with peripheral neuropathies. Three variants were found in canine *MPZ*. The first variant is a heterozygous c.-4G>A in the 5' untranslated region (UTR). The variant is not predicted to introduce a new start codon. The second variant in *MPZ* is a heterozygous synonymous mutation, p.Ser17Ser (c.51A>G); although unlikely, a pathogenic effect of synonymous mutations cannot be ruled out (Taioli, Cabrini, Cavallaro, Simonati, et al., 2011). The c.-4G>A and p.Ser17Ser variants were found in the Golden Retriever with generalised peripheral nerve disease. A third variant, c.625-5dupC was found in the homozygous state in the Golden Retriever and in the heterozygous state in the Leonberger with unspecified familial peripheral neuropathy. None of these variants were found in dbSNP. Although this was not performed in this study, transcriptional analysis would be useful to rule out a potential effect of the c.625-5dupC variant on splicing. We did not have access to a large cohort of canine controls to screen for these variants in healthy dogs of the same breed.

3.4.5 *Mitofusin 2* (*MFN2*) screen in Papillon dog with neuroaxonal dystrophy and cerebellar abiotrophy (NAD-CA)

Three homozygous synonymous variants were found in *MFN2* in the Papillon dog with NAD-CA: p.Val112Val (c.336A>G), p.Phe240Phe (c.720T>C) and p.Ala507Ala (c.1521G>A). Only the p.Phe240Phe was found in dbSNP (rs8738884), although the frequency of this variant is not available. None of these variants are predicted to be pathogenic as they do not lead to an amino acid change.

3.5 Discussion

The prevalence of *EGR2* mutations in our selected cohort of CMT1 patients from the UK negative for the Chr17p11.2 duplication was 2.96% (4/135). Although *EGR2* mutations are a rare cause of CMT in our cohort (Murphy, Laura, et al., 2012), this frequency nonetheless represents a non-negligible number of CMT patients who have now received a genetic diagnosis. The frequency of *EGR2* mutations is in agreement with previous studies of the European/UK and USA populations, which have found *EGR2* mutations in 0.1-2% of CMT1 cases (Boerkoel et al., 2001; Mostacciuolo et al., 2001; Saporta et al., 2011; Timmerman et al., 1999; Vandenberghe et al., 2002). CMT1 patients with *EGR2* mutations in our cohort generally had more severe and complex forms of CMT1, although one patient with the p.Arg381Cys mutation had a CMT2-like MNCV. This screening uncovered one novel mutation in *EGR2*, p.Arg426Gln.

PMP22 and *EGR2* mutations were found in 2.3% and 1.2% of our cohort of Greek CMT1 patients respectively, therefore mutations in these genes are likely to be a rare cause of disease in Greek CMT1 patients. As mentioned above, this is in accordance with the consensus in the literature. Small *PMP22* duplications and deletions may be more common in the Greek population. *LITAF* and *NEFL* mutations were not found in our Greek cohort. These low frequencies are similar to previously published reports in other populations (Abe et al., 2009; Jordanova et al., 2003; Latour et al., 2006; Murphy, Laura, et al., 2012; Pareyson & Marchesi, 2009). A genetic diagnosis was obtained in 3.5% of our Greek cohort previously found negative for Chr17p11.2 duplication as well as *MPZ* and *GJB1* mutations. One HNPP patient previously

misdiagnosed as CMT1 was found to carry a mutation in *PMP22* (Koutsis et al., 2012; Koutsis et al., 2013).

In the Greek cohort, we have identified three novel micromutations in *PMP22*, two in CMT1 patients and one in an HNPP patient. In our study, as in previous reports, *PMP22* small deletions and duplications displayed high phenotypic variability (Koutsis et al., 2012; Taioli, Cabrini, Cavallaro, Acler, et al., 2011). The first mutation, a splice site mutation before exon 3, is predicted to cause skipping of exon 3 and frameshift leading to a premature stop codon and was associated with an HNPP phenotype. Although analysis at the RNA level was not possible in our patient, frameshift changes leading to delayed or premature stop codons in *PMP22* are usually associated with HNPP (Reilly et al., 2011; Taioli, Cabrini, Cavallaro, Acler, et al., 2011). An exception occurs when the premature stop codon is not expected to undergo NMD, which may cause CMT1 or DSD (Choi et al., 2004; Ionasescu, Searby, Ionasescu, Reisin, et al., 1997; Koutsis et al., 2012; Numakura et al., 2002), as well as HNPP (Taioli, Cabrini, Cavallaro, Acler, et al., 2011). The second mutation, an in-frame 6 bp deletion, caused severe CMT1/DSD. The third mutation is an in-frame 21 bp duplication; there was high intra-familial phenotypic variability associated with this mutation (Koutsis et al., 2012). In agreement with our study, in-frame deletions and duplications in *PMP22* are generally associated with a CMT1 phenotype (Ekici et al., 2000; Koutsis et al., 2012; Mersiyanova et al., 2000; Park et al., 2006; Sambuughin et al., 2003; Taioli, Cabrini, Cavallaro, Acler, et al., 2011).

The *EGR2* p.Arg381His mutation found in the Greek cohort is usually associated with variably severe CMT1 phenotypes with or without cranial involvement (Pareyson et al., 2000; Vandenberghe et al., 2002). Our patient had severe CMT1 but no cranial involvement, however cranial palsies may be seen later in the patient's life as with previous cases carrying this mutation (Koutsis et al., 2013; Pareyson et al., 2000).

The large majority of CMT1 patients in our Greek cohort remain without a genetic diagnosis, indicating that many novel causative genes are yet to be uncovered in the Greek CMT1 population (Koutsis et al., 2013). The well-defined geographical

location of the Greek population may point to a higher frequency of AR causes of CMT disease; therefore, AR causes of CMT may be explored in cases where AD inheritance cannot be fully ascertained (Koutsis et al., 2013). We have also suggested that the low frequency of mutations in CMT1 genes in our cohort may be explained by the cut-off of 40 m/s used to discriminate CMT1 from CMT2 in this particular cohort of patients. Consequently, it is possible that some CMT2 patients were mistakenly included in our gene screening (Koutsis et al., 2012; Koutsis et al., 2013). Phenotypic variability between patients carrying the same mutation as in our Greek family with the in-frame 21 bp duplication in *PMP22* further complicates prognosis and confirms that genetic modifiers are likely to play a role in disease severity in CMT.

The screening of *PMP22*, *GJB1* and *EGR2* in the Yakutsk CMT1 cohort revealed one *GJB1* variant out of the 10 patients tested for this gene. In a study of Russian patients, *GJB1* mutations accounted for 7.4% of CMT1, 3.1% of CMT2 and 17.6% of unspecified CMT cases (Mersiyanova et al., 2000). Although the pathogenicity of this novel variant is unclear and our cohort was small, the finding of a *GJB1* mutation in our Yakutsk CMT1 patients confirms that *GJB1* mutations are likely to be an important cause of disease in Yakutsk CMT patients and perhaps in other provinces of Russia.

Some important issues previously discussed in studies of CMT and other genetic diseases have once again been highlighted in this study. Segregation of mutations in families, the use of in-silico prediction software like Polyphen-2 and SIFT, assessment of conservation of amino acids across species and screening of the variant in control groups remain insufficient to prove pathogenicity. Furthermore, previous publication in scientific journals does not establish pathogenicity, as some mutations once thought to be deleterious have now been categorized as polymorphisms. Although functional studies are usually thought to be the gold standard in assessing pathogenicity of mutations, some mutations causing dysfunction in vitro have been found in healthy individuals (Kochañski, 2006). Finally, screening the coding exons and flanking intronic sequences of genes does not completely rule out the possibility of that gene being involved in the disease.

Variants in the 5'UTR and 3'UTR regions and deep intronic or synonymous variants may cause disease by affecting microRNA binding, splicing, stability of mRNA or translational efficiency, or they may modify protein structure and activity (Parmley & Hurst, 2007). For example, a synonymous mutation in *MPZ* in a DSD patient was found to activate a cryptic splice site leading to an in-frame partial deletion of one exon (Taioli, Cabrini, Cavallaro, Simonati, et al., 2011).

In the future, gene panels, exome sequencing and whole genome sequencing will become faster and more affordable, thus single gene testing as performed herein may become obsolete. In the meantime however, the diagnostic guidelines described in Section 3.1.1 should be followed to avoid inappropriate genetic tests (Amato & Reilly, 2011). Genotype-phenotype correlations and assessment of subtype frequencies in different populations such as those presented in this study should also guide clinicians in their task.

Although the causative genes have not been identified in our canine peripheral neuropathy cases as well as in the canine with NAD-CA, our screen was only preliminary. Screening of other demyelinating and axonal CMT genes targeted according to the dog's phenotype is warranted, including the genes associated with AR inheritance (Granger, 2011). Sequencing of *MTMR2* and *MTMR13* should be prioritised in future molecular studies of the Schnauzer dogs with demyelinating polyneuropathy and focally folded myelin sheaths (Vanhaesebrouck et al., 2008).

Granger (2011) also highlights some differences between human CMT and CMT-like disease in canines: there is no equivalent of the 38 m/s MNCV cut-off value to delineate demyelinating from axonal forms of CMT in canines; only AR cases have been described in canines, while AD forms are more common in humans; demyelinating forms of neuropathies with onion bulbs are much less frequent in canines than they are in humans. These differences should be kept in mind in studies linking canine and human CMT disease (Granger, 2011).

The finding of new disease-associated genes would provide strong candidates for the human forms of the disease and would allow us to gain further insight into the pathogenesis of disease, especially as the collection of tissue such as nerve and

muscle will be easier than in humans. The causative gene in the Papillon dog may be a candidate gene for AR infantile NAD in humans. We have obtained DNA from five unrelated control Schnauzer dogs in addition to the two affected Schnauzers with AR demyelinating CMT-like polyneuropathy with focally folded myelin sheaths which were screened in this study. We also now have 5 affected, 31 unaffected and 1 obligate carrier of the highly-inbred Papillon dogs with NAD-CA. Future studies will involve genotyping of these two cohorts on the Illumina HD Canine array (Illumina). Because both the Schnauzers and the Papillon dog are part of highly inbred families, we will search for mutant homozygous alleles identical by descent located in a large region of homozygosity shared by the affected dogs and not shared with unaffected dogs, as was done in the Drögemüller et al (2010) study. The array will also allow us to detect large duplications or deletions that may be disease-causing. Recent studies have shown that genes underlying Mendelian traits in dogs can be uncovered by genome-wide association analysis using just 10 affected and 10 control dogs (Karlsson et al., 2007; Matiasek & Drögemüller, 2011).

3.6 Conclusion

In conclusion, this study has provided additional data on the frequency of CMT genetic subtypes in three populations: the UK, Greece and the Yakutsk province in Russia. It has widened the spectrum of phenotypes associated with particular mutations in CMT genes, and has confirmed that in-frame deletions and duplications in *PMP22* cause CMT1 while nonsense mutations are usually associated with HNPP. Such gene screening studies and phenotype-genotype descriptions are essential in elucidating the natural history of disease and providing accurate counselling to patients. We have also highlighted some issues associated with pathogenicity assessments of mutations; these issues apply not only to CMT but to most other genetic diseases as well. Solving these issues will become more important as we identify thousands of new variants in “next-generation sequencing” (NGS) studies.

This study has also ruled out *PMP22* and *MPZ* mutations in a cohort of dogs with peripheral neuropathy and *MFN2* mutations in a dog with NAD-CA. Although the genetic cause of disease remains unexplained in these dogs, it has provided a stepping ground for further genetic research including sequencing of other CMT

genes and homozygosity mapping. These studies may result in a new canine model of CMT in the near future.

This Chapter has highlighted the phenotypic and genotypic heterogeneity of CMT. The next Chapter will focus on one particular CMT subtype, CMT1A, which displays high variability in disease severity despite all patients carrying the Chr17p11.2 duplication.

Chapter 4 Genetics modifiers of the CMT1A phenotype

4.1 Introduction

4.1.1 Phenotypic variability in CMT1A

As discussed in Section 1.4.4, most CMT1A patients carry the same sized Chr17p11.2 duplication, yet they exhibit a wide range of severities both within and between families. Age of onset, weakness and wasting, NCVs and sensory signs are the most variable features (Birouk et al., 1997; Garcia et al., 1995; Kaku et al., 1993; Thomas et al., 1997). As highlighted in Section 1.4.2, several cases of CMT1A and other CMT subtypes have been reported to display coexistent CIDP-like inflammatory features, with abrupt worsening of disease in some instances. This association is thought to occur more often that would be expected by chance (Ginsberg et al., 2004). The high intra- and interfamilial variability in disease severity in CMT1A and other CMT subtypes renders it difficult for clinicians to advise patients on disease progression and family planning. The phenotypic heterogeneity in CMT1A suggests that genetic factors as well as epigenetic, stochastic and environmental effects may influence disease severity as identical twins have shown disparate phenotypes (Boerkoel et al., 1999; Fraga et al., 2005; Garcia et al. 1995). As discussed in Section 1.4.4, comorbid conditions such as diabetes may worsen the CMT1A phenotype (Sheth et al., 2008), however most of the disease variability is likely to be due to genetic background or epigenetics as no environmental factor has been found to contribute significantly to disease severity (Pareyson & Marchesi, 2009).

4.1.2 Genetic modifiers of disease

Although not disease-causing on their own, common variants may act as genetic modifiers of a phenotype by modulating the effect of a disease-associated variant (Génin et al., 2008). Genetic modifiers are defined as genes that influence the phenotypic expression of another gene; they may be monogenic, where variation in one gene explains most of the variability, or multi-factorial, where several genes are involved in modifying a disease phenotype (Génin et al., 2008). The multi-factorial model is likely to be more common (Génin et al., 2008). The past few years have witnessed an increased interest in finding potential genetic modifiers of various

diseases including hereditary neuropathies. Detecting biomarkers of disease severity in CMT will help provide more accurate disease prognoses and further clues about CMT disease pathways. Modifiers may influence a patient's response to treatment and may also be disease-causing in other forms of inherited neuropathy. The mechanism of disease modification will be a potential therapeutic target (Fledrich, Schlotter-Weigel, et al., 2012; Reilly et al., 2011).

4.1.3 Genetic modifiers in CMT1A

Genes such as *PMP22* which cause disease via a gene dosage mechanism may be especially sensitive to the effect of genetic modifiers and the environment (Boerkoel et al., 1999). Genetic modifiers of CMT1A disease have not been extensively studied. Variants in other genes within the Chr17p11.2 duplication may modify the CMT1A phenotype, however given the restricted phenotype of CMT1A, these genes are probably not very sensitive to gene dosage, and most are only expressed in foetal tissues (Inoue et al., 2001; Murakami et al., 1997). A study of CMT1A rats has identified lipid metabolism genes such as *peroxisome proliferator-activated receptor gamma* (*Pparg*) that are dysregulated in sciatic nerve transcriptomes; these genes may be modifiers of disease progression. Skin biopsy studies of CMT1A patients confirmed some of the results found in the rat, and also found that the age of the patient, as well as the mRNA levels of *glutathione S-transferase theta 2* (*GSTT2*) and *cathepsin A* (*CTSA*) together could account for 47% of the variance in the patients' CMTNS (Fledrich, Schlotter-Weigel, et al., 2012).

A concomitant mutation in another CMT gene is likely to affect the phenotype of CMT1A patients. Patients with compound forms of CMT carrying a Chr17p11.2 duplication as well as a *GJB1*, *LITAF* or *MPZ* mutation in the compound heterozygous state have been described. These patients had severe phenotypes likely due to an additive effect of the two genetic defects (Hodapp et al., 2006; Meggouh et al., 2005; Young et al., 2013). A p.Ser72Leu *PMP22* point mutation on the same chromosome as a CMT1A duplication has been found in a CMT1A family with unusual and mild disease (Gouvea et al., 2010). These compound forms of CMT may remain undetected as CMT1A patients are not usually tested for point mutations in *PMP22* and other CMT genes. Although they are probably rare, additional mutations

in CMT genes may account for a minor portion of the phenotypic variability in CMT1A. It may be worthwhile to search for additional pathogenic variants in atypically severe or mild CMT cases (Hodapp et al., 2006). To illustrate, we collaborated on the investigation of a patient with a severe DSD phenotype and additional features including congenital hip dysplasia, partial craniosynostosis and respiratory failure. This patient was found to carry a *PMP22* point mutation and a microdeletion on chromosome 3q23. The genes located within this deletion may be candidate genetic modifiers of the phenotype in other CMT patients, especially in severely affected patients with respiratory involvement (Voermans et al., 2012).

4.1.4 A role for the immune system in CMT1A phenotypic heterogeneity

As described in Section 1.4.2, various cases of superimposed inflammatory neuropathy have been reported in CMT1A, and immunological mechanisms may play a role in disease pathogenesis. The immune system in humans detects foreign agents to protect against disease and therefore needs to be able to differentiate "self" from "non-self" agents such as antigens. Its two main components are the innate immune response, which is non-specific but immediate, and the adaptive immune response, which is specific to certain pathogens and antigens and develops a memory to improve its response over time. Macrophages, a type of leukocyte, are an important part of the innate immune system; macrophages remove debris by phagocytosis and may also act as antigen-presenting cells to activate the adaptive immune system (Male et al., 2006). Lymphocytes, another type of leukocyte, are important cells in the adaptive immune response. B-cells and T-cells are types of lymphocytes; B-cells mediate humoral immunity, which involves antibody production in response to an antigen, while T-cells mediate cell-mediated immunity, which results in the activation of macrophages, the release of cytokines and the production of cytotoxic CD8-positive T-cells in response to an antigen. T-cells require antigen presentation by a major histocompatibility complex (MHC) molecule. The MHC is a group of cell surface molecules encoded by a large set of genes in humans, the most well-known of which are the nine principal human leukocyte antigen (HLA) genes: *HLA-A, HLA-B, HLA-C, HLA-DPA, HLA-DPB, HLA-DQA, HLA-DQB, HLA-DRA,* and *HLA-DRB* (Male et al., 2006). The MHC, composed of class I, II and III, is a 7.6 Mb region on chromosome 6p21-22

containing a dense cluster of 224 loci (128 of which are expressed) in high linkage disequilibrium (LD). Approximately half of the expressed loci in the MHC region play a significant role in the immune system and its associated diseases (Gough & Simmonds, 2007; MHC Sequencing consortium, 1999). Inflammatory and autoimmune diseases are disorders of the immune system. In autoimmune diseases, the immune response is mistargeted towards the body's own healthy tissue, specifically the myelin sheath in CIDP. Although the triggering antigen remains unknown in CIDP, it is suggested that antigens in non-compact myelin and at the axolemma are attacked by the immune system (Dalakas, 2011; Pollard & Armati, 2011).

Several models of myelin-mutant mice have reported an involvement of the immune system in CMT disease pathogenesis. Heterozygous knockout *MPZ* mice and *GJB1*-deficient mice both have a demyelinating neuropathy with presence of CD8-positive T-lymphocytes and activation of macrophages with myelin-macrophage interactions. In both cases, demyelination was less severe and macrophages were not upregulated when mice were crossbred with immunodeficient mice, indicating that macrophages and CD8-positive T-cells may play an active role in the demyelinating process in this animal model of neuropathy (Carenini et al., 2001; Ip et al., 2006; Mäurer et al., 2002; Schmid et al., 2000). In *PMP22* overexpressing mice, levels of macrophages were also increased in demyelinated nerves and macrophages were noted to phagocytose intact myelin; however, CD8-positive T-lymphocytes were not found to mediate demyelination in this mouse model of CMT1A (Kobsar et al., 2005; Kohl et al., 2010). It is possible that the immune system is activated in CMT1A during early stages of demyelination in animal models (Kobsar et al., 2005; Ip et al., 2006). Of course, it may be that the involvement of immune cells in peripheral nerves of *PMP22* mutant mice is neuroprotective rather than pathogenic (Ip et al., 2006). The animal models mentioned here do not show a CIDP-like phenotype, do not respond to anti-inflammatory drugs, and unlike in CMT1 patients with CIDP-like features, T-cells are mainly CD8-positive rather than CD4-positive (Martini & Toyka, 2004). Hence, it is likely that the involvement of the immune system in these CMT1 animal models is chronic and does not model CIDP-like disease in human CMT1. It may however suggest that immune-mediated components of disease could be present in

typical CMT1 at a subclinical level (Martini & Toyka, 2004).

Vasculitis and infiltration of macrophages and CD4-positive T-lymphocytes close to myelinated axons have been reported on some nerve biopsies in CMT1A and unspecified AD CMT1 (Carvalho et al., 2005; Ginsberg et al., 2004; Malandrini et al., 1999; Martini & Toyka, 2004; Pál et al., 2009; Vital et al., 1992; Vital et al., 2003; Williams et al., 1993). These patients typically develop CIDP-like acute or sub-acute worsening of symptoms and often respond well to steroids or IVIG treatment (Dyck et al., 1982; Malandrini et al., 1999). Another study found upregulation of MHC class II molecules and activation of macrophages but no lymphocytic infiltration in eight CMT1A patient nerve biopsies; however, it is unknown whether these patients had CIDP-like features clinically (Stoll et al., 1998). Inflammatory infiltration on nerve biopsy was not seen in a large cohort of CMT1A patients without CIDP-like features, therefore these findings may not be a common phenomenon in typical CMT1A (Gabriel et al., 2002).

Interestingly, autoantibodies against PMP22 were present in 66% of CMT1A, 75% of CMT1 and 60% of CMT2 patients; however they were also present in 23% of controls (Ritz et al., 2000). In another study, anti-PMP22 antibodies were more frequent in CMT1A patients than in controls, especially in those with stepwise progression of disease, but not more frequent than in patients with other neuropathies. It is possible that anti-PMP22 antibodies are merely a response to nerve damage rather than a primary cause of pathology (Gabriel et al., 2002). It is noteworthy that the presence of anti-PMP22 antibodies and the concentration of cytokines in the serum did not correlate with disease severity in CMT1A (Gabriel et al., 2002). Exposure to PMP22 in rats was able to induce experimental autoimmune neuritis, an animal model of immune-mediated neuropathy (Gabriel et al., 1998). PMP22 autoantibodies were found in 50% of CIDP patients in the Ritz et al. (2000) study. One study similarly found antibodies against PMP22 in 35% of patients with CIDP and in none of the controls (Gabriel et al., 2000). However, myelin protein peptides did not elicit immune responses in CIDP patients (Sanvito et al., 2009). It is still uncertain whether PMP22 may play a role in the pathogenesis of inflammatory neuropathy (Gabriel et al., 2000).

Some CMT1A patients may develop a superimposed acquired inflammatory neuropathy because of exposure to damaged components of myelin, leading to increased susceptibility to autoimmune reactions against this myelin debris and healthy myelin (Martini & Toyka, 2004). This mechanism has been suggested to explain the co-existence of CIDP in other CMT subtypes, including CMT4C (Houlden et al., 2009), CMT1B (Donaghy et al., 2000) and CMT1X (Ginsberg et al., 2004). A dysimmune reaction against PMP22 due to increased dosage is a possible explanation for the development of CIDP in CMT1A; however, as discussed above, PMP22 antibodies have also been found at high levels in other inherited neuropathies and the presence of PMP22 antibodies in CMT1A is not correlated to disease severity, therefore a nonspecific response to nerve damage may be a more plausible explanation (Gabriel et al., 2000; Vital et al., 2003). The peripheral nerve may also have increased susceptibility or fragility due to the hereditary neuropathy leading to activation of macrophages by Schwann cell-related factors, facilitating additional immune-mediated demyelination (Ben Youssef-Turki et al., 2011; Ginsberg et al., 2004; Mäurer et al., 2002). Alternatively, immunogenic neuritogens may be exposed as a result of myelin damage (Kobsar et al., 2005; Martini & Toyka, 2004). It remains unclear how the activation of the immune system in CMT1A may sometimes lead to an additional inflammatory autoimmune disease (Kobsar et al., 2005).

The involvement of the immune system in the pathogenesis of inherited neuropathies is considered debatable. Indeed, it is still undetermined whether autoimmune involvement concerns most CMT1 patients at a subclinical level, or a selection of patients who develop a secondary acquired autoimmune-mediated neuropathy (Martini & Toyka, 2004). As previously mentioned, most CMT1 patients do not improve with immunosuppressant therapy, therefore the former is perhaps less likely (Ginsberg et al., 2004; Martini & Toyka, 2004). It remains possible that SNPs associated with autoimmune and inflammatory diseases may modulate disease severity in CMT1A (Ginsberg et al., 2004). Although the exact function of all the genes located within the CMT1A duplicated region has not been elucidated, none of the genes with known function are thought to be involved in the immune system. Therefore, an Immunochip (Illumina) array was used herein to study the association

of inflammatory markers with the CMT1A phenotype and determine whether certain SNPs are associated with severe or mild disease. This methodology employs a candidate gene approach to genetic modifier identification; a candidate gene approach involves studying genes either in the same disease pathway, or as in this case, genes located in another pathway which are involved in somewhat more indirect disease consequences (Génin et al., 2008).

4.1.5 Description of the Immunochip

The Immunochip is an Illumina Infinium customised genotyping chip that contains 196,524 common and rare variants (195,806 SNPs and 718 small insertions-deletions (indels)). The Immunochip was designed by the WTCCC for deep replication of genome-wide association studies (GWAS) of autoimmune and inflammatory diseases, as well as fine mapping of the significant loci identified in various GWAS studies by leading investigators. The majority of these variants have been previously found to be associated with autoimmune and inflammatory diseases including multiple sclerosis, rheumatoid arthritis, Type 1 Diabetes, Crohn's disease, systemic lupus erythematosus (SLE), ankylosing spondylitis, autoimmune thyroid disease, celiac disease, ulcerative colitis and psoriasis. SNPs in the HLA region are especially well covered on the Immunochip (Cortes & Brown, 2011). SNPs from GWAS of non-immunological diseases performed by the WTCCC are also included. The chip requires only a small amount of DNA, and is relatively inexpensive compared to whole-genome chip-based SNP assays (Cortes & Brown, 2011). The chip contains 20 SNPs located within the Chr17p11.2 duplicated region, one of which is located within the *PMP22* gene (dbSNP ID rs3785651).

4.2 Aims of this study

The principal aim of this study was to identify the genetic factors modifying the CMT1A phenotype. Specifically, this Chapter seeks to determine whether alleles associated with immune-related mechanisms and diseases may be responsible for some of the heterogeneity in CMT1A disease severity. It is hoped that this work will be a stepping stone in identifying novel drug targets and will help in predicting CMT1A disease progression during patient counselling.

4.3 Methods

4.3.1 CMT1A patient cohort

CMT1A patients were recruited and clinically evaluated by consultant neurologists leading CMT clinics around the world, including Professor Mary Reilly and Dr Matilde Laurá at the NHNN, Professor Mike Shy at the University of Iowa, USA and Professor Wilson Marques Jr. at the University of São Paulo, Brazil.

CMT1A was diagnosed based on physical examination, electrophysiological tests and genetic tests (microsatellites and/or MLPA) performed by consultant neurologists and laboratories at the corresponding centres. DNA was either obtained from the Neurogenetics diagnostic laboratory at the NHNN or was sent to our centre from the participating centres mentioned above. Details of ethics approval and patient consent are found in Section 2.1.1. Purity and concentration of DNA samples were assessed using a NanoDrop as described in Section 2.1.5

4.3.2 Patient disease severity assessment

The CMT examination scores (CMTES) as well as the CMTNS, where possible, were calculated for each patient by the consultant neurologist. As discussed in Section 1.3.1, the CMTNS is measured on a scale of 0 to 36; patients with mild, intermediate and severe disability typically have a CMTNS between 1–10, 11–20 and 21 or greater, respectively. The CMTES is a sub-score of the CMTNS and is calculated out of 28 points. It contains the sum of the symptoms plus the signs, but does not include the electrophysiological results (Murphy, Herrmann, et al., 2011). Either the first or second version of the CMTNS and/or CMTES was calculated for each patient due to variability in year and location of clinical assessment. The components that were found to differ the most between these two versions in the Murphy, Herrmann and colleagues (2011) study include sensory symptoms, motor symptoms in the arms, sensibility to pinprick, arm strength, and SNAPs.

4.3.3 Confirmation of Chr17p11.2 duplication by quantitative polymerase chain reaction (qPCR)

Before cases were genotyped, the Chr17p11.2 duplication was confirmed in CMT1A cases where a proof of genetic diagnosis could not be obtained. Dosage of *PMP22*

exon 4 was assessed by qPCR using SYBR Green chemistry (Applied Biosystems) and the StepOnePlus Real-Time PCR System (Applied Biosystems) as described in Section 2.1.6. The delta-delta C_t method (described in Section 2.1.6) was used for relative quantitation of *PMP22* exon 4; *ACTBL2* was used as the housekeeping gene. Primer sequences for *PMP22* and *ACTBL2* can be found in Appendix IV Table IV-1.

4.3.4 Adjustment of CMT examination score (CMTES) for age at examination (AAE)

A study of CMT1A patients found an increase in disease severity of 0.257 CMTNS points per year and a Pearson correlation coefficient of 0.4 between age at examination (AAE) and CMTNS (Steiner et al., 2008). Another study has found the age-adjusted CMTNS of CMT1A patients to increase by 0.686 points per year (Shy et al., 2008). To determine whether AAE should be taken into account when considering the CMTES in the Immunochip association study, the AAE for each CMT1A patient in the cohort was plotted against their CMTES. A linear regression was performed to confirm the pattern between the CMTES and AAE.

As expected, the AAE had a non-negligible positive linear correlation with the CMTES (Figure 4-1), with an increase of 0.1557 CMTES points per year and a Pearson correlation coefficient of 0.29.

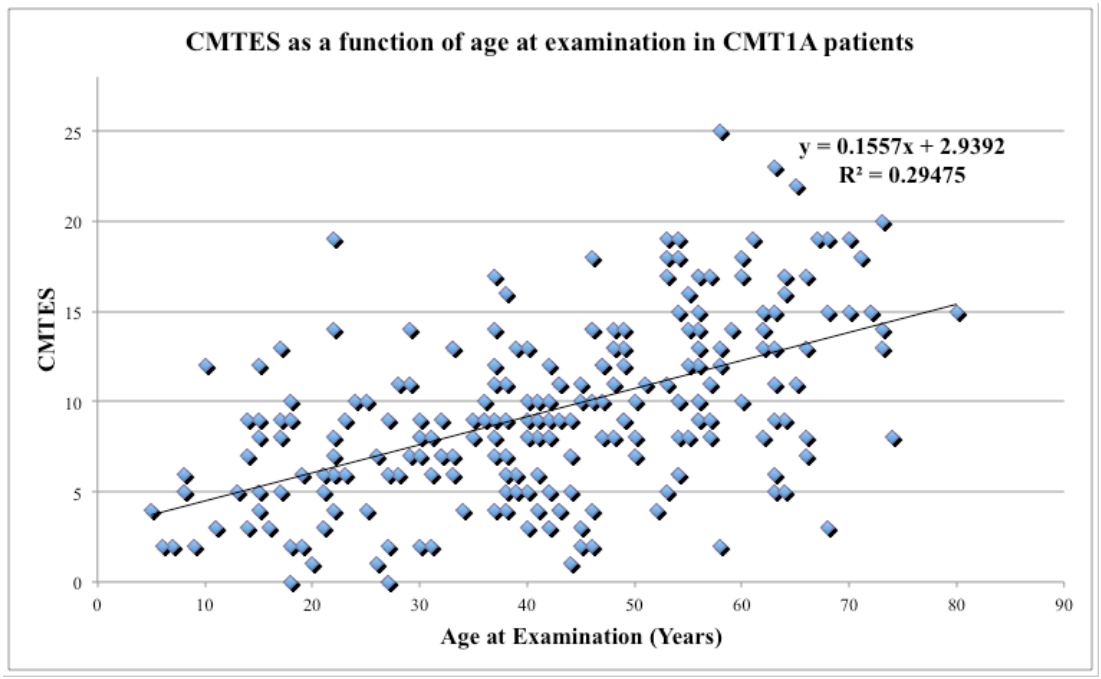

Figure 4-1 Graph of CMTES as a function of AAE in CMT1A patients.

The graph of the residuals after regression shows that once AAE is accounted for, the positive linear trend disappears, confirming the effect of AAE on CMTES. The residual of the regression was then used as the age-corrected CMTES. Negative values (values falling below the regression line) and positive values (values falling above the regression line) represent patients with a phenotype milder and more severe than expected for their AAE, respectively (Figure 4-2).

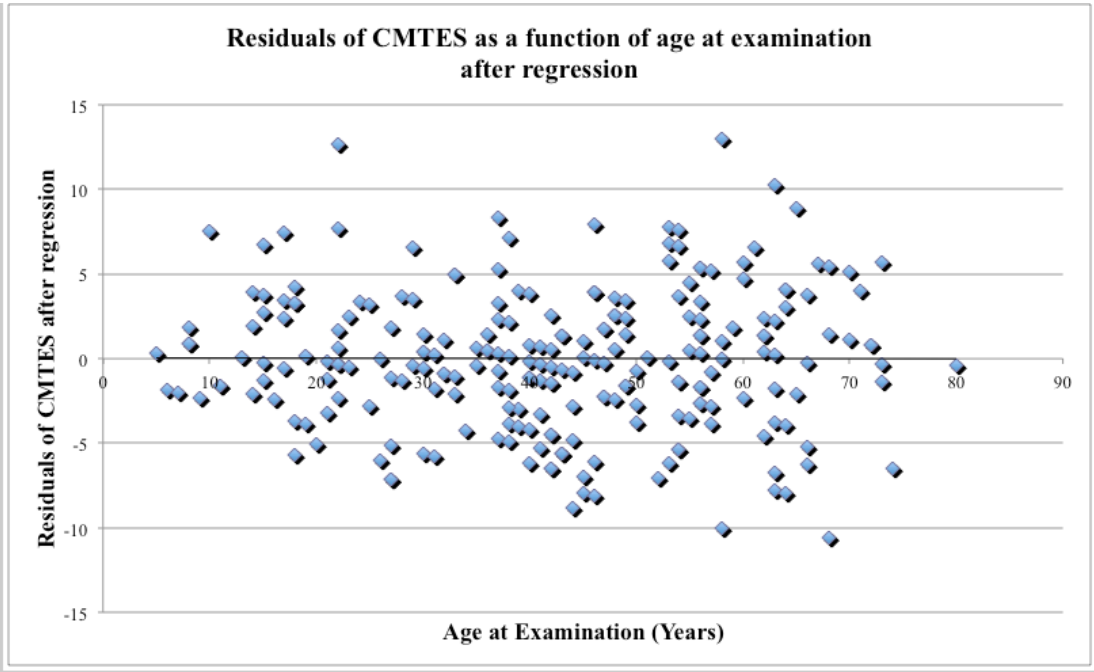

Figure 4-2 Graph of the residuals of age-corrected CMTES as a function of AAE after regression in CMT1A patients.

Although there is a minor increase in variance in age-corrected CMTES distribution in the older CMT1A patients, the age-corrected CMTES is mostly independent in value and variance from the AAE (Figure 4-3).

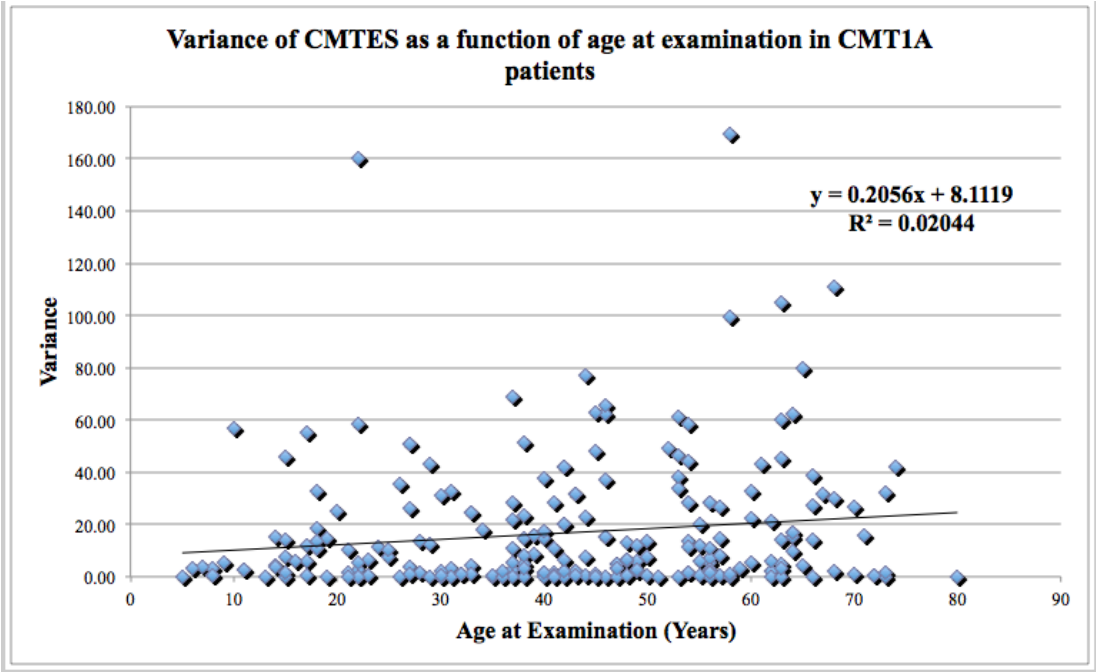

Figure 4-3 Graph of the variance of age-corrected CMTES as a function of AAE in CMT1A patients.

4.3.5 Assessment of intrafamilial and interfamilial variability in CMT1A

To characterize the extent of intrafamilial variability in our patient cohort, the age-corrected CMTES (Section 4.3.4) of one family member was plotted against the age-corrected CMTES of another member of that family in a total of 36 CMT1A families with two to nine family members each.

To assess the extent of intra- and interfamilial variability, the difference in age-corrected CMTES between members of the same family was compared to the difference in age-corrected CMTES of unrelated CMT1A patients. The difference of one member from the rest of the group refers to the mean of the absolute value of the difference between the age-corrected CMTES of that individual compared to every single member of that group. The average size of a CMT1A family in our study was 2.57 members. Using the R software package, 100,000 groups of an average size of 2.57 individuals were randomly created using 185 unrelated CMT1A patients. It was critical that similar-sized groups were compared for analysis of related and unrelated CMT1A patients.

4.3.6 Immunochip association study: patient cohort

A total of 366 CMT1A patients (120 UK, 151 USA, and 95 Brazil patients), 135 CIDP patients and 150 controls were included in the Immunochip association study before quality control was performed. Additional details regarding the CMT1A patient cohort are available in Section 4.3.1. CIDP patients were recruited and clinically evaluated by consultant neurologists at the NHNN and other specialist centres throughout the UK. CIDP cases were analysed in this study to test for shared immune-related disease mechanisms with CMT1A. Control Immunochip data for healthy individuals of Northern European ancestry were provided by the WTCCC2.

4.3.7 Immunochip association study: patient classification and severity scoring

The CMTES was available for all patients in the Immunochip cohort and was therefore used as a measure of disease severity. For the association study, CMT1A patients were classified as mild or severe. According to our categorization, mildly affected patients have a CMTES of 0-8, inclusive and severe patients have a CMTES of 11 or above. Any patient with CMTES of 9 or 10 was excluded to avoid false negative results and to more clearly delineate the two categories. Similarly, using the age-corrected CMTES, any patient with a score between -1 and 1 was excluded. Patients with age-corrected CMTES of -1 and below were considered mild; patients with age-corrected CMTES of 1 and above were considered severe.

4.3.8 Immunochip association study: genotyping

Genotyping of samples on the Illumina Infinium HD Human Immuno BeadChip (Illumina) was performed entirely by UCL Genomics according to the manufacturer's protocol using 300 ng of gDNA. Further details of the genotyping protocol are available in Appendix II. GenomeStudio (v.2010.1, Illumina) was used to extract data files in the PED and MAP file formats for compatibility with the gPLINK software, an open-source C/C++ tool set used here for data quality control and association analyses. A description of gPLINK is available in Section 2.6.

4.3.9 Immunochip association study: data quality control

GenomeStudio (Illumina) was used to examine the X chromosome of all samples (except controls for which gender was not available) and discard individuals with discordant sex information in the eventuality that sample processing errors had occurred. B allele frequencies (defined in Section 2.1.13) of the male X chromosome indicate widespread hemizygosity while the female X chromosome has a much higher rate of heterozygous SNPs (Figure 4-4).

Male X chromosome

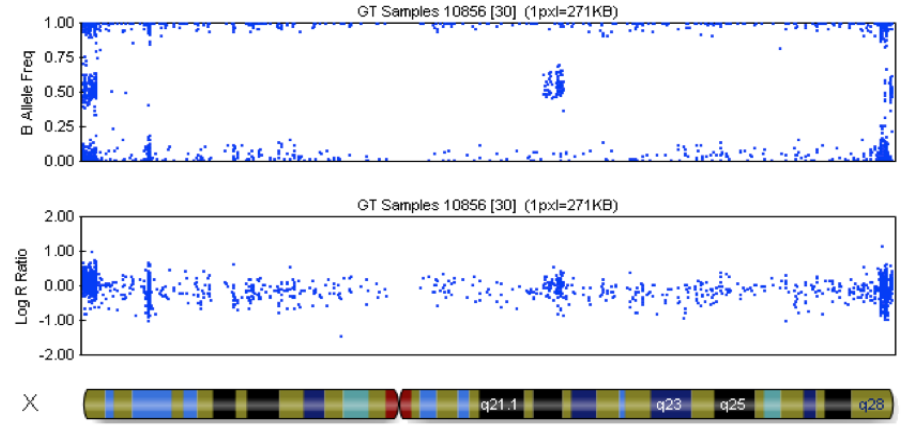

Female X chromosome

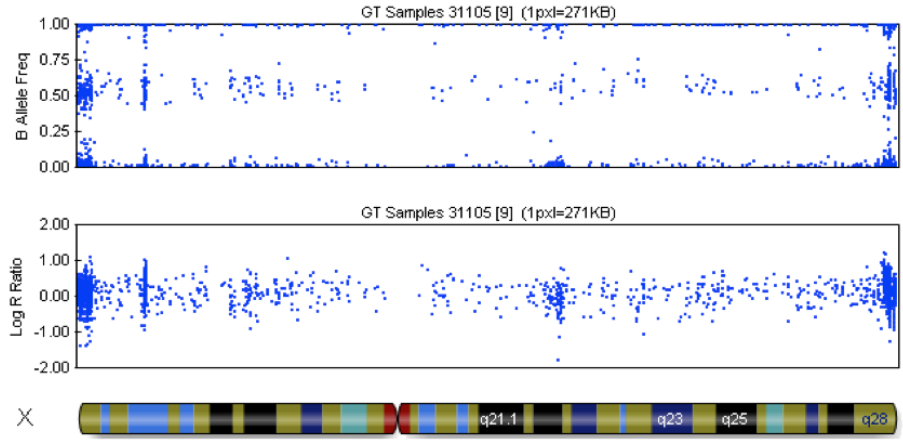

Figure 4-4 B allele frequencies and log R ratios of sample male and female X chromosomes. The B allele frequency is used to infer genotype calls as it is a measure of the allelic intensity ratio of two alleles. The log R ratio is the total signal intensity for two alleles of a SNP. X chromosomes with B allele frequencies (top panels) indicating male (top) and female (bottom) gender in GenomeStudio.

Command lines used in gPLINK for quality control are found in Appendix IV. PED and MAP files from GenomeStudio were converted to binary PED (BED) files using the gPLINK software. PED files contain the sample ID, affectation status and genotypes while MAP files contain SNP information including the chromosome, marker ID, genetic distance and physical position. "Per individual" and "per SNP" quality control measures were performed in gPLINK to eliminate bias and errors as described by Anderson et al. (2010). Any CMT1A patient of non-Northern European

origin including all patient DNA obtained from the University of São Paulo in Brazil were excluded to avoid population stratification or spurious associations due to ethnicity-based rather than disease-based differences in allele frequencies. Individuals with incomplete phenotypic grading, those with more than 10% missing genotypes and individuals with CMTES falling between the mild and severe categories were also removed from the analysis. One member of each family was randomly selected; other family members were excluded to avoid introducing bias and over-representing a particular genotype. Gender was ignored in all analyses as it was not available for the control group; gender is not believed to be linked to disease severity in CMT1A (Swan et al., 2007). A total of 187 CMT1A cases, 125 CIDP cases and 150 controls remained after the exclusion criteria were applied: 103 individuals were of unmatched ethnicity, 12 had incomplete phenotypic grading, 67 were excluded based on familial relationship and 4 had high rates of missing genotypes. 33 CMT1A patients with CMTES of 9 or 10 were excluded from the mild versus severe, mild versus controls and severe versus controls analyses; 40 CMT1A patients with unavailable AAE or an age-corrected CMTES between -1 and 1 were excluded from the corresponding age-corrected analyses. The gender, AAE and CMTES (non-age-corrected and age-corrected) of the 187 CMT1A patients who passed the quality control measures are found in Appendix IV Table IV-3.

SNPs showing a significant deviation from Hardy-Weinberg equilibrium (HWE) in controls were discarded from further analyses as these may indicate genotype-calling errors or selection; the significance threshold used in this test was 0.001 (Anderson et al., 2010). Other "per SNP" quality control filters used in gPLINK to reduce the probability of genotype-induced artefacts included exclusion of SNPs with a genotype rate below 90% and removal of all markers with a very low MAF (MAF<0.01). A total of 138,103 SNPs remained for analysis after data quality control: 1,588 SNPs showed deviation from HWE (in controls only), 6085 SNPs had a genotyping rate lower than 90% and 51,965 SNPs had a MAF less than 0.01 in the CMT1A/CIDP/control combined dataset.

The R software package was used to construct QQ plots of p-value distributions to check for systematic sources of bias such as the possibility of population

stratification. QQ plots show the expected distribution of p-values for all SNPs tested on the x-axis, against the observed p-values for these SNPs on the y-axis. A deviation of p-values from the x=y line indicates a deviation from the null hypothesis of no association. A deviation in the bottom 90% of the values from the x=y line suggests the presence of spurious associations due to bias (persistent differences between cases and controls throughout the entire genome). A sharp deviation from the x=y line in the top right hand corner (smallest p-values) indicates a true association or a false positive association (Balding, 2006). Command lines used to construct QQ plots in the R software are found in Appendix IV.

4.3.10 Immunochip association study: association analyses

All association analyses were performed using specific command lines in gPLINK (Appendix IV). Two sets of standard case/control allelic association analyses based on Chi-squared (Clarke et al., 2011) were performed: one using the non-age-corrected CMTES, and a second using the age-corrected CMTES. Age-correction of CMTES is described in Section 4.3.4. For the non-age-corrected set, analyses were performed between: CMT1A cases (n=187) and controls (n=150); mild (n=69) and severe (n=85) CMT1A cases; severe CMT1A cases (n=85) and controls (n=150); mild CMT1A cases (n=69) and controls (n=150). Allelic association tests using age-corrected CMTES were also performed on mild (n=66) versus severe (n=81) CMT1A cases, severe CMT1A cases (n=81) versus controls (n=150), and mild CMT1A cases (n=66) versus controls (n=150). Association tests were performed between mild CMT1A and controls as well as between severe CMT1A and controls to ensure that any significant difference in allele frequency in the mild versus severe CMT1A analysis was not specific to that population; any variant significantly associated with mild or severe CMT1A cases needed to be significantly associated either in the mild CMT1A versus controls or severe CMT1A versus controls analysis. An allelic association analysis was also performed for CMT1A cases (n=187) versus CIDP cases (n=125), and controls (n=150) versus CIDP cases (n=125). For each analysis above, association was performed on the entire chip (138,103 SNPs), on the HLA region (7,969 SNPS), and on the HLA region after pruning of SNPs in LD (1,094 SNPs). SNPs in LD have alleles which are non-randomly associated (Anderson et al., 2010). Including only tagging SNPs in the

HLA region and excluding ones in LD (i.e. "pruning") is preferable for small sample sizes as it decreases the number of tests and therefore increases power. The NCBI website was used to find the chromosomal position of the HLA region in Genome Build 36.1.

The pointwise and genome-wide p-values were calculated for each SNP. Pointwise p-values represent the probability of observing a test statistic greater than or equal to the observed test statistic at that particular locus under the null hypothesis (Balding, 2006). Given the large number of SNPs tested, a correction for multiple testing was needed to avoid false-positive results (Génin et al., 2008). The significance thresholds obtained using the Bonferroni correction for multiple testing ($\alpha=0.05/n$; α is the significance threshold and n is the number of comparisons) would be somewhat conservative as this correction assumes independence between tests and is not appropriate when LD may be present, as is the case in the HLA region. Instead, the genome-wide p-value was used to correct for multiple testing by performing 100,000 random permutations of case and control labels (Balding, 2006). The genome-wide p-value represents the probability of observing the test statistic or higher at any locus across the genome by chance. The pointwise and genome-wide p-value significance thresholds were set at $\alpha=0.05$. SNPs in which the MAF is significantly lower in cases (or severe cases) compared to controls (or mild cases) indicates a protective effect of the allele; in this case, the odds ratio (OR) is lower than 1. The OR is a measure of the relative odds of the occurrence of an outcome of interest given exposure to a particular variable. SNPs in which the MAF is significantly higher in cases (or severe cases) compared to controls (or mild cases) indicates susceptibility to disease; in this case, the OR is higher than 1. A 95% confidence interval (CI) was used for the OR. The UCSC, dbSNP, NCBI, UniProtKB and Ensembl browsers were used to search for SNP and gene information.

4.4 Results

4.4.1 Confirmation of Chr17p11.2 duplication

The RQ was greater than 1.3 in all tested CMT1A cases (refer to Section 2.1.6 for an explanation of RQ), thus confirming the presence of the Chr17p11.2 duplication in cases where the genetic diagnosis could not be confirmed.

4.4.2 Assessment of intrafamilial and interfamilial variability in CMT1A

Determining the extent of intra- and interfamilial variability in our patient cohort provided an estimation of the importance of genetic factors in modulating the disease phenotype. If familial relationship could predict disease severity, we would expect a larger number of data points in the bottom left (both family members are mild) and top right (both family members are severe) quadrants in the graph in Figure 4-5. As no such pattern is seen and the Pearson correlation coefficient is 0.00059, disease severity of one family member cannot be predicted from that of a second family member.

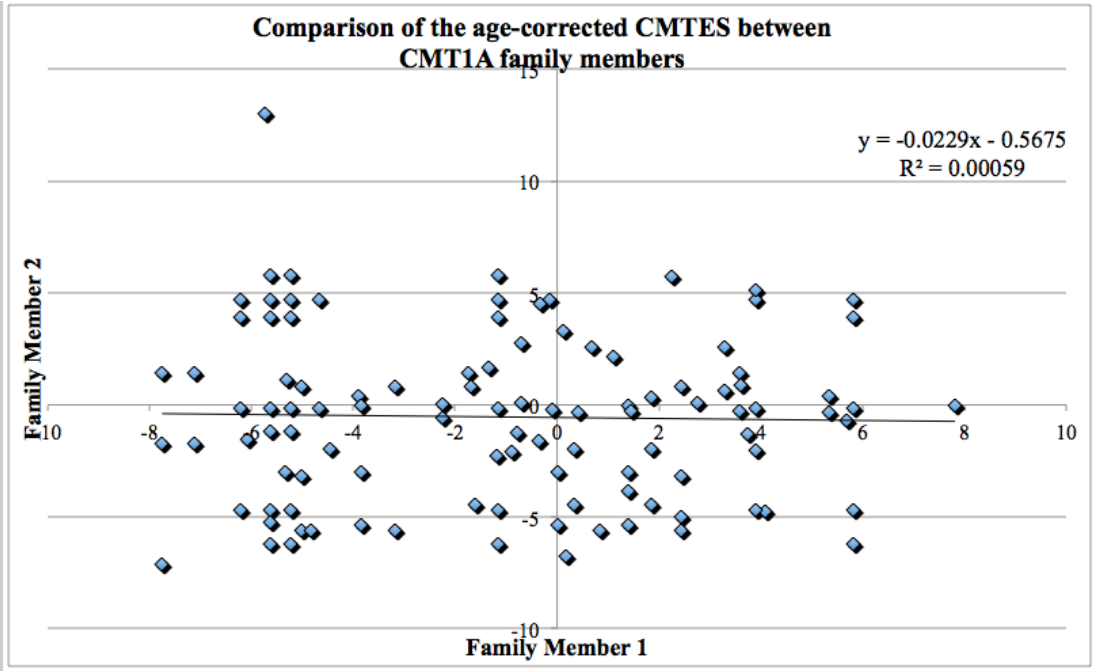

Figure 4-5 Comparison of the age-corrected CMTES between CMT1A family members.

Given the low concordance between family members, *trans*-acting rather than *cis*-acting modifying factors are probably involved in causing CMT1A phenotypic variability. By the same logic, genetic modifiers in CMT1A are most likely multi-factorial rather than monogenic (Génin et al., 2008).

Although as shown above there is high intrafamilial phenotypic variability in CMT1A, if genetic factors are modulating the CMT1A phenotype, variability

between families should still be greater than variability within families (Génin et al., 2008). The average difference in age-corrected CMTES between one individual and the other members of his family was 3.96 age-corrected CMTES points. In comparison, the corresponding value for unrelated CMT1A patients was 4.87 age-corrected CMTES points. The density graph shown in Figure 4-6 shows the distribution of the difference in age-corrected CMTES for members of the same family and unrelated patients. Excluding one outlier, the distribution of the difference in CMTES within families appears to be centred closer to zero and is narrower than the difference in CMTES between unrelated individuals, suggesting that interfamilial variability is greater than intrafamilial variability in CMT1A.

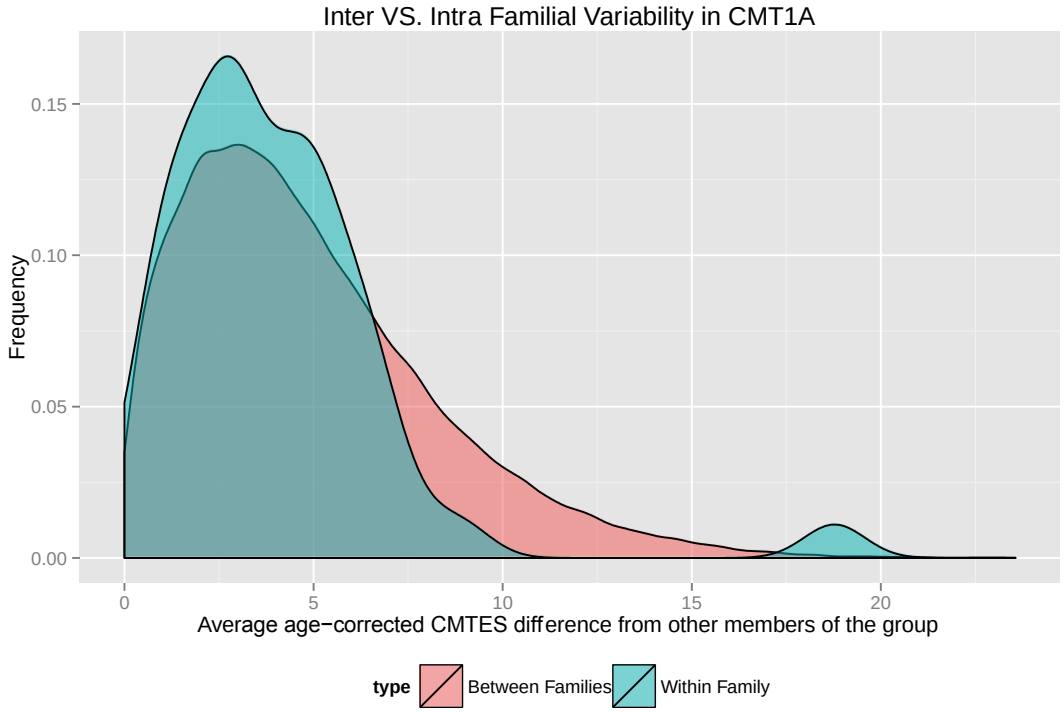

Figure 4-6 Density graph showing the distribution of the difference in age-corrected CMTES for members of the same family and unrelated patients.

4.4.3 Immunochip association study of variants associated with autoimmune and inflammatory diseases in CMT1A patients

The QQ plots generated for further quality control are represented in Appendix IV Figure IV-1; an example is shown below in Figure 4-7.

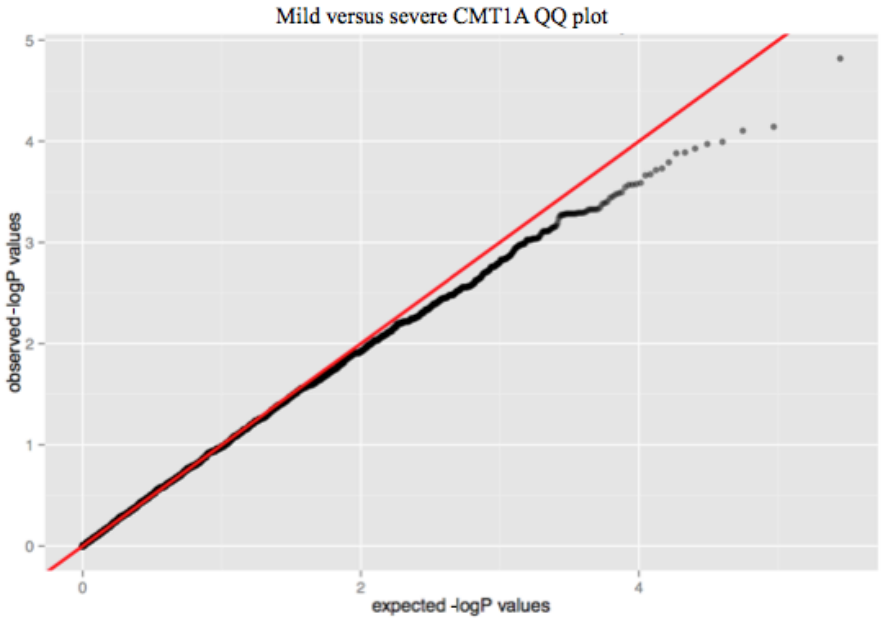

Figure 4-7 QQ plot of the mild versus severe CMT1A allelic association analysis.

The QQ plots showed that the CMT1A cases, CIDP cases and controls were generally appropriately matched. The p-values adhere relatively closely to the x=y line (i.e. null hypothesis) for the bottom 90% of the values for most of the analyses. As some data points do deviate from the x=y line in some analyses, such as the age-corrected severe CMT1A versus controls analysis, results from these analyses should be interpreted with caution. Points deviating from the x=y line in the top right hand corner (lowest p-values), which are most evident in the QQ plot for the CIDP versus controls analysis, may indicate real associations or false associations due to genotyping errors. Therefore, SNPs reaching significance were checked individually for accurate calling of genotypes using the genotype cluster plots in GenomeStudio (Illumina) (see Appendix IV Figure IV-2 for cluster plots and call rates of all top hit SNPs on the Immunochip). SNPs reaching significance but which showed poor clustering were excluded.

The results of the CMT1A versus controls, mild versus severe CMT1A, and CIDP versus controls allelic association analyses are shown in Tables 4-1 to 4-3. The results of the remaining allelic association analyses are located in Appendix IV Table IV-4 but are also described below. Chromosomal positions refer to Genome Build 36.1. In analyses in which no SNP had both a pointwise and genome-wide p-value

below α=0.05, the SNPs with the two lowest genome-wide p-values are provided and written in italics. If the SNP was not located within a gene, the closest protein-coding gene(s) to the SNP is given. Where available, the MAF in the 1000 Genomes European population is provided for each SNP. For selected SNPs, the MAFs in other cohorts from our study are provided for reference. For the CIDP versus controls analyses, the potential effect of the allele on the disease state (i.e. causative or protective) is given for significantly associated SNPs; a question mark is written when the 1000 Genomes MAF is in conflict with the MAF found in our control group.

Table 4-1 Results of top hits in the mild versus severe CMT1A allelic association analysis on the Immunochip.

CHR	SNP	Gene	Base pair	A1	Severe CMT1A MAF	Mild CMT1A MAF	Controls MAF	1000 Genomes MAF (Europeans)	CIDP MAF	A2	CHISQ	P-value	OR	SE	L95	U95	Pointwise P-value	Genome-wide P-value after 100000 permutations
Severe CMT1A versus mild CMT1A- whole chip																		
9	*rs1933038*	*Close to DMRT2*	*1156086*	*A*	*0.2059*	*0.4348*	*0.2181*	*0.272*	*0.2944*	*G*	*18.71*	*1.52E-05*	*0.337*	*0.256*	*0.2041*	*0.557*	*8.00E-05*	*0.4905*
3	*rs13059662*	*Close to ZDHHC19*	*197392725*	*A*	*0.1824*	*0.0362*	*0.12*	*0.119*	*0.068*	*G*	*15.76*	*7.21E-05*	*5.932*	*0.497*	*2.24*	*15.71*	*2.00E-05*	*0.9551*
Severe CMT1A versus mild CMT1A- HLA region																		
6	*rs7771432*	*Close to HLA-C*	*31388729*	*A*	*0.02976*	*0.1397*	*0.0685*	*0.067*	*0.0565*	*G*	*12.49*	*0.000408*	*0.189*	*0.517*	*0.0686*	*0.52*	*0.00098*	*0.4264*
6	*1kg_6_30051248/ rs1128306*	*Close to HLA-A*	*30051248*	*A*	*0.1905*	*0.0625*	*0.13*	*0.144*	*0.1452*	*G*	*10.18*	*0.001419*	*3.529*	*0.415*	*1.566*	*7.955*	*0.00284*	*0.7932*
Severe CMT1A versus mild CMT1A- HLA region (pruned)																		
6	*rs7771432*	*Close to HLA-C*	*31388729*	*A*	*0.02976*	*0.1397*	*0.0685*	*0.067*	*0.0565*	*G*	*12.49*	*0.000408*	*0.189*	*0.517*	*0.0686*	*0.52*	*0.00138*	*0.1678*
6	*rs3819299*	*HLA-B*	*31430345*	*C*	*0.02381*	*0.1087*	*0.0604*	*0.102*	*0.0391*	*A*	*9.374*	*0.0022*	*0.2*	*0.575*	*0.0648*	*0.618*	*0.00238*	*0.6232*
Age-corrected severe CMT1A versus mild CMT1A- whole chip																		
14	*1kg_14_34817568 /rs61988272*	*PSMA6*	*34817568*	*G*	*0.216*	*0.0379*	*0.12*	*0.117*	*0.12*	*A*	*19.64*	*9.33E-06*	*7*	*0.494*	*2.657*	*18.44*	*7.00E-05*	*0.3183*
3	*rs957215*	*Close to LRRC3B*	*26608282*	*G*	*0.2778*	*0.5303*	*0.4633*	*0.443*	*0.4234*	*A*	*19.48*	*1.02E-05*	*0.341*	*0.247*	*0.2098*	*0.553*	*3.00E-05*	*0.3382*
Age-corrected severe CMT1A versus mild CMT1A- HLA region																		
6	*1kg_6_30131847/ rs3869070*	*C6orf12*	*30131847*	*G*	*0.321*	*0.5379*	*0.4867*	*0.493*	*0.52*	*A*	*14.06*	*0.000177*	*0.406*	*0.243*	*0.2525*	*0.653*	*0.00047*	*0.2245*
6	*1kg_6_30083432/ rs2240619*	*HLA-A*	*30083432*	*A*	*0.6296*	*0.4242*	*0.4533*	*0.476*	*0.428*	*C*	*12.34*	*0.000443*	*2.307*	*0.24*	*1.442*	*3.691*	*0.00135*	*0.4433*
Age-corrected severe CMT1A versus mild CMT1A- HLA region (pruned)																		
6	*rs2523776*	*Close to HLA-G*	*29917173*	*C*	*0.1543*	*0.0455*	*0.0667*	*0.092*	*0.088*	*A*	*9.139*	*0.002502*	*3.832*	*0.471*	*1.522*	*9.647*	*0.00553*	*0.652*
6	*rs9366752*	*C6orf12*	*30132656*	*A*	*0.1481*	*0.2879*	*0.2718*	*0.28*	*0.272*	*G*	*8.534*	*0.003486*	*0.43*	*0.293*	*0.2422*	*0.764*	*0.00687*	*0.7704*

Chr: chromosome; SNP: SNP identifier; A1: minor allele; MAF: minor allele frequency; A2: major allele; Chisq: basic allele test Chi-square value; P-value: asymptotic p-value for this test; OR: estimated odds ratio for A1; SE: standard error of estimated odds ratio; L95: lower bound of 95% confidence interval for odds ratio; U95: upper bound of 95% confidence interval for odds ratio; N/A: not available

Groups being compared in each association analysis are coloured in grey; MAFs for corresponding SNPs in other groups are provided for reference.

Table 4-2 Results of top hits in the CMT1A versus controls allelic association analysis on the Immunochip.

CHR	SNP	Gene	Base pair	A1	CMT1A MAF	Controls MAF	1000 Genomes MAF (Europeans)	Mild CMT1A MAF (MAF in age-corrected analysis)	Severe CMT1A MAF (MAF in age-corrected analysis)	CIDP MAF	A2	CHISQ	P-value	OR	SE	L95	U95	Pointwise P-value	Genome-wide P-value after 100000 permutations
CMT1A versus controls- whole chip																			
12	*imm_12_9700708*	*PRB4*	*9700708*	*C*	*0.05618*	*0.16*	*N/A*	*0.0625 (0.05833)*	*0.04938 (0.05769)*	*0.122*	*A*	*18.89*	*1.39E-05*	*0.313*	*0.279*	*0.181*	*0.54*	*1.00E-05*	*0.4879*
1	*imm_1_150937361 /rs11582063*	*Close to LCE2A*	*150937361*	*A*	*0.1709*	*0.3154*	*0.299*	*0.1452 (0.175)*	*0.197 (0.1846)*	*0.2564*	*G*	*17.52*	*2.85E-05*	*0.447*	*0.195*	*0.305*	*0.655*	*0.00012*	*0.7499*
CMT1A versus controls- HLA region																			
6	*rs9258740*	Close to *HLA-G*	*29935878*	*A*	*0.2219*	*0.1007*	*0.194*	*0.1884 (0.1667)*	*0.2706 (0.284)*	*0.1585*	*G*	*17.43*	*2.98E-05*	*2.548*	*0.229*	*1.626*	*3.993*	*9.00E-05*	*0.05104*
6	*rs4607472*	Close to *HLA-G*	*29918522*	*G*	*0.1123*	*0.03667*	*0.09*	*0.1087 (0.1136)*	*0.1176 (0.1111)*	*0.075*	*A*	*13.14*	*0.0002885*	*3.324*	*0.348*	*1.68*	*6.576*	*0.0006*	*0.3365*
CMT1A versus controls- HLA region (pruned)																			
6	*rs4607472*	Close to *HLA-G*	*29918522*	*G*	*0.1123*	*0.03667*	*0.09*	*0.1087 (0.1136)*	*0.1176 (0.1111)*	*0.075*	*A*	*13.14*	*0.0002885*	*3.324*	*0.348*	*1.68*	*6.576*	*0.00074*	*0.142*
6	*rs2394180*	Close to *HLA-G*	*29913178*	*G*	*0.1524*	*0.07333*	*0.12*	*0.1449 (0.1439)*	*0.1588 (0.1728)*	*0.116*	*A*	*10.06*	*0.001516*	*2.272*	*0.264*	*1.354*	*3.813*	*0.00355*	*0.5337*

Chr: chromosome; SNP: SNP identifier; A1: minor allele; MAF: minor allele frequency; A2: major allele; Chisq: basic allele test Chi-square value; P-value: asymptotic p-value for this test; OR: estimated odds ratio for A1;
SE: standard error of estimated odds ratio; L95: lower bound of 95% confidence interval for odds ratio; U95: upper bound of 95% confidence interval for odds ratio; N/A: not available
Groups being compared in each association analysis are coloured in grey; MAFs for corresponding SNPs in other groups are provided for reference.

Table 4-3 Results of top hits in the CIDP versus controls allelic association analysis on the Immunochip.

CHR	SNP	Gene	Base pair	A1	CIDP MAF	Controls MAF	1000 Genomes MAF (Europeans)	A2	CHISQ	P-value	OR	SE	L95	U95	Pointwise P-value	Genome-wide P-value after 100000 permutations	Potential effect of allele on CIDP
CIDP versus controls- whole chip																	
3	imm_3_58370541	*PXK*	58370541	G	0.5574	0.2333	N/A	A	60.05	9.24E-15	4.138	0.1877	2.864	5.978	1.00E-05	1.00E-05	Causative
8	1kg_8_11183638/ rs4841519	*MTMR9*	11183638	A	0.56	0.2099	0.471	T	66.49	3.52E-16	4.79	0.1981	3.249	7.063	1.00E-05	1.00E-05	?
CIDP versus controls- HLA region																	
6	*rs2242659*	*PRRC2A*	*31709492*	*G*	*0.2642*	*0.41*	*0.379*	*A*	*12.72*	*0.0003614*	*0.5168*	*0.1863*	*0.3587*	*0.7445*	*0.00057*	*0.3991*	*N/A*
6	*rs1046089*	*PRRC2A*	*31710946*	*A*	*0.26*	*0.4033*	*0.458*	*G*	*12.52*	*0.0004032*	*0.5198*	*0.1861*	*0.3609*	*0.7486*	*0.00064*	*0.4238*	*N/A*
CIDP versus controls- HLA region (pruned)																	
6	*rs3778630*	*PSORS1C1*	*31199307*	*A*	*0.0726*	*0.01667*	*0.033*	*G*	*10.56*	*0.001158*	*4.617*	*0.5131*	*1.689*	*12.62*	*0.00093*	*0.4482*	*N/A*
6	*1kg_6_30214416*	*TRIM40*	*30214416*	*G*	*0.072*	*0.01667*	*N/A*	*A*	*10.42*	*0.001247*	*4.578*	*0.5131*	*1.675*	*12.51*	*0.00452*	*0.4735*	*N/A*

Chr: chromosome; SNP: SNP identifier; A1: minor allele; MAF: minor allele frequency; A2: major allele; Chisq: basic allele test Chi-square value; P-value: asymptotic p-value for this test; OR: estimated odds ratio for A1; SE: standard error of estimated odds ratio; L95: lower bound of 95% confidence interval for odds ratio; U95: upper bound of 95% confidence interval for odds ratio; N/A: not available
Groups being compared in each association analysis are coloured in grey.

The aims of this association study were to determine whether alleles at SNPs associated with inflammatory and autoimmune diseases and/or CIDP may modulate disease severity in CMT1A, and whether these alleles may be involved more generally in CMT1A pathogenesis. To confirm the first hypothesis, we would expect a significant association of some Immunochip SNPs with mild or severe CMT1A in the mild versus severe CMT1A analysis. No SNP had both pointwise and genome-wide p-values below 0.05 in the mild versus severe CMT1A analysis (Table 4-1). The lowest (but non-significant) genome-wide p-value for the mild versus severe CMT1A analysis was found in the non-age-corrected analysis on the pruned HLA region (p-value=0.1678 for rs7771432 at chr6:31,388,729). It is worth noting that none of the top hits in the mild versus severe CMT1A analysis was common to both the age-corrected and non-age-corrected analyses, suggesting that age-correction of the CMTES modifies the mild and severe categories considerably. If an overlap of CIDP with CMT1A could explain some phenotypic variability, some alleles significantly associated with CIDP in the CIDP versus controls analysis should also be significantly associated with either mild or severe CMT1A. No top hit SNP was found in both the CIDP versus controls and the mild versus severe CMT1A analyses.

To confirm the second hypothesis that some alleles at SNPs on the Immunochip may play a role in CMT1A disease, we would expect a significant association of some Immunochip SNPs with CMT1A in the CMT1A versus controls analysis. No SNP had both pointwise and genome-wide p-values below 0.05 in the CMT1A versus controls analysis (Table 4-2). One SNP on the pruned HLA region, rs9258740, was close to reaching significance; the CMT1A and controls MAF were 0.2219 and 0.1007, respectively (genome-wide p-value=0.05104; OR=2.548; 95% CI of OR=1.626-3.993). This SNP is located close to *HLA-G*, a non-classical MHC class I gene. However, the MAF in the 1000 Genomes European population (0.194) was similar to that found in our CMT1A cohort (0.2202), therefore it is unlikely to be causative for CMT1A disease.

Two SNPs were significantly associated with CIDP in the CIDP versus controls analysis on the entire chip, supporting the role of the immune system in the pathogenesis of CIDP (Table 4-3). Both SNPs also have significantly different MAF

in the CMT1A versus CIDP analysis, where CMT1A cases have a similar MAF to controls. One SNP (imm_3_58370541 at chr3:58,370,541) is predicted to be causative for CIDP (genome-wide p-value=0.00001; OR=4.138; 95% CI of OR=2.864-5.978). This SNP is located within an intron of the *PX domain containing serine/threonine kinase* (*PXK*) gene, which encodes a Phox PXK homology domain–containing serine-threonine kinase; it may have a role in trafficking of the epidermal growth factor receptor. This *PXK* locus is unlikely to be a risk allele for CMT1A as CMT1A patients had similar MAF to controls (MAF in CMT1A=0.2204; controls=0.2333; CIDP=0.5574).

In Europeans, this gene contains known susceptibility loci for systemic sclerosis (rs2176082 at chr3:58,306,226 (Martin et al., 2013)), rheumatoid arthritis (rs13315591 at chr3:58,531,881 (Stahl et al., 2010)) and SLE (rs2176082, as well as rs6445975 at chr3:58,345,217 (Martin et al., 2013; SLEGEN et al., 2008)). In the GWAS of SLE patients versus controls, association was also found with SNPs within the HLA region, in genes previously associated with SLE, and with several other loci (SLEGEN et al., 2008). In the Martin et al. (2013) study, a pan-meta-GWAS combining both systemic sclerosis and SLE patients, the association with the *PXK* locus was common to both groups of patients. Several novel susceptibility loci were also identified in this study (Martin et al., 2013). The Stahl et al. (2010) study identified new risk loci for rheumatoid arthritis, and confirmed associations with previously known rheumatoid arthritis and other autoimmune disease risk loci. In my study, approximately 230 SNPs located within the *PXK* exons, introns, upstream and downstream regions were included in the Immunochip association analysis (including rs6445975 and rs2176082); however, no other SNP in this gene or nearby regions besides the chr3:58,370,541 SNP was significantly associated with CIDP.

The effect could not be predicted for the second significantly associated SNP (rs4841519); the MAF in the 1000 Genomes database (0.471) was closer to the MAF in CIDP (0.56) than to the MAF in our control group (0.2099), suggesting that this difference in MAF between our control group and CIDP patients may not be real. No SNPs reached significance on the HLA region or pruned HLA region in the CIDP versus controls analysis.

If CMT1A and CIDP shared certain risk alleles and therefore perhaps some disease mechanisms, some alleles significantly associated with CIDP in the CIDP versus controls analysis should also be associated with CMT1A in the CMT1A versus controls analysis. No SNP fulfilled this criterion.

Interestingly, none of the top hit SNPs in any of the CMT1A analyses was located in the Chr17p11.2 duplicated region; this finding would suggest that alleles at SNPs located in this area of the genome on the Immunochip are unlikely to play a role in CMT1A pathogenesis or in modifying the CMT1A phenotype. However, this conclusion is premature given the small number of samples and other limitations of our study, which will be discussed in Section 4.5.2.

4.5 Discussion

4.5.1 Assessment of intrafamilial and interfamilial variability in CMT1A

The inability to predict disease severity in one family member given the CMTES of another family member confirms the high intrafamilial phenotypic variability in CMT1A families, and supports a role of the environment and epigenetics in modulating the phenotype. However, as interfamilial variability was found to be greater than intrafamilial variability, genetic modifying factors are nonetheless likely to be involved to some extent in modifying the CMT1A phenotype.

4.5.2 Association study of inflammatory and autoimmune disease-associated SNPs in CMT1A

When considering both age-corrected and non-age-corrected analyses of the mild versus severe CMT1A groups, no Immunochip SNPs genotyped in CMT1A patients showed an association with disease severity after 100,000 permutations. Furthermore, no SNP significantly associated with CIDP (as compared to controls) was amongst the SNPs with the lowest genome-wide p-values in the mild versus severe CMT1A analysis. It seems unlikely that alleles associated with CIDP and with autoimmune and inflammatory diseases are modifying the CMT1A phenotype. No SNP reached genome-wide significance in the CMT1A versus controls analysis. No SNP was found to be significantly associated with both CIDP in the CIDP versus controls analysis and with CMT1A in the CMT1A versus controls analysis,

suggesting that SNPs associated with CIDP are probably not involved in CMT1A pathogenesis. One SNP within the *PXK* gene was associated with CIDP (but not with CMT1A); this gene also contains susceptibility loci for other autoimmune diseases. If the association of CIDP with the *PXK* locus identified in our study (chr3:58,370,541) can be replicated in a larger cohort, this would suggest that CIDP shares a susceptibility locus (and perhaps disease mechanisms) with other autoimmune diseases.

These results suggest that there is no evidence for a role of the immune system in CMT1A or in modifying the CMT1A phenotype. However, the results of this study are very preliminary, and any SNP close to reaching significance in this study should be considered for future studies with larger cohorts of patients. The substantial limitations of this study are discussed below.

One important limitation of this study is the considerable lack of power due to insufficient patient numbers. Association studies are usually performed on much larger cohorts of patients. However, obtaining both DNA and complete phenotypic details for unrelated CMT1A cases of matching ethnicity is not trivial. Significant findings from this study need to be replicated in a larger cohort of patients for validation.

In one set of Immunochip analyses, the CMTES were corrected for AAE. However, one assumption of this model is that CMT1A progresses in a steady manner (Shy et al., 2008; Steiner et al., 2008), which is generally true except when there is an overlapping inflammatory neuropathy. There is also a suggestion of a slight increase in rate of disease progression with age (Shy et al., 2008) and of anticipation or increase in disease severity over successive generations (Steiner et al., 2008). The model used for age-correction in this study assumed linearity of disease progression and therefore may not be appropriate if disease progression is no longer linear in the older CMT1A population. This model also assumes that the CMTES scale is linear, which is not necessarily the case (Steiner et al., 2008). These assumptions are further drawbacks of this study.

The CMTES used to describe the "severe" and "mild" categories do not follow the traditional description of severe and mild CMT; however, because most of the patients in our cohort were mildly affected, and because the two categories needed to contain similar numbers of patients, we had to adjust what we considered mild and severe disease so that it would be appropriate to our cohort. It must also be kept in mind that the exclusion of gender in our analysis precludes us from validating any associations located on the X chromosome; therefore, analysis of association data was limited to autosomes. Finally, the association tests performed herein are qualitative and only consider individual alleles; further association tests could be performed, including a genotype association test and a quantitative trait analysis.

Unlike a GWAS, the use of the Immunochip is focused and hypothesis-driven, and may suffer from bias as the markers are a selection of SNPs already found to be associated with autoimmune disorders. Indeed, a more appropriate method of identifying genetic modifiers of disease would be to perform a GWAS. This powerful approach makes no a priori assumptions about which genes are involved in producing or modifying a given phenotype. To this end, we have contributed CMT1A DNA samples to collaborators in the USA to perform a GWAS. Although GWAS studies are less biased as they involve a systematic approach, the sheer number of potential interactions (i.e. loci modifying the phenotype) it involves reduces statistical power. A more pragmatic methodology would be to predict genetic interactions via "network-guided modifier screening" using functional gene networks and to test specifically for associations of these loci with the phenotype (Lee et al., 2010).

4.5.3 Supplementary study into genetic modifiers of the CMT1A phenotype

A supplementary study was conducted in the cohort of CMT1A patients described in this Chapter to assess the involvement of additional genetic factors in modifying the CMT1A phenotype. The other potential sources of phenotypic modification in CMT1A studied therein include: variants in the nerve-specific *PMP22* promoter and 5'UTR region, concomitant pathogenic variants in the *PMP22* coding region, the presence of the *PMP22* p.Thr118Met variant, and the size of the Chr17p11.2 duplication. The results of this supplementary study are:

- Sequencing of the nerve-specific *PMP22* promoter and 5'UTR revealed very few rare variants.
- No concomitant pathogenic variants were found in the *PMP22* coding region.
- The frequency of the *PMP22* p.Thr118Met variant with ambiguous pathogenicity was comparable to that reported in control databases.
- The small number of CMT1A patients with duplications of an atypical size had a classic CMT1A phenotype.

Due to space restrictions and the significant limitations of this particular study, further details are available in Appendix VIII.

4.6 Conclusion

In conclusion, this Chapter has emphasised the phenotypic heterogeneity of CMT1A and has assessed the potential contribution of alleles associated with inflammatory and autoimmune diseases in modifying the CMT1A phenotype. The discovery of disease severity markers is critical for identification of drug targets as well as for patient counselling (Reilly et al., 2011). The next Chapter will seek to elucidate the genetic cause of disease in CMT patients who remain without a genetic diagnosis.

Chapter 5 Exome sequencing in CMT

5.1 Introduction

The recent shift from traditional "first-generation" Sanger sequencing and linkage analysis to high-throughput NGS methods such as exome sequencing and whole-genome sequencing has revolutionised gene discovery and diagnostics for Mendelian and complex diseases (Choi et al., 2009; Metzker, 2010). NGS requires only 1-2 µg of gDNA and allows the investigation of small families and isolated individuals who could not have been studied using linkage or positional cloning (Singleton, 2011).

Exome sequencing involves target enrichment and high-throughput re-sequencing of nearly all protein-coding regions of the genome, including exons and flanking intronic sequences. Protein-coding regions make up only 1% of the genome and yet account for the vast majority (85%) of mutations associated with Mendelian diseases (Choi et al., 2009; Montenegro et al., 2011). Exome sequencing is more cost-efficient and less data-intensive than whole-genome sequencing, requiring only 5% of the sequencing needed for an entire human genome (Ng et al., 2010). Exome sequencing generally uncovers approximately 20,000 variants in a single European individual; on average, about 2% of these variants are novel (Bamshad et al., 2011). In 2009 and 2010, Choi et al. (2009) and Ng et al. (2010) demonstrated two of the first applications of exome sequencing and found the disease-causing gene in a small number of cases with rare monogenic disorders.

CMT disease is an excellent example of a Mendelian disease which has greatly benefited from the advent of NGS technologies. Indeed, the number of genes to be associated with peripheral neuropathies has nearly doubled in the past few years (Rossor et al., 2013). This NGS technology is especially time and cost-effective in highly penetrant, phenotypically and genetically heterogeneous diseases like CMT (Singleton, 2011). NGS may also uncover mutations in known but rare CMT genes for which testing is often restricted to the research setting (Montenegro et al., 2011). Novel CMT-associated genes or new mutations in known CMT genes were successfully identified using exome sequencing and whole-genome sequencing. In the early years of NGS, whole-genome sequencing was used to identify a mutation in a known CMT gene, *SH3TC2*, in an AR CMT family that did not carry mutations in

some of the common CMT genes (Lupski et al., 2010). Exome sequencing was also used to perform a comprehensive diagnostic screen in an undiagnosed CMT patient; the patient was found to carry a mutation in *GJB1*, a known CMT gene (Montenegro et al., 2011). One early example of a novel CMT gene identified with exome sequencing is *DYNC1H1*, a cause of axonal CMT (Weedon et al., 2011). In the past few years, many additional studies have used NGS to identify the genetic cause of disease in CMT patients. A recent study has performed exome sequencing in 25 unrelated CMT patients without the Chr17p11.2 duplication/deletion or mutations in major CMT genes; they focused on genes previously linked to CMT and found mutations in 32% of patients, thus highlighting the usefulness of exome sequencing in CMT (Choi et al., 2012).

Although the advent of NGS has enabled many CMT patients to receive a genetic diagnosis, many cases remain genetically undiagnosed. As discussed in Chapter 3, the UK study by Murphy, Laura, et al. (2012) determined that 62.6% of CMT patients seen at the inherited neuropathy clinic in Queen Square (London) received a genetic diagnosis; the proportion was 80.4% and 25.2% for CMT1 and CMT2 patients, respectively. In the Saporta et al. (2011) study, 67% of CMT patients were successfully assigned a genetic subtype. Therefore, many CMT genes remain to be unveiled, especially in CMT2. As highlighted previously, obtaining a genetic diagnosis is essential for patient counselling, family planning, and to exclude treatable acquired causes of neuropathy (Reilly et al., 2011).

Over 60 genes or loci have been associated with CMT (Braathen et al., 2011; Reilly et al., 2011). As discussed in the introduction to this Thesis, proteins encoded by CMT genes are involved in a wide array of cellular functions, some of which include myelin structural components, mitochondrial fusion and fission, endocytosis, intracellular protein sorting and quality control, transcription factors and regulation of gene expression, ion channels, protein synthesis, cytoskeletal dynamics, axonal transport and vesicular motility (Pandraud, in press; Patzkó & Shy, 2011). Furthermore, the expression of many CMT genes is not restricted to neurones or Schwann cells, and several genes had no prior known role in Schwann cells or axons (Scherer & Wrabetz, 2008). Ubiquitously expressed CMT genes include *FIG4*,

DNM2, *LMNA*, the t-RNA synthetases, *MTMR2*, *MTMR13*, *MFN2*, *RAB7*, *HSPB1*, *HSPB8* and others. The variety of protein functions and ubiquitous expression of many CMT genes render it difficult to identify the causative variant leading to peripheral nerve degeneration within the exome sequencing data. Identifying novel CMT genes and carrying out functional studies expands the list of pathomechanisms involved in CMT, allowing for a better understanding of peripheral nerve biology and neurodegeneration along with the discovery of potential drug targets (Azzedine et al., 2012).

5.2 Aims of this study

The first aim of this study was to identify the disease-causing gene in two CMT families without a genetic diagnosis; the second aim was to provide further evidence for the pathogenicity of a mutation in a candidate gene by screening this gene in a cohort of CMT patients.

5.3 Methods: exome sequencing of CMT families

5.3.1 CMT families for exome sequencing

Patients in this study were recruited from the inherited neuropathy clinic at the NHNN. DNA extracted from peripheral blood using standard procedures was obtained from the NHNN Neurogenetics Unit. Details of ethics approval and patient consent are found in Section 2.1.1.

Although comparatively less expensive and data-intensive than whole-genome sequencing, families for exome sequencing do have to be chosen strategically to maximise the probability of identifying the causative gene with this technology. Selection is often based on the number of previous genetic tests performed as well as availability of DNA and detailed phenotypes. Two CMT families were selected for exome sequencing in this study. Family IS was chosen because DNA and comprehensive phenotypes were available for three affected siblings; this family was negative for many CMT genes (detailed below). The second family, family AD, has dominantly inherited demyelinating CMT and most of the common genes have been excluded by Sanger sequencing; this family is therefore particularly interesting to

study as the vast majority of CMT1 patients have received a genetic diagnosis (Murphy, Laura, et al., 2012).

CMT family IS is from the United Kingdom; three siblings had late-onset CMT2 disease with intermediate NCVs. They had slowly progressive sensory symptoms in the lower limbs and mild walking difficulties starting in the fifth or sixth decade of life. One of the siblings required ankle-foot orthoses for mobility in the seventh decade of life; the other two siblings could walk without aid. Upon neurological examination of the index case (individual II-2 in Figure 5-1) at age 64, the patient had distal weakness, normal tone, lack of ankle jerk reflexes and reduced pinprick sensation in the feet. At age 53 his brother, individual II-3, had normal muscle power and tone in the upper and lower limbs, lack of right ankle jerk reflex, reduced pinprick sensation and reduced vibration sense to the knees in the lower limbs. At age 67 their sister, individual II-1, had bilateral foot drop, distal muscle wasting in the upper and lower limbs, normal ankle plantar flexion, and absent reflexes at the left ankle. Pinprick sensation was reduced in the hands and normal in the lower limbs. Vibration sense was reduced to the ankles bilaterally but normal in the upper limbs. All three siblings had similar neurophysiological results consistent with a length-dependent sensory-motor axonal neuropathy. Some of the motor NCVs were within the intermediate range; median NCVs were 37 m/s for individual II-2, 34 m/s for individual II-3 and 41 m/s for individual II-1. A fourth sibling (individual II-4) may be affected. According to his children's account, the father (individual I-2) developed bilateral foot drop in his early sixties, and required splints at the age of 65 years. Inheritance is presumed to be AD, however as the father was not examined in our clinic, AR inheritance cannot be ruled out. DNA was available on three affected siblings (individuals II-1, II-2 and II-3). One of the siblings was genetically tested and was negative for rearrangements on Chr17p11.2 and for mutations in *PMP22*, *MPZ*, *MFN2*, *EGR2*, *GDAP1*, *NEFL*, *TRPV4*, *HSPB1*, *HSPB8* and *GJB1*.

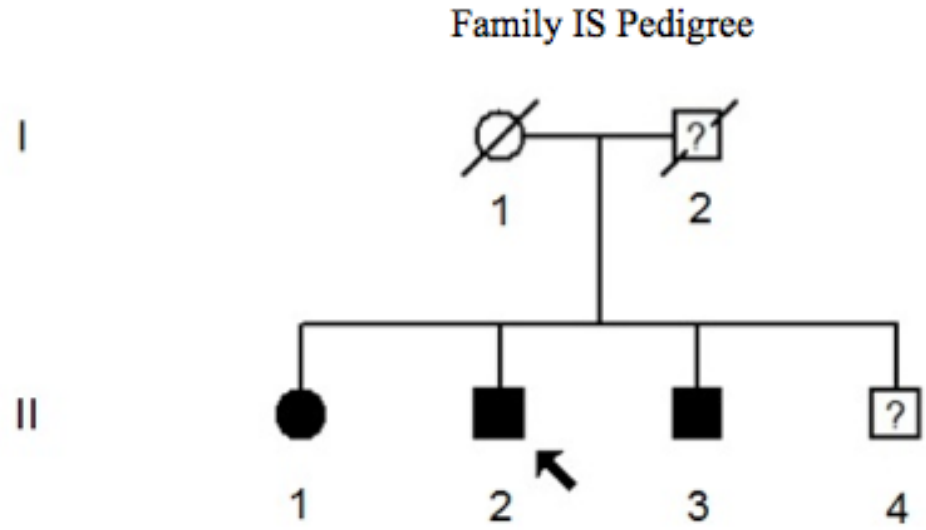

Figure 5-1 Pedigree of CMT family IS.

Affected members of CMT family AD, also from the United Kingdom, consisted of a mother (individual I-2 in Figure 5-2) and her daughter (individual II-I) who both had severe CMT1. The index case (individual I-2) was a 37-year old woman who presented with slowly progressive distal weakness and sensory loss in the upper and lower limbs. She walked abnormally from 13 months and was never able to run. She developed high arches during the first decade and had several operations to her feet. Her motor and sensory symptoms were slowly progressive. At 15 years old, her MNCV was 8.4 m/s in her right ulnar nerve. At the age of 37, she required crutches to walk and used a scooter for mobility outdoors. She had numbness in the lower limbs distally and occasional pain as well as pins and needles. On examination, she had distal muscle wasting in all limbs and no movement below the ankles. She had reduced pinprick sensation to the elbows and the top of the thighs, as well as no reflexes or plantar responses. She had inexcitable nerves on neurophysiology, except for the facial nerves for which she had reduced CMAP amplitudes and prolonged distal motor latencies.

DNA was available on the affected mother (individual I-2) and her affected daughter (individual II-1). Inheritance is predicted to be AD or X-linked (Figure 5-2). The consanguinity on the mother's side of the family is not predicted to be relevant. It

remains possible that inheritance is AR in this family if individual I-1 (father of II-1) and individual I-2 belong to an inbred population and are therefore distantly related, in which case individual I-1 may be a heterozygous carrier for the homozygous disease-causing mutation in individuals I-2 and II-1. However, this possibility is rather unlikely. Individual I-2 tested negative for rearrangements on Chr17p11.2 and for mutations in *PMP22*, *MPZ*, *EGR2*, *LITAF*, *NEFL*, *GJB1*, *GDAP1*, and *SH3TC2*.

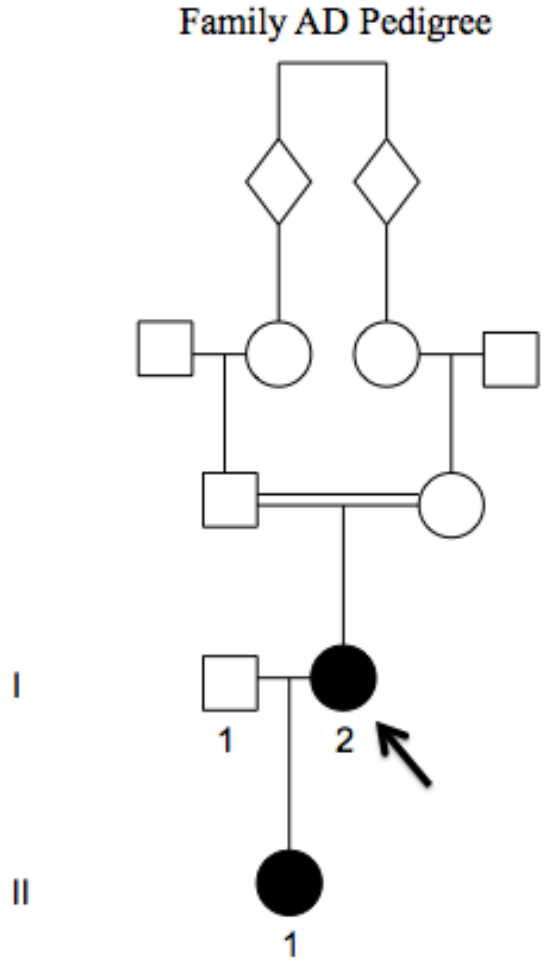

Figure 5-2 Pedigree of CMT family AD.

Given the previous successes of exome sequencing in CMT and the exclusion of several common CMT genes by Sanger sequencing, this NGS technology was used in this study. Exome sequencing was performed on individuals II-1, II-2 and II-3 in CMT family IS, and individuals I-2 and II-2 in CMT family AD.

5.3.2 Exome sequencing and variant calling

Purity and concentration of DNA samples were assessed as described in Section 2.1.5. gDNA (2 μg) was sent to the Wellcome Trust Sanger Institute in Hinxton, UK for exome sequencing. Exome sequencing was performed as part of the UK10K Project at the Wellcome Trust Sanger Institute. DNA was sheared to 100-400 bp segments using a Covaris E210 or LE220 (Covaris, USA). Sheared DNA was subjected to Illumina paired-end DNA library preparation and enriched for target sequences (Agilent Technologies, USA; Human All Exon 50 Mb - ELID S02972011) according to manufacturer's recommendations (Agilent Technologies; SureSelectXT Automated Target Enrichment for Illumina Paired-End Multiplexed Sequencing). Exome-enriched libraries were sequenced on the HiSeq platform as paired-end 75 base reads with v.3 chemistry according to the manufacturer's protocol (Illumina). Further details on the exome sequencing protocol are found in Section 2.1.15. Variant calling was performed by both the Wellcome Trust Sanger Institute and Dr Alan Pittman at the UCL ION.

5.3.3 Assessment of gene coverage and read depth in neuropathy genes

As described in Section 2.1.16, gene coverage and read depths were assessed for all known inherited neuropathy genes using the exome sequencing BAM files and Golden Helix GenomeBrowse software. The coverage could not be determined for individual II-2 in CMT family IS and individual I-2 in CMT family AD as no BAM files could be obtained.

5.3.4 Exome data filtering and variant prioritisation

The exome variant filtering steps are described in Section 2.1.17. Variants not found in all affected family members (three affected siblings in CMT family IS and affected mother/daughter pair in CMT family AD) were filtered out. Given the uncertainty of the inheritance pattern in CMT family IS, both heterozygous variants (AD model) and homozygous/compound heterozygous variants (AR model) were filtered independently. In CMT family AD, only heterozygous variants were selected in order to fit with the presumed AD or X-linked mode of inheritance. Next, synonymous mutations were filtered out. For all exome datasets, all known inherited neuropathy genes, including genes associated with HSP, were inspected for

potentially pathogenic variants. For the AD model in CMT families IS and AD, a MAF of 0.005 was used as a cut-off point for the EVS and 1000 Genomes control reference databases; a MAF of 0.01 was used as a cut-off point for the CG69 database as this database is known to contain variants at frequencies higher than that observed in other much larger control databases. A cut-off MAF of 0.005 is conservative compared to the 0.001 cut-off usually used in AD disorders (Bamshad et al., 2011). However, this higher cut-off was used to make certain that the potentially pathogenic variant would not be filtered out. In addition, the disease in CMT family IS was relatively mild. For the AR model in CMT family IS, a MAF cut-off of 0.01 was used for the EVS, 1000 Genomes and CG69 databases. A MAF of 0.01 still provides sufficient power in AR models (Bamshad et al., 2011). Any variant within a segmental duplication region with identity greater than or equal to 96% was removed. SNP chromosomal locations are based on Genome Build 37.3.

Candidate genes were searched in the literature for any known prior disease-association. The GEM.app, provided by University of Miami's Miller School of Medicine and described in Section 2.6, was used to search for variants in the candidate genes in families with similar phenotypes. Conservation between species of the mutated amino acid, location within the protein structure, and in-silico pathogenicity predictions were determined for variants of interest as described in Section 2.6. Gene expression data was obtained from the Human Protein Atlas as described in Section 2.6.

5.4 Methods: Sanger sequencing of a candidate gene from a previous exome sequencing study

A family with CMT2 (CMT family BJ) from our inherited neuropathy clinic in Queen Square was exome sequenced by the Department of Human Genetics and Hussman Institute for Human Genomics at University of Miami's Miller School of Medicine as part of a collaboration. The index case (individual IV-1 in Figure 5-3) suffered from falls, high arches and lower limb wasting from the age of two. He had slowly progressive distal wasting and sensory loss in the feet. Examination showed an unsteady gait, lack of reflexes, sensory loss in the hands, inability to stand on heels or toes, and mild proximal and distal weakness in the upper and lower limbs. An axonal sensory-motor neuropathy in the lower limbs was evident on NCS and

denervation and reinnervation were seen on muscle biopsy. The index case in this family was negative for mutations in *PMP22, MPZ, GJB1, MFN2, TRPV4, HSPB1, HSPB8, GDAP1,* and *BSCL2,* and for common mutations in the *polymerase (DNA directed), gamma* (*POLG*) and *progressive external ophthalmoplegia 1* (*PEO1*) genes. He also tested negative for common point mutations and large-scale rearrangements of mitochondrial DNA in the muscle.

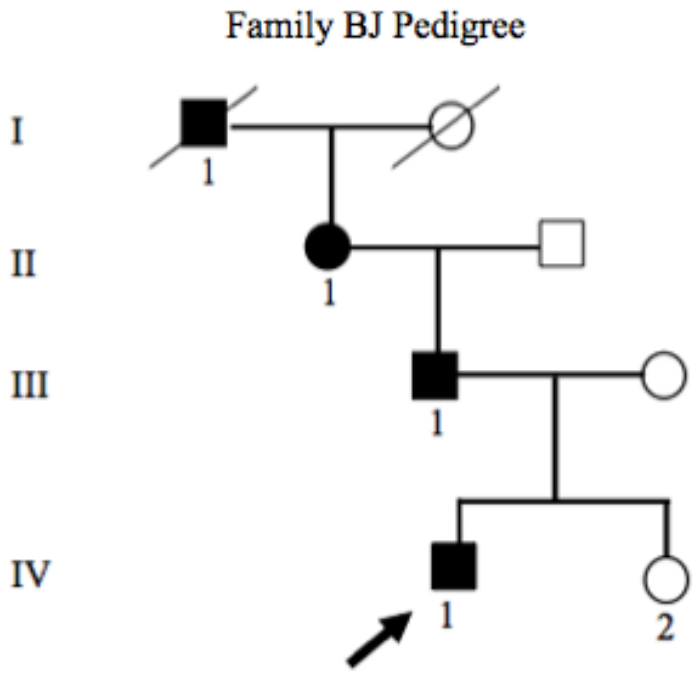

Figure 5-3 Pedigree of CMT family BJ.

One of the candidate genes emerging from the variant filtering performed by our colleagues was *mitochondrial fission factor* (*MFF*), encoding a protein with a role in mitochondrial fission (Gandre-Babbe & van der Bliek, 2008). The variant identified by our collaborators was p.Arg118His in exon 5 and was not found in over 2,000 controls. In an effort to provide additional evidence for the pathogenicity of this variant, I screened all coding exons and flanking intronic sequences of *MFF* in 48 CMT2 cases. Exon 5 was also screened in 285 additional patients with CMT2, dHMN or HSP. These additional 285 patients had a complex phenotype similar to that seen in CMT family BJ; these patients were selected by Professors Mary Reilly and Henry Houlden, consultant neurologists and professors in Clinical Neurology at

the NHNN. DNA was available at the NHNN Neurogenetics Unit. Purity and concentration of DNA samples were assessed as described in Section 2.1.5. PCR, agarose gel electrophoresis, purification of PCR products, Sanger sequencing, dye removal and sequencing analysis were performed using standard conditions as described in Sections 2.1.9-2.1.12. Sequences of *MFF* primers and PCR cycling conditions can be found in Appendix V Table V-1.

5.5 Results

5.5.1 The challenges of exome variant interpretation in CMT

In the exome data analysis of both CMT families in this study, hundreds of candidate genes containing variants of unknown significance still remained after the filtering steps described in Section 5.3.4. Predicted protein function and gene expression have been used in the past to select candidate genes in exome sequencing, however this is not always practical in diseases such as CMT. The discovery of over 60 CMT genes has provided a list of pathways which may be involved in disease pathogenesis. It remains difficult to stratify candidate genes based on the biological role of the protein because the defective biological process involved in a particular case of CMT may have never been previously described to cause inherited neuropathies (Azzedine et al., 2012; Bamshad et al., 2011). Of course, proteins with known roles in CMT-related processes were prioritised. For CMT family IS with ICMT, the protein function would be expected to involve both Schwann cells and axons (Azzedine et al., 2012); for CMT family AD with AD CMT1, myelin structural components and transcription factors regulating myelin gene expression would be potential candidate genes (Scherer & Wrabetz, 2008).

Transcriptional profiles of the PNS may provide a list of candidate genes for inherited peripheral neuropathies, however these lists are incomplete (De Jonge et al., 2003; Giambonini-Brugnoli et al., 2005). Genes therefore cannot be excluded on the basis that they are not found in transcriptional profiles of the PNS. In any case, it is difficult to exclude variants based on expression profiles as many CMT genes are ubiquitously expressed and not nerve-specific (Azzedine et al., 2012). Variants predicted to have a more severe functional impact on the protein such as stop-gain, stop-loss, indels, frameshift coding, and essential splice-site variants may be

prioritised, however there is a risk of eliminating potentially disease-causing missense variants.

5.5.2 Exome sequencing in an intermediate CMT (ICMT)/CMT2 family

The exome sequencing for individual II-1 of family IS resulted in a total of 75,912,176 reads. The mean target coverage was 83.7X (the definition of mean target coverage is provided in Section 2.1.16); 91.2% of the bases had at least 2-fold coverage, 84.3% of bases had at least 10-fold coverage and 72.3% of the bases had at least 30-fold coverage. The exome sequencing in individual II-3 of family IS produced a total of 74,978,099 reads. The mean target coverage was 81.4X; 91% of the bases had at least 2-fold coverage, 83.8% of bases had at least 10-fold coverage and 70.8% of the bases had at least 30-fold coverage. As mentioned in Section 5.3.3, the coverage could not be assessed for individual II-2 as the BAM file was not available.

Please see Appendix V Table V-2 for a list of poorly covered exons in inherited neuropathy genes in individuals II-1 and II-3 of CMT family IS. Overall, 21 inherited neuropathy genes had at least one poorly covered exon: *PMP22, MPZ, NEFL, NDRG1, PRX, FIG4, CTDP1, GARS, DNM2, DYNC1H1, LRSAM1, serine palmitoyltransferase, long chain base subunit 2* (*SPTLC2*), *LMNA, MTMR13, IGHMBP2, pyruvate dehydrogenase kinase, isozyme 3* (*PDK3*), *septin 9* (*SEPT9*), *DNA (cytosine-5-)-methyltransferase 1* (*DNMT1*), *HSPB1, kinesin family member 1A* (*KIF1A*) and *kinesin family member 5A* (*KIF5A*). In total, 19,681 variants were found in individual II-1, 20,593 in II-2 and 19,219 in II-3. The three affected siblings in CMT family IS shared 8,904 variants, 4,865 and 4,039 of which were homozygous and heterozygous, respectively. After filtering out synonymous mutations, 4,369 variants remained (2,394 homozygous and 1,975 heterozygous). Variants found in known inherited neuropathy genes among these 4,369 variants are summarized in Table 5-1. A total of 18 non-synonymous variants in 12 different neuropathy genes were found in CMT family IS, but none are likely to be the real pathogenic variant as the variants either had a high MAF in control databases, or the gene did not fit with the phenotype of the patient. Of course, it remains possible that mutations in a particular gene may result in a new phenotype. As mentioned in Section 5.3.4, both

an AD and an AR model were followed independently for variant filtering in CMT family IS. For the AD model, 93 heterozygous variants remained after filtering out variants in segmental duplications and those found in control databases using the frequency filters mentioned in Section 5.3.4. For the AR model, 28 compound heterozygous and 27 homozygous variants remained after applying these same filters. As mentioned in Section 5.1, choosing candidate genes based on protein function in CMT is potentially erroneous, as genes with a wide array of functions have been involved in this disease. Without exome data for additional family members, it is extremely difficult to narrow down the list of variants any further.

One variant, located in the *tubulin-specific chaperone cofactor E-like protein* (*TBCEL*) gene was however retained for further analysis. This gene was considered a candidate gene because a mutation in a related but unpublished gene, *tubulin, beta 8 class VIII* (*TUBB8*) found in a family with CMT2, was recently reported at the 5th International CMT Consortium Meeting in Antwerp, Belgium in June 2013 by a research group at University of Miami's Miller School of Medicine, USA.

All affected members of CMT family IS had a heterozygous non-synonymous mutation in the last coding exon of *TBCEL*, p.Met357Val (c.1069A>G) (Ensembl Transcript ID: ENST00000422003). The depth and quality of this variant were 55 and 772 in individual II-1, 34 and 418 in individual II-2, and 81 and 1,355 in individual II-3, respectively. The mutation is predicted to be located in a potential coiled-coil region of the ubiquitin-like domain (UniProtKB ID: Q5QJ74). This variant was not found in dbSNP, 1000 Genomes, CG69 or EVS control databases. It was predicted benign by SIFT and PolyPhen-2 (score=0.009), but disease-causing by Mutation Taster (score=0.57, probability=0.98694). It is conserved in vertebrates but not in *Drosophila melanogaster* or *Caenorhabditis elegans* (GERP score=2.93). Two families with peripheral neuropathy were found to carry mutations in this gene in the GEM.app. One family with pure HSP had a p.Ile359Val (c.1075A>G) mutation and one family with unspecified CMT carried a p.Trp242Stop (c.725G>A) mutation. In both cases, inheritance was AD and mutations segregated with the phenotype. The MAF in the GEM.app were 0.06 and 0.03 for p.Ile359Val and p.Trp242Stop, respectively.

TBCEL, located on chromosome 11, is 424 amino acids long and has eight exons, seven of which are coding exons. It contains seven leucine-rich domains, one leucine-rich C-terminal domain and one ubiquitin-like domain. According to the Human Protein Atlas, TBCEL is expressed ubiquitously at low to moderate levels, and is most highly expressed in the male reproductive system. TBCEL is moderately expressed in neuronal and glial cells in the cerebral cortex and peripheral nerve.

TBCEL is thought to play a role in spermatogenesis in animals (Nuwal et al., 2012). When overexpressed in-vitro, TBCEL depolymerises microtubules and targets tubulin to the proteasome for degradation; therefore, it is also thought to be involved in regulation of tubulin turnover and microtubule organisation (Bartolini et al., 2005). A non-synonymous mutation in *TBCEL* may cause microtubule disorganisation via a gain-of-function mechanism. Microtubules form part of the cytoskeleton and are essential for intracellular transport, including axonal transport. Many CMT genes encode proteins involved in the axon cytoskeleton, in vesicle formation and/or in axonal transport, and several CMT mutations result in defective axonal transport. These include such genes as *NEFL, RAB7, DNM2, DYNC1H1, HSPB1, heat shock 27kDa protein 3* (*HSPB3*), *HPSB8, LMNA*, *KIF1B* and *MFN2* (D'Ydewalle et al., 2012).

TBCEL shows sequence homology to *tubulin-specific chaperone cofactor E* (*TBCE*). In the mouse, a homozygous mutation in the *tubulin-specific chaperone E* (*Tbce*) gene causes a progressive motor neuronopathy associated with shortened axons and axonal swelling due to defects in tubulin assembly (Bommel et al., 2002). In humans, *TBCE* mutations cause Sanjad–Sakati syndrome, an AR disease characterised by hypoparathyroidism, mental retardation and dysmorphism (Padidela et al., 2009).

Further assessment of this candidate gene will be taken forward by another member of staff as this work was out of the remit of this PhD. To this end, the variant in *TBCEL* in CMT family IS has now been confirmed by Sanger sequencing to ensure that the mutation was not an artefact of exome sequencing.

5.5.3 Exome sequencing in a severe CMT1 family

The exome sequencing in individual II-1 of CMT family AD produced a total of 119,890,846 reads. The mean target coverage was 98X; 87.3% of the bases had at least 2-fold coverage, 80.7% of bases had at least 10-fold coverage and 72.5% of the bases had at least 30-fold coverage. As explained in Section 5.3.3, the coverage could not be assessed for individual I-2 as no BAM file could be obtained.

Please see Appendix V Table V-3 for a list of poorly covered exons in inherited neuropathy genes in individual II-1 of family AD. Overall, 24 inherited neuropathy genes had at least one poorly covered exon: *PMP22, NEFL, EGR2, NDRG1, PRX, FIG4, CTDP1, TRPV4, GARS, DNM2, DYNC1H1, LRSAM1, SPTLC1, SPTLC2, histidyl-tRNA synthetase* (*HARS*), *LMNA, MTMR13, IGHMBP2, PDK3, MARS, SEPT9, DNMT1, HSPB1* and *KIF1A*. In total, 19,619 variants were found in individual I-2 and 18,161 variants in individual II-1. These two individuals shared 10,339 variants. After filtering for the heterozygous variants, 5,207 variants remained. 2,614 variants were left after filtering out synonymous mutations. Variants found in known inherited neuropathy genes amongst these 2,614 variants are summarized in Table 5-2. A total of 8 non-synonymous variants in 7 different neuropathy genes were found; no variant was predicted to be the disease-causing variant as all variants were either found at a high MAF in control databases, or the gene did not fit with the patient's clinical description. A total of 181 variants remained after filtering out variants in areas of segmental duplication as well as variants found in control databases using the frequency filters mentioned in Section 5.3.4.

Amongst the list of remaining variants, a variant in *rho guanine nucleotide exchange factor 11* (*ARHGEF11*) was retained for further analysis. Mutations in *rho guanine nucleotide exchange factor 10* (*ARHGEF10*) were reported in an ICMT family and a CMT2 family at the 5th International CMT Consortium Meeting in Antwerp, Belgium in June 2013 (unpublished). A mutation in *ARHGEF10* with AD inheritance was also associated with slowed nerve conduction and thinly myelinated axons (Verhoeven et al., 2003).

Both individuals I-2 and II-1 of CMT family AD had a heterozygous non-synonymous mutation in *ARHGEF11*, p.Gly1393Arg (c.4177G>A) (Ensembl Transcript ID: ENST00000368194). This variant (dbSNP ID rs142548089) has a MAF of 0.001 in Europeans and 0.006 in individuals from Great Britain according to the 1000 Genomes database. Its MAF is 0.001047 in Europeans in the EVS database; it is not found in the CG69 database. This variant is not found in the GEM.app database; only common SNPs are reported for this gene in CMT patients in this database. SIFT, Polyphen-2 and Mutation Taster in-silico analyses predicted this variant to be pathogenic (Polyphen-2 score=0.995 (probably damaging); Mutation Taster score=3.41 with probability of 0.85118). This amino acid is highly conserved, with a GERP score of 4.92. According to the Human Protein Atlas, the ARHGEF11 protein is ubiquitously expressed with moderate to high expression in neuronal and glial cells in the brain and moderate expression in peripheral nerve. The depth and quality of this variant were 41 and 293.92 in individual I-2, and 47 and 678.29 in individual II-1, respectively.

ARHGEF11, located on chromosome 1, is 1,562 amino acids long and has 41 exons, all of which are coding exons. It acts as a guanine nucleotide exchange factor for RhoA GTPase. ARHGEF11 activates Rho/Rho kinase signalling and is involved in neurite retraction and actin cytoskeleton reorganisation (Banerjee & Wedegaertner, 2004; Togashi et al., 2000). GTPases of the Rho subfamily play a role in myelination in the nervous system; furthermore, mutations in the Rho GTPase guanine nucleotide exchange factor *Frabin/FGD4* are known to cause CMT (Stendel et al., 2007).

Additional analysis of *ARHGEF11* will be performed by another member of staff, as is the case for the candidate gene in CMT family IS. The *ARHGEF11* mutation in CMT family AD needs to be confirmed by Sanger sequencing. For both CMT families IS and AD, segregation of the variants in the families needs to be performed. If the candidate variants do not segregate, additional family members for which DNA is available could be exome sequenced to further narrow down the list of remaining variants. Exome sequencing of the father (individual I-2) in family IS would reduce the final list of remaining variants by about 50%, and exome sequencing the fourth, possibly affected sibling (individual II-4) would reduce it by

about 25%. Performing exome sequencing on both parents of individual I-2 in family AD would have been ideal as parent-child trios are very informative in identifying de novo mutations; indeed, multiple de novo events within a single gene or pathway are rare (Bamshad et al., 2011). Unfortunately, DNA was not available for these individuals. Furthermore, *TBCEL* and *ARHGEF11* should be screened in a large number of in-house CMT cases with a similar phenotype, as well as in controls of matching ethnicity. The exons of CMT genes poorly covered by exome sequencing should also be Sanger sequenced. Finally, functional studies will be necessary to provide further evidence of pathogenicity.

Table 5-1 Variants identified in known inherited neuropathy genes in CMT family IS.

Gene	Position	Reference allele	Observed allele	Amino acid change	Type	Functional change	Call	1000 Genomes MAF	EVS MAF	CG69 MAF	dbSNP ID
PRX	40900865	C	T	p.Gly1132Arg	exonic	nonsynonymous	hom	0.96	0.953791	0.942	rs268674
HK1	71060610	A	G	p.His7Arg	exonic	nonsynonymous	hom	0.91	0.920655	0.826	rs906220
LRSAM1	130242166	A	G	p.Asn318Asp	exonic	nonsynonymous	hom	0.74	0.741809	0.703	rs1539567
ASAH1	17918934	A	G	p.Val262Ala	exonic	nonsynonymous	hom	0.86	0.8666	0.833	rs10103355
GALC	88401213	T	C	p.Thr641Ala	exonic	nonsynonymous	hom	0.94	0.959477	0.942	rs421262
IGHMBP2	68678962	T	C	p.Leu201Ser	exonic	nonsynonymous	het	0.7	0.778565	0.775	rs560096
IGHMBP2	68705674	C	A	p.Thr879Lys	exonic	nonsynonymous	het	0.23	0.210117	0.196	rs17612126
WNK1	994487	G	C	p.Cys1506Ser	exonic	nonsynonymous	hom	0.99	0.986083	0.993	rs7955371
SCN9A	167099158	A	G	p.Trp1150Arg	exonic	nonsynonymous	hom	0.89	0.877448	0.855	rs6746030
SETX	135203231	C	T	p.Gly1252Arg	exonic	nonsynonymous	hom	0.59	0.693065	0.645	rs1183768
SETX	135202829	T	C	p.Ile1386Val	exonic	nonsynonymous	hom	0.59	0.693757	0.645	rs543573
SETX	135203409	A	C	p.Asp1192Glu	exonic	nonsynonymous	hom	0.66	0.792942	0.739	rs1185193
ZFYVE26	68234539	T	C	p.Asn1891Ser	exonic	nonsynonymous	hom	0.92	0.941719	0.92	rs3742883
DST	56463410	T	C	p.Gln1308Arg	exonic	nonsynonymous	het	0.34	0.381045	0.391	rs4712138
DST	56470551	T	A	p.Thr2422Ser	exonic	nonsynonymous	het	0.27	0.307263	0.29	rs13194995
DST	56471402	G	A	p.Pro2464Leu	exonic	nonsynonymous	het	0.37	0.432662	0.442	rs9382658
DST	56482801	C	G	p.Val2011Leu	exonic	nonsynonymous	het	0.4	0.469245	0.449	rs6459166
ATM	108183167	A	G	p.Asn1983Ser	exonic	nonsynonymous	hom	1	N/A	1	rs659243

Table 5-2 Variants identified in known inherited neuropathy genes in CMT family AD.

Gene	Position	Reference allele	Observed allele	Amino acid change	Type	Functional change	Call	1000 Genomes MAF	EVS MAF	CG69 MAF	dbSNP ID
KARS	75661803	G	C	p.Thr623Ser	exonic	nonsynonymous	het	0.11	0.136504	0.13	rs6834
SBF2	9879838	C	T	p.Glu679Lys	exonic	nonsynonymous	het	0.06	0.078522	0.065	rs7102464
GAN	81411091	C	G	p.Pro562Ala	exonic	nonsynonymous	het	0.0037	0.003384	NA	rs79901179
AP4B1	114438951	A	G	p.Leu480Ser	exonic	nonsynonymous	het	0.35	0.437952	0.312	rs1217401
WNK1	990912	A	C	p.Thr1056Pro	exonic	nonsynonymous	het	0.85	0.852606	0.826	rs956868
SPG11	44918690	C	T	p.Ala695Thr	exonic	nonsynonymous	het	0.01	0.009698	N/A	rs78183930
SPG11	44944037	C	T	p.Glu370Lys	exonic	nonsynonymous	het	0.01	0.014624	N/A	rs77697105
ZFYVE26	68249499	C	T	p.Cys1457Tyr	exonic	nonsynonymous	het	0.19	0.263494	0.167	rs2235967

5.5.4 Sanger sequencing of a candidate gene from a previous exome sequencing study

The p.Arg118His variant in *MFF* was not detected in our cohort of 333 CMT2/HSP/dHMN patients. All variants detected in *MFF* in this cohort were known polymorphisms and were not predicted to be pathogenic (refer to Appendix V Table V-4 for list of variants found in *MFF*). *MFF* was one of several candidate genes retained for further analysis by colleagues at University of Miami's Miller School of Medicine in this CMT family. Upon additional genetic and functional studies, another candidate gene, *trafficking protein kinesin binding 2* (*TRAK2*), was subsequently considered more likely to be the true disease-causing variant in CMT family BJ (unpublished). *TRAK2* encodes a protein needed for mitochondrial transport in axons and dendrites; specifically, it connects mitochondria to motors on microtubules (Van Spronsen et al., 2013). However, studies in other CMT families performed by the University of Miami's Miller School of Medicine now suggest that *TRAK2* is in fact unlikely to be the causative gene. *MFF*, which had not been firmly excluded, as well as other candidate genes, are being further evaluated by our colleagues.

5.6 Discussion

This study has identified candidate disease-causing variants in two CMT families who have so far remained without a genetic diagnosis. These results are very preliminary; as mentioned previously, further assessment of pathogenicity will be carried out by another member of staff as this work could not be carried out within the timeframe of this study.

Although exome sequencing is often considered the gold standard for identifying novel disease genes or assigning novel phenotypes to known disease genes, this view is perhaps biased as negative exome sequencing results are rarely published (Bamshad et al., 2011). In our experience, many families for which exome sequencing has been performed remain without a genetic diagnosis. In the event that a suitable candidate gene is selected for further study, there remains the significant hurdle of proving its pathogenicity. Comparative genomics are sometimes considered one of the most accurate measures of deleteriousness, although there are some

exceptions (Bamshad et al., 2011). In vitro studies may be helpful but are not definitive; a deleterious effect on the molecular level will not always cause a phenotype in an organism. Using an inappropriate cell type or outcome measure may also lead to false negative or false positive results (Bamshad et al., 2011). Furthermore, severe functional disturbances in vitro have been known to occur as a result of mutations found in control individuals; similarly, certain known pathogenic mutations have not been found to cause defects in vitro (Kochañski, 2006).

It is possible that the mutation causing CMT in these two families was not detected. Exome sequencing will not reveal large indels, duplications, translocations and repeat sequences (Singleton, 2011). Variants outside of coding regions which may be disease-causing are also not detected, such as in introns, promoters, microRNAs or UTRs. Another limitation of exome sequencing is that coverage is not always sufficient or homogeneous throughout the genome; for example, the first exon in a gene is commonly missed (Azzedine et al., 2012; Bamshad et al., 2011; Singleton, 2011). Synonymous mutations were excluded during filtering but the effect of these variants is not necessarily neutral (Parmley & Hurst, 2007). The mutation may also be located in a poorly covered gene or in an as-of-yet uncharacterised gene. Technical problems with mapping or alignment cannot be discarded as well (Bamshad et al., 2011).

In addition to its role in novel-gene identification, exome sequencing allows simultaneous testing of all CMT genes with relatively little DNA, and in this regard is faster and cheaper than Sanger sequencing of individual genes (Rossor et al., 2013). It may uncover variants in CMT genes which were previously screened but in which the variant was missed. Although the cost of exome sequencing, as well as the lack of complete gene coverage, prevent it from being used for routine testing at present, it is predicted that exome sequencing will become a diagnostic screening tool within the next few years (Azzedine et al., 2012). As discussed in Chapter 3, since 92% of CMT patients in the Saporta et al. (2011) study had a Chr17p11.2 duplication/deletion or mutation in *MPZ, GJB1,* or *MFN2*, these genes should still be tested by Sanger sequencing first, as appropriate for each patient (Amato & Reilly,

2011). In addition to identifying rare variants, exome sequencing may become a useful tool to detect modifier genes and risk factors.

5.7 Conclusion

This Chapter has highlighted the difficulties of exome sequencing, particularly in diseases such as CMT caused by defects in a wide array of biological pathways. An undisputable challenge of exome sequencing is to identify the disease-causing variant among the large number of potentially pathogenic variants remaining after extensive filtering. The mutations in the candidate genes identified in this study will be subject to further genetic and functional analyses to support their pathogenicity. Despite its limitations, exome sequencing remains an effective way to identify causal variants in CMT patients who are negative for the common CMT genes. The advantages of exome sequencing include rapidity, low cost and the possibility of screening nearly all protein-coding regions of the genome in parallel with only 2 μg of DNA.

Chapter 6 Screening of riboflavin transporter genes and searching for novel genetic causes of BVVL and related neuropathies

6.1 Introduction

6.1.1 Riboflavin transporter mutations as a novel cause of hereditary sensory-motor neuropathy

Exome sequencing has been used by our group and colleagues to identify the genetic cause of disease in patients suffering from BVVL. As described in Section 1.6.1, BVVL syndrome is a childhood-onset, progressive pontobulbar palsy with sensory-motor neuropathy, bilateral sensorineural hearing loss and respiratory insufficiency; it is often fatal in childhood due to respiratory failure (Brown, 1894; Van Laere, 1966; Vialetto, 1936). The phenotype of BVVL may overlap with that of ALS and SMA, as discussed previously (Green et al., 2010; Horvath et al., 2012), and is also likely allelic with FL syndrome (Fazio, 1892; Londe, 1893; Londe, 1894). As detailed in Section 1.6.3, homozygous and compound heterozygous mutations in *SLC52A2* and *SLC52A3*, encoding human riboflavin transporters RFVT2 and RFVT3 respectively, have recently been found in several BVVL patients using exome and Sanger sequencing (Anand et al., 2012; Bandettini di Poggio et al., 2013; Bosch et al, 2011; Ciccolella et al., 2012; Ciccolella et al. 2013; Dezfouli et al., 2012; Green et al., 2010; Haack et al., 2012; Johnson, Gibbs, et al., 2010; Johnson et al., 2012; Koy et al., 2012; Yamamoto et al., 2009; Yao et al., 2010). Haploinsufficiency in *SLC52A1*, encoding RFVT1, was associated with mild maternal riboflavin deficiency and a riboflavin-responsive MADD (RR-MADD)-like biochemical profile in her newborn infant (Chiong et al., 2007; Ho et al., 2010; Yonezawa et al., 2008). No treatment had previously proven successful in BVVL patients (Sathasivam, 2008); these genetic discoveries have uncovered high-dose riboflavin therapy as a potential treatment for BVVL patients with riboflavin transporter mutations, with clinical and biochemical improvements evident in most patients (Bosch et al., 2012). It is likely that many patients with mutations in these riboflavin transporters who may benefit from riboflavin therapy remain to be identified.

Defective riboflavin transport as a result of mutations in the riboflavin transporters causes decreased intracellular levels of riboflavin and its active coenzyme forms, FAD and FMN (Bosch et al., 2011). FAD and FMN are components of

flavoenzymes and flavoproteins and are therefore needed for a wide range of cellular functions, including energy metabolism, glutathione recycling, oxidative protein folding, DNA repair, and others (Section 1.6.6) (Lienhart et al., 2013; Massey, 2000).

The mechanisms of riboflavin absorption, transport, metabolism and homeostasis will now be described; this will be followed by a description of the mutations which have been described to date in the riboflavin transporters.

6.1.2 Riboflavin absorption, transport and metabolism

As mentioned in Section 1.6.6, unlike plants and many microorganisms, humans cannot synthesise riboflavin and thus need to obtain it from exogenous sources in the diet (McCormick, 1989; Northrop-Clewes & Thurnham, 2012). The riboflavin synthesized by the microflora of the large intestine in humans provides only a minor percentage of the riboflavin needed for health (Powers, 2003). Although a small amount of riboflavin is actually required by the body, the symptoms associated with riboflavin deficiency (as delineated in Section 1.6.4) clearly demonstrate that this vitamin is an essential micronutrient (Northrop-Clewes & Thurnham, 2012).

Most riboflavin in food is found in the form of FAD, and a lesser portion is found as FMN and free riboflavin. FAD and FMN must be released from flavoproteins by gastric proteases during digestion, and hydrolysed by pyrophosphatases and phosphatases to free riboflavin for absorption (Henriques et al., 2010; McCormick, 1989; Powers, 2003, Said & Mohammed, 2006). Free riboflavin is then absorbed at the luminal surface of the epithelial cells in the proximal small intestine (Levy & Jusko, 1966); the riboflavin uptake process via specialised transporters will be described below. In the blood, the riboflavin level increases fastest in the plasma, and slowly equilibrates between the plasma and the blood erythrocytes (Stripp, 1965). Upon entering circulation, riboflavin is distributed throughout the body and into target tissues. In the plasma, most of the free riboflavin associates with other proteins such as albumin and immunoglobulins (McCormick, 1989). In humans, a very low amount of riboflavin is stored in the body; the highest levels of its coenzyme forms FMN and FAD were found in kidney and liver (Burch et al., 1956; McCormick,

1989). It is also stored in the spleen and cardiac muscle in minute quantities (Depeint et al., 2006). The kidney controls riboflavin excretion as a large portion of filtered riboflavin is re-absorbed at the luminal surface of renal urinary ducts; when plasma concentrations of riboflavin are too high (above 0.5 μM), the excess is excreted in the urine (Kumar et al., 1998; Moriyama, 2011; Spector & Johanson, 2006). Therefore, the intestines and kidney are critical in maintaining riboflavin homeostasis in the body (Subramanian et al., 2013).

Riboflavin is absorbed very rapidly in humans (Levy & Jusko, 1966; Zempleni et al., 1996); given the size of this substance (molecular weight of 376.36) and its lipid-insoluble nature, a specialised transport mechanism was suspected to be more likely than absorption by passive diffusion only (Levy & Jusko, 1966). The amount of riboflavin that would be allowed through by passive diffusion would likely not be sufficient to meet the cell's requirement (Fujimura et al., 2010). Indeed, the majority of in vitro studies using various human cell lines have found evidence of an energy-dependent, largely Na^+-independent, highly specific, and saturable carrier-mediated system for riboflavin uptake (Foraker et al., 2003; Huang & Swaan, 2001; Kansara et al., 2005; Kumar et al., 1998; Levy & Jusko, 1966; Said & Ma, 1994; Said et al., 1998). Riboflavin synthesised by bacteria in the colon is also absorbed efficiently by a similar mechanism (Said & Mohammed, 2006). When given orally, absorption decreased with increasing dose, showing evidence of tissue saturation (Levy & Jusko, 1966; Zempleni et al., 1996); the excretion rate decreased exponentially with time and the absorption half-life was 1.1 h on average (Levy & Jusko, 1966). Pharmacokinetic variables for riboflavin absorption did not exhibit gender differences (Zempleni et al., 1996). A fraction of the administered riboflavin was rapidly eliminated early on, while a second fraction was excreted more slowly after several hours; this was not significantly dependent on dose or route of administration and suggests the presence of a peripheral compartment (likely uptake into cells and tissues) in riboflavin distribution (Levy & Jusko, 1966; Zempleni et al., 1996). Although a saturable carrier system predominated when intake of riboflavin was low or normal, at higher intakes or when plasma concentrations were higher than 12 nM, transport occurred principally by passive diffusion (Feder et al., 1991; Foraker et al., 2003; McCormick, 1989). It has been suggested that the maximal absorption for

pharmacological doses of riboflavin administered orally is 25-27 mg per dose, and that unused riboflavin is excreted within 8 to 24 h following the intake (Gregersen, 1985; Zempleni et al., 1996). However, there is enhanced absorption of higher doses of riboflavin when taken orally after a meal, possibly due to decreased transit in the intestine and therefore prolonged exposure to intestinal sites of absorption (Levy & Jusko, 1966).

Once inside the cell, riboflavin kinase converts riboflavin to FMN, most of which is then converted to FAD by FAD synthetase in an ATP-dependent process (Henriques et al., 2010; McCormick, 1989). Whether the conversion of riboflavin to FMN and FAD occurs only in the cytosol has long been a subject of controversy; however, recent evidence suggests that FAD synthesis can also occur in the mitochondria and in the nucleus after uptake of riboflavin into these organelles via an uncharacterised carrier-mediated process (Barile et al., 2000; Depeint et al., 2006; Giancaspero et al., 2013; Henriques et al., 2010; McCormick, 1989). FAD in the mitochondria can be incorporated into flavoproteins or reconverted to free riboflavin in the outer mitochondrial membrane by FAD pyrophosphatase and FMN phosphohydrolase (Bafunno et al., 2004; McCormick, 1989). The *FLX1* gene in *Saccharomyces cerevisiae* encodes an FAD transporter protein on the mitochondrial membrane necessary for the balance of flavin nucleotides in yeast mitochondria (Bafunno et al., 2004; Tzagoloff et al., 1996). The human orthologue of FLX1, the mitochondrial folate transporter (MFT), is a mitochondrial FAD transporter which may be involved in FAD export from the mitochondria (Spaan et al., 2005). Although the studies described above would suggest a riboflavin-FAD cycle in the cell as a recycling pathway (Barile et al., 2000), the exact mechanism used by the cell to maintain flavin homeostasis is still uncertain, and no mammalian mitochondrial or nuclear riboflavin transporter has been characterised to date (Giancaspero et al., 2013).

As with many membrane-bound transporter systems, riboflavin uptake is thought to be regulated by signalling pathways including the protein kinase A (PKA) pathway and the calcium/calmodulin-mediated pathways with variations between tissues (Foraker et al., 2003; Kansara et al., 2005; Kumar et al., 1998; Patel et al., 2012; Said et al., 1994). Calmodulin inhibitors, as well as compounds such as forskolin which

activate the PKA pathway by increasing intracellular cyclic adenosine monophosphate (cAMP) levels, were found to decrease riboflavin uptake (Foraker et al., 2003; Kansara et al., 2005; Patel et al., 2012; Said et al., 1994). Riboflavin transport was also regulated by extracellular levels of riboflavin; deficiency and high-dose supplementation of riboflavin led to up and down-regulation of riboflavin uptake in the intestine, respectively (Said & Ma, 1994; Said & Mohammed, 2006).

The minimal required daily intake of riboflavin is determined by factors including tissue growth/metabolic demand, respiratory infections, age, dietary intake/fasting, absorption and transport, FMN/FAD synthesis, and mitochondrial metabolism and transport (Hustad et al., 2002; Vergani et al., 1999). Growing children and pregnant women have a higher demand for riboflavin (Gregersen, 1985). Riboflavin was mobilised from tissue to blood during respiratory infections in humans and mice, and urinary excretion of riboflavin increased (Hustad et al., 2002; Prasad et al., 1991). These studies may provide an explanation for the observation that BVVL is often initiated or worsened by events such as viral infection and fever, as discussed in Section 1.6.1.

The median baseline blood plasma concentrations of riboflavin, FMN and FAD in human subjects were determined to be 10.5 nM, 6.6 nM and 74 nM, respectively, with riboflavin displaying much greater variability (Hustad et al., 2002; Zempleni et al., 1996). Although riboflavin and FMN levels increased significantly upon riboflavin supplementation in riboflavin-deficient individuals, levels of FAD in plasma did not increase. FAD levels have also been found to remain relatively more stable compared to riboflavin levels during the development of riboflavin deficiency in humans and monkeys (Burch et al., 1956; Hustad et al., 2002). A homeostatic mechanism probably exists to regulate and maintain levels of flavin coenzymes in the tissues, especially that of FAD (Hustad et al., 2002).

6.1.3 Identification and characterisation of the riboflavin transporters

Riboflavin transporters have been identified in other species, including the RibU protein in *Lactobacillus lactis* (Burgess et al., 2006) and the Mch5p protein in *Saccharomyces cerevisiae* (Reihl & Stolz, 2005). Although a carrier-mediated

mechanism for transport of riboflavin and homeostasis of riboflavin levels throughout the body had been suspected for decades from studies of human-derived cell lines (Foraker et al., 2003; Huang & Swaan, 2001; Kansara et al., 2005; Kumar et al., 1998; Levy & Jusko, 1966; Said & Ma, 1994; Said et al., 1998), human riboflavin transporters (encoded by *SLC52A1, SLC52A2* and *SLC52A3*) were only recently cloned from human tissues (Fujimura et al., 2010; Subramanian, Subramanya, et al., 2011; Yamamoto et al., 2009; Yao et al., 2010; Yonezawa et al., 2008). These transporters showed no similarity to riboflavin transporters described in other species or to other SLC transporters (Foraker et al., 2003; Yonezawa et al., 2008; Yonezawa & Inui, 2013).

RFVT1 was the first member of this new mammalian riboflavin transporter family to be identified based on its similarity to the rat rRFVT1 with which it shares 87% similarity (Yonezawa et al., 2008). This transporter is encoded by *SLC52A1*, a gene with five exons (four coding exons) on Chr17p13.3. This gene was first known as *GPR172B*, however it is not related to G-protein coupled receptor proteins (Yao et al., 2010). *SLC52A1* has two mRNA transcript variants (GenBank accession numbers NM_017986 and NM_001104577); the two transcripts differ only in the 5'UTR and encode the same protein of 448 amino acids (NP_001098047.1 and NP_060456.3). The protein is predicted to have eleven transmembrane domains (TMHMM v.2 prediction). RFVT1 is most highly expressed in the placenta and also has high expression in the small intestine and in the colon. It has very low expression in the CNS, and overall is expressed at lower levels throughout the body than RFVT2 and RFVT3 (Yao et al., 2010; Yonezawa et al., 2008). Expression in the small intestine suggests a role of RFVT1 in riboflavin uptake from food into the blood. Furthermore, its expression in the colon suggests it is important for absorption of riboflavin synthesized by the bacterial microflora of the large intestine (Yonezawa et al., 2008). It is worthy of note that RFVT1 is highly expressed in the placenta, which may explain the phenotype seen in the infant of a riboflavin-deficient mother with haploinsufficiency of *SLC52A1* (Chiong et al., 2007; Ho et al., 2010).

RFVT3, encoded by *SLC52A3*, was the second member of the riboflavin transporter family to be identified based on its 83% similarity to the rat rRFVT3 (Fujimura et al.,

2010; Yamamoto et al., 2009). The rat rRFVT3, highly expressed in the small intestine, was originally identified due to its similarity to a putative bacterial riboflavin transporter, impX (Yamamoto et al., 2009). *SLC52A3* has five exons (four coding exons) and is located on Chr20p13 (GenBank accession number NM_033409). The encoded protein is 469 amino acids long (NP_212134.3) and is predicted to have eleven transmembrane domains (TMHMM v.2 prediction). RFVT3 is highly conserved across species. It is most highly expressed in the testes, and is also highly expressed in the small intestine and prostate (Yao et al., 2010); its expression was also detectable in skeletal muscle, spinal cord, colon, kidney and stomach (Fujimura et al., 2010; Yamamoto et al., 2009). RFVT3 is moderately expressed in the CNS, with minimal expression in the brain (Yamamoto et al., 2009; Yao et al., 2010). Polymorphisms in this gene have been found to modulate susceptibility to oesophageal squamous cell carcinoma (Wei et al., 2013); similarly, decreased plasma riboflavin levels resulting from defective expression of *SLC52A3* have been associated with development of gastric carcinoma (Eli et al., 2012). Two orthologues of RFVT3 encoded by the riboflavin transporter genes *rft-1* and *rft-2* have been recently identified in *Caenorhabditis elegans*, which also lack the ability to synthesise riboflavin. Both of these orthologues are expressed in the intestine and rft-1 shared transport characteristics with RFVT3. Knocking down these transporters resulted in a severe loss of fertility. As expected, there was a drop in *rft-1* mRNA when worms were supplemented with riboflavin (Biswas et al., 2013).

SLC52A2 encodes RFVT2, the third riboflavin transporter to be identified. *SLC52A2*, a gene with five exons (four coding) on Chr8q24.3, was discovered on the basis of its homology to *SLC52A1* (Yao et al., 2010). The gene has three mRNA transcript variants (GenBank accession numbers NM_024531.4, NM_001253816.1 and NM_001253815.1); the transcripts differ only in the 5'UTR and encode the same protein of 445 amino acids (NP_001240745.1, NP_078807.1 and NP_001240744.1) with eleven predicted transmembrane domains (TMHMM v.2 prediction). Unlike RFVT1 and RFVT3, RFVT2 is expressed ubiquitously but is particularly highly expressed in the brain, foetal brain, spinal cord and salivary gland (Yao et al., 2010). RFVT1 and RFVT2 were initially reported to act as receptors for porcine endogenous retrovirus subgroup A, but their function had not been fully elucidated

until recently (Ericsson et al., 2003). RFVT3 shares 43% amino acid identity with RFVT1, while RFVT2 shares 87% and 44% amino acid identity with RFVT1 and RFVT3, respectively (Yamamoto et al., 2009; Yao et al., 2010).

Initial experiments in transfected HEK293 cells confirmed localisation of all transporters at the cellular plasma membrane (Yao et al., 2010). The uptake of [^{3}H]-riboflavin via all three transporters increased in a time and concentration-dependent manner (Yao et al., 2010). In human intestinal epithelial cells in vitro, riboflavin uptake via RFVT3 was significantly higher than uptake via RFVT1 and RFVT2 (Subramanian, Subramanya, et al., 2011). RFVT1 had low riboflavin transport activity in Caco-2 cells (Yonezawa et al., 2008). RFVT1, RFVT2 and RFVT3 had similar substrate specificities and uptake for all three transporters was independent of extracellular Na^{+} and Cl^{-} (Yao et al., 2010). Although certain previous in vitro studies had found riboflavin transport to be independent of extracellular Na^{+}, other carrier-mediated mechanisms for riboflavin uptake in intestinal cells had been found to be Na^{+}-dependent, suggesting that other transporters of riboflavin may exist (Foraker et al., 2003; Fujimura et al., 2010). Riboflavin transport via RFVT3 in HEK293 cells favoured a slightly acidic pH, while transport via RFVT1 and RFVT2 was pH-independent (Yamamoto et al., 2009; Yao et al., 2010). Transport via all three transporters was strongly inhibited by riboflavin and riboflavin analogues such as lumiflavin, and was moderately inhibited by FMN. FAD only slightly inhibited uptake via the RFVT2 transporter therefore it is likely that riboflavin is principally carried across the plasma membrane. Transport through all transporters was not inhibited by D-ribose, indicating that the isoalloxazine ring of riboflavin is necessary for transporter recognition (Fujimura et al., 2010; Yao et al., 2010; Yonezawa & Inui, 2013). Therefore, both the amino acid sequence and mechanistic characteristics of riboflavin transport of RFVT2 are more similar to that of RFVT1 than that of RFVT3 (Yao et al., 2010). Overall however, additional research is needed to further elucidate the riboflavin transport mechanisms via the RFVTs (Moriyama, 2011).

In the enterocyte of the intestine, riboflavin is transported first across the apical brush-border membrane domain, and subsequently across the basolateral membrane domain (Subramanian, Subramanya, et al., 2011). RFVT3 was located exclusively at

the apical brush border membrane domain in human-derived Caco-2 cells and in the renal MDCK cell line, therefore RFVT3 is likely responsible for riboflavin uptake on the luminal surface of the small intestine (Fujimura et al., 2010; Subramanian, Rapp, et al., 2011; Yoshimatsu et al., 2014). In these cell lines, intracellular trafficking of RFVT3 involved vesicular structures and required an intact microtubule network; the velocity of the vesicles was temperature-dependent (Subramanian, Rapp, et al., 2011). In Caco-2 cells and MDCK cells, RFVT1 was mainly localised at the basolateral membrane of polarised enterocytes, although some RFVT1 was retained in intracellular vesicles; RFVT2 was localised mostly in intracellular vesicles (most likely endosomes) but was also found at the basolateral membrane of some cells (Subramanian, Subramanya, et al., 2011; Yao et al., 2010). While the intracellular trafficking vesicles containing tagged RFVT1 and RFVT2 co-localised with lysosomal-associated membrane protein 1 (LAMP1), a late endosomal and lysosomal marker, RFVT3 did not co-localise with LAMP1 (Subramanian, Subramanya, et al., 2011). The localisation of RFVT2 within endosomes of intestinal cells may suggest that its translocation to and from the basolateral membrane can be regulated (Subramanian, Subramanya, et al., 2011).

Given their high expression in the small intestine, RFVT1 and RFVT3 are probably mainly responsible for distribution of riboflavin from the intestinal lumen (i.e. from food) into the blood by intestinal epithelial cells, although RFVT3 was the most efficient at transporting riboflavin in native human intestinal cells (Fujimura et al., 2010; Subramanian, Subramanya, et al., 2011; Yao et al., 2010). The different localisation of RFVT1 and RFVT3 in polarised epithelial cells suggests that transport of riboflavin from the lumen to the bloodstream occurs via two transporters sequentially: RFVT3 followed by RFVT1. It is probable that *SLC52A1* and *SLC52A3* mutations result in deficient uptake of riboflavin from food, leading to the decreased plasma flavin levels seen in these BVVL patients (Bennett, 2012). It may be that the effects of haploinsufficiency of RFVT1 can be prevented via compensation by RFVT3, however this remains to be investigated. RFVT2 may provide further opportunity for regulating riboflavin homeostasis in the intestine and is likely to be important for riboflavin homeostasis and energy metabolism in the brain (Fujimura et al., 2010; Subramanian, Subramanya, et al., 2011; Yao et al., 2010). Its lower

expression in the small intestine may provide a rationalisation for the normal levels of flavins in the plasma of most BVVL patients with *SLC52A2* mutations (Bennett, 2012). As discussed previously however, it is likely that some riboflavin uptake may occur via passive diffusion when riboflavin intake is high (Foraker et al., 2003).

Transporters of nutrients possess targeting motifs and signals which are often located within the COOH terminus (Subramanian, Rapp, et al., 2011). Accordingly, the COOH-terminal sequence was shown to be necessary for cell surface expression of RFVT3 and riboflavin uptake via this transporter in transfected Caco-2 cells. In particular, mutation of the cysteine residues 463 and 467 in the COOH-terminal caused defective riboflavin uptake with retention of the construct in the endoplasmic reticulum (ER), which is the site of synthesis, folding, and assembly of transmembrane and secretory proteins in the cell (Sevier & Kaiser, 2008). A potential disulphide bridge was also predicted between the cysteine residues at amino acids 386 and 463. Indeed, when cysteine 386 was mutated the construct was also retained intracellularly, supporting the role of the disulphide bridge in membrane localisation and proper function of this transporter (Subramanian, Rapp, et al., 2011). The amino acids encompassing the COOH-terminals in human RFVT1, RFVT2 and RFVT3 are amino acids 430-448, 427-445 and 451-469, respectively (Subramanian, Rapp, et al., 2011).

Although rodents carry the *Slc52a2* and *Slc52a3* genes (encoding RFVT2 and RFVT3, respectively), no orthologue encoding a third riboflavin transporter has been identified in rodents. The characteristics of riboflavin uptake via the mouse mRFVT2 were similar to that of human RFVT2. mRFVT2 shares approximately 80% of its amino acids with both human RFVT1 and RFVT2 and is therefore predicted to be an orthologue of both these human transporters (Yao et al., 2013). Since higher animals such as humans, chimpanzees (*Pan troglodytes*) and rhesus monkeys (*Macaca mulatta*) have three riboflavin transporters, the third riboflavin transporter has likely evolved more recently in evolution (Yonezawa & Inui, 2013). Experiments suggest mRFVT3 may be important for riboflavin transport under acidic conditions (Yao et al., 2013). mRFVT2 is expressed at a higher level in the mouse liver than mRFVT3. Riboflavin deprivation in mice led to decreased intracellular concentration of

riboflavin in the plasma but not in the liver, concomitant with upregulation of *Slc52a2* but not *Slc52a3* mRNA expression in this organ (Yao et al., 2013). mRFVT2 likely plays an important role in riboflavin uptake in various tissues including the liver. As acyl-CoA dehydrogenase was found to be highly expressed in the liver, defective riboflavin transport in this tissue may explain the biochemical abnormalities in BVVL patients (Yao et al., 2013).

Studies of riboflavin uptake in the rat have shown the mRNA expression of rRFVT3 to be upregulated in the small intestine of rats fed a riboflavin-deficient diet, likely as an adaptive response; this response is common to several B vitamin transporters in the intestine (Fujimura et al., 2010). Interestingly, mRNA expression of rRFVT2 was not upregulated in response to riboflavin deprivation, providing evidence that its role in intestinal absorption in the rat is limited (Fujimura et al., 2010).

Chronic alcohol consumption is often associated with riboflavin deficiency in humans. In rats, chronic alcohol intake was found to inhibit carrier-mediated transport of riboflavin across brush border and basolateral membranes of the intestine and kidney, and was associated with decreased mRNA and protein levels of the rat riboflavin transporters rRFVT2 and rRFVT3 in the intestine and kidney. Thus intestinal absorption and renal re-absorption of riboflavin is impaired by elevated alcohol consumption, and this mechanism involves the aforementioned riboflavin transporters in the rat (Subramanian et al., 2013).

6.1.4 Riboflavin homeostasis in the brain

In addition to the saturable absorption system in the gut, and excretion system in the kidney, riboflavin entry and exit is also controlled in the CNS by a saturable transport system. Transport mechanisms of essential nutrients into the brain have often developed independently from intestinal transporters used for absorption of nutrients from food (Yao et al., 2010). Riboflavin can cross the blood-brain barrier while FAD and FMN are unable to do so (Nagatsu et al., 1967). Over 85% of the total riboflavin (riboflavin, FAD and FMN) in rat brain as well as in rabbit brain and choroid plexus was present as FMN or FAD (the major flavin in the brain), therefore riboflavin is rapidly converted into FMN and FAD which are metabolically trapped

within the cell (Nagatsu et al., 1967; Spector, 1980b). The concentration of total riboflavin in rabbit brain was approximately fifty times higher than in rabbit plasma (Nagatsu et al., 1967; Spector, 1980a). Riboflavin homeostasis appears to be particularly tightly regulated in the brain (Spector & Johanson, 2006). Indeed, unlike other organs such as the liver, the levels of FMN and FAD in the brain have been found to stay relatively constant during severe riboflavin deficiency and after elevated doses of riboflavin (Burch et al., 1956; Nagatsu et al., 1967). Although riboflavin is quickly transported from the plasma into the brain, the stable intracellular levels of total riboflavin seen in the brain could possibly be explained by the slow turnover of total riboflavin in this organ (about 1% per hour) (Nagatsu et al., 1967; Spector, 1980b; Spector & Johanson, 2006).

Several mechanisms at the level of the blood-brain barrier, in the brain cells, and across the choroid plexus are likely to maintain riboflavin homeostasis in the brain. Entry via the blood-brain barrier is thought to be the predominant passageway for riboflavin into the CNS (Spector & Johanson 2006). In rabbit brain slices, riboflavin transport was saturable and riboflavin accumulation was inhibited by other flavins (Spector, 1980a; Spector, 1980b). The characteristics of riboflavin accumulation in rabbit brain slices were similar to that of human RFVT2, which is highly expressed in the brain (Spector, 1980a; Spector, 1980b; Yao et al., 2010). Transport was suspected to occur by facilitated diffusion first through the blood-brain barrier, and subsequently into the brain cells; both these systems prevent excessive amounts of riboflavin from reaching the brain (Spector & Johanson, 2006).

A saturable, high-affinity carrier-mediated riboflavin uptake system on the luminal side of rat brain capillary endothelial cells was recently described. Uptake was temperature, energy and Na^+-dependent but pH-independent; uptake was inhibited by structural analogues of riboflavin but not D-ribose and was modulated by the $Ca^{2+/}$calmodulin and PKA pathways. A second transport system via the rRFVT3 was considered unlikely to be functional in the rat brain capillary endothelial cells (Patel et al., 2012). Since uptake via RFVT1, RFVT2 and RFVT3 was independent of extracellular Na^+ (Yao et al., 2010), it may be that an additional as-yet-unknown riboflavin transporter exists in rat, and possibly human, brain capillary endothelial

cells. Although RFVT2 is highly expressed in the human brain and may play a role in riboflavin uptake into neurons and astrocytes, the transport mechanism via RFVT2 remains uncharacterised in human brain tissue and neuronal models (Moriyama, 2011; Yao et al., 2010).

The choroid plexus, the region of the blood-CSF barrier, is thought to play a major role in transport of riboflavin between the brain and the blood through the CSF (Spector, 1980b; Spector, 1980c; Spector & Johanson 2006). The choroid plexus is critical for clearance of riboflavin from the CSF (Spector, 1980b; Spector, 1980c; Spector & Johanson, 2006). In rabbits, riboflavin was suspected to be transported from the CSF into the blood via two carrier-mediated systems in the choroid plexus: one located at the apical membrane (likely via the organic acid transporter 3 carrier) for influx into the CSF, and one at the basolateral membrane for efflux into blood via an unknown carrier. These riboflavin carriers were thought to have broad specificity and to function by facilitated diffusion (Spector, 1980b; Spector, 1980c; Spector & Johanson, 2006).

When levels of riboflavin were low in rabbit plasma, for example during starvation, higher levels of riboflavin were transported to the choroid plexus and the brain from the plasma to counteract the lower riboflavin levels; in contrast, when riboflavin concentration was high in the plasma, the transport system was saturated and less riboflavin was able to enter via the blood-CSF and blood-brain barriers. This observation may further explain how total riboflavin levels remain stable in the brain (Burch et al., 1956; Spector, 1980b). Riboflavin transport in the peripheral nerve has not yet been extensively studied.

6.1.5 *Solute carrier family 52, riboflavin transporter member 1* (*SLC52A1*), *SLC52A2* and *SLC52A3* mutations in BVVL syndrome

Thus far, non-synonymous, stop-gain, frameshift and splice site altering pathogenic variants have been identified in the homozygous or compound heterozygous state in *SLC52A3*; only non-synonymous mutations in the homozygous or compound heterozygous state have been reported in *SLC52A2* up until now (Appendix VI Table VI-1) (Bosch et al., 2012; Spagnoli et al., 2014). Mutations in both *SLC52A2* and *SLC52A3* were spread throughout the genes and were located in transmembrane,

intracellular and extracellular loops (Dezfouli et al., 2012). Besides the deletion of two exons in *SLC52A1* causing mild maternal riboflavin deficiency, no other pathogenic mutations associated with MADD or BVVL have been reported in this gene (Chiong et al., 2007; Ho et al., 2010). A table of polymorphisms located in *SLC52A1*, *SLC52A2* and *SLC52A3* is available in Appendix VI Table VI-2.

As mutations in these riboflavin transporters have only recently been associated with BVVL, phenotype-genotype correlations are not yet possible. However, in agreement with the findings highlighting the importance of the RFVT3 COOH-terminal (Subramanian, Rapp, et al., 2011), preliminary observations indicate that mutations causing pre-mature truncations of *SLC52A3* or non-synonymous mutations in the COOH-terminal of *SLC52A3* may be associated with increased disease severity and lower levels of riboflavin in the plasma (Bosch et al., 2011; Ciccolella et al., 2012; Green et al., 2010; Subramanian, Rapp, et al., 2011).

6.2 Aims of this study

The finding by our group and colleagues of a homozygous mutation in *SLC52A2* in two families with BVVL-like MND without mutations in *SLC52A3* (Johnson et al., 2012) has prompted us to screen this gene and the other two riboflavin transporters in a larger cohort of patients. Indeed, although the recent identification of mutations in riboflavin transporters in BVVL patients has revealed the genetic cause of disease in several individuals, it is likely that many patients remain to be uncovered. The first aim of this Chapter was to detect unrecognised cases of BVVL, thereby facilitating access to early treatment with high doses of riboflavin and widening the phenotype associated with riboflavin transporter mutations. To fulfil this aim, the three known riboflavin transporters were screened in a cohort of BVVL, BVVL-like and spinal muscular atrophy with respiratory distress (SMARD)-like patients. As will be discussed later on in this Chapter, results of this study were combined with findings from other centres and resulted in a publication (Foley et al., 2014). A second aim of this Chapter was to use exome sequencing to identify the genetic cause of disease in patients with BVVL-like phenotypes and in patients with AR polyneuropathy with a predominant motor component without mutations in the three genes encoding the riboflavin transporters. Any novel genes identified in this study may also contribute

to diseases such as ALS and spinal muscular atrophy/SMARD, as their phenotypes overlap with BVVL.

6.3 Methods

6.3.1 BVVL and BVVL-like patient cohort

This study was an important collaboration of many clinicians and scientists in the UK and rest of the world.

Amongst patients known to the NHNN, we selected 35 patients that had BVVL-like features, with two of the following four criteria: severe cranial neuropathy, sensory-motor neuropathy, deafness, and respiratory insufficiency. A total of 35 patients were screened for mutations in *SLC52A1*, *SLC52A2*, and *SLC52A3*. The majority of patients in this cohort were from the UK. DNA or blood had already been or was subsequently sent to the NHNN Neurogenetics Unit. Patients had previously had diagnostic testing of genes associated with related disorders (e.g. ALS, CMT, and/or SMA genes, mitochondrial DNA mutations); patients had been found negative for mutations in these genes.

A second cohort of patients studied herein consisted of 57 patients (including two pairs of siblings (55 probands)) referred specifically for research genetic testing of riboflavin transporters. Most of these patients were expressly referred for *SLC52A2* sequencing as their phenotype was very similar to that described in the first report of *SLC52A2*-mutated patients (Foley et al., 2014; Johnson et al., 2012). DNA for this second cohort was obtained from the NHNN Neurogenetics Unit or was sent to our centre from hospitals worldwide. Institutions which sent DNA included: the Dubowitz Neuromuscular Centre and MRC Centre for Neuromuscular Disorders, UCL ICH and GOSH in London, UK, the Evelina Children's Hospital, King's College Hospital, St George's Hospital, Royal London Hospital, Guy's Hospital and St. Thomas' Hospital in London, UK, the Royal Manchester Children's Hospital in Manchester, UK, the Royal Aberdeen Children's Hospital in Aberdeen, UK, the Institute of Genetic Medicine at the University of Newcastle upon Tyne, UK, the Southern General Hospital and the Royal Hospital for Sick Children in Glasgow, Scotland, UK, the Sheffield Children's Hospital in Sheffield, UK, the St. James's

University Hospital in Leeds, UK, the Children's University Hospital and Beaumont Hospital in Dublin, Ireland, the Vrije Universiteit Medical Centre in Amsterdam, the Netherlands, the Université Saint Joseph in Beirut, Lebanon, the University of Sao Paulo in Ribeirão Preto, Brazil, the National University Hospital at the University of Iceland, Iceland, the Institut de Myologie, Groupe Hospitalier Pitié-Salpêtrière in Paris, France, the Gothenburg University in Sweden, the Mater Dei Hospital in Malta, the Sakhalin Hospital in Russia and the Children's Hospital of Pittsburgh at the University of Pittsburgh Medical Centre in Pittsburgh, USA.

Sequencing results from these two patient cohorts were combined with results obtained by collaborators at the University of Sydney and Institute for Neuroscience and Muscle Research at the Children's Hospital at Westmead, Sydney, Australia and at the University of Miami's Miller School of Medicine in the USA. Where available, clinical information for the patients in whom variants were found is included in the appropriate section.

6.3.2 Spinal muscular atrophy with respiratory distress (SMARD)-like and atypical diaphragmatic weakness patient cohort

As discussed in Section 1.6.1, SMARD1 patients share some clinical features with BVVL patients. DNA was available for four patients with SMARD-like disease and/or atypical diaphragmatic weakness without mutations in the known SMARD genes. Patient AHH had a severe peripheral neuropathy with distal denervation and reinnervation. These features resembled that seen in SMARD, however disease onset was later than expected. This patient also had scoliosis, as well as bulbar and respiratory problems. Patient MM had motor and respiratory weakness, with severe reduction of CMAPs, severe decrease of MNCVs in the legs and preserved sensory responses. This patient showed evidence of denervation in the muscles of the leg, but also muscles involving the diaphragm and the tongue; these features are also suggestive of SMARD. Patient HS had cataracts, sensorineural deafness, failure to thrive and respiratory failure. A detailed phenotype was not available for the fourth patient. DNA for the four patients in this cohort was obtained from GOSH in London, UK.

6.3.3 Patients for exome sequencing

Exome sequencing was performed for three families in this study. Individual II-10 of family SP and individuals III-3 and III-8 of family TB were part of the BVVL patient cohort (Section 6.3.1), thus mutations in the three known riboflavin transporters had been excluded. Sanger sequencing of the three riboflavin transporters was not performed in individual III-3 of family MO. DNA for family SP was obtained from Dr Jose Berciano at the University Hospital Marqués de Valdecilla in Santander, Spain. DNA for families TB and MO was obtained from the Dubowitz Neuromuscular Centre and MRC Centre for Neuromuscular Disorders, UCL ICH in London, UK. Affected members of family SP had a BVVL-like phenotype with pontobulbar palsy and AR inheritance. Families MO and TB had an AR polyneuropathy with a predominant motor component. Although the clinical picture is not that of classical BVVL in families MO and TB, there are some overlapping features.

Family SP is of Spanish origin. Three siblings (individuals II-3, II-7 and II-10) were affected in this family; the parents were unaffected and there was no known consanguinity in the family (Figure 6-1).

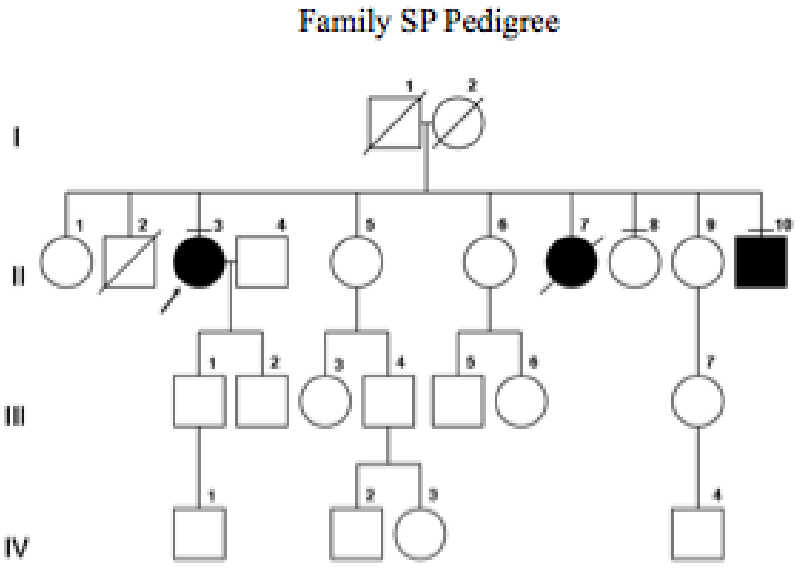

Figure 6-1 Pedigree of family SP.

The proband, individual II-3 is now in her seventies. She had progressive dysarthria, intermittent dysphagia, bilateral pes cavus, toe clawing and walking clumsiness since infancy. She had mild amyotrophy of the hand and lower leg. The patient was not able to walk on her heels and there was minimal spasticity while walking. She did not notice any deafness, however pure-tone audiometry studies showed a subclinical high-frequency deficit. She had tongue weakness and atrophy, as well as furrowing of the tongue with occasional fasciculations. Her tendon reflexes were brisk except for absent plantar and ankle reflexes. This patient had sensory abnormalities with stocking hypoesthesia. Bilateral palatal and facial paresis were seen, along with an absent gag reflex. Laboratory investigations including cranio-spinal MRI, electrocardiogram and thoracic X-rays were normal. Electrophysiological studies showed chronic denervation and features of an axonal sensory-motor neuropathy. She also displayed evidence of a central sensory axonopathy with delayed central motor conduction times. She had fatty atrophy of distal foot muscles on MRI. Mutations in *X25/frataxin* and *SMN1* had been previously excluded. Both individuals II-7 and II-10 had a similar clinical picture to the proband. The working diagnosis was FL syndrome, although BVVL was also considered possible given the pure-tone audiometry findings.

Individual III-3, the proband in family MO was the only affected member of the family. This patient is from the UK and was born to non-consanguineous parents; the pedigree is compatible with an AR mode of inheritance (Figure 6-2).

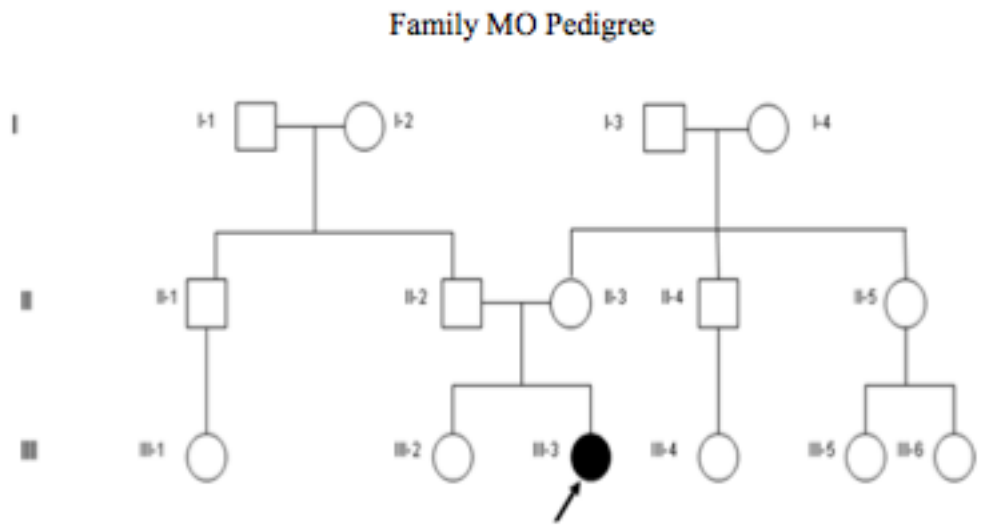

Figure 6-2 Pedigree of family MO.

At three months, the proband had progressive hypotonia leading to breathing difficulties therefore she was put on invasive ventilator support. She had cataracts and renal tubulopathy at five months of age. At seven months, she had recurring unexplained fevers. A severe progressive sensory-motor axonal neuropathy, demyelination and axonal degeneration were seen on nerve biopsy; denervation was evident on muscle biopsy, with no sign of reinnervation. MRI brain scans, MRC enzyme activity and plasma amino acids were normal. Urine organic acids and intermittent lactic acidosis suggested a mitochondrial disorder. Maleic acid was present in the urine. Urine amino acids showed strong generalised aminoaciduria and liver ultrasonography showed hepatomegaly. At nine months of age, she remained ventilator-dependent and was minimally responsive. She had facial weakness and muscle weakness, absent deep tendon reflexes and decreased light touch sensation. Her acylcarnitine profile showed raised hydroxybutyrylcarnitine; fatty acid β-oxidation studies were normal. Her electroencephalogram (EEG) had encephalopathic patterns. Treatment included dichloroacetate, riboflavin, ascorbic acid and CoQ_{10} since a mitochondrial disorder was suspected. Acquired neuromuscular causes were excluded. Mitochondrial DNA sequencing was negative for *POLG*, *mpv17 mitochondrial inner membrane protein* (*MPV17*) (exons 2-8), *PEO1*, *ribonucleotide reductase M2B* (*RRM2B*), *deoxyguanosine kinase* (*DGUOK*) (exons 1-7) and *Twinkle* (partial sequencing). Further sequencing of SMA (*SMARD1*,

SMN1), myotonic dystrophy (*dystrophia myotonica 1* (*DM1*)), Emery-Dreifuss muscular dystrophy (*Lamin A/C*), CMT (*DNM2*, *PMP22*, *MPZ*, *EGR2*) and congenital central hypoventilation syndrome (*paired-like homeobox 2b* (*PHOX2B*)) genes was negative. Prader-Willi syndrome as well as peroxisomal and nutritional disorders were also ruled out. A deficiency of maleylacetoacetate isomerase (MAAI, also known as glutathione-5-transferase zeta-1 (GSTZ1)) was suspected given the presence of maleic acid in the urine and the renal tubulopathy. MAAI catalyses the last step in the catabolism of tyrosine to fumarate. It remained unclear whether these metabolic abnormalities might have occurred as a result of treatments administered to this patient. The motor neurone dysfunction remained the most important feature in the proband.

Family TB is from the UK and Greece. The two affected individuals in family TB are cousins. The parents of individual III-8 are consanguineous, however there is no known consanguinity on individual III-3's side of the family (Figure 6-3).

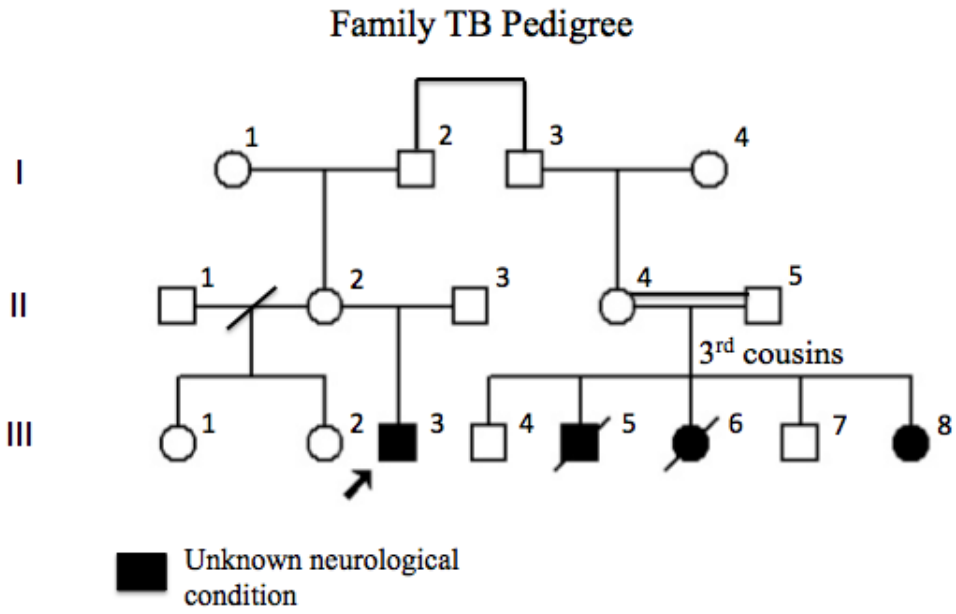

Figure 6-3 Pedigree of family TB.

The proband, individual III-3, had a clinically-relapsing motor neuropathy. He asked to be fed frequently in infancy and showed personality changes if not fed regularly. At 18 months, he had episodes of vomiting and became too weak to walk; he subsequently made an almost complete recovery. At 2.5 years, he had an infection leading to leg weakness. A further infection at age three caused arm and leg weakness. At 4.5 years, he had a viral infection leading to paralysis, compromised breathing and speech loss. At 9.5 years, there was weakness of movement of palate and tongue as well as weakness of all limb muscles. He also had absent deep tendon reflexes at this stage. Electrophysiological studies showed features of an axonal neuropathy, including reduced CMAP amplitudes and slight reduction of median NCVs. Muscle biopsy showed severely atrophic fibres and denervation and reinnervation; the nerve biopsy was normal. He had low plasma acetylcarnitines and low fibroblast fatty acid β-oxidation. Activities of MRC complexes II/III and IV were normal. He had low plasma serine with possible evidence of increased serine catabolism. There was mitochondrial DNA depletion on muscle biopsy. A fatty acid β-oxidation defect or a carnitine acetyl transferase deficiency was suspected. The proband was administered carnitine and riboflavin; he showed a slow improvement. He was then given L-serine and displayed improvement in speech and in antigravity movement in all limbs.

Individual III-8, his cousin, developed normally in her first year. At age two, she had an upper respiratory tract infection, leading to generalized weakness and hypotonia. Her ulnar and median NCVs were decreased and there was evidence of a demyelinating polyneuropathy. Her nerve biopsy was normal. Individual III-8 was initially diagnosed with CIDP, with overlapping features of CMT1. At age four, she had another attack of generalized weakness with involvement of respiratory muscles. A more severe attack at age six put the patient in intensive care. She made a partial recovery with IVIG and steroids. She had weakness of face, trunk, and limb muscles, which was more distal than proximal. She had absent reflexes and no sensory impairment. A year later, she showed some improvement. Further studies showed prominent neuropathy affecting mostly the motor fibres. There were some sensory changes and a severe decrease in CMAPs. She was diagnosed with “familial, episodic, primarily motor peripheral neuropathy” of unknown cause. Additional

studies of urine organic acids showed increased excretion of urate. The organic acid results of individuals III-3 and III-8 had some similarities such as raised glycolate and citrate, but were not identical. Furthermore, unlike her cousin, individual III-8's plasma serine levels were normal. She was left wheelchair-bound with severe scoliosis, reduced muscle bulk, and no antigravity movement in her arms. Her brother (individual III-5) had seizures from six months of age and he died at 15 months. Her sister (individual III-6) had delayed walking. Individual III-6 became weak after a flu-like illness at 3.5 years of age. At seven years of age, individual III-6 had a widespread infection, increasing weakness and a rash on her trunk and arms, and did not survive. It remains possible that the biochemical changes (low serine and acetyl carnitine) seen in individual III-3 and individual III-8 were secondary to loss of motor neurones.

6.3.4 Patient consent and DNA samples

Details of ethics approval and patient consent for all patients described in Sections 6.3.1-6.3.3 are found in Section 2.1.1. Purity and concentration of DNA samples were assessed as described in Section 2.1.5.

6.3.5 DNA extraction from human saliva

For one BVVL sample, DNA was extracted from human saliva as described in Section 2.1.3.

6.3.6 PCR and Sanger sequencing of three riboflavin transporters

PCR, agarose gel electrophoresis, purification of PCR products, Sanger sequencing, dye removal and sequencing analysis were performed in all cohorts using standard conditions as described in Sections 2.1.9-2.1.12. Coding exons and flanking intronic sequences were sequenced for human *SLC52A1*, *SLC52A2* and *SLC52A3*. Transcript references used for primer design, as well as sequences of gene-specific primers and PCR cycling conditions can be found in Appendix VI Table VI-3. The sequences for all *SLC52A3* primers and some *SLC52A2* primers were obtained from Johnson et al., 2012. However, some *SLC52A3* primers used by Johnson and colleagues (2012) had to be redesigned; the primer binding was inefficient due to a common SNP being present at one of the primer-binding bases, which would have caused potential

mutations to be missed. SNP chromosomal locations are based on Genome Build 37.3. In-silico analyses were performed as described in Section 2.6. Variants were searched in the dbSNP, 1000 Genomes and/or EVS databases. To assess conservation among species of the mutated amino acid residues, Ensembl was used to retrieve the sequences and the Clustal Omega software was used for multiple sequence alignment. TMHMM v.2 was used to predict transmembrane domains and intracellular/extracellular loops. Where DNA was available, segregation analysis of variants in family members was performed.

6.3.7 Sanger Sequencing and exome sequencing performed by collaborators

Our collaborators used Sanger and exome sequencing to screen for *SLC52A1, SLC52A2* and *SLC52A3* mutations in their BVVL patients. Patients A1 and A2 were Sanger sequenced at the University of Sydney as described in Foley et al., 2014. Exome sequencing for patients A3, A4, U1 and U2 was performed by the University of Miami. Briefly, exome sequencing was carried out using the SureSelect Human All Exon 50 Mb exome capture kit (Agilent Technologies) and was sequenced on the Illumina HiSeq2000 (Illumina). Sequence data analysis was performed by the University of Miami as described in Foley et al., 2014. Patients A5-A7 were exome sequenced by BGI Inc (USA; http://www.genomics.cn/en/index) using the NimbleGen sequence capture exome array kit (44Mb) (Roche). Exome sequencing was carried out on the Illumina HiSeq2000 instrument (Illumina) by BGI Inc. Sequence data analysis was performed by the University of Sydney as described in Foley et al., 2014.

6.3.8 High-dose oral riboflavin therapy

High-dose oral riboflavin therapy was commenced in the majority of patients who were found to carry riboflavin transporter mutations in the combined cohort. Generally, patients were initially treated with 10 mg/kg/day of oral riboflavin and this was increased to a maximum of 50 mg/kg/day in children and 1500 mg/day in adults, as recommended by Dr Annet Bosch (Department of Paediatrics, University of Amsterdam, the Netherlands) and published online (http://www.bvvl international.org/B2_Therapy_Protocol.html). Clinical and biochemical

examinations were performed by the patients' respective neurological care teams before and following the start of treatment, where possible (Foley et al., 2014).

6.3.9 HumanCytoSNP-12 BeadChip analysis

As will be discussed in Section 6.4.5, one patient was found to carry a homozygous mutation in *SLC52A2*, however there was no reported consanguinity in this particular family. Although the patient's mother was a carrier for the mutation, paternal DNA was not available to confirm the father's carrier status. A HumanCytoSNP-12 v.2.1 BeadChip (Illumina) was therefore used to exclude a large deletion on the other allele and to assess the likelihood of the mutation truly being homozygous by evaluating the frequency of homozygous genotypes in the surrounding genomic region. The array data was analysed using GenomeStudio (v.2010.1, Illumina). Further details on the HumanCytoSNP-12 v.2.1 BeadChip and the data analysis are available in Section 2.1.13.

6.3.10 Haplotype analysis in Lebanese patients carrying the homozygous *SLC52A2* p.Gly306Arg mutation

Several BVVL cases in the combined cohort were of Lebanese origin and carried the *SLC52A2* p.Gly306Arg mutation in the homozygous state. To assess whether this mutation was inherited as a shared ancestral allele, haplotype analysis was performed in these BVVL patients, as well as in obligate carriers (parents) and unaffected siblings for whom DNA was available. While our collaborators used a SNP-based array to establish the haplotype, I genotyped 11 SNPs upstream and downstream of the *SLC52A2* gene using Sanger sequencing in the remaining families. Four SNPs were located within or downstream of *F-box and leucine-rich repeat protein 6* (*FBXL6*) and seven SNPs were located within or downstream of *aarF domain containing kinase 5* (*ADCK5*); these genes are upstream and downstream of *SLC52A2*, respectively. PCR and sequencing were performed as described in 6.3.6. Sequences of primers used to determine the genotype at the 11 SNPs, as well as PCR cycling conditions can be found in Appendix VI Table VI-4. The carrier status of the p.Gly306Arg variant was also confirmed by re-sequencing of the appropriate *SLC52A2* exon, following procedures described in Section 6.3.6.

6.3.11 *SLC52A2* patient fibroblasts

Patient skin biopsies were performed by the patients' neurologists and fibroblasts grown from these biopsies were sent to our centre. For biopsies performed at the NHNN/GOSH, patient fibroblasts were grown from skin biopsies by Diana Johnson, as described in Section 2.2.2. Five BVVL patient fibroblast lines (patients E1-E4 and I1), one carrier fibroblast line (mother of patient E1) and three age-matched control fibroblast lines were available for transcriptional analysis of *SLC52A2* mutations (see Section 2.2.2 for full details of control fibroblast lines). Details of consent are available in Section 2.2.1.

6.3.12 Cell culture of fibroblasts

Patient, carrier and control fibroblasts were cultured in regular DMEM as described in Section 2.2.3.

6.3.13 Transcriptional analysis

RNA was extracted from patient, carrier and control fibroblasts, and cDNA was synthesized as described in Sections 2.2.9-2.2.10. cDNA was sequenced according to the Sanger sequencing protocol as described in Section 2.1.12. Sequences of primers and cycling conditions used for cDNA sequencing can be found in Appendix VI Table VI-5.

6.3.14 Exome sequencing

Exome sequencing was performed on individuals II-3 and III-1 of family SP, individual III-3 of family MO, and individuals III-3 and III-8 of family TB. Exome sequencing for families SP and TB was performed by Oxford Gene Technology (UK). Exome sequencing for family MO was performed at the UCL ION by Dr Deborah Hughes and Dr Alan Pittman. In both instances, 2 μg of gDNA was supplied.

The exome sequencing carried out by Oxford Gene Technology used Agilent's SureSelect protocol v.1.2 (Agilent Technologies) for library preparation and enrichment of samples. Sequencing was performed on the Illumina HiSeq 2000 platform using the TruSeq v.3 chemistry (Illumina). For the exome sequencing

performed in-house at the UCL ION, library preparation for exome sequencing was performed as per the TruSeq (Illumina) sample-preparation protocol. DNA libraries were hybridized to exome-capture probes with TruSeq chemistry (Illumina). Samples were clustered on a cBot (Illumina) and exome-enriched libraries were sequenced on the HiSeq 1000 (Illumina). Variant calling was performed by both Oxford Gene Technology and Dr Alan Pittman at the UCL ION. Further details on the exome sequencing protocol are found in Section 2.1.15.

6.3.15 Assessment of gene coverage and read depth

As described in Section 2.1.16, gene coverage and read depths were assessed for all three known riboflavin transporter genes using the exome sequencing BAM files and Golden Helix GenomeBrowse software. The coverage and read depth of the *GSTZ1* gene was also assessed for individual III-3 in family MO.

6.3.16 Exome data filtering and variant prioritisation

The exome variant filtering steps are described in Section 2.1.17. Briefly, synonymous mutations were first filtered out. Following this step, all three riboflavin transporter genes, as well as the *GSTZ1* gene in individual III-3 of family MO, were inspected for potentially pathogenic variants. For all three families, the pedigrees were consistent with AR inheritance. In families SP and MO, the variant was predicted to be compound heterozygous as there was no known consanguinity in the family. In family TB, consanguinity was only thought to be present on individual III-8's side of the family. Three possibilities were considered in the exome data analysis for this family. The disease-causing variant could be in the homozygous state in both individual III-3 and III-8; alternatively, individual III-3 and III-8 may carry compound heterozygous mutations in the same gene. In the latter case, the two individuals may share one or both variants in the compound heterozygous state. In the third scenario, individual III-8 may be homozygous for the disease-causing variant, and individual III-3 may carry the same variant in the compound heterozygous state with another mutation in the same gene. For all families, a lower MAF of 0.01 was used as a cut-off point for the control reference databases (1000 Genomes, CG69 and EVS). Any variant within a segmental duplication region with identity greater than or equal to 96% was removed. SNP chromosomal locations are

based on Genome Build 37.3. For certain variants of interest, the conservation of the amino acid between species, location within the protein structure, and in-silico pathogenicity predictions were assessed as explained in Section 2.6. Gene expression data was obtained from the Human Protein Atlas as described in Section 2.6. Candidate genes were searched in the literature for any known association to disease.

Candidate genes for families SP, MO and TB were predicted to be highly expressed in the brain and spinal cord. Potential candidates included genes encoding enzymes involved in riboflavin, FAD and FMN synthesis and metabolism. Additionally, riboflavin transporters found in other species were evident candidates. For example, Mch5p functions as a plasma membrane riboflavin transporter in yeast *Saccharomyces cerevisiae* which operates via a facilitated diffusion mechanism (Reihl & Stolz, 2005); *solute carrier family 16, member 12* (*SLC16A12*), the human homologue of *Mch5p,* is also thought to encode a monocarboxylate transporter that causes juvenile cataract with microcornea and renal glycosuria when mutated (Kloeckener-Gruissem et al., 2008). The gene encoding the human mitochondrial FAD transporter, *MFT,* was another candidate gene (Spaan et al., 2005), as well as genes encoding proteins responsible for FAD and FMN homeostasis in the mitochondria (Rhead et al., 1993). Genes encoding flavoproteins and proteins with a role in FAD or FMN-dependent pathways, in mitochondrial fatty acid β-oxidation, or more generally in cell energy metabolism were also possible candidates. Given the phenotypic overlap, juvenile ALS genes and SMA genes were also considered in the exome analysis. Other candidate genes for family TB included serine transporters or enzymes involved in serine metabolism or synthesis. Additional candidate genes specifically for individual III-3 of family MO included the *GSTZ1* gene, as discussed above, as well as the three known riboflavin transporters as these genes were not sequenced in this patient.

6.4 Results

6.4.1 Results of Sanger sequencing of *SLC52A1, SLC52A2* and *SLC52A3* in the BVVL, BVVL-like and SMARD-like cohorts

The screening of the three riboflavin transporters in BVVL and BVVL-like patients has resulted in a publication in collaboration with colleagues in Australia (Sydney

Children's Hospitals Network) and the USA (University of Miami's Miller School of Medicine) (see Foley et al., 2014). For simplicity, IDs used herein for patients with *SLC52A2* mutations refer to those used in our recent publication (Foley et al., 2014). Since this publication, two additional patients carrying mutations in *SLC52A2* have been identified as part of this thesis (E8 and B1), and several patients with heterozygous *SLC52A3* mutations have been found, as will be discussed below. In the combined cohort, a total of 19 patients were found to carry compound heterozygous or homozygous mutations in *SLC52A2*, ten of which were sequenced at our centre for this PhD thesis work. All ten patients in our cohort were unrelated. Nine of the ten patients (patients E2-E6, E8, L1, I1 and B1) were part of the cohort of patients specifically referred for research testing of *SLC52A1*, *SLC52A2* and *SLC52A3* (9/55 probands or 16.4%); one patient (patient E7) was part of the cohort of patients with BVVL-like features as determined by a database search (1/35 probands or 2.9%). The nine additional patients identified by our collaborators to carry *SLC52A2* mutations were spread across four families; two patients (one proband) were identified by Sanger sequencing (A1 and A2) and seven were found using exome sequencing (A3-A7 and U1-U2, three of which are probands; A5 and A6 are identical twins). Therefore, the 19 patients found to carry *SLC52A2* mutations in this study were from 14 different families (Foley et al., 2014). We will also discuss herein a patient (patient E1) who has been previously described and found to carry a homozygous *SLC52A2* mutation using Sanger sequencing (Johnson et al., 2012). Patients E1-E8 are from the UK, patients A1-A7 are from Australia, patients U1 and U2 are from the USA, I1 is from Ireland, L1 is from Lebanon and B1 is from Brazil. The female to male ratio was 13:7, which is lower than the reported 3:1 female to male ratio in BVVL (Foley et al., 2014; Sathasivam, 2008).

In total, nine non-synonymous mutations and one premature stop were identified in *SLC52A2* in our combined cohort; details of the *SLC52A2* mutations are listed in Table 6-1. The p.Gly306Arg and p.Leu339Pro mutations have been previously reported (Haack et al., 2012; Johnson et al., 2012); all other mutations are novel. The most frequent mutation was p.Gly306Arg, which was found both in the homozygous and compound heterozygous states. All mutations were predicted not tolerated by SIFT; all variants were predicted probably damaging by Polyphen-2, except the

p.Ser128Leu and p.Ala284Asp which were predicted possibly damaging. Six of the mutations were located within predicted transmembrane domains. Three of the mutations were found in the EVS and dbSNP databases (p.Ser128Leu; p.Leu339Pro; p.Ala420Thr), but at a very low frequency (MAF≤0.0002). All mutations were located at amino acids highly conserved between species and in human RFVT1 and RFVT3, except for the p.Gln234Stop and p.Ala284Asp mutations. The nonsense mutation was only conserved in the *Gorilla gorilla* and in RFVT1; the p.Ala284Asp mutation was not conserved in *Danio rerio* (Foley et al., 2014). None of the *SLC52A2* mutations were localised in the COOH terminal domain. The predicted transmembrane domains and intracellular/extracellular loops of RFVT2, as well as the *SLC52A2* gene structure and location of mutations identified in the combined cohort are displayed in Figure 6-4. The conservation of affected amino acid residues in RFVT2 across species and in human RFVT1 and RFVT3 is illustrated in Figure 6-5.

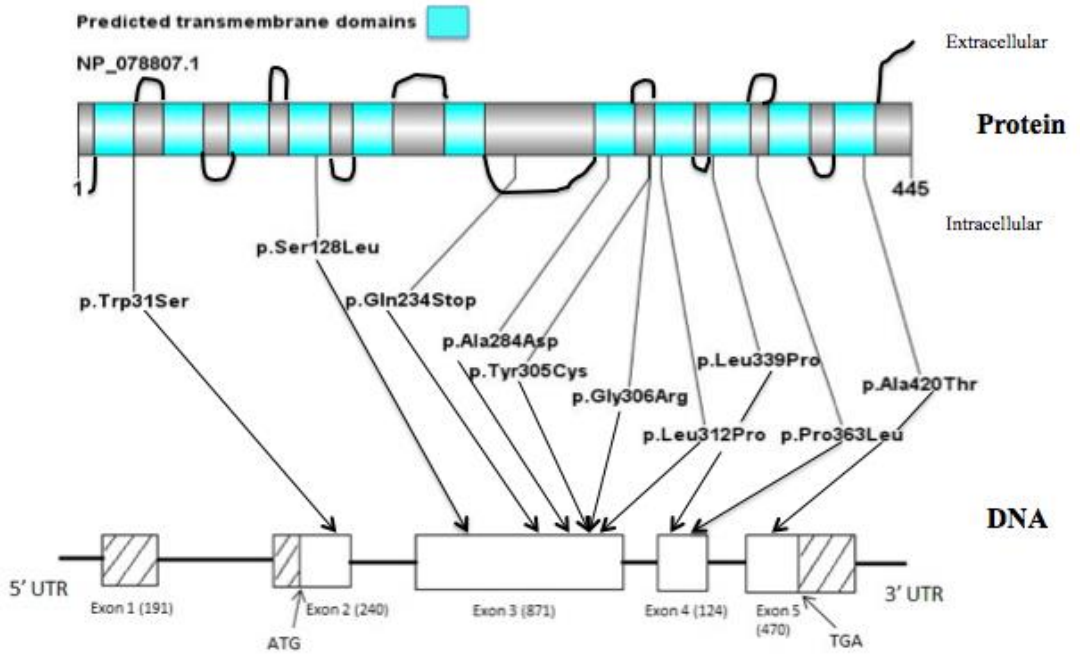

Figure 6-4 Location of *SLC52A2* mutations identified in this study with respect to gene structure and predicted transmembrane domains, intracellular and extracellular loops in RFVT2 (as predicted by TMHMM v.2; produced using the DOG2.0 software (Ren et al., 2009)). Reference sequence NM_024531.4 (adapted from Foley et al., 2014).

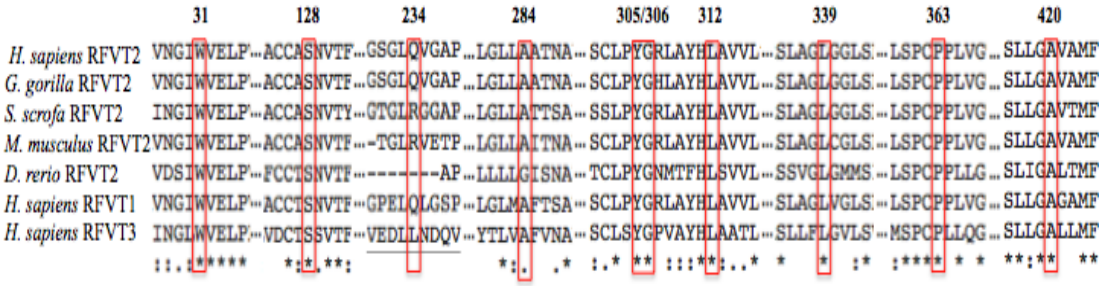

Figure 6-5 Structural conservation of relevant amino acid residues in RFVT2 (ENSP00000333638) across species and in RFVT1 (ENSP00000254853) and RFVT3 (ENSP00000217254). The Ensembl protein IDs for the RFVT2 orthologous sequences reported are: ENSGGOP00000028056, ENSSSCP00000028741, ENSMUSP00000023220 and ENSDARP00000045674. An * (asterisk) indicates positions which have a single, fully conserved residue. A : (colon) indicates conservation between groups of strongly similar properties. A . (period) indicates conservation between groups of weakly similar properties (Adapted from Foley et al., 2014).

Segregation analysis was performed for the families of patients E2-E6, L1, I1, E1, E7 (only maternal DNA tested in family of E1 and E7) and B1 (only paternal DNA tested in family of B1). Where DNA was available, all mutations segregated within the families with all parents tested found to be heterozygous carriers. Pedigrees, along with sequencing chromatograms of affected and unaffected family members are available in Appendix VI Figure VI-1 (Foley et al., 2014). Phenotypic details of the patients with *SLC52A2* mutations will be discussed in Section 6.4.2. Results of functional evaluations of some of the *SLC52A2* mutations found in this study will be presented in Chapter 7.

Seven patients (RDB, NDB, JG, HM, LF, KG, and LS; RDB and NDB are siblings (6 probands)) were found to carry heterozygous non-synonymous mutations in *SLC52A3*, representing six different mutations in total. No other mutation was detected in *SLC52A3* or the other riboflavin transporters in these patients. All patients with *SLC52A3* mutations belonged to the cohort of patients referred for BVVL research testing. Therefore, the frequencies of mutations in *SLC52A3* in the cohort of patients with BVVL-like features as determined by a database search and in patients specifically referred for BVVL testing were 0% (0/35 probands) and

10.9% (6/55 probands), respectively. Details of these mutations are listed in Table 6-1. The pathogenicity of these mutations is unclear, as BVVL patients usually carry riboflavin transporter mutations on both alleles. Four of the mutations (p.Gly13Arg, p.Glu36Lys, p.Thr125Asn, and p.Phe457Leu) were predicted damaging by both the SIFT and Polyphen-2 in-silico analyses. The p.Ile20Leu variant was predicted tolerated by SIFT but probably damaging by Polyphen-2. The p.Thr135Ala mutation was predicted benign by both prediction programmes. The p.Gly13Arg, p.Ile20Leu and p.Phe457Leu mutations were found at very low MAF in the EVS database (MAF of 0.0001, 0.0001 and 0.0007, respectively); the other mutations were not found in the EVS database. All mutations except the p.Thr125Asn and p.Thr135Ala mutations were found in dbSNP, however in all cases, no MAF was provided. The p.Gly13Arg, p.Glu36Lys, p.Thr125Asn, and p.Phe457Leu mutations alter amino acids evolutionarily conserved from humans to *Danio rerio* and also conserved in the other two human riboflavin transporters. The p.Ile20Leu variant alters an amino acid conserved from humans to *Danio rerio* but not conserved in the human RFVT1 and RFVT2. The p.Thr135Ala mutation affects an amino acid conserved from humans to *Mus musculus* but not conserved in *Danio rerio*, human RFVT1 and RFVT2 (Figure 6-6). The p.Gly13Arg, p.Ile20Leu, p.Thr125Asn, and p.Thr135Ala variants are located within transmembrane domains of RFVT3; the p.Glu36Lys is located in an extracellular loop. The p.Phe457Leu mutation is located in the COOH terminal domain in the extracellular tail. As mentioned in Section 6.1.3, the COOH-terminal sequence was determined to be essential for cell surface expression of RFVT3 and therefore for riboflavin uptake via this transporter in human intestinal epithelial cells (Subramanian, Rapp, et al., 2011). The amino acid residue 457 is one of the four residues within the COOH-terminal sequence to be entirely conserved in rat and mouse and in the other two riboflavin transporters (Subramanian, Rapp, et al., 2011). The p.Gly13Arg, p.Ile20Leu, and p.Thr135Ala variants are novel, although mutations have been described at nearby amino acids (p.Trp17Arg (Bosch et al., 2011); p.Asn21Ser (Dezfouli et al., 2012); p.Arg132Trp (Green et al., 2010)). The p.Thr125Asn variant has been previously found by a London-based diagnostic laboratory; the mutation was in the compound heterozygous state with a heterozygous pathogenic mutation in *SLC52A3* (C. Ridout, personal communication). The p.Glu36Lys and p.Phe457Leu variants have been previously

found in BVVL patients (Green et al., 2010; Johnson et al., 2012), as will be described in Section 6.4.3.

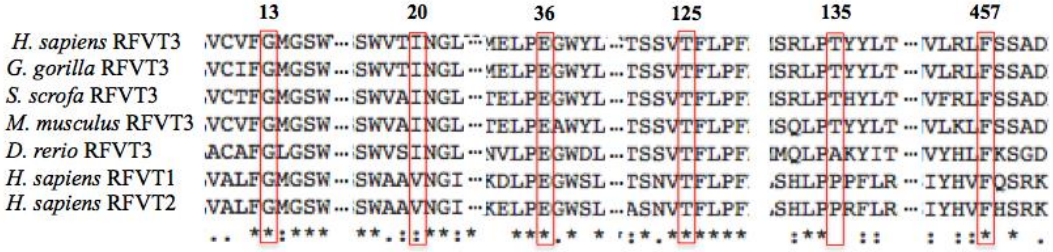

Figure 6-6 Structural conservation of relevant amino acid residues in RFVT3 across species and in RFVT1 and RFVT2. The Ensembl protein IDs for the RFVT3 orthologous sequences reported are: ENSGGOP00000004951, ENSSSCP-00000007667, ENSMUSP00000072961 and ENSDARP00000062715. An * (asterisk) indicates positions which have a single, fully conserved residue. A : (colon) indicates conservation between groups of strongly similar properties. A . (period) indicates conservation between groups of weakly similar properties.

DNA was available for both unaffected parents of patient HM. While the father was a carrier of the heterozygous p.Glu36Lys variant, no mutation was found in *SLC52A3* in the mother of patient HM. DNA was available for the unaffected father of patient LF, who was found to be a carrier of the heterozygous p.Thr125Asn mutation. DNA for the mother of patient LF was not available. Segregation analysis could not be performed for the other five patients with heterozygous *SLC52A3* mutations. Sequencing chromatograms from individuals carrying heterozygous *SLC52A3* mutations are available in Appendix VI Figure VI-2. Phenotypic details of patients with *SLC52A3* mutations will be discussed in Section 6.4.3.

All mutations identified in *SLC52A1* in both cohorts of patients were common polymorphisms. None of the SMARD and SMARD-like patients described in Section 6.3.2 had pathogenic mutations in any of the three riboflavin transporters; all identified variants were commonly found in control populations.

Table 6-1 Summary of mutations identified in *SLC52A2* and *SLC52A3* in our cohort and by our collaborators.

MUTATION SUMMARY

Gene	Mutation	Type	SIFT prediction	Polyphen-2 Prediction	Region (TMHMM prediction)	EVS MAF in Europeans	1000 Genomes/dbSNP
SLC52A2	c.92G>C; p.Trp31Ser	Non-synonymous	Not tolerated	Probably damaging	Transmembrane	N/A	N/A
SLC52A2	c.383C>T; p.Ser128Leu	Non-synonymous	Not tolerated	Possibly damaging	Transmembrane	0.0002	rs374071862 (no MAF)
SLC52A2	c.700C>T; p.Gln234Stop	Stop-gained	Not tolerated	Probably damaging	Intracellular loop	N/A	N/A
SLC52A2	c.851C>A; p.Ala284Asp	Non-synonymous	Not tolerated	Possibly damaging	Transmembrane	N/A	N/A
SLC52A2	c.914A>G; p.Tyr305Cys	Non-synonymous	Not tolerated	Probably damaging	Extracellular loop	N/A	N/A
SLC52A2	c.916G>A; p.Gly306Arg	Non-synonymous	Not tolerated	Probably damaging	Extracellular loop	N/A	N/A
SLC52A2	c.935T>C; p.Leu312Pro	Non-synonymous	Not tolerated	Probably damaging	Transmembrane	N/A	N/A
SLC52A2	c.1016T>C; p.Leu339Pro	Non-synonymous	Not tolerated	Probably damaging	Transmembrane	0.0002	rs148234606 (no MAF)
SLC52A2	c.1088C>T; p.Pro363Leu	Non-synonymous	Not tolerated	Probably damaging	Extracellular loop	N/A	N/A
SLC52A2	c.1258G>A; p.Ala420Thr	Non-synonymous	Not tolerated	Probably damaging	Transmembrane	0.0001	rs368924997 (no MAF)
SLC52A3	c.37G>A; p.Gly13Arg	Non-synonymous	Not tolerated	Probably damaging	Transmembrane	0.0001	rs146302587 (G>C change, no MAF)
SLC52A3	c.58A>C; p.Ile20Leu	Non-synonymous	Tolerated	Probably damaging	Transmembrane	0.0001	rs148387972 (no MAF)
SLC52A3	c.106G>A; p.Glu36Lys	Non-synonymous	Not tolerated	Probably damaging	Extracellular loop	N/A	rs267606686 (no MAF)
SLC52A3	c.374C>A; p.Thr125Asn	Non-synonymous	Not tolerated	Probably damaging	Transmembrane	N/A	N/A
SLC52A3	c.403A>G; p.Thr135Ala	Non-synonymous	Tolerated	Benign	Transmembrane	N/A	N/A
SLC52A3	c.1371C>G; p.Phe457Leu	Non-synonymous	Not tolerated	Probably damaging	Extracellular tail	0.0007	rs145431028 (no MAF)

6.4.2 Phenotypes of patients with *SLC52A2* mutations

The phenotype descriptions below refer to all patients with *SLC52A2* mutations in our study, with the exception of patient B1, for whom an extensive phenotype could not be obtained. Patient B1 had a persistent lactic acidemia, respiratory insufficiency, as well as moderate to severe deafness requiring hearing aids.

Phenotypes of patients with *SLC52A2* mutations are provided in Table 6-2. The phenotype of patient L1, as well as that of his affected sister is also extensively described in the recent clinical report by Urtizberea et al. (2013). Nearly half of the patients presented with a sensory ataxic gait (9/19 or 47%) associated with a progressive sensory neuropathy. The earliest symptom reported occurred at seven months (nystagmus), while the latest age of onset was eight years of age and an ataxic gait was the presenting symptom. Bilateral sensorineural hearing loss was evident in 18/19 (95%) patients; patient E8 died at two years of age, therefore any impairment might not have developed by this time. Optic atrophy was seen in 15/16 (93.8%) patients for whom ophthalmologic studies had been performed. Tongue fasciculations were noted in 11 of 19 patients. Almost all patients had severe, rapidly progressive weakness of axial and upper limb muscles with no antigravity movement. Neck and distal upper limb muscles were affected before the proximal upper limbs (Figure 6-7). However, patients generally had mild lower limb weakness with preserved ability to walk with head and trunk support. Deep tendon reflexes were usually absent, and a flexor plantar response was present in the majority of cases. Fourteen patients had respiratory insufficiency; ventilator support did not suffice to prevent respiratory failure and death in patients A3 and E8. None of the patients suffered from cognitive dysfunction (Foley et al., 2014).

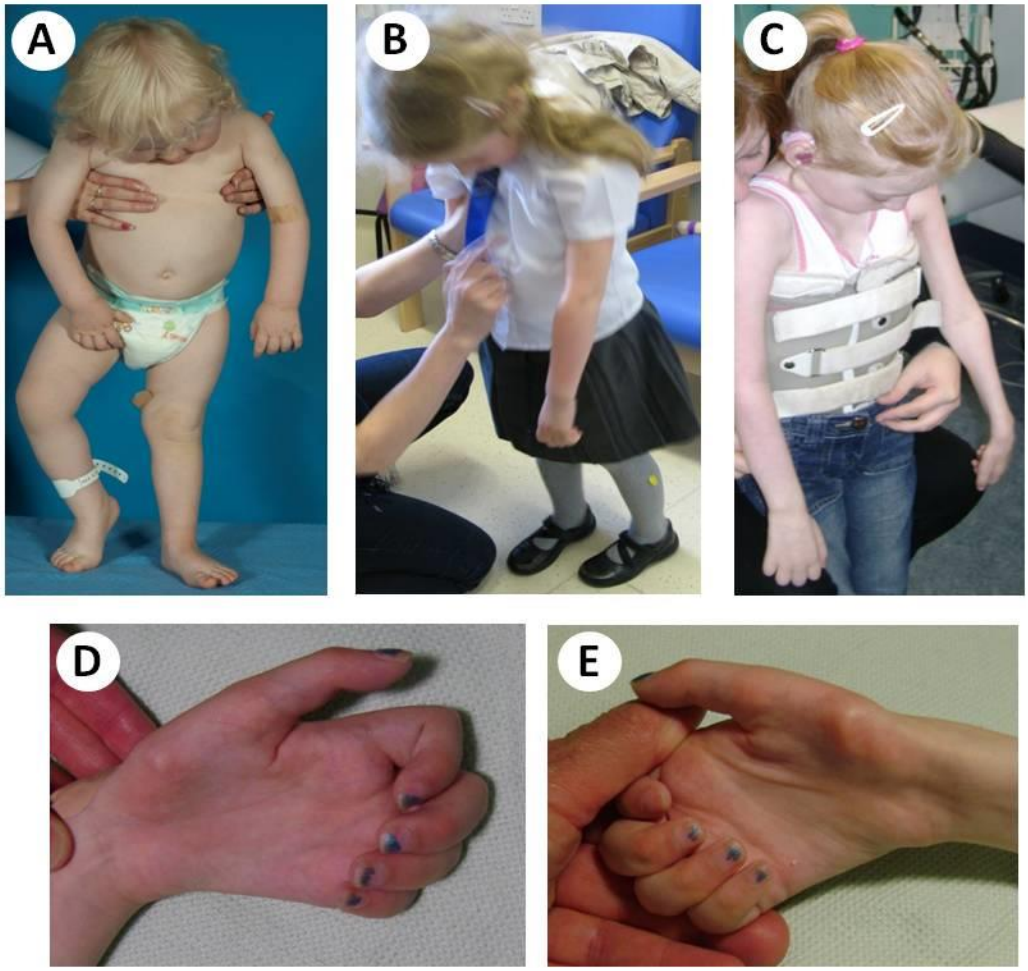

Figure 6-7 Clinical features of BVVL patients with *SLC52A2* mutations. A) Patient I1 at 1.8 years old displaying severe weakness of neck extension and upper limbs, with relative preservation of lower limb strength. B) Patient E4 at 5.8 years old. C) Patient E1 at 8.6 years old. D) and E) Patient E1's left and right hands at 10.5 years old showing symmetric atrophy of intrinsic hand muscles (reproduced from Foley et al., 2014).

Table 6-2 Clinical and genetic features of patients with mutations in *SLC52A2* at the time of diagnosis (prior to riboflavin therapy) (from Foley et al., 2014).

Patient	E1	E2	E3	E4	E5	E6
***SLC52A2* mutations**	homozygous: c.[916G>A]; p.[(Gly306Arg)]	compound heterozygous: c.[92G>C]; [935T>C] p.[(Trp31Ser)]; [(Leu312Pro)]	compound heterozygous: c.[700C>T]; [1258G>A] p.[(Gln234Stop)]; [(Ala420Thr)]	compound heterozygous: c.[916G>A]; [1016T>C] p.[(Gly306Arg)]; [(Leu339Pro)]	compound heterozygous: c.[916 G>A]; [1016T>C] p.[(Gly306Arg)]; [(Leu339Pro)]	compound heterozygous: c.[935T>C]; [1016T>C] p.[(Leu312Pro]; [(Leu339Pro)]
Sex	female	female	female	female	female	female
Ethnicity	Scottish	English and Icelandic	English	English and Scottish	Scottish	English
Consanguinity	not reported	no	no	no	no	no
First symptom	ataxic gait	ataxic gait	ataxic gait	right-sided ptosis	upper limb weakness	nystagmus
Age at first symptom	1.5 years	1 year	3.5 years	1.5 years	3 years	0.6 years
Optic atrophy	yes	yes	yes	yes	not done	yes
Sensorineural hearing loss	yes	yes	yes	yes	yes	yes
Sensorimotor neuropathy (based on NCS)	yes	yes	yes	yes	yes	yes
Distribution of weakness	upper limbs>lower limbs; neck extension	upper limbs>lower limbs; neck extension	upper limbs>lower limbs; neck extension	upper limbs>lower limbs; neck extension	upper limbs>lower limbs; neck extension	upper limbs>lower limbs; neck extension
Overall maximal motor function	independent ambulation	independent ambulation	independent ambulation	independent ambulation	independent ambulation	independent ambulation
Maximal motor function at the time of diagnosis (prior to riboflavin therapy)	taking a few steps with head and trunk supported	unable to sit	walking if trunk supported	walking if trunk supported	taking a few steps with head and trunk supported	taking a few steps with head and trunk supported
Respiratory function	nocturnal non-invasive ventilation	ventilator dependent	ventilator dependent	nocturnal non-invasive ventilation	nocturnal non-invasive ventilation	nocturnal non-invasive ventilation
Feeding	by mouth	by gastrostomy only	by mouth and gastrostomy	by mouth	by gastrostomy only	by mouth and gastrostomy
Age at genetic diagnosis	10 years	6 years	5 years	5 years	12 years	17.5 years

Patient	E7	E8	B1	I1	L1	Family 1 A1	Family 1 A2
***SLC52A2* mutations**	compound heterozygous: c.[916 G>A]; [1258G>A] p.[(Gly306Arg)]; [(Ala420Thr)]	homozygous: c.[935T>C] p.[(Leu312Pro]	compound heterozygous: c.[383C>T]; [1088C>T] p.[(Ser128Leu)]; [(Pro363Leu)]	compound heterozygous: c.[914A>G]; [916G>A] p.[(Tyr305Cys)]; [(Gly306Arg)]	homozygous: c.[916G>A]; p.[(Gly306Arg)]	homozygous: c.[916G>A]; p.[(Gly306Arg)]	homozygous: c.[916G>A]; p.[(Gly306Arg)]
Sex	male	female	female	male	male	female	female
Ethnicity	English	English	Brazilian	Irish	Lebanese	Lebanese	Lebanese
Consanguinity	no	no	unknown	no	yes	yes	yes
First symptom	hearing loss	horizontal nystagmus and motor-developmental arrest	unknown	nystagmus	hearing loss	ataxic gait	ataxic gait
Age at first symptom	2 years	7 months	unknown	1.3 years	3 years	8 years	3 years
Optic atrophy	yes	yes	unknown	yes	not done	no	yes
Sensorineural hearing loss	yes	no	yes	yes	yes	yes	yes
Sensorimotor neuropathy (based on NCS)	yes	yes	unknown	yes	yes	sensory only	yes
Distribution of weakness	upper limbs>lower limbs	upper limbs>lower limbs	unknown	upper limbs>lower limbs; neck extension	upper limbs>lower limbs; neck extension	none detected	upper limbs
Overall maximal motor function	independent ambulation	crawling, pulling to stand, could hold objects with pincer grip	unknown	independent ambulation	independent ambulation	independent ambulation	independent ambulation
Maximal motor function at the time of diagnosis (prior to riboflavin therapy)	taking a few steps with head and trunk supported	hypotonic, deteriorated arm function	unknown	sitting	independent ambulation	independent ambulation	independent ambulation
Respiratory function	nocturnal non-invasive ventilation	ventilator dependent	respiratory insufficiency	ventilator dependent	normal	normal	normal
Feeding	by mouth and gastrostomy	by gastrostomy only	unknown	by nasogastric tube only	by mouth	by mouth	by mouth
Age at genetic diagnosis	21.5 years	deceased (2.1 years)	24 years	1.9 years	6 years	10 years	9 years

Patient	Family 2		Family 3			Family 4	
	A3	**A4**	**A5**	**A6**	**A7**	**U1**	**U2**
***SLC52A2* mutations**	compound heterozygous: c.[916G>A]; [1016T>C] p.[(Gly306Arg)]; [(Leu339Pro)]	compound heterozygous: c.[916G>A]; [1016T>C] p.[(Gly306Arg)]; [(Leu339Pro)]	homozygous: c.[916G>A]; p.[(Gly306Arg)]	homozygous: c.[916G>A]; p.[(Gly306Arg)]	homozygous: c.[916G>A]; p.[(Gly306Arg)]	compound heterozygous: c.[851C>A]; [916G>A] p.[(Ala284Asp)]; [(Gly306Arg)]	compound heterozygous: c.[851C>A]; [916G>A] p.[(Ala284Asp)]; [(Gly306Arg)]
Sex	female	female	male	male	male	female	male
Ethnicity	English and Scottish	English and Scottish	Lebanese	Lebanese	Lebanese	Native American, Scottish, Irish, English and German	Native American, Scottish, Irish, English and German
Consanguinity	no	no	yes	yes	yes	no	no
First symptom	ataxic gait and upper limb weakness	hearing loss	ataxic gait and hearing loss	ataxic gait and hearing loss	ataxic gait	respiratory failure	vision loss
Age at first symptom	2 years	5 years	3 years	3 years	5 years	2 years	4 years
Optic atrophy	not done	yes	yes	yes	yes	yes	yes
Sensorineural hearing loss	not done	yes	yes	yes	yes	yes	yes
Sensorimotor neuropathy (based on NCS)	yes	yes	yes	yes	yes	yes	yes
Distribution of weakness	upper limbs	upper limbs; neck extension	upper limbs; neck extension	upper limbs; neck extension	upper limbs	upper limbs>lower limbs	upper limbs>lower limbs
Overall maximal motor function	independent ambulation	independent ambulation	independent ambulation	independent ambulation	independent ambulation	independent ambulation	independent ambulation
Maximal motor function at the time of diagnosis (prior to riboflavin therapy)	taking a few steps with head and trunk supported	independent ambulation	taking a few steps with head and trunk supported	taking a few steps with head and trunk supported	independent ambulation	independent ambulation	walking with a cane
Respiratory function	decreased; on ventilator at the time of death	decreased; nocturnal non-invasive ventilation recommended	ventilator dependent	nocturnal non-invasive ventilation	normal	nocturnal non-invasive ventilation	normal
Feeding	by mouth	by mouth	by gastrostomy only	by gastrostomy only	by mouth	by mouth	by mouth
Age at genetic diagnosis	deceased (3.5 years)	15 years	16 years	16 years	21 years	52 years	44 years

Plasma acylcarnitine profiles were abnormal prior to riboflavin therapy in 10 out of 17 patients tested (59%). Acylcarnitine profiles and plasma concentrations of riboflavin, FAD and FMN prior to riboflavin therapy are available for patients E1-E7, A1-A7, U1-U2 and I1 (Appendix VI Table VI-7). Activity of MRC complexes in muscle was determined in seven patients (E1, E2, E5, E6, E8, I1 and A6). Three patients had complex activities falling outside the normal range: E2 had decreased complex IV activity (0.012 (reference range: 0.014-0.034)), E6 had decreased complex I activity (0.089 (reference range: 0.104-0.268)) and I1 had decreased complex II/III activity (0.026 (reference range: 0.040-0.204)). Electrophysiological studies revealed an axonal sensory-motor neuropathy for all 19 patients. In all cases, the motor neuropathy was more severe in the upper limbs than the lower limbs. The sensory neuropathy appeared earlier than the motor neuropathy in patients for whom multiple tests were performed. Neurophysiological findings for patients E1-E7, A1-A7, U1-U2, L1 and I1 are detailed in Appendix VI Table VI-8. Sural nerve biopsies were available for patients E2, E3, E5, A3, A6 and I1; findings revealed a chronic axonal neuropathy with fibrosis and continuous degeneration with no regeneration. The absence of regeneration may be more suggestive of a neuronopathy. Preferential involvement of large myelinated fibres may explain the sensory ataxia and areflexia. No signs of inflammation, hypomyelination or demyelination were seen on the biopsies. The remaining axons were mostly normal or atrophic in a few cases (Appendix VI Table VI-9) (Foley et al., 2014).

Brain MRI was normal in the 15 patients in whom it was performed. Brain MRI is usually normal in BVVL although several reports have noted structural and signal abnormalities, as described in Section 1.6.1 (Ciccolella et al., 2012; Dakhil et al., 2010; Foley et al., 2014; Francis et al., 1993; Koul et al., 2006; Koy et al., 2012; Malheiros et al., 2007; Sathasivam, 2008).

6.4.3 Phenotypes of patients with *SLC52A3* mutations

Limited phenotypes could be obtained for the patients with heterozygous *SLC52A3* mutations. The siblings RDB and NDB carried the heterozygous p.Gly13Arg *SLC52A3* mutation. These siblings are the product of a consanguineous marriage;

both patients have a typical BVVL phenotype with sensorineural hearing loss and LMN disease with bulbar signs.

Patient JG carried the heterozygous p.Ile20Leu mutation in *SLC52A3*; there is consanguinity in this patient's family and inheritance is likely AR. The two most likely diagnoses were considered to be AR spastic ataxia of Charlevoix-Saguenay and X-linked bulbospinal muscular atrophy. Patient JG had optic nerve pressure from two years of age; his gait was abnormal from the age of five. He had multiple system involvement suggesting a mitochondrial abnormality including peripheral neuropathy, some myopathy with neck flexion and extension weakness, ptosis, cerebellar signs with some bulbar involvement (speech), mild dysdiadochokinesis, spasticity, gaze-evoked nystagmus, tonic pupils and raised pressure in the eye. This patient also had some oral facial myokymia, diplopia, oxycephaly, possible mild hearing loss, slurred speech, and difficulty chewing and swallowing. At age 25, walking was increasingly difficult with unsteadiness, fatigue and falls. He also had distal upper limb weakness, proximal and distal lower limb weakness, distal muscle atrophy as well as bilateral facial weakness. Pinprick sensation was reduced in the extremities, and temperature sensation was reduced in the forearm and lower leg. Reflexes were absent at the ankles.

Patient HM, who carried the heterozygous p.Glu36Lys mutation in *SLC52A3* had a very mild phenotype with bilateral optic and auditory neuropathies; sequencing of the full mitochondrial DNA and *optic atrophy 1* (*OPA1*) were negative. No further clinical details were available. The same mutation has been found in the cis configuration with a heterozygous p.Val413Ala mutation in *SLC52A3*. The patient presented in his twenties with peripheral neuropathy and could walk a short distance with a stick in his fifties. He had muscle wasting, truncal ataxia, sensorineural deafness but no respiratory compromise. As the p.Val413Ala mutation was tolerated by SIFT, it was suggested to be a possible polymorphism, which would fit with the milder phenotype of the patient in that study (Green et al., 2010) and in our study.

Patient LF carried the heterozygous p.Thr125Asn mutation in *SLC52A3*. This patient is currently 12 years of age; the principal phenotypic features include poor hearing, neuropathy, ataxia, weight loss, and breathing problems. Patient KG carried the

heterozygous p.Thr135Ala variant. This patient is a 15 year-old girl who presented with a partial right third nerve palsy and hemi-atrophy of the right side of her tongue. An MRI scan was normal. There was no history of deafness. Over 6-8 weeks, she developed progressive weakness starting in the face, progressing to the shoulders and eventually the lower limbs. She also developed significant neuromuscular scoliosis requiring spinal surgery. The patient required a wheelchair and a nasogastric tube for feeding. NCS was suggestive of an axonal neuropathy. The patient was treated with IVIG with no significant improvement, but she showed dramatic improvement in her strength when treated with steroids. After the first course (four months) of steroids, this patient's condition returned to the baseline level of functioning. Investigations for CMT1, HNPP, and Friedreich's Ataxia were all negative. Riboflavin was recently trialled with no dramatic improvement, but treatment with steroids has been successfully weaned down.

Patient LS carried the heterozygous p.Phe457Leu mutation. No detailed phenotype is available but the patient was described as having a typical BVVL phenotype with stabilisation on high-dose riboflavin therapy. As mentioned in 6.1.5, mutations located in the COOH terminal such as this one are usually associated with severe phenotypes (Bosch et al., 2011; Ciccolella et al., 2012; Green et al., 2010; Subramanian, Rapp, et al., 2011). The p.Phe457Leu mutation has been previously found in the homozygous state in two patients (Green et al., 2010; Johnson et al., 2012). In the Green et al. (2010) study, the patient presented at three months and had breathing difficulties, deafness, respiratory compromise and generalised weakness, leading to death at 11 months (Green et al., 2010). No phenotype was provided in the Johnson et al. (2012) study.

It is possible that another mutation in the compound heterozygous state in *SLC52A3* was missed. However, single heterozygous mutations in *SLC52A3* causing BVVL disease have been described in several studies (Ciccolella et al., 2012; Dezfouli et al., 2012). In the Dezfouli et al. (2012) study, the two heterozygous *SLC52A3* mutations each found in one patient were located at highly conserved amino acids. The two patients had later disease onset; however, inheritance was unlikely to be AD as the parents were unaffected (Dezfouli et al., 2012; Houlden, 2012). AD inheritance has

only rarely been described in BVVL (De Grandis et al., 2005; Hawkins et al., 1990). Incomplete penetrance has been considered in some BVVL families where affected siblings of BVVL patients showed a very mild phenotype (Dezfouli et al., 2012; Hawkins et al., 1990). In the Ciccolella et al. (2012) study, a BVVL patient carried a heterozygous *SLC52A3* p.Cys432Stop mutation and no other mutation in the coding region and UTRs; the authors suggested that the protein may be partially functional. As suggested by these authors, BVVL patients with heterozygous *SLC52A3* mutations may have a heterozygous copy number variant on the other allele or a pathogenic mutation in a non-coding region of *SLC52A3* such as a deep intronic or promoter variant (Ciccolella et al., 2012; Dezfouli et al., 2012). Although this could not be carried out during this study, the DNA of these patients will be run on a custom array to determine whether copy number defects are present in *SLC52A3*. Analysing the cDNA and performing family segregation studies would also help assess the pathogenicity of the *SLC52A3* mutations identified in this study.

Where this information was available, a brief clinical description of patients who tested negative for all three riboflavin transporters in both cohorts screened at our centre is available in Appendix VI Tables VI-12 and VI-13. The phenotypes of individual II-10 of family SP and individuals III-3 and III-8 of family TB who were part of the patient cohort specifically referred to us for BVVL testing are available in Section 6.3.3.

6.4.4 Response of BVVL patients to high-dose oral riboflavin treatment

High-dose oral riboflavin therapy was commenced in 16 patients with *SLC52A2* mutations, with treatment durations lasting from one month to 20 months. There were no reported adverse events or toxicity. One patient did not agree to administration of the therapy and two died (patients A3 and E8) prior to the genetic diagnosis. Stable function or significant, sustained improvement clinically and biochemically was reported in 15 of the 16 patients in whom high-dose oral riboflavin was administered; one patient could not be followed-up. The therapy was effective after just four weeks of treatment in patient I1 and proved to be life-saving; this is likely due to the fact that the therapy was initiated near to symptom-onset in this patient. For all nine patients with abnormal plasma acylcarnitine profiles in

whom repeat tests were performed, the acylcarnitine profile normalised upon treatment with riboflavin (within two weeks after the first riboflavin dose in patient I1). The levels of riboflavin, FAD and FMN (or FAD only, when measured on its own) increased in 9/10 patients with tests performed before and after the start of treatment. Partial acylcarnitine profiles and plasma concentrations of riboflavin, FAD and FMN following riboflavin therapy are available for patients E1, E3, E4, E7, A1-A2, A4, A5-A7, U1-U2 and I1 (Appendix VI Table VI-10). Observed responses to riboflavin therapy including treatment dose and duration for patients E1-E4, E6, E7, A1-A2, A4-A7, U1-U2, I1 and L1 are summarised in Appendix VI Table VI-11. Detailed clinical responses to therapy were available for patients E1 and I1 and are described below (Foley et al., 2014).

Patient E1 was first described in the report by Johnson et al. (2012). This patient initially presented at 18 months of age with a sensory ataxia; at age six, there was progressive weakness in the upper limbs, vision and hearing loss, and respiratory insufficiency. The homozygous *SLC52A2* p.Gly306Arg mutation was detected at age 10; following this finding, treatment with 10 mg/kg/day of riboflavin was commenced. Over a period of 12 weeks, the dose was steadily increased up to 50 mg/kg/day. Patient E1 showed improvement in biochemical and clinical tests performed three months after initiation of treatment, including normalization of the acylcarnitine profile, improved visual evoked potentials, audiometry testing and pulmonary function (Table 6-3). These last three tests had previously shown steady deterioration prior to treatment. Although patient E1's hair, shoe size, weight and height had stayed stable between the ages of six and ten, these measures have also shown an improvement with riboflavin therapy. She remains stable after 20 months of therapy and has shown particularly significant improvement in motor function; she can now sit and stand on her own, something she had not been able to do for three years (Foley et al., 2014).

Table 6-3 Response to high-dose riboflavin therapy in patient E1 (reproduced from Foley et al., 2014).

Testing Modality	Prior to Riboflavin	After 3 Months of Riboflavin
Audiometry	80db at 8 kilohertz	40-55db at 8 kilohertz
Visual Evoked Potentials	Size Both eyes open 200' degraded 100' 10uV at 176 milliseconds 50' 14uV at 175 milliseconds	Size Both eyes open 200' 16uV at 160 milliseconds 100' 16uV at 154 milliseconds 50' 8uV at 131 milliseconds
Forced Vital Capacity	0.51 Litres (29%)	0.56 Litres (33%)
Acylcarnitine Profile	Mimicking MADD	Normal

A thorough report on response to high-dose riboflavin treatment was also available for patient I1. At 22 months of age, this patient presented with a six-month history of nystagmus, four-month history of ataxic gait and rapidly progressive weakness of hand and bulbar muscles over the preceding three weeks. Upon first evaluation, patient I1 could not walk or hold a bottle. Respiratory failure and severe swallowing difficulties quickly followed. Further examinations revealed bilateral optic atrophy, vision loss and bilateral sensorineural hearing loss. The C6, C8, C10 and C14:1 carnitine species were raised in plasma (Appendix VI Table VI-7). Riboflavin treatment with a dose of 10 mg/kg/day was initiated only eight days after first presentation; dosage was increased to 50 mg/kg/day over a four-week period. Respiratory support was no longer necessary only ten days after the start of treatment, and the patient has remained stable since this time. After four weeks of treatment, he could hold his head upright, grab objects, feed by mouth and walk with trunk support (Foley et al., 2014).

6.4.5 Array analysis of *SLC52A2* and surrounding region in patient E1

As described in Section 6.3.9, the HumanCytoSNP-12 v.2.1 BeadChip was used to provide further evidence that the *SLC52A2* p.Gly306Arg variant was indeed homozygous in patient E1 despite there being no known consanguinity in the family. Although the BeadChip array did not contain SNPs within the *SLC52A2* gene, the

SLC52A2 gene was located within a large 2 Mb region of homozygosity in this patient. It is worth noting that Sanger sequencing in this patient did not reveal any heterozygous bases in *SLC52A2* exons or flanking intronic sequences. The log R ratio did not support the possibility of a large deletion encompassing the *SLC52A2* gene or exons. It is likely that the p.Gly306Arg mutation was indeed homozygous in this patient. Due to time constraints, such an assessment could not be carried out in patient E8 with the homozygous *SLC52A2* p.Leu312Pro mutation who also had no reported consanguinity in her family.

6.4.6 Haplotype analysis of patients of Lebanese origin carrying the homozygous *SLC52A2* p.Gly306Arg mutation

The haplotype was established around the *SLC52A2* p.Gly306Arg mutation in the families of Lebanese origin including A1-A2, A5-A7, L1 (proband L1, his unaffected parents and affected sister) and in the family described in Mégarbané et al (2000) (proband, two unaffected siblings, unaffected father and affected cousin). In all these families, the heterozygous and homozygous state of the mutation was confirmed in all unaffected parents and affected individuals, respectively. The haplotype analysis showed all affected patients to be homozygous at all 11 genotyped SNPs (Appendix VI Table VI-6). The Australian families of Lebanese origin A1-A2 and A5-A7 had a different genotype at one SNP located close to the end of the analysed segment (dbSNP ID: rs4993862). If the mutation is a founder mutation and has its origins on a common haplotype in the Lebanese population, it would imply that there must have been a recent recombination event between the two variants, or that the variant located at rs4993862 has arisen after the p.Gly306Arg mutation (Foley et al., 2014). The haplotype around the homozygous p.Gly306Arg mutation in patient E1, who is of non-Lebanese origin, has previously been established to be different from the haplotype in the family described by Mégarbané et al. (2000) (Johnson et al., 2012).

6.4.7 Transcriptional analysis of mutations in BVVL patients

In all patients for whom fibroblasts were available (patients E1-E4 and I1) and in the carrier fibroblast line (mother of E1), the cDNA analysis did not show aberrant transcripts. With the exception of the stop mutation in patient E3 discussed below,

the cDNA sequencing confirmed all mutations found at the genomic level. In patient E3, the p.Ala420Thr mutation was confirmed by cDNA analysis; however, only the WT allele was present on analysis of the cDNA for the p.Gln234Stop mutation, suggesting that this mutation results in NMD (Figure 6-8).

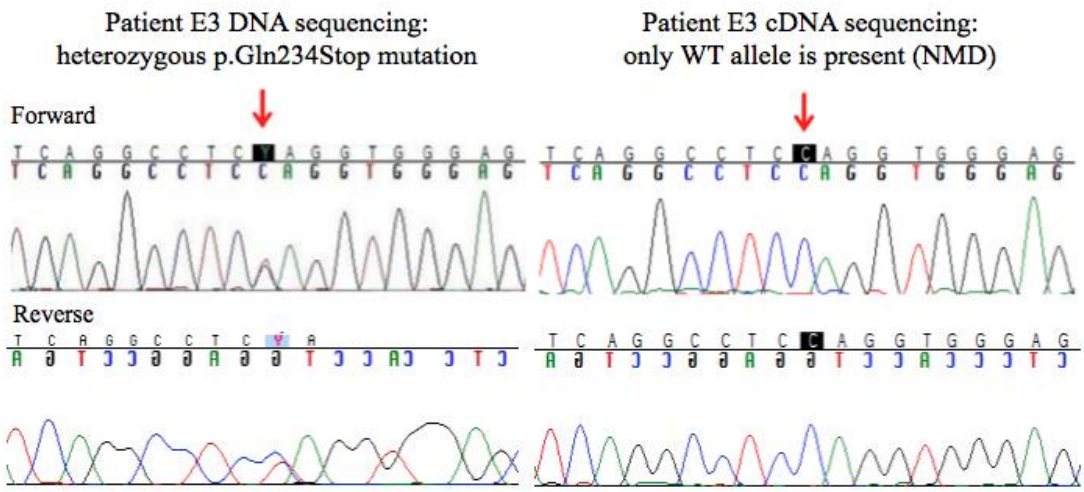

Figure 6-8 DNA and cDNA sequencing of *SLC52A2* exon 3 in patient E3 showing NMD at the cDNA level.

6.4.8 Exome sequencing

The reader is referred to Appendix VI Table VI-14 for a list of poorly covered exons in the three known riboflavin transporter genes for families SP, MO and TB. The only poorly covered exons in these three genes were exons 4 in *SLC52A2* and *SLC52A3* in individual III-3 of family MO. The *GSTZ1* gene, a candidate gene in individual III-3 of family MO, was well covered in this individual.

The exome sequencing for individual II-3 of family SP resulted in a total of 47,212,177 reads. The mean target coverage was 58.9X; 95.7% of the bases had at least 2-fold coverage, 89.9% of bases had at least 10-fold coverage and 68.6% of the bases had at least 30-fold coverage. There were a total of 49,049,895 reads in the exome sequencing of individual III-1 in family SP. The mean target coverage was 63X; 95.8% of the bases had at least 2-fold coverage, 90.5% of bases had at least 10-fold coverage and 70.9% of the bases had at least 30-fold coverage. A total of 22,925 variants were found in individual II-3. After filtering out synonymous variants, 11,589 variants remained. In agreement with the Sanger sequencing results, no

variant amongst these was located in *SLC52A2* or *SLC52A3*; two non-synonymous variants were found in *SLC52A1*, however both variants are common polymorphisms (Appendix VI Table VI-15). After filtering out homozygous variants, 6,974 variants remained. 505 variants remained after removing variants in segmental duplications and those found in control databases using the frequency filters mentioned in Section 6.3.16. By selecting only variants in the compound heterozygous state with at least one other variant in the same gene, 60 variants in 28 different genes remained. The unaffected son of individual II-3, individual III-1 should only carry one of the two variants found in the compound heterozygous state in his mother. Individual III-1 carried the same two common non-synonymous variants in *SLC52A1* as those found in his mother. For 14 out of the 28 genes remaining, the son did not carry any of the same variants as his mother; for six of these genes, the son carried all the same variants in a particular gene as his mother. Therefore, eight genes remained in which individual II-3 had at least two variants, and individual III-1 did not carry at least one of the variants found in his mother. The genes remaining included *titin* (*TTN*), *transmembrane protein 184A* (*TMEM184A*), *mucin 6* (*MUC6*), *olfactory receptor, family 4, subfamily C, member 45* (*OR4C45*), *achalasia, adrenocortical insufficiency, alacrima syndrome* (*AAAS*), *phosphatidylinositol glycan anchor biosynthesis, class Q* (*PIGQ*), *tektin 5* (*TEKT5*) and *dynein, axonemal, heavy chain 17* (*DNAH17*). Based on protein function, the most likely candidate gene amongst these was *AAAS*; the protein encoded by this gene, ALADIN, is a nucleoporin of the nuclear pore complex and is a member of the WD-repeat family of regulatory proteins. It is thought to be involved in the development of the CNS and PNS (Handschug et al., 2001; Koehler et al., 2013; Tullio-Pelet et al., 2000). Homozygous and compound heterozygous mutations in this gene cause Achalasia-Addisonianism-Alacrima Syndrome (AAAS), also known as Triple-A syndrome or Allgrove syndrome (Handschug et al., 2001; Tullio-Pelet et al., 2000).

Individual II-3 carried two heterozygous non-synonymous mutations in the first exon of *AAAS*, p.Gln15Lys (c.43G>T) and p.Tyr19Cys (c.56T>C) (Ensembl Transcript ID: ENST00000209873). The proband's son, individual III-1, only carried the p.Gln15Lys (c.43G>T) variant in the heterozygous state in this gene, along with a synonymous mutation. The depth and quality of the p.Gln15Lys variant were 69 and

194 respectively in individual II-3; corresponding values for the p.Tyr19Cys variant were 68 and 201. Neither of the two variants is located within a WD-repeat region (UniProtKB ID: Q9NRG9). The p.Gln15Lys variant may be in a region needed for AAAS protein β-strand stability (Sandrini et al., 2001). The p.Gln15Lys variant was found in dbSNP (ID: rs121918549), however it was classified as pathogenic and no frequency data was available. Its MAF in the EVS database was 0.000186; it was not found in the CG69 or 1000 Genomes databases. The p.Tyr19Cys was not found in the dbSNP, 1000 Genomes, CG69 or EVS control databases. The p.Gln15Lys variant was predicted benign by SIFT, possibly damaging by PolyPhen-2 (score=0.779), and disease-causing by Mutation Taster (score=1.45, probability=0.977). The p.Tyr19Cys variant was predicted benign by SIFT and PolyPhen-2 (score=0), but disease-causing by Mutation Taster (score=5.29, probability=0.995). However, SIFT had low confidence in its prediction ability at these amino acids. Furthermore, the specificity of the Polyphen-2 prediction for p.Tyr19Cys was zero, therefore the prediction cannot be trusted in this case. Both amino acids altered in *AAAS* in individual II-3 are conserved in *Pan troglodytes, Macaca mulatta, Mus musculus, Felis catus* and *Xenopus tropicalis*; there is no homologue or alignment for *Drosophila melanogaster* and *Caenorhabditis elegans*. The GERP scores were 3.33 and 4 for p.Gln15Lys and p.Tyr19Cys, respectively, confirming that the two amino acids are under evolutionary constraint.

Triple-A syndrome is a rare, AR multi-system disease. The main features include alacrima, achalasia and adrenal failure (Allgrove et al., 1978). However, neurologic features involving the CNS, PNS and autonomic nervous system have been reported. These features include wasting and weakness of distal limb muscles, brisk tendon reflexes with absent ankle jerks, inability to walk on toes, pes cavus, dysarthria, autonomic abnormalities, hyperreflexia, amyotrophy, ataxia, gait disturbance, optic atrophy, cognitive deficits and sensory impairment (Dixit et al., 2011; Houlden et al., 2002; Sandrini et al., 2001; Tullio-Pelet et al., 2000; Vallet et al., 2012). These reports have also highlighted the phenotypic heterogeneity and the variable disease severity which may be seen in Triple-A syndrome; indeed, patients may only have a subset of the typical clinical problems usually associated with the disease (Houlden et al., 2002). Both sensory-motor axonal and demyelinating neuropathies have been

reported (Dixit et al., 2011; Dumić et al., 2011). Neurological symptoms are especially predominant in late-onset cases; endocrine and gastrointestinal issues may be minor in these cases (Vallet et al., 2012). Alacrima, adrenal abnormalities and autonomic involvement were not reported in individual II-3 in family SP; however, the patient did have prominent neurological involvement with several of the features noted above including: dysarthria, pes cavus, gait disturbance, amyotrophy, brisk tendon reflexes with absent ankle jerks, sensory deficits and an axonal sensory-motor neuropathy. Individual II-3 also had dysphagia, one of the features of achalasia. Palatal paresis, atrophic furrowed tongue with fasciculations and prolonged central motor conduction times as seen in individual II-3 have also been previously described in the literature in Triple-A syndrome (Houlden et al., 2002).

The p.Gln15Lys variant in *AAAS* has been previously reported in the homozygous and compound heterozygous state in cases of Triple-A syndrome (Handschug et al., 2001; Houlden et al., 2002; Sandrini et al., 2001; Vallet et al., 2012). When found in the homozygous state, this mutation led to a milder phenotype and was associated with alacrima, achalasia, learning disabilities, neurologic deficiencies and glucocorticoid deficiency (Sandrini et al., 2001). The other mutation p.Tyr19Cys is novel. Most mutations in this gene lead to a truncated protein and are therefore predicted to act via a loss of function mechanism (Handschug et al., 2001). Frameshift and nonsense mutations are generally associated with a more severe phenotype (Houlden et al., 2002), which may explain the milder phenotype seen in our patient.

AAAS, located on chromosome 12, is 546 amino acids long and has 16 coding exons. It contains four WD-repeat regions. It is ubiquitously expressed although it is most highly expressed in a subset of cells in the CNS, as well as in gastrointestinal structures, in the blood and immune system, heart muscle, kidney, endocrine glands and the male reproductive system (Handschug et al., 2001; http://www.proteinatlas.org). It is weakly expressed in peripheral nerve (http://www.proteinatlas.org). Nucleoporins such as ALADIN are responsible for transport of macromolecules between the cell nucleus and cytoplasm. ALADIN is needed for the import of several factors into the cell nucleus, including aprataxin,

DNA ligase I, and ferritin heavy chain, and is important for preventing DNA damage and associated oxidative stress (Koehler et al., 2013). In fibroblasts of Triple-A syndrome patients, several genes associated with antioxidant defence and oxidative stress were differentially regulated; it was postulated that Triple-A syndrome patients have a defective response to oxidative stress (Koehler et al., 2013). We believe that Triple-A syndrome due to mutations in the *AAAS* gene is likely to be the cause of the neuropathy in family SP.

The exome sequencing for individual III-3 of family MO resulted in a total of 64,488,853 reads. The mean coverage was 47.7X; 93% of the bases had at least 2-fold coverage, 87.1% of bases had at least 10-fold coverage and 67.1% of the bases had at least 30-fold coverage. Individual III-3 of family MO had severe progressive sensory-motor axonal neuropathy, tubulopathy and cataracts. In total, 21,468 variants were found in this proband. After filtering out synonymous variants, 10,901 variants remained. Amongst these variants, no variants were found in *SLC52A2*. Two non-synonymous variants were found in *SLC52A1* and *GSTZ1*, and three non-synonymous variants were detected in *SLC52A3*; however, all of these variants were common polymorphisms (Appendix VI Table VI-16). 6,671 variants remained after filtering out homozygous variants. 418 variants remained after filtering out variants in segmental duplications and those found in control databases using the frequency filters mentioned in Section 6.3.16. After selecting only variants in the compound heterozygous state with at least one other variant in the same gene, 47 variants in 21 different genes remained.

The most probable candidate gene amongst these 21 genes based only on protein function was *neurofilament heavy polypeptide* (*NEFH*). *NEFH*, located on chromosome 22, has four exons and encodes a protein of 1,020 amino acids. According to the Human Protein Atlas, NEFH is highly expressed in neuronal cells of the CNS and in the salivary gland, and is moderately expressed in the peripheral nerve, pancreas and liver. Neurofilaments, the intermediate filaments of neurons, are structural proteins involved in stability of the cytoskeleton and in determination of the axon diameter (Lariviere & Julien, 2004; Lees et al., 1988).

Individual III-3 of family MO carried a heterozygous non-frameshift insertion p.Lys651_Ala652insProLysSerProGluLys (c.1953_1954insCCCAAGTCCCCTGA-GAAG) and a heterozygous non-frameshift substitution p.Glu658delinsProSer-ProHisArgArg (c.1972_1973insCCAAGTCCCCATAGA-AGG), both located in the fourth exon of *NEFH* (Ensembl Transcript ID: ENST00000310624). The depth and quality of both variants were 217 and 113, respectively. The variants identified in our study are located within a repeat region of the Lys-Ser-Pro sequence motif in the heavily phosphorylated tail domain of the NEFH protein (UniProtKB ID: Q9NRG9). A common polymorphism results in either 43 or 44 of these repeats. Neither of the two variants was found in the dbSNP, 1000 Genomes, CG69 or EVS control databases. Although similar in-frame insertions and deletions are reported in these databases between amino acids 525 and 832, most have no frequency data.

The tail domain is involved in forming cross-links between filaments (Figlewicz et al., 1994). Phosphorylation of this domain has been involved in determining the density of the neurofilament and the axonal calibre (Lariviere & Julien, 2004; Lees et al., 1988). The variants identified herein could disrupt the phosphorylation pattern, thus dysregulating the filament crosslinking and the assembly of the neurofilaments, potentially leading to abnormal protein accumulation within neurons (Figlewicz et al., 1994; Tomkins et al., 1998). Mice overexpressing the human *NEFH* gene develop a progressive neuronopathy with impairment of neurofilament transport causing axonopathy and muscle atrophy, suggesting that regulation of this gene is crucial for neuronal health (Côté et al., 1993). Although the common 43/44 repeat polymorphism mentioned above is neutral, other deletions and insertions in the repeat domain were found in sporadic ALS patients and were not found in controls in several studies (Lariviere & Julien, 2004; Tomkins et al., 1998). Mutations in the *neurofilament light polypeptide* (*NEFL*) gene causing defects in neurofilament assembly are associated with CMT2E (Rossor et al., 2013). Additional studies are required before it can be concluded that *NEFH* mutations are the cause of the neuropathy in individual III-3 of family MO.

There were a total of 45,866,011 reads in the exome sequencing of individual III-3 in family TB. The mean target coverage was 57.6X; 95.6% of the bases had at least 2-

fold coverage, 89.6% of bases had at least 10-fold coverage and 67.9% of the bases had at least 30-fold coverage. The exome sequencing for individual III-8 of family TB resulted in a total of 49,890,292 reads. The mean coverage was 62.5X; 95.7% of the bases had at least 2-fold coverage, 90.2% of bases had at least 10-fold coverage and 70.6% of the bases had at least 30-fold coverage. Individuals III-3 and III-8 in family TB had an AR, predominantly motor polyneuropathy. A total of 22,950 variants were found in individual III-8. After filtering out synonymous variants, 11,767 variants remained. As expected, no variant amongst these was found in *SLC52A2* or *SLC52A3*; two common non-synonymous variants were found in *SLC52A1*, neither of which is likely to be pathogenic (Appendix VI Table VI-17). 770 variants remained after removing variants in segmental duplications and those found in control databases using the frequency filters mentioned in Section 6.3.16. A total of 22,767 variants were found in individual III-3 of family TB. After filtering out synonymous variants, 11571 variants remained. Again, no variant amongst these was found in *SLC52A2* or *SLC52A3*; the same two common *SLC52A1* variants as in individual III-8 were detected. 596 variants remained in individual III-3 after removing variants in segmental duplications and those found in control databases using the frequency filters mentioned in Section 6.3.16.

Three models were then followed. In the eventuality that both cousins carried the same mutation in the homozygous state, all heterozygous variants were filtered out in individuals III-3 and III-8: 89 variants and 86 variants remained for individuals III-3 and III-8, respectively. 39 homozygous variants in 38 different genes were common to both individuals. The number of homozygous variants in common between the two individuals could not be further reduced; no variant was considered especially likely to be disease-causing based on protein function. For the second model, homozygous variants were filtered out from the list of 596 variants remaining for individual III-3; 507 heterozygous variants remained. Twenty genes had at least two variants in the compound heterozygous state. Upon searching for variants in the compound heterozygous state in individual III-3 for which one of the two variants was also found in the homozygous state in individual III-8, no variants remained. For the third model, homozygous variants were filtered out from the list of 770 variants remaining in individual III-8, and only compound heterozygous variants were

selected out of the list of 684 remaining heterozygous variants. Amongst these, a total of 33 genes had at least two heterozygous variants in individual III-8. Three genes were common to both lists of compound heterozygous variants in individuals III-3 and III-8 (*MUC6, OR4C45* and *dentin sialophosphoprotein* (*DSPP*)); however, none of the variants in *DSPP* were found in both individuals, and *OR4C45* and *MUC6* are unlikely to be the cause of disease based on their predicted protein function in UniProtKB.

6.5 Discussion

SLC52A2 mutations were more frequent than mutations in *SLC52A3* and *SLC52A1* in both cohorts of patients screened for BVVL genes in our study. Amongst patients screened at our centre as part of this Thesis, *SLC52A2* mutations were found in 16.4% of the cohort of patients specifically referred for BVVL testing and 2.9% of the cohort designed by a database-search of patients with BVVL-like features; corresponding values for *SLC52A3* mutations were 10.9% and 0%, although the pathogenicity of the heterozygous *SLC52A3* mutations remains uncertain. Therefore, frequencies of mutations in *SLC52A2* and *SLC52A3* were higher in the referred patient series compared to the series of patients selected from the NHNN database. *SLC52A2* mutations have only very recently been associated with BVVL, yet from our gene screening and that of our collaborators, it now appears that they may be a common cause of BVVL. Given the high proportion of patients in both cohorts who were found to be negative for mutations in the three known riboflavin transporters, it is likely that novel genetic causes of this disease remain to be uncovered, especially as some negative patients had phenotypes typical for BVVL. Admittedly, copy number changes and mutations in introns, UTRs and promoter regions cannot be ruled out in patients found to be negative for mutations in all three riboflavin transporters.

This study also confirms previous findings that *SLC52A1* mutations are rare in BVVL patients (Johnson et al., 2012). This study has identified the first stop mutation in *SLC52A2*, which was found to cause NMD at the mRNA level. In agreement with previous studies, mutations in *SLC52A2* and *SLC52A3* were spread

throughout the genes and were found in intracellular and extracellular loops as well as in transmembrane domains (Dezfouli et al., 2012).

All patients with *SLC52A2* mutations in our cohort had rapidly progressive axonal sensory-motor neuropathy causing sensory ataxia, upper limb and trunk weakness, and respiratory insufficiency. There was also involvement of the cranial nerves, as evidenced by optic atrophy (cranial nerve II), hearing loss (cranial nerve VIII) and tongue fasciculations with or without weakness and atrophy (cranial nerve XII). Patients had severe weakness in the upper limb and axial muscles, with preservation of lower limb strength. Although the upper limb predominance contrasts with length-dependent inherited sensory-motor polyneuropathies, some inherited neuropathies do have predominant upper extremity weakness such as those associated with *BSCL2* mutations (Rossor et al., 2013). Of course, *SLC52A2*-mutated patients differ from those with *BSCL2* mutations with regards to the mode of inheritance and associated features specific to BVVL such as hearing loss, sensory neuropathy, optic atrophy and respiratory insufficiency. In contrast to genetically uncharacterized BVVL cases and patients with *SLC52A3* mutations who usually have a more generalised disease onset (Green et al., 2010; Bosch et al., 2011), our patients with *SLC52A2* mutations had early-onset weakness of the neck and upper limbs. *SLC52A2* patients were also unique in that they did not exhibit UMN signs in the lower limbs, which are commonly reported in BVVL and *SLC52A3* patients (De Grandis et al., 2005; Dipti et al., 2005; Francis et al., 1993; Gallai et al., 1981; Green et al., 2010; Hawkins et al., 1990; Koul et al., 2006; Voudris et al., 2002). Although most reports have cited bilateral hearing loss as the presenting symptom in BVVL (Gallai et al., 1981; Sathasivam, 2008), ataxic gait and nystagmus were the two most frequent presenting symptoms in our cohort of *SLC52A2*-mutated patients. Some patients with pathogenic mutations in *SLC52A2* in our study had normal acylcarnitine profiles; this finding has been previously noted in patients with *SLC52A2* and *SLC52A3* mutations (Bosch et al., 2012; Ciccolella et al., 2012; Ciccolella et al., 2013; Koy et al., 2012). Interestingly, although NCS do not always show abnormalities in BVVL patients (Dipti et al., 2005; Koul et al., 2006; Voudris et al., 2002), an axonal sensory-motor neuropathy was seen in our patients with *SLC52A2* mutations. However, it remains unclear whether the axonal damage in the *SLC52A2* patients is due to a neuronopathy

of the dorsal root ganglia and anterior horn neurons, or to a primary axonopathy causing hearing loss, optic atrophy and a sensory-motor neuropathy (Foley et al., 2014). Plasma FAD levels were normal in all patients with *SLC52A2* mutations in whom testing was performed. This finding is in agreement with the role of RFVT2 in uptake of riboflavin from the blood into target cells (Ciccolella et al., 2012; Haack et al., 2012).

Only limited clinical information was available for the patients with heterozygous *SLC52A3* mutations. The phenotype was typical of BVVL in siblings RDB and NDB and in patient LS. Patient LF also had a typical BVVL phenotype including hearing loss, neuropathy, ataxia and impaired breathing. Although patient HM had mild disease with bilateral optic and auditory neuropathies, both of which may be seen in BVVL, the phenotypic details available for this patient were limited. Patient KG had some features of BVVL including tongue atrophy, axonal neuropathy and facial weakness progressing distally to the limbs, although no hearing loss was present. This patient also had a third cranial nerve palsy; palsies of the oculomotor nerve have been reported in BVVL, although these remain relatively rare (Sathasivam et al., 2000; Sathasivam, 2008; Vialetto, 1936). In the recent review by Bosch and colleagues, palsies of the III, IV or VI cranial nerves combined were seen in 32% of BVVL patients (Bosch et al., 2012). Patient JG had a complex phenotype with several features of BVVL including AR inheritance, gait abnormalities, peripheral neuropathy, bilateral facial weakness, weakness of the neck muscles, distal limb weakness, ptosis, cerebellar signs with bulbar involvement, reduced reflexes, sensory abnormalities, nystagmus, mild hearing loss, speech abnormalities and difficulty swallowing. Plasma flavin levels could not be obtained for the patients with *SLC52A3* mutations in our cohort. Some studies have reported normal plasma flavin levels in *SLC52A3* mutated patients; in this case, the effect of the *SLC52A3* mutations on localisation or expression of RFVT3 was suggested to be restricted to the CNS via an unknown mechanism (Ciccolella et al., 2012). Further studies are needed to determine whether the heterozygous *SLC52A3* mutations are the cause of BVVL disease in the patients identified herein.

Given the distinct phenotypes associated with defects in the three riboflavin transporters, Bosch and colleagues had suggested to rename these subtypes of BVVL as riboflavin transporter deficiency, type 1 (*SLC52A1*-encoded RFVT1, previously hRFT1), type 2 (*SLC52A3*-encoded RFVT3, previously hRFT2) and type 3 (*SLC52A2*-encoded RFVT2, previously hRFT3) to better delineate them clinically (Bosch et al., 2012). However, given the new protein nomenclature, we have suggested that type 2 should refer to *SLC52A2*-associated forms of BVVL and type 3 to *SLC52A3*-associated BVVL (Foley et al., 2014).

In agreement with the majority of previous findings in patients with mutations in *SLC52A2* (Haack et al., 2012) and *SLC52A3* (Anand et al., 2012; Bosch et al., 2011; Bosch et al., 2012; Ciccolella et al., 2012) (Section 1.6.5), our study has shown that BVVL associated with *SLC52A2* mutations is potentially treatable with high-dose oral riboflavin (Foley et al., 2014). While the literature suggests that high-dose riboflavin supplementation can apparently benefit both *SLC52A2* and *SLC52A3*-mutated patients if administered early on, treatment should be trialled in a greater number of patients to assess whether BVVL cases associated with each of these genetic subtypes respond differently to therapy.

In accordance with previous observations, in our study the therapy was effective even in patients with normal plasma flavin levels (Bosch et al., 2011; Bosch et al., 2012). No adverse events associated with the therapy were seen in our cohort. Siblings of affected patients should be screened soon after the genetic finding to allow for pre-symptomatic initiation of therapy, if necessary (Foley et al., 2014). As discussed in Section 1.6.5, high-dose oral riboflavin therapy should be initiated as soon as BVVL is suspected and before results of genetic studies are obtained to prevent irreparable damage (Bosch et al., 2011; Spagnoli & De Sousa, 2011), especially as riboflavin is not known to be toxic at high doses (Alhadeff et al., 1984; Foley et al., 2014; McCormick, 1989). The effectiveness of the therapy in older patients with a long disease duration is unknown. Patients in our cohort who showed stable functioning as opposed to improvement with high-dose riboflavin therapy were largely the patients who were older at the time of treatment initiation. It is likely that the extent of neurological damage was too advanced in these patients for

riboflavin therapy to be effective (Bosch et al., 2012; Foley et al., 2014; Spagnoli & De Sousa, 2011). Finally, the trial period of treatment should be continued even if no improvement is seen initially as severely affected patients usually show more gradual improvement (Bosch et al., 2012).

The lack of toxicity may be due to the fact that riboflavin is rapidly excreted in the urine when present at very high concentrations in the blood (Gregersen, 1985; Haack et al., 2012). Although patients in our study were treated with 10-50 mg/kg/day of oral riboflavin or 1,500 mg/day in adults, as discussed in Section 6.1.2 the maximal absorption for pharmacological doses of riboflavin administered orally is 25-27 mg per dose (Gregersen, 1985: Zempleni et al., 1996). Due to the potentially saturable nature of the transporters, further studies are needed to determine how to best optimise the uptake of riboflavin via diffusion or via the other two functional riboflavin transporters, RFVT1 and RFVT3 (Bosch et al., 2012; Foley et al., 2014). Furthermore, the optimal dose, frequency and length of treatment, as well as the best method of administration of riboflavin treatment remains to be elucidated (Bosch et al., 2012; Foley et al., 2014).

While none of the SMARD-like patients carried mutations in the three riboflavin transporters, further studies are warranted to fully exclude riboflavin transporter mutations in other SMARD patients given the positive response to riboflavin treatment reported in this and other studies. Mutations in these genes could also be linked to other overlapping syndromes including ALS (especially infantile or early-onset familial ALS), Nathalie syndrome, Boltshauser syndrome and Madras MND; screening of the BVVL-associated genes in these patients is also justified (Green et al., 2010). The riboflavin transporters should also be screened in children with optic atrophy and/or sensory ataxia as well as in children with some BVVL-like features, even if the phenotype is not typical of BVVL (Houlden, 2012).

Although the exome sequencing results in family SP are still very preliminary, our study would confirm previous findings that *AAAS* mutations should be considered in patients with complex axonal neuropathy (Dixit et al., 2011; Houlden et al., 2002). For both families SP and MO, additional assessments of pathogenicity of the candidate genes could not be performed within the timeframe of this Thesis. The

variants detected in the *AAAS* and *NEFH* genes should be confirmed by Sanger sequencing and screened in a large cohort of controls. Segregation studies should be carried out in additional family members. The poorly covered exons in *SLC52A2* and *SLC52A3* in individual III-3 of family MO should be Sanger sequenced. The pathogenic nature of the mutations found in *AAAS* and *NEFH* needs to be confirmed in vitro. We also highlight again the difficulties associated with exome sequencing data analysis. As discussed in Chapter 5, the causative variant in these three families may have been missed by the exome sequencing; reasons may include poor coverage, if the variant was a large deletion, insertion, duplication, translocation or repeat sequence, or if it was located in a non-coding region. The pathogenic variant in families SP and MO may have been in the homozygous state, although this is unlikely given the absence of reported consanguinity in these families. Finally, it is possible that individuals III-3 and III-8 of family TB were suffering from diseases with different aetiologies.

6.6 Conclusion

In conclusion, this study has highlighted the relatively high frequency of *SLC52A2* mutations in BVVL patients and has expanded the range of clinical phenotypes associated with riboflavin transporter mutations. Importantly, patients in our cohort found to carry mutations in *SLC52A2* were immediately initiated on high-dose riboflavin therapy following the genetic finding. Riboflavin may also be an effective treatment in other MNDs with overlapping phenotypes, such as those described in Section 1.6.1.

Defects of riboflavin transporters represent a new genetic cause of neuropathy associated with a previously largely unknown disease pathway. However, the question remains as to how mutations in these proteins may cause a complex syndrome involving a sensory-motor neuropathy. The next Chapter will seek to elucidate the pathomechanisms leading to BVVL disease in patients with *SLC52A2* mutations and to understand how this disease pathway may differ from that associated with nutritional riboflavin deficiency.

Finally, although further proof of pathogenicity is required, exome sequencing was

used in this study to ascribe mutations in a known gene, *AAAS*, to a relatively atypical phenotype. It is unlikely that this gene would have been deliberately screened in this family.

Chapter 7 BVVL: A functional investigation of a treatable neuropathy

7.1 Introduction

7.1.1 Riboflavin transporter mutations in BVVL, a novel neuropathy-associated disease pathway

The genetic screening of *SLC52A1, SLC52A2,* and *SLC52A3* mutations in a cohort of BVVL patients (Chapter 6) has unveiled *SLC52A2* mutations as a significant cause of this disease. The requirement for three genes encoding riboflavin transporters suggests that this pathway is indispensable. In contrast to the phenotype associated with nutritional riboflavin deficiency, which either remains subclinical or is primarily dermatological in nature (Foraker et al., 2003), BVVL patients present with a severe and complex phenotype characterised by early-onset progressive pontobulbar palsy with bilateral sensorineural hearing loss, sensory-motor neuropathy and respiratory insufficiency (Brown, 1894; Van Laere, 1966; Vialetto, 1936). The patients with *SLC52A2* mutations in our cohort shared a phenotype of rapidly progressive axonal sensory-motor neuropathy leading to sensory ataxia, upper limb and trunk weakness, and respiratory insufficiency, with involvement of selected cranial nerves. It remains unknown how the pathomechanisms leading to BVVL may differ from that of riboflavin deficiency associated with low intakes of riboflavin in the diet.

A selection of the cellular pathways in which riboflavin and its cofactor forms FMN and FAD are involved will now be described in detail. Studies of riboflavin supplementation in riboflavin-responsive metabolic and mitochondrial diseases will also be discussed, to be followed by a summary of the effects of riboflavin deprivation in various human cell lines and animal models. Finally, results of the limited previous studies into the functional effect of riboflavin transporter mutations will be presented.

7.1.2 Cellular energy metabolism

FAD and FMN serve as cofactors in a variety of cellular energy metabolism processes and play crucial roles in aerobic respiration (McCormick, 1989). Aerobic respiration is the process by which eukaryotes use O_2 to release the energy stored in

food in the form of substrates like glucose, fatty acids, and amino acids to generate ATP. During glycolysis, glucose is converted to pyruvate in the cytosol. In the mitochondria, there are two main enzyme systems for cellular metabolism and energy generation: the Krebs cycle and the MRC. Prior to entering the Krebs cycle, the pyruvate from glycolysis is converted to acetyl-CoA by the pyruvate dehydrogenase complex, a flavoprotein which uses FAD as an electron carrier (Duchen, 2004). Acyl-CoA fatty acids are metabolised in the mitochondrial matrix to acetyl-CoA via fatty acid β-oxidation. In the first instance, the fatty acid moiety is oxidised by acyl-CoA dehydrogenase, a flavoprotein with a bound FAD molecule, forming a fatty acyl-CoA molecule two carbons shorter. Electrons are transferred first to the FAD in ETF in the matrix and then to the FAD in ETF:QO in the inner mitochondrial membrane (Henriques et al., 2010). During the Krebs cycle, acetyl-CoA produced by the breakdown of pyruvate, fatty acids and amino acids is catabolised, resulting in the production of CO_2, NADH and reduced flavin adenine dinucleotide ($FADH_2$). A small amount of ATP is produced by glycolysis and the Krebs cycle by substrate-level phosphorylation (Duchen, 2004).

Mitochondria are the power plants of the cell, as they provide the cell with most of its energy in the form of ATP via the MRC and subsequent oxidative phosphorylation (Cozzolino & Carrì, 2012). The MRC is composed of four membrane-bound electron-transporting multimeric protein complexes, complexes I-IV. The complex II enzyme is the only complex which is also part of the Krebs cycle, where succinate dehydrogenase (SDH) catalyses the oxidation of succinate to fumarate and reduces FAD to $FADH_2$ in the process. The NADH and $FADH_2$ generated during glycolysis, pyruvate processing, fatty acid β-oxidation and the Krebs cycle serve as reducing equivalents for the MRC. Complexes I and II are both flavin-dependent complexes of the MRC. Complex I (NADH: ubiquinone oxidoreductase), the largest MRC complex with 45 subunits, is a major point of entry into the MRC and is considered to be the rate-limiting complex. Its FMN moiety, located within the soluble fraction of the complex along with the iron protein subunit, accepts electrons from NADH; these electrons then travel through a series of iron-sulphur centres. Complex II (succinate: ubiquinone oxidoreductase)/SDH is the simplest complex and is the sole complex to be only encoded by nuclear DNA. It is

made up of four subunits, SDHA, SDHB, SDHC, and SDHD; the SDHA subunit contains a succinate binding site, as well as the covalently attached FAD, which serves as the initial electron acceptor (Cecchini, 2003). Formation of the covalent linkage of FAD to SDH occurs in a complex process (Baker & Tarnopolsky, 2003; Cecchini, 2003; Distelmaier et al., 2009; Duchen, 2004).

NADH and $FADH_2$ are therefore oxidised to NAD^+ and FAD in complexes I and II, respectively. High-energy electrons from these molecules are transferred from iron-sulphur centres in complexes I and II to ubiquinone (CoQ), which is reduced to ubiquinol. CoQ, a mobile electron carrier, is a lipid-soluble molecule located in the inner mitochondrial membrane. Electrons in $FADH_2$ are also donated into the MRC by ETF:QO of fatty acid β-oxidation to CoQ, thus providing a link between fatty acid metabolism and the MRC. Ubiquinol is oxidised by complex III (ubiquinone-cytochrome *c* oxidoreductase), which contains cytochromes *b* and *c*. Electrons are carried by cytochrome *c* to complex IV (cytochrome *c* oxidase), the terminal cytochrome oxidase, before being donated to O_2, the terminal electron acceptor, which is reduced to H_2O. In the process, protons are pumped out of the matrix into the intermembrane space at complexes I, III and IV against their concentration gradient, generating an electrochemical gradient across the mitochondrial inner membrane known as the ΔΨm (Section 2.2.18). Complex II and ETF:QO are mechanistically unable to pump protons across the inner membrane. Complex V, also known as ATP-synthase or F_1F_0-ATPase, uses this gradient to phosphorylate adenosine diphosphate (ADP) and produce ATP by allowing protons to translocate back into the matrix (Duchen, 2004).

Monovalent cationic fluorescent dyes such as TMRM can be used to monitor the ΔΨm in vitro, as described in Section 2.2.18. A common technique to specifically assess the implication of complex I in maintaining the ΔΨm in live cells is to monitor the TMRM intensity after the addition of rotenone, a toxin which blocks the transfer of electrons from the iron-sulphur cluster in complex I to ubiquinone by binding to the CoQ binding site (Murphy, 2009).

Inhibition of respiration, impaired respiratory complex activity, reduced substrate supply and mitochondrial uncoupling are some of the mechanisms which may affect the ΔΨm by decreasing or dysregulating proton pumping (Duchen, 2004). A loss of ΔΨm leads to reduced cellular ATP levels and mitochondrial dysfunction, which can result in cellular dysfunction or cell death (Distelmaier et al., 2009; Duchen, 2004; Grad & Lemire, 2006; Mancuso et al., 2010). Mitochondrial depolarisation can lead to swelling of the mitochondria and release of cytochrome c and apoptosis (Duchen, 2004).

When the ΔΨm dissipates as a result of damage or inhibition of respiration (e.g. due to a decrease in MRC complex activities), in certain conditions ATP synthase may act in reverse mode to preserve the ΔΨm. In this case, it can function as an ATPase by hydrolysing glycolytic ATP to pump protons out across the inner membrane against the gradient (Nicholls, 2002). Determining whether ATP synthase is operating in reverse is a common way of assessing mitochondrial function in neurodegenerative diseases (Abramov et al., 2010; Gandhi et al., 2009). This is usually achieved by monitoring the ΔΨm using the TMRM dye, and observing the response to the mitochondrial toxin oligomycin, an inhibitor of the ATP synthase (Abramov et al., 2010). In healthy cells, oligomycin causes a slight transient hyperpolarisation (due to build-up of the proton gradient) or no response, suggesting that the ΔΨm is maintained by the MRC. If oligomycin results in depolarisation, the ΔΨm is being maintained by the hydrolysis of ATP due to reversal of ATP synthase (Abramov et al., 2010). Because this reversal process is harmful to cells as it uses ATP stores, binding of the initiation factor 1 (IF1) protein to this enzyme can serve as a defence mechanism to prevent the ATPase from operating in reverse mode, at the expense of the ΔΨm (Cecchini, 2003; Duchen, 2004).

Inhibition of the MRC due to a genetic defect or other source of damage may cause the respiration rate to decrease, NADH to accumulate, and the NADH: NAD^+ ratio to increase. Calculating the NADH: NAD^+ ratio is another common way of assessing mitochondrial function (Bartolome et al., 2013). As discussed in Section 2.2.19, the NADH: NAD^+ ratio is measured in vitro by monitoring NADH fluorescence after the addition of the uncoupler drug FCCP, which reversibly depolarises the mitochondria,

maximises respiration and minimises NADH levels, followed by addition of NaCN, which completely inhibits respiration and maximises NADH levels (Bartolome et al., 2013; Duchen, 2004).

If aerobic respiration is defective, the cell may use anaerobic respiration to compensate and meet its energy requirements. However, anaerobic respiration causes pyruvate, the end product of glycolysis, to accumulate, and eventually to be reduced to lactate by NADH instead of being oxidised to acetyl-CoA and entering the Krebs cycle. Pyruvate can also accumulate if the activity of the pyruvate dehydrogenase complex is low (Bernsen et al., 1993; Grad & Lemire, 2006; Mackay & Robinson, 2007). The lactate/pyruvate ratio measured in blood, CSF or cells such as fibroblasts is often used to detect MRC dysfunction. An increased lactate/pyruvate ratio is a typical finding in mitochondrial disorders (Bernsen et al., 1993; Mackay & Robinson, 2007). In order to compensate for a defect in mitochondrial respiration, cells may also upregulate glycolysis to maintain ATP levels, more or less effectively depending on the cell type. The relative expression of the β subunit of the F_1-ATPase compared to that of GAPDH, a glycolytic enzyme, has been previously used as a marker of change in bioenergetics to determine whether cells predominantly obtain ATP from glycolysis or oxidative phosphorylation (Yao et al., 2011).

A defect in mitochondrial function can cause a large range of phenotypes, but often results in muscular and neurological problems as muscle, brain nerve cells and peripheral nerves contain a large number of mitochondria to support their high energy demands (Federico et al., 2012; McInnes, 2013). The long axons of neurones, and especially of motor neurones, imply that molecules have to be transported over great distances efficiently. Furthermore, low levels of glycolysis in neurones make them especially reliant on oxidative phosphorylation; glycolysis alone would not provide sufficient ATP in these cells (Burchell et al., 2010; Davey, 1998). When neurones do not produce sufficient energy, calcium signalling, synaptic transmission, neurotransmitter release and therefore overall nervous system function is affected, eventually leading to apoptosis or necrosis (Burchell et al., 2010).

The specific effect of defective oxidative phosphorylation and energy metabolism in the brain remains unclear. A study of synaptic mitochondria in the brain has

determined that the activities of complexes I, III and IV could be decreased by 25%, 80%, and 70%, respectively, before oxygen consumption and synthesis of ATP were significantly compromised. Complex I was found to have the greatest control on oxidative phosphorylation compared to other complexes in synaptic mitochondria, however this is known to vary between tissues (Davey, 1998; Pathak & Davey, 2008). In non-synaptic mitochondria of neuronal and astrocytic cells, the equivalent thresholds for complexes I, III and IV were 72%, 70% and 60%, which may explain why degeneration may preferentially take place at synapses (Pathak & Davey, 2008). It should be noted that these results were obtained from isolated mitochondria, and it is not known whether similar thresholds would be observed in vivo.

7.1.3 Reactive oxygen species (ROS) and oxidative stress in the mitochondria

Besides energy metabolism, mitochondria are also involved in other cellular processes, which are closely linked and are significantly dependent on one another (Burchell et al., 2010). Therefore, proper function of these complex structures is critical for overall cell health. Some of these functions include intracellular signalling, calcium homeostasis and activation of apoptosis (Cozzolino & Carrì, 2012; McInnes, 2013). Furthermore, mitochondria are an important source of antioxidants; however, in many cell types, mitochondria are also a source of ROS production. Decreased ATP generation and increased ROS production are two of the central mechanisms leading to neurodegeneration. These free radicals are produced by the reaction of unpaired electrons generated during oxidative phosphorylation with O_2, leading to superoxide ions which are highly reactive (Duchen, 2004; Nicholls, 2002). ROS are normally produced in small quantities in the cells and increasingly as we age; however, when antioxidant defences are unable to keep the ROS levels down low enough, oxidative stress ensues which further damages the MRC. ROS are damaging to lipids, nucleic acids and proteins, and impair the mitochondria's ability to produce ATP (Murphy, 2009). ROS are especially hurtful to neurones due to their post-mitotic nature and high rate of oxygen consumption (Burchell et al., 2010; Mancuso et al., 2010). When the MRC is impaired, electrons which become blocked early on in the transport chain (especially in complex I) accumulate and are more likely to form ROS (Duchen, 2004; Mancuso et al., 2010; Murphy, 2009). Substrate accumulation in complex I as evidenced by a high NADH:

NAD^+ ratio in the mitochondrial matrix is often associated with significant ROS production (Abramov et al., 2010; Murphy, 2009). This phenomenon has been reported in patient fibroblasts with isolated complex I deficiency (Distelmaier et al., 2009; Duchen, 2004). Therefore, oxidative stress and energy metabolism dysfunction are closely linked (Baker & Tarnopolsky, 2003).

The cell is dependent on efficient antioxidants to protect it against ROS (Abramov et al., 2010). In addition to its role in the MRC, CoQ_{10}, the predominant form of CoQ, is also an antioxidant and free radical scavenger in its reduced form ubiquinol, and thereby protects against oxidative damage (Mancuso et al., 2010). CoQ_{10} was able to maintain the $\Delta\Psi m$ in neuronal cells undergoing oxidative stress (Mancuso et al., 2010). Interestingly, a monooxygenase involved in the biosynthesis of CoQ_{10} is FAD-dependent (Baker & Tarnopolsky, 2003; Lienhart et al., 2013). Furthermore, GSH is another important antioxidant in the CNS. Glutathione reductase, the enzyme responsible for regenerating GSH from the oxidised form GSSG, is a flavoprotein with a bound FAD molecule therefore riboflavin acts indirectly as an antioxidant (Depeint et al., 2006; Henriques et al., 2010). High ROS production often leads to glutathione depletion, which in turn makes the cells more vulnerable to oxidative stress (Abramov et al., 2010). Therefore, as is seen in many neurodegenerative diseases, disturbed glutathione homeostasis may be a consequence or a cause of oxidative stress. Indeed, various studies have provided evidence that a decrease in glutathione levels in neuronal cells increases ROS production, causes defects in the $\Delta\Psi m$, loss of mitochondrial function, and may cause cell death (Schulz et al., 2000). Interestingly, in neuronal, non-synaptic mitochondria, depletion of GSH in vitro abolished the complex I threshold mentioned in Section 7.1.2, and oxygen consumption started to be impaired at much lower levels of complex I inhibition, suggesting that maintenance of antioxidant status may be necessary for the preservation of energy thresholds in the mitochondria (Davey, 1998).

7.1.4 Riboflavin and CoQ_{10} therapy in metabolic and mitochondrial disorders

Riboflavin therapy has been shown to improve to variable extents the symptoms of a subgroup of MADD patients (RR-MADD). Deficiencies of aerobic metabolism in these patients were restored to normal with riboflavin supplementation; riboflavin

was suggested to activate the aerobic pathway (Gianazza et al., 2006; Henriques et al., 2010; Olsen et al., 2007; Peluchetti et al., 1991; Vergani et al., 1999). In contrast to non-riboflavin responsive forms of MADD, fibroblasts of patients with RR-MADD were found to have milder folding defects, normal or supranormal fatty acid β-oxidation, and normal oxidation of flavoprotein-dependent substrates when cultured in riboflavin-supplemented medium (1010 nM or 5310 nM) (Cornelius et al., 2012; S. Olpin, personal communication; Olsen et al., 2007; Rhead et al. 1993). In parallel to these findings, vitamin B_6 in the cell medium has been found to obscure the interpretation of in-vitro assays in fibroblasts of patients with vitamin B_6-responsive homocystinuria (Lipson et al., 1980).

Riboflavin has also been used with some success clinically and biochemically in a subgroup of patients with defects of complex I and/or complex II (Baker & Tarnopolsky, 2003; Bernsen et al., 1993; Bugiani et al., 2006; Gerards et al., 2011; Gianazza et al., 2006; Jain-Ghai et al., 2013; Marriage et al., 2003; Ogle et al., 1997; Olsen et al., 2007; Peluchetti et al., 1991; Scholte et al., 1995; Vergani et al., 1999). Riboflavin therapy has also proven beneficial in some patients with mutations in *acyl-CoA dehydrogenase family, member 9* (*ACAD9*), which encodes an FAD-dependent acyl-CoA dehydrogenase in fatty acid β-oxidation with a potential role in complex I assembly. In these patients, supplementation of the cell medium for three days with 5300 nM riboflavin led to a two-fold increase in complex I activity in patient fibroblasts, but not in control fibroblasts (Gerards et al., 2011; Haack et al., 2010; Horvath, 2012; Scholte et al., 1995).

Some explanations which have been proposed for riboflavin responsiveness and improved mitochondrial respiration in complex I and/or II deficiency include the stimulation of an alternative pathway via complex I, II or ETF:QO by providing these enzymes with FAD molecules, and increasing electron transfer to CoQ. Another rationale involves reduced degradation of complex I followed by increased enzymatic activity of the complex (Ogle et al., 1997; Vergani et al., 1999). Riboflavin was also suggested to have a general stabilising effect on complex assembly (Bar-Meir et al., 2001).

Riboflavin has often been used in conjunction with CoQ_{10} in mitochondrial and metabolic disorders. CoQ_{10} deficiencies may either be primary, such as those due to mutations in CoQ_{10} biosynthesis genes or secondary, due to mutations in genes not involved in CoQ_{10} biosynthesis such as *aprataxin* (*APTX*) or *ETFDH* (Quinzii et al., 2008). Four main phenotypes are associated with CoQ_{10} deficiencies; these include encephalomyopathy with defects of the MRC, the cerebellar type with ataxia and atrophy (with or without neuropathy), the multisystemic infantile type, and the pure myopathy with lipid storage myopathy (Quinzii et al., 2008). In fibroblasts of patients with CoQ_{10} deficiency, there was reduced activity of complexes I-IV, decreased $\Delta\Psi m$ and increased ROS production; these defects were nearly normalised upon CoQ_{10} supplementation (Quinzii et al., 2008; Spindler et al., 2009).

Secondary CoQ_{10} deficiency in muscle has been reported in some RR-MADD patients with a myopathic phenotype due to *ETFDH* mutations. These patients also had decreased activities of complexes I, II-III and IV, as well as increased lactate levels, all of which improved with riboflavin and CoQ_{10} combination therapy (Gempel et al., 2007). In MADD patients, the dehydrogenation of acyl-CoA molecules is impaired due to defects in the transport of electrons from acyl-CoA to CoQ in the MRC (Horvarth, 2012). It has been proposed that the CoQ_{10} deficiency in these patients may be due to feedback inhibition and a downregulation of CoQ_{10} synthesis as a result of a loss of ETF:QO activity; alternatively, a defect in ETF:QO may impair binding to CoQ_{10} and cause increased degradation of CoQ_{10} (Cornelius et al., 2013; Gempel et al., 2007; Gregersen et al., 2008; I. Hargreaves, personal communication).

7.1.5 In vitro and in vivo effects of riboflavin deprivation

Several lines of evidence from in vitro and in vivo models suggest that nutritional riboflavin deficiency leads to defects of cellular energy metabolism, with variable involvement between tissues. Moderately and severely riboflavin-deficient rats have abnormal amino acid metabolism and decreased fatty acid β-oxidation mainly due to impaired activity of acyl-CoA dehydrogenase activity (Brady & Hoppel, 1985; Goodman, 1981; Olpin & Bates, 1982; Sakurai et al., 1982).

Rats subjected to acute, severe riboflavin deficiency ceased to grow early on in the deficiency period. The activity of SDH decreased early on in the deficiency state in the brain, liver, and intestine, although this was found to be due to starvation and not specific to riboflavin deficiency in the latter two tissues. The magnitude of decrease of SDH activity was smaller in brain and skin compared to other tissues. There was no decline in the activity of NADH dehydrogenase in brain and skin. In the kidney and heart, neither SDH nor NADH dehydrogenase activities decreased. Levels of flavins decreased significantly in the liver in the first two weeks of riboflavin deficiency. Although FAD levels were more conserved than FMN levels due to increased activity of FAD synthetase in the liver, the FAD levels were not maintained to the same extent as in other tissues. The activity of flavokinase was decreased early on in the liver, which led to a greater concentration of riboflavin than FMN in this tissue. In the kidney, the decline in flavin levels was less steep, and FAD levels were also preferentially maintained (Prentice & Bates, 1981a).

In man, nutritional riboflavin deficiency is most often chronic in nature and associated with suboptimal levels of riboflavin intake. Therefore, in a subsequent study of marginal chronic deficiency in rats, hepatic and renal flavin levels were proportional to dietary intake of riboflavin. FAD levels were again more conserved than FMN levels. SDH activity decreased with decreasing riboflavin intake in the liver, but this decrease was smaller or less specific in the brain, skin and intestine. The activity of NADH dehydrogenase declined in liver and intestine, but not in skin and brain. Despite large variability between tissues, marginal chronic riboflavin deficiency in the rat primarily affected the growth, food intake, tissue flavin levels and the glutathione reductase status. The second most affected parameter was SDH activity in the liver. Finally, the least sensitive variable was activity of NADH dehydrogenase in the liver. Overall, the kidney and brain were the least sensitive tissues amongst those assayed in the study (Powers, 2003; Prentice & Bates, 1981b). Another study showed that FAD levels fell to 25% of controls and FMN to less than 5% of controls in riboflavin-deficient rats. In liver mitochondria, activity of NADH dehydrogenase was 35-50% of normal and that of SDH was 25% of normal. Oxygen consumption decreased by 34-48%, further suggesting that the MRC is impaired in

riboflavin-deficient liver (Burch et al., 1960). Riboflavin-deficient rats supplemented with riboflavin had improved mitochondrial respiration (Depeint et al., 2006).

In a subsequent study, in addition to a reduction of 50% in the activity of liver SDH in riboflavin-deficient rats, the rates of mitochondrial oxidation via the FAD-dependent dehydrogenases of succinate, beta-hydroxybutyrate, alpha-ketoglutarate, glutamate, and the complex I-linked substrates pyruvate and malate were also decreased by 50%. Although the MRC was impaired, the efficiency of oxidative phosphorylation was unaffected (Zaman & Verwilghen, 1975). A study by Hoppel et al. (1979) provided somewhat similar results. In accordance with other studies (Brady & Hoppel, 1985; Nagao & Tanakas, 1992), the most dramatic mitochondrial effect of moderate riboflavin deficiency in rat liver was on fatty acid β-oxidation (Hoppel et al., 1979). In comparison, the oxidation of non-fatty acid substrates such as succinate was affected only three weeks after the initiation of riboflavin deprivation. In contrast to previous studies, the oxidations of glutamate, pyruvate, and alpha-ketoglutarate were not affected (Hoppel et al., 1979). Overall, while fatty acid oxidation is clearly severely impaired in riboflavin deficiency in rats, oxidative phosphorylation is preserved; findings regarding the Krebs cycle are contradictory.

The preservation of FAD levels in most tissues except liver is in agreement with previous findings in humans and monkeys of stable FAD levels after riboflavin deprivation and supplementation (Burch et al., 1956; Hustad et al., 2002). As mentioned in Section 6.1.4, levels of FAD and FMN had been determined to remain particularly stable in the brain during severe deficiency; this was associated with increased riboflavin transport into the brain to compensate for the decrease in brain flavin levels (Burch et al., 1956; Spector, 1980b; Spector & Johanson, 2006). These observations are consistent with the relative preservation of SDH and NADH dehydrogenase activities described herein in riboflavin-deficient rat brain. Although ATP production was preserved in brain during riboflavin deficiency, other less essential FAD and FMN-dependent pathways such as iron metabolism and the first step of fatty acid β-oxidation were affected (Depeint et al., 2006; Ross & Hansen, 1992).

As expected given the role of FAD in recycling of the antioxidant glutathione and in protein folding, riboflavin deficiency was found to cause cell stress in vitro (Werner et al., 2005). Interestingly, glutathione reductase was determined to lose FAD faster than other enzymes involved in energy metabolism during riboflavin deprivation (Hustad et al., 2002; Ross & Hansen, 1992), therefore oxidative stress may occur early on in nutritional riboflavin deficiency. Within four days of growth in moderately riboflavin-deficient medium (3.1 nM), the activity of glutathione reductase decreased by 98% in HepG2 liver cells compared to those grown in riboflavin-replete medium (532 nM) (Werner et al., 2005). The resulting decrease in cellular levels of GSH was associated with increased DNA strand breaks and oxidative damage (Camporeale & Zempleni, 2003; Manthey et al., 2005). In an intestinal cell model of riboflavin depletion, defects in energy generation with inhibition of cell growth and reduced ATP levels were followed by an increase in ROS production (Lee et al., 2013). Not surprisingly, riboflavin was determined to be necessary for development of the gastrointestinal tract, and in adults with low riboflavin intake, there was impaired proliferation of crypt cells in the colon (Nakano et al., 2011).

That nutritional riboflavin deficiency in humans is associated with relatively mild symptoms would suggest that the levels of riboflavin in the body are indeed tightly regulated (Foraker et al., 2003). Evidence from animal and cell models of riboflavin deficiency suggests that certain cells may adapt their rate of riboflavin uptake via the transporters according to the extracellular levels of riboflavin. In lymphoid cells, HepG2 liver cells, renal epithelial cells and Caco-2 intestinal epithelial cells, transport rates of riboflavin were elevated in moderately and severely riboflavin-deficient medium compared to cells grown in medium with physiological and pharmacological levels of riboflavin (Camporeale & Zempleni, 2003; Kumar et al., 1998; Said & Ma, 1994; Werner et al., 2005). As mentioned in Section 6.1.3, the mRNA expression of rRFVT3 was upregulated in the intestine of riboflavin-deficient rats (Fujimura et al., 2010).

As most of the aforementioned studies were carried out in animal models or in cell lines, it is unclear whether these findings reflect the pathology of nutritional

riboflavin deficiency in humans (Olpin & Bates, 1982). In addition, the aforementioned in vitro and in vivo effects of nutritional riboflavin deficiency likely represent only a fraction of the consequences of nutritional riboflavin deficiency. As has been highlighted previously, FAD and FMN are components of a wide range of flavoproteins, which are involved in a large array of biochemical processes and are located in various cellular compartments including in the cytosol, peroxisome, lysosomes and mitochondria. The activity of any or all flavoproteins could theoretically be affected by reduced intracellular levels of riboflavin and its cofactors, as seen in nutritional riboflavin deficiency and BVVL (Henriques et al., 2010; Lienhart et al., 2013; Massey, 2000; Powers, 2003). Since nutritional riboflavin deficiency usually occurs in conjunction with a deficiency of other vitamins rather than in isolation, the effect of additional deficiencies may influence the phenotype of nutritional riboflavin deficiency. In fact, it has been suggested that some of the features of nutritional riboflavin deficiency such as dermatitis may result from concomitant deficiencies of vitamins such as B_6 and niacin (McCormick, 1989; National Research Council, 1998).

In vitro studies have highlighted the variability in the riboflavin levels required by different cell types and tissues. While HepG2 liver cells and murine macrophage cells were found to be especially sensitive to deficiency with cell cycle arrest and apoptosis within four days of growth in 3.1 nM riboflavin medium (Manthey et al., 2005; Mazur-Bialy et al., 2013), lymphoid cells were comparatively more resistant (Werner et al., 2005). The sensitivity of different tissues to deficiency may be different in humans. Indeed, it remains unknown whether ATP-generating pathways are also selectively preserved in the brain of riboflavin-deficient humans.

7.1.6 Previous in vitro functional studies of mutations in *SLC52A2* and *SLC52A3*

As the discovery of the riboflavin transporter mutations in BVVL patients is relatively recent, very little work has been undertaken to elucidate the pathomechanisms of disease in BVVL. Indeed, little is known about the function of these proteins in the nervous system and how mutations in these genes affect the function of the transporter and lead to the BVVL phenotype.

In accordance with in vitro findings in fibroblasts of RR-MADD patients described in Section 7.1.4, Bosch et al. (2011) reported normal fatty acid oxidation results in fibroblasts of patients with *SLC52A3* mutations when these cells were grown in medium with high concentrations of riboflavin; the authors had postulated that riboflavin in the cell medium may have corrected the defect.

One study has examined the effects of clinically-relevant *SLC52A3* mutations, including the p.Glu36Lys mutation identified in our cohort in Chapter 6, in human-derived intestinal epithelial Caco-2 cells. They found a significant decrease in riboflavin uptake, which was apparently not due to a reduction in transcription and/or translation of *SLC52A3* since mRNA and protein levels were similar in intestinal epithelial cells expressing the mutant and WT *SLC52A3*. Some of the mutant proteins (including p.Glu36Lys) were retained in the ER and not targeted to the plasma membrane (Nabokina et al., 2012). As previously mentioned in Section 6.1.3, certain mutations such as those located in the COOH terminal domain of RFVT3 may affect its cell surface expression (Subramanian, Rapp, et al., 2011).

Haack et al. (2012) found reduced riboflavin uptake when the *SLC52A2* p.Leu123Pro and p.Leu339Pro mutations were expressed in HEK293 cells. In the Ciccolella et al. (2013) study, there was also reduced riboflavin uptake in fibroblasts of a patient with the p.[Gly419Ser];[Ser52Phe] mutations in *SLC52A2*, with residual activity at 29% of controls when cells were grown in low riboflavin medium (0.4 nM). In this patient, there was a significant reduction (45%) in the *SLC52A2* mRNA expression, while the mRNA expression of *SLC52A1* was unaffected; however, the protein levels of both RFVT1 and RFVT2 were undetectable. In vitro studies of the parents' fibroblasts suggested that the p.Ser52Phe mutation may impair the *SLC52A2* mRNA stability, while the p.Gly419Ser mutation may affect the protein function. The authors suggested that the reduction in protein expression of both the RFVT1 and RFVT2 transporters might suggest a potential cooperation between these two transporters. The two mutations identified in this patient are localised at a polar-xx-polar motif, where the polar amino acids are serine residues, and a GxxxG motif; these were found in transmembrane helices 2 and 10 of the RFVT2 protein,

respectively. The authors proposed that these motifs might be needed for the formation of heterodimers with the RFVT1 protein (Ciccolella et al., 2013).

Where this assay was performed, activities of MRC enzyme complexes in muscle were normal in patients with *SLC52A2* and *SLC52A3* mutations (Haack et al., 2012; Koy et al, 2012; Mégarbané et al., 2000). However, in some patients presenting with FL syndrome with no genetic diagnosis, muscle biopsies revealed a deficiency of MRC complexes I and III and decreased ATP production, however these results were not seen in patient fibroblasts. These patients also had elevated plasma lactate (Roeleveld-Versteegh et al., 2004). Elevations in lactate levels have been reported in some cases (Bosch et al., 2011; Dipti et al., 2005). Furthermore, the infant born to an *SLC52A1*-haploinsufficient mother was found to have lactic acidosis (Chiong et al., 2007). Overall however, lactate levels in the blood and/or CSF have generally been reported to be normal in patients with *SLC52A2* and *SLC52A3* mutations, and in patients without a genetic diagnosis (Ciccolella et al., 2012; Koy et al., 2012; Mégarbané et al., 2000; Sathasivam et al., 2000; Voudris et al., 2002). Finally, although FAD is a cofactor for glutathione reductase as discussed in Section 7.1.3, one study found no difference in the blood levels of GSH and GSSG between *SLC52A3* patients and controls (Ciccolella et al., 2012).

Our collaborators, Dr Yonezawa and colleagues at the Kyoto University Hospital in Japan, have carried out a preliminary functional evaluation of some of the *SLC52A2* mutations identified in our BVVL genetic study. These results were included in our publication (Foley et al., 2014). Dr Yonezawa and colleagues determined the ^{3}H-riboflavin transport activities and protein expression in HEK293 cells transiently expressing the following *SLC52A2* mutations: p.Trp31Ser, p.Gln234Stop, p.Ala284Asp, p.Tyr305Cys, p.Gly306Arg, p.Leu312Pro, and p.Leu339Pro. The WT and mutants had similar transfection efficiencies, as determined by RT-PCR. Cells expressing the p.Trp31Ser, p.Gln234Stop, p.Ala284Asp, p.Tyr305Cys, and p.Leu339Pro mutations displayed the greatest reduction in riboflavin uptake compared to WT cells. The p.Gly306Arg and p.Leu312Pro mutations showed a moderate but significant decrease in riboflavin transport compared with WT. Western blot on the crude membrane of the transiently expressing HEK293 cells

revealed that the expression levels of all *SLC52A2* mutants were reduced compared to WT, except the p.Trp31Ser mutant which remained expressed near WT levels in the plasma membrane; the protein expression levels in the plasma membrane were well correlated with the riboflavin uptake data (Foley et al, 2014; Figure 7-1).

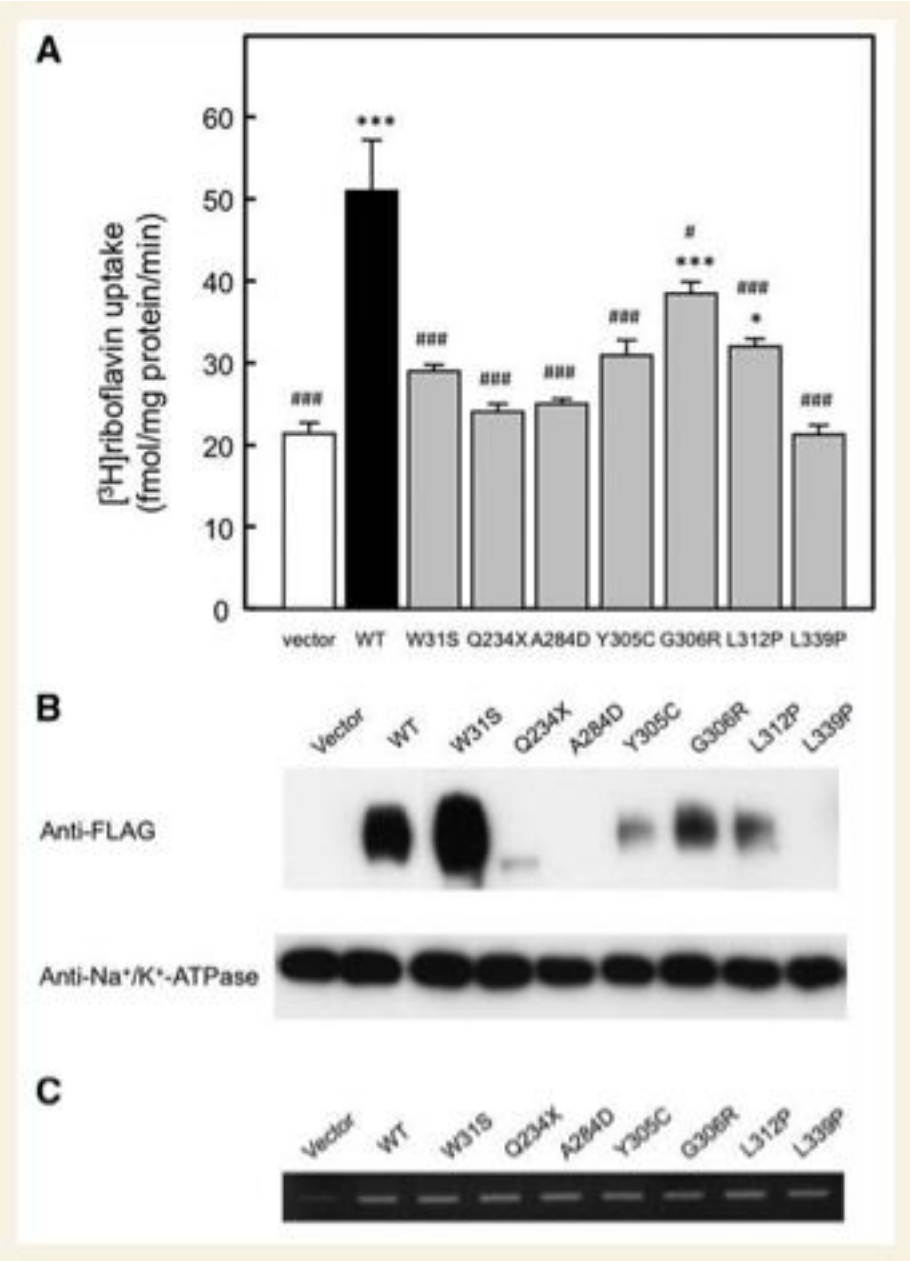

Figure 7-1 Functional studies of *SLC52A2* mutations carried out by Dr Yonezawa and colleagues. (A) Uptake of ^{3}H-riboflavin by HEK293 cells transfected with empty vector (Vector), WT *SLC52A2* (WT), *SLC52A2* (92G>C; W31S), *SLC52A2* (700C>T; Q234X), *SLC52A2* (851C>A; A284D), *SLC52A2* (914A>G; Y305C), *SLC52A2* (916G>A; G306R), *SLC52A2* (935T>C; L312P) and *SLC52A2* (1016T>C; L339P). The cells were incubated with 5 nM ^{3}H-riboflavin (pH 7.4) for 1 min at 37˚C. Each bar represents the mean ± standard error of the mean (SEM), n=3. Data were analysed by Dunnett's two-tailed test after one-way ANOVA. *$p < 0.05$, ***$p < 0.001$ means significantly different from vector-transfected cells. $^{\#}p < 0.05$, $^{\#\#\#}p <$

0.001 means significantly different from *SLC52A2* (WT)-transfected cells. (B) Western blot analysis was performed using the crude membrane of HEK293 cells expressing empty vector, *SLC52A2* (WT) and *SLC52A2* variants. The crude membrane fractions were subjected to Western blotting using antibodies against FLAG and Na^+/K^+-ATPase. Na^+/K^+-ATPase was used as an IS. (C) RNA expression of *SLC52A2* in HEK293 cells transfected with empty vector, *SLC52A2* (WT) and *SLC52A2* variants. RT-PCR analysis was carried out using specific primer sets (reproduced from Foley et al., 2014).

7.2 Aims of this study

Following our genetic investigation in a cohort of BVVL patients, the aim of this study was to understand how mutations in the *SLC52A2*-encoded riboflavin transporter RFVT2 lead to neurodegeneration, and specifically a sensory-motor neuropathy. Given that nutritional riboflavin deficiency has a very different clinical phenotype from that of BVVL, it was initially thought that the function of the riboflavin transporters was unlikely to be related to the disease mechanism (Green et al., 2010). That riboflavin supplementation improves the symptoms of BVVL patients supports the hypothesis that the disease is at least in part due to decreased availability of riboflavin and subsequently FMN and FAD, and that the role of the proteins as riboflavin transporters is likely to be important in disease pathogenesis (Bosch et al., 2011). In keeping with the role of FMN and FAD in cellular energy metabolism, mitochondrial dysfunction was primarily investigated as a potential pathway leading to neuronal damage in BVVL.

Fibroblasts of selected patients from our cohort of BVVL patients with *SLC52A2* mutations were used in this study. Preliminary investigations in *SLC52A2*-KD SH-SY5Y cells and in *Slc52a2* and *Slc52a3*-KD primary mixed ventral horn cultures were also carried out. Investigating the disease pathomechanisms in BVVL may provide clues into novel BVVL-associated genes, and may help identify new therapeutic targets for this fatal infantile MND. Finally, elucidating the disease pathways in BVVL could help understand related MNDs such as ALS as well as the function of the mutated proteins.

7.3 Methods: *SLC52A2* patient fibroblasts

7.3.1 *SLC52A2* patient, carrier and control fibroblasts

Details regarding the source of the skin biopsies and establishment of patient, carrier and control fibroblast cultures are described in Sections 2.2.2 and 6.3.11. Five BVVL patient fibroblast lines (patients E1-E4 and I1), one p.Gly306Arg carrier fibroblast line (mother of patient E1) and three age-matched control fibroblast lines were available for study (see Section 2.2.2 for full details of control fibroblast lines). As determined in Chapter 6, patients carried the following mutations: E1: p.[Gly306Arg];[Gly306Arg]; E2: p.[Trp31Ser];[Leu312Pro]; E3: p.[Gln234Stop]; [Ala420Thr]; E4: p.[Gly306Arg];[Leu339Pro]; I1: p.[Tyr305Cys]; [Gly306Arg]. The mother of patient E1 carried the p.Gly306Arg mutation in the heterozygous state. Details of consent are available in Section 2.2.1.

7.3.2 Cell culture of fibroblasts

Fibroblast cells from control, p.Gly306Arg carrier, and patient fibroblasts were cultured as described in Section 2.2.3.

7.3.3 Assessment of *SLC52A2* messenger ribonucleic acid (mRNA) expression levels in fibroblasts

Although gene expression studies carried out by Dr Mina Ryten at the ION had indicated that *SLC52A2* is expressed in human fibroblasts (M. Ryten, personal communication), the RT-qPCR experiment carried out in this study also served to confirm that *SLC52A2* is indeed expressed in human fibroblasts, and that, in this respect, this cell type is suitable to use for the experiments that follow. To assess whether the stability of the *SLC52A2* mRNA was affected by the *SLC52A2* variants, RNA was extracted from patient, p.Gly306Arg carrier, and control fibroblasts grown in regular DMEM, and cDNA was synthesized as described in Sections 2.2.9 and 2.2.10. RT-qPCR of *SLC52A2* was performed as detailed in Section 2.2.11. Details of the Taqman probes used for RT-qPCR of *SLC52A2* and the housekeeping gene *ACTB* can be found in Section 2.2.11.

7.3.4 Optimisation of riboflavin concentration in fibroblast culture medium

Based on studies of riboflavin-responsive diseases discussed in Section 7.1.4, which demonstrated that supraphysiological concentrations of riboflavin in the cell medium could correct the enzymatic defects in vitro, and given the improvement seen in BVVL patients upon administration of high-dose riboflavin, it was likely that any metabolic abnormalities would not be detectable in our patient fibroblasts if grown in regular cell medium which has a high riboflavin concentration (concentration in DMEM=1.06 M). However, as discussed in Section 7.1.5, if the medium is severely riboflavin-depleted, it will not be able to support normal fatty acid oxidation and other cellular functions for which riboflavin is required, both in healthy control cells as well as in patient cells. Therefore, it was necessary to establish the threshold of riboflavin concentration in the fibroblast culture medium which would uncover any potential defect in patient cells but which would not negatively affect control cells.

For medium optimisation, MRC complex I and II activities were used as a measure of cell health in control fibroblasts grown in varying concentrations of riboflavin. Therefore, the activities of complexes I and II of the MRC as well as CS were assayed in control fibroblasts as described in Sections 2.2.15-2.2.17. Medium optimisation is detailed in Section 2.2.8. Unless otherwise specified, all fibroblast lines were grown for four days in modified DMEM containing physiological concentrations (12.6 nM) of riboflavin, followed by four days in modified DMEM which was either riboflavin-supplemented (300.6 nM) or low riboflavin medium (3.1 nM). For assessment of ATP5β and GAPDH expression levels by Western blot, cells were grown for four days in physiological concentrations (12.6 nM) of riboflavin, followed by four days in low riboflavin medium (3.1 nM) only.

7.3.5 Total protein determination

The protein content of the cell lysates obtained from patient, p.Gly306Arg carrier, and control fibroblasts required for some of the experiments below was determined by the Bradford method as described in Section 2.2.7.

7.3.6 Assessment of human riboflavin transporter 2 (RFVT2) protein levels in fibroblasts

To establish whether the *SLC52A2* mutations affect the RFVT2 protein expression, the expression levels of endogenous RFVT2 protein were measured by Western blot in patient, p.Gly306Arg carrier, and control fibroblasts grown in regular DMEM as described in Section 2.2.22.

7.3.7 Subcellular localisation of RFVT2 in fibroblasts

To determine whether the *SLC52A2* mutations cause mislocalisation of the plasma membrane RFVT2 protein, the subcellular localization of endogenous RFVT2 was assessed by immunocytochemistry in patient, p.Gly306Arg carrier, and control fibroblasts grown in regular DMEM, as detailed in Section 2.2.13.

7.3.8 Uptake assay of [^{3}H]-riboflavin in fibroblasts

The effect of the *SLC52A2* mutations on uptake of [^{3}H]-riboflavin was assessed using scintillation counting in patient, p.Gly306Arg carrier, and control fibroblasts grown in modified DMEM with variable riboflavin concentrations, as described in Section 2.2.12.

7.3.9 Assessment of intracellular FMN and FAD levels in fibroblasts

To establish whether patient fibroblasts had reduced intracellular levels of FMN and FAD, FMN and FAD levels were measured by HPLC in patient, p.Gly306Arg carrier, and control fibroblasts, as described in Section 2.2.14. Peak integration and data analysis on the HPLC were performed with the help of Marcus Oppenheim.

7.3.10 MRC complex I and II activities in fibroblasts

To test for impaired activity of flavin-dependent complexes in *SLC52A2* mutant fibroblasts, the activities of complexes I and II of the MRC as well as CS were assayed in patient, p.Gly306Arg carrier, and control fibroblasts, as described in Sections 2.2.15-2.2.17.

7.3.11 Basal ΔΨm measurement and response to inhibitors in fibroblasts

TMRM was used to determine the Δψm, an indicator of mitochondrial state, by live cell imaging in patient, p.Gly306Arg carrier and control fibroblasts with and without inhibition of glycolysis, as explained in Section 2.2.18. The mechanism maintaining the Δψm was investigated by studying the sensitivity of the Δψm to selected mitochondrial inhibitors, including oligomycin, rotenone, and FCCP, as described in Section 2.2.18.

7.3.12 Measurement of NADH redox index in fibroblasts

To further study the functional effect of *SLC52A2* mutations on the activity of the MRC as well as the rate of substrate supply, the resting levels of NADH autofluorescence were measured using an epifluorescence inverted microscope in patient, p.Gly306Arg carrier and control fibroblasts, as described in Section 2.2.19. The NADH redox index was calculated by calibration of the NADH fluorescence signal with the mitochondrial inhibitors NaCN and FCCP, as described in Section 2.2.19.

7.3.13 Assessment of ATP-synthase β (ATP5β) and glyceraldehyde-3-phosphate dehydrogenase (GAPDH) levels in fibroblasts

To determine whether *SLC52A2* patient fibroblasts increase their rate of glycolysis to compensate for a potential impairment in energy production, the expression levels of ATP5β, a subunit of the mitochondrial ATP-synthase/complex V, and GAPDH, a glycolytic enzyme, were assessed by Western blot in patient, p.Gly306Arg carrier and control fibroblasts grown in low riboflavin medium, as described in Section 2.2.22.

7.3.14 Quantification of CoQ_{10} levels in fibroblasts

To investigate a potential effect of *SLC52A2* mutations upon CoQ_{10} status, CoQ_{10} content was determined in patient, p.Gly306Arg carrier and control fibroblasts using reversed-phase HPLC with UV detection or tandem mass spectrometry as described in Section 2.2.21. The majority of this work was performed by Dr Kate Duberley.

7.3.15 Assessment of lactate/pyruvate ratio in fibroblasts

To further establish whether aerobic respiration is defective in *SLC52A2* patient fibroblasts, the lactate/pyruvate ratio was measured in cell medium aliquots obtained from patient, p.Gly306Arg carrier and control fibroblasts, as described in Section 2.2.20. This assay was performed by the Neurometabolic Unit at the NHNN.

7.3.16 Statistical analysis

For the experiments in fibroblasts, all statistical analyses were performed separately for the riboflavin-supplemented and low riboflavin conditions. For the statistical analysis of most experiments, the data had to be normalized to the average of the controls in order to eliminate variability between experiments (riboflavin-supplemented and low riboflavin considered independently). However, wherever possible and for graphical purposes only, the data were normalized to the average of the controls in both riboflavin-supplemented and low riboflavin conditions combined in order to visualize the impact of the addition of riboflavin on the dependent variable. All results are expressed as mean ± SEM. Further details regarding the statistical analysis are provided in Section 2.5.

7.4 Methods: *SLC52A2*-shRNA KD SH-SY5Y cells

7.4.1 Cell culture of SH-SY5Y cells

Human neuroblastoma SH-SY5Y cells were cultured as described in Section 2.3.2.

7.4.2 Generation and transfection of *SLC52A2*-shRNA KD constructs

After confirming by RT-PCR that *SLC52A2* is expressed in SH-SY5Y cells (Section 2.3.9), plasmid DNA for human pGIPZ lentiviral shRNAmir clones with empty control, scrambled control, and *SLC52A2*-targeting (*SLC52A2*-shRNA1 and *SLC52A2*-shRNA2) hairpin sequences was prepared as described in Sections 2.3.4-2.3.6. Quality control was performed as described in Section 2.3.6. Empty control, scrambled control, and *SLC52A2*-shRNA KD cells were generated by stable transfection with subsequent puromycin selection, as described in Section 2.3.7. The two *SLC52A2*-KD shRNAs were either pooled or transfected as individual shRNAs. Sequences of shRNA clones are available in Appendix VII Table VII-3.

7.4.3 Assessment of KD in *SLC52A2*-KD SH-SY5Y cells

To assess the level of *SLC52A2*-KD achieved, RNA was extracted from empty control, scrambled control, and *SLC52A2*-KD shRNA SH-SY5Y cells grown in regular DMEM, and cDNA was synthesized as described in Sections 2.3.8-2.3.9. RT-qPCR of *SLC52A2* was performed as detailed in Section 2.3.10. Details of the Taqman probes used for RT-qPCR of *SLC52A2* and the housekeeping gene *ACTB* can be found in Section 2.2.11.

7.4.4 Total protein determination

The protein content of cell lysates obtained from empty control, scrambled control, and *SLC52A2*-KD shRNA SH-SY5Y cells was determined by the Bradford method as described in Section 2.2.7.

7.4.5 Optimisation of riboflavin concentration in SH-SY5Y culture medium

Given the previously published findings showing correction of the metabolic defect upon riboflavin supplementation in fibroblasts of riboflavin-responsive patients (Section 7.1.4), an effect of riboflavin in the SH-SY5Y culture medium on our parameters of interest could not be excluded. It was again necessary to establish the threshold of riboflavin concentration in the SH-SY5Y culture medium which would uncover any potential defect in *SLC52A2*-KD shRNA cells, but which would not negatively affect empty and scrambled control shRNA cells. For medium optimisation, MRC complex I and II activities were used as a measure of cell health in empty control, scrambled control, and *SLC52A2*-KD shRNA (clones 1, 2 and 1+2 combined) SH-SY5Y cells grown in varying concentrations of riboflavin. Therefore, the activities of complexes I and II of the MRC as well as CS were assayed in empty control, scrambled control shRNA and *SLC52A2*-shRNA KD clones in SH-SY5Y cells, as described in Section 2.3.14-2.3.16. Medium optimisation for SH-SY5Y cells is further detailed in Section 2.3.11.

7.5 Methods: *SLC52A2*-mutant SH-SY5Y cells

7.5.1 Cell culture of SH-SY5Y cells

Human neuroblastoma SH-SY5Y cells were cultured as described in Section 2.3.2.

7.5.2 Generation and transfection of myc-DDK-tagged *SLC52A2*-mutant constructs

To determine the pathogenic effect of the *SLC52A2* mutations in SH-SY5Y cells, the open-reading frame of human *SLC52A2* containing a C-terminal myc-DDK tag in a pCMV6 expression vector was purchased from Origene (USA). The following mutations were introduced by site-directed mutagenesis: c.92G>C (p.Trp31Ser), c.700C>T (p.Gln234Stop), c.916G>A (p.Gly306Arg), c.935T>C (p.Leu312Pro), c.1016T>C (p.Leu339Pro), and c.1258G>A (p.Ala420Thr). Primer sets used for the mutagenesis are available in Appendix VII Table VII-7. SH-SY5Y cells were transfected with an empty vector and vectors containing *SLC52A2*^{WT}, *SLC52A2*$^{92G>C}$, *SLC52A2*$^{700C>T}$, *SLC52A2*$^{916G>A}$, *SLC52A2*$^{935T>C}$, *SLC52A2*$^{1016T>C}$, and *SLC52A2*$^{1258G>A}$ with subsequent stable selection with G-418 antibiotic. Detailed methods are available in Appendix II.

Studies using the myc-DDK-tagged *SLC52A2* mutant constructs in SH-SY5Y cells were not pursued further; instead, to maximise the impact of this PhD work, studies in primary mixed ventral horn cultures were prioritised as primary neuronal cells are a more appropriate model for in vitro studies of neurodegeneration.

7.6 Methods: studies in wild-type (WT) primary mixed ventral horn cultures and WT mouse embryonic fibroblasts (MEFs)

7.6.1 The riboflavin transporters in the mouse

As mentioned in Section 6.1.3, the mouse has two riboflavin transporters, *Slc52a2* and *Slc52a3*, encoding mRFVT2 and mRFVT3, respectively. No orthologue encoding a third riboflavin transporter has been recognised in the mouse, therefore the third riboflavin transporter present in higher animals must have evolved more recently in evolution (Yao et al., 2013; Yonezawa & Inui, 2013). The protein mRFVT3 shares 41% identity with mRFVT2. The mouse mRFVT3 (NCBI Reference Sequence NP_081448.2) is the orthologue for the human RFVT3, with which it shares 75% identity. The mouse mRFVT2 (NCBI Reference Sequence NP_083919, ambiguously also called Gpr172b) is the orthologue for both the human RFVT1 and RFVT2, with which it shares approximately 80% of its amino acids (Yao et al., 2013; Yonezawa et al., 2008; Yonezawa & Inui, 2013). Characteristics of

riboflavin transport via the mRFVT2 and mRFVT3 have been previously described in Section 6.1.3.

7.6.2 Culture of WT primary mixed ventral horn cultures

Mixed ventral horn cultures from spinal cords of WT embryonic mice were obtained and cultured as described in Section 2.4.2. This work was performed with the help of Dr Bernadett Kalmar.

7.6.3 Assessment of *Slc52a2* and *Slc52a3* mRNA expression levels in WT primary mixed ventral horn cultures and MEFs

To establish the relative mRNA expression levels of *Slc52a2* and *Slc52a3* in WT primary mixed ventral horn cultures and WT MEFs, RNA was extracted from WT primary mixed ventral horn cultures and WT MEFs, and cDNA was synthesized as described in Sections 2.4.9-2.4.10. RT-qPCR of *Slc52a2* and *Slc52a3* was performed as detailed in Section 2.4.11. Details of the Taqman probes used for RT-qPCR of *Slc52a2* and *Slc52a3* as well as the housekeeping gene *Actb* can be found in Section 2.4.11.

7.6.4 Total protein determination

The protein content of the lysates obtained from primary mixed ventral horn cultures was determined by the Bradford method as described in Section 2.4.13.

7.6.5 Determining the effect of riboflavin deprivation on MRC complex I and II activities in WT primary mixed ventral horn cultures

The WT primary mixed ventral horn cultures were grown for nine DIV in modified DMEM containing variable concentrations of riboflavin, as detailed in Section 2.4.2. Cells were also grown in regular CNB medium for comparison, as explained in Section 2.4.2. The activities of complexes I and II of the MRC as well as CS were assayed on cell lysates as described in Sections 2.4.14-2.4.16.

7.6.6 Determining the effect of riboflavin deprivation on basal ΔΨm in WT primary motor neurones

TMRM was used to determine the Δψm by live cell imaging in WT primary motor neurones grown either in regular CNB medium, in riboflavin-supplemented or 99% riboflavin-deficient modified DMEM for nine DIV as described in Section 2.4.17.

7.7 Methods: *Slc52a2* and *Slc52a3*-KD in primary mixed ventral horn cultures

7.7.1 Culture of primary mixed ventral horn cultures

Mixed ventral horn cultures from spinal cords of WT embryonic mice were obtained and cultured as described in Section 2.4.2. This work was performed with the help of Dr Bernadett Kalmar.

7.7.2 Generation of lentiviruses and viral transduction of shRNA constructs

Plasmid DNA for empty control, scrambled control, *Slc52a2*-targeting (*Slc52a2*-1) and *Slc52a3*-targeting (*Slc52a3*-1 and *Slc52a3*-2) hairpin sequences were prepared as described in Section 2.4.4-2.4.6. Lentiviral particles for empty control, scrambled control, *Slc52a2*-targeting (*Slc52a2*-1) and *Slc52a3*-targeting (*Slc52a3*-1 and *Slc52a3*-2) hairpin sequences were generated by packaging in HEK293T cells, as described in Section 2.4.7. Empty control, scrambled control, *Slc52a2*-shRNA and *Slc52a3*-shRNA KD cells were generated by transduction of primary mixed ventral horn cultures, MEFs, or HEK293T cells, as described in Section 2.4.7. The viral titre was determined in HEK293T cells as well as in primary motor neurones as described in Section 2.4.8.

7.7.3 Assessment of *Slc52a2* and *Slc52a3*-KD in MEFs

To assess the level of *Slc52a2* and *Slc52a3*-KD achieved, RNA was extracted from MEFs transduced with either empty control, scrambled control, *Slc52a2*-KD (*Slc52a2*-1) or one of two *Slc52a3*-KD (*Slc52a3*-1 and *Slc52a3*-2) shRNA lentiviral vectors, and grown in regular CNB medium with subsequent puromycin selection, as described in Section 2.4.9. cDNA was synthesized and RT-qPCR of *Slc52a2* and *Slc52a3* was performed as detailed in Sections 2.4.10-2.4.11. Details of the Taqman

probes used for RT-qPCR of *Slc52a2* and *Slc52a3* as well as the housekeeping gene *Actb* can be found in Section 2.4.11.

7.7.4 Basal measurement and response to inhibitors in *Slc52a2* and *Slc52a3*-KD primary motor neurones

TMRM was used to determine the Δψm by live cell imaging in primary motor neurones transduced with empty control, scrambled control, *Slc52a2*-KD (*Slc52a2*-1) or one of two *Slc52a3*-KD (*Slc52a3*-1 and *Slc52a3*-2) shRNA lentiviral vectors, and grown in 99% riboflavin-deficient modified DMEM for seven DIV as described in Section 2.4.17. The mechanism maintaining the Δψm was investigated by studying the sensitivity of Δψm to selected mitochondrial inhibitors, as described in Section 2.4.17.

7.7.5 Statistical analysis

Statistical analysis was performed as described in Section 2.5.

7.8 Results: *SLC52A2* patient fibroblasts

7.8.1 *SLC52A2* mRNA expression levels in fibroblasts

Patient E3 had significantly reduced *SLC52A2* mRNA expression levels compared to controls (51.2 ± 4.8% of controls; p-value=0.00754). This finding is consistent with the fact that this patient carries a premature stop mutation (p.Gln234Stop) in the compound heterozygous state, which leads to NMD as described in Chapter 6. Although the *SLC52A2* mRNA expression levels were also lower than controls in all other patients and in the p.Gly306Arg carrier, the reduction did not reach statistical significance in these individuals (patient E1: 89.2 ± 12.4% of controls; patient E2: 78.9 ± 9.2% of controls; patient E4: 73 ± 8.5% of controls; patient I1: 81.4 ± 12.9% of controls; p.Gly306Arg carrier: 93.3 ± 16.3% of controls) (Figure 7-2).

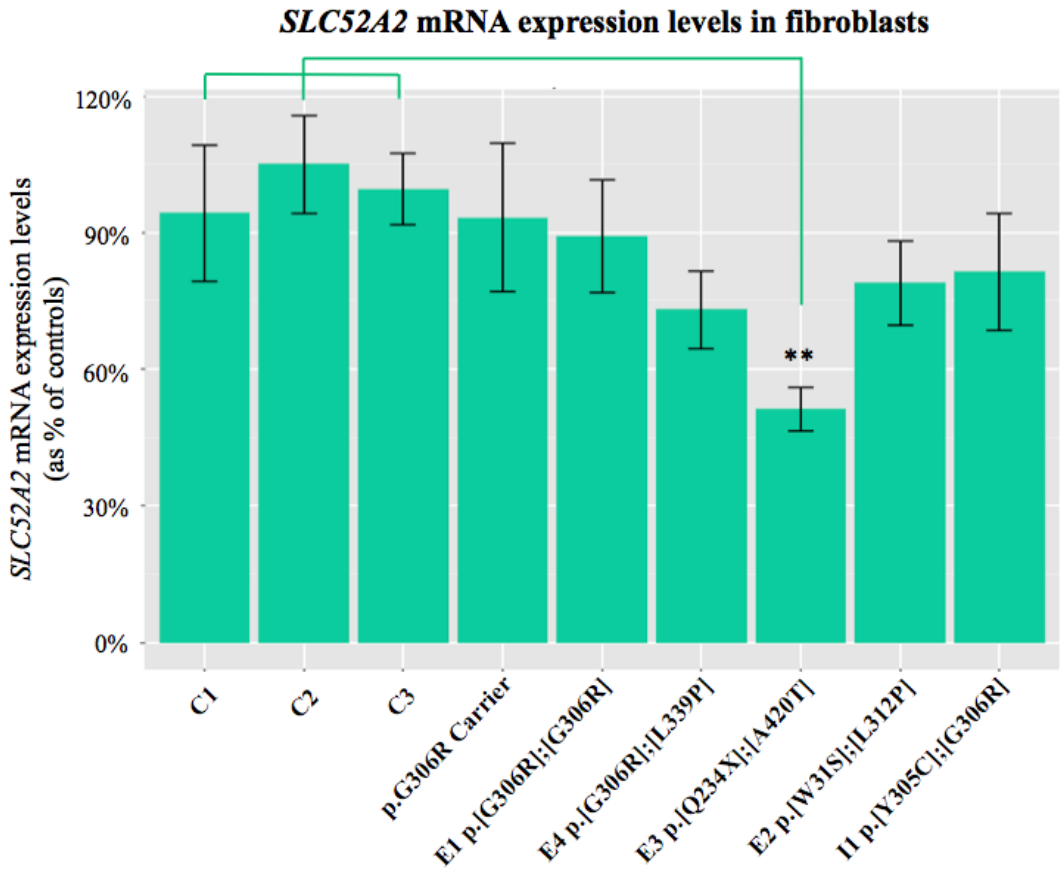

Figure 7-2 *SLC52A2* mRNA expression levels in patient, p.Gly306Arg carrier, and control fibroblasts. Results are expressed as mean ± SEM; data were normalised to control fibroblasts. Statistical analysis was carried out using one-way ANOVA with Dunnett's post-hoc test; level of significance compared to control cells: **: $p<0.01$. Data are the mean of three separate PCR determinations performed on at least three different occasions.

7.8.2 Intracellular FMN and FAD levels in fibroblasts

All patients had reduced levels of FMN compared to controls when grown in low riboflavin medium. This reduction reached significance at the $p<0.1$ level for patient E3 (64.1 ± 7.6% of controls in low riboflavin medium; $p=0.0736$), at the $p<0.05$ level for patient E4 (58.8 ± 1.6% of controls in low riboflavin medium; $p=0.0308$), and at the $p<0.001$ level for patient E2 and I1 (19 ± 3.6% and 36 ± 6.7% of controls in low riboflavin medium, respectively). The reduction was not significant in patient E1 (75.4 ± 19.4% of controls in low riboflavin medium). The p.Gly306Arg carrier

also did not have significantly reduced FMN levels in this condition (95.4 ± 13.9% of controls in low riboflavin medium).

When cells were grown in riboflavin-supplemented medium, FMN levels were not significantly different from controls for patients E1, E3, E4 and I1 (patient E1: 115.5 ± 11.3%, patient E3: 128.9 ± 16.6%, patient E4: 70.7 ± 6.1%, and patient I1: 90.7 ± 15.1% of controls in riboflavin-supplemented medium), as well as for the p.Gly306Arg carrier (134.9 ± 25.6% of controls in riboflavin-supplemented medium). FMN levels remained significantly lower than controls for patient E2 in the supplemented medium (58 ± 14.1% of controls in riboflavin-supplemented medium; p=0.0265). For all fibroblast lines including controls, the FMN levels were higher in the riboflavin-supplemented condition compared to the low riboflavin condition (Figure 7-3).

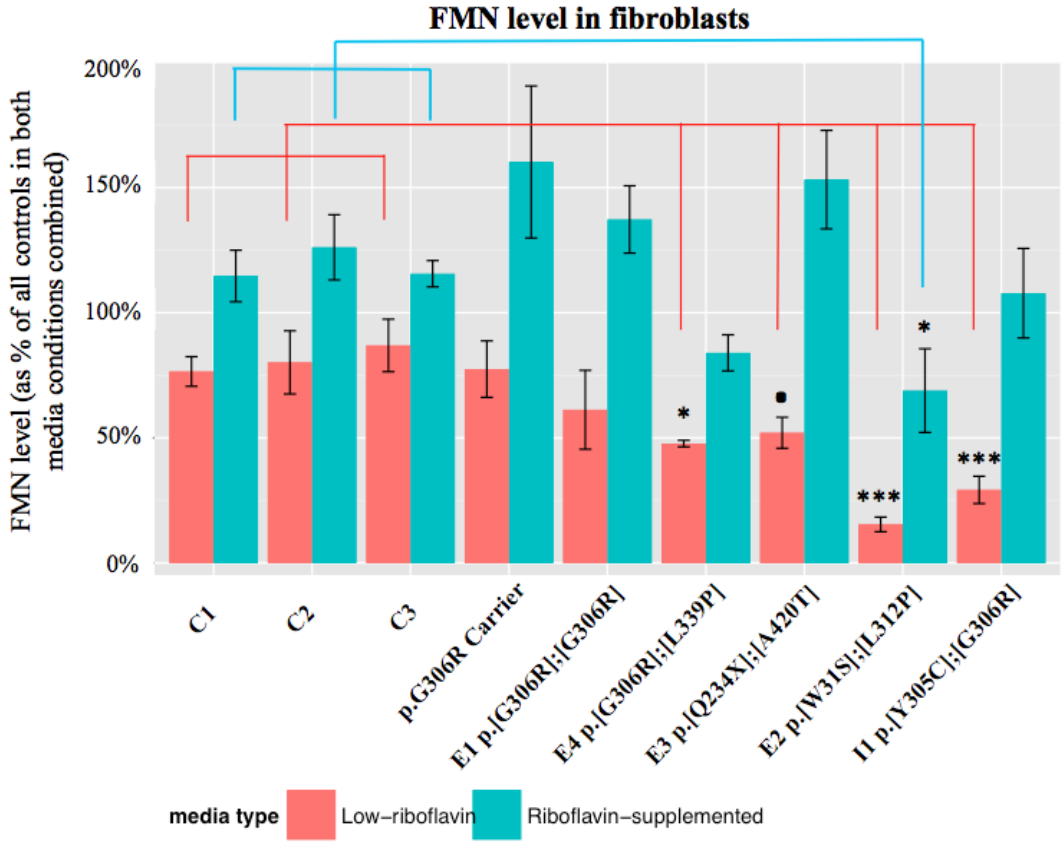

Figure 7-3 Intracellular FMN levels in patient, p.Gly306Arg carrier, and control fibroblasts. Results are expressed as mean ± SEM; for graphical purposes only, data were normalised to control fibroblasts in both media conditions combined. Statistical analysis was carried out using one-way ANOVA with Dunnett's post-hoc test for each medium condition independently; levels of significance compared to control cells: ".": $p<0.1$, *: $p<0.05$, ***: $p<0.001$. Data were generated from a minimum of three independent experiments.

All patients had reduced levels of FAD compared to controls when grown in low riboflavin medium, although to varying extents. This reduction reached significance for patients E2 and I1 (28.7 ± 6.1% and 39.1 ± 7.1% of controls in low riboflavin medium, respectively; $p<0.0001$). The reduction was not significant in all other patients (patient E1: 79.6 ± 4.5%, patient E3: 79.1 ± 2.4%, patient E4: 75.8 ± 12.1% of controls in low riboflavin medium). The p.Gly306Arg carrier had mildly reduced FAD levels (90.7 ± 5.3% of controls in low riboflavin medium); this was not statistically significant. When cells were grown in riboflavin-supplemented medium, FAD levels remained significantly lower than controls for patient E2 (63.9 ± 16.5%

of controls in riboflavin-supplemented medium; p=0.0731). FAD levels were not (or no longer) significantly lower than controls for all other patients as well as the p.Gly306Arg carrier (patient E1: 100.6 ± 11.9%, patient E3: 115.1 ± 11.8%, patient E4: 90.8 ± 4.7%, patient I1: 92.9 ± 16.3%, p.Gly306Arg carrier: 114.6 ± 15.1% of controls in riboflavin-supplemented medium). For all fibroblast lines including controls, the FAD levels were higher in the riboflavin-supplemented condition compared to the low riboflavin condition (Figure 7-4).

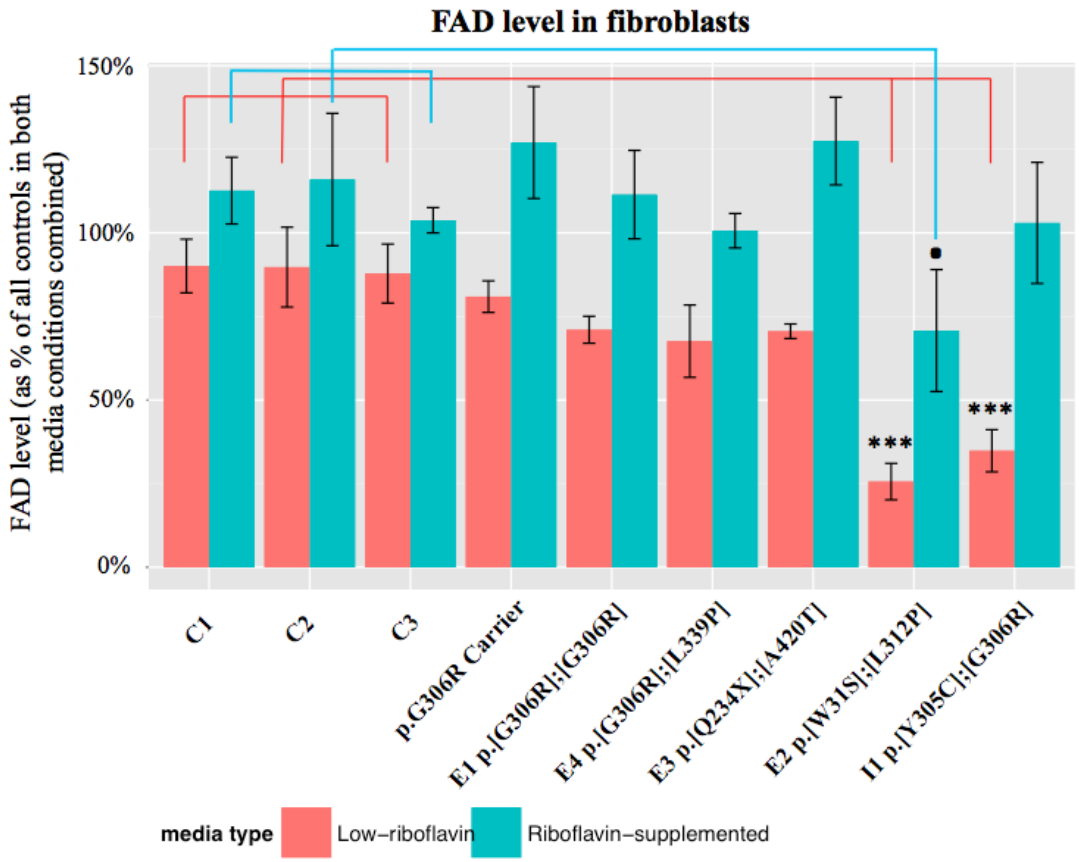

Figure 7-4 Intracellular FAD levels in patient, p.Gly306Arg carrier, and control fibroblasts. Results are expressed as mean ± SEM; for graphical purposes only, data were normalised to control fibroblasts in both media conditions combined. Statistical analysis was carried out using one-way ANOVA with Dunnett's post-hoc test for each medium condition independently; levels of significance compared to control cells: ".": $p<0.1$, ***: $p<0.001$. Data were generated from a minimum of three independent experiments.

7.8.3 MRC complex I and II activities in fibroblasts

All MRC complex activities are expressed as a ratio to CS activity, a mitochondrial marker enzyme, to normalise for mitochondrial enrichment (Hargreaves et al., 1999). All patients had reduced activities of MRC complex I compared to controls when grown in low riboflavin medium. This reduction reached significance at the $p<0.1$ level for patient E1 (47.3 ± 8.8% of controls in low riboflavin medium; $p=0.0639$) and at the $p<0.05$ level for patients E3 (24 ± 11.6% of controls in low riboflavin medium; $p=0.0101$), E4 (29.8 ± 10.6% of controls in low riboflavin medium; $p=0.0195$) and I1 (27.1 ± 8.9% of controls in low riboflavin medium; $p=0.0144$). The reduction was not significant in patient E2 (57.5 ± 20.1% of controls in low riboflavin medium). The complex I activity of the p.Gly306Arg carrier was not significantly different from controls in the low riboflavin medium (87.2 ± 50.1% of controls in low riboflavin medium). When cells were grown in riboflavin-supplemented medium, MRC complex I activities were restored at least to control levels for all patients (patient E1: 151.3 ± 20.8% SEM, patient E2: 141.6 ± 20.1%, patient E3: 113.5 ± 29.4%, patient E4: 107.3 ± 35.5%, patient I1: 124.6 ± 27.4% of controls in riboflavin-supplemented medium). In the supplemented medium, complex I activity was also not significantly different from controls for the p.Gly306Arg carrier (142.2 ± 24.2% of controls in supplemented medium). For all fibroblast lines, the MRC complex I activity was consistently higher in the riboflavin-supplemented condition compared to the low riboflavin condition (Figure 7-5).

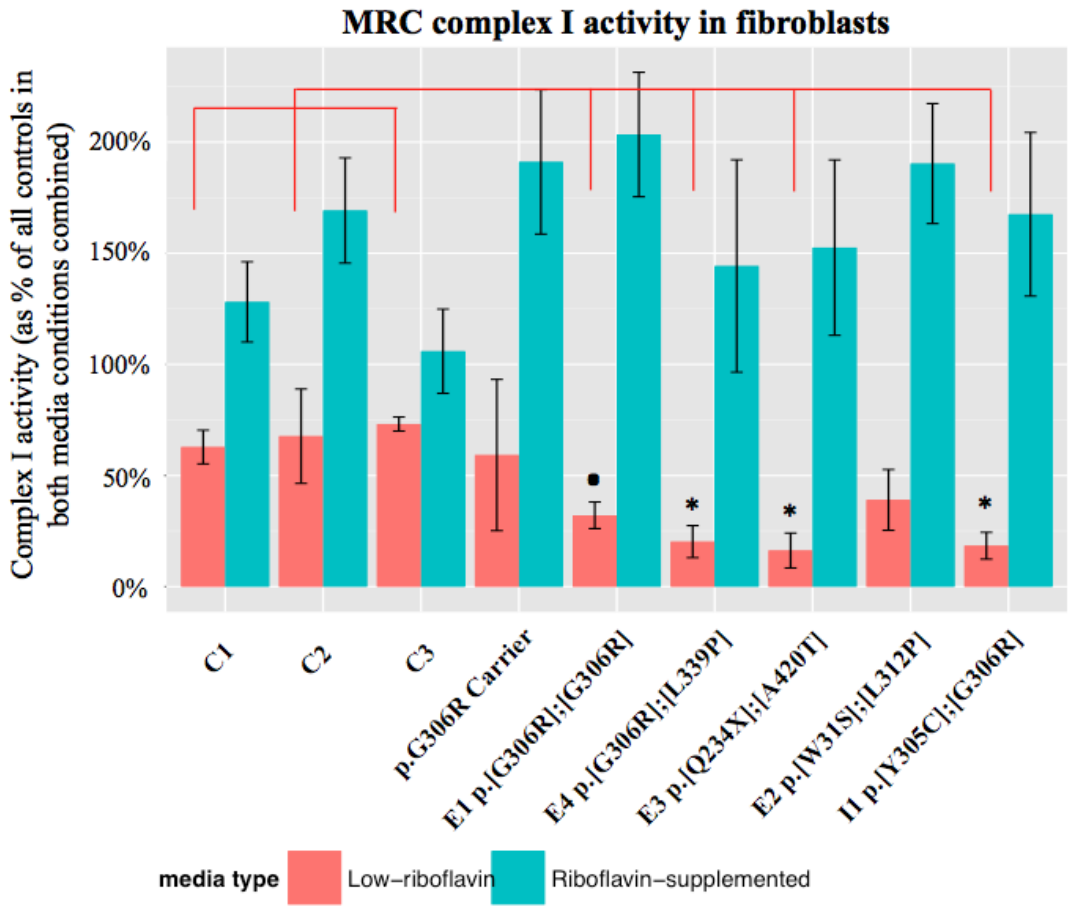

Figure 7-5 MRC complex I activity in patient, p.Gly306Arg carrier, and control fibroblasts. All MRC complex activities are expressed as a ratio to CS activity to normalise for mitochondrial enrichment (Hargreaves et al., 1999). Results are expressed as mean ± SEM; for graphical purposes only, data were normalised to control fibroblasts in both media conditions combined. Statistical analysis was carried out using one-way ANOVA with Dunnett's post-hoc test for each medium condition independently; levels of significance compared to control cells: ".": $p<0.1$, *: $p<0.05$. Data were generated from a minimum of three independent experiments.

All patients as well as the p.Gly306Arg carrier had reduced activities of MRC complex II compared to controls when grown in low riboflavin medium. This reduction reached significance at the $p<0.05$ level for patients E1 (53.8 ± 17.7% of controls in low riboflavin medium; $p=0.0135$), E3 (48.6 ± 2% of controls in low riboflavin medium; $p=0.0155$) and E4 (56.3 ± 15.2% of controls in low riboflavin medium; $p=0.0495$), at the $p<0.01$ level for patient I1 (42.5 ± 1.2% of controls in low riboflavin medium; $p=0.0059$), and at the $p<0.001$ level for patient E2 (33.5 ± 22.1%

of controls in low riboflavin medium; p=0.0003). The reduction was not significant in the p.Gly306Arg carrier (62.8 ± 11.9% of controls in low riboflavin medium).

When cells were grown in riboflavin-supplemented medium, MRC complex II activities were no longer significantly different from controls for all patients (patient E1: 105 ± 4.5%, patient E2: 112.7 ± 22.3%, patient E3: 78.2 ± 14.1%, patient E4: 88.4 ± 19.9%, patient I1: 89.3 ± 6.8% of controls in riboflavin-supplemented medium). In this condition, complex II activity was also not significantly different from controls for the p.Gly306Arg carrier (82.5 ± 32.1% of controls in supplemented medium). Again, for all fibroblast lines, the MRC complex II activity was consistently higher in the riboflavin-supplemented condition compared to the low riboflavin condition (Figure 7-6).

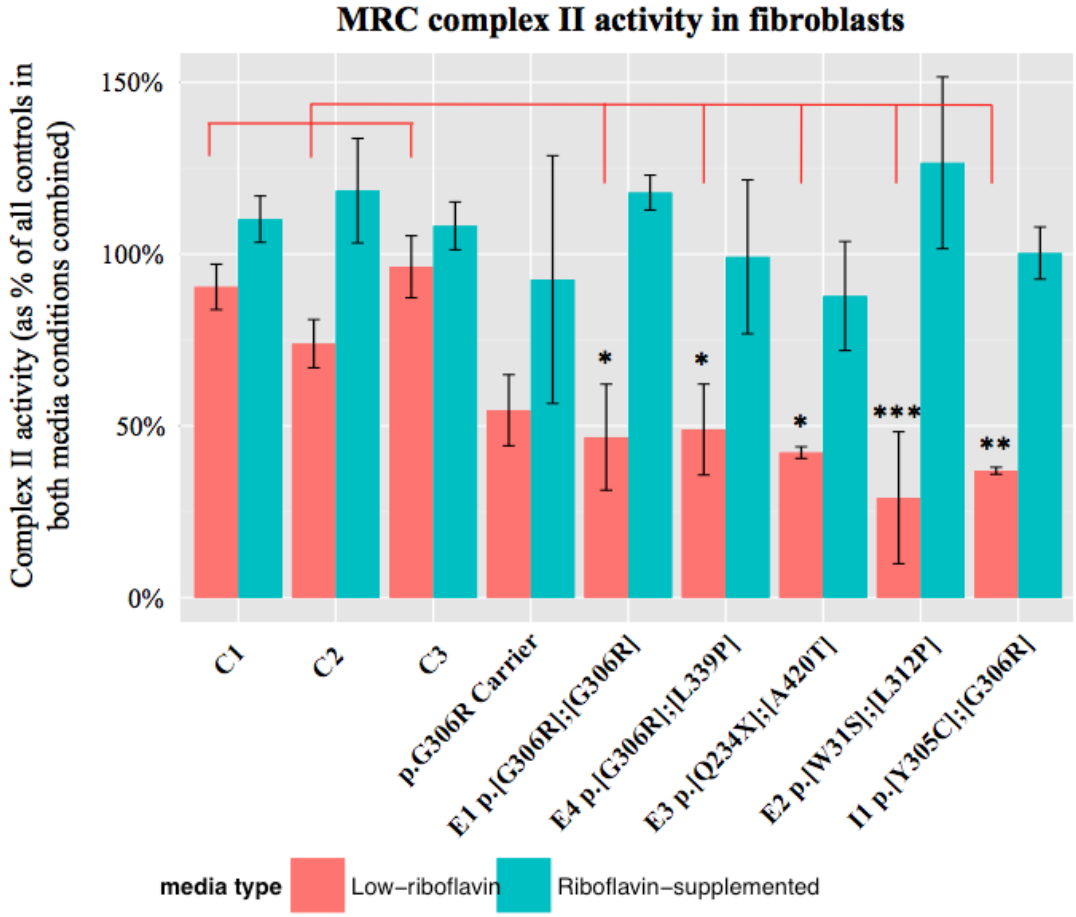

Figure 7-6 MRC complex II activity in patient, p.Gly306Arg carrier, and control fibroblasts. All MRC complex activities are expressed as a ratio to CS activity to normalise for mitochondrial enrichment (Hargreaves et al., 1999). Results are expressed as mean ± SEM; for graphical purposes only, data were normalised to control fibroblasts in both media conditions combined. Statistical analysis was carried out using one-way ANOVA with Dunnett's post-hoc test for each medium condition independently; levels of significance compared to control cells: *: $p<0.05$, **: $p<0.01$, ***: $p<0.001$. Data were generated from a minimum of three independent experiments.

7.8.4 Basal ΔΨm measurement and response to inhibitors in fibroblasts

The Δψm serves as an indicator of mitochondrial health and function. Accumulation of TMRM within the inner membrane of healthy mitochondria is driven by the $\Delta\Psi_m$; it leads to increased TMRM-associated red fluorescence. Therefore, intensity measurements indicate how well mitochondria are able to maintain the potential

across their membrane, and therefore serve to assess MRC function (Bartolome et al., 2013; Duchen, 2004). When cells were grown in low riboflavin medium, the TMRM fluorescence signal measured in the presence of glucose (normal conditions) was only significantly decreased compared to controls in patient I1 (85.1 ± 5.9% of controls in low riboflavin medium; p=0.0985), suggesting that basal $\Delta\psi m$ was decreased in this patient. The TMRM fluorescence signal measured in the presence of glucose was not significantly different from controls in patients E1, E2, E3 and E4 and in the p.Gly306Arg carrier in the low riboflavin medium (patient E1: 107.1 ± 6.3%, patient E2: 102.3 ± 6.6%, patient E3: 106.1 ± 3.6%, patient E4: 110.9 ± 7.2%, p.Gly306Arg carrier: 100.7 ± 4.5% of controls in low riboflavin medium).

When cells were grown in riboflavin-supplemented medium, the TMRM fluorescence signal was restored to control levels for patient I1 (109.5 ± 2.6% of controls in low riboflavin medium) and remained not significantly different from controls for patients E1, E3 and E4 as well as the p.Gly306Arg carrier (patient E1: 100.7 ± 4.1%, patient E3: 104.2 ± 8.3%, patient E4: 110.8 ± 8.6%, p.Gly306Arg carrier: 105 ± 4% of controls in riboflavin-supplemented medium). Patient E2 had significantly higher TMRM fluorescence signal compared to controls in this medium (118.9 ± 5.9% of controls in riboflavin-supplemented medium; p=0.0132) (Figure 7-7).

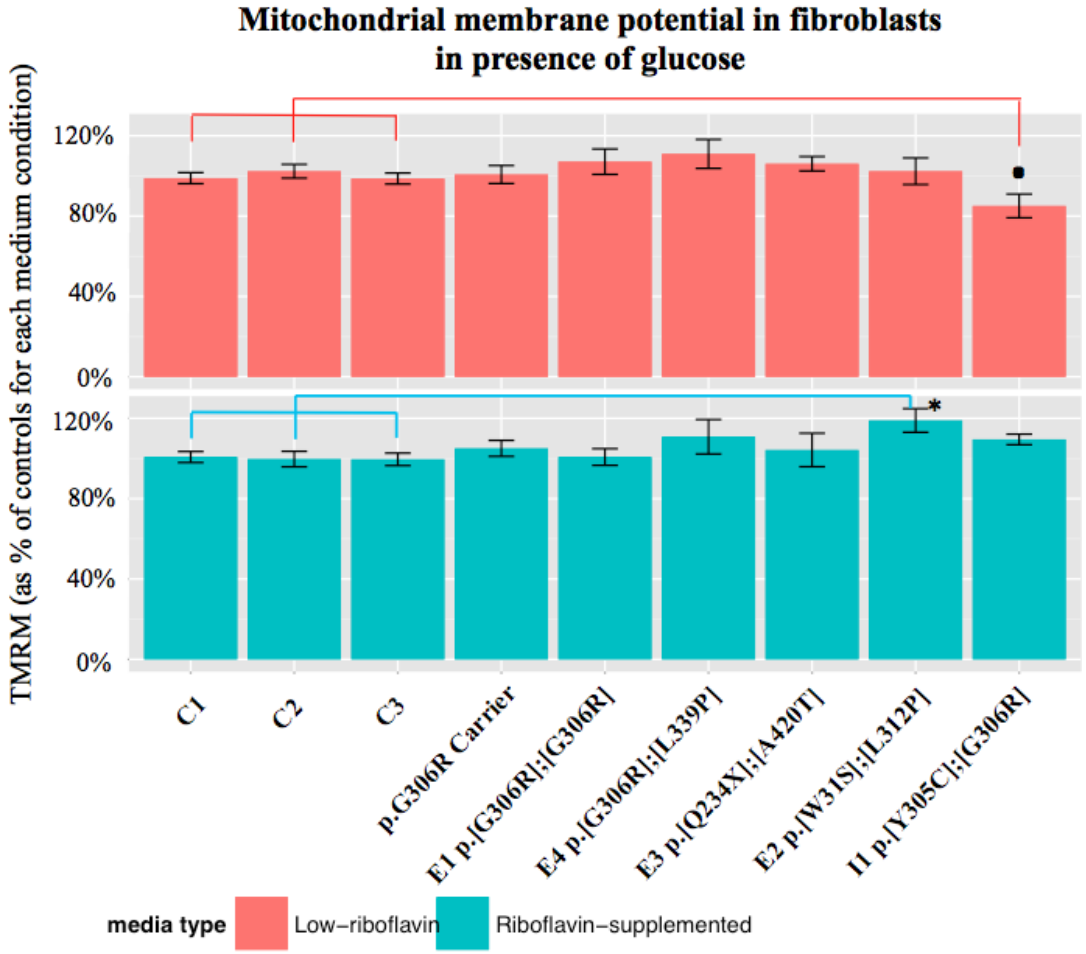

Figure 7-7 Basal ΔΨm in patient, p.Gly306Arg carrier, and control fibroblasts in the presence of glucose using TMRM in the redistribution mode. Results are expressed as mean ± SEM; data were normalised to control fibroblasts in each medium condition independently. Statistical analysis was carried out using one-way ANOVA with Dunnett's post-hoc test for each medium condition independently; levels of significance compared to control cells: ".": $p<0.1$, *: $p<0.05$. Data were generated from a minimum of 20 cells on a single coverslip in each of three independent experiments.

To investigate the mechanism of maintenance of the ΔΨm in the patient fibroblasts, the sensitivity of the Δψm was assessed following the addition of selected mitochondrial inhibitors, including oligomycin (ATP-synthase inhibitor), rotenone (MRC complex I inhibitor), and FCCP (uncoupler of oxidative phosphorylation to obtain complete depolarisation). This experiment was carried out in the presence of glucose in the fibroblasts grown in the low riboflavin and riboflavin-supplemented

media. Results are expressed as the change in TMRM intensity after addition of each toxin as a percentage of basal intensity (basal=baseline $\Delta\psi m$ – $\Delta\psi m$ after FCCP). For the fibroblasts grown in the low riboflavin medium, patient E2 showed a significantly greater reduction in TMRM fluorescence intensity following addition of oligomycin compared to controls, although this was not consistent across experiments (13.6 ± 9.8% reduction in TMRM intensity, p=0.0791). Following addition of rotenone, patient E1 showed a significantly smaller reduction in TMRM fluorescence intensity compared to controls (48.9 ± 13.3% reduction in TMRM intensity, p=0.0646). Responses to FCCP for patient fibroblasts grown in low riboflavin conditions did not differ significantly from controls; although patient E1 did had a comparatively stronger depolarisation in response to FCCP in this medium (45.2 ± 14.9% reduction in TMRM intensity), this did not reach statistical significance (Figure 7-8).

For the fibroblasts grown in the riboflavin-supplemented medium, responses to oligomycin for patient fibroblasts did not differ significantly from controls. Similarly, responses to rotenone for patient fibroblasts did not differ significantly from controls; patient E1 had a comparatively smaller depolarisation in response to rotenone in this medium (39.2 ± 2.8% reduction in TMRM intensity), however this was not statistically significant. Patient E1 showed a significantly greater reduction in TMRM fluorescence intensity following addition of FCCP compared to controls (62.9 ± 5% reduction in TMRM intensity, p=0.0783) (Figure 7-8). Representative TMRM traces from patient E2 and control-1 in low riboflavin medium and in the presence of glucose are shown in Figure 7-9.

A.

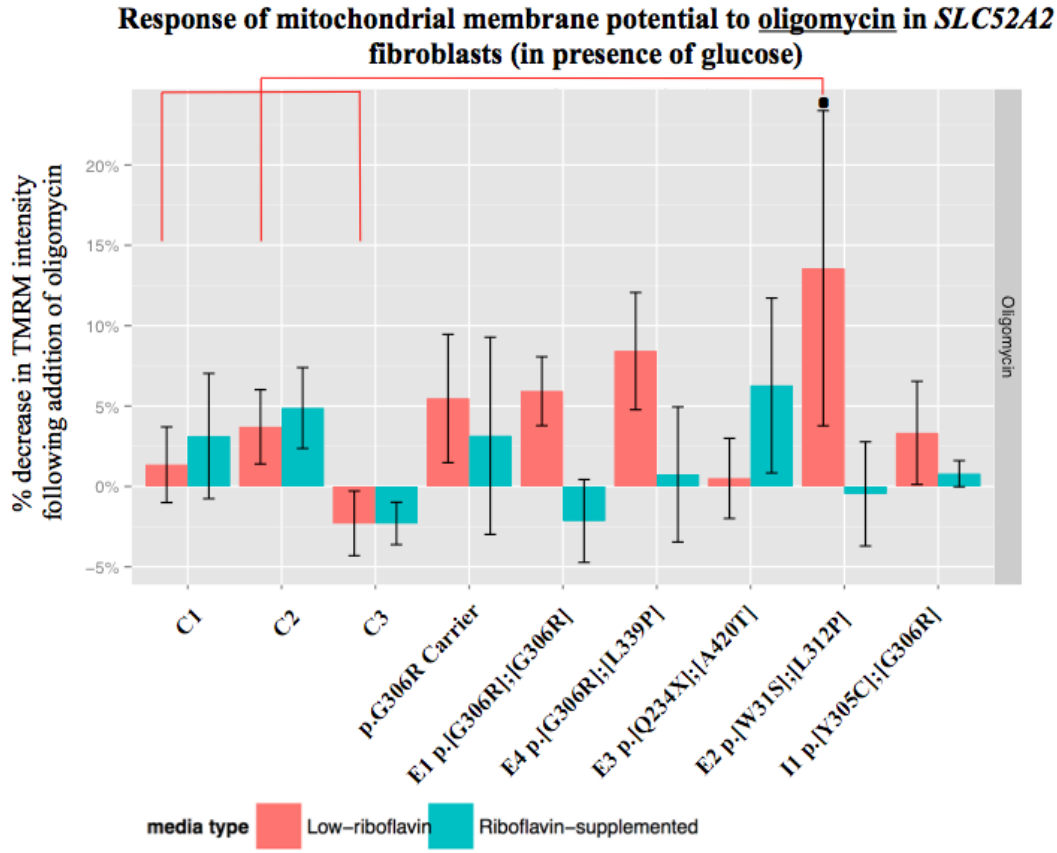
Response of mitochondrial membrane potential to oligomycin in SLC52A2 fibroblasts (in presence of glucose)
% decrease in TMRM intensity following addition of oligomycin
20%
15%
10%
5%
0%
−5%
Oligomycin
C1
C2
C3
p.G306R Carrier
E1 p.[G306R];[G306R]
E4 p.[G306R];[L339P]
E3 p.[Q234X];[A420T]
E2 p.[W31S];[L312P]
I1 p.[Y305C];[G306R]
media type
Low−riboflavin
Riboflavin−supplemented

B.

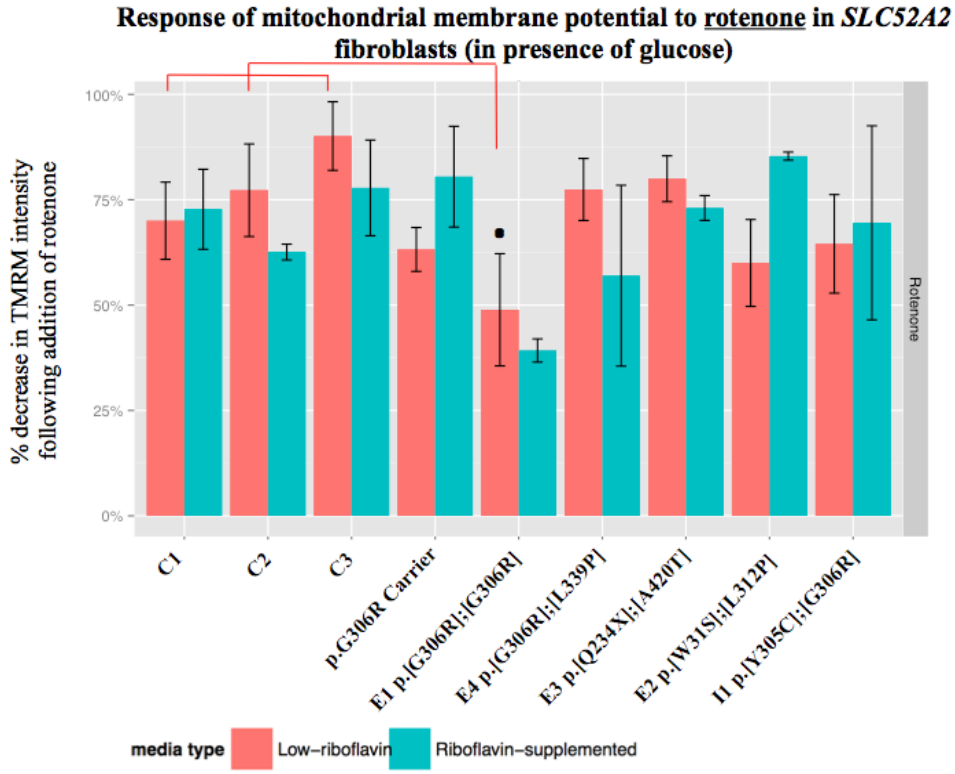
Response of mitochondrial membrane potential to rotenone in SLC52A2 fibroblasts (in presence of glucose)
% decrease in TMRM intensity following addition of rotenone
100%
75%
50%
25%
0%
Rotenone
C1
C2
C3
p.G306R Carrier
E1 p.[G306R];[G306R]
E4 p.[G306R];[L339P]
E3 p.[Q234X];[A420T]
E2 p.[W31S];[L312P]
I1 p.[Y305C];[G306R]
media type
Low−riboflavin
Riboflavin−supplemented

C.

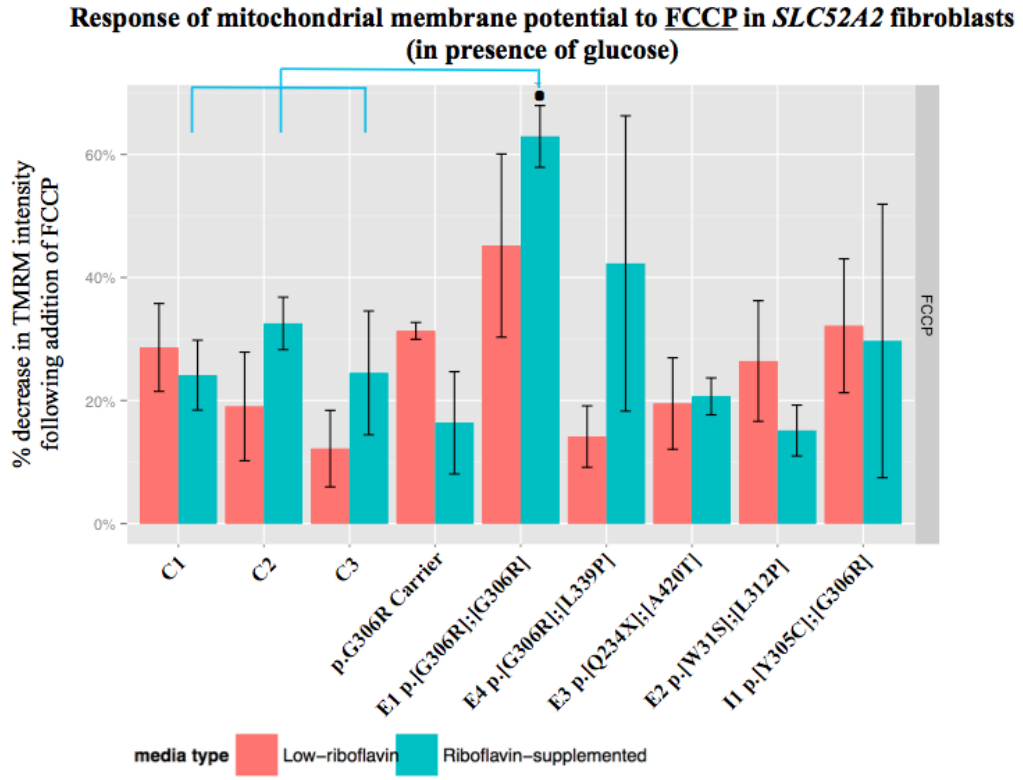

D.

	Oligomycin		Rotenone		FCCP	
Fibroblast line	**Low riboflavin**	**Riboflavin-supplemented**	**Low riboflavin**	**Riboflavin-supplemented**	**Low riboflavin**	**Riboflavin-supplemented**
C1	1.4 ± 2.4 %	3.1 ± 3.9 %	70 ± 9.2 %	72.7 ± 9.5 %	28.6 ± 7.1 %	24.1 ± 5.7 %
C2	3.7 ± 2.3 %	4.9 ± 2.5 %	77.2 ± 11 %	62.6 ± 1.9 %	19 ± 8.8 %	32.5 ± 4.3 %
C3	-2.3 ± 2 %	-2.2 ± 1.3 %	90.1 ± 8.1 %	77.8 ± 11.4 %	12.2 ± 6.2 %	24.5 ± 10 %
p.G306R carrier	5.5 ± 4 %	3.2 ± 6.1 %	63.2 ± 5.2 %	80.4 ± 12 %	24.5 ± 10.1 %	31.3 ± 1.4 %
E1 p.[G306R];[G306R]	5.9 ± 2.1 %	-2.1 ± 2.6 %	**48.9 ± 13.3 % (.)**	39.2 ± 2.8 %	45.2 ± 14.9 %	**62.9 ± 5 % (.)**
E4 p.[G306R];[L339P]	8.4 ± 3.6 %	0.7 ± 4.2 %	77.4 ± 7.4 %	57 ± 21.5 %	14.1 ± 5 %	42.3 ± 24 %
E3 p.[Q234X];[A420T]	0.5 ± 2.5 %	6.3 ± 5.4 %	80 ± 5.4 %	73 ± 2.9 %	19.5 ± 7.4 %	20.7 ± 3 %
E2 p.[W31S];[L312P]	**13.6 ± 9.8 % (.)**	-0.5 ± 3.2 %	60 ± 10.3 %	85.3 ± 1 %	26.4 ± 9.8 %	15.1 ± 4.1 %
I1 p.[Y305C];[G306R]	3.3 ± 3.2 %	0.8 ± 0.8 %	64.5 ± 11.7 %	69.5 ± 23 %	32.1 ± 10.9 %	29.7 ± 22.2 %

Figure 7-8 Percentage decrease in TMRM intensity after addition of oligomycin (2 µg/ml; A), rotenone (10 µM; B) and FCCP (1 µM; C) in patient, p.Gly306Arg carrier, and control fibroblasts using TMRM in the redistribution mode and in the presence of glucose. Negative values indicate hyperpolarisation. Results are expressed as mean ± SEM. Data were generated from 10-15 cells on a single coverslip in each of three independent experiments. Statistical analysis was carried out using one-way ANOVA with Dunnett's post-hoc test for each medium condition independently. Values of percentage decrease in TMRM intensity are shown in the table (D). Values in bold represent statistically significant results compared to controls; level of significance compared to control cells: ".": $p<0.1$.

A.

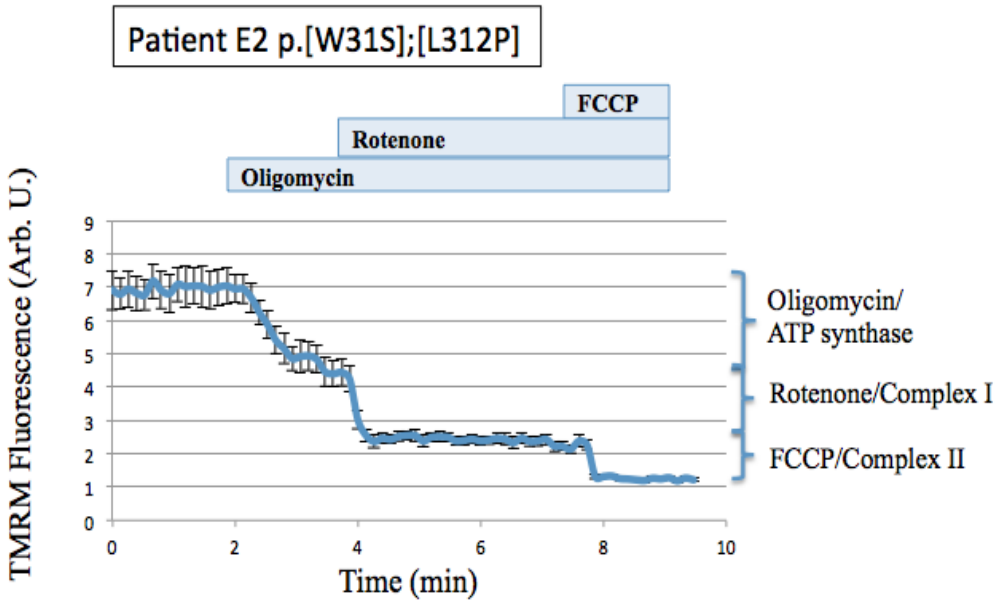

B.

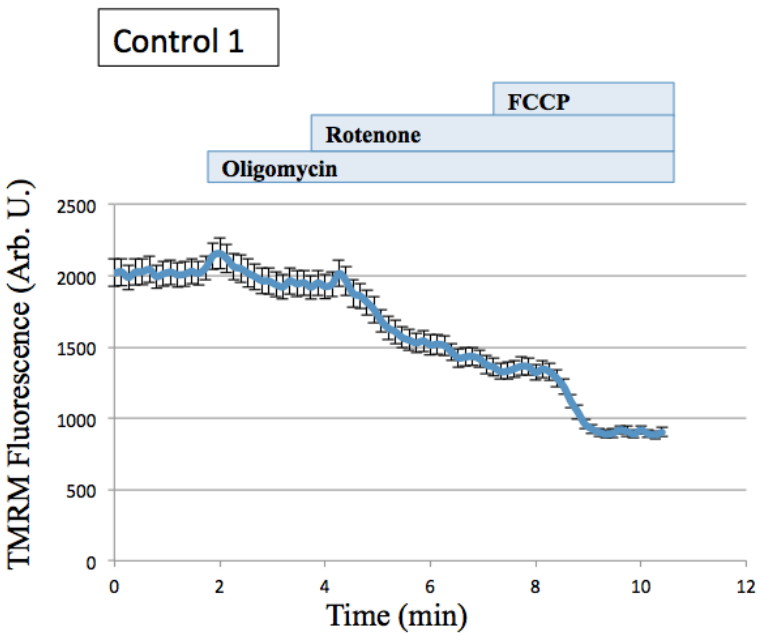

Figure 7-9 Representative TMRM traces (in the presence of glucose) from patient E2 (A) and control-1 (B) grown in low riboflavin medium showing responses to oligomycin (2 μg/ml), rotenone (10 μM) and FCCP (1 μM). Data represent results from 10-15 cells on a single coverslip. Error bars represent the SEM.

In a follow-up experiment, glycolysis was inhibited by using glucose-free incubation medium supplemented with 2-deoxy-D-glucose for the duration of the TMRM experiment. Glycolysis was blocked to enhance the cells' reliance on mitochondrial respiration via oxidative phosphorylation for ATP production, in the hope that any deficiency in respiration may become more evident. Fibroblasts have a high glycolytic capacity, thus a compensatory mechanism for defective respiration would be very efficient in these cells (Yao et al., 2011). The TMRM fluorescence signal measured in the absence of glucose was significantly decreased compared to controls in patients E1 (90.6 ± 2.9% of controls in low riboflavin medium; p=0.0077) and E2 (92.9 ± 1% of controls in low riboflavin medium; p=0.0528) when cells were cultured in low riboflavin medium. Although not significant in the other patients, there was a general trend for decreased $\Delta\psi m$ in patients and in the p.Gly306Arg carrier compared to controls in these conditions (patient E3: 94.9 ± 1%, patient E4: 93.4 ± 4.3%, patient I1: 96.5 ± 2.6%, p.Gly306Arg carrier: 95.3 ± 4.6% of controls in low riboflavin medium).

When cells were grown in riboflavin-supplemented medium, the TMRM fluorescence signal measured in glucose-free conditions was restored to control levels for all patients (patient E1: 98.6 ± 2.2%, patient E2: 105.5 ± 2.9%, patient E3: 102.1 ± 4.4%, patient E4: 102.6 ± 3.3%, patient I1: 109.5 ± 3.7%, p.Gly306Arg carrier: 104.6 ± 4.6% of controls in riboflavin-supplemented medium); none of the patient fibroblast lines were significantly different from controls in this condition (Figure 7-10).

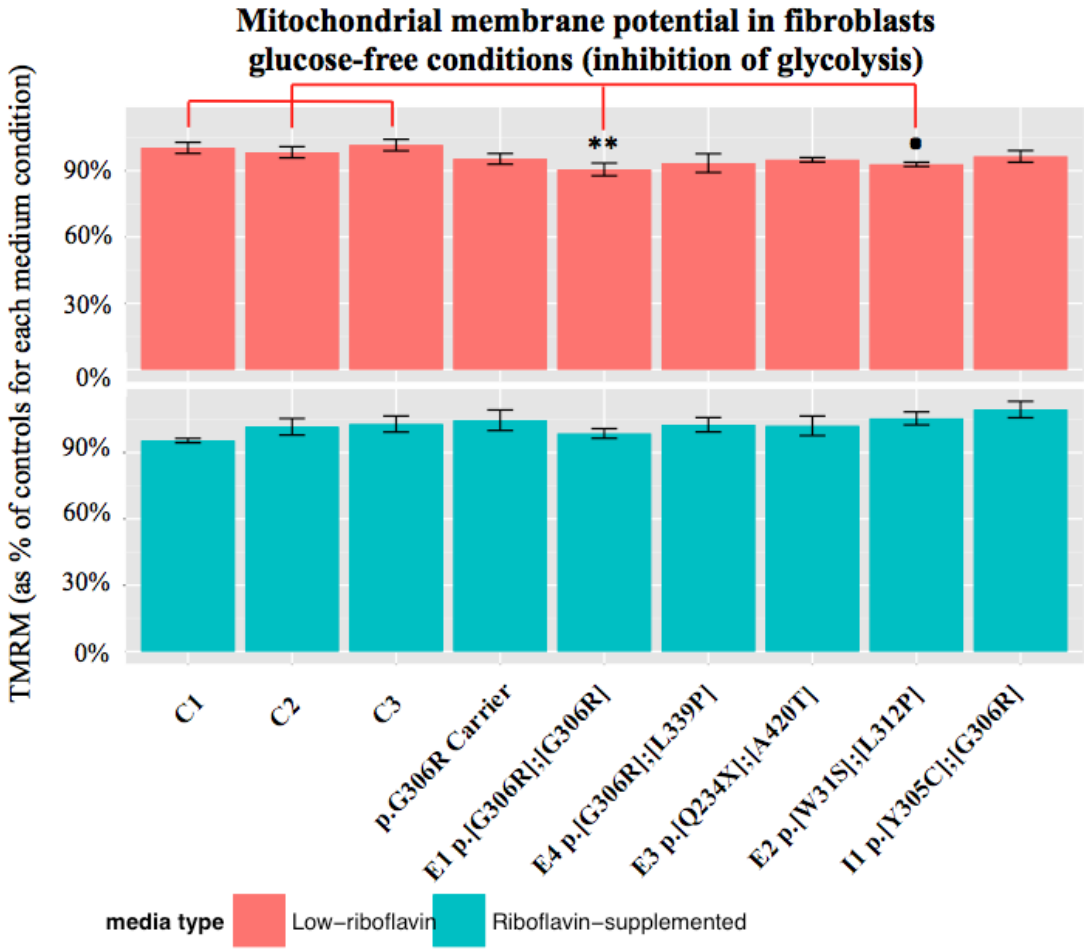

Figure 7-10 Basal ΔΨm in patient, p.Gly306Arg carrier, and control fibroblasts using TMRM in the redistribution mode and with inhibition of glycolysis. Results are expressed as mean ± SEM; data were normalised to control fibroblasts in each medium condition independently. Statistical analysis was carried out using one-way ANOVA with Dunnett's post-hoc test for each medium condition independently; levels of significance compared to control cells: ".": $p<0.1$, **: $p<0.01$. Data were generated from a minimum of 20 cells on a single coverslip in each of three independent experiments.

As before, the sensitivity of the Δψm was assessed in glucose-free conditions following the addition of selected mitochondrial inhibitors, including oligomycin, rotenone, and FCCP; this experiment was carried out only in fibroblasts grown in low riboflavin medium. Results are expressed as the change in TMRM intensity after addition of each toxin as a percentage of basal intensity. Patient E1 showed a significantly greater reduction in TMRM intensity following addition of oligomycin

compared to controls, although there was variability between experiments (17.6 ± 14.7% reduction in TMRM intensity, p=0.0093). Upon subsequent addition of both rotenone and FCCP, responses for patient fibroblasts did not significantly differ from controls (Figure 7-11). Representative TMRM traces from patient E1 and control-3 in low riboflavin medium and with inhibition of glycolysis are shown in Figure 7-12.

A.

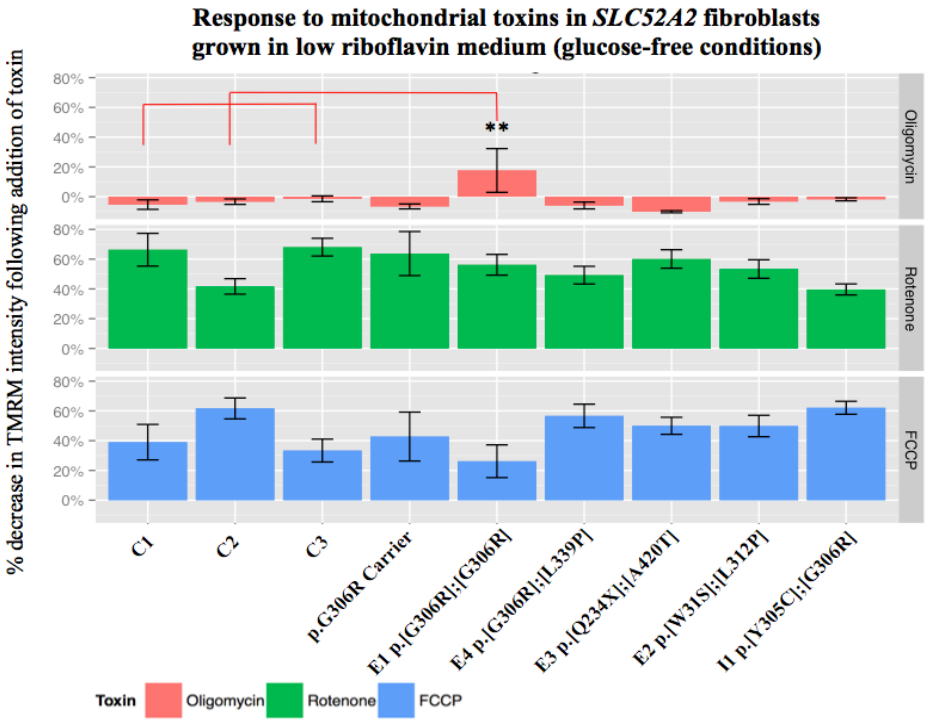

B.

Fibroblast line	Oligomycin Low riboflavin	Rotenone Low riboflavin	FCCP Low riboflavin
C1	-5.3 ± 3.18 %	66.3 ± 11 %	39 ± 11.9 %
C2	-3.3 ± 1.8 %	41.7 ± 5.2 %	61.7 ± 7 %
C3	-1.4 ± 2 %	68.1 ± 5.9 %	33.3 ± 7.7 %
p.G306R carrier	-6.5 ± 1.7 %	63.8 ± 14.8 %	42.8 ± 16.5 %
E1 p.[G306R];[G306R]	**17.6 ± 14.7 % (**)**	56.2 ± 7 %	26.2 ± 11 %
E4 p.[G306R];[L339P]	-5.9 ± 2.3 %	49.3 ± 5.9 %	56.7 ± 7.9 %
E3 p.[Q234X];[A420T]	-10.1 ± 0.73 %	60.1 ± 6.2 %	50 ± 5.7 %
E2 p.[W31S];[L312P]	-3.2 ± 1.9 %	53.4 ± 6.2 %	49.8 ± 7.2 %
I1 p.[Y305C];[G306R]	-1.8 ± 1 %	39.6 ± 3.7 %	62.1 ± 4.4 %

Figure 7-11 Percentage decrease in TMRM intensity after addition of oligomycin (2 µg/ml), rotenone (10 µM) and FCCP (1 µM) in patient, p.Gly306Arg carrier, and control fibroblasts using TMRM in the redistribution mode and with inhibition of glycolysis (A). Negative values indicate hyperpolarisation. Results are expressed as mean ± SEM. Data were generated from 10-15 cells on a single coverslip in each of three independent experiments. Statistical analysis was carried out using one-way ANOVA with Dunnett's post-hoc test. Values of percentage decrease in TMRM intensity are shown in the table (B). Values in bold represent statistically significant results compared to controls; level of significance compared to control cells: **: $p<0.01$.

A.

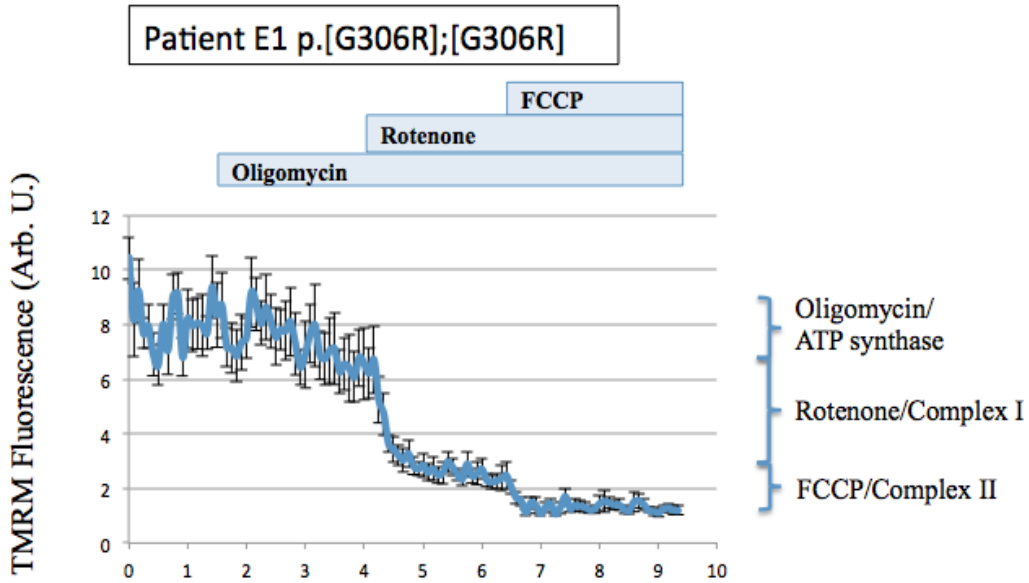

B.

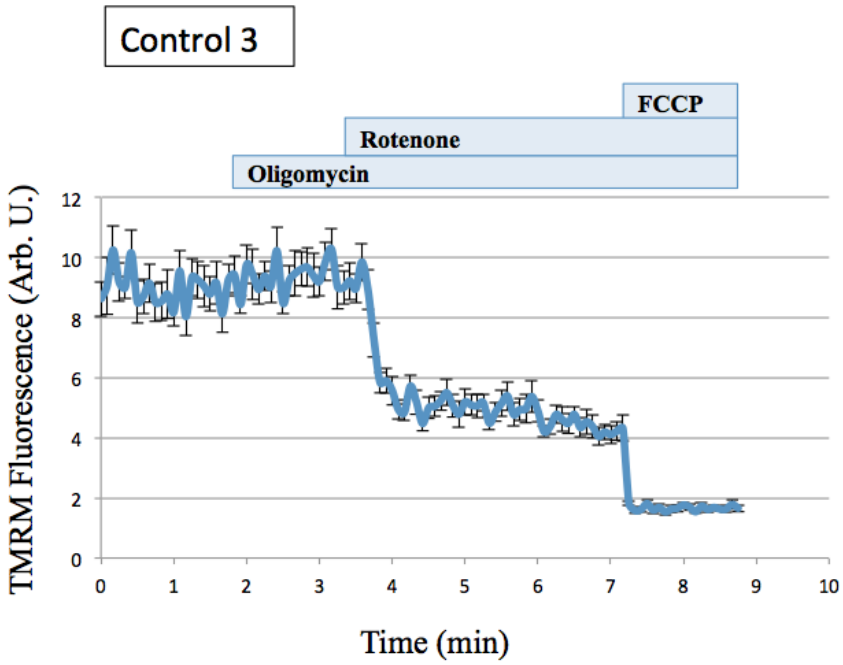

Figure 7-12 Representative TMRM traces (with inhibition of glycolysis) from patient E1 (A) and control-3 (B) grown in low riboflavin medium showing responses to oligomycin (2 μg/ml), rotenone (10 μM) and FCCP (1 μM). Data represent results from 10-15 cells on a single coverslip. Error bars represent the SEM.

7.8.5 NADH redox index and NADH pool in fibroblasts

The redox state of NADH reflects the rate of substrate supply as well as the activity of the MRC (Bartolome et al., 2013; Duchen, 2004). As discussed in Section 7.1.2, complex I deficiency may lead to decreased electron transfer, reduced NADH oxidation, and accumulation of NADH (Duchen, 2004). To assess the redox state of NADH in the *SLC52A2* patient fibroblasts, the NADH autofluorescence was monitored in all fibroblast lines and the NADH redox index was calculated as described in Section 2.2.19. Unfortunately, the FAD^{2+} redox state could not be assessed in the fibroblasts as these cells inherently have very low levels of FAD^{2+} autofluorescence (Bartolome et al., 2013).

When cells were grown in low riboflavin medium, the NADH redox index was significantly increased compared to controls in patient E2 only (172.7 ± 18.1% of controls in low riboflavin medium; $p<0.0001$). The NADH redox index was marginally increased compared to controls in patient E3 in this medium type (125.1 ± 8.5% of controls in low riboflavin medium), however this elevation did not reach statistical significance. The NADH redox index was as follows in the remaining patients and the carrier: patient E1: 94.9 ± 9.5%, patient E4: 117.2 ± 14.2%, patient I1: 113.6 ± 8.4%, p.Gly306Arg carrier: 108.2 ± 13.1% of controls in low riboflavin medium.

When cells were grown in riboflavin-supplemented medium, the NADH redox index decreased to below control levels for patient E2 (73.8 ± 8.6% of controls in the supplemented medium). In this medium type, the NADH redox index was also not significantly different from controls for all other patients as well as the p.Gly306Arg carrier (patient E1: 105.3 ± 32.5%, patient E3: 94.5 ± 13.6%, patient E4: 84 ± 20.7%, patient I1: 71.6 ± 12.8%, p.Gly306Arg carrier: 107 ± 8.5% of controls in riboflavin-supplemented medium) (Figure 7-13).

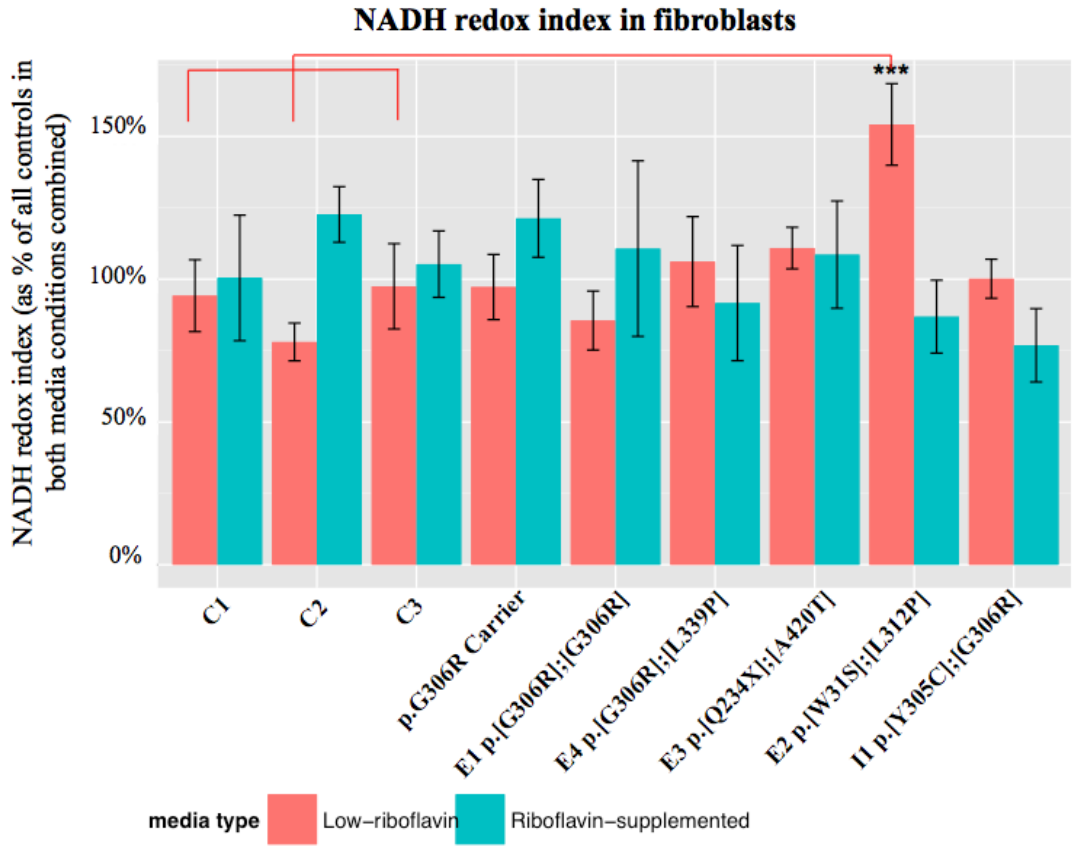

Figure 7-13 NADH redox index in patient, p.Gly306Arg carrier, and control fibroblasts. Results are expressed as mean ± SEM; for graphical purposes only, data were normalised to control fibroblasts in both media conditions combined. Statistical analysis was carried out using one-way ANOVA with Dunnett's post-hoc test for each medium condition independently; level of significance compared to control cells: ***: $p<0.001$. Data were generated from a minimum of 20 cells on a single coverslip in at least three independent experiments.

Representative traces of average NADH autofluorescence from patient E2 and control-1 grown in low riboflavin medium are illustrated in Figure 7-14. The trace for patient E2 displays an increased NADH redox index compared to control-1 under basal conditions.

A.

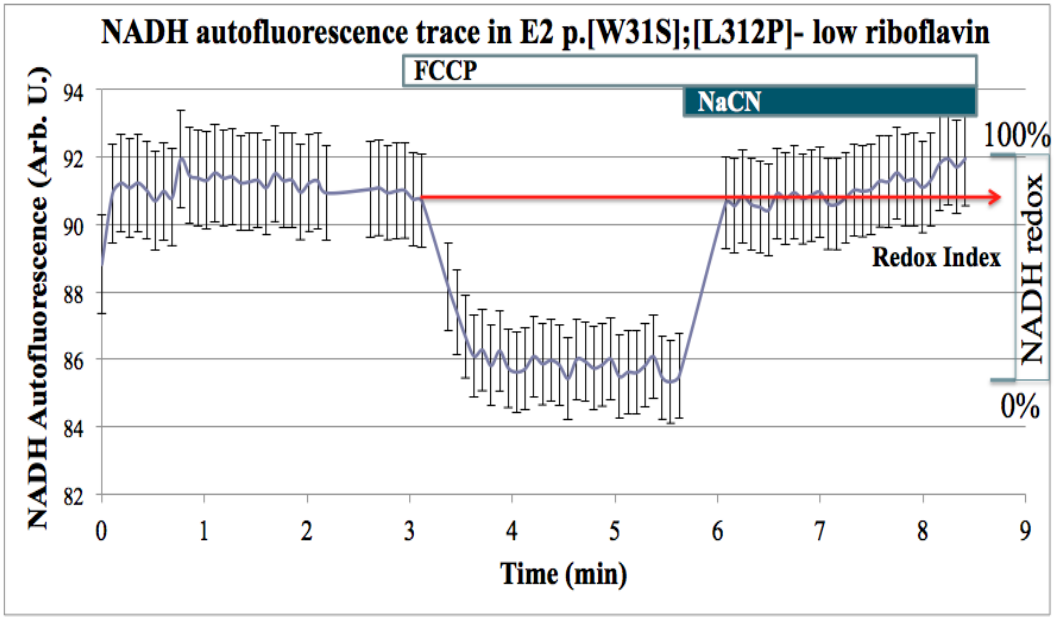

B.

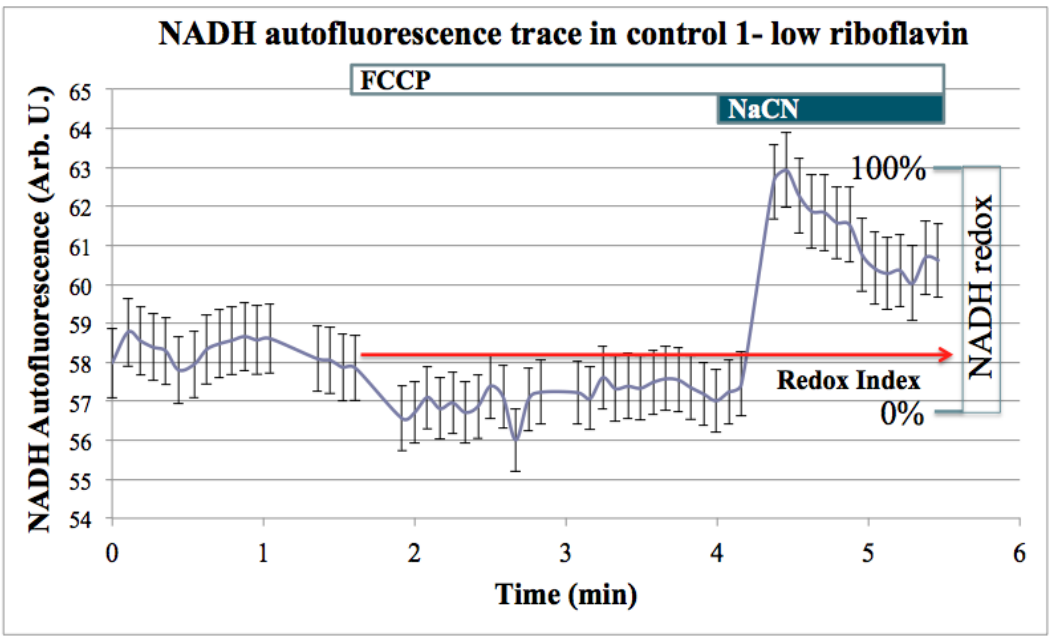

Figure 7-14 Representative traces of average NADH autofluorescence from a minimum of 20 cells on a single coverslip in patient E2 (A) and control-1 (B) after addition of FCCP (2 µM) and NaCN (2 mM). The NADH redox index (the initial NADH autofluorescence expressed as a percentage of the range) is illustrated graphically. Both traces were obtained from cells grown in low riboflavin medium. Error bars represent the SEM.

The NADH pool indicates how effective the Krebs cycle is in making NADH in the mitochondria. The NADH pool was not statistically different between patients/p.Gly306Arg carrier and controls for cells grown in the low riboflavin medium (patient E1: 113.5 ± 9.9%; patient E2: 100.1 ± 15.6%; patient E3: 108.8 ± 12.1%; patient E4: 95.1 ± 12%; patient I1: 123.1 ± 17.2%; p.Gly306Arg carrier: 98.9 ± 6.1% of controls in low riboflavin medium), as well as in the riboflavin-supplemented medium (patient E1: 105.3 ± 10.4%; patient E2: 96 ± 9.9%; patient E3: 102.9 ± 10.8%; patient E4: 98.1 ± 10.8%; patient I1: 86.6 ± 7.9%; p.Gly306Arg carrier: 107.1 ± 13% of controls in riboflavin-supplemented medium) (Figure 7-15).

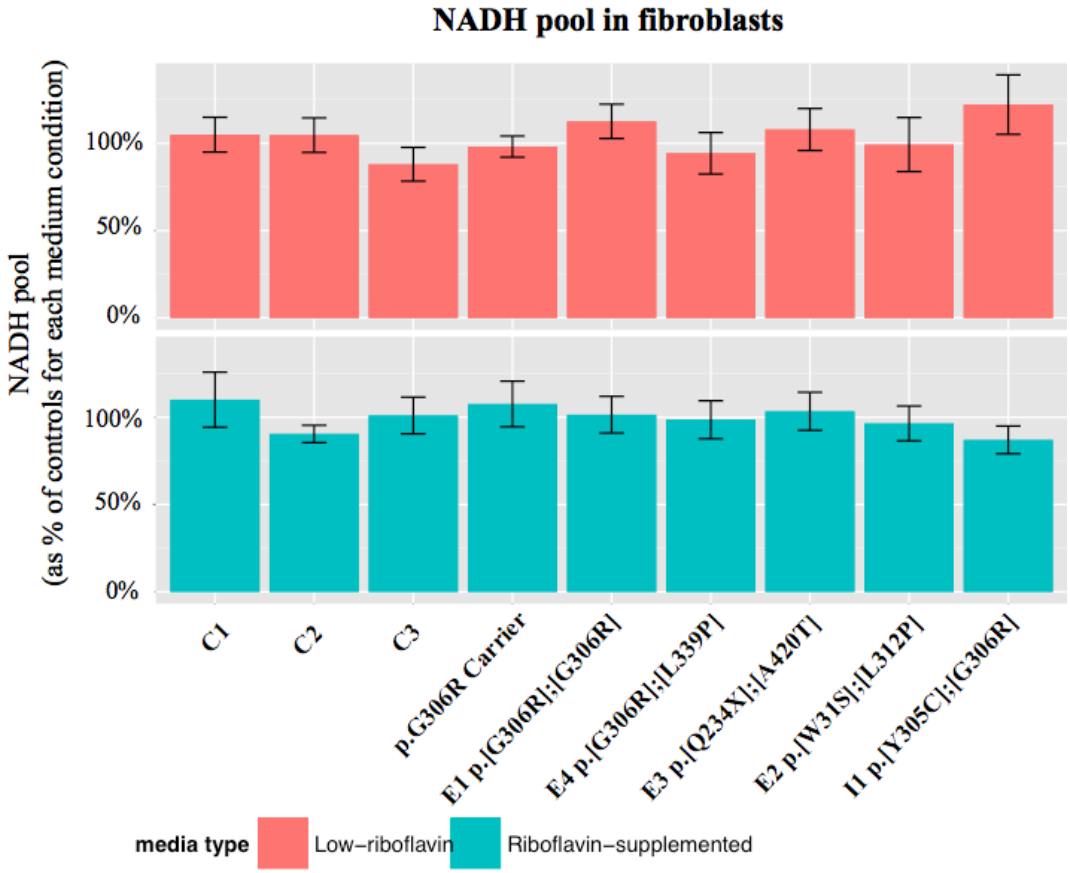

Figure 7-15 NADH pool in patient, p.Gly306Arg carrier, and control fibroblasts. Results are expressed as mean ± SEM; data were normalised to control fibroblasts in each medium condition independently. Statistical analysis was carried out using one-way ANOVA with Dunnett's post-hoc test for each medium condition independently. Data were generated from a minimum of 20 cells on a single coverslip in each of three independent experiments.

7.8.6 ATP5β and GAPDH levels in fibroblasts

The protein levels of ATP5β and GAPDH were qualitatively assessed by Western blot to establish whether *SLC52A2* fibroblasts increase their rate of glycolysis relative to their rate of oxidative phosphorylation to maintain ATP levels (Yao et al., 2011). Although this data was generated from only two independent experiments and was not quantified, the protein levels of GAPDH did not increase in patient and p.Gly306Arg carrier fibroblasts compared to controls when grown in low-riboflavin medium. The protein levels of ATP5β did not decrease in most patient fibroblasts compared to controls when grown in low-riboflavin medium, although patient E2 and I1 had mildly reduced ATP5β levels compared to controls. Within each individual, the protein levels of ATP5β and GAPDH were comparable; only patient I1 displayed a possible, very mild increase of GAPDH expression relative to ATP5β. A representative Western blot is shown in Figure 7-16, with β-actin as a loading control.

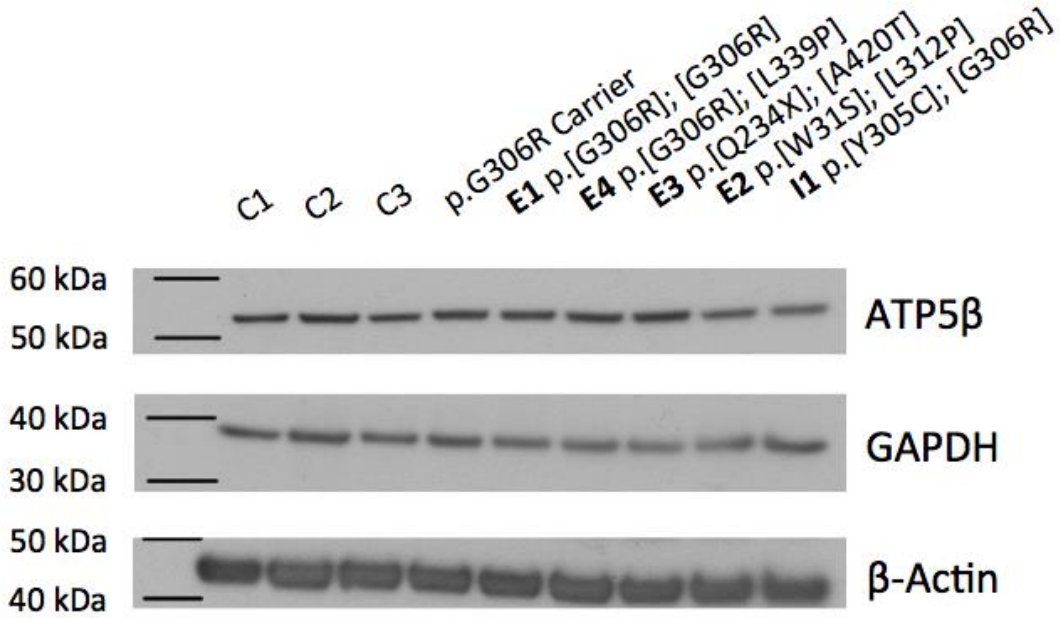

Figure 7-16 A representative Western blot of ATP5β and GAPDH expression in control, p.Gly306Arg carrier and patient fibroblasts grown in low riboflavin medium. The housekeeping protein β-actin was used as a loading control. Data were generated from two independent experiments.

7.8.7 CoQ_{10} levels in fibroblasts

CoQ_{10} is an antioxidant and a mobile electron carrier which accepts electrons from MRC complexes I and II and from fatty acid β-oxidation, and transfers them to complex III. As discussed in Section 7.1.4, some MADD patients carrying *ETFDH* mutations have defective fatty acid β-oxidation and reduced activity of complexes I, II-III and IV, along with secondary CoQ_{10} deficiency; the explanation for this secondary CoQ_{10} deficiency remains unknown, although a negative feedback mechanism is one possibility amongst others which have been proposed, as discussed earlier in this Chapter (Gempel et al., 2007). With the decrease in FAD availability observed in patients with *SLC52A2* mutations, the ETF:QO activity in the ETC would be expected to decrease along with the defect in fatty acid β-oxidation, which in turn may lead to a secondary CoQ_{10} deficiency in these patients (I. Hargreaves, personal communication).

For the riboflavin-supplemented condition in this experiment, the CoQ_{10} levels of the controls differed significantly from each other ($p<0.01$) as determined by an ANOVA, therefore a Tukey's two-tailed post-hoc test was performed for pairwise comparison between each control and patient/carrier individually. The highest p-value resulting from each of the three control-patient and control-carrier comparisons was used to assess significance.

The CoQ_{10} levels in controls grown in low riboflavin medium were 99.2 ± 11.3 pmol/mg in control-1, 84 ± 4.4 pmol/mg in control-2, and 79.4 ± 1.9 pmol/mg in control-3. When grown in this medium, patient E1, E3, E4 and the p.Gly306Arg carrier had CoQ_{10} levels which were not significantly different from controls (patient E1: 93.5 ± 6 pmol/mg; patient E3: 113.9 ± 10.7 pmol/mg; patient E4: 84.7 ± 4 pmol/mg; p.Gly306Arg carrier: 92.7 ± 10.4 pmol/mg); patient E2 had significantly reduced CoQ_{10} levels compared to controls in the low riboflavin medium (43 ± 15.8 pmol/mg; 51.8% reduction; $p=0.0029$).

When the cells were grown in riboflavin-supplemented medium, the CoQ_{10} levels in controls were 96.8 ± 19.2 pmol/mg in control-1, 94.6 ± 9.7 pmol/mg in control-2, and 69.3 ± 2.1 pmol/mg in control-3. In this medium type, CoQ_{10} levels were not

significantly different from controls for patient E1, E3, E4 and the p.Gly306Arg carrier (patient E1: 82.4 ± 21.6 pmol/mg, patient E3: 120 ± 18 pmol/mg, patient E4: 79.3 ± 6.8 pmol/mg, p.Gly306Arg carrier: 89.3 ± 33.8 pmol/mg). CoQ_{10} levels were restored to control levels for patient E2 (94.3 ± 17.2 pmol/mg) (Figure 7-17). A reference range for CoQ_{10} levels in fibroblasts was established by Dr Kate Duberley using the tandem mass spectrometry method (57-121.6 pmol/mg; n=50) (Duberley et al., 2013). In agreement with our findings above, only the CoQ_{10} levels in patient E2 fell below this reference range in the low riboflavin medium; after addition of riboflavin to the medium, the CoQ_{10} levels of this patient were within the reference range.

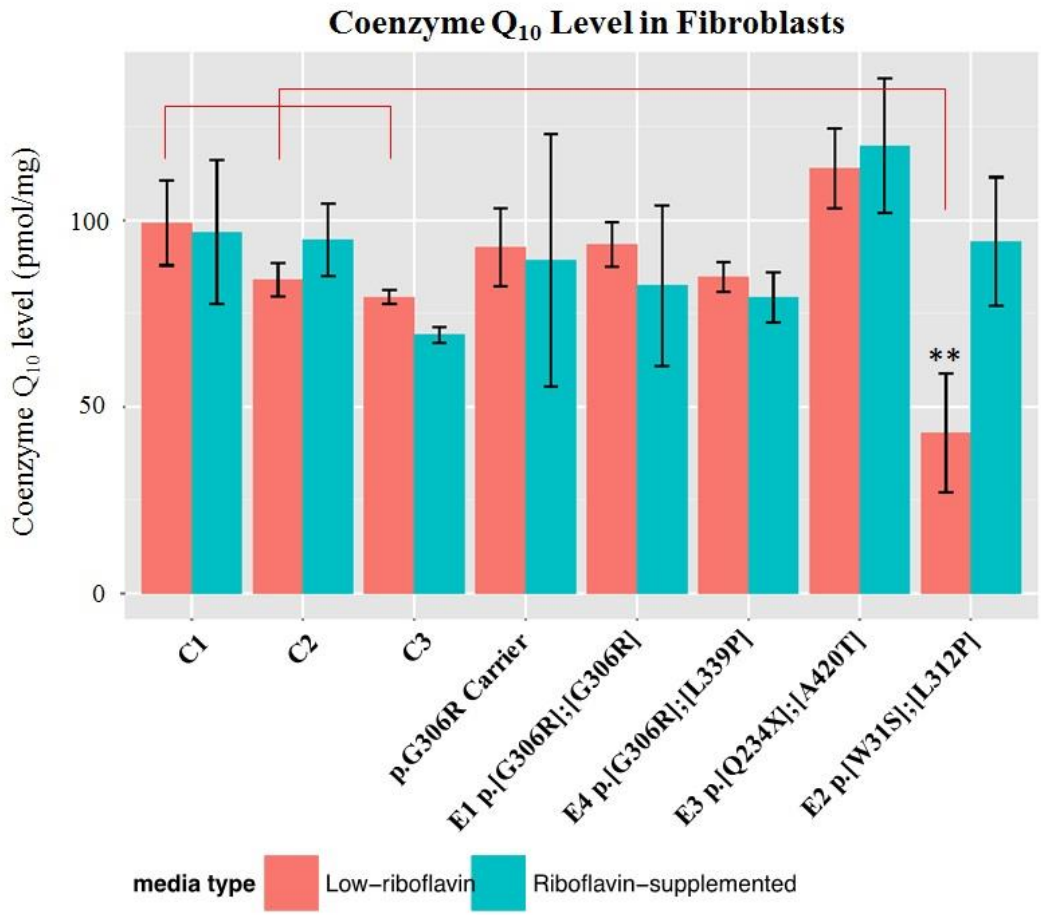

Figure 7-17 CoQ_{10} levels in patient, p.Gly306Arg carrier, and control fibroblasts. Results are expressed as mean ± SEM; statistical analysis was carried out using one-way ANOVA with Dunnett's (low riboflavin) or Tukey's (riboflavin-supplemented) post-hoc tests for each medium condition independently; level of significance compared to control cells: **: $p<0.01$. Data were generated from a minimum of three independent experiments.

In this study, all fibroblast lines except patient I1 were assessed using the tandem mass spectrometry method described in Section 2.2.21. Levels of CoQ_{10} in patient I1 had to be assessed by the reversed-phase HPLC with UV detection method due to equipment unavailability. A study has compared the HPLC-UV and mass spectrometry methods; both methods were found to give similar results for CoQ_{10} levels in muscle, indicating that these analytical methods may be comparable for CoQ_{10} measurements in this tissue. Although this has not been confirmed in fibroblasts, we tentatively had to use the reference range for fibroblasts established using the mass spectrometry method for patient I1. The CoQ_{10} level in patient I1 was 180.7 ± 24.5 pmol/mg in low riboflavin medium and 189.7 ± 11 pmol/mg in riboflavin-supplemented medium. These values are above the upper limit of the reference range in fibroblasts determined by the mass spectrometry method; the higher CoQ_{10} levels observed for patient I1 are likely due to the different methodology used. However, it can reasonably be established that patient I1 does not have decreased CoQ_{10} in either medium condition.

7.8.8 Lactate/pyruvate ratio in fibroblasts

As discussed in Section 7.1.2, the cell may switch to anaerobic respiration when aerobic respiration is inefficient. In the process, pyruvate accumulates and is converted to lactate, leading to an increase in the lactate/pyruvate ratio (Bernsen et al., 1993; Grad & Lemire, 2006; Mackay & Robinson, 2007). In this experiment, for both the low riboflavin and riboflavin-supplemented conditions, an ANOVA suggested that the lactate/pyruvate ratio of the controls differed significantly from each other ($p<0.01$), therefore a Tukey's two-tailed post-hoc test was performed for pairwise comparison between each control and patient/carrier individually. The highest p-value resulting from each of the three control-patient and control-carrier comparisons was used to assess significance.

When fibroblasts were grown in low riboflavin medium, the lactate/pyruvate ratio was significantly increased compared to control-2 only in patient E2 (320 ± 80.8% of controls in low riboflavin medium; $p=0.0188$). The lactate/pyruvate ratio was increased compared to controls in patient E3 (210.2 ± 16.9% of controls in low riboflavin medium), although this increase did not reach significance with respect to

control-2. The lactate/pyruvate ratio was not significantly different from controls in the other patients and the carrier when grown in low riboflavin medium: patient E1: 146.2 ± 10.4%, patient E4: 100.4 ± 11.9%, patient I1: 97 ± 35.7%, p.Gly306Arg carrier: 151.1 ± 13.5% of controls in low riboflavin medium.

When cells were grown in riboflavin-supplemented medium, the lactate/pyruvate ratio was restored to below control levels for patient E2 (87.2 ± 14.1% of controls in riboflavin-supplemented medium). The lactate/pyruvate ratio was as follows in the other patients and the carrier grown in riboflavin-supplemented medium: patient E1: 120.4 ± 10.6%, patient E3: 147.8 ± 20.5%, patient E4: 87.4 ± 12.5%, patient I1: 82.5 ± 28.2%, p.Gly306Arg carrier: 139.7 ± 22.3% of controls in riboflavin-supplemented medium. For all patients, the addition of riboflavin to the medium tended to decrease the lactate/pyruvate ratio (Figure 7-18).

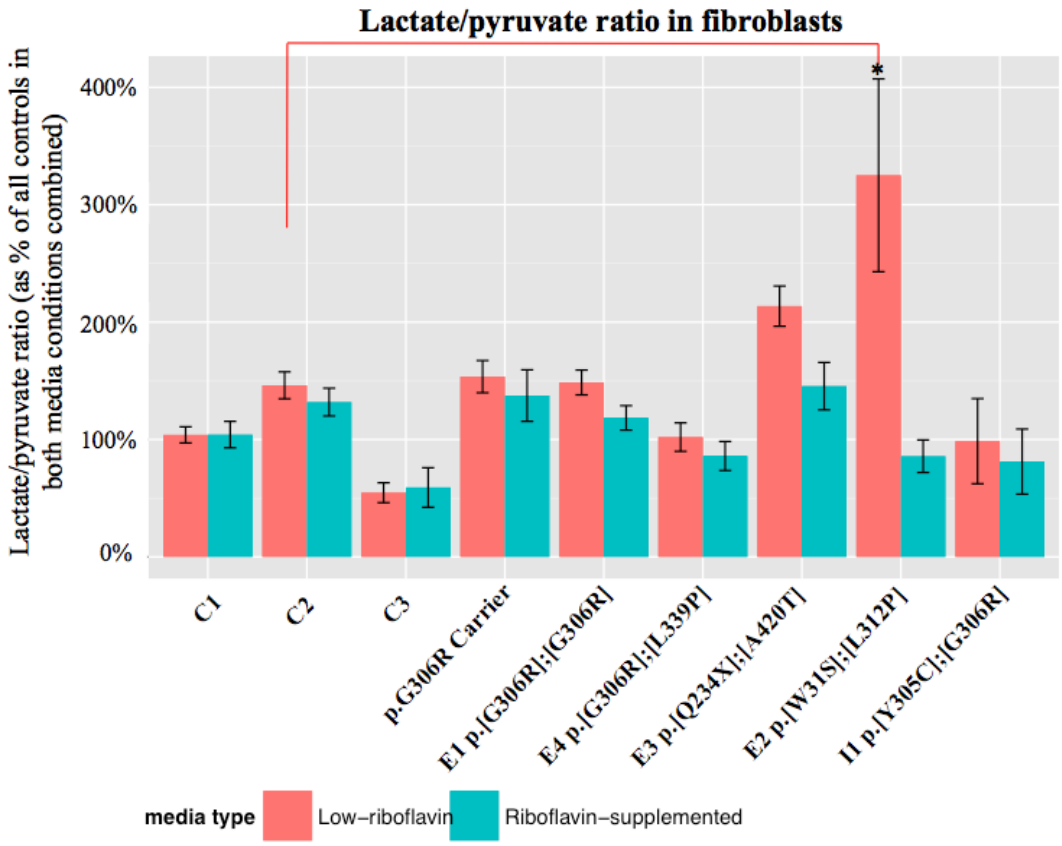

Figure 7-18 Lactate/pyruvate ratio in patient, p.Gly306Arg carrier, and control fibroblasts. Results are expressed as mean ± SEM; for graphical purposes only, data were normalised to control fibroblasts in both media conditions combined. Statistical analysis was carried out using one-way ANOVA with Tukey's post-hoc test for each medium condition independently; level of significance compared to control-2: *: $p<0.05$. Data were generated from a minimum of three independent experiments.

7.9 Results: *SLC52A2*-KD SH-SY5Y cells

Given the findings discussed in Section 7.1.6 of reduced riboflavin uptake in fibroblasts of BVVL patients and in cells transfected with clinically relevant riboflavin transporter mutations, we had hypothesised that the riboflavin transporter mutations may cause BVVL via a loss of function mechanism. Therefore, in an effort to model the potential disease mechanism in vitro, the *SLC52A2* gene was transiently silenced in SH-SY5Y cells. The mRNA expression levels of *SLC52A2* in SH-SY5Y cells transfected with *SLC52A2*-shRNA1 or *SLC52A2*-shRNA2 were 42.5 ± 3% and 77.6 ± 8.2% of scrambled control, respectively. Therefore, the *SLC52A2*-shRNA2

was less efficient at knocking down *SLC52A2* than *SLC52A2*-shRNA1. When the SH-SY5Y cells were transfected with both *SLC52A2*-shRNA 1 and 2 combined, the mRNA expression level of *SLC52A2* was 41.2 ± 9.1% of scrambled control; therefore, pooling the two shRNAs only mildly improved the level of *SLC52A2*-KD in comparison to exclusively using the *SLC52A2*-shRNA1. The empty clone had similar *SLC52A2* mRNA expression levels to the scrambled control clone (97.4 ± 6% of scrambled control) (Figure 7-19). It would be mathematically incorrect to test for statistical significance in this experiment as there is only a single control sample (scrambled control shRNA) which has zero variance (control is set at 100% on all experimental days).

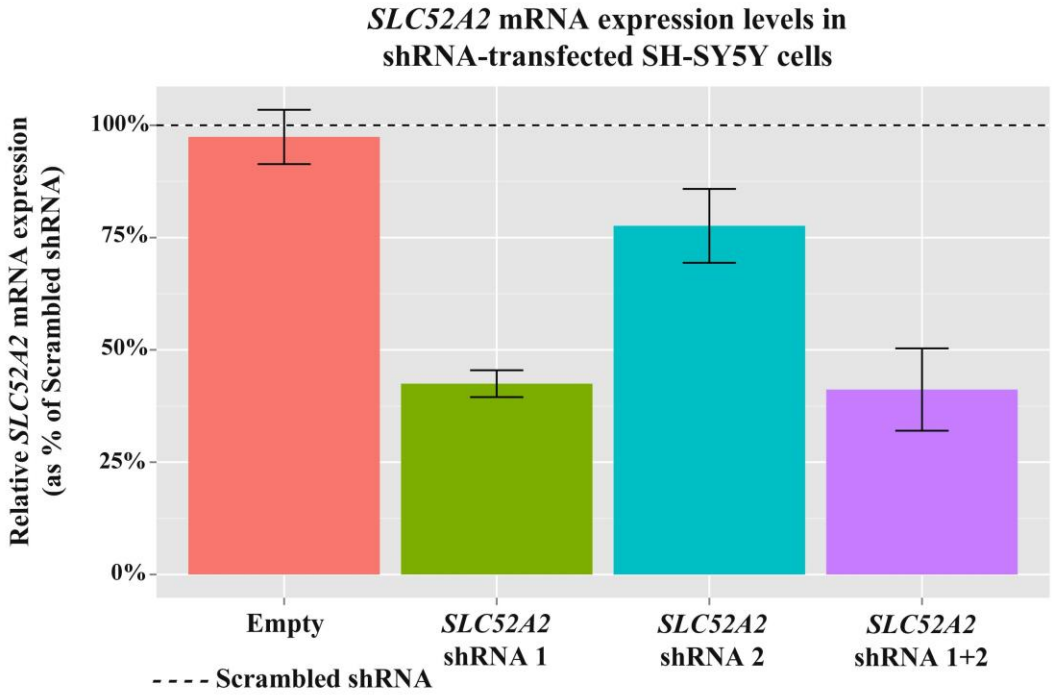

Figure 7-19 *SLC52A2* mRNA expression levels in shRNA-transfected SH-SY5Y cells. Results are expressed as mean ± SEM. Data were normalised to the scrambled control shRNA. Data are the mean of three separate PCR determinations performed on at least three different occasions.

To establish the riboflavin concentration in the medium that would unmask any defect in *SLC52A2*-KD shRNA cells without affecting the empty control and scrambled control shRNA cells, activities of complexes I and II of the MRC were

measured and used as a measure of cell health in empty control, scrambled control shRNA and *SLC52A2*-shRNA KD clones in SH-SY5Y cells. Five independent optimisation trials were carried out, as described in Section 2.3.11 and Appendix VII Table VII-5. In none of the experimental conditions did any of the *SLC52A2*-KD shRNA clones show a reproducible reduction in complex I and/or II activities. In all of the cell lines (empty control, scrambled control, and *SLC52A2*-KD shRNA (clones 1, 2 and 1+2 combined) SH-SY5Y cells), there was a mild trend for reduced complex I and/or complex II activities in the low riboflavin concentration medium compared to the medium containing a higher riboflavin concentration, however this was not consistently the case. This latter finding is unexpected, and may suggest that SH-SY5Y cells are relatively resistant to riboflavin deprivation; this would be in line with previous studies in brain tissue which suggested that ATP production is relatively preserved in this tissue during riboflavin deficiency (Depeint et al., 2006; Ross & Hansen, 1992).

Overall, the riboflavin concentration in the SH-SY5Y cell medium could not be successfully optimised. There are several possible explanations for these results, some of which may include: 1) insufficient KD, as haploinsufficiency (equivalent to 50% KD) does not cause overt disease in humans, 2) KD was not efficient at the protein level; this could not be assessed due to poor antibody specificity, 3) in contrast to fibroblasts, *SLC52A2* KD may not inherently lead to a decrease in complex I and/or II activities in SH-SY5Y cells, and 4) the optimisation protocol did not test the appropriate combination of extent and length of riboflavin deprivation. Studies in the *SLC52A2*-KD SH-SY5Y cells were not pursued further following these observations.

7.10 Results: studies in WT primary mixed ventral horn cultures and WT MEFs

7.10.1 *Slc52a2* and *Slc52a3* mRNA expression levels in WT primary mixed ventral horn cultures and WT MEFs

As the relative mRNA expression levels of *Slc52a2* and *Slc52a3* in mouse tissues are relatively unknown, the mRNA expression levels of both mouse riboflavin transporters were measured in WT primary mixed ventral horn cultures and WT

MEFs. Results from two independent experiments show that the mRNA expression level of *Slc52a3* was 94.8% of the mRNA expression level of *Slc52a2* in WT MEFs. In WT primary mixed ventral horn cultures, the mRNA expression level of *Slc52a3* was 30.9% of the mRNA expression level of *Slc52a2*. Therefore, although both riboflavin transporters are expressed at very similar levels in WT MEFs, *Slc52a2* is much more highly expressed than *Slc52a3* in primary mixed ventral horn cultures. Examining the data further, it can be determined that the mRNA expression of *Slc52a2* in WT primary mixed ventral horn cultures is 170.4% of that in WT MEFs; the mRNA expression of *Slc52a3* in WT primary mixed ventral horn cultures is 55.6% of that in WT MEFs. In other words, *Slc52a2* is expressed at higher levels in WT primary mixed ventral horn cultures than in WT MEFs, and *Slc52a3* is expressed at higher levels in WT MEFs than in WT primary mixed ventral horn cultures (Figure 7-20).

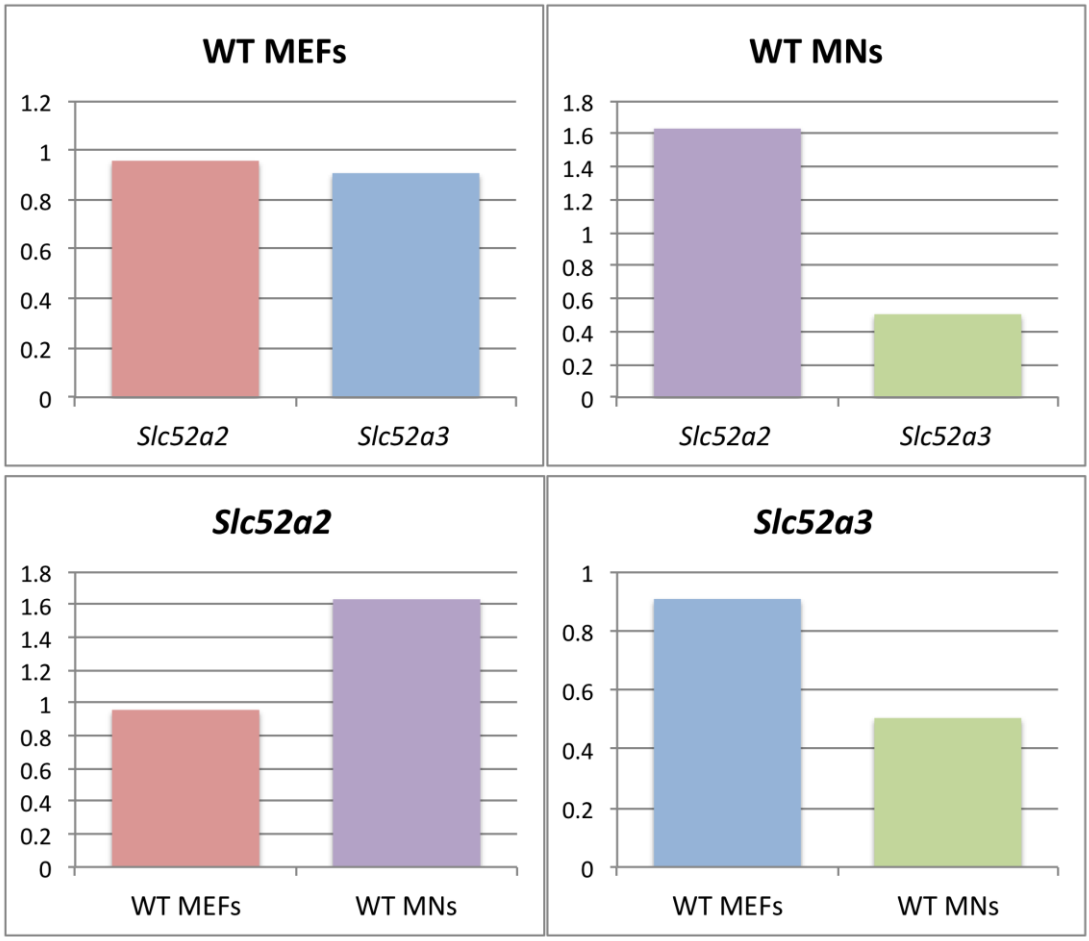

Figure 7-20 *Slc52a2* and *Slc52a3* mRNA expression levels as determined by RT-qPCR in WT MEFs and primary mixed ventral horn cultures. Data were generated from two independent experiments. Units are arbitrary; data were normalised to 100%.

7.10.2 Effect of riboflavin deprivation on MRC complex I and II activities in WT primary mixed ventral horn cultures

As a preliminary assessment of the sensitivity of WT primary mixed ventral horn cultures to riboflavin deprivation, cultures were grown in modified DMEM containing 1,005 nM riboflavin (=100% or no deprivation) and 502.5 nM riboflavin (50% deprivation). As in previous bioenergetics experiments, all MRC complex activities are expressed as a ratio to CS activity to normalise for mitochondrial enrichment (Hargreaves et al., 1999). When the WT primary mixed ventral horn cultures were grown for nine DIV in modified DMEM with 50% deprivation of

riboflavin, there was no decrease in MRC complex I and II activities compared to mixed ventral horn cultures grown in the riboflavin-supplemented medium (n=1) (Table 7-1).

Table 7-1 MRC Complex I and II activities in WT primary mixed ventral horn cultures grown in riboflavin-supplemented and 50% riboflavin-deficient medium. Data were generated from a single experiment.

Medium Type	MRC Complex I activity	MRC Complex II activity
Riboflavin-supplemented WT mixed ventral horn cultures	0.061259606	0.052108236
50% riboflavin-deficient WT mixed ventral horn cultures	0.065121624	0.052887169

To further test the susceptibility of the mixed ventral horn cultures to riboflavin deficiency, the WT primary mixed ventral horn cultures were grown for nine DIV in modified DMEM with 99% deprivation (0.98 nM) of riboflavin; this caused a reduction in MRC complex I and II activities in deprived mixed ventral horn cultures (0.98 nM) compared to the riboflavin-supplemented mixed ventral horn cultures (1,005 nM). Residual activities of complexes I and II in riboflavin-deprived cells were 65.7 ± 6.2% and 84.1 ± 4.8% of cells grown in riboflavin-supplemented medium, respectively. It is mathematically incorrect to assess statistical significance in this case as the experiment has a single control sample (riboflavin-supplemented medium) which has no variance (control is set to 100% on all experimental days).

Of note, simply changing the medium from regular CNB medium to riboflavin-supplemented modified DMEM (both 1,005 nM riboflavin) caused a decrease in MRC complex I and II activities, although both media contained the same concentration of riboflavin (complex I and II activities of WT primary mixed ventral horn cultures in regular CNB medium: 195.8 ± 8% and 119.4 ± 13.2% of cells grown in riboflavin-supplemented medium) (Figures 7-21 and 7-22). Therefore, nutrients found in CNB medium and not in riboflavin-supplemented modified DMEM are essential for cellular energy metabolism.

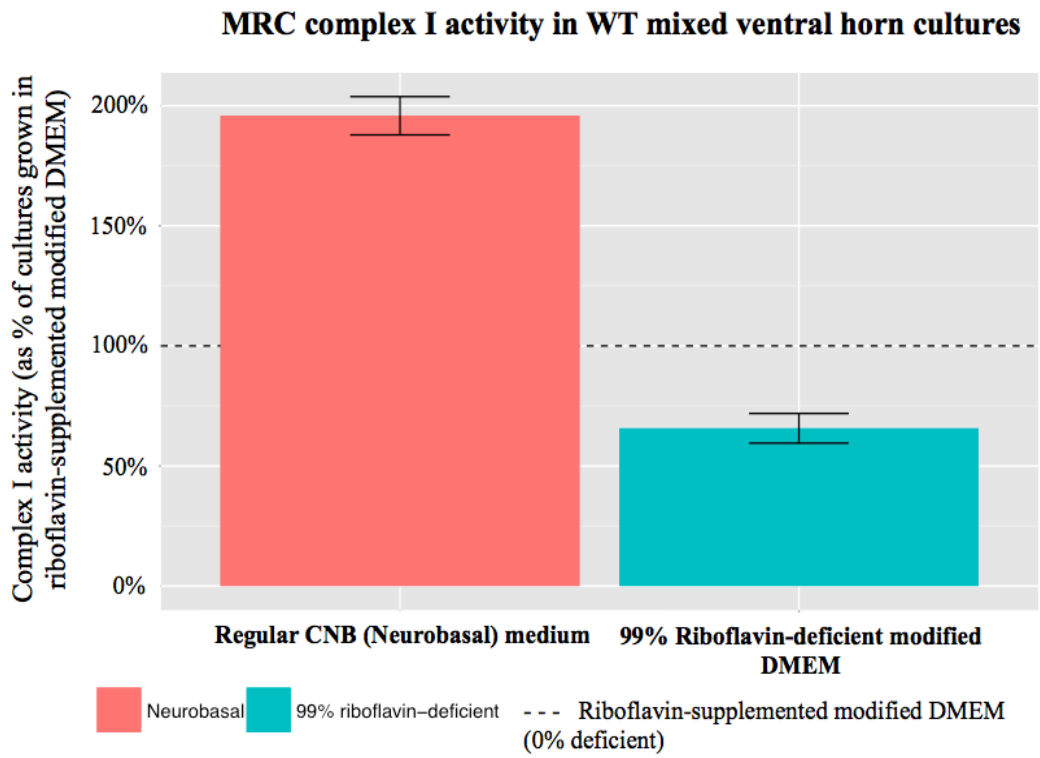

Figure 7-21 MRC complex I activity in WT primary mixed ventral horn cultures grown in regular CNB medium, in riboflavin-supplemented modified DMEM (both 1,005 nM), or in 99% riboflavin-deficient modified DMEM (0.98 nM). All MRC complex activities are expressed as a ratio to CS activity to normalise for mitochondrial enrichment (Hargreaves et al., 1999). Results are expressed as mean ± SEM; data were normalised to WT primary mixed ventral horn cultures grown in riboflavin-supplemented modified DMEM. Data were generated from a minimum of three independent experiments.

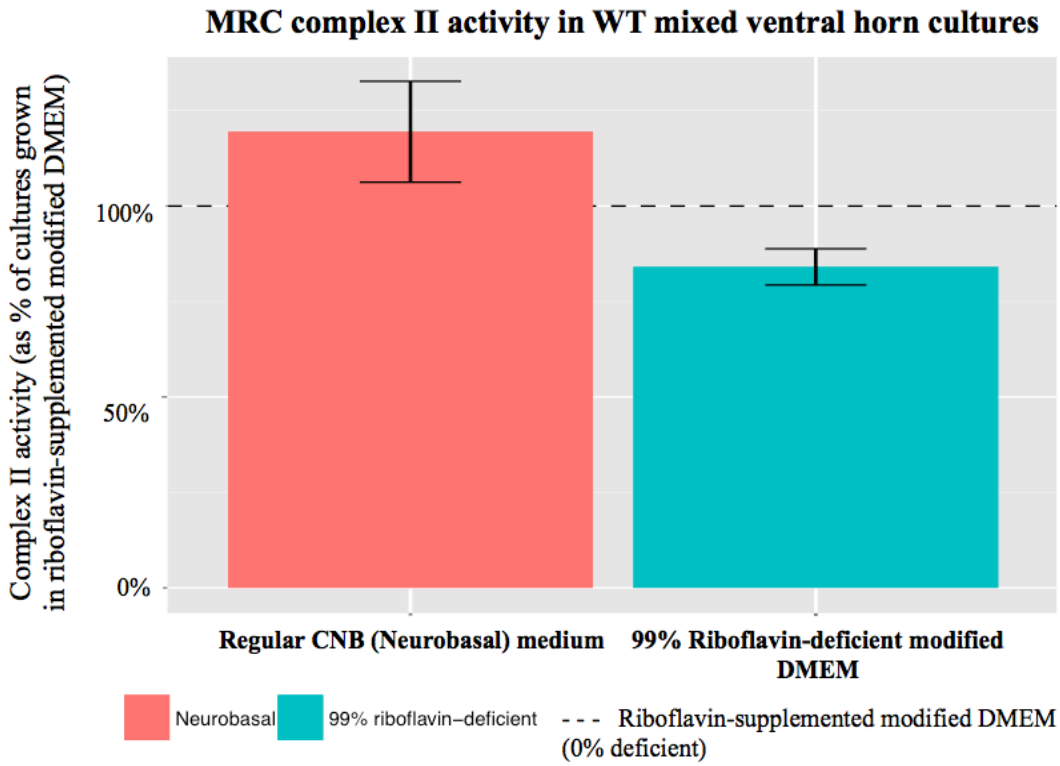

Figure 7-22 MRC complex II activity in WT primary mixed ventral horn cultures grown in regular CNB medium, in riboflavin-supplemented modified DMEM (both 1,005 nM), or in 99% riboflavin-deficient modified DMEM (0.98 nM). All MRC complex activities are expressed as a ratio to CS activity to normalise for mitochondrial enrichment (Hargreaves et al., 1999). Results are expressed as mean ± SEM; data were normalised to WT primary mixed ventral horn cultures grown in riboflavin-supplemented modified DMEM. Data were generated from a minimum of three independent experiments.

7.10.3 Effect of riboflavin deprivation on basal ΔΨm in WT primary motor neurones

To determine whether the reduction in MRC complex I and II activities observed with 99% riboflavin deprivation causes an impairment in the maintenance of the Δψm in WT primary motor neurones, basal TMRM fluorescence was assessed in WT primary motor neurones grown in riboflavin-supplemented modified DMEM (1,005 nM), 99% riboflavin-deficient modified DMEM (0.98 nM), and regular CNB medium (1,005 nM). The TMRM fluorescence signal in WT primary motor neurones grown in 99% riboflavin-deficient medium was 96.9 ± 7.5% of the TMRM

fluorescence signal observed in those grown in riboflavin-supplemented medium. The TMRM fluorescence signal in WT primary motor neurones grown in regular CNB medium was 100.1 ± 5.5% of the TMRM fluorescence signal observed in those grown in riboflavin-supplemented medium (Figure 7-23). Again, it is mathematically incorrect to assess statistical significance in this case as the experiment has a single control sample (riboflavin-supplemented medium) with zero variance (control is set to 100% on all experimental days). However, these data strongly suggest that the basal Δψm is not affected by riboflavin deprivation in WT motor neurones.

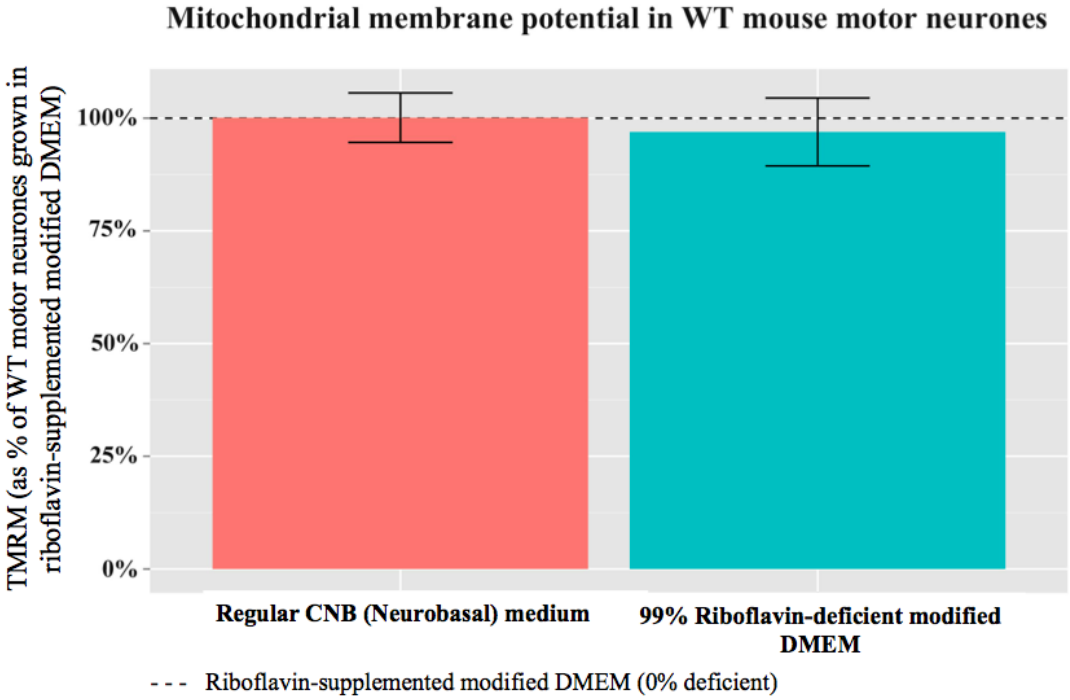

Figure 7-23 Basal ΔΨm in WT primary motor neurones grown in regular CNB medium, in riboflavin-supplemented modified DMEM (both 1,005 nM), or in 99% riboflavin-deficient modified DMEM (0.98 nM), using TMRM in the redistribution mode. Results are expressed as mean ± SEM; data were normalised to WT primary motor neurones grown in riboflavin-supplemented modified DMEM. Data were generated from a minimum of 5-10 motor neurones on 1-2 coverslips in each of a minimum of three independent experiments.

7.11 Results: *Slc52a2* and *Slc52a3*-KD in primary mixed ventral horn cultures

7.11.1 Viral titre in HEK293T cells and primary motor neurones

The viral titres for the empty control, scrambled control, *Slc52a2*-KD (*Slc52a2*-1) and *Slc52a3*-KD (*Slc52a3*-1 and *Slc52a3*-2) shRNAs transduced into HEK293T cells were: 1.27 x 10^5 TU/ml (empty control clone); 2.65 x 10^5 TU/ml (scrambled control clone); 1.35 x 10^5 TU/ml (clone *Slc52a2*-1); 2.58 x 10^5 TU/ml (clone *Slc52a3*-1); 1.15 x 10^5 TU/ml (clone *Slc52a3*-2). Although the viral titre is officially the titre as determined in HEK293T cells, the titre in primary motor neurones was also determined as this cell type is more relevant to this study. The viral titres for the clones transduced into primary motor neurones were: 1.57 x 10^5 TU/ml (empty control clone); 0.70 x 10^5 TU/ml (scrambled control clone); 0.48 x 10^5 TU/ml (clone *Slc52a2*-1); 2.06 x 10^5 TU/ml (clone *Slc52a3*-1); 2.81 x 10^5 TU/ml (clone *Slc52a3*-2). Due to the poor transduction efficiency observed with all clones in the primary motor neurones, experiments were limited to single-cell measurements (single-cell TMRM); the activity of the MRC complexes could not be determined in the shRNA-transduced mixed ventral horn cultures for this reason.

7.11.2 KD efficiency in *Slc52a2* and *Slc52a3*-KD MEFs

With the aim of modelling *SLC52A2* and *SLC52A3*-associated BVVL disease in primary neuronal cells, the mouse *Slc52a2* and *Slc52a3* riboflavin transporters were independently silenced in WT primary mixed ventral horn cultures. MEFs grown in regular CNB medium were used to assess KD efficiency, as this cell type is less susceptible than motor neurones to selection of transduced cells with puromycin antibiotic. The mRNA expression levels of *Slc52a2* and *Slc52a3* in *Slc52a2*-1 shRNA MEFs were 64.7 ± 8.7% and 70.8 ± 8.5% of scrambled control, respectively; although this shRNA is intended to target *Slc52a2*, the mRNA expression of both mouse riboflavin transporters was affected to similar extents. The mRNA expression levels of *Slc52a2* and *Slc52a3* in *Slc52a3*-1 shRNA MEFs were 96.6 ± 32.6% and 33.6 ± 6.4% of scrambled control, respectively, therefore this shRNA appropriately targeted *Slc52a3* without affecting the mRNA levels of *Slc52a2*. Finally, the mRNA expression levels of *Slc52a2* and *Slc52a3* in *Slc52a3*-2 shRNA MEFs were 80.3 ± 7.7% and 50.4 ± 5.3% of scrambled control, respectively. This shRNA targeted *Slc52a3* and decreased its mRNA expression levels; however, the mRNA levels of

Slc52a2 were also marginally decreased with this shRNA. The empty control clone had similar *Slc52a2* and *Slc52a3* mRNA expression levels to the scrambled control clone (88.6 ± 5.9% and 94.5 ± 9% of scrambled control, respectively) (Figures 7-24 and 7-25). The statistical significance cannot be assessed as the experiment has a single control sample (scrambled control shRNA) with zero variance (control is set to 100% on all experimental days).

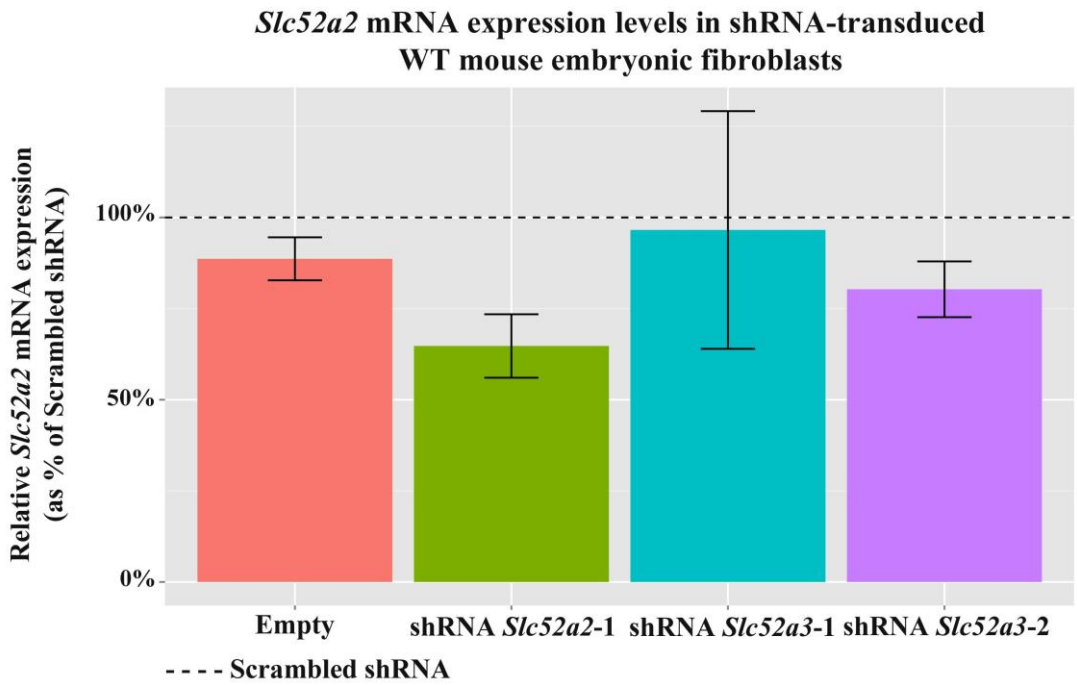

Figure 7-24 *Slc52a2* mRNA expression levels in shRNA-transduced WT MEFs. Results are expressed as mean ± SEM. Data were normalised to the scrambled control shRNA. Data were generated from three independent experiments.

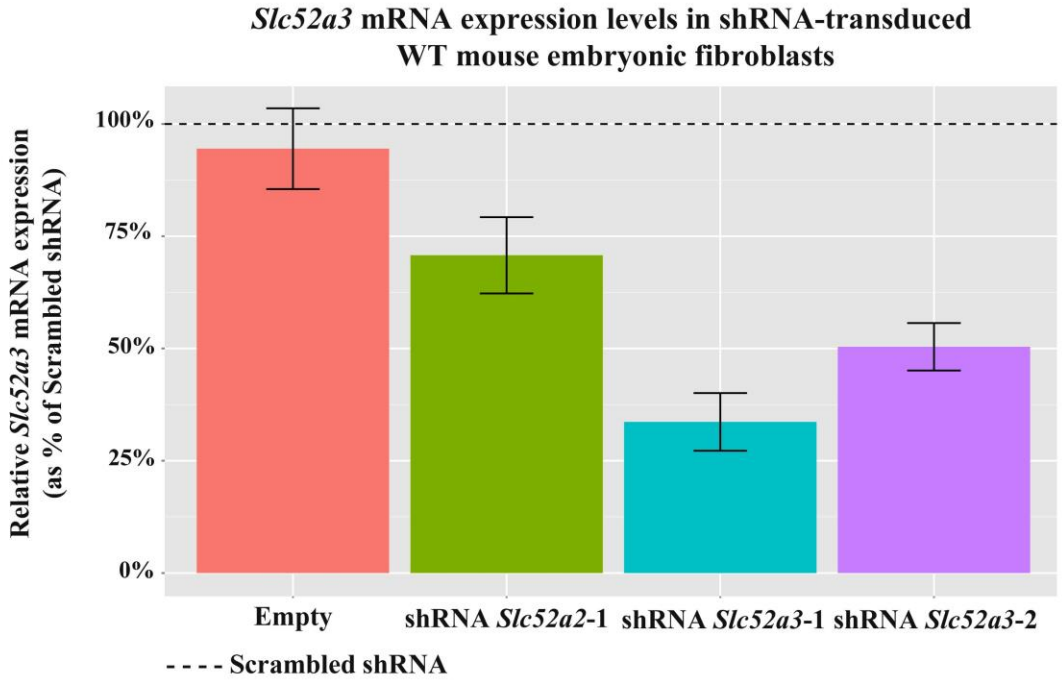

Figure 7-25 *Slc52a3* mRNA expression levels in shRNA-transduced WT MEFs. Results are expressed as mean ± SEM. Data were normalised to the scrambled control shRNA. Data were generated from three independent experiments.

7.11.3 Basal ΔΨm measurement and response to inhibitors in *Slc52a2* and *Slc52a3*-KD primary motor neurones

The Δψm was estimated in empty control, scrambled control, *Slc52a2*-KD and *Slc52a3*-KD primary motor neurones grown in 99% riboflavin-deficient modified DMEM (0.98 nM). Cultures were grown in this medium to avoid the risk of masking any defects with supplementation of riboflavin; furthermore, 99% riboflavin deprivation was not found to affect the Δψm in WT primary motor neurones (Section 7.10.3). The TMRM fluorescence signal was 106.5 ± 15.9% of scrambled control for the *Slc52a2*-1 shRNA motor neurones, 97.1 ± 16.2% of scrambled control for the *Slc52a3*-1 shRNA motor neurones, and 100.6 ± 3.5% of scrambled control for the *Slc52a3*-2 shRNA motor neurones (Figure 7-26). The statistical significance cannot be assessed as the experiment has a single control sample (scrambled control shRNA) with zero variance (control is set to 100% on all experimental days).

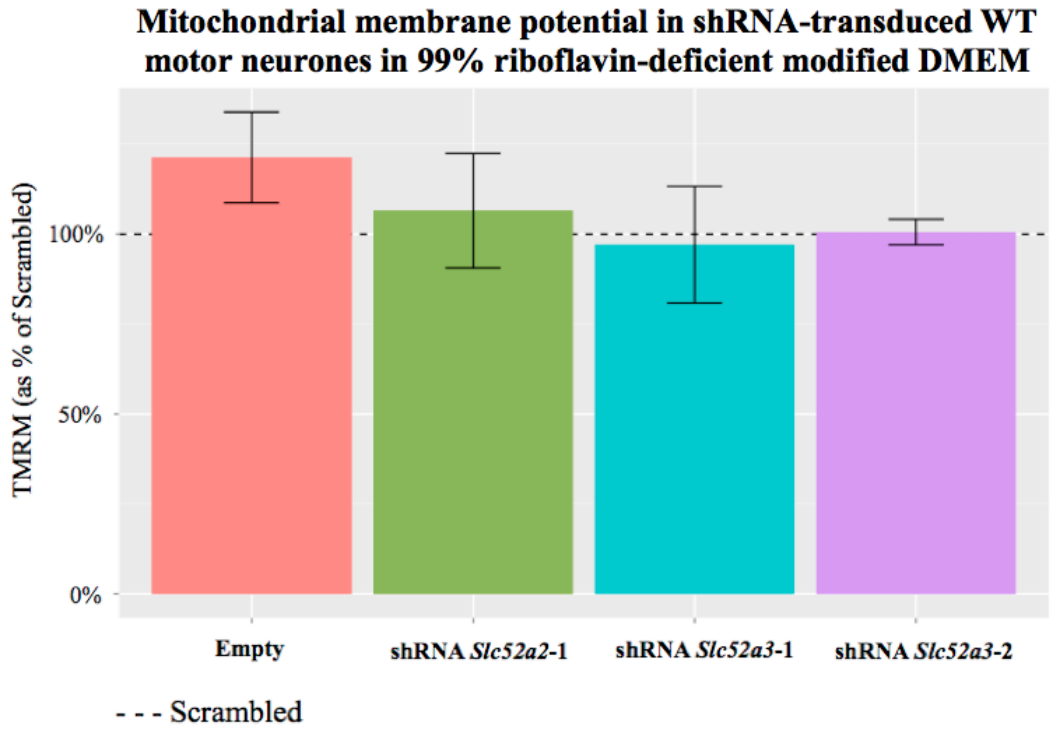

Figure 7-26 Basal ΔΨm in *Slc52a2* and *Slc52a3*-KD primary motor neurones grown in 99% riboflavin-deficient modified DMEM (0.98 nM), using TMRM in the redistribution mode. Results are expressed as mean ± SEM; data were normalised to scrambled control shRNA. Data were generated from a minimum of 3-8 transduced motor neurones on a single coverslip in each of four independent experiments.

The sensitivity of the Δψm was assessed following the addition of oligomycin, rotenone, and FCCP in the empty control, scrambled control, *Slc52a2*-KD and *Slc52a3*-KD primary motor neurones grown in the 99% riboflavin-deficient modified DMEM. Results are expressed as the change in TMRM intensity after addition of each toxin as a percentage of basal (basal=baseline Δψm – Δψm after FCCP). None of the responses to oligomycin, rotenone, and FCCP in the *Slc52a2*-KD and *Slc52a3*-KD mouse motor neurones were significantly different from scrambled control shRNA. Although the primary motor neurones transduced with shRNAs *Slc52a3*-1 and *Slc52a3*-2 showed strong depolarisation after oligomycin compared to the scrambled control, this finding was not observed consistently across experiments and is therefore not statistically significant (Figure 7-27).

Furthermore, due to the very low transduction efficiency, these data represent only a total of three transduced motor neurones (single motor neurone in each of three independent experiments), and results are therefore extremely preliminary. In addition, the depolarisation observed after oligomycin, which is especially strong in cells transduced with shRNAs *Slc52a3*-1 and *Slc52a3*-2, is likely due to leakage of dye from the mitochondria as TMRM intensity was seen to decrease from the beginning of the experiment. Representative TMRM traces from scrambled shRNA and *Slc52a3*-2 shRNA are displayed in Figure 7-28. In conclusion, further experiments are required to be able to confidently draw conclusions regarding the potential reversal of ATP synthase in *Slc52a2* and *Slc52a3*-KD motor neurones.

A.

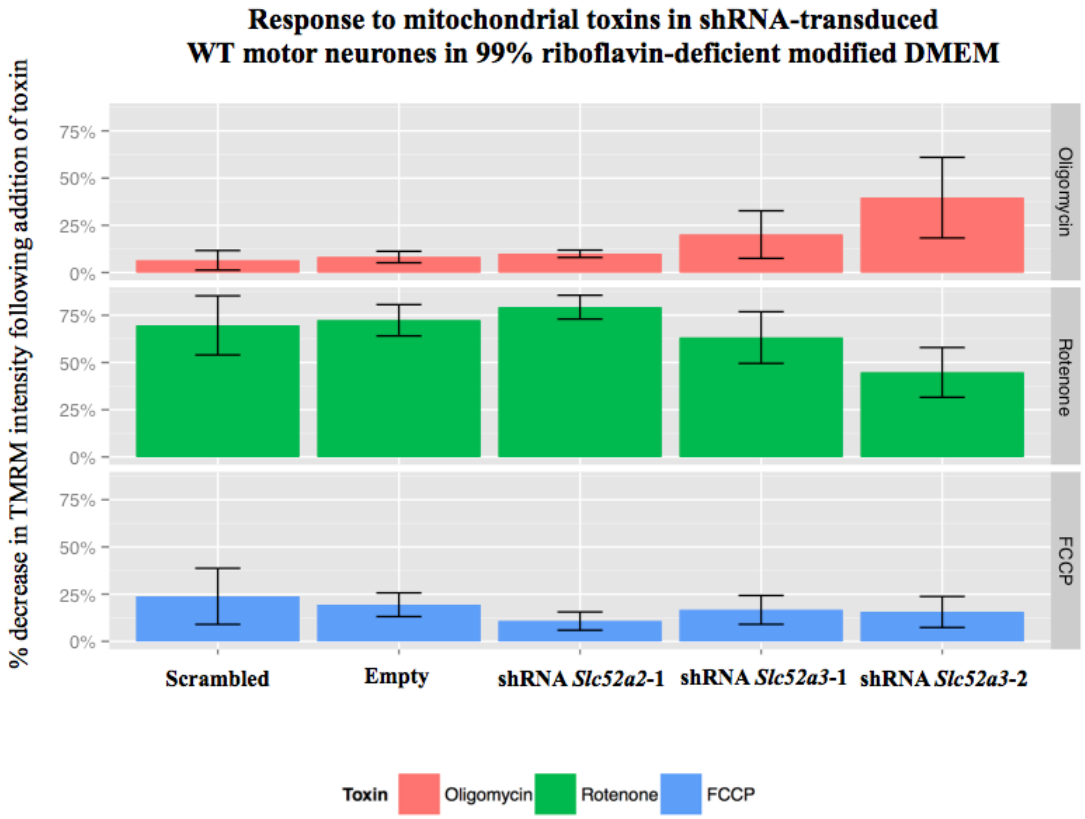

B.

Clone	Oligomycin 99% riboflavin deficient	Rotenone 99% riboflavin deficient	FCCP 99% riboflavin deficient
Scrambled	6.5 ± 5.2 %	69.7 ± 15.6 %	23.9 ± 14.8 %
Empty	8.2 ± 3.1 %	72.4 ± 8.3 %	19.4 ± 6.3 %
shRNA *Slc52a2*-1	9.9 ± 2 %	79.3 ± 6.3 %	10.8 ± 4.8 %
shRNA *Slc52a3*-1	20.1 ± 12.6 %	63.2 ± 13.7 %	16.7 ± 7.6 %
shRNA *Slc52a3*-2	39.6 ± 21.4 %	44.8 ± 13.2 %	15.6 ± 8.2 %

Figure 7-27 Percentage decrease in TMRM intensity after addition of oligomycin (2 μg/ml), rotenone (5 μM) and FCCP (1 μM) in empty control, scrambled control, *Slc52a2*-KD and *Slc52a3*-KD primary motor neurones grown in the 99% riboflavin-deficient modified DMEM using TMRM in the redistribution mode. Results are expressed as mean ± SEM. Data were generated from a single motor neurone in each of three independent experiments (A). Statistical analysis was carried out using one-way ANOVA with Dunnett's post-hoc test. Values of percentage decrease in TMRM intensity are shown in the table (B).

A.

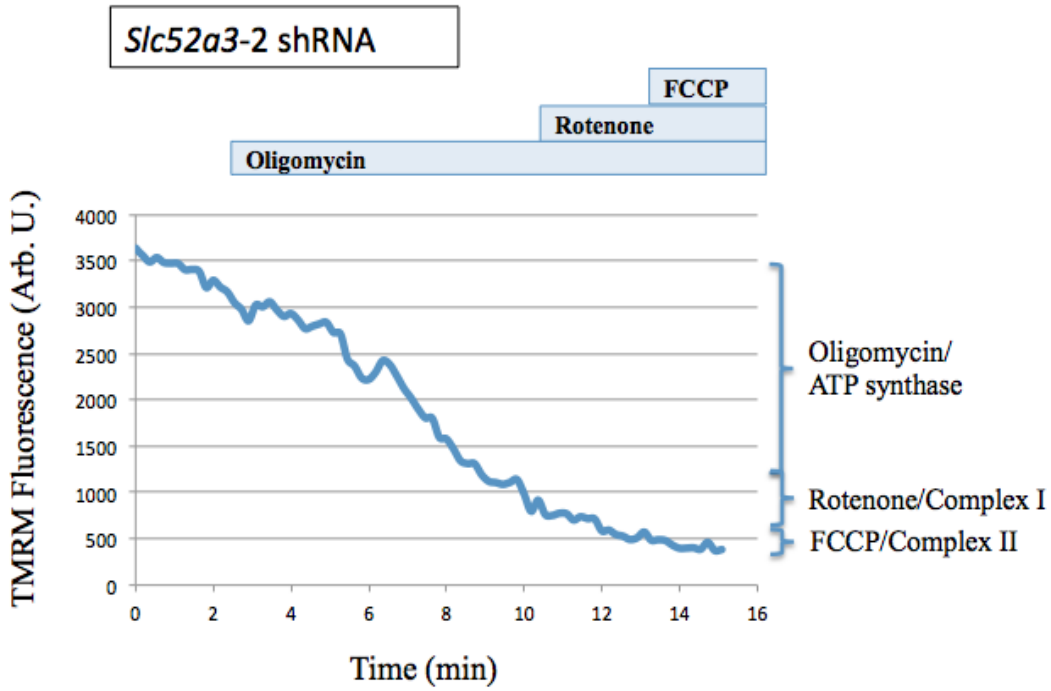

B.

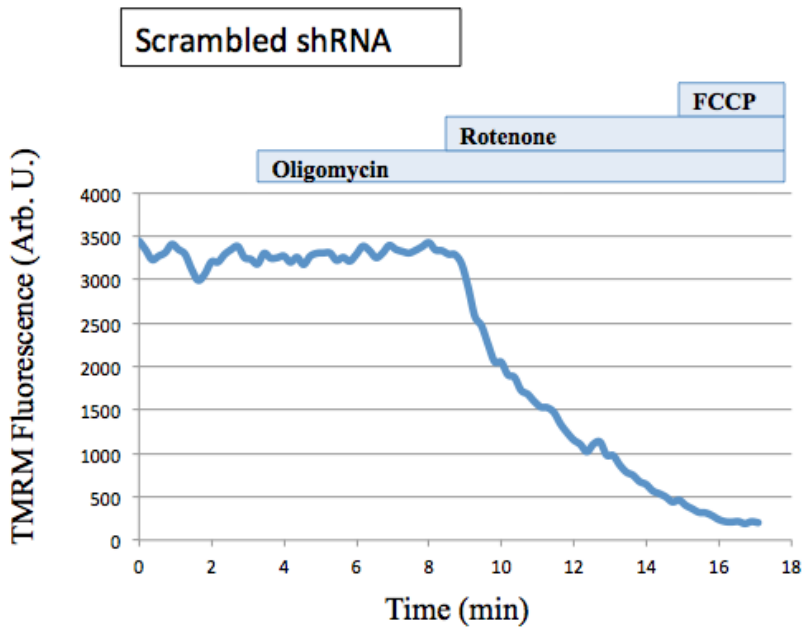

Figure 7-28 Representative TMRM traces from *Slc52a3*-KD (A) and scrambled control (B) primary motor neurones grown in the 99% riboflavin-deficient modified DMEM showing responses to oligomycin (2 μg/ml), rotenone (5 μM) and FCCP (1 μM). Data represent results from a single cell on one coverslip.

7.12 Discussion

In this study, I primarily investigated the in vitro effects of *SLC52A2* mutations on cellular energy metabolism and mitochondrial function using several approaches in fibroblasts of patients with *SLC52A2* mutations. Furthermore, after determining the relative distribution of the two mouse riboflavin transporters in MEFs and primary mixed ventral horn cultures, I have performed preliminary studies to explore the effects on mitochondrial function of riboflavin deprivation in primary mixed ventral horn cultures. Finally, as a stepping ground for future studies, I have silenced the mouse riboflavin transporters *Slc52a2* and *Slc52a3* in mixed ventral horn cultures and have started assessing the impact on basal ΔΨm in these cells.

7.12.1 Studies in *SLC52A2* patient fibroblasts

I have shown that patient E3 has significantly reduced levels of the *SLC52A2* transcript compared to controls. This patient carries the p.Gln234Stop mutation in the compound heterozygous state, which leads to a premature truncation codon and likely destabilizes the mRNA transcript via NMD (as found in Chapter 6), thus leading to decreased abundance of this transcript. All other patients had mildly reduced levels of the *SLC52A2* transcript, especially patients E2, E4 and I1, suggesting that the stability of the *SLC52A2* mRNA transcript may be reduced in some of these patients.

In low riboflavin conditions, FMN levels were most strongly reduced in patients E2 and I1, and moderately reduced in patients E3 and E4. The mild reduction in FMN levels in patient E1 did not reach significance. FAD levels were strongly reduced in patients E2 and I1, and mildly (not significantly) reduced in all other patients. The addition of riboflavin to the cell medium normalised the FMN and FAD levels in all patients, except for patient E2 in whom both FMN and FAD remained lower than controls. It should be noted that FMN and FAD were measured in whole cell lysates rather than isolated mitochondria, and therefore represent the cellular FMN and FAD content rather than the co-enzymes levels found in the mitochondria exclusively.

MRC complex I activity in low riboflavin medium was strongly reduced in all patients except patient E2. However, patient E2 had the most prominent reduction in

MRC complex II activity, followed by patient I1. All other patients had moderately but significantly reduced complex II activities. Riboflavin supplementation caused MRC complex I and II activities to increase to control levels.

Notably, patients E2 and I1 who had the most significant decreases in complex II activities in low riboflavin medium also had the two lowest FAD (as well as FMN) levels in this medium, which is in line with the role of FAD as an electron acceptor in complex II. Although complex I activity was not significantly decreased in patient E2, patient I1 had one of the lowest complex I activities compared to controls. Interestingly, although the riboflavin co-enzyme levels were not restored in patient E2 by addition of riboflavin to the medium, the complex I and II activities were successfully normalised to the control level in this patient. Patient E1 was the only patient for whom both FMN and FAD levels were not significantly decreased; this patient also showed some of the smallest decreases in complex I and II activities, suggesting that the p.Gly306Arg mutation may have a milder phenotype in vitro. Finally, as expected from previous studies discussed in Sections 7.1.4-7.1.5, the intracellular FMN and FAD levels as well as the MRC complex I and II activities were affected by riboflavin deprivation in the control fibroblasts as well, although to a lesser extent than in patient fibroblasts.

As described in Chapter 6, the MRC complex activities (complexes I, II/III and IV) of patients E1, E2 and I1 (as well as patients E5, E6, E8 and A6) had been determined in muscle as part of our genetic investigation. E2 had mildly decreased complex IV activity (not measured in fibroblasts in this study), E6 had moderately decreased complex I activity, and I1 had moderately decreased complex II/III activity (see Chapter 6 for values). MRC complex activities were normal for patients E1, E5, E8 and A6. The reason for the discrepancy between findings in muscle and fibroblasts remains unclear.

These biochemical deficiencies may provide a rationale for FL patients being previously diagnosed with mitochondrial cytopathy due to MRC defects in complexes I and II, and other FL patients showing ragged red fibres on muscle biopsy (Roeleveld-Versteegh et al., 2004; Spagnoli & De Sousa, 2011).

When TMRM was measured in the presence of glucose, the Δψm was significantly decreased only in patient I1 in the low riboflavin medium. Despite the difference in TMRM intensity being relatively small, a small decrease in the Δψm may still appreciably influence the function of the mitochondria and ATP production (Nicholls, 2002). It is worthy of note that this patient was also on the severe end of the spectrum with regards to FMN and FAD levels, as well as complex I and II activities.

In these conditions, with the exception of patient I1, the decrease in activity of respiratory complexes I and II in patient fibroblasts was not sufficiently severe to cause a decrease in basal Δψm in patients when glucose was present. However, the Δψm in patient E2 was significantly decreased upon addition of oligomycin, suggesting that the Δψm may be maintained by ATP hydrolysis by the F_1F_0-ATPase, and that oxidative phosphorylation is impaired when this patient's fibroblasts are grown in low riboflavin conditions. This patient had the most marked decrease in FMN and FAD levels, as well as complex II activities. The fact that a muscle sample from this patient showed reduced activity of the non-flavin dependent complex IV is quite notable; indeed, in *Caenorhabditis elegans* complex I deficiency due to complex I mutations was found to destabilise complex IV via an unknown mechanism, but possibly as a consequence of the effect of complex I deficiency on the Δψm and subsequent damaging effect on complex IV assembly (Grad & Lemire, 2006). Impairment of complex IV has also been noted in RR-MADD patients. Since heme deficiency has been found to affect complex IV assembly and activity, in these patients it was suggested that impaired function of the FAD-dependent protoporphyrinogen oxidase, an enzyme of the heme biosynthetic pathway, may be responsible for the complex IV deficiency (Olsen et al., 2007).

When the fibroblasts of patient E1 when grown in low riboflavin medium and TMRM was performed in the presence of glucose, there is a suggestion that this patient's fibroblasts activated the complex II pathway, and switched from complex I to complex II. Indeed, the response to rotenone, a complex I inhibitor, was significantly smaller than in controls, and the response to FCCP (which represents the remaining contribution to the Δψm by complex II) was larger than in controls,

although the latter was not significant. In line with these findings, patient E1's fibroblasts had a relatively mild decrease in complex II activity compared to controls and other patients.

Upon supplementation of the medium with riboflavin, there was a trend for increased Δψm compared to controls, with normalisation of the Δψm in patient I1, and significantly increased Δψm in patient E2 compared to controls. The fibroblasts of patient E2 no longer operated in reverse mode, as blocking the proton channel of ATP synthase with oligomycin did not result in depolarisation in this case. With supplementation of riboflavin, compensation by complex II was once again apparent in patient E1.

Interestingly, when cells were grown in low riboflavin medium, inhibiting glycolysis revealed a deficiency in maintaining the Δψm in patient E1 and E2, which was not evident when this experiment was carried out in the presence of glucose. Oligomycin caused a significant depolarisation in patient E1's fibroblasts compared to controls; this would suggest that, instead of activating complex II as was seen in the presence of glucose, ATP synthase operates in reverse mode to try to maintain the Δψm in patient E1 when glucose is not available for efficient glycolysis. Patient E2's fibroblasts no longer operated in reverse mode when glucose was absent. Growing these cells in riboflavin-supplemented medium corrected the Δψm in both patients E1 and E2 when measuring the Δψm with inhibition of glycolysis.

The Δψm in the other patient fibroblast lines was not significantly different from controls when grown in low riboflavin medium and with inhibition of glycolysis, possibly due to endogenous glucose remaining. There is nonetheless a clear trend for reduced Δψm in all patient cell lines. It is possible that, when the cells are grown in low riboflavin conditions, glycolysis may help to compensate for a deficiency in MRC activity in most of the patient fibroblast lines. However, except for patient I1, Western blot analysis of ATP5β and GAPDH does not support the hypothesis that *SLC52A2* patient fibroblasts increase their rate of glycolysis to compensate for a potential energy deficit when grown in low riboflavin medium. Although no fatty acids were present in the cell medium for the TMRM experiment, in vivo, increased fatty acid metabolism may also serve as a compensatory mechanism.

It should be noted that, in all conditions, inhibition of complex I by rotenone caused an immediate partial depolarisation in all fibroblast lines including controls, suggesting that complex II was at least still partly functional. The mitochondrial uncoupler FCCP caused complete depolarisation in patient, p.Gly306Arg carrier and control fibroblasts, as expected.

In the fibroblasts of patients E3, E4 and I1, the finding of a normal basal $\Delta\psi m$ and lack of a response or slight hyperpolarisation to oligomycin in all experimental conditions suggest that ATP was not hydrolysed by the F_1F_0-ATPase and the $\Delta\psi m$ was still maintained by the activity of the MRC with contribution from both complexes I and II in these cells (Abramov et al., 2010). As discussed in Section 7.1.2, if the damage in the mitochondria is less severe, it is possible that the reverse mode was prevented from operating by overexpression of the IF1 protein in these cells (Cecchini, 2003; Duchen, 2004). Furthermore, whether the defect in MRC activities is severe enough to affect oxidative phosphorylation is thought to be dependent on the type of mitochondria affected (Pathak & Davey, 2008); it is possible that fibroblasts are relatively resistant to MRC damage.

We observed a significant increase in NADH redox index compared to control cells in patient E2, and a very mild elevation in the NADH redox index in patient E3. The increase in basal levels of NADH in low riboflavin conditions may be due to increased substrate delivery and faster respiration, or to decreased NADH consumption due to slower respiration (Distelmaier et al., 2009; Gandhi et al., 2009). The latter would imply functional inhibition of complex I, which may be secondary to reduced substrate supply or to defective MRC complexes. Given the reduction in intracellular FMN and FAD levels and decreased MRC complex I and II activities, the latter explanation is more likely to account for the increase in NADH redox index in these two patients. In patient E2, this is consistent with the mild decrease in ATP5β protein expression witnessed by Western blot. In both patients E2 and E3, there was no activation of glycolysis relative to oxidative phosphorylation in low riboflavin medium on the Western blot, providing further evidence that increased substrate delivery is unlikely to account for the elevation in the NADH redox index in these cells. Finally, as there was no difference in the NADH pool between patients

and controls in either medium condition, this suggests that there is no deficit in the Krebs cycle in patient fibroblasts compared to controls, and reduced NADH supply is therefore improbable in patients E2 and E3. Therefore, respiration is probably inhibited in the fibroblasts of patients E2 and E3 in low riboflavin conditions.

Riboflavin addition greatly lowered the NADH redox index in patient E2, potentially by activating respiration or by increasing the rate of glycolysis. Given that there is no significant difference in the NADH pool between patient E2 and control fibroblasts in the riboflavin-supplemented condition, substrate supply does not appear to be increased therefore it is perhaps more likely that riboflavin is able to normalise the NADH redox index by increasing the rate of respiration in this case. Inhibition of respiration as seen in fibroblasts of patients E2 and E3 under low riboflavin conditions is consistent with the increased lactate/pyruvate ratio observed in both of these patient cell lines in this medium and suggests that there is severe damage to the MRC in these patients, which is responsive to riboflavin supplementation. Although patient E2 did appear to operate in reverse mode to maintain the $\Delta\Psi m$ in low riboflavin conditions, it is surprising that the $\Delta\Psi m$ was maintained normally in patient E3 in these circumstances.

CoQ_{10} levels were decreased only in patient E2 in low riboflavin medium; this defect was riboflavin-responsive as well. CoQ_{10} deficiency associated with low complex IV activity as seen in patient E2 has been previously observed in some patient biopsies; the reason for this association remains unclear (I. Hargreaves, personal communication). Secondary CoQ_{10} deficiency associated with decreased MRC complex activities and increased lactate levels, all of which were responsive to riboflavin, has been described in some RR-MADD patients with mutations in *ETFDH*. As previously discussed, CoQ_{10} deficiency in these patients has been suggested to result either from feedback inhibition, downregulation of CoQ_{10} synthesis, or increased degradation of CoQ_{10}. In patient E2, a loss of activity in *ETFDH*-encoded ETF:QO resulting from decreased intracellular FAD levels may also cause CoQ_{10} deficiency via one of the above mechanisms; alternatively, oxidative stress due to complex I and II inhibition may affect the CoQ_{10} levels (Cornelius et al., 2013; Gempel et al., 2007; Gregersen et al., 2008; I. Hargreaves,

personal communication). Indeed, as previously mentioned, high basal levels of NADH due to substrate accumulation in complex I are often associated with oxidative stress (Abramov et al., 2010; Murphy, 2009). Finally, CoQ_{10} deficiency may be caused by a defect in the function of the FAD-dependent monooxygenase, which is needed for CoQ_{10} biosynthesis (Baker & Tarnopolsky, 2003; Lienhart et al., 2013).

Oxidative stress may also be a consequence rather than a cause of CoQ_{10} deficiency. CoQ_{10} deficiency in cells of patients with genetic defects of CoQ_{10} biosynthesis has been found to cause increased ROS production and cell death and/or defects of ATP synthesis depending on the magnitude of CoQ_{10} decrease (Quinzii et al., 2010). A decrease in CoQ_{10} may therefore cause oxidative stress in patient E2, further contributing to pathophysiology in this patient, however this remains to be investigated.

It is worth mentioning that, although this was not statistically significant, CoQ_{10} levels were increased in patient E3 compared to controls in the low riboflavin medium. This patient also displayed the greatest decrease in complex I activity. It may be that levels of CoQ_{10}, an antioxidant, are increased in this patient to compensate for ROS production due to complex I inhibition. Again, levels of ROS would need to be assessed to confirm this hypothesis.

In this study, patient fibroblasts carried the following mutations: patient E1- p.[Gly306Arg];[Gly306Arg]; patient E2- p.[Trp31Ser];[Leu312Pro]; patient E3- p.[Gln234Stop]; [Ala420Thr]; patient E4- p.[Gly306Arg]; [Leu339Pro]; patient I1- p.[Tyr305Cys];[Gly306Arg]. As described in Chapter 6, all of the mutations carried by the *SLC52A2* patient fibroblasts studied here-in had been predicted not tolerated by SIFT and probably damaging by Polyphen-2, and all except p.Gln234Stop were located at amino acids highly conserved between species and in the other two riboflavin transporters. The p.Trp31Ser, p.Leu312Pro, p.Leu339Pro, and p.Ala420Thr mutations are located in transmembrane domains, the p.Gln234Stop variant is localised within an intracellular loop, and the p.Tyr305Cys and p.Gly306Arg are located in an extracellular loop (Section 6.4.1).

As discussed in Section 7.1.6, in vitro work by Dr Yonezawa and colleagues performed as part of our publication in Brain had found that HEK293 cells transiently transfected with the p.Trp31Ser, p.Gln234Stop, p.Tyr305Cys, and p.Leu339Pro mutations showed the strongest decrease in riboflavin uptake compared to WT, while the p.Gly306Arg and p.Leu312Pro mutations showed a moderate but significant decrease (p.Ala420Thr was not assessed). Protein expression of all mutants except p.Trp31Ser was decreased in the crude membrane fraction compared to WT, and was most reduced for the p.Gln234Stop and p.Leu339Pro mutants (Foley et al., 2014). In light of these findings, it is plausible that for most mutants besides p.Trp31Ser, the genetic defect causes impaired delivery of RFVT2 to the plasma membrane.

Due to the poor quality and specificity of the commercial RFVT2 endogenous antibodies used for Western blot and immunocytochemistry, whether the *SLC52A2* mutations affected the protein expression and subcellular localisation of the RFVT2 protein could not be assessed in the fibroblasts. Additional details regarding troubleshooting of these experiments are provided in Sections 2.2.13 and 2.2.22. Similarly, despite numerous trials, the uptake assay of [^{3}H]-riboflavin using scintillation counting could not be successfully optimised; details are available in Section 2.2.12.

It remains unknown whether the defects identified in this study in these patients extend to other tissues and whether they parallel the situation in vivo. In addition, as most patients in this study carried compound heterozygous mutations, it is difficult to dissect the effect of individual *SLC52A2* mutations. However, such patient cell lines remain of substantial value because the mutations are in the context of a particular genetic background, which is unique to each patient (Distelmaier et al., 2009). Although fibroblasts are not neuronal cells and are not a particularly vulnerable tissue, metabolic and mitochondrial abnormalities are commonly studied in patient fibroblasts (Distelmaier et al., 2009; Olsen et al., 2007; Rhead et al., 1993).

Given the relatively mild phenotype of the p.Leu312Pro mutation in HEK293 cells, it is somewhat surprising to note that this patient's fibroblasts showed the most impressive defects. Clinically, patient E2 was also particularly severely affected; she

had her first symptom (ataxic gait) at one year of age, and prior to riboflavin therapy, was unable to sit, was ventilator-dependent, and could only be fed by gastrostomy. These observations would suggest that the p.Trp31Ser causes severe dysfunction despite still being expressed in the plasma membrane (Foley et al., 2014). The p.Trp31Ser mutation may cause an impairment in the regulation of riboflavin uptake or may directly inhibit RFVT2 function via an unknown mechanism (Chiong et al., 2007).

The milder phenotype of the p.Gly306Arg mutation in HEK293 cells is consistent with findings in the fibroblasts of patient E1 who carried this mutation in the homozygous state. This patient had the mildest reductions in riboflavin cofactor levels and in MRC complex activities. As evidenced by the TMRM results in the presence of glucose, patient E1's fibroblasts may be able to activate the complex II pathway to maintain MRC function due to its relatively preserved levels of FAD, with this no longer being the case when glycolysis is inhibited. The fact that the p.Gly306Arg mutation causes only partial impairment of RFVT2 function and is found in most patients either in the homozygous or compound heterozygous state may suggest that partial RFVT2 function is necessary for survival. With these considerations in mind, as the fibroblasts of patient E3 had a mild phenotype in vitro, it is probable that the p.Ala420Thr retains at least partial function since the other *SLC52A2* mutation carried by this patient (p.Gln234Stop) causes NMD associated with a severe reduction in riboflavin uptake in HEK293 cells (Foley et al., 2014).

In vivo, in addition to differences arising from the nature of the mutations themselves, phenotypic differences between patients may also arise from variability in intracellular riboflavin homeostasis; indeed, differences in rates of tissue growth, metabolic demand, episodes of fasting, FMN and FAD synthesis, rate of catabolism of FAD and FMN, or differences in metabolism of FMN and FAD in the mitochondria and transport of these coenzymes into the mitochondria could all account for some of the inter-patient heterogeneity (Ross & Hansen, 1992; Vergani et al., 1999).

It is worth remembering that different tissues and cell types may respond differently to MRC defects, and it is usually very difficult to correlate patient phenotypes to results obtained in a cell culture system (Distelmaier et al., 2009). For example, two patients with isolated complex I deficiency and a similar disease course displayed substantially different physiological findings in fibroblasts; however, the authors noted that some exceptions can occur when a patient is very severely affected (Distelmaier et al., 2009), as seen for patient E2 in our study. It could also be argued that the fibroblast studies in this Chapter are not replicating the situation in vivo, as the cells need to be placed in what is considered to be riboflavin-deficient medium to show abnormalities, while patients develop a phenotype with normal dietary intakes of riboflavin.

In addition, growing the fibroblasts in low riboflavin medium and with dialysed FBS (which lacks many other nutrients besides riboflavin) may cause a multitude of other effects not directly related to the riboflavin transporter defect (Lee et al., 2013). As riboflavin uptake is known to be modulated by extracellular levels of riboflavin available (Camporeale & Zempleni, 2003; Fujimura et al., 2010; Said & Ma, 1994; Said & Mohammed, 2006), it is also unclear whether patient and control fibroblasts would initiate similar up and downregulation of riboflavin uptake in low riboflavin and riboflavin-supplemented media, respectively. To circumvent these issues, lumiflavin, a structural analogue of riboflavin which competitively inhibits riboflavin transport but is not expected to affect riboflavin transporter mRNA expression, could have been added to the medium, as has been recently suggested (Lee et al., 2013).

It should also be borne in mind that experiments in which cells derived from different sources (patient-derived and control fibroblasts) are being directly compared are subject to error, as variables unrelated to the disease state may influence the cells' behaviour. In order to control for any such confounding variable, rescue experiments in which the patient fibroblasts are transfected with the WT *SLC52A2* gene should allow us to determine whether the phenotype observed in the patient fibroblasts is actually due to loss of function of the mutated gene-encoded protein. Another possible source of error concerns the quantification of fluorescence by microscopy, specifically the large variability in the raw data values in different

cells and between experiments, reflected by the need to transform the data to percentages. Such data analysis renders it difficult to assess the significance of any observed decrease or increase in fluorescence. An internal control for the fluorescence within each well assessing potential confounds such as mitochondrial mass and mitochondrial localisation (for instance using the Mitotracker dye) would provide reassurance that the wells to be measured are comparable. Finally, as has been discussed previously, obtaining a commercial antibody to probe the function of the endogenous transporters is of utmost importance. The suitability of the available commercial antibody for RFVT2 could have been verified by transiently expressing epitope-tagged proteins in tissue cell lines. As mentioned in Section 7.5, myc-DDK-tagged *SLC52A2* mutant constructs were prepared during this PhD with the aim of transfecting the constructs in SH-SY5Y cells. Although this work was not carried out to prioritise studies in the mouse motor neurones, assessing the intracellular localisation of the RFVT2 riboflavin transporter in cells transfected with the WT and mutant epitope-tagged constructs would have certainly complemented the data on mitochondrial dysfunction in the fibroblasts.

7.12.2 Studies in WT, *Slc52a2* and *Slc52a3*-KD primary mixed ventral horn cultures

Studies in WT, *Slc52a2*-KD and *Slc52a3*-KD mixed ventral horn cultures presented herein aimed only to provide a foundation for forthcoming studies in primary motor neurones. The relative mRNA expression levels of *Slc52a2* and *Slc52a3*, encoding the two mouse riboflavin transporters mRFVT2 and mRFVT3 (orthologues of the human RFVT2/RFVT1 and RFVT3, respectively), were investigated in WT MEFs and WT primary mixed ventral horn cultures. It is interesting to note that both transporters were expressed at similar levels in the MEFs, while *SLC52A3* is not expressed in fibroblasts in humans (Ciccolella et al., 2012). The mouse *Slc52a2* was more highly expressed in WT mixed ventral horn cultures than in WT MEFs, and was expressed at higher levels than *Slc52a3* in the mixed ventral horn cultures, which perhaps parallels the high expression of the human RFVT2 in the brain and spinal cord (Yao et al., 2010).

The susceptibility of WT primary mixed ventral horn cultures to riboflavin deprivation in the medium was then assessed. Although mixed ventral horn cultures were not affected by a decrease from 1,005 nM to 502.5 nM riboflavin (50% deprivation) after nine DIV, activities of complexes I and II for mixed ventral horn cultures grown in 0.98 nM riboflavin (99% deprivation) were approximately 66% and 84% of those grown in 1,005 nM riboflavin for nine DIV. In comparison, results of the medium optimisation in control human fibroblasts had shown that the threshold for maintaining the metabolism in control human fibroblasts lies between 0.85 nM and 3.1 nM riboflavin in the medium (Section 2.2.8).

Given the high energy demands, low levels of glycolysis, and reliance on oxidative phosphorylation in neurones (Burchell et al., 2010; Davey, 1998; Federico et al., 2012; McInnes, 2013), one would expect motor neurones to be relatively sensitive to nutritional riboflavin deficiency. However it would seem that motor neurones are relatively resistant to riboflavin deprivation in the medium compared to fibroblasts, although a titration of riboflavin concentration should be performed in these cells to assess the exact threshold at which the MRC is impaired. Furthermore, after nine DIV motor neurones only represent approximately 40% of the mixed ventral horn culture, therefore it may be that other cells present in the lysate (interneurons, astrocytes, fibroblasts, etc.) may be more resistant to deficiency and mask a more substantial defect in the motor neurones. Alternatively, the reduction in complex activities may not be specific to motor neurones in this experiment. Finally, as complex activities were strongly affected by the switch from CNB to modified DMEM medium (both 1,005 nM riboflavin), it is possible that the lack of certain nutrients damaged the MRC to such an extent that the effect of riboflavin deficiency was rendered negligible and was underestimated.

The decrease in complex I and II activities observed in mixed ventral horn cultures grown in 99% riboflavin-deficient medium as well as those grown in riboflavin-replete modified DMEM did not translate to a reduction in basal $\Delta\psi m$ compared to motor neurones grown in the CNB medium. As the TMRM experiments were performed by exclusively imaging motor neurones, other cells within the culture could not have masked a defect in maintaining the $\Delta\psi m$ in motor neurones. Hence it

could be that the motor neurones are indeed resistant to riboflavin deficiency and that the decrease in complex activities was in fact not specific to motor neurones. Although an issue with the experimental procedure itself cannot be ruled out, another possibility is that complex I and II activities were actually affected by riboflavin deficiency, but that inhibition of complex activity was not sufficient to cause an impairment of Δψm and respiration; such thresholds have been previously described in brain mitochondria (Davey, 1998; Pathak & Davey, 2008) (Section 7.1.2).

Similarly, *Slc52a2*-KD and *Slc52a3*-KD in primary motor neurones did not cause a reduction in the Δψm compared to scrambled control when cells were grown in 99% riboflavin-deficient medium, and the ATP synthase was not found to operate in reverse mode in these cells. However, this study was performed on very few motor neurones due to the poor transduction efficiency, therefore these results should be interpreted with caution. As the Δψm was not affected in WT motor neurones grown in 99% riboflavin-deficient medium, it is unlikely that the Δψm was already too greatly reduced by the nutritional riboflavin deficiency in scrambled control to uncover a difference with the *Slc52a2*-KD and *Slc52a3*-KD motor neurones. Some more likely explanations include that KD of the riboflavin transporters was not efficient in motor neurones since KD efficiency was only assayed in MEFs, that KD was insufficient to cause damage, or that it was not efficient at protein level. Another possibility is that the findings observed in fibroblasts do not recapitulate what is happening in motor neurones with deficiencies of riboflavin transport.

7.12.3 Mitochondrial dysfunction in other neurodegenerative diseases

Although defects in mitochondria were once thought to occur secondary to the primary disease mechanism, it is now thought that mitochondrial dysfunction may perhaps play a role in disease onset and evolution in certain neurodegenerative diseases (McInnes, 2013). Decreased activity of one or more MRC complexes and oxidative stress have been reported in tissues, cell models and/or animals models of Alzheimer's disease, Parkinson's disease and Huntington's disease patients (Burchell et al., 2010; McInnes, 2013). Overall, it is still unclear whether mitochondrial dysfunction is a cause or consequence of the neurodegenerative process in these diseases (Federico et al., 2012).

Due to their high metabolic rate and role in neuromuscular activity, motor neurones are particularly susceptible to impaired energy metabolism (Cozzolino & Carrì, 2012; Martin, 2011; Shaw, 2005). Deficiencies of cellular energy metabolism are thought to underlay neuronal damage in several MNDs such as SMA and ALS (Acsadi et al., 2009; Ciccolella et al., 2013; Martin, 2011). In a cell culture model of SMA, there was evidence of decreased ATP production and increased generation of ROS (Acsadi et al., 2009). Along with other mechanisms including impaired axonal transport and protein aggregation (Shaw, 2005), mitochondrial dysfunction with alteration of the MRC and increased oxidative stress are known to be involved in the pathomechanism of neurodegeneration in ALS patients (Cozzolino & Carrì, 2012; Federico et al., 2012; Martin, 2011). In the spinal cord of superoxide dismutase 1 (SOD1) mutant mouse, before disease onset and during disease progression, there was evidence of decreased MRC complex activities, particularly in complex I in the ventral horn (Jung et al., 2002). Electron microscopy studies have revealed structural abnormalities in mitochondria in several tissues of ALS patients including spinal motor neurones (Martin, 2011). The findings that mutations in cytochrome *c* oxidase subunit 1 and in a mitochondrial tRNA gene were associated with an MND phenotype provide further evidence for the involvement of defective oxidative metabolism in ALS (Martin, 2011). Recently, mutations in *valosin-containing protein* (*VCP*), which plays a role in the ubiquitin-proteasome system and may be important for regulating cellular ATP levels, were found to cause AD ALS (Johnson, Mandrioli, et al., 2010). In vitro studies revealed that VCP deficiency causes mitochondrial depolarisation, mitochondrial uncoupling, decreased ATP production and increased mitochondrial respiration as evidenced by decreased basal levels of NADH (Bartolome et al., 2013).

Interestingly, RT-qPCR in blood samples of ALS patients revealed decreased mRNA levels of FAD synthetase and other electron transport proteins including riboflavin kinase, cytochrome C1 (a subunit of complex III) and the complex II subunit SDHB. Of course, it remains possible that these changes occurred as a result of inactivity and downregulation of energy metabolism (Lin et al., 2009). On the basis that riboflavin is thought to improve energy efficiency in mitochondria and to bear antioxidant properties, SOD1 mutant ALS mice were treated with riboflavin;

riboflavin supplementation was not found to alter disease onset and progression in this study (Moges et al., 2009).

As discussed in Section 1.6.1, the phenotypes of SMA and ALS may overlap with the BVVL phenotype (Horvath, 2012; Sathasivam, 2008). Furthermore, although motor neurones are affected the earliest and the most severely in ALS, ALS pathology is not exclusive to the motor system and may involve the sensory and spinocerebellar tracts as well (Shaw, 2005). It may be that there is an overlap in the pathways leading to neuronal vulnerability in BVVL and other MNDs and neuropathies.

7.12.4 Disease mechanisms in BVVL versus nutritional riboflavin deficiency

In vitro studies of riboflavin deprivation discussed in Section 7.1.5 as well as results from this study confirm that sufficient uptake of riboflavin is crucial for cellular energy metabolism in most cell types, and that fibroblasts of patients with *SLC52A2* mutations are even more susceptible than control fibroblasts to such a deficiency. A crucial question that has arisen from the discovery of riboflavin transporter mutations in BVVL patients is to explain why nutritional riboflavin deficiency and BVVL cause such disparate phenotypes despite both being associated with reduced levels of riboflavin in the body and deficient energy metabolism in vitro.

As discussed in Section 1.6.4, nutritional riboflavin deficiency is usually only observed at the biochemical level. When the deficiency does manifest clinically, symptoms are usually mainly dermatological, although neuropathy has been observed in some cases (Depeint et al., 2006; Foraker et al., 2003; Powers, 2003; Spagnoli & De Sousa, 2011). It must be that unique disease pathways are likely to be operating in BVVL and nutritional riboflavin deficiency. Due to the involvement of the riboflavin cofactors in a wide array of biochemical reactions (detailed in Section 1.6.6), it is probable that cellular systems and pathways are selectively or differentially affected by nutritional riboflavin deficiency or by a problem with transport of riboflavin (Henriques et al., 2010; Lienhart et al., 2013). An understanding of how the mechanism of disease in BVVL may differ from that of

nutritional riboflavin deficiency is crucial in providing additional therapy options for BVVL patients.

Why is it, then, that BVVL patients present with a severe and complex phenotype of progressive pontobulbar palsy with bilateral sensorineural hearing loss, sensory-motor neuropathy and respiratory insufficiency (Brown, 1894; Van Laere, 1966; Vialetto, 1936)? Since carrier fibroblasts in vitro as well as humans who are heterozygous carriers of an *SLC52A2* mutation do not develop a phenotype, it must be that a certain bottom threshold of riboflavin uptake must be attained to cause disease. It is possible that RFVT2 has an additional, as-yet-unknown function in the nervous system which may account for the discrepancy with the phenotype of nutritional riboflavin deficiency. As described in Section 7.1.6, levels of FMN and FAD are selectively preserved in rat brain during severe riboflavin deficiency due to a compensatory increase in riboflavin uptake. Although upregulation of riboflavin transport following riboflavin deficiency has been observed in several cell types in vitro, preservation of the levels of riboflavin and its cofactors was the most striking in the brain (Burch et al., 1956; Camporeale & Zempleni, 2003; Fujimura et al., 2010; Said & Ma, 1994; Said & Mohammed, 2006; Spector, 1980b; Spector & Johanson, 2006). As *SLC52A2* is highly expressed in the brain, mutations in this transporter may compromise this compensatory mechanism in the brain of *SLC52A2*-mutated BVVL patients. However, the extent to which *SLC52A3* mutations could also affect regulation of riboflavin levels in the brain is unknown, as this transporter is only moderately expressed in the CNS (Yamamoto et al., 2009; Yao et al., 2010).

In contrast, the FMN and FAD levels in the brains of patients with low dietary intakes of riboflavin might remain stable, thereby protecting the brain from nutritional riboflavin deficiency. Although depriving WT primary mixed ventral horn cultures of riboflavin led to a decrease in complex I and II activities, it was not associated with defects of $\Delta\psi m$ maintenance in primary motor neurones. One of the key questions to answer is whether the MRC is damaged in neurones in vivo during nutritional riboflavin deficiency states. Although in vitro studies of riboflavin deprivation in animals had shown that the MRC was impaired (albeit this varied between tissues), the most dramatic effects were seen at the level of the less critical

FAD and FMN-dependent pathways, such as iron metabolism and fatty acid β-oxidation (Depeint et al., 2006; Hoppel et al., 1979; Ross & Hansen, 1992).

As previously mentioned, the highest levels of riboflavin cofactors are found in the kidney and liver (Burch et al., 1956; McCormick, 1989). *SLC52A2* as well as *SLC52A3* are not particularly highly expressed in these tissues (Yao et al., 2010). It is possible that kidney and liver are preferentially affected in nutritional riboflavin deficiency. Indeed, fatty degeneration of the kidney and liver has been observed in riboflavin deficiency states in animals (Foraker et al., 2003). Riboflavin deficiency in weanling rats caused increased gastrointestinal iron loss and altered gastrointestinal development; the latter was also seen in riboflavin-deficient humans and may in turn affect the absorption of a variety of other nutrients besides riboflavin (Nakano et al., 2011; Powers, 2003). Deficiencies of iron handling are known be involved in the development of anaemia in riboflavin-deficient individuals, a symptom which is not seen in BVVL. As the levels of riboflavin in the intestinal lumen of BVVL patients are not expected to be altered with normal dietary intakes of riboflavin, this may explain why BVVL patients do not display symptoms of iron deficiency (Powers, 2003).

7.12.5 Riboflavin supplementation in vitro and in BVVL patients, and other potential therapies for BVVL

How might riboflavin supplementation ameliorate the phenotype in *SLC52A2*-mutant fibroblasts and in BVVL patients despite the defect in riboflavin transport via RFVT2? Over-supplementation with riboflavin is thought to be associated with a downregulation of riboflavin transporters. This may explain why previous studies had noted that at higher intakes of riboflavin or when plasma concentrations were high (above 12 nM), transport mainly occurred by a passive diffusion mechanism (Feder et al., 1991; Foraker et al., 2003; McCormick, 1989). It is possible that in BVVL patients and in BVVL fibroblasts supplemented with high doses of the vitamin, riboflavin is transported across the cell membrane primarily via passive diffusion, thus circumventing the riboflavin transporter defect. However, several systems in the brain are thought to prevent excessive amounts of riboflavin from reaching the brain (Spector & Johanson, 2006); therefore, if riboflavin treatment

does manage to reach the brain in BVVL patients, this mechanism must somehow be bypassed if the therapy is to be effective.

Another question which remains to be answered is whether or not expression of the other two riboflavin transporters is upregulated in patients with BVVL, and if so, why this does not compensate for defective riboflavin uptake via RFVT2. As discussed in Section 7.1.6, Ciccolella and colleagues (2013) had found that the *SLC52A1*-encoded RFVT1 transporter expression was decreased in the fibroblasts of a patient with *SLC52A2* mutations, therefore in this case RFVT1 could perhaps not have compensated for deficient riboflavin uptake. However, other studies have not yet confirmed that RFVT1 and/or RFVT3 expression is decreased in patients with *SLC52A2* mutations; this would warrant further investigation. It may be that RFVT1 and RFVT3 expression is normal but that the uptake via these transporters is simply not optimised prior to riboflavin therapy in *SLC52A2*-mutated patients; this may be due to the relatively low expression of both these transporters in the CNS (Yao et al., 2010).

As discussed in Section 7.1.4, riboflavin therapy is effective in a wide range of metabolic and mitochondrial disorders. The mechanisms underlying this beneficial effect of riboflavin remain unknown, although various hypotheses have been put forward, as highlighted previously. Riboflavin supplementation may feed FMN and FAD molecules to complex I, complex II and/or to ETF:QO in the MRC, thus improving energy metabolism by providing electrons to CoQ. In addition to activating the MRC enzymes, riboflavin may also promote the synthesis or prevent the breakdown of the complexes (Bernsen et al., 1993).

Although high-dose riboflavin therapy has only been trialled for extended periods and/or was started soon following symptom-onset in a relatively small number of BVVL patients (Anand et al., 2012; Bosch et al., 2011; Bosch et al., 2012; Ciccolella et al., 2012; Foley et al., 2014; Haack et al., 2012), it is unlikely that this therapy will be able to reverse damage which has already occurred and restore normal function in patients following motor neurone degeneration. Therefore, high-dose riboflavin should be administered as soon as possible following, or ideally prior to disease-onset, to prevent further axonal damage (Foley et al., 2014).

Therapies that have been trialled in patients with mitochondrial disorders could possibly benefit BVVL patients. Indeed, due to the mitochondrial abnormalities observed in BVVL patient fibroblasts, CoQ_{10} or idebenone, an analogue of CoQ_{10} (Kerr, 2013), could be trialled in BVVL. This therapy would be especially relevant in patient E2 who has decreased levels of CoQ_{10}. CoQ_{10} treatment may increase the level of antioxidants and/or may foster the transfer of electrons from complexes I and II to complex III and thereby potentially bypass deficiencies in complex I and/or II (Baker & Tarnopolsky, 2003; Burchell et al., 2010; Mancuso et al., 2010; Spindler et al., 2009). In addition to those described in Section 7.1.4, CoQ_{10} deficiency has been reported in many neuromuscular and neurodegenerative disorders such as ALS, Alzheimer's disease, Parkinson's disease and Huntington's disease, in which mitochondrial dysfunction and oxidative stress are thought to be involved. In patient fibroblasts, in in vitro models of oxidative stress, as well as in animal models of neurodegenerative diseases, there is limited evidence for neuroprotective effects of CoQ_{10}. Small patient clinical trials have shown variable efficacy (Burchell et al., 2010; Mancuso et al., 2010; Spindler et al., 2009).

Additional potential therapies for BVVL may include other antioxidants besides CoQ_{10} such as vitamin C and E to target potential oxidative stress (Burchell et al., 2010). In addition to administering antioxidants, oxidative stress could also be mediated by increasing the expression of endogenous antioxidants. Upregulation of nuclear respiratory factor 2 (Nrf2), which is part of the antioxidant response element /Nrf2/kelch-like ECH-associated protein 1 signalling pathway involved in regulation of expression of antioxidant enzymes, has been suggested as a potential treatment for Parkinson's disease and other neurodegenerative diseases (Burchell et al., 2010). Finally, therapies for BVVL could also be directed at the bioenergetics dysfunction. One such example is dichloroacetate, a structural analogue of pyruvate which activates the pyruvate dehydrogenase complex and decreases lactate production arising from defective oxidative phosphorylation. Dichloroacetate was somewhat beneficial to some patients with congenital lactic acidosis in several clinical trials, although side effects were not negligible (Kerr, 2013). This therapy may be especially applicable to BVVL patients displaying an elevated lactate/pyruvate ratio as seen in this Thesis. Administration of creatine, which promotes ATP production

and may help compensate for energy deficiency, has shown some evidence of neuroprotection in studies of Parkinson's disease and Huntington's disease (Burchell et al., 2010).

7.12.6 Future studies

The work presented in this Chapter merely provides a basis for future studies that could be performed in vitro, some of which have already been mentioned. It would be interesting to determine whether the expression of the other riboflavin transporters is upregulated in BVVL patient fibroblasts. As mentioned previously, oxidative stress which may result from MRC complex inhibition, decreased CoQ_{10} levels, and/or decreased levels of the antioxidant glutathione (the recycling of which is FAD-dependent) should also be investigated in *SLC52A2* patient fibroblasts by measuring ROS production both in the cytosol and mitochondrial matrix (Gandhi et al., 2009). Perhaps the most important studies to be performed next would involve measuring oxygen consumption and ATP levels to determine whether the MRC dysfunction is impairing oxidative phosphorylation. Examining the morphology of the mitochondria in vitro would also provide valuable information regarding the health of the mitochondria. It would also be valuable to determine whether concomitant addition of riboflavin with CoQ_{10} or other agents mentioned in Section 7.12.5 to the fibroblast cell medium further improves the phenotype in vitro. Again, much work remains to be done in the primary mixed ventral horn cultures, and perhaps in dorsal root ganglion cultures given the sensory component of BVVL.

High-dose riboflavin treatment in BVVL is still in its early days, and very little is known about the mechanism of riboflavin transport via RFVT2 in the brain (Moriyama, 2011; Yao et al., 2010). It is clear that the uptake mechanism in the CNS, the optimal riboflavin dose to be administered, and potential uptake enhancers should be investigated in models such as in primary motor neurones and in riboflavin transporter-knockout animal models. Uptake enhancers may include H-89, an inhibitor of the PKA pathway which was found to potentiate riboflavin uptake in a human-derived retinoblastoma cell line (Kansara et al., 2005). Studies should also be carried out to determine how to best optimise riboflavin uptake via the other two transporters and via passive diffusion (Foley et al., 2014).

7.13 Conclusion

The recent identification of riboflavin transporter mutations has provided clues for a novel mechanism leading to neurodegeneration. The principal aim of this study was to begin to investigate the disease pathway in BVVL patients with *SLC52A2* mutations, with a particular focus on the effect of riboflavin transporter mutations on mitochondrial function. Compared to age-matched control fibroblasts, patient fibroblasts had decreased MRC complexes I and II activities as a possible consequence of a deficit in FMN and FAD status. One patient was found to have decreased CoQ_{10} along with an increased lactate/pyruvate ratio compared to controls. The $\Delta\psi m$ was decreased in some patient fibroblasts, and was maintained by ATP hydrolysis by the F_1F_0-ATPase in certain cases. Inhibition of complex I as evidenced by an increased NADH redox index was most obvious in one patient. These deficits were rescued to varying extents upon treatment of the cells with riboflavin.

Given the role of riboflavin, FMN, and FAD in maintenance of energy metabolism and antioxidant status, it is possible that this relatively novel genetic defect may have overlapping disease mechanisms with other MNDs with known involvement of mitochondrial dysfunction and oxidative stress. A more profound understanding of BVVL pathogenesis may also shed light on disease pathways in other neurodegenerative diseases and especially in MNDs, in which riboflavin therapy could potentially provide some benefit.

Chapter 8 General conclusions

This Thesis has utilised a variety of genetics and molecular biology-based techniques to investigate two inherited peripheral neuropathies, CMT and BVVL.

CMT is characterised by high phenotypic and genotypic heterogeneity; with the advent of novel sequencing technologies, the number of genes and loci associated with CMT has increased significantly in the past decade, thus complicating genetic diagnosis (Pandraud et al., 2012; Patzkó & Shy, 2011; Reilly et al., 2011; Rossor et al., 2013). Targeting genetic tests according to inheritance pattern, neurophysiology, outstanding phenotypic features, as well as frequency of CMT subtypes in particular ethnic backgrounds is therefore essential. Following diagnostic algorithms prevents the use of costly and unneeded genetic tests; these algorithms have proven extremely useful, whereby 70% of CMT patients have received a genetic diagnosis (Pareyson & Marchesi, 2009; Reilly et al., 2011; Rossor et al., 2013; Saporta et al., 2011). Nevertheless, the frequency of CMT subtypes has not been well established in many populations, especially that of the rare genes which are not routinely tested.

To provide additional frequency data and expand phenotype-genotype correlations in CMT1, in Chapter 3, I have screened known CMT1-associated genes in CMT1 patients from three populations: the UK, Greece, and the Yakutsk province in Russia. Mutation frequencies in the studied genes were generally in agreement with those previously reported in the literature. The genetic cause of disease remained unknown in many Greek CMT1 patients. Performing exome sequencing in these patients should uncover novel CMT-associated genes (Koutsis et al., 2013), though it remains possible that variants in non-coding regions of the genes or synonymous variants may have been disease-causing in these patients (Parmley & Hurst, 2007; Taioli, Cabrini, Cavallaro, Simonati, et al., 2011). Although future studies of this nature would likely benefit from using NGS instead of Sanger sequencing of single genes to enable more patients to be diagnosed, the cost of these technologies remains too prohibitive to use in large cohorts of patients at this time. Nonetheless, this study has widened the phenotypes associated with particular CMT genes/mutations, thus contributing to our understanding of the disease. This study also provided further evidence that, while in-frame deletions and duplications in *PMP22* lead to CMT1,

nonsense mutations are generally associated with HNPP. In addition, although this study generated frequency data for only a few selected populations and CMT genes, it has enabled an important number of patients to receive a genetic diagnosis, and represents one of the few (Greek cohort) or only (Yakutsk cohort) studies on CMT subtype frequencies in these populations. Finally, this Chapter has gathered important natural history data for CMT. While identifying the genetic cause of disease is important for patient counselling and family planning, diagnosis will become imperative following the development of treatments specific to particular CMT subtypes and/or to shared mechanisms of peripheral nerve degeneration (Amato & Reilly, 2011; Bouhy & Timmerman, 2013; Pandraud et al., 2012; Reilly et al., 2011; Reilly & Shy, 2009).

Another aim of Chapter 3 was to screen selected CMT genes in canines with naturally occurring peripheral neuropathy or NAD-CA. CMT-like neuropathies have been reported in many dog breeds (Granger, 2011). Canines with mutations in CMT genes would provide an animal model of peripheral neuropathy which may more closely parallel the human disease than models in other, more distant species (Karlsson et al., 2007). While no mutations were found, this study has provided a basis for future investigations, specifically in the Schnauzer and Papillon dogs for which a reasonable number of DNA samples are available for homozygosity mapping and/or whole genome sequencing. Recently, whole genome sequencing was used to identify the disease-causing gene in a single affected dog with AR spinocerebellar ataxia and unaffected controls (Gilliam et al., 2013). In the future, a similar study in our cohort of canines with peripheral neuropathies may give clues for novel human CMT genes.

Chapter 4 focused on the most common subtype of CMT, CMT1A. While most CMT1A patients carry Chr17p11.2 duplications of the same size, it remains unknown why patients exhibit such marked intra- and interfamilial heterogeneity in disease severity, thus making patient counselling challenging in these families. Interfamilial variability was determined to be greater than intrafamilial variability in my CMT1A cohort, providing further evidence that genetic factors may be involved in modifying disease severity. In addition to providing more accurate counselling,

genetic modifying factors of the CMT1A phenotype could serve as drug targets (Reilly et al., 2011).

Given the coexistent CIDP-like inflammatory features reported in several CMT1A cases, as well as evidence for the involvement of the immune system in several animal models of CMT, in this Chapter I performed an association study using an Immunochip to determine whether SNPs associated with immune-related mechanisms and diseases could influence disease severity in CMT1A. Overall, results of this study suggest that alleles associated with CIDP and with autoimmune and inflammatory diseases are unlikely to modify the CMT1A phenotype or to be involved more generally in CMT1A pathogenesis. Given these preliminary results and the fact that most CMT1A patients do not respond to immunosuppressant therapy (Ginsberg et al., 2004; Martini & Toyka, 2004), it seems unlikely that autoimmune involvement is common to most CMT1A patients. However, it remains possible that a superimposed inflammatory neuropathy may worsen the phenotype in a small subset of CMT1A patients. The association study did reveal a potential susceptibility locus for CIDP, located within an intron of the *PXK* gene, a gene containing known susceptibility loci for other autoimmune diseases including systemic sclerosis, rheumatoid arthritis, and SLE. This finding may suggest that CIDP shares some pathomechanisms with these diseases. The SNP within the *PXK* gene was found at a similar frequency in CMT1A and control cases, therefore it is unlikely to be associated with CMT1A. This study suffers from several limitations (discussed in Section 4.5.2), including a significant lack of power; top hits from all analyses should be replicated in a much larger study. However, although DNA for over 1,000 CMT1A patients may be readily available, it is difficult to acquire detailed phenotypes obtained in a consistent manner for all patients. Studies of CMT1A genetic modifiers performed by collaborators on our cases and others are now focusing on whole genome sequencing of CMT1A cases with phenotypes on either end of the severity spectrum.

In Chapter 5, exome sequencing was used to search for the causative gene in two CMT families without a known genetic cause of disease. The shift from "first generation" Sanger sequencing to high-throughput NGS methods, including exome

and whole-genome sequencing (Choi et al., 2009; Metzker, 2010), has dramatically increased the number of CMT-associated genes and has expanded the CMT phenotype (Rossor et al., 2013). Despite these advances, a proportion of CMT patients still remain without a known genetic cause, especially in CMT2 (Rossor et al., 2013). In this study, two candidate genes, *TBCEL* and *ARHGEF11*, were retained for further genetic and functional studies to be performed by another member of staff as these findings are very preliminary.

Perhaps equally important, the exome sequencing study in CMT has highlighted the benefits and disadvantages of this NGS technology which should be borne in mind prior to undertaking this type of study. It is important to remember that exome sequencing may miss variants due to insufficient coverage or to the nature or location of the mutation (Bamshad et al., 2011; Singleton, 2011). Furthermore, although novel gene finding by exome sequencing can be performed in single individuals or in only two family members (Singleton, 2011), these studies often result in long lists of variants of unknown pathogenicity despite extensive filtering. From our experience, unless linkage analysis was performed in parallel, our research group has usually had little success with exome sequencing in singletons and very small families. This problem is especially pertinent to CMT, for which causative genes may be ubiquitously expressed and are involved in a broad range of cellular functions (Patzkó & Shy, 2011; Scherer & Wrabetz, 2008). In addition, as is the case for variants identified via Sanger sequencing of single genes, it remains extremely difficult to prove pathogenicity of candidate genes identified via exome sequencing (Bamshad et al., 2011; Kochañski, 2006). To illustrate, in this Chapter I also attempted to provide additional evidence for the pathogenicity of a mutation in a previously identified candidate gene, *MFF*, by screening this gene in a cohort of CMT patients. Genetic and functional studies of this gene and another candidate gene *TRAK2* have thus far been inconclusive and their pathogenicity is still uncertain.

Although novel gene finding using exome sequencing does present some challenges, its advantages, including time and cost-efficiency, as well as the small amount of DNA required, are evident. This technology is particularly useful in diseases such as

CMT which are phenotypically and genetically heterogeneous with a large number of rare genes which could not reasonably be tested individually (Singleton, 2011). Following further reduction in cost and an improvement in the depth and coverage achieved, NGS technologies will surely be used in the diagnostic setting (Azzedine et al., 2012; Rossor et al., 2013). Finally, identifying novel CMT genes via NGS increases our understanding of the disease and provides clues for novel drug targets (Azzedine et al., 2012).

Identifying novel genes via exome sequencing may be considered more straightforward for diseases with a clearer pathological process. For example, the finding of decreased plasma levels of riboflavin, FAD and FMN in BVVL patients, which was not attributable to a nutritional riboflavin deficiency (Bosch et al., 2011), suggested that riboflavin transporters may be involved in the pathological process of this severe infantile neuropathy. This theory was confirmed by our group and colleagues through the discovery of mutations in genes encoding riboflavin transporters using exome sequencing. These findings in turn led to the recommendation that high-dose riboflavin therapy should be trialled in BVVL patients, for whom no treatment had been available to date (Sathasivam, 2008). Shortly thereafter, I undertook a study (Chapter 6) to identify unrecognised BVVL cases by screening the three riboflavin transporters, thereby prompting the initiation of riboflavin therapy in patients found to carry mutations. Mutations in *SLC52A2* were more frequent than *SLC52A1* and *SLC52A3* mutations in patients with BVVL and BVVL-like disease. As all *SLC52A3* mutations identified were in the heterozygous state, further studies are required to assess their pathogenicity. A significant proportion of the BVVL cohort did not carry mutations in any of the three genes, thus the next step would be to perform exome sequencing in these patients and their family members to search for novel genes.

Patients with *SLC52A2* mutations generally had a complex and severe phenotype including axonal sensory-motor neuropathy, respiratory insufficiency, optic atrophy, and bilateral sensorineural hearing loss with upper limb and trunk weakness but preservation of lower limb strength; most of these patients initially presented with ataxic gait or nystagmus. Importantly, all patients found to carry *SLC52A2* mutations

were immediately treated with high-dose riboflavin therapy. Clinical and biochemical improvements were seen in most patients, however the earlier this therapy was initiated, the more likely it was to be effective. Therefore, early genetic screening of suspected BVVL patients is essential. This treatment could also be useful in diseases with overlapping phenotypes, including ALS and SMA (Green et al., 2010; Horvath et al., 2011). Future studies should focus on optimising the riboflavin dose, the method of administration, and the length of treatment. Given the availability of this potentially life-saving treatment, additional patients with a broader range of BVVL-like phenotypes should be screened.

Exome sequencing was also used in this Chapter to search for novel genes in patients who had a BVVL-like phenotype or an AR polyneuropathy with prevalent motor involvement, and whom were negative for mutations in the riboflavin transporters. The challenges of data analysis in exome sequencing were also noted in this study. However, mutations in a promising candidate gene, *AAAS*, were found in one out of the three families studied with complex axonal neuropathy. These results are preliminary and additional genetic and functional assessments of pathogenicity are required. Nonetheless, this finding provides an example of the benefits of exome sequencing, whereby a previously unsuspected gene which would not otherwise have been screened, was found to be associated with a similar but somewhat atypical phenotype.

The discovery of riboflavin transporter mutations in BVVL patients has uncovered a novel pathway leading to neuropathy. In Chapter 7, I primarily used fibroblasts from patients with *SLC52A2* mutations as well as primary mixed ventral horn cultures from embryonic mice to begin to elucidate how deficiencies in riboflavin transport may lead to neurodegeneration. The scarce in vitro studies available to date had determined that riboflavin uptake was reduced for most *SLC52A2* and *SLC52A3* mutants, and some of the mutant proteins were retained in the ER and not targeted to the plasma membrane (Ciccolella et al., 2013; Haack et al., 2012; Nabokina et al., 2012). In this Chapter, I have shown that fibroblasts of BVVL patients with *SLC52A2* mutations had reduced MRC complex I and II activities, likely as a result of the observed reduction in intracellular FMN and FAD levels. Unfortunately, the

riboflavin uptake could not be measured in the fibroblasts due to technical difficulties; however, reduced uptake was subsequently confirmed by our collaborators, Dr Yonezawa and colleagues, in HEK293 cells expressing most of the *SLC52A2* mutations identified in Chapter 6 (Foley et al., 2014). Some patient fibroblast lines had reduced $\Delta\psi m$ with reversal of the ATP synthase, suggesting a deficiency in the MRC and cellular energy metabolism. CoQ_{10} levels were decreased, and the lactate/pyruvate ratio as well as NADH redox index were increased most evidently in the fibroblasts of one patient with a particularly severe phenotype. Notably, all defects described above were at least partially, if not completely, rescued in vitro by addition of high doses of riboflavin to the cell medium; admittedly, the mechanism by which riboflavin supplementation corrects these defects in the patient fibroblasts is not certain.

Data from these in vitro studies support the role of riboflavin in maintaining cellular energy metabolism, and have provided additional suggestions for prospective therapies in BVVL, as described in Section 7.12.5. A significant limitation of these studies is that patient fibroblasts had to be deprived of riboflavin in order to uncover the metabolic defects, thus perhaps mimicking an additional nutritional riboflavin deficiency. However, it may be that fibroblasts have relatively low requirements for riboflavin, and that the concentration of riboflavin in the low riboflavin medium is in fact sufficient for normal cellular energy metabolism in these cells. Data from this study may or may not be applicable to other cell types and to the disease pathway in vivo.

Although mitochondrial dysfunction was the focus of my investigations given the role of riboflavin and its metabolites in the MRC, these flavoproteins are involved in a wide range of cellular functions (Henriques et al., 2010; Lienhart et al., 2013; Massey, 2000; Powers, 2003). The experiments performed in this study were restricted in scope, thus it would be worthwhile to explore other biochemical processes which may be affected in BVVL. For example, ER stress could be investigated as a potential pathomechanism in BVVL; ER stress occurs when the function of the ER is disrupted, its folding capacity is exceeded, and unfolded or misfolded proteins accumulate and aggregate in this cellular compartment (Kanekura

et al., 2009). Disulphide bond formation is critical for protein biogenesis and proper secretion of proteins in the cell. In mammals, ER oxidoreductin 1 (Ero1), which is localized in the ER and has a role in oxidative protein folding and disulphide bond formation, uses FAD as an electron acceptor (Camporeale & Zempleni, 2003; Manthey et al., 2005; Papp et al., 2005; Varsányi et al., 2004; Werner et al., 2005). In yeast, FAD also promotes disulphide bridge formation by Ero1p (Tu & Weissman, 2002), and depletion of riboflavin causes an impairment of oxidative folding (Tu et al., 2000; Tu & Weissman, 2002). Furthermore, FAD binding was determined to be necessary for the assembly and folding of some flavoproteins, including acyl-CoA dehydrogenases (Nagao & Tanakas, 1992; Saijo & Tanaka, 1995). Accordingly, it was suggested that flavin deficiency might cause accumulation of unfolded proteins and ER stress (Camporeale & Zempleni, 2003; Tu et al., 2000).

Other cellular models besides patient fibroblasts were trialled as part of this Thesis. The in vitro work involving *SLC52A2*-KD SH-SY5Y cells was not pursued following difficulties with optimising the riboflavin concentration in the cell medium. Mutant *SLC52A2* SH-SY5Y cells were also prepared as part of this Thesis; however, upon further consideration it was deemed more appropriate to use primary mixed ventral horn cultures from embryonic mice for subsequent in vitro studies. The ideal cell model to use would have been to grow induced pluripotent stem (IPS) cells from the BVVL patient fibroblasts and differentiate them into neurones. However, developing the model itself takes nearly a year, thus given the time constraints, this model could not be utilised here. IPS cells grown from patient fibroblasts as well as riboflavin transporter-knockout animal models should be prioritised for future studies into the pathomechanism of BVVL.

Mitochondrial function was briefly assessed in the WT mixed ventral horn cultures deprived of riboflavin as a preliminary investigation of the resistance of these cells to riboflavin withdrawal. Although complex I and II activities were affected by riboflavin deficiency in the mixed culture, these observations did not translate to a defect of $\Delta\psi m$ maintenance in individual motor neurones. Future studies may wish to purify the cultures for enrichment of motor neurones as the presence of other cell types within the mixed ventral horn culture may have been a confounding variable.

Other possible explanations for this discrepancy are discussed in Section 7.12.2. The mouse riboflavin transporters *Slc52a2* and *Slc52a3* were also independently silenced in this cell model; results from measurements of basal $\Delta\psi m$ and response to mitochondrial toxins were inconclusive due to the small number of cells assessed as a result of poor transduction efficiency.

At this time, how mutations in riboflavin transporters can lead to a phenotype which so markedly differs from that of nutritional riboflavin deficiency is still unresolved. Possible additional functions of the riboflavin transporters should be investigated. Although it has been proposed that the brain is specifically protected against low intakes of riboflavin in the diet, mutations in riboflavin transporters may disrupt the ordinarily tightly regulated pathway (Foraker et al., 2003) and prevent the compensatory increase in riboflavin transport observed during nutritional riboflavin deficiency (Burch et al., 1956; Camporeale & Zempleni, 2003; Fujimura et al., 2010; Said & Ma, 1994; Said & Mohammed, 2006; Spector, 1980b; Spector & Johanson, 2006). Evidently, more studies are needed to characterise the riboflavin transporters and their uptake mechanisms both in vitro and in vivo.

Additional suggestions for future in vitro and in vivo studies of BVVL are detailed in Section 7.12.6. As previously mentioned, elucidating the BVVL pathway could putatively help to understand other MNDs and may generate more ideas for therapies. Similarly, it is likely that BVVL and other neurodegenerative diseases share some pathomechanisms, as the riboflavin metabolites play a role in several pathways already known to be involved in ALS, Parkinson's disease, and Alzheimer's disease, such as oxidative stress, ER stress and mitochondrial dysfunction.

With respect to the initial aims of the Thesis, the above experiments have:

- **Chapter 3:** 1) Established mutation frequencies for selected CMT1 genes in cohorts from the UK, Greece, and Russia, 2) expanded the phenotypes associated with defects in these genes, 3) enabled the genetic diagnosis of a group of CMT1 patients, and 4) ruled out several CMT genes as a cause of canine peripheral neuropathy and NAD-CA.

- **Chapter 4**: 1) Determined that alleles associated with CIDP and other autoimmune diseases are unlikely to modulate disease severity in CMT1A or to play a role in CMT1A in general, therefore a superimposed inflammatory neuropathy is probably not a common modifier of the phenotype in CMT1A, and 2) discovered a potential susceptibility locus in the *PXK* gene in CIDP patients.

- **Chapter 5**: Uncovered two possible candidate genes in two undiagnosed CMT families using exome sequencing.

- **Chapter 6**: 1) Detected riboflavin transporter mutations in unrecognised cases of BVVL, thus facilitating access to early treatment with high-dose riboflavin therapy, 2) extended the phenotype previously associated with BVVL, and 3) identified a strong candidate gene by exome sequencing in a previously undiagnosed family with complex axonal neuropathy.

- **Chapter 7**: 1) Established that *SLC52A2* patient fibroblasts show evidence of mitochondrial dysfunction, which could be rescued in vitro by supplementation with riboflavin, and 2) suggested additional therapies for BVVL based on results obtained in vitro.

Appendices

APPENDIX I

Table I-1: Classification of CMT, dHMN and HSAN (Adapted from Pandraud et al., 2012 and Rossor et al., 2013).

CMT1		
Subtype	**Gene/Locus**	**Phenotype**
ADCMT1		
CMT1A	*PMP22* (Duplication 17p11.2)	classic CMT1
	PMP22 (Point mutation)	CMT1/DSD/CHN (rarely recessive)
CMT1B	*MPZ*	CMT1/CMT2/DSD/CHN (rarely recessive)
CMT1C	*LITAF (SIMPLE)*	classic CMT1
CMT1D	*EGR2*	CMT1/DSD/CHN
CMT1F	*NEFL*	CMT2, motor NCV can be in CMT1 range (rarely recessive)
Other	*SOX10*	CMT1/CHN/Waardenburg-Hirschsprung disease
	FBLN5	age-related macular degeneration/hyperextensible skin/HMN
	GJB3 (Cx31)	bilateral high-frequency hearing loss/sensory polyneuropathy/variable penetrance
ARCMT1 (CMT4)		
CMT4A	*GDAP1*	severe CMT1/CMT2/DSD/possible vocal cord and diaphragm paralysis/rare AD families
CMT4B1	*MTMR2*	severe CMT1/facial weakness/bulbar palsy/focally-folded myelin
CMT4B2	*MTMR13 (SBF2)*	severe CMT1/glaucoma/focally-folded myelin
CMT4B3	*MTMR5 (SBF1)*	CMT1/pain/scoliosis/focally-folded myelin
CMT4C	*SH3TC2*	severe CMT1/scoliosis
CMT4D/HMSN-Lom	*NDRG1*	severe CMT1/gypsy/deafness/tongue atrophy
CMT4E	*EGR2*	CMT1/DSD/CHN
CMT4F	*PRX*	CMT1 with more sensory involvement/rare AD families/focally-folded myelin
CMT4G/HMSN Russe	*HK1*	severe CMT1/early-onset/possible proximal weakness/gypsy
CMT4H	*FGD4* (Frabin)	classic CMT1
CMT4J	*FIG4*	CMT1/progressive/mainly motor
CCFDN	*CTDP1*	CMT1/gypsy/cataracts/dysmorphic features
Other	*SURF1*	allelic with encephalopathy/CNS involvement (nystagmus, ataxia, hearing loss)/scoliosis

CMT2		
Subtype	**Gene/Locus**	**Phenotype**
ADCMT2		
CMT2A	*MFN2*	CMT2/more progressive/optic atrophy/tremor (rarely recessive)
CMT2B	*RAB7*	CMT2 with predominant sensory involvement and sensory complications
CMT2C	*TRPV4*	CMT2/dHMN (congenital SMA)/scapuloperoneal SMA/respiratory involvement/ arthrogryposis, laryngomalacia and vocal cord paresis
CMT2D	*GARS*	CMT2 with predominant hand wasting
CMT2E	*NEFL*	CMT2, motor NCV can be in CMT1 range (rarely recessive)
CMT2F	*HSP27 (HSPB1)*	CMT2/motor predominance
CMT2I	*MPZ*	late-onset CMT2
CMT2J	*MPZ*	CMT2/hearing loss/pupillary abnormalities
CMT2K	*GDAP1*	late-onset CMT2 (dominant)/severe CMT2 (recessive)
CMT2L	*HSP22 (HSPB8)*	CMT2/motor predominance
CMT2M	*DNM2*	ICMT/CMT2/cataracts/ophtalmoplegia/ptosis
CMT2N	*AARS*	classic CMT2
CMT2O	*DYNC1H1*	early-onset CMT2
CMT2P	*LRSAM1*	mild/slowly progressive/sensory predominance/CMT2 (dominant and recessive)
CMT2Q	*DHTKD1*	classic CMT2
HMSN-P	*TFG*	CMT2 with proximal involvement
Other	*MARS*	late-onset CMT2
	HARS	CMT2
	GJB3 (Cx31)	deafness/peripheral neuropathy
	KIF5A	CMT2/hereditary spastic paraplegia (SPG10)
	MT-ATP6	CMT2/pyramidal signs/relapsing
	IFRD1	ataxia/nystagmus
ARCMT2		
CMT2B1	*LMNA*	CMT2 with proximal involvement/rapid progression/muscular dystrophy/cardiomyopathy/lipodystrophy
CMT2B2	*MED25*	classic CMT2
Other	*HINT1*	predominantly motor/axonal neuropathy/neuromyotonia
	TRIM2	infantile-onset CMT2/poor growth/hypotonia

X-linked CMT		
Subtype	**Gene/Locus**	**Phenotype**
CMTX1	*GJB1 (Cx32)*	CMT1/CMT2/I-CMT, male motor NCVs < female motor NCVs
CMTX4/Cowchock syndrome	*AIFM1*	CMT2/infantile-onset/deafness/learning disability/developmental delay
CMTX5	*PRPS1*	severe CMT2/deafness/optic atrophy
CMTX6	*PDK3*	CMT2/hand tremor/mild or asymptomatic females
Dominant intermediate CMT (DI-CMT)		
Subtype	**Gene/Locus**	**Phenotype**
DI-CMTA	10q24.1-25.1	CMT2
DI-CMTB	*DNM2*	ICMT/CMT2/cataracts/ophtalmoplegia/ptosis
DI-CMTC	*YARS*	ICMT
DI-CMTD	*MPZ*	ICMT
DI-CMTE	*INF2*	ICMT/glomerulopathy/end-stage renal failure
DI-CMTF	*GNB4*	ICMT/more severe motor NCV changes in males
Other	*ARHGEF10*	hypomyelination/most patients asymptomatic
Recessive intermediate CMT (RI-CMT)		
Subtype	**Gene/Locus**	**Phenotype**
RI-CMTA	*GDAP1*	ICMT
RI-CMTB	*KARS*	ICMT/dysmorphic features/developmental delay/vestibular schwannoma
RI-CMTC	*PLEKHG5*	ICMT/allelic with distal SMA 4
Others		
Subtype	**Gene/Locus**	**Phenotype**
Hereditary neuralgic amyotrophy (HNA)	*SEPT9*	recurrent neuralgic amyotrophy
HNPP	Deletion 17p11.2/some *PMP22* point mutations	typical hereditary neuropathy with liability to pressure palsies

HSAN			
Subtype	**Inheritance**	**Gene/Locus**	**Phenotype**
HSAN1A	AD	*SPTLC1*	HSN/variable distal motor involvement/acromutilation/adolescent-onset
HSAN1C	AD	*SPTLC2*	HSN//variable distal motor involvement/acromutilation/adult-onset
CMT2B	AD	*RAB7*	sensory-motor with sensory complications/loss of nociception
HSN1D/SPG3A	AD	*ATL1*	HSN/trophic skin and nail changes/acromutilation/spasticity/adult-onset
HSN1E	AD	*DNMT1*	HSN/acromutilations/sensorineuronal hearing loss/dementia/adult-onset
HSAN2A	AR	*WNK1*	HSN/mutilations in hands and feet/acropathy/congenital or early childhood onset/severe
HSAN2B/HSAN1B	AR	*FAM134B*	HSN/impaired nociception/progressive mutilating ulceration of hands and feet/osteomyelitis/childhood onset
HSN2C/SPG30	AR	*KIF1A*	HSN/impaired position and vibration sense/acromutilations/minor distal weakness/childhood to adolescent-onset
HSAN3/Riley-Day	AR	*IKBKAP*	HSN/prominent autonomic involvement with vasomotor instability and hyperhidrosis/absent fungiform papillae/congenital/Ashkenazi Jewish
Channelopathy-associated insensitivity to pain/small-fibre neuropathy	AR and AD	*SCN9A*	congenital insensitivity to pain(recessive)/erythromelalgia, small-fibre neuropathy/paroxysmal extreme pain disorder (dominant)
CIPA/HSAN4	AR	*NTRK1*	congenital insensitivity to pain with anhydrosis/episodic fever/ skin and corneal lesions/joint deformities/mental retardation/unmyelinated fibres mainly affected
HSAN5	AR	*NGF-B*	insensitivity to pain/severe loss of deep pain perception/minimal autonomic/painless fractures, joint deformities/no mental retardation/mainly unmyelinated fibres affected
HSAN and dementia	AD	*PRNP*	autonomic dysfunction/dementia/sensory loss
Hereditary sensory neuropathy with spastic paraplegia	AR	*CCT5*	HSN/acromutilation/spastic paraplegia

dHMN			
Subtype	**Inheritance**	**Gene**	**Phenotype**
HMN2A	AD	*HSPB8/HSP22*	classical HMN
HMN2B	AD	*HSPB1/HSP27*	classical HMN
HMN2C	AD	*HSPB3*	classical HMN
HMN with pyramidal features/ALS4	AD	*SETX*	HMN/pyramidal signs/early-onset
DSMA5	AR	*DNAJB2 (HSJ1)*	classical HMN
HMN5A/SPG17	AD	*BSCL2*	hand wasting/silver syndrome/sensory involvement as in CMT2D
HMN5A	AD	*GARS*	hand wasting/slowly progressive
HMN5B/SPG31	AD	*REEP1*	hand wasting/pyramidal signs
HMN6/SMARD1	AR	*IGHMBP2*	infantile-onset/respiratory distress
HMN7A	AD	*SLC5A7*	classical HMN/vocal cord palsy
HMN7B	AD	*DCTN1*	HMN/adult-onset/bulbar and facial weakness
SMAX3	X-linked	*ATP7A*	classical HMN
SMALED	AD	*BICD2*	contractures/congenital/pyramidal signs/lower-limb predominance
SMALED	AD	*DYNC1H1*	contractures/congenital/pyramidal signs/lower-limb predominance/learning difficulties/cortical migration defects
PNMHH	AD	*MYH14*	typical HMN/hoarseness/distal myopathy/hearing loss
SPSMA	AD	*TRPV4*	HMN/adult-onset/vocal cord palsy/scapular winging
HMN	AD	*AARS*	typical HMN

Table I-2: CMT genes and associated predicted protein functions (Adapted from Azzedine et al., 2012; Pandraud, in press; Rossor et al., 2013; Tazir et al., 2013).

Gene	Predicted Protein Function
PMP22	Myelin structural component, myelin formation, Schwann cell differentiation
MPZ	Myelin structural component, adhesion, compaction and maintenance of myelin
LITAF (SIMPLE)	Protein sorting at the early endosome
EGR2	Transcription factor, regulation of myelination program
NEFL	Organization and assembling of neurofilaments, mitochondrial dynamics
MFN2	GTPase, mitochondrial fusion and transport
PRX	Myelin structural component, membrane-protein interactions, extracellular matrix signaling during myelination
SOX10	Transcription factor, regulation of myelination program
FBLN5	Elastic fiber assembly
GJB3 (Cx31)	Gap junction membrane protein
GDAP1	Glutathione metabolism, mitochondrial fission
MTMR2	Lipid phosphatase, membrane trafficking, endocytosis and control of myelination
MTMR13 (SBF2)	Pseudophosphatase, membrane trafficking
MTMR5 (SBF1)	Probably pseudophosphatase
SH3TC2	Rab11 effector, endocytic recycling
NDRG1	Signalling and membrane trafficking
HK1	Regulation of energy metabolism and cell survival, glucose metabolism
FGD4	Guanine nucleotide exchange factor, cytoskeletal remodelling
FIG4	Lipid phosphatase, membrane trafficking
CTDP1/FCP1	Phosphatase/RNA metabolism
SURF1	Mitochondrial, biogenesis of cytochrome C oxidase complex
KIF1B	Motor protein, vesicle trafficking
RAB7	GTPase, vesicle trafficking between late endosomes and lysosomes
TRPV4	Cation channel, transduction of sensory inputs
GARS	T-RNA synthetase, protein synthesis

(continued)	
HSP27 (HSPB1)	Chaperone, protein folding/quality control, neurofilament network organization
HSP22 (HSPB8)	Chaperone, protein folding, stress response, and regulation of apoptosis
DNM2	GTPase, cellular fusion and fission, vesicle trafficking, endocytosis
AARS	T-RNA synthetase, protein synthesis
DYNC1H1	Motor protein, retrograde axonal transport
LRSAM1	E3 ubiquitin ligase, receptor endocytosis
DHTKD1	Part of the 2-oxoglutarate dehydrogenase complex
TFG	Located at endoplasmic reticulum exit sites, possibly involved in vesicle trafficking
MARS	T-RNA synthetase, protein synthesis
HARS	T-RNA synthetase, protein synthesis
KIF5A	Anterograde axonal transport of organelles
MT-ATP6	ATP synthase subunit 6 in the mitochondrial membrane
IFRD1	Transcriptional co-activator/repressor
LMNA	Nuclear envelope structure, genomic stability, axonal survival and development
MED25	Transcriptional co-activator
HINT1	Purine phosphoramidase; binds to lysyl-tRNA synthetase
TRIM2	E3 ubiquitin ligase, ubiquitinates NEFL
GJB1 (Cx32)	Myelin structural component, cell membrane channel, formation of intracellular gap junctions between the folds of the Schwann cell cytoplasm
AIFM1	Oxidoreductase, role in apoptosis
PRPS1	Metabolic enzyme, nucleotide biosynthesis and purine metabolism
PDK3	Mitochondrial, regulates pyruvate dehydrogenase complex, bioenergetic pathway
YARS	T-RNA synthetase, protein synthesis
INF2	Cytoskeleton remodelling, regulator of actin polymerisation
GNB4	Guanine nucleotide-binding protein, cell signalling
ARHGEF10	Guanine nucleotide exchange factor, cytoskeletal remodelling
KARS	T-RNA synthetase, protein synthesis
PLEKHG5	Nuclear factor κB–activator

APPENDIX II

DNA extraction from human saliva using Oragene kit (OraSure technologies)

Briefly, 500 µl of the mixed Oragene/saliva sample was added to an Eppendorf tube. The tube was incubated at 50°C and spun briefly. 20 µl of Oragene Purifier was added to the tube and contents were vortexed. The tube was incubated on ice for 10 min and centrifuged at room temperature for 5 min at 13,000 rpm. The clear supernatant was transferred to a fresh tube. 500 µl of 95-100% ethanol was added to 500 µl of supernatant, and the contents were mixed gently by inverting 10 times. The tube was allowed to sit at room temperature for 10 min. The tube was centrifuged at room temperature for 2 min at 13,000 rpm. The supernatant was discarded, and 50 µl of Tris-EDTA buffer was added to the pellet. The tube was vortexed for 5 s and incubated at 50°C for 1 hr.

Quantitative polymerase chain reaction for confirmation of the Chr17p11.2 duplication

PMP22 primer concentrations were optimised (900 nM final concentration for both forward and reverse primers); optimal final primer concentrations for *ACTBL2* had been previously determined to be 500 nM for both forward and reverse primers. Similar amplification efficiency of reference (*ACTBL2*) and target (*PMP22*) genes was confirmed. All samples were run in triplicates. Each qPCR reaction for *PMP22* amplification contained 10 µl Power SYBR Green PCR master mix (Applied Biosystems), 3.6 µl of both forward and reverse primers at 5 µM, 0.8 µl autoclaved dH_2O and 2 µl DNA at 10 ng/µl. qPCR reactions for *ACTBL2* amplification contained 10 µl Power SYBR Green PCR master mix (Applied Biosystems), 1 µl of both forward and reverse primers at 10 µM, 6 µl autoclaved dH_2O and 2 µl DNA at 10 ng/µl. MicroAmp Fast Optical 96-well reaction plates were sealed with MicroAmp Optical Adhesive Film (Applied Biosystems). Samples were run along with a no template control and two control samples (negative for the Chr17p11.2 duplication) on the StepOnePlus Real-Time PCR System (Applied Biosystems). Thermalcycling conditions were as follows: 10 min at 95°C, followed by 40 cycles of 15 s at 95°C and 60 s at 60°C, and a final dissociation step. Cycles 28-30 were

excluded from the analysis as amplification was no longer linear at these cycles. Analysis of the dissociation curve eliminated the possibility of contamination and non-specific PCR products.

Illumina Infinium HD Human Immuno BeadChip Genotyping

Following an initial quality check, 300 ng of DNA sample was whole-genome amplified and incubated overnight at 37°C. The following day, the amplified DNA was fragmented at 37°C for 1 h and 15 min. Following alcohol precipitation and resuspension of DNA in hybridisation buffer, the samples were denatured. Samples were hybridised to the BeadChip and the DNA annealed to locus-specific 50-mers linked to one of more than 300,000 beadtypes, followed by overnight incubation at 48°C. One beadtype represents one allele per SNP locus. The next day, the probes on the chip were extended by a single hapten-labelled ddNTP base complementary to the hybridised DNA. 2',3'-dideoxyadenosine-5'-triphosphate (ddATP) and 2',3'dideoxythymidine-5'-triphosphate (ddTTP) bases were labelled with 2,4-dinitrophenol (DNP); 2',3'-dideoxycytidine-5'-triphosphate (ddCTP) and 2',3'-dideoxyguanosine-5'-triphosphate (ddGTP) were labelled with biotin. Formamide was then used to strip the DNA sample off the chip. For the staining procedure, the signal was amplified by multi-layer immunohistochemical staining. Streptavidin and an anti-DNP primary antibody conjugated to green and red fluorophores respectively (STM reagent, Illumina) were used to detect the haptens. To amplify the fluorescent signal, these were then counterstained with biotinylated anti-steptavidin and a DNP-labelled secondary antibody to the anti-DNP primary antibody (ATM reagent, Illumina). The STM reagent, containing the fluorophores to allow signal detection, was the last layer of the stain. The stained chips were covered in a glue-like substance to protect the dyes. A Freedom EVO liquid handling robot (Tecan Ltd, Switzerland) was used for hybridisation and staining procedures by an automated protocol; all processing prior to hybridization was carried out manually. The intensity of the fluorescence from the beads was detected by an iScan scanner system with autoloader (Illumina).

Data was initially analysed using the Illumina GenomeStudio software (cnvPartition v3.1.6, Illumina). For quality control, samples were assessed for their call rate which

should be >98%, and >99% average across the batch. Every array contained both sample-dependent and sample-independent control probes. Sample-independent probes tested the quality of the processing while sample-dependent probes assessed the DNA quality. The B-allele frequency plots and copy number analysis results were checked to identify potentially contaminated samples. This work was performed entirely by Kerra Pearce.

Exome sequencing protocol and data processing

For the exome sequencing performed at the UCL ION by Dr Deborah Hughes and Dr Alan Pittman, the sequencing data was mapped to the human reference genome build UCSC hg19 by Novoalign Software (Novocraft, Malaysia). After removal of PCR duplicates using Picard (http://picard.sourceforge.net) as well as reads without a unique mapping location, variants were extracted using the Maq model in SAMtools and filtered by the following criteria: consensus quality >30, SNP quality >30 and root mean square mapping quality >30. These variants were further filtered against the dbSNP 135 and 1000 Genomes databases by use of Annovar (http://www.openbioinformatics.org /annovar/).

The data processing for the exome sequencing performed by the Wellcome Trust Sanger Institute in Hinxton, UK was carried out as described in Cirak et al., 2013. Briefly, sequencing reads that failed quality control were eliminated using the Illumina Genome Analyser Pipeline (Illumina). The Burrows-Wheeler Aligner was used for alignment to the human reference genome build UCSC hg19; PCR duplicates were removed using Picard. Calling of variants was performed in target regions plus or minus a 100 bp window using both SAMtools (v.0.1.17) and Genome Analysis Tool Kit (GATK) Unified Genotyper (v.1.1-5). Base quality recalibration and indel realignment was done with GATK. SNPs and indels were called using the GATK Unified Genotyper, and labelled with dbSNP132 ID numbers. GATK Variant Filtration was applied and variants were assigned to quality tranches by GATK. Vcf-filter was used to filter the variants called by each method separately and the resulting files were merged. Variant calls were annotated using the earliest version of dbSNP containing this call, dbSNP132 ID numbers, and allele frequencies in the

1000 Genomes population (June 2011 release). Several functional scores were annotated to help in the filtering of variants.

The data processing for the exome sequencing performed by Oxford Gene Technology was carried out as follows. Read files were generated from the sequencing platform via the manufacturer's proprietary software. Reads were mapped to the human reference genome build UCSC hg19 using the Burrows-Wheeler Aligner package v.0.6.1. Local realignment of the mapped reads around potential indel sites was carried out with GATK v.1.6. Picard v.1.62 was used to mark duplicate reads. Additional BAM file manipulations were performed with SAMtools v.0.1.18. Base quality scores were recalibrated using GATK's covariance recalibration. The GATK Unified Genotyper was used to call SNP and indel variants, and variants were compared against dbSNP135. Ensembl was used to annotate genes and gene function for all variants.

cDNA synthesis

Briefly, the following was added to each well of a nuclease-free plate: 1 µl of 150 ng/µl random primers, 1 µl dNTP mix (each at 10 mM), 500 ng RNA, and autoclaved dH_2O to a total volume of 12 µl. The plate was heated to 65°C for 5 min and chilled on ice. 4 µl of 5X First-Strand buffer and 2 µl of 0.1 M DTT were added to each well. Contents were mixed and the plate was incubated at 25°C for 2 min. 1 µl (200 units) of SuperScript II Reverse transcriptase (200 U/µl; Life Technologies) was added to all wells except the "no RT" control. Contents were mixed and the plate was incubated at 25°C for 10 min, 42°C for 50 min, and 70°C for 15 min.

Optimisation of [^{3}H]-Riboflavin uptake assay in fibroblasts

Precautions required for working with radioactive material were followed throughout the procedure. Cells and incubation buffer were pre-warmed to 37°C. Uptake of [^{3}H]-Riboflavin (30 Ci/mmol, 99% purity; American Radiolabelled Chemicals, USA) was measured by removing the medium and pre-incubating the cells with 200 µl of incubation buffer at pH 7.4 (see below for recipe) for 10 min at 37°C. After removal of the buffer, 200 µl of incubation buffer with either 5 nM or 10 nM final

concentration of [^{3}H]-Riboflavin was added per well. Control wells (no added [^{3}H]-Riboflavin) were used in parallel. The cells were incubated for either 2.5 min or 30 min at 37°C, followed by two washes of the monolayers with 1 ml ice-cold incubation buffer to quench uptake. 500 µl of 0.5 M sodium hydroxide (NaOH) was added to solubilise the cells; half the wells were neutralised with 2.5 M hydrochloric acid (HCl). Success of the lysis was verified under a light microscope. Radioactive content of 300 µl aliquots of samples and standards of known radioactive content was assessed by liquid scintillation counting on a Packard Tri-Carb scintillation counter using QuantaSmart software (PerkinElmer) with 3 min assay time per vial.

In previous studies of [^{3}H]-Riboflavin uptake in *SLC52A1* or *SLC52A2*-mutant HEK293 cells, cells were incubated with either 5 nM or 10 nM [^{3}H]-Riboflavin for 1 min (Foley et al., 2014; Haack et al., 2012; Ho et al., 2010), but riboflavin concentration in the culture medium was not specified in these studies. Another study using *SLC52A2*-mutant fibroblasts had grown cells for 24 h in growth medium containing 0.4 nM riboflavin and incubated cells with 5 nM [^{3}H]-Riboflavin for a maximum of 30 min (Ciccolella et al., 2013). Despite the similar protocol used in this PhD work and the longer incubation time trialled, the [^{3}H]-Riboflavin uptake assay could not be successfully optimized within the timeframe of this PhD. Decreasing the amount of riboflavin in the growth medium, increasing the amount of added [^{3}H]-Riboflavin from 5 nM to 10 nM, and neutralising with HCl had no substantive effect on [^{3}H]-Riboflavin uptake. Possible issues include insufficient number of cells, inappropriate culturing conditions (length of time and riboflavin concentration), inappropriate incubation time or [^{3}H]-Riboflavin concentration. Although the pH of the buffer may affect uptake, it was verified before each assay, and uptake via RFVT1 and RFVT2 is known to be pH-independent (Yamamoto et al., 2009; Yao et al., 2010). The lower concentration of riboflavin (0.4 nM) in the culture medium compared to the 3.1 nM riboflavin medium used in other experiments in this PhD was trialled in order to increase levels of radioactivity detected and accuracy. Indeed, evidence from animal and in vitro studies of riboflavin deficiency suggests that some cells increase transport rates of riboflavin when grown in low riboflavin conditions as a compensatory mechanism (Section 7.1.5) (Camporeale & Zempleni, 2003; Kumar et al., 1998; Said & Ma, 1994a; Said

& Mohammed, 2006). Although cells did take up some [^{3}H]-Riboflavin since dpm values in wells with added [^{3}H]-Riboflavin were somewhat higher than in the control wells, the dpm values were not sufficiently higher than basal levels to allow for accurate determination of [^{3}H]-Riboflavin uptake.

Western blot optimisation: Endogenous RFVT2 protein levels in fibroblasts

To measure the expression levels of endogenous RFVT2 protein, both pellet and supernatant fractions of the cell lysates were used as RFVT2 expression has been identified in various cellular locations (Subramanian, Subramanya, et al., 2011; Yao et al., 2010; Section 6.1.3). A whole-cell sample was also used for comparison. For the supernatant fraction, the protein concentration was assayed as described in Section 2.2.7 and the sample was prepared as described in Section 2.2.22. Pellet and whole cell fractions were sonicated and samples were prepared in 4X SDS buffer so as to be representative of the supernatant fraction. The Western blot was performed as described in Section 2.2.22 with the following primary antibodies: rabbit polyclonal anti-RFVT2 (1:1,000; Sigma) and goat polyclonal anti-RFVT2 (D-13) (1:200; Santa Cruz Biotechnology). A donkey anti-goat IgG-HRP secondary antibody (1:5,000; Santa Cruz Biotechnology) was used with the Santa Cruz Biotechnology primary antibody. Thorough optimisation of the RFVT2 antibodies was carried out, with modifications in amount of protein loaded, transfer time, blocking agent and time, antibody concentration and incubation time, as well as developing time. It should be noted that this experiment was also trialled in SH-SY5Y cells, in the event that fibroblasts did not express sufficient amounts of RFVT2 to be detected by Western blot. However, no bands appeared at the expected molecular weight (46 kilodaltons) either in the pellet, supernatant or whole-cell lysate fractions for any of the primary antibodies or cell types used, suggesting that these antibodies are not appropriate for use in this study. Unfortunately, the number and quality of the commercially available antibodies for RFVT2 was very limited.

Preparation of *SLC52A2*-mutant SH-SY5Y cells

Cell line and cell culture:

Please refer to Sections 2.3.1 and 2.3.2 for a description of the SH-SY5Y cell line and culturing conditions.

Description of pCMV6-*SLC52A2*-myc-DDK plasmid:

Full-length C-terminal Myc-DDK-tagged *SLC52A2* cDNA (GenBank accession number NM_024531) in a pCMV6 entry plasmid (RC202512) was obtained from Origene. The myc-DDK tag is attached to the C-terminal of the protein and the open-reading frame is flanked by a polyA signal at the 3' end. The expression of *SLC52A2* is driven by a CMV promoter. A kanamycin resistance gene is the antibiotic selection marker for *Escherichia coli* and a neomycin (G-418) resistance gene provides antibiotic selection in mammalian cells (Figure II-1).

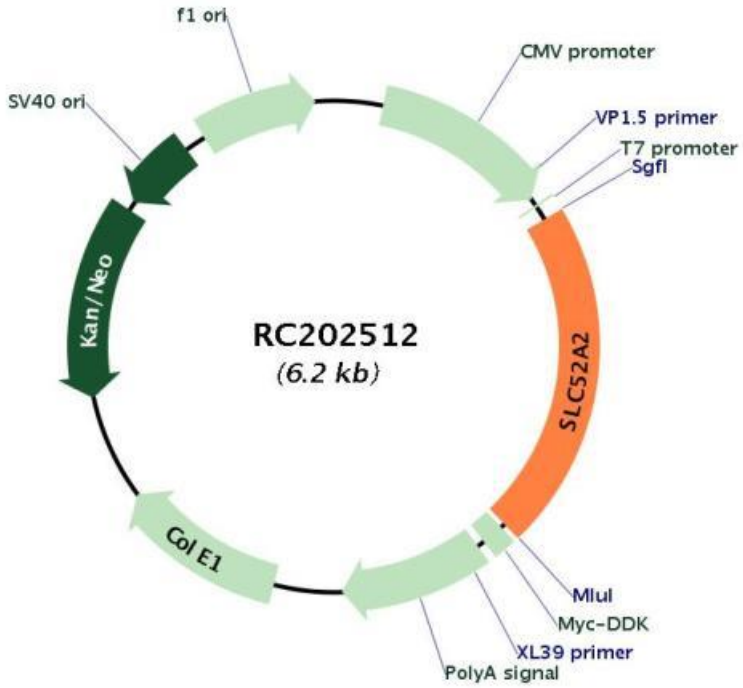

Figure II-1: Vector map for the pCMV6-*SLC52A2*-myc-DDK plasmid (reproduced from Origene website).

Quality control of pCMV6-*SLC52A2*-myc-DDK plasmid:

The entire *SLC52A2* open reading frame of the pCMV6-*SLC52A2*-myc-DDK plasmid described above was sequenced by the UCL DNA sequencing service and was confirmed to be free of mutations (see Appendix VII Table VII-6 for sequences of pCMV6 vector primers). A restriction digest was performed for further quality control. The digest reaction contained: 2 µl 10X restriction enzyme buffer 3 (NEB), 2 µl 10X BSA, 0.5 µl restriction enzyme SalI or DraIII (20 U; NEB), 300 ng plasmid DNA, made up to 20 µl final volume with dH_2O. The reaction was mixed and incubated at 37°C for 2 h. 10 µl of the digested samples were loaded onto a 1% w/v agarose gel with 1 Kb DNA ladder (NEB). Uncut samples were run alongside the digested samples for comparison. As expected, three bands of the expected size were obtained when using the DraIII restriction enzyme, and two bands of the correct size were obtained when using SalI.

Preparation of empty vector:

An empty pCMV6 vector was prepared from the pCMV6-*SLC52A2*-myc-DDK plasmid. The digest reaction contained 5 µl 10X restriction enzyme buffer 3 (NEB), 5 µl 10X BSA, 1 µg plasmid DNA, 2.5 µl each of XhoI and SalI restriction enzymes (20 U) (NEB), made up to 50 µl with dH_2O. The reaction was incubated for 3 h at 37°C. 50 µl of the digest was mixed with 10 µl 5X loading dye (Qiagen) and loaded onto a 1% w/v agarose gel with 10 µl of 1 Kb ladder (NEB). Samples were electrophoresed for 1 h at 60 V and visualized under a UV transilluminator. The band corresponding to the empty vector (4.9 Kb) was excised from the agarose gel with a sharp scalpel and the DNA was extracted using the QIAquick gel extraction kit (Qiagen). DNA purity and concentration were determined as described in Section 2.1.5. Vector ligation was performed using 1.5 µl ligase buffer, 1.5 µl T4 ligase, 100 ng DNA, made up to 15 µl in dH_2O. The reaction was left to incubate for 2 h at room temperature.

Site-directed mutagenesis of pCMV6-*SLC52A2*-myc-DDK plasmid:

Primers for mutagenesis of the pCMV6-*SLC52A2*-myc-DDK plasmid for selected *SLC52A2* mutations (c.92G>C (p.Trp31Ser), c.700C>T (p.Gln234Stop), c.916G>A (p.Gly306Arg), c.935T>C (p.Leu312Pro), c.1016T>C (p.Leu339Pro), and c.1258G>A (p.Ala420Thr)) were designed using the QuikChange primer design program (Agilent Technologies) (see Appendix VII Table VII-7 for mutagenesis primer sequences). Mutagenesis primers, two complimentary oligonucleotides containing the desired mutation with unmodified nucleotide sequence on either side, were synthesized by Sigma. It was thereafter noted that, as the myc tag is located downstream of the p.Ala420Thr stop mutation, the myc tag could not be expressed in cells transfected with this mutant plasmid. Rather, a truncated cDNA sequence should have been introduced into the pCMV6 entry vector.

SLC52A2 mutations were introduced by site-directed mutagenesis using the Stratagene QuikChange II XL Site-Directed Mutagenesis Kit (Agilent Technologies). Briefly, 5 µl of 10X reaction buffer, 10 ng plasmid DNA, 125 ng of forward primer, 125 ng of reverse primer, 1 µl dNTP mix, 3 µl QuikSolution, made up to 50 µl with dH_2O and 1 µl of PfuUltra High Fidelity DNA polymerase (2.5 U/µl) was mixed in a thin-walled PCR tube. PCR thermalcycling conditions were as follows: 1 min at 95 °C, followed by 18 cycles of 50 s at 95°C, 50 s at 60°C and 6 min at 68°C before a final 7 min elongation stage at 68°C. The reactions were placed on ice for 2 min. 1 µl (10 U/µl) of DpnI restriction enzyme (NEB) was then added to the mutagenesis reactions and incubated at 37°C for 1 h to digest the parental DNA.

Transformation of chemically competent cells:

A 50 µl vial of One Shot Top 10 chemically competent *Escherichia coli* cells (Life Technologies) was thawed on ice. 5 µl of the mutagenesis reaction (or 50 ng of DNA for the empty and WT plasmids) was incubated in one vial of competent cells on ice for 30 min before being heat-shocked at 42°C for 30 s. The vial of competent cells was placed on ice for 2 min and 350 µl of pre-warmed SOC medium (Life Technologies) was added aseptically. The vial was placed in an incubator at 37°C and shaken at 225 rpm for 1 h. 100 µl aliquots were pipetted onto pre-warmed

selective agar plates (25 μg/ml kanamycin) and spread throughout the plate. The plates were then inverted and incubated overnight at 37°C. The following day, single colonies were picked aseptically and inoculated into a tube containing 2 ml of LB broth with 25 μg/ml kanamycin. These starter cultures were grown for 7 h on a shaking (225 rpm) incubator at 37°C. 300 μl of starter culture was aseptically added to a 500 ml flask containing 150 ml of LB broth (1:500 dilution) with 25 μg/ml kanamycin and grown overnight at 37°C in a shaking (225 rpm) incubator. Glycerol stocks of all clones were prepared by mixing 500 μl of the overnight culture with 500 μl glycerol at 50% v/v and freezing at -80°C. Overnight cultures were harvested by centrifugation at 4°C at 3,000 rpm for 20 min; the pellet was frozen at -80°C until needed for the Maxiprep.

Maxiprep isolation of plasmid DNA:

To obtain high-quality plasmid DNA for mammalian cell transfection, DNA for the empty, WT and the mutant pCMV6-*SLC52A2*-myc-DDK plasmids was purified from the cell pellets obtained from the overnight bacterial cultures using the Qiagen Plasmid Maxi kit (Qiagen) as per the manufacturer's instructions. Plasmid DNA purity and concentration were determined as described in Section 2.1.5. The entire *SLC52A2* open-reading frame was sequenced by the UCL DNA sequencing service (see Appendix VII Table VII-6 for primer sequences) to confirm insertion of the correct mutations and absence of additional mutations which may have arisen during the mutagenesis and transformation procedures.

To verify that the empty vector was indeed empty following the Maxiprep above, enzyme digests of the WT pCMV6-*SLC52A2*-myc-DDK plasmid and the empty vector were performed using 2 μl of restriction enzyme buffer 4 (NEB), 2 μl of 10X BSA, 300 ng plasmid DNA, 0.5 μl XmaI restriction enzyme (20 U; NEB), made up to 20 μl in dH_2O. The reaction was incubated at 37°C for 2 h. 10 μl of the digested samples were loaded with 2 μl 5X loading dye (Qiagen) onto a 1% w/v agarose gel with 1 Kb DNA ladder (NEB). Two bands of the expected sizes were obtained, confirming that the empty vector did not contain the *SLC52A2* open reading frame. The empty vector was also confirmed to be empty by sequencing as described above.

Stable transfection of pCMV6-*SLC52A2*-myc-DDK plasmids:

SH-SY5Y cells were stably transfected with the empty pCMV6 vector and the pCMV6-*SLC52A2*-myc-DDK vectors containing *SLC52A2*^{WT}, *SLC52A2*$^{92G>C}$, *SLC52A2*$^{700C>T}$, *SLC52A2*$^{916G>A}$, *SLC52A2*$^{935T>C}$, *SLC52A2*$^{1016T>C}$, and *SLC52A2*$^{1258G>A}$. The night before transfection, cells were plated at approximately 50% confluence in 6-well plates and incubated under normal conditions. The transfection procedure was performed as described in Section 2.3.7. The SH-SY5Y cells were maintained in selective medium containing 700 μg/ml G-418 antibiotic (PAA Laboratories- GE Healthcare) from 48 h after transfection to eliminate cells not expressing the vector.

Recipes

LB agar: 35 g of LB agar powder (Sigma) dissolved in 1 L dH_2O, followed by autoclaving.

LB broth: 20 g of LB broth powder (Sigma) dissolved in 1 L dH_2O, followed by autoclaving.

Orange G loading dye: 60% glycerol, 40% dH_2O, teaspoon of orange G powder (Sigma).

Agarose gel: 75 ml 1X TBE, 1 g agarose powder (Roche), 2 μl of 10 mg/ml ethidium bromide (Promega).

10X TBE (for 1 L; pH to 8.3): 121.1 g Tris (Sigma), 61.8 g anhydrous boric acid (Merck-Millipore), 7.4 g EDTA (VWR), made up with dH_2O.

Fibroblast freezing medium: 20% DMSO (Sigma), 80% FBS.

Western blot lysis buffer: 50 mM Tris (pH 7.4), 0.1 mM ethylene glycol tetraacetic acid (EGTA) (pH 7.4), 1 mM EDTA (pH 7.4), 1% Triton X-100 neat (Sigma), 92 mg/ml sucrose, 0.1% β-mercaptoethanol, and 100 μl/ml each of 10X Complete

EDTA-free protease inhibitor cocktail tablets (Roche) and PhosSTOP phosphatase inhibitor cocktail tablets (Roche).

Western blot running buffer: 100 ml 20X NuPAGE MES SDS running buffer (Life Technologies) in 1,900 ml dH_2O.

Western blot Tris transfer buffer: 20% methanol, 10% Tris-glycine electroblotting buffer 10X (National Diagnostics, USA), 70% dH_2O.

PBS Tween: 2 PBS tablets (Life Technologies), 1 ml Tween 20 (for electrophoresis, Sigma) dissolved in 1 L of dH_2O.

Incubation buffer for [^{3}H]-Riboflavin uptake assay (from Ciccolella et al., 2013): 145 mM NaCl**,** 3 mM KCl, 1 mM $CaCl_2$, 0.5 mM $MgCl_2$, 5 mM D-glucose, 5 mM 4-(2-hydroxyethyl)-1-piperazineethanesulfonic acid (HEPES), dissolved in dH_2O, pH to 7.4 and sterile-filtered.

Glucose-free HBSS: 1.26 mM anhydrous $CaCl_2$, 0.493 mM $MgCl_2$ x $6H_2O$, 0.407 mM $MgSO_4$ x $7H_2O$, 5.33 mM KCl, 0.441 mM KH_2PO_4, 4.17 mM $NaHCO_3$, 137.93 mM NaCl, 0.338 mM Na_2HPO_4, 5.56 mM 2-deoxy-D-glucose (Sigma), dissolved in dH_2O, pH to 7.35-7.4.

CNB medium (for 200 ml): 191.1 ml 1X Neurobasal Medium (Gibco), 4 ml 50X B-27 serum-free supplement (Gibco), 2 µl of 10 µg/ml brain-derived neurotrophic factor (Alomone labs, Israel), 2 µl of 10 µg/ml glial cell line-derived neurotrophic factor (Alomone labs), 20 µl of 5 µg/ml ciliary neurotrophic factor (Alomone labs), 500 µl of 200 mM glutamine, 100 µl 0.05% β-mercaptoethanol (Gibco), 4 ml heat-inactivated horse serum (Sigma), 2 ml P/S (Life Technologies).

TMRM RM for mixed ventral horn cultures: 156 mM NaCl, 10 mM HEPES (Thermo Fisher Scientific), 10 mM D-glucose, 3 mM KCl, 2 mM $MgSO_4$, 2 mM $CaCl_2$, 1.25 mM $KHPO_4$, dissolved in dH_2O and pH to 7.35 with NaOH.

APPENDIX III

Table III-1: Sequences of primers used to amplify the human *PMP22*, *EGR2*, *LITAF*, *GJB1*, and *NEFL* genes. All *GJB1* primers have M13 tails.

Gene	Ensembl transcript	Exon	Direction	Primer sequence (5' to 3')	Annealing temperature	PCR protocol	Amplicon length (bp)
PMP22	ENST00000312280	2	forward	aaaagcaaaagatgttcc	52°C	Qiagen	461
PMP22	ENST00000312280	2	reverse	actgtctgcaaataacac			
PMP22	ENST00000312280	3	forward	tgtgcatgtggaacttctcc	65-60°C	Roche	397
PMP22	ENST00000312280	3	reverse	caacgacattctggcttgtg			
PMP22	ENST00000312280	4	forward	cttctgcttctgctgcctgt	62-52°C	Roche	388
PMP22	ENST00000312280	4	reverse	catccagtggggagactcat			
PMP22	ENST00000312280	5	forward	tcaattctggacctggaagc	65-60°C	Roche	406
PMP22	ENST00000312280	5	reverse	gggattttgggctagctctt			
EGR2	ENST00000242480	1	forward	aagtgtggagggcaaaagga	65-60°C	Roche	403
EGR2	ENST00000242480	1	reverse	agtcagcaccgtccacctg			
EGR2	ENST00000242480	2-1	forward	ttggactttgccacagctc	65-60°C	Roche	630
EGR2	ENST00000242480	2-1	reverse	atcattgggaagagacctgg			
EGR2	ENST00000242480	2-2	forward	aggagacctctaccaggacc	65-60°C	Roche	634
EGR2	ENST00000242480	2-2	reverse	gatatgggtggtgaggtgg			
EGR2	ENST00000242480	2-3	forward	ccaacagacccagcaagac	65-60°C	Roche	591
EGR2	ENST00000242480	2-3	reverse	cagtgctagctccaccaaag			
LITAF	ENST00000339430	2	forward	cagaaagaaaattgaagacttaggtg	62-52°C	Roche	425
LITAF	ENST00000339430	2	reverse	tggaacgtactggcacttca			
LITAF	ENST00000339430	3	forward	actggtgttccttccccttt	65-60°C	Qiagen	432
LITAF	ENST00000339430	3	reverse	cctgaatgtcaagcatggtg			
LITAF	ENST00000339430	4	forward	cctcttcttctaaggtcattgg	62-52°C	Roche	402
LITAF	ENST00000339430	4	reverse	tggagaggtgagaccacca			
GJB1	ENST00000361726	2-1	forward	tgggacacaagtgctctgtg	58°C	Roche	521
GJB1	ENST00000361726	2-1	reverse	actcttccaagagccagtag			
GJB1	ENST00000361726	2-2	forward	gaggtcaagtcaagtgagtg	58°C	Roche	571
GJB1	ENST00000361726	2-2	reverse	ttcacctcctccaggtgtag			
GJB1	ENST00000361726	2-3	forward	ctgcagctcatcctagtttc	58°C	Roche	551
GJB1	ENST00000361726	2-3	reverse	atgtctttcagggagccatc			
GJB1	ENST00000361726	2-4	forward	aggtggtgtacctcatcatc	58°C	Roche	524
GJB1	ENST00000361726	2-4	reverse	ccatctcttgtacccagtgg			
NEFL	ENST00000221169	1-1	forward	cacacagccatccatcctc	60-50°C	Roche	493
NEFL	ENST00000221169	1-1	reverse	atggctcggagtgcttctg			
NEFL	ENST00000221169	1-2	forward	ctccagctctggatcgttg	60-50°C	Roche	556
NEFL	ENST00000221169	1-2	reverse	gatctgcgcgtactggatc			
NEFL	ENST00000221169	1-3	forward	tgaagaggaggtgctgagc	60-50°C	Roche	633
NEFL	ENST00000221169	1-3	reverse	gccaagccctatccctaag			
NEFL	ENST00000221169	2	forward	acaggaagttattctaggagag	60-50°C	Roche	412
NEFL	ENST00000221169	2	reverse	ttcttggaagaagccaaa			
NEFL	ENST00000221169	3-1	forward	tttctggtctccatcaaa	60-50°C	Roche	350
NEFL	ENST00000221169	3-1	reverse	caatggtttcctccacttcg			
NEFL	ENST00000221169	3-2	forward	agagctcccaggtctttgg	60-50°C	Roche	419
NEFL	ENST00000221169	3-2	reverse	ttcagagtagatgccttaggaa			
NEFL	ENST00000221169	4	forward	tcatggcaagctttgtctgt	55-52°C	Roche	402
NEFL	ENST00000221169	4	reverse	tcacatagaatctggaactcaa			

Table III-2: Sequences of primers used to amplify the canine *PMP22*, *MPZ*, and *MFN2* genes.

Gene	Ensembl transcript	Exon	Direction	Primer sequence (5' to 3')	Annealing temperature	PCR protocol	Amplicon length (bp)
PMP22	ENSCAFT00000028432	1	forward	ctccgctgagcaccactc	60-50°C	Roche	318
PMP22	ENSCAFT00000028432	1	reverse	catgaatctgctcgggtttt			
PMP22	ENSCAFT00000028432	2	forward	aggctggctagatgagtgga	60°C	Roche	300
PMP22	ENSCAFT00000028432	2	reverse	gactttggagccgtgtcttc			
PMP22	ENSCAFT00000028432	3	forward	gccagctcttcctaacctga	60°C	Roche	431
PMP22	ENSCAFT00000028432	3	reverse	ggaccttccttccagactcc			
PMP22	ENSCAFT00000028432	4	forward	agattgggcgatatggtctg	65-60°C	Qiagen	423
PMP22	ENSCAFT00000028432	4	reverse	ctggtttccttcctcccttt			
MPZ	ENSCAFT00000020580	1	forward	ggttactggctcaggacagc	60°C	Roche	476
MPZ	ENSCAFT00000020580	1	reverse	tttcctaccatgcgacaaca			
MPZ	ENSCAFT00000020580	2-1	forward	tcagttagcccggacagagt	60-50°C	Qiagen	319
MPZ	ENSCAFT00000020580	2-1	reverse	ctccccgtactcaccgagat			
MPZ	ENSCAFT00000020580	2-2	forward	cctttctgcttgcagtgct	60-50°C	Roche	275
MPZ	ENSCAFT00000020580	2-2	reverse	gtcccccagtgtccctctat			
MPZ	ENSCAFT00000020580	3	forward	ctgaggctagacccacaagc	60°C	Roche	457
MPZ	ENSCAFT00000020580	3	reverse	taggaggggagggaagagaa			
MPZ	ENSCAFT00000020580	4	forward	gtgaggggctctgggaata	60°C	Roche	366
MPZ	ENSCAFT00000020580	4	reverse	gcagagagggagccagact			
MPZ	ENSCAFT00000020580	5	forward	gaggctcaggtaaggggagt	60°C	Roche	390
MPZ	ENSCAFT00000020580	5	reverse	agccccttggacttcttttc			
MPZ	ENSCAFT00000020580	6	forward	aaggggaaattgcacaagg	65-60°C	Qiagen	418
MPZ	ENSCAFT00000020580	6	reverse	gttcttgaggctggttctgc			
MFN2	ENSCAFT00000026136	2	forward	tgctgacccaggtctagtc	55°C	Roche	451
MFN2	ENSCAFT00000026136	2	reverse	ggtgacaacctatctggg			
MFN2	ENSCAFT00000026136	3	forward	gtagggatccagcctttg	55°C	Roche	330
MFN2	ENSCAFT00000026136	3	reverse	cctggtaagaggttaatatc			
MFN2	ENSCAFT00000026136	4	forward	gagactttgggcttcgag	55°C	Roche	329
MFN2	ENSCAFT00000026136	4	reverse	cctggttggtctaagctc			
MFN2	ENSCAFT00000026136	5	forward	gtgtgaaatggaagaaggg	55°C	Roche	367
MFN2	ENSCAFT00000026136	5	reverse	cagtctaagcaatgacagg			
MFN2	ENSCAFT00000026136	6-7	forward	tttgtactcctttgcctg	55°C	Roche	516
MFN2	ENSCAFT00000026136	6-7	reverse	tggtgaactcagtcatagg			
MFN2	ENSCAFT00000026136	8	forward	ttagaagaaaggcacagg	55°C	Roche	320
MFN2	ENSCAFT00000026136	8	reverse	ctgcctcactctcagaac			
MFN2	ENSCAFT00000026136	9-10	forward	ctgtctgcttagctttgg	55°C	Roche	476
MFN2	ENSCAFT00000026136	9-10	reverse	gatgaggcgatcacttc			
MFN2	ENSCAFT00000026136	11	forward	gtgtgaaactgctgaggc	55°C	Roche	348
MFN2	ENSCAFT00000026136	11	reverse	cttctggaaggctgagag			
MFN2	ENSCAFT00000026136	12	forward	ctcagggaaacttgtgcg	55°C	Roche	300
MFN2	ENSCAFT00000026136	12	reverse	ccctgaatcactgtcctg			
MFN2	ENSCAFT00000026136	13	forward	ttccttgtcccttggctc	55°C	Roche	295
MFN2	ENSCAFT00000026136	13	reverse	actaactcgttgtcaaagg			
MFN2	ENSCAFT00000026136	14	forward	ctgacgtggcttctcctcat	60°C	Roche	492
MFN2	ENSCAFT00000026136	14	reverse	gggtgcctcagtcagctaag			
MFN2	ENSCAFT00000026136	15	forward	tttgggaattgaagagcc	55°C	Roche	332
MFN2	ENSCAFT00000026136	15	reverse	actgagccaaagcaggag			
MFN2	ENSCAFT00000026136	16	forward	aactagggctcttgggaagg	65-60°C	Qiagen	495
MFN2	ENSCAFT00000026136	16	reverse	ccaacccaggacataaggtg			
MFN2	ENSCAFT00000026136	17	forward	gaagtttctgcggaactgg	55°C	Roche	366
MFN2	ENSCAFT00000026136	17	reverse	cccaagacagacaagcag			
MFN2	ENSCAFT00000026136	18	forward	tcacgggagcttagaatag	55°C	Roche	311
MFN2	ENSCAFT00000026136	18	reverse	tcaaaacggtatgagacg			

Table III-3: Sequences of primers used to amplify the 391 bp-long cDNA region of interest in *PMP22* for the small duplication and deletion identified in the Greek CMT1 cohort. *An 18 bp oligonucleotide was tagged to this primer.

Gene	Position	Direction	Primer sequence (5' to 3')
PMP22	exon 4	forward	cctgtcgatcatcttcagca
PMP22	3' UTR	reverse	gggattttgggctagctctt*

Table III-4: Variants identified in the UK CMT1 cohort along with pathogenicity predictions.

Gene	Exon	Nucleotide substitution	Heterozygous/ Homozygous	Amino acid change	Frequency in our UK CMT1 cohort	Frequency in our UK control cohort	dbSNP ID (1000 Genomes MAF)	NHLBI EVS MAF	Polyphen-2 prediction	SIFT prediction	Conservation across species	Literature references	Pathogenicity
EGR2	2	c.627A>G	heterozygous	p.Pro209Pro	1/135 (0.74%)	N/A	rs224083 (0.013)	0.018	-	-	-	-	unlikely
EGR2	2	c.644C>T	heterozygous	p.Thr215Met	2/135 (1.48%)	1/255 (0.39%)	rs139147487 (0.001)	0.0007	benign	unknown	not conserved	-	unlikely
EGR2	2	c.1075C>T	heterozygous	p.Arg359Trp	1/135 (0.74%)	N/A	rs104894161 (-)	-	probably damaging	not tolerated	highly conserved	Boerkoel et al., 2001; Choi et al., 2004; Chung et al., 2005; Taroni et al., 1999; Timmerman et al., 1999; Warner et al., 1999	likely
EGR2	2	c.1086A>C	heterozygous	p.Arg362Arg	6/135 (4.44%)	N/A	rs45602133 (0.065)	0.04	-	-	-	Choi et al., 2004; Timmerman et al., 1999	unlikely
EGR2	2	c.1141C>T	heterozygous	p.Arg381Cys	2/135 (1.48%)	0/257 (0%)	-	-	probably damaging	not tolerated	highly conserved	Briani et al., 2010; Yoshihara et al., 2001	likely
EGR2	2	c.1277G>A	heterozygous	p.Arg426Gln	1/135 (0.74%)	0/264 (0%)	-	-	possibly damaging	not tolerated	partially conserved	-	likely
EGR2	2	c.1352G>T	heterozygous	p.Gly451Val	1/135 (0.74%)	1/185 (0.54%)	rs138967272 (-)	-	unknown	unknown	unknown	Takashima et al., 2001	unlikely

Table III-5: Variants identified in the Greek CMT1 cohort along with pathogenicity predictions.

Gene	Exon	Nucleotide substitution	Heterozygous/ Homozygous	Amino acid change	Frequency in our Greek CMT1 cohort	Frequency in our Greek control cohort	dbSNP ID (1000 Genomes MAF)	NHLBI EVS MAF	Polyphen-2/ Spliceview prediction	SIFT prediction	Conservation across species	Literature References	Pathogenicity
PMP22	Splice site, intron 2-3	c.79-2A>G	heterozygous	p.(Gln27_Asn59del_Glu60AsnfsX10)	1/86 (1.2%)	0/225 (0%)	-	-	disrupts acceptor site	-	-	this study (Koutsis et al., 2012)	likely
PMP22	4	c.296_301delCTGGAA	heterozygous	p.Thr99_Gly100del	1/86 (1.2%)	0/225 (0%)	-	-	-	-	-	this study (Koutsis et al., 2012)	likely
PMP22	5	c.328_348dup21	heterozygous	p.Val110_Ile116dup	1/86 (1.2%)	0/225 (0%)	-	-	-	-	-	this study (Koutsis et al., 2012)	likely
EGR2	2	c.1086A>C	heterozygous	p.Arg362Arg	8/86 (9.3%)	-	rs45602133 (0.065)	0.04	-	-	-	Choi et al., 2004; Timmerman et al., 1999	unlikely
EGR2	2	c.1142A>G	heterozygous	p.Arg381His	1/86 (1.2%)	-	rs281865137 (-)	-	probably damaging	not tolerated	highly conserved	Pareyson et al., 2000; Vandenberghe et al., 2002	likely
EGR2	2	c.1352G>T	heterozygous	p.Gly451Val	1/86 (1.2%) †	0/225 (0%)	rs138967272 (-)	-	unknown	unknown	unknown	Takashima et al., 2001	unlikely
EGR2	2	c.1352G>A	heterozygous	p.Gly451Asp	1/86 (1.2%) ‡	1/225 (0.4%)	-	8E-05	unknown	unknown	unknown	this study (Koutsis et al., 2012)	unlikely
LITAF	3	c.234G>A	heterozygous	p.Thr78Thr	4/86 (4.6%)	-	rs9282774 (0.01)	0.01	-	-	-	Latour et al., 2006	unlikely
LITAF	3	c.274A>G	both	p.Ile92Val	33/86 het. (38.4%); 3/86 hom. (3.49%)	-	rs4280262(0.13)	0.2	-	-	-	Latour et al., 2006	unlikely
LITAF	3	c.333C>T	heterozygous	p.Ala111Ala	2/86 (2.3%)	-	rs34448402 (0.003)	0.0026	-	-	-	Latour et al., 2006	unlikely
NEFL	1	c.667C>T	heterozygous	p.Leu223Leu	1/86 (1.2%)		rs60156239 (0.003)	0.0037	-	-	-	Jordanova et al., 2003	unlikely
NEFL	3	c.1402G>A	heterozygous	p.Asp468Asn	1/86 (1.2%)	-	rs57153321 (0.002)	0.0013	unknown	tolerated	unknown	Jordanova et al., 2003	unlikely
NEFL	4	c.1579_1581delGAG	heterozygous	p.Glu527del	1/86 (1.2%)	0/225	rs3832558 (-)	-	-	-	-	Abe et al., 2009; Jordanova et al., 2003; Yamamoto et al., 2004; Yoshihara et al., 2002	unlikely

† parents of proband are asymptomatic with normal NCS, mother carries c.1352G>T; ‡ parents of proband are asymptomatic with normal NCS, father carries c.1352G>A.

Table III-6: Variants identified in the Yakutsk CMT1 cohort along with pathogenicity predictions.

Gene	Exon	Nucleotide substitution	Heterozygous/ Homozygous	Amino acid change	Frequency in our Russian CMT1 cohort	dbSNP ID (1000 Genomes MAF)	NHLBI EVS MAF	Polyphen-2 prediction	SIFT prediction	Conservation across species	Literature References	Pathogenicity
PMP22	*No variants identified*											
EGR2	2	c.627A>G	homozygous	p.Pro209Pro	2/54 (3.70%)	rs224083 (0.013)	0.018	-	-	-	-	unlikely
EGR2	2	c.1086A>C	both	p.Arg362Arg	7/54 het. (13.0%); 1/54 hom. (1.85%)	rs45602133 (0.065)	0.04	-	-	-	Choi et al., 2004; Timmerman et al., 1999	unlikely
GJB1	2	c.839G>C	hemizygous	p.Cys280Ser	1/10 (10%)	-	-	benign	not tolerated	partially conserved	-	likely

APPENDIX IV

Table IV-1: Primer sequences for *PMP22* exon 4 (obtained from Kim et al., 2003) and housekeeping gene *ACTBL2* for confirmation of the Chr17p11.2 duplication in CMT1A cases using SYBR Green I chemistry.

Gene	Ensembl transcript	Exon	Direction	Primer sequence (5' to 3')	Amplicon length (bp)
PMP22	ENST00000312280	4	forward	tctgtccaggccaccatga	75
PMP22	ENST00000312280	4	reverse	gaagagttggcagaagaacagga	
ACTBL2	ENST00000423391	1	forward	ttgagtccagtgggatccat	110
ACTBL2	ENST00000423391	1	reverse	catggtgctccctccagata	

Table IV-2: Sequences of primers used to amplify the *PMP22* upstream promoter region and non-coding exon 1A.

Gene	Ensembl transcript	Fragment	Direction	Primer sequence (5' to 3')	Annealing temperature	PCR protocol	Amplicon length (bp)
PMP22	ENST00000312280	fragment 1	forward	aggcaggtaacagggagtc	62-52°C	Roche	744
PMP22	ENST00000312280	fragment 1	reverse	tcttgtaaagcataggcacac			
PMP22	ENST00000312280	fragment 2	forward	gcttcagttacagggagcacc	62-52°C	Roche	215
PMP22	ENST00000312280	fragment 2	reverse	acatcacccagaggcacagtt			

Table IV-3: Phenotypes of the 187 CMT1A patients who passed the quality control measures in the Immunochip association study. Scores in bold were excluded from the mild versus severe CMT1A, mild CMT1A versus controls and severe CMT1A versus controls analyses.

Gender	AAE	CMTES	Age-corrected CMTES
F	22	6	**-0.364267**
F	42	8	-1.477967
F	15	8	2.725528
M	41	**9**	**-0.322282**
M	57	**9**	-2.813242
M	15	5	**-0.274472**
M	46	2	-8.100707
F	20	1	-5.052897
M	55	12	**0.498128**
M	14	7	1.881213
M	14	3	-2.118787
F	27	0	-7.142692
F	8	5	**0.815323**
M	80	15	**-0.393997**
F	30	2	-5.609747
M	15	12	6.725528
F	56	13	1.342443
F	16	3	-2.430157
F	66	13	**-0.214407**
M	23	**9**	2.480048
M	24	**10**	3.324363
M	56	17	5.342443
M	45	11	1.054978
M	23	6	**-0.519952**
F	48	13	2.587923
M	39	5	-4.010912
F	62	14	1.408333
F	64	17	4.096963
F	73	20	5.695798
F	52	13	1.965183
M	42	**10**	**0.522033**
F	40	14	4.833403
M	36	**9**	**0.456143**
M	58	**10**	-1.968927
M	17	**9**	3.414158
M	44	7	-2.789337
F	33	8	**-0.076802**
M	18	2	-3.741527
F	14	**9**	3.881213
F	54	18	6.653813
M	56	15	3.342443

Gender	AAE	CMTES	Age-corrected CMTES
F	57	17	5.186758
F	59	14	1.875388
M	49	8	-2.567762
M	60	17	4.719703
F	63	11	-1.747352
F	64	**9**	-3.903037
F	43	4	-5.633652
F	46	14	3.899293
F	28	11	3.701623
M	54	8	-3.346187
F	47	8	-2.256392
F	56	**10**	-1.657557
F	58	13	1.031073
M	40	3	-6.166597
F	62	8	-4.591667
F	54	15	3.653813
F	17	**10**	4.414158
F	56	**9**	-2.657557
F	43	11	1.366348
F	65	22	8.941278
M	60	**10**	-2.280297
F	65	11	-2.058722
F	31	8	**0.234568**
F	30	**9**	1.390253
F	42	**9**	**-0.477967**
F	56	**10**	-1.657557
F	62	13	**0.408333**
M	38	8	**-0.855227**
F	47	11	**0.743608**
F	62	13	**0.408333**
M	34	4	-4.232487
F	27	**9**	1.857308
F	40	7	-2.166597
F	41	4	-5.322282
M	43	11	1.366348
M	55	14	2.498128
M	48	1	-9.412077
M	56	17	5.342443
F	54	6	-5.346187
F	53	11	**-0.190502**

Gender	AAE	CMTES	Age-corrected CMTES
F	56	8	-3.657557
M	47	12	1.743608
F	35	**9**	**0.611828**
F	73	14	**-0.304202**
F	63	**9**	-3.747352
F	49	**9**	-1.567762
M	56	12	**0.342443**
F	45	**10**	**0.054978**
M	32	**9**	1.078883
F	66	15	1.785593
F	33	7	-1.076802
M	15	4	-1.274472
M	54	**10**	-1.346187
F	29	11	3.545938
M	45	3	-6.945022
F	37	11	2.300458
M	64	17	4.096963
M	9	2	-2.340362
F	68	3	-10.525777
M	42	12	2.522033
M	8	5	**0.815323**
F	48	8	-2.412077
M	N/A	3	**N/A**
F	40	**10**	**0.833403**
F	N/A	7	**N/A**
F	11	3	-1.651732
M	45	2	-7.945022
M	70	19	5.162853
F	62	15	2.408333
M	53	19	7.809498
F	58	2	-9.968927
M	74	8	-6.459887
M	30	7	**-0.609747**
F	37	14	5.300458
M	61	19	6.564018
M	58	25	13.031073
F	63	6	-6.747352
M	39	13	3.989088
M	67	19	5.629908
F	10	12	7.503953
M	66	17	3.785593

Gender	AAE	CMTES	Age-corrected CMTES
F	64	5	-7.903037
F	42	5	-4.477967
M	73	13	-1.304202
M	25	**10**	3.168678
M	5	4	**0.282378**
M	44	1	-8.789337
M	6	2	-1.873307
F	55	16	4.498128
M	48	13	2.587923
F	42	3	-6.477967
M	55	8	-3.501872
F	38	16	7.144773
F	27	6	-1.142692
M	22	8	1.635733
F	49	14	3.432238
F	29	14	6.545938
M	36	**9**	**0.456143**
M	64	16	3.096963
M	18	**10**	4.258473
M	71	16	2.007168
M	72	15	**0.851483**
M	58	6	-5.968927
F	61	12	**-0.435982**
M	57	15	3.186758
M	63	13	**0.252648**
F	56	14	2.342443
M	43	11	1.366348
M	63	23	10.252648
F	53	5	-6.190502
F	51	11	**0.120868**
F	50	8	-2.723447
M	57	11	**-0.813242**
F	40	5	-4.166597
F	53	19	7.809498
F	22	4	-2.364267
F	46	4	-6.100707
F	48	13	2.587923
M	41	**10**	**0.677718**
F	22	14	7.635733
F	54	**10**	-1.346187
M	32	7	**-0.921117**

Gender	AAE	CMTES	Age-corrected CMTES
F	41	6	-3.322282
M	78	7	-8.082627
F	22	19	12.635733
F	37	17	8.300458
M	68	15	1.474223
F	53	7	-4.190502
M	24	8	1.324363
F	55	12	**0.498128**
M	70	11	-2.837147
M	60	15	2.719703
M	56	15	3.342443
F	40	**10**	**0.833403**
M	20	**9**	2.947103
F	56	7	-4.657557
F	39	11	1.989088
F	47	**10**	**-0.256392**
M	55	21	9.498128
F	36	8	**-0.543857**
M	48	8	-2.412077
M	42	12	2.522033
F	30	12	4.390253
F	29	14	6.545938
M	60	18	5.719703
M	54	19	7.653813

Command lines used in gPLINK for Immunochip file conversion and quality control:

1) To create a BED file set for combined control and CMT1A/CIDP data using "generate fileset" → "standard input" → "select PED and MAP files" ("allow no sex" option is used to ignore gender):

"working directory" --map "MAP file with data" --ped "PED file with data" --allow-no-sex --make-bed --out "name of output file" –gplink

2) To create file with controls only:

“working directory” --keep “Text file with list of control IDs” –bfile “BED file created in step 1” --allow-no-sex --make-bed --out "name of output file" –gplink

3) To apply HWE threshold in BED file with control data:

“working directory” --hwe 0.001 --bfile "BED file with control data created in step 2" --allow-no-sex --make-bed --out “name of output file" –gplink

4) To create a list of SNPs found in the control BED file (after filtering using HWE threshold) using “create plink command”:

“working directory” --bfile "BED file with filtered control data created in step 3" –-allow-no-sex --write-snplist --out "name of output file" –gplink

5) To exclude CMT1A samples which failed the “per individual” quality control measures:

“working directory” --remove “Text file with list of IDs to exclude” –bfile “BED file created in step 1” --allow-no-sex --make-bed --out "name of output file" –gplink

6) To keep only SNPs which passed HWE test in the control dataset (list created in step 4) in the combined controls/CMT1A/CIDP BED file:

“working directory” --extract "SNP list created in step 4" --bfile " BED file created in step 5" --allow-no-sex --make-bed --out "name of output file" --gplink

7) To perform further “per SNP” and “per individual” quality control measures in controls, CIDP and CMT1A (all three combined) including removal of all markers with a very low MAF (MAF<0.01), exclusion of SNPs with a genotype rate below 90%, and removal of all individuals with more than 10% missing genotypes:

“working directory” --maf 0.01 --geno 0.1 --mind 0.1 --bfile "BED file created in step 6" --allow-no-sex --make-bed --out "name of output file" –gplink

8) Using FAM file updated in step 7, modify file as appropriate for association analyses: in fourth column, label cases (or severe cases) as “2”, controls (or mild cases) as “1” and samples to exclude as “-9”.

Command lines used in gPLINK for Immunochip allelic association analyses:

9) To perform allelic association test on entire chip with 95% CI, QQ plot option and 100,000 permutations:

“working directory” --bfile "BED file modified in step 8" --assoc --ci 0.95 --mperm 100000 --adjust --allow-no-sex --qq-plot --out "name of output file" –gplink

10) To select for HLA region:

“working directory” --chr 6 --from-kb 25900 --to-kb 33500 --bfile "BED file modified in step 8" --allow-no-sex --make-bed --out "name of output file" --gplink

11) To perform allelic association test on HLA region with 95% CI, QQ plot option and 100,000 permutations:

“working directory” --bfile "BED file modified in step 10" --assoc --ci 0.95 --mperm 100000 --adjust --allow-no-sex --qq-plot --out "name of output file" –gplink

12) To extract SNPs in LD in HLA region:

“working directory” --bfile "BED file modified in step 10" --indep 50 5 2 --allow-no-sex --out "name of output file" –gplink

13) To keep only pruned in SNPs (SNPs not in LD):

“working directory” --extract "file with prune.in extension created in step 12" --bfile "BED file modified in step 10" --allow-no-sex --make-bed --out "name of output file" --gplink

14) To perform allelic association test on pruned HLA region with 95% CI, QQ plot option and 100,000 permutations:

“working directory” --bfile "BED file created in step 13" --assoc --ci 0.95 --mperm 100000 --adjust --allow-no-sex --qq-plot --out "name of output file" –gplink

Code used in R software package for QQ plot creation:

```
data=read.table("file with .adjusted extension from association analyses in gPLINK", header=TRUE)
data$QQ=-log(data$QQ, 10)
data$UNADJ=-log(data$UNADJ,10)
p <- ggplot(data) +geom_point(aes(x=data$QQ,y=data$UNADJ),alpha=.5) +
  xlab("expected-logP values") + ylab("observed -logP values") +
  labs(title=file) +
  geom_abline(slope = 1, intercept = 0, color="red",size=1)
```

Table IV-4: Results of remaining allelic association analyses on the Immunochip.

CHR	SNP	Gene	Base pair	A1	Mild CMT1A MAF	Controls MAF	1000 Genomes MAF (Europeans)	Severe CMT1A MAF	CIDP MAF	A2	CHISQ	P-value	OR	SE	L95	U95	Pointwise P-value	Genome-wide P-value after 100000 permutations
Mild CMT1A versus controls- whole chip																		
9	rs1933038	Close to DMRT2	1156086	A	0.4348	0.2181	0.272	0.2059	0.2944	G	21.65	0.000003271	2.757	0.2217	1.786	4.258	0.00001	0.2072
15	rs8035074	EHD4	40027071	G	0.6377	0.41	0.45	0.5	0.4879	A	19.63	0.00000942	2.533	0.2125	1.67	3.841	0.00001	0.4708
Mild CMT1A versus controls- HLA region																		
6	rs2859448	Close to MICB	31544252	G	0.3913	0.2133	0.215	0.2588	0.216	A	15.21	9.62E-05	2.371	0.2242	1.527	3.679	0.0003	0.157
6	rs6923313	HLA-B	31349349	G	0.5072	0.33	0.358	0.3588	0.348	A	12.53	0.0004002	2.09	0.2099	1.385	3.154	0.00058	0.4399
Mild CMT1A versus controls- HLA region (pruned)																		
6	rs7750059	Close to COL11A2	33211151	G	0.05147	0	0.768	0.0625	0	A	15.18	9.80E-05	N/A	N/A	N/A	N/A	0.00018	0.06812
6	1kg_6_30524746 /rs4959049	Close to HLA-E	30524746	C	0.05072	0.003333	0.025	0.02941	0.016	A	11.84	0.00058	15.98	1.074	1.946	131.2	0.0039	0.3019
Age-corrected mild CMT1A versus controls- whole chip																		
3	rs12107036	TP63	191082854	A	0.3182	0.5278	0.453	0.5062	0.492	G	16	6.34E-05	0.418	0.221	0.271	0.6439	5.00E-05	0.9789
6	imm_6_106725478 /rs9486298	Close to ATG5	106725478	A	0.2197	0.08333	0.106	0.1543	0.16	C	15.58	7.89E-05	3.097	0.2964	1.733	5.536	6.00E-05	0.9914
Age-corrected mild CMT1A versus controls- HLA region																		
6	rs2859448	Close to HCP5	31544252	G	0.3939	0.2133	0.215	0.2531	0.216	A	15.22	9.55E-05	2.397	0.2271	1.536	3.741	0.00033	0.162
6	rs2844507	Close to HCP5	31544560	A	0.3864	0.2162	0.214	0.2654	0.2114	G	13.45	0.000245	2.282	0.2278	1.46	3.567	0.00052	0.3208
Age-corrected mild CMT1A versus controls- HLA region (pruned)																		
6	1kg_6_30524746/ rs4959049	Close to HLA-E	30524746	C	0.05303	0.003333	0.025	0.03704	0.016	A	12.46	0.0004166	16.74	1.074	2.039	137.5	0.00329	0.2388
6	rs4607472	Close to HLA-G	29918522	G	0.1136	0.03667	0.09	0.1111	0.075	A	9.601	0.001945	3.368	0.4118	1.503	7.55	0.00906	0.6628

Chr: chromosome; SNP: SNP identifier; A1: minor allele; MAF: minor allele frequency; A2: major allele; Chisq: basic allele test Chi-square value; P-value: asymptotic p-value for this test; OR: estimated odds ratio for A1; SE: standard error of estimated odds ratio; L95: lower bound of 95% confidence interval for odds ratio; U95: upper bound of 95% confidence interval for odds ratio; N/A: not available
Groups being compared in each association analysis are coloured in grey; MAFs for corresponding SNPs in other groups are provided for reference.

CHR	SNP	Gene	Base pair	A1	Severe CMT1A MAF	Controls MAF	1000 Genomes MAF (Europeans)	Mild CMT1A MAF	CIDP MAF	A2	CHISQ	P-value	OR	SE	L95	U95	Pointwise P-value	Genome-wide P-value after 100000 permutations
Severe CMT1A versus controls- whole chip																		
6	*rs9258740*	*Close to HLA-G*	*29935878*	*A*	*0.2706*	*0.1007*	*0.194*	0.1884	*0.1585*	*G*	*22.98*	*1.64E-06*	*3.314*	*0.259*	*1.996*	*5.501*	*4.00E-05*	*0.0871*
5	*rs10071484*	*Close to IRX1*	*3742527*	*G*	*0.3471*	*0.1633*	*0.211*	*0.2319*	*0.2*	*A*	*20.7*	*5.38E-06*	*2.723*	*0.224*	*1.754*	*4.227*	*1.00E-05*	*0.2503*
Severe CMT1A versus controls- HLA region																		
6	rs9258740	Close to *HLA-G*	29935878	A	0.2706	0.1007	0.194	0.1884	0.1585	G	22.98	1.64E-06	3.314	0.259	1.996	5.501	1.00E-05	0.0041
Severe CMT1A versus controls- HLA region (pruned)																		
6	*rs4607472*	Close to *HLA-G*	*29918522*	*G*	*0.1176*	*0.03667*	*0.09*	*0.1087*	*0.075*	*A*	*11.55*	*0.00068*	*3.503*	*0.389*	*1.635*	*7.503*	*0.0025*	*0.3024*
6	*1kg_6_30227055*	*Close to TRIM10*	*30227055*	*A*	*0.0765*	*0.01667*	*N/A*	*0.02899*	*0.016*	*G*	*10.54*	*0.00117*	*4.885*	*0.535*	*1.711*	*13.95*	*0.00246*	*0.464*
Age-corrected severe CMT1A versus controls- whole chip																		
6	rs9258740	Close to *HLA-G*	29935878	A	0.284	0.1007	0.194	0.1667	0.1585	G	25.56	4.29E-07	3.543	0.26	2.13	5.893	1.00E-05	0.02545
Age-corrected severe CMT1A versus controls- HLA region																		
6	rs9258740	Close to *HLA-G*	29935878	A	0.284	0.1007	0.194	0.1667	0.1585	G	25.56	4.29E-07	3.543	0.26	2.13	5.893	1.00E-05	0.00121
6	rs2517887	Close to *HLA-G*	29915372	G	0.3272	0.14	0.212	0.1894	0.204	C	22.56	2.04E-06	2.987	0.236	1.881	4.744	2.00E-05	0.00497
6	rs2735003	Close to *HLA-G*	29916613	C	0.3272	0.14	0.212	0.1894	0.204	A	22.56	2.04E-06	2.987	0.236	1.881	4.744	2.00E-05	0.00497
6	rs2735014	Close to *HLA-G*	29913788	A	0.3272	0.1395	0.212	0.1894	0.204	C	22.49	2.12E-06	3	0.238	1.884	4.779	2.00E-05	0.00515
6	rs3893538	*HLA-A*	30032404	G	0.2975	0.1267	0.199	0.1667	0.204	A	19.98	7.84E-06	2.919	0.246	1.803	4.726	3.00E-05	0.01704
Age-corrected severe CMT1A versus controls- HLA region (pruned)																		
6	*1kg_6_30227055*	*Close to TRIM10*	*30227055*	*A*	*0.0864*	*0.01667*	*N/A*	*0.0303*	*0.016*	*G*	*12.98*	*0.00032*	*5.581*	*0.531*	*1.973*	*15.79*	*0.00076*	*0.1609*
6	*rs6924186*	*Close to HLA-A*	*29978801*	*C*	*0.1062*	*0.02685*	*0.053*	*0.04098*	*0.0766*	*A*	*12.72*	*0.00036*	*4.309*	*0.441*	*1.817*	*10.22*	*0.00082*	*0.1785*

Chr: chromosome; SNP: SNP identifier; A1: minor allele; MAF: minor allele frequency; A2: major allele; Chisq: basic allele test Chi-square value; P-value: asymptotic p-value for this test; OR: estimated odds ratio for A1; SE: standard error of estimated odds ratio; L95: lower bound of 95% confidence interval for odds ratio; U95: upper bound of 95% confidence interval for odds ratio; N/A: not available

Groups being compared in each association analysis are coloured in grey; MAFs for corresponding SNPs in other groups are provided for reference.

CHR	SNP	Gene	Base pair	A1	CMT1A MAF ("cases")	CIDP MAF ("controls"	Controls MAF	1000 Genomes MAF (Europeans)	A2	CHISQ	P-value	OR	SE	L95	U95	Pointwise P-value	Genome-wide P-value after 100000 permutations
SNPs in bold in the CMT1A versus CIDP analysis indicate SNPs also significantly associated in the controls versus CIDP analysis																	
CMT1A versus CIDP- whole chip																	
3	**imm_3_58370541**	*PXK*	58370541	G	0.2204	0.5574	0.2333	N/A	A	73.16	1.19E-17	0.2245	0.1796	0.1579	0.3193	1.00E-05	1.00E-05
8	**1kg_8_11183638/ rs4841519**	*MTMR9*	11183638	A	0.2312	0.56	0.2099	0.471	T	69.88	6.29E-17	0.2363	0.1771	0.167	0.3343	1.00E-05	1.00E-05
CMT1A versus CIDP- HLA region																	
6	*rs424232*	*Close to NOTCH4*	*32316302*	*A*	*0.361*	*0.22*	*0.2833*	*0.263*	*G*	*14.06*	*0.0001771*	*2.003*	*0.1868*	*1.389*	*2.888*	*0.0002*	*0.2729*
6	*rs3130304*	*Close to NOTCH4*	*32315159*	*A*	*0.2649*	*0.136*	*0.22*	*0.202*	*G*	*13.85*	*0.0001976*	*2.29*	*0.2263*	*1.469*	*3.568*	*0.00036*	*0.3021*
CMT1A versus CIDP- HLA region (pruned)																	
6	*rs3115630*	*Close to HLA-G*	*29902480*	*A*	*0.03652*	*0.1057*	*0.07667*	*0.095*	*G*	*11.49*	*0.0006999*	*0.3207*	*0.3505*	*0.1613*	*0.6374*	*0.00113*	*0.3559*
6	*1kg_6_30214416*	*TRIM40*	*30214416*	*G*	*0.01872*	*0.072*	*0.01667*	*N/A*	*A*	*11.06*	*0.0008814*	*0.2458*	*0.4533*	*0.1011*	*0.5977*	*0.00499*	*0.4114*

Chr: chromosome; SNP: SNP identifier; A1: minor allele; MAF: minor allele frequency; A2: major allele; Chisq: basic allele test Chi-square value; P-value: asymptotic p-value for this test; OR: estimated odds ratio for A1; SE: standard error of estimated odds ratio; L95: lower bound of 95% confidence interval for odds ratio; U95: upper bound of 95% confidence interval for odds ratio; N/A: not available

Groups being compared in each association analysis are coloured in grey; MAFs for corresponding SNPs in other groups are provided for reference.

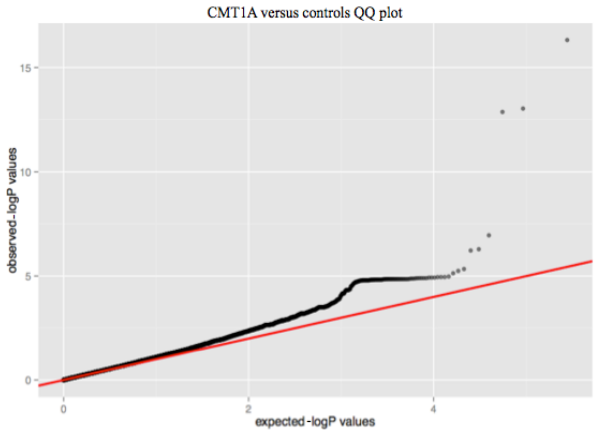
CMT1A versus controls QQ plot
observed -logP values
expected -logP values

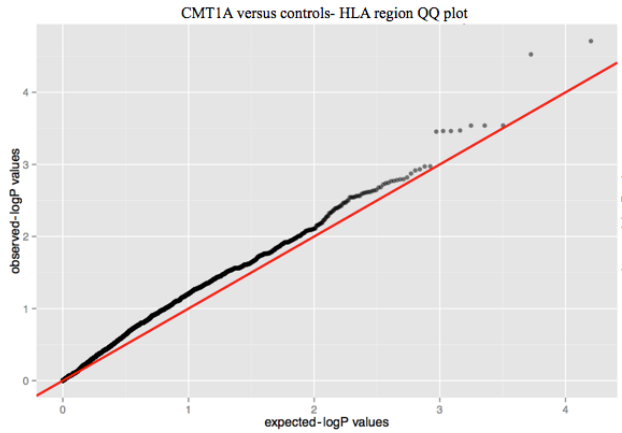
CMT1A versus controls- HLA region QQ plot
observed -logP values
expected -logP values

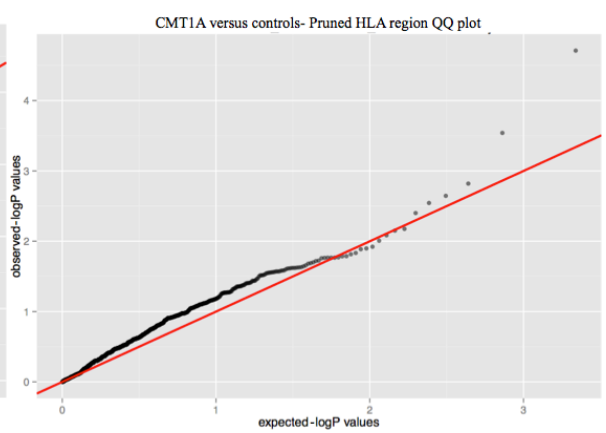
CMT1A versus controls- Pruned HLA region QQ plot
observed -logP values
expected -logP values

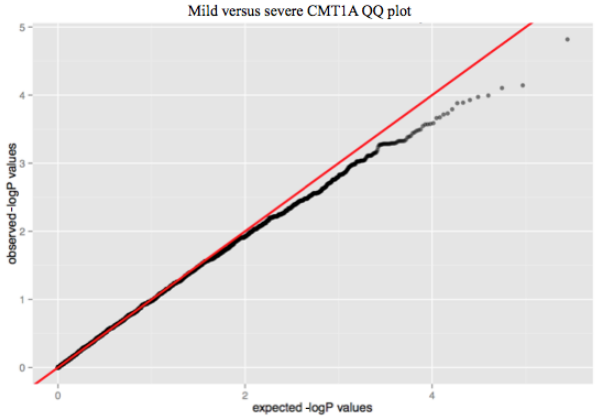
Mild versus severe CMT1A QQ plot
observed -logP values
expected -logP values

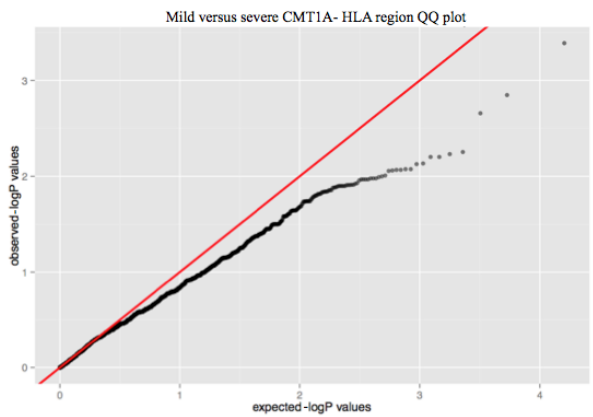
Mild versus severe CMT1A- HLA region QQ plot
observed -logP values
expected -logP values

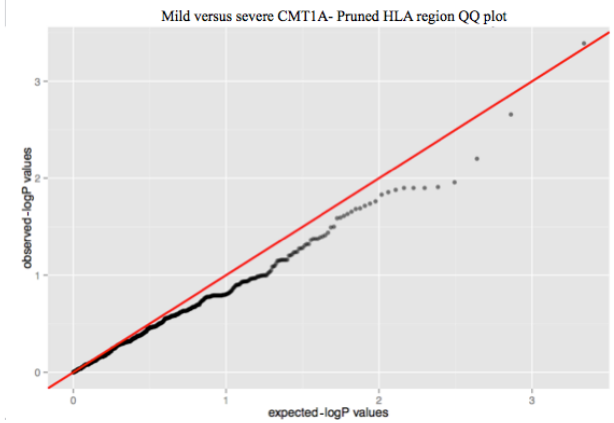
Mild versus severe CMT1A- Pruned HLA region QQ plot
observed -logP values
expected -logP values

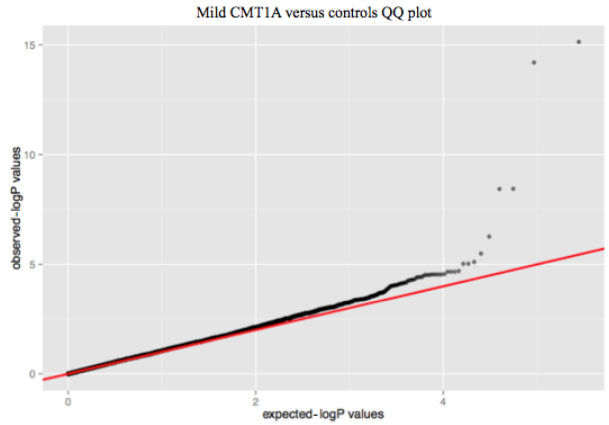
Mild CMT1A versus controls QQ plot
observed -logP values
expected -logP values

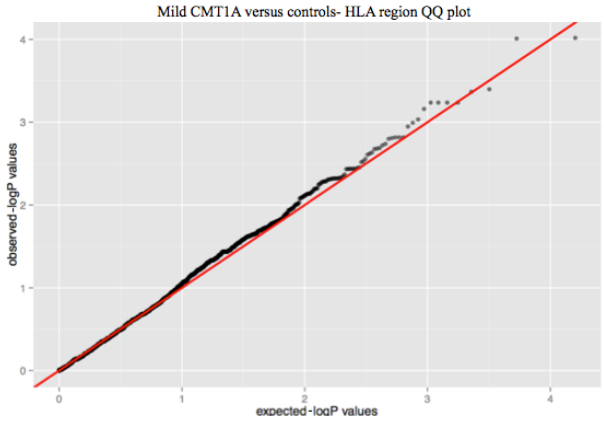
Mild CMT1A versus controls- HLA region QQ plot
observed -logP values
expected -logP values

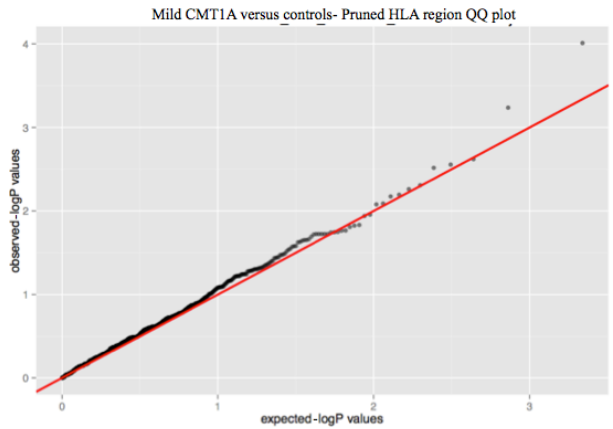
Mild CMT1A versus controls- Pruned HLA region QQ plot
observed -logP values
expected -logP values

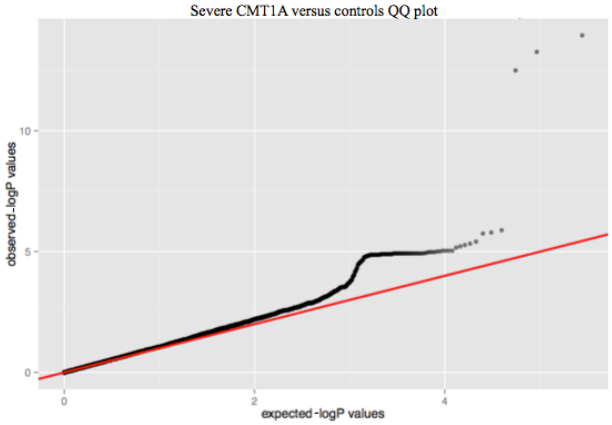
Severe CMT1A versus controls QQ plot
observed -logP values
expected -logP values

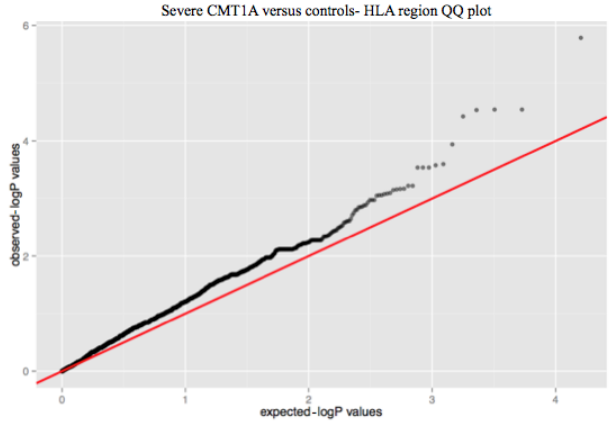
Severe CMT1A versus controls- HLA region QQ plot
observed -logP values
expected -logP values

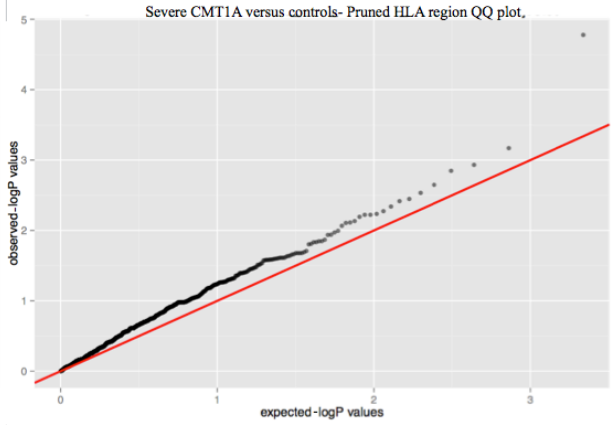
Severe CMT1A versus controls- Pruned HLA region QQ plot,
observed -logP values
expected -logP values

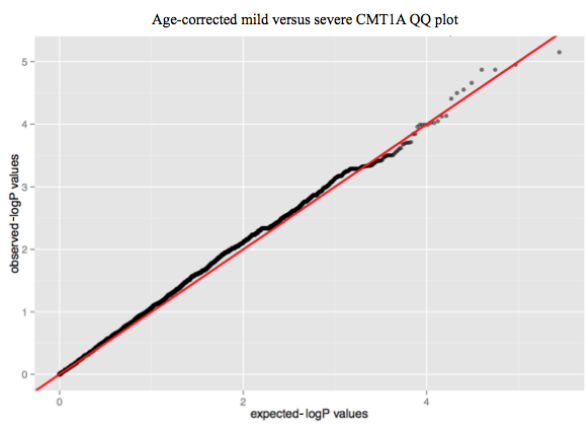
Age-corrected mild versus severe CMT1A QQ plot
observed -logP values
expected -logP values

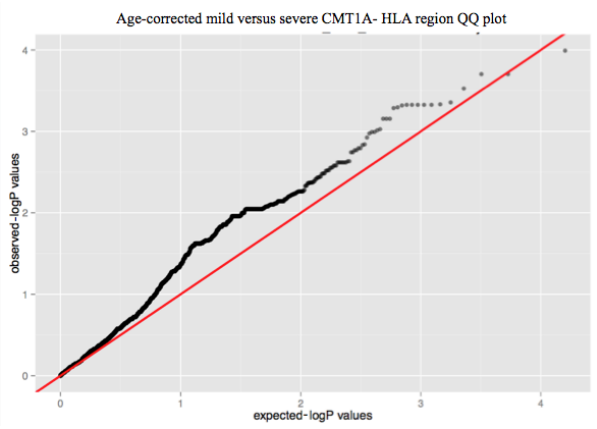
Age-corrected mild versus severe CMT1A- HLA region QQ plot
observed -logP values
expected -logP values

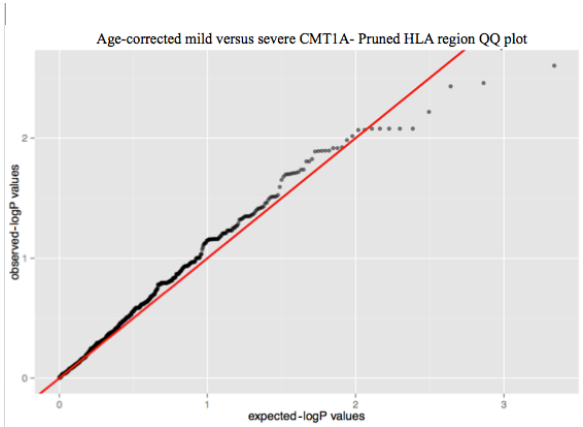
Age-corrected mild versus severe CMT1A- Pruned HLA region QQ plot
observed -logP values
expected -logP values

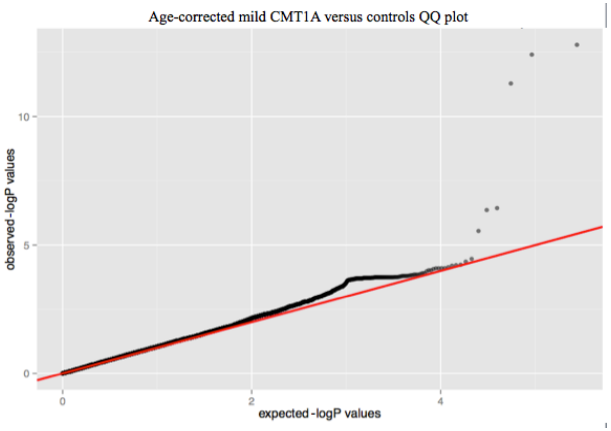
Age-corrected mild CMT1A versus controls QQ plot
observed -logP values
expected -logP values

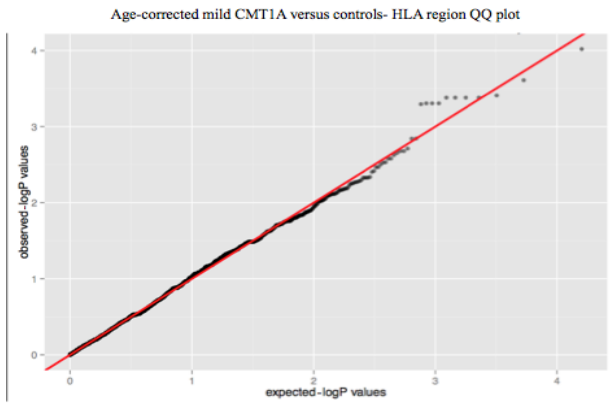
Age-corrected mild CMT1A versus controls- HLA region QQ plot
observed -logP values
expected -logP values

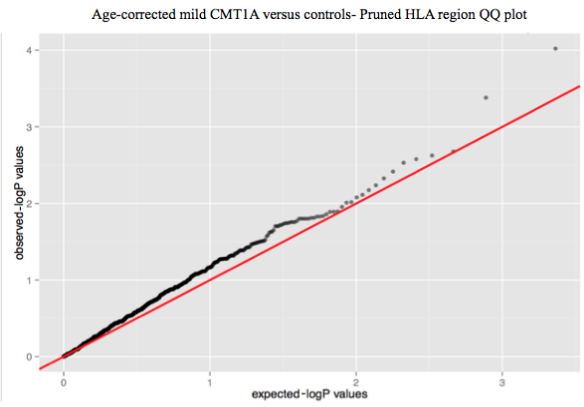
Age-corrected mild CMT1A versus controls- Pruned HLA region QQ plot
observed -logP values
expected -logP values

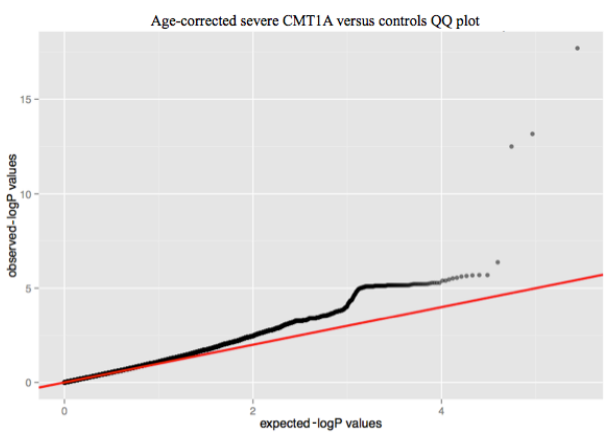
Age-corrected severe CMT1A versus controls QQ plot
observed -logP values
expected -logP values

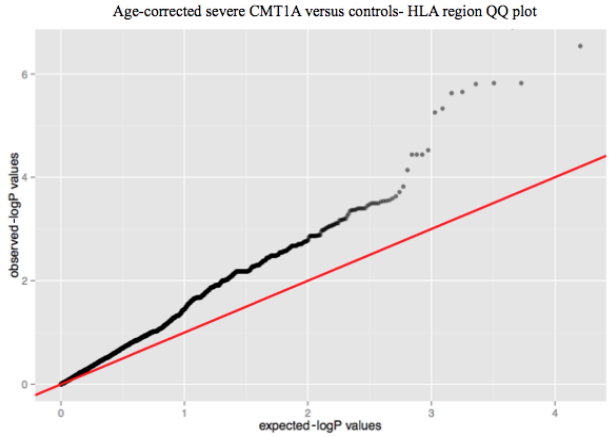
Age-corrected severe CMT1A versus controls- HLA region QQ plot
observed -logP values
expected -logP values

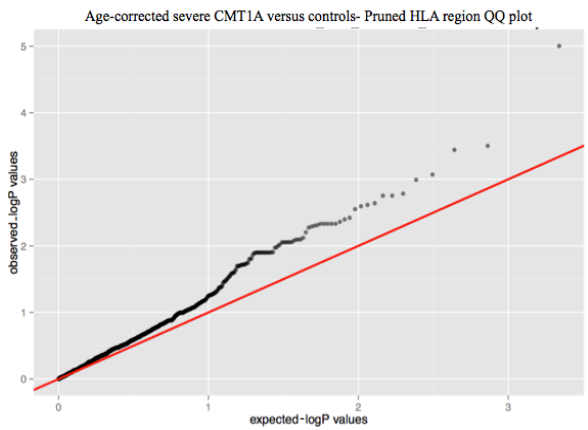
Age-corrected severe CMT1A versus controls- Pruned HLA region QQ plot
observed -logP values
expected -logP values

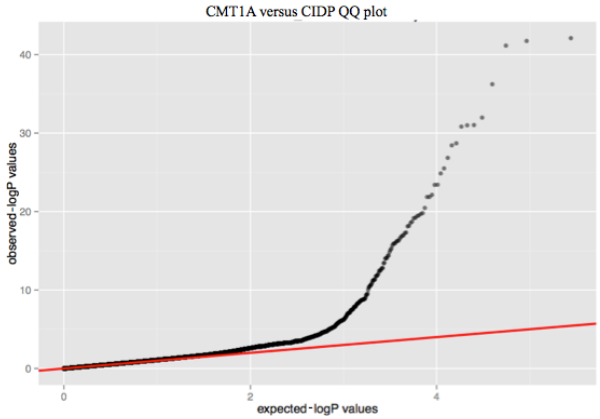
CMT1A versus CIDP QQ plot
observed -logP values
expected -logP values

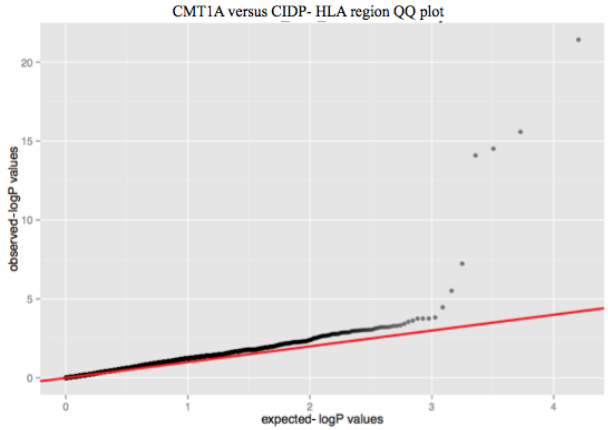
CMT1A versus CIDP- HLA region QQ plot
observed -logP values
expected- logP values

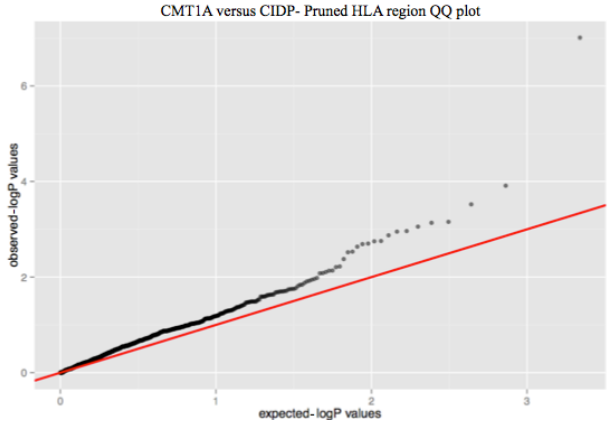
CMT1A versus CIDP- Pruned HLA region QQ plot
observed -logP values
expected- logP values

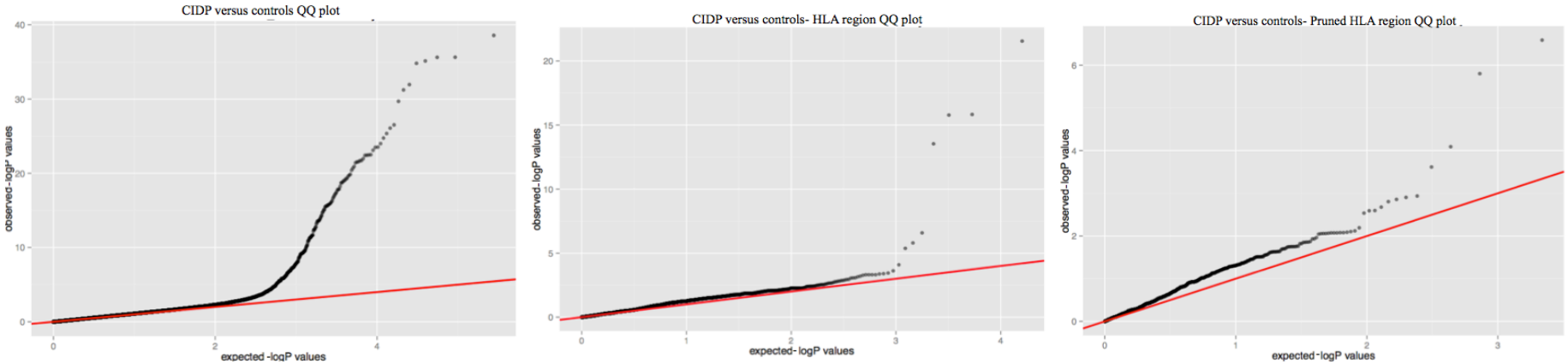

Figure IV-1: QQ plots generated for further quality control of Immunochip allelic association analyses.

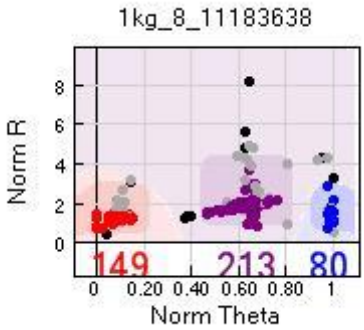

Call rate: 93.8%

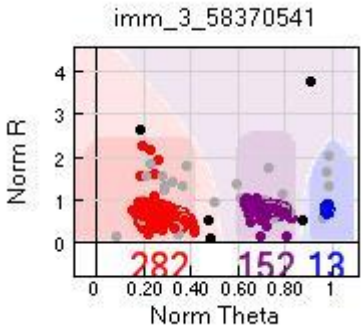

Call rate: 94.9%

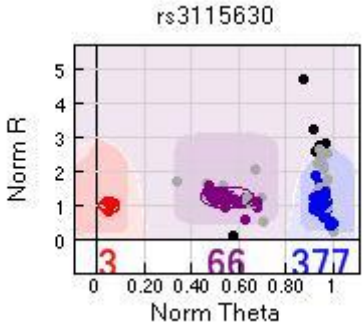

Call rate: 94.7%

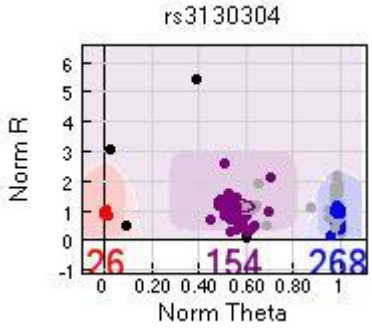

Call rate: 95.1%

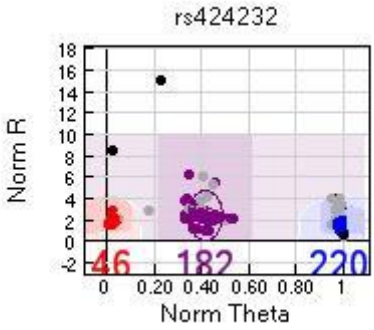

Call rate: 95.1%

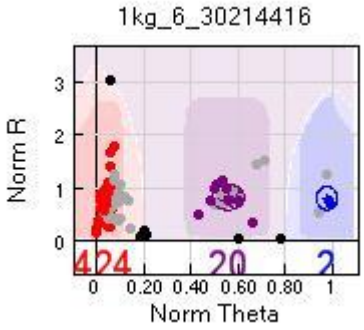

Call rate: 94.7%

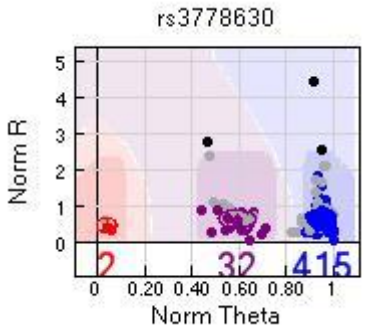

Call rate: 95.3%

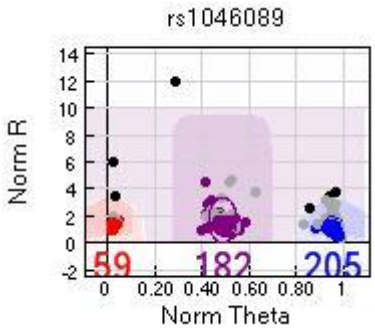

Call rate: 94.7%

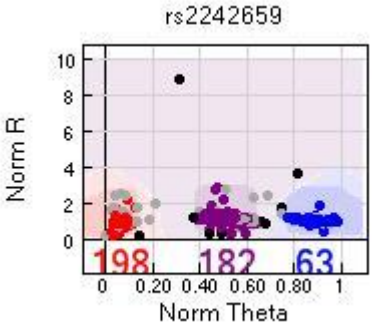

Call rate: 94.1%

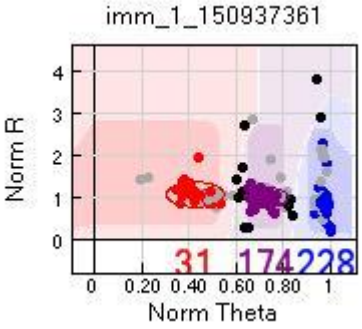

Call rate: 91.9%

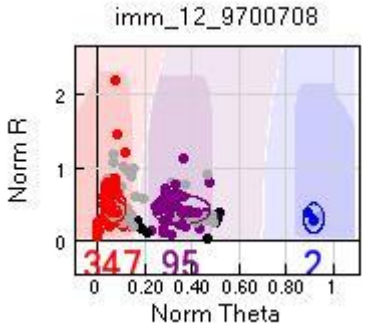

Call rate: 94.3%

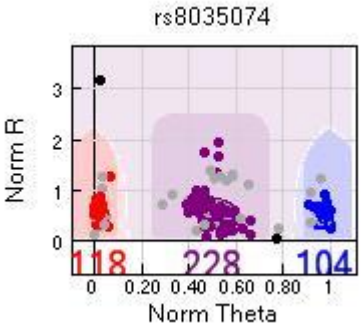

Call rate: 95.5%

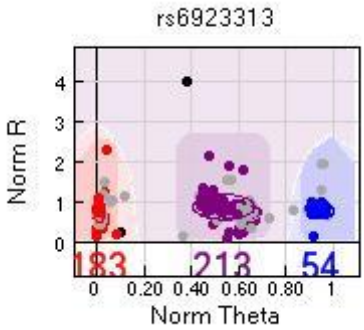

Call rate: 95.5%

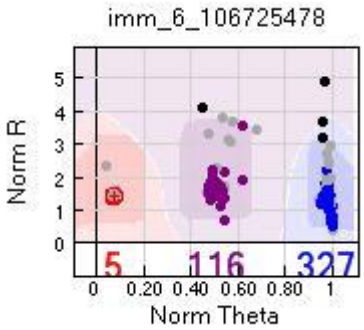

Call rate: 95.1%

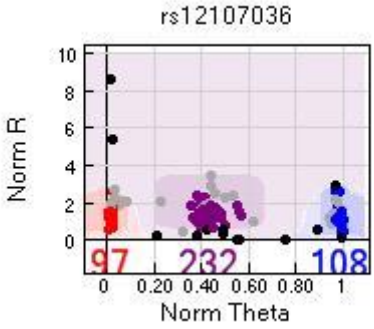

Call rate: 92.8%

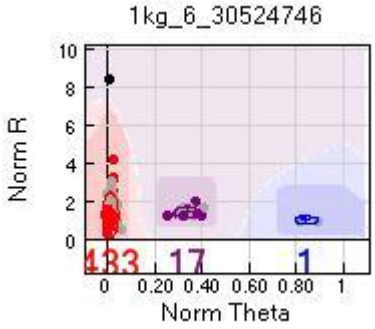

Call rate: 95.8%

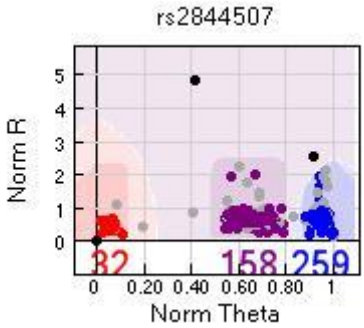

Call rate: 95.3%

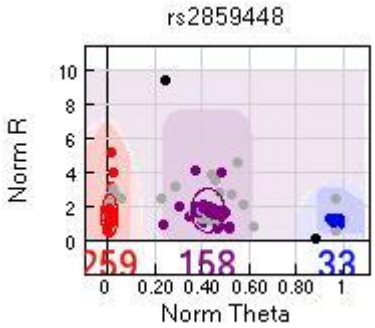

Call rate: 95.5%

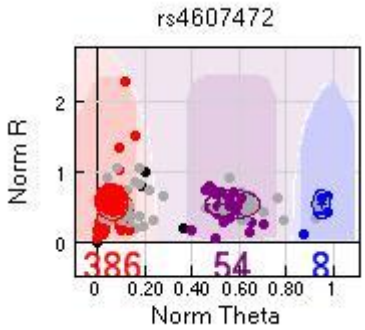

Call rate: 95.1%

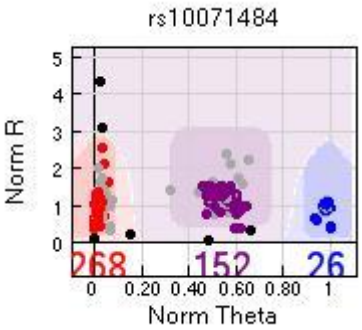

Call rate: 94.7%

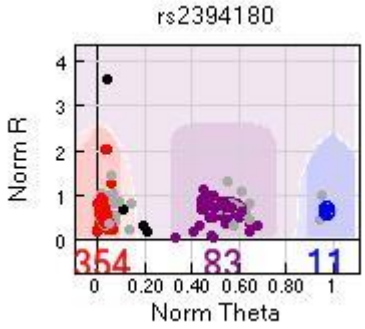

Call rate: 95.1%

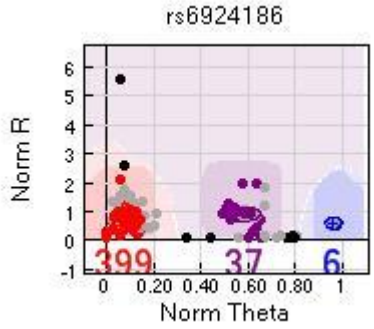

Call rate: 93.8%

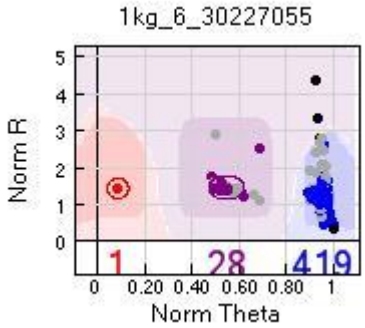

Call rate: 95.1%

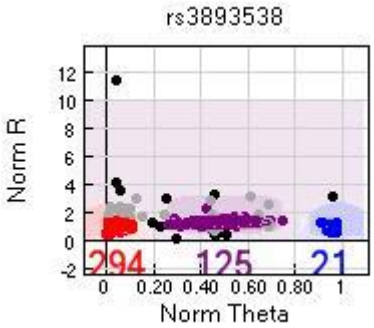

Call rate: 93.4%

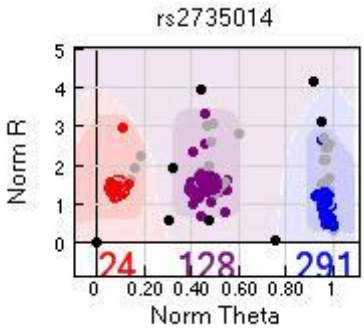

Call rate: 94.1%

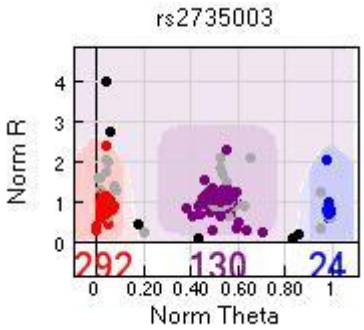

Call rate: 94.7%

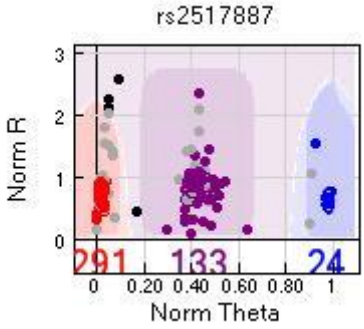

Call rate: 95.1%

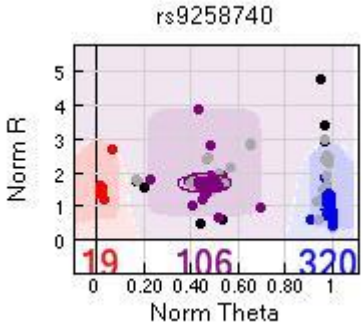

Call rate: 94.5%

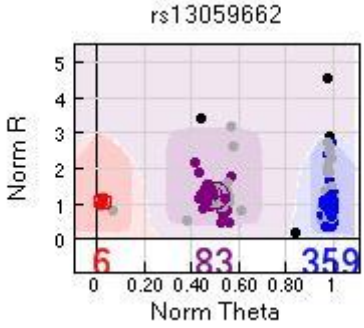

Call rate: 95.1%

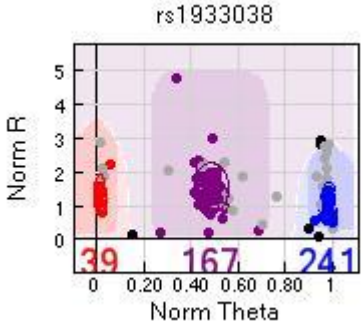

Call rate: 94.9%

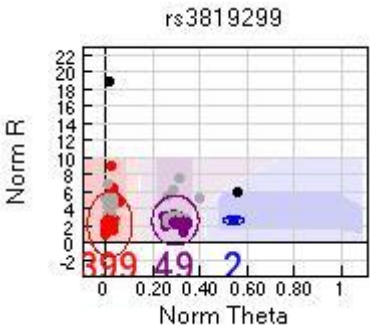

Call rate: 95.5%

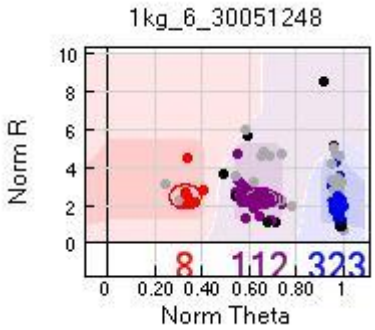

Call rate: 94.1%

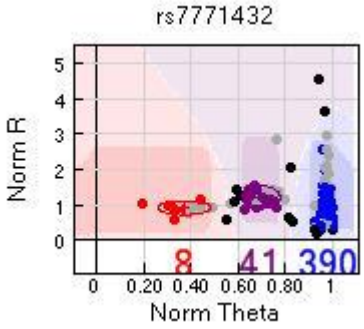

Call rate: 93.2%

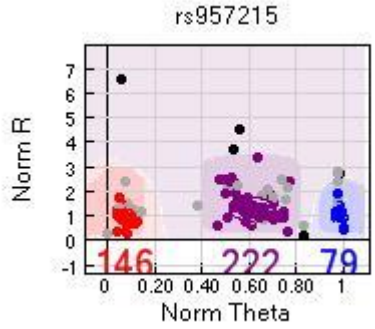

Call rate: 94.9%

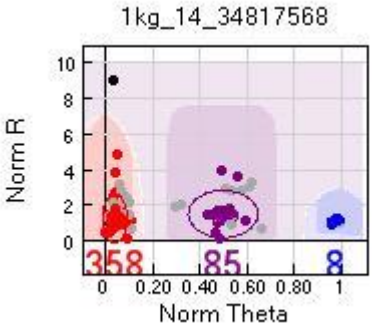

Call rate: 95.8%

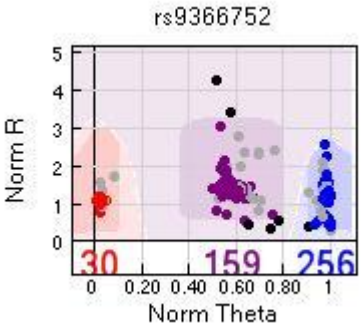

Call rate: 94.5%

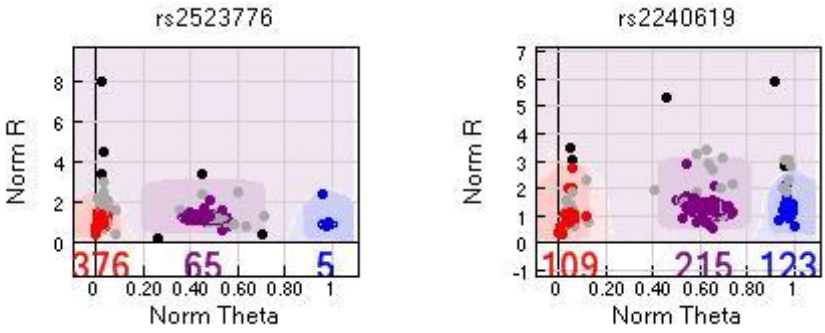

Call rate: 94.7%

Call rate: 94.9%

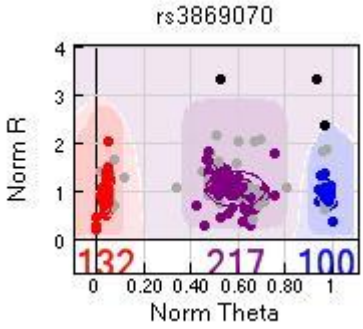

Call rate: 95.3%

Figure IV-2: SNP cluster plots and call rates of all top hits (SNPs) in the Immunochip allelic association analyses (from GenomeStudio). Dots in red, purple and blue represent the three possible genotypes; dots in grey represent individuals excluded by quality control measures; dots in black represent a SNP which did not fit in any of the three genotype clusters in an individual (genotype was not called for this SNP for this individual).

APPENDIX V

Table V-1: Transcript references used for primer design, as well as primer sequences and PCR cycling conditions for *MFF* primers.

Gene	Ensembl transcript	Exon	Direction	Primer sequence (5' to 3')	Annealing temperature	PCR protocol	Amplicon length (bp)
MFF	ENST00000353339	3	forward	ttcaaatccaaaagtcattttacg	65-60°C	Roche	399
MFF	ENST00000353339	3	reverse	ccgccaatacaaaagctgat			
MFF	ENST00000353339	4	forward	tgagaagtttcctttcgctctt	65-60°C	Roche	440
MFF	ENST00000353339	4	reverse	tgcattttccaactccttttc			
MFF	ENST00000353339	5	forward	tgggtggtataattcaaaagca	65-60°C	Roche	390
MFF	ENST00000353339	5	reverse	aagctttcatgacatattgctaaaga			
MFF	ENST00000353339	6	forward	gcaattcttggttgcctttt	65-60°C	Roche	394
MFF	ENST00000353339	6	reverse	gaccaacaaaatggccaga			
MFF	ENST00000353339	7	forward	gggtatgagagcaggagcac	65-60°C	Roche	398
MFF	ENST00000353339	7	reverse	tttgagaaatcctgaaacagagg			
MFF	ENST00000353339	8	forward	ggaaaggggcaagaacacta	65-60°C	Roche	400
MFF	ENST00000353339	8	reverse	gctgtttcaaatcattgcatct			
MFF	ENST00000353339	9	forward	ggaggacacatgagacaagga	65-60°C	Roche	356
MFF	ENST00000353339	9	reverse	tcgaggaaagctgtagaaacaa			
MFF	ENST00000353339	10	forward	tgtagacagttgtcattttaagctttt	65-60°C	Roche	389
MFF	ENST00000353339	10	reverse	tttgatagtcccacaggagagaa			
MFF	ENST00000353339	11	forward	caaatgaaactttccatgtttgt	65-60°C	Roche	357
MFF	ENST00000353339	11	reverse	tggcatacaatgcagagaca			

Table V-2: Coverage in neuropathy genes in individuals II-1 and II-3 of CMT family IS (only genes with at least one poorly covered exon are shown).

Gene	Poorly covered exon(s)
PMP22	exon 2
MPZ	exon 1
NEFL	exon 1
NDRG1	exon 16
PRX	exons 5 and 7
FIG4	exon 1
CTDP1	exon 8
GARS	exon 1
DNM2	exons 1 and 21
DYNC1H1	exon 1
LRSAM1	exons 10, 16, and 25
SPTLC2	exon 1
LMNA	exon 1
MTMR13	exon 1
IGHMBP2	exons 1 and 9 to 11
PDK3	exon 12
SEPT9	exons 1, 7, 9
DNMT1	poor coverage throughout
HSP27	exon 1
KIF1A	poor coverage throughout
KIF5A	exons 12, 14, 16, 21, 24, 26 a nd 28

Table V-3: Coverage in neuropathy genes in individual II-1 of family AD (only genes with at least one poorly covered exon are shown).

Gene	Poorly covered exon(s)
PMP22	exon 2
NEFL	exon 1
EGR2	exon 3
NDRG1	exon 16
PRX	poor coverage throughout
FIG4	exon 1
CTDP1	exon 8
TRPV4	exon 11
GARS	exon 1
DNM2	exons 1 and 21
DYNC1H1	exon 1
LRSAM1	exons 16 and 25
SPTLC1	exon 1
SPTLC2	exon 1
HARS	exon 1
LMNA	poor coverage throughout
MTMR13	exon 1
IGHMBP2	poor coverage throughout
PDK3	exon 1
MARS	exon 1
SEPT9	poor coverage throughout
DNMT1	poor coverage throughout
HSP27	exon 1
KIF1A	poor coverage throughout

Table V-4: Variants identified in *MFF* candidate gene in CMT2/dHMN/HSP patients.

Gene	Nucleotide substitution	Amino acid change	dbSNP ID	1000 Genomes MAF
MFF	c.19A>T	p.Ser7Cys	rs3211097	0.196
MFF	c.363G>A	p.Thr121Thr	rs11557342	0.074
MFF	c.921A>G	p.Leu307Leu	rs74713223	0.147

APPENDIX VI

Table VI-1: Reported pathogenic mutations found in the homozygous or compound heterozygous state in *SLC52A1*, *SLC52A2* and *SLC52A3* (adapted from Bosch et al., 2012). *c.106G>A and c.1237T>C were found in the cis configuration; only the c.106G>A change was predicted to be pathogenic. **considered unlikely to be pathogenic and/or found in unaffected individuals. ***found in the heterozygous state; no other mutation found in gene. ****c.1127A>G and c.1203instT were found in the cis configuration.

Gene	Exon	Nucleotide substitution	Mutation type	Amino acid change	Predicted region	References
SLC52A1	2-3	Deletion of exons 2-3	Deletion	Unknown	N/A	Ho et al., 2010
SLC52A2	2	c.155C>T	Non-synonymous	p.Ser52Phe	Transmembrane	Ciccolella et al., 2013
SLC52A2	3	c.368T>C	Non-synonymous	p.Leu123Pro	Transmembrane	Haack et al., 2012
SLC52A2	3	c.916G>A	Non-synonymous	p.Gly306Arg	Extracellular loop	Johnson et al., 2012
SLC52A2	3	c.1016T>C	Non-synonymous	p.Leu339Pro	Transmembrane	Haack et al., 2012
SLC52A2	5	c.1255G>A	Non-synonymous	p.Gly419Ser	Transmembrane	Ciccolella et al., 2013
SLC52A3	2	c.49T>C	Non-synonymous	p.Trp17Arg	Transmembrane	Bosch et al., 2011
SLC52A3	2	c.62A>G	Non-synonymous	p.Asn21Ser	Transmembrane	Dezfouli et al., 2012
SLC52A3	2	c.82C>A	Non-synonymous	p.Pro28Thr	Extracellular loop	Johnson et al., 2010
SLC52A3	2	c.106G>A*	Non-synonymous	p.Glu36Lys	Extracellular loop	Green et al., 2010
SLC52A3	2	c.160G>A	Non-synonymous	p.Gly54Arg	Transmembrane	Johnson et al., 2012
SLC52A3	2	c.173T>A	Non-synonymous	p.Val58Asp	Transmembrane	Ciccolella et al., 2012
SLC52A3	2	c.211G>A	Non-synonymous	p.Glu71Lys	Intracellular loop	Johnson et al., 2010
SLC52A3	2	c.211G>T	Stop-gained	p.Glu71Stop	Intracellular loop	Green et al., 2010
SLC52A3	2	c.224T>C	Non-synonymous	p.Ile75Thr	Transmembrane	Johnson et al., 2012
SLC52A3	2	c.394C>T	Non-synonymous	p.Arg132Trp	Intracellular loop	Green et al., 2010
SLC52A3	Intron 2-3	c.568-18_19 insCTGATTGAC**	Insertion	Unknown	N/A	Ciccolella et al., 2012
SLC52A3	3	c.639C>G	Stop-gained	p.Tyr213Stop	Extracellular loop	Bosch et al., 2011; Green et al., 2010; Johnson et al., 2010
SLC52A3	3	c.659C>A***	Non-synonymous	p.Pro220His	Extracellular loop	Dezfouli et al., 2012
SLC52A3	3	c.670T>C	Non-synonymous	p.Phe224Leu	Transmembrane	Green et al., 2010
SLC52A3	3	c.796C>T	Non-synonymous	p.Arg266Trp	Intracellular loop	Ciccolella et al., 2012
SLC52A3	3	c.935C>T	Non-synonymous	p.Ala312Val	Transmembrane	Dezfouli et al., 2012
SLC52A3	3	c.955C>T	Non-synonymous	p.Pro319Ser	Extracellular loop	Ciccolella et al., 2012
SLC52A3	3	c.989G>T	Non-synonymous	p.Gly330Val	Extracellular loop	Koy et al., 2012
SLC52A3	3	c.1048T>A*	Non-synonymous	p.Leu350Met	Transmembrane	Green et al., 2010
SLC52A3	4	c.1081C>G**	Non-synonymous	p.Leu361Val	Intracellular loop	Bandettini Di Poggio et al., 2013
SLC52A3	4	c.1124G>A***	Non-synonymous	p.Gly375Asp	Transmembrane	Dezfouli et al., 2012
SLC52A3	4	c.1127A>G****	Non-synonymous	pTyr376Cys	Transmembrane	Bandettini Di Poggio et al., 2013
SLC52A3	Intron 4-5	c.1198-2A>G	Splicing change	Unknown	N/A	Bosch et al., 2011
SLC52A3	5	c.1203insT****	Frameshift insertion	Protein 56 amino acids longer than WT	Transmembrane	Bandettini Di Poggio et al., 2013
SLC52A3	5	c.1237T>C*	Non-synonymous	p.Val413Ala	Transmembrane	Green et al., 2010
SLC52A3	5	c.1238T>C	Non-synonymous	p.Val413Ala	Transmembrane	Ciccolella et al., 2012
SLC52A3	5	c.1296C>A***	Stop-gained	p.Cys432Stop	Transmembrane	Ciccolella et al., 2012
SLC52A3	5	c.1325_1326delTG	Frameshift deletion	p.Leu442ArgfsX35	Transmembrane	Green et al., 2010
SLC52A3	5	c.1371C>G	Non-synonymous	p.Phe457Leu	Extracellular tail	Green et al., 2010; Johnson et al., 2012
SLC52A3	Unknown	Unknown	Frameshift mutation	Unknown	Unknown	Spagnoli et al., 2014
SLC52A3	Unknown	Unknown	Non-synonymous	Unknown	Unknown	Spagnoli et al., 2014
SLC52A3	Unknown	Unknown	Unknown	Unknown	Unknown	Anand et al., 2012

Table VI-2: Polymorphisms reported in *SLC52A1*, *SLC52A2*, and *SLC52A3* in the UCL HEX, EVS, dbSNP and 1000 Genomes databases.

Gene	dbSNP ID	Position	Alleles	Type	Amino acid change	HEX genotype count	EVS MAF (%)	dbSNP/1000 Genomes MAF
SLC52A1	rs200539588	4936262	C/A	non-synonymous	C446F	N/A	N/A	0.001
SLC52A1	rs377601117	4936272	C/A	non-synonymous	V443L	N/A	0.0077	N/A
SLC52A1	rs148979394	4936278	C/G	non-synonymous	D441H	N/A	0.0846	0.002
SLC52A1	rs72822610	4936336	A/T	synonymous	L421L	AA=130/AT=49/TT=3	14.1	0.115
SLC52A1	rs148131990	4936339	C/T	synonymous	L420L	N/A	N/A	0.001
SLC52A1	rs202032568	4936345	G/A	synonymous	G418G	N/A	N/A	0.001
SLC52A1	rs147687964	4936358	G/A	non-synonymous	A414V	N/A	0.0077	N/A
SLC52A1	rs142353672	4936359	C/T	non-synonymous	A414T	N/A	0.0077	N/A
SLC52A1	rs112874988	4936370	G/T	non-synonymous	A410E	N/A	0.0538	0.001
SLC52A1	rs148063153	4936376	A/G	non-synonymous	L408S	N/A	0.077	N/A
SLC52A1	rs373765126	4936382	G/A	non-synonymous	P406L	N/A	0.0154	N/A
SLC52A1	rs377522935	4936403	A/G	non-synonymous	L399P	N/A	0.0077	N/A
SLC52A1	rs187609896	4936443	G/C	non-synonymous	L386V	N/A	N/A	0.002
SLC52A1	rs201578619	4936457	G/A	non-synonymous	S381L	N/A	N/A	0.002
SLC52A1	rs370773962	4936460	A/G	non-synonymous	L380P	N/A	0.077	N/A
SLC52A1	N/A	4936468	C/T	splice variant	N/A	N/A	N/A	N/A
SLC52A1	rs192857700	4936572	G/A	non-synonymous	A373V	N/A	N/A	N/A
SLC52A1	rs140906879	4936585	C/T	non-synonymous	V369M	N/A	0.077	N/A
SLC52A1	rs200594561	4936587	A/G	non-synonymous	L368P	N/A	N/A	0.002
SLC52A1	N/A	4936597	N/A	frameshift	C365Afs*28	N/A	0.0479	N/A
SLC52A1	N/A	4936627	N/A	frameshift	Y355Tfs*2	N/A	0.1678	N/A
SLC52A1	rs375892458	4936667	C/T	synonymous	G341G	N/A	0.0077	N/A
SLC52A1	rs150164483	4936784	C/T	non-synonymous	V334M	N/A	0.0231	0.001
SLC52A1	rs374646797	4936785	G/A	synonymous	G333G	N/A	0.0077	N/A
SLC52A1	rs184838357	4936793	C/G	non-synonymous	A331P	N/A	N/A	0.001
SLC52A1	rs200412989	4936813	T/G	non-synonymous	N324T	N/A	N/A	0.001
SLC52A1	rs140073463	4936818	G/A	synonymous	A322A	N/A	N/A	0.001
SLC52A1	rs9897165	4936855	C/T	non-synonymous	R310H	N/A	0.8458	0.006
SLC52A1	rs141719111	4936861	T/C	non-synonymous	Y308C	N/A	0.0538	N/A
SLC52A1	rs2304445	4936898	C/T	non-synonymous	V296M	CC=132/CT=44/TT=6	15.44	0.268
SLC52A1	rs367746302	4936899	G/A	synonymous	G295G	N/A	0.0077	N/A
SLC52A1	N/A	4936934	N/A	insertion	L283_G284 insL	N/A	0.008	N/A
SLC52A1	rs137917213	4936969	T/A	non-synonymous	H272L	N/A	0.0308	N/A
SLC52A1	rs346821	4936972	G/A	non-synonymous	A271V	GG=24/GA=75/AA=83	31.1779	0.445
SLC52A1	rs371915134	4936980	G/A	synonymous	D268D	N/A	0.0077	N/A
SLC52A1	rs143848711	4936984	G/A	non-synonymous	P267L	N/A	0.0077	N/A
SLC52A1	rs200049864	4937013	C/T	synonymous	P257P	N/A	N/A	0.001
SLC52A1	rs199704379	4937014	G/A	non-synonymous	P257L	N/A	0.0077	N/A
SLC52A1	rs148611457	4937029	G/A	non-synonymous	P252L	N/A	0.0154	N/A
SLC52A1	rs369106349	4937051	T/C	non-synonymous	K245E	N/A	0.0077	N/A
SLC52A1	rs142480426	4937067	T/C	synonymous	G239G	N/A	0.0077	N/A
SLC52A1	rs150901297	4937075	A/G	non-synonymous	S237P	N/A	0.0154	N/A
SLC52A1	rs373793198	4937105	C/T	non-synonymous	G227R	N/A	0.0077	N/A
SLC52A1	rs377338075	4937149	C/T	non-synonymous	R212Q	N/A	0.0077	N/A
SLC52A1	rs370188723	4937150	G/A	non-synonymous	R212W	N/A	0.0077	N/A
SLC52A1	rs373142659	4937151	G/A	synonymous	F211F	N/A	0.0077	N/A
SLC52A1	rs376918815	4937153	A/G	non-synonymous	F211L	N/A	0.0077	N/A
SLC52A1	rs139373407	4937156	C/T	non-synonymous	A210T	N/A	0.0384	0.001
SLC52A1	rs145524474	4937169	G/C	synonymous	V205V	N/A	0.0154	N/A
SLC52A1	N/A	4937196	N/A	frameshift	F196Sfs*5	N/A	0.016	N/A

SLC52A1	rs200459465	4937203	C/T	non-synonymous	S194N	N/A	N/A	0.001
SLC52A1	rs147698089	4937222	G/A	non-synonymous	P188S	N/A	0.0077	N/A
SLC52A1	rs142091289	4937231	G/A	non-synonymous	L185F	N/A	N/A	0.001
SLC52A1	rs144716094	4937274	G/A	synonymous	L170L	N/A	0.1538	0.001
SLC52A1	rs201198708	4937279	G/A	non-synonymous	R169C	N/A	N/A	0.001
SLC52A1	rs374197009	4937311	G/A	non-synonymous	P158L	N/A	0.0077	N/A
SLC52A1	rs368344539	4937331	C/G	non-synonymous	Q151H	N/A	0.0154	N/A
SLC52A1	rs370325558	4937349	C/T	synonymous	R145R	N/A	0.0077	N/A
SLC52A1	rs374174324	4937350	C/T	non-synonymous	R145Q	N/A	0.0077	N/A
SLC52A1	rs56126318	4937351	G/T	synonymous	R145R	GG=157/GT=24/TT=1	6.3125	0.07
SLC52A1	rs200268874	4937368	A/G	non-synonymous	L139P	N/A	N/A	N/A
SLC52A1	rs148924968	4937379	G/A	synonymous	F135F	N/A	0.0077	N/A
SLC52A1	rs143199804	4937388	G/C	non-synonymous	F132L	N/A	0.0077	N/A
SLC52A1	rs146289149	4937413	G/A	non-synonymous	A124V	N/A	0.5382	0.009
SLC52A1	rs140348114	4937414	C/T	non-synonymous	A124T	N/A	0.0077	N/A
SLC52A1	rs368167047	4937420	C/T	non-synonymous	A122T	N/A	0.0077	N/A
SLC52A1	rs371340617	4937481	G/A	synonymous	H101H	N/A	0.0077	N/A
SLC52A1	N/A	4937481	G/C	non-synonymous	H101Q	GG=180/GC=2/CC=0	N/A	N/A
SLC52A1	rs375943631	4937492	G/A	synonymous	L98L	N/A	0.0077	N/A
SLC52A1	rs187721459	4937505	G/A	synonymous	A93A	N/A	0.0077	0.001
SLC52A1	rs145407203	4937534	C/T	non-synonymous	V84I	CC=181/CT=1/TT=0	N/A	N/A
SLC52A1	N/A	4937539	N/A	frameshift	Q82Gfs*47	N/A	0.008	N/A
SLC52A1	rs376978383	4937555	C/T	non-synonymous	E77K	N/A	0.0077	N/A
SLC52A1	rs201983129	4937565	C/T	synonymous	P73P	N/A	0.0077	0.002
SLC52A1	rs137937212	4937566	G/A	non-synonymous	P73L	N/A	0.0077	N/A
SLC52A1	rs346822	4937575	T/C	non-synonymous	Q70R	TT=0/TC=18/CC=164	4.498	0.074
SLC52A1	rs150112294	4937576	G/A	stop-gained	Q70*	N/A	0.0077	N/A
SLC52A1	rs201707443	4937595	C/T	synonymous	L63L	N/A	N/A	0.001
SLC52A1	rs138410039	4937617	G/A	non-synonymous	A56V	N/A	0.1384	N/A
SLC52A1	rs200242588	4937777	G/A	non-synonymous	P42L	N/A	N/A	N/A
SLC52A1	rs372498524	4937779	A/G	synonymous	L41L	N/A	0.0077	N/A
SLC52A1	rs199742635	4937817	C/T	non-synonymous	G29R	N/A	N/A	0.001
SLC52A1	rs377033431	4937818	G/A	synonymous	N28N	N/A	0.0077	N/A
SLC52A1	rs201477941	4937879	C/T	non-synonymous	R8H	N/A	0.0077	0.001

Gene	dbSNP ID	Position	Alleles	Type	Amino acid change	HEX genotype count	EVS MAF (%)	dbSNP/1000 Genomes MAF
SLC52A2	rs141698844	145583036	A/G	non-synonymous	N28S	N/A	0.0308	0.001
SLC52A2	rs200102613	145583037	T/C	synonymous	N28N	N/A	N/A	0.002
SLC52A2	rs150137023	145583309	G/C	non-synonymous	V53L	N/A	0.0077	N/A
SLC52A2	rs372988060	145583329	C/T	synonymous	N59N	N/A	0.0077	N/A
SLC52A2	rs201213634	145583330	C/T	synonymous	L60L	N/A	N/A	0.001
SLC52A2	rs201246554	145583344	G/C	synonymous	V64V	N/A	N/A	0.001
SLC52A2	rs111588500	145583380	C/T	synonymous	D76D	N/A	0.123	0.002
SLC52A2	rs377110942	145583397	G/A	non-synonymous	R82Q	N/A	0.077	N/A
SLC52A2	N/A	145583444	N/A	frameshift	H100Pfs*13	N/A	0.0399	N/A
SLC52A2	rs146256291	145583461	C/T	synonymous	A103A	N/A	N/A	0.002
SLC52A2	rs376031054	145583470	A/G	synonymous	A106A	N/A	0.0077	N/A
SLC52A2	rs370812676	145583504	G/A	non-synonymous	A118T	N/A	0.0077	N/A
SLC52A2	rs117500243	145583505	C/A	non-synonymous	A118D	CC=181/CA=1/AA=0	0.3076	0.002
SLC52A2	rs74445699	145583511	T/C	non-synonymous	V120A	N/A	N/A	0.004
SLC52A2	rs146274588	145583522	G/T	non-synonymous	A124S	N/A	N/A	N/A
SLC52A2	rs200753132	145583523	C/T	non-synonymous	A124V	N/A	N/A	0.001
SLC52A2	rs374071862	145583535	C/T	non-synonymous	S128L	N/A	0.0154	N/A
SLC52A2	rs140003920	145583536	G/A	synonymous	S128S	N/A	0.0384	N/A

SLC52A2	rs199864300	145583562	G/A	non-synonymous	S137N	N/A	N/A	N/A
SLC52A2	rs377740960	145583573	C/T	non-synonymous	P141S	N/A	0.0077	N/A
SLC52A2	rs371376526	145583608	C/T	synonymous	G152G	N/A	0.0077	N/A
SLC52A2	rs376026812	145583615	G/T	non-synonymous	A155S	N/A	0.0077	N/A
SLC52A2	rs141953803	145583630	G/A	non-synonymous	V160M	N/A	0.0154	N/A
SLC52A2	rs142879103	145583686	C/T	synonymous	N178N	N/A	0.0077	N/A
SLC52A2	rs151081625	145583687	G/A	non-synonymous	G179S	N/A	0.0615	0.001
SLC52A2	rs202232509	145583703	C/A	non-synonymous	P184Q	N/A	N/A	0.001
SLC52A2	rs74370046	145583707	C/T	synonymous	L185L	N/A	0.0615	0.023
SLC52A2	rs201705744	145583720	C/T	non-synonymous	R190C	N/A	N/A	0.001
SLC52A2	rs200455766	145583750	C/T	synonymous	L200L	N/A	N/A	0.001
SLC52A2	rs187632310	145583758	C/T	synonymous	A202A	N/A	N/A	0.001
SLC52A2	rs144883729	145583765	G/A	non-synonymous	V205I	N/A	0.0154	N/A
SLC52A2	rs367886725	145583787	A/T	non-synonymous	Q212L	N/A	0.0077	N/A
SLC52A2	rs147954962	145583795	C/T	synonymous	L215L	N/A	0.1	0.001
SLC52A2	rs370367859	145583802	T/A	non-synonymous	L217Q	N/A	0.0077	N/A
SLC52A2	rs374006728	145583808	C/T	non-synonymous	P219L	N/A	0.0077	N/A
SLC52A2	rs141909863	145583809	G/A	synonymous	P219P	N/A	0.0077	N/A
SLC52A2	rs367852733	145583841	G/A	non-synonymous	G230E	N/A	0.0077	N/A
SLC52A2	rs373923619	145583861	G/C	non-synonymous	A237P	N/A	0.0077	N/A
SLC52A2	rs200533281	145583932	C/T	synonymous	T260T	N/A	N/A	0.001
SLC52A2	rs372057075	145583958	A/G	non-synonymous	Y269C	N/A	0.0077	N/A
SLC52A2	rs375088539	145583960	C/T	stop-gained	Q270*	N/A	0.0077	N/A
SLC52A2	rs145009003	145583974	C/A	synonymous	A274A	N/A	0.0077	N/A
SLC52A2	rs144912258	145583976	G/A	non-synonymous	R275H	N/A	0.0692	N/A
SLC52A2	rs368287241	145584004	C/T	synonymous	A284A	N/A	0.0077	N/A
SLC52A2	rs372376214	145584033	T/C	non-synonymous	L294P	N/A	0.0077	N/A
SLC52A2	rs375399467	145584040	C/T	synonymous	A296A	N/A	0.0077	N/A
SLC52A2	rs369031014	145584048	G/C	non-synonymous	S299T	N/A	0.0077	N/A
SLC52A2	rs149050347	145584070	G/A	synonymous	G306G	N/A	0.0077	N/A
SLC52A2	rs143091206	145584072	G/A	non-synonymous	R307H	N/A	0.0385	0.001
SLC52A2	rs370929795	145584100	G/A	synonymous	L316L	N/A	0.0154	N/A
SLC52A2	rs371669411	145584131	C/G	non-synonymous	L327V	N/A	0.0077	N/A
SLC52A2	rs148234606	145584264	T/C	non-synonymous	L339P	N/A	0.0154	N/A
SLC52A2	rs140307485	145584265	G/C	synonymous	L339L	N/A	0.0077	N/A
SLC52A2	rs145502954	145584287	G/A	non-synonymous	V347M	N/A	0.1	0.001
SLC52A2	N/A	145584295	N/A	frameshift	G351Afs*3	N/A	0.008	N/A
SLC52A2	rs200618841	145584313	G/T	synonymous	A355A	N/A	N/A	0.001
SLC52A2	rs138107380	145584314	C/T	synonymous	L356L	N/A	0.1076	N/A
SLC52A2	rs142697341	145584322	C/T	synonymous	V358V	N/A	0.0308	N/A
SLC52A2	rs146292053	145584337	G/A	synonymous	P363P	GG=178/GA=1 /AA=1	0.2384	0.005
SLC52A2	rs138160033	145584354	C/T	non-synonymous	S369L	N/A	0.0154	N/A
SLC52A2	rs149575570	145584361	G/A	synonymous	G371G	N/A	0.0231	N/A
SLC52A2	rs374615555	145584362	G/T	non-synonymous	V372L	N/A	0.0077	N/A
SLC52A2	rs200631895	145584364	G/C	synonymous	V372V	N/A	N/A	0.001
SLC52A2	rs200245353	145584366	T/G	non-synonymous	V373G	N/A	N/A	0.002
SLC52A2	rs144290224	145584370	C/T	synonymous	L374L	N/A	0.0615	0.002
SLC52A2	rs71691497	145584373	N/A	deletion	N/A	N/A	N/A	N/A
SLC52A2	rs376552382	145584490	G/A	non-synonymous	V385M	N/A	0.0077	N/A
SLC52A2	rs148754028	145584500	A/G	non-synonymous	Y388C	N/A	0.0461	0.001
SLC52A2	rs370533575	145584501	C/T	synonymous	Y388Y	N/A	0.0077	N/A
SLC52A2	rs374011301	145584510	G/A	synonymous	V391V	N/A	0.0231	N/A
SLC52A2	rs368448590	145584528	G/A	synonymous	L397L	N/A	0.0077	N/A
SLC52A2	rs144821688	145584534	C/T	synonymous	G399G	N/A	0.0077	N/A
SLC52A2	rs371806077	145584541	C/T	non-synonymous	R402W	N/A	0.0077	N/A
SLC52A2	rs374612342	145584546	G/A	synonymous	P403P	N/A	0.0077	N/A
SLC52A2	rs368749792	145584558	A/T	synonymous	A407A	N/A	0.0077	N/A
SLC52A2	rs371456902	145584561	C/T	synonymous	A408A	N/A	0.0077	N/A
SLC52A2	rs147518188	145584564	C/T	synonymous	G409G	N/A	0.0154	0.001
SLC52A2	rs140177553	145584576	G/A	synonymous	Q413Q	N/A	0.0077	N/A
SLC52A2	rs199767089	145584594	C/T	synonymous	G419G	N/A	0.0077	0.001
SLC52A2	rs368924997	145584595	G/A	non-synonymous	A420T	N/A	0.0077	N/A
SLC52A2	N/A	145584601	N/A	frameshift	A422Vfs*67	N/A	0.008	N/A

SLC52A2	rs201673476	145584614	C/T	non-synonymous	P426L	CC=181/CT=1/TT=0	N/A	0.001
SLC52A2	rs184190914	145584630	C/T	synonymous	H431H	N/A	N/A	0.001
SLC52A2	rs202178971	145584631	G/A	non-synonymous	V432M	N/A	N/A	0.001
SLC52A2	rs372200881	145584644	G/A	non-synonymous	R436K	N/A	0.0077	N/A
SLC52A2	rs189845609	145584657	A/G	synonymous	A440A	N/A	N/A	0.001
SLC52A2	rs75165898	145584658	G/T	non-synonymous	D441Y	N/A	N/A	N/A

Gene	dbSNP ID	Position	Alleles	Type	Amino acid change	HEX genotype count	EVS MAF (%)	dbSNP/1000 Genomes MAF
SLC52A3	rs369872639	741694	G/T	non-synonymous	F462L	N/A	0.008	N/A
SLC52A3	rs140360713	741699	C/A	non-synonymous	D461Y	CC=172/CA=1/AA=0	0.0397	0.002
SLC52A3	N/A	741706	C/A	synonymous	S458S	CC=172/CA=1/AA=0	N/A	N/A
SLC52A3	rs145431028	741709	G/C	non-synonymous	F457L	N/A	0.0548	N/A
SLC52A3	rs371883183	741741	T/C	non-synonymous	M447V	N/A	0.0078	N/A
SLC52A3	rs138169890	741760	C/T	synonymous	S440S	N/A	0.0078	N/A
SLC52A3	rs149534355	741792	A/G	synonymous	L430L	N/A	0.0234	N/A
SLC52A3	rs113063693	741796	G/A	non-synonymous	A428A	N/A	N/A	N/A
SLC52A3	rs139137879	741802	G/A	synonymous	R426R	N/A	0.0234	0.001
SLC52A3	rs369230517	741810	G/A	non-synonymous	L424F	N/A	0.0078	N/A
SLC52A3	rs200665228	741815	C/G	non-synonymous	R422P	N/A	N/A	0.001
SLC52A3	rs267606687	741842	A/G	non-synonymous	V413A	N/A	N/A	N/A
SLC52A3	rs910857	741847	A/G	synonymous	S411S	AA=24/AG=58/GG=95	29.77	0.392
SLC52A3	rs370820845	742370	C/T	non-synonymous	G391D	N/A	0.0077	N/A
SLC52A3	rs374085235	742426	G/A	synonymous	C372C	N/A	0.0077	N/A
SLC52A3	rs148181353	742440	C/T	non-synonymous	V368M	N/A	0.0077	N/A
SLC52A3	rs367957442	742459	C/G	synonymous	L361L	N/A	0.0077	N/A
SLC52A3	rs76947760	744167	A/T	non-synonymous	L350M	N/A	1.6992	0.018
SLC52A3	rs147369439	744168	C/T	synonymous	S349S	CC=181/CT=1/TT=0	0.0769	0.002
SLC52A3	rs139542858	744206	C/T	non-synonymous	A337T	N/A	0.0077	N/A
SLC52A3	rs376546378	744228	A/G	synonymous	Y329Y	N/A	0.0154	N/A
SLC52A3	rs62641669	744234	C/G	synonymous	L327L	N/A	0.1076	0.016
SLC52A3	rs368434500	744246	G/A	synonymous	T323T	N/A	0.0077	N/A
SLC52A3	rs147508914	744261	C/T	synonymous	L318L	N/A	0.0077	N/A
SLC52A3	rs200604650	744263	G/A	synonymous	L318L	N/A	N/A	0.001
SLC52A3	rs372400886	744269	C/T	non-synonymous	G316S	N/A	0.0077	N/A
SLC52A3	rs139430185	744270	G/A	synonymous	N315N	N/A	0.0308	N/A
SLC52A3	rs6054602	744279	C/T	synonymous	A312A	N/A	0.1153	0.002
SLC52A3	rs374661714	744281	C/T	non-synonymous	A312T	N/A	0.0077	N/A
SLC52A3	rs145194879	744287	C/T	non-synonymous	V310I	N/A	0.0154	N/A
SLC52A3	rs201254395	744301	G/T	non-synonymous	T305N	N/A	N/A	0.001
SLC52A3	rs3746802	744308	T/C	non-synonymous	I303V	TT=141.TC=41/CC=0	9.9185	0.096
SLC52A3	rs373350870	744324	C/T	synonymous	P297P	N/A	0.0077	N/A
SLC52A3	rs201990981	744325	G/A	non-synonymous	P297L	N/A	0.0231	N/A
SLC52A3	rs142265627	744350	C/T	non-synonymous	E289K	N/A	0.0692	N/A
SLC52A3	rs3746803	744382	G/A	non-synonymous	T278M	GG=141/GA=41/AA=0	9.9185	0.093
SLC52A3	rs374137295	744389	C/A	non-synonymous	A276S	N/A	0.0077	N/A
SLC52A3	rs377559449	744401	C/G	non-synonymous	D272H	N/A	0.0077	N/A
SLC52A3	rs111912321	744412	C/T	non-synonymous	R268Q	N/A	N/A	N/A
SLC52A3	rs145498634	744413	G/T	synonymous	R268R	N/A	0.0461	N/A
SLC52A3	rs146474751	744414	C/T	synonymous	P267P	N/A	0.0231	N/A
SLC52A3	rs3746804	744415	G/A	non-synonymous	P267L	GG=108/GA=69/AA=5	19.61	0.213
SLC52A3	rs370499474	744419	G/A	non-synonymous	R266W	N/A	0.0077	N/A
SLC52A3	rs150159842	744428	G/A	non-synonymous	H263Y	N/A	0.0154	N/A

SLC52A3	rs3746805	744450	G/A	synonymous	L255L	GG=43/GA=108/AA=31	37.52	0.323
SLC52A3	rs199909033	744453	G/T	non-synonymous	D254E	N/A	N/A	0.001
SLC52A3	rs192438170	744462	G/A	synonymous	S251S	N/A	0.0077	0.001
SLC52A3	rs148832841	744482	G/T	non-synonymous	P245T	N/A	0.0077	N/A
SLC52A3	rs183391382	744504	C/T	synonymous	A237A	N/A	N/A	0.001
SLC52A3	rs3746806	744510	G/A	synonymous	L235L	N/A	1.0995	0.014
SLC52A3	rs369075038	744522	C/G	non-synonymous	M231I	N/A	0.0077	N/A
SLC52A3	rs373044162	744527	T/G	non-synonymous	M230L	N/A	0.0077	N/A
SLC52A3	rs143511669	744539	G/A	non-synonymous	L226F	N/A	0.0077	N/A
SLC52A3	rs267606685	744545	A/G	non-synonymous	F224L	N/A	N/A	N/A
SLC52A3	rs202130911	744569	C/T	non-synonymous	A216T	N/A	N/A	0.001
SLC52A3	rs6054605	744570	G/A	synonymous	P215P	GG=160/GA=22/AA=00	4.8901	0.135
SLC52A3	rs16992990	744615	G/A	synonymous	P200P	GG=177/GA=5/AA=0	0.7388	0.021
SLC52A3	rs142019192	744618	G/A	synonymous	L199L	N/A	0.0231	N/A
SLC52A3	rs113864305	745868	T/C	non-synonymous	E184G	N/A	N/A	N/A
SLC52A3	rs150702278	745871	C/T	non-synonymous	R183K	N/A	0.0077	N/A
SLC52A3	rs139965967	745873	C/T	synonymous	T182T	N/A	0.0846	N/A
SLC52A3	rs201100567	745874	G/A	non-synonymous	T182M	N/A	N/A	0.001
SLC52A3	rs143641819	745894	G/A	synonymous	S175S	N/A	0.0154	N/A
SLC52A3	rs6054614	745898	T/C	non-synonymous	D174G	N/A	1.0918	0.008
SLC52A3	rs201479216	745905	T/C	non-synonymous	I172V	N/A	N/A	0.001
SLC52A3	rs139629967	745908	C/T	non-synonymous	E171K	N/A	0.0077	N/A
SLC52A3	rs200356747	745912	G/A	non-synonymous	V169V	N/A	N/A	0.001
SLC52A3	rs112034541	745920	C/T	non-synonymous	V167I	N/A	0.0154	N/A
SLC52A3	rs377618514	745921	G/A	synonymous	C166C	N/A	0.0077	N/A
SLC52A3	rs113754514	745936	G/A	synonymous	S161S	N/A	N/A	N/A
SLC52A3	rs199778195	745941	C/T	non-synonymous	G160S	N/A	N/A	0.001
SLC52A3	rs3746807	745963	G/A	synonymous	P152P	GG=144/GA=38/AA=0	10.63	0.13
SLC52A3	rs146492942	745971	G/A	non-synonymous	L150F	N/A	0.0077	N/A
SLC52A3	rs149076913	745981	T/C	synonymous	G146G	N/A	0.0154	0.001
SLC52A3	rs142157418	746024	C/T	non-synonymous	R132Q	N/A	0.0077	0.001
SLC52A3	rs267606684	746025	G/A	non-synonymous	R132W	N/A	N/A	N/A
SLC52A3	rs11477762	746051	G/-	frameshift	N/A	N/A	N/A	N/A
SLC52A3	rs151229044	746080	G/A	synonymous	F113F	N/A	0.0461	N/A
SLC52A3	rs140391358	746091	C/A	non-synonymous	V110F	N/A	0.0077	N/A
SLC52A3	rs3746808	746098	G/A	synonymous	A107A	GG=81/GA=80/AA=21	25.57	0.252
SLC52A3	rs370718326	746100	C/T	non-synonymous	A107T	N/A	0.0077	N/A
SLC52A3	rs201152444	746108	T/C	non-synonymous	H104R	N/A	N/A	0.001
SLC52A3	rs137861276	746116	G/A	synonymous	D101D	N/A	0.0154	N/A
SLC52A3	rs369152341	746125	C/G	non-synonymous	W98C	N/A	0.0077	N/A
SLC52A3	rs142064992	746169	C/T	non-synonymous	V84I	N/A	0.0077	N/A
SLC52A3	rs200606057	746170	G/A	synonymous	T83T	N/A	0.0077	0.001
SLC52A3	rs34376836	746179	G/A	synonymous	G80G	N/A	1.3872	0.011
SLC52A3	rs35655964	746197	G/C	non-synonymous	I74M	GG=147/GC=35/CC=0	6.9526	0.04
SLC52A3	rs267606683	746208	C/A	stop-gained	E71*	N/A	N/A	N/A
SLC52A3	rs149622425	746216	C/G	non-synonymous	C68S	N/A	0.0154	N/A
SLC52A3	rs144337813	746225	C/T	non-synonymous	R65Q	N/A	0.0077	N/A
SLC52A3	rs373887707	746284	C/T	synonymous	T45T	N/A	0.0154	N/A
SLC52A3	rs267606686	746313	C/T	non-synonymous	E36K	N/A	N/A	N/A
SLC52A3	rs199861879	746322	C/G	non-synonymous	E33Q	N/A	N/A	0.001
SLC52A3	rs267606688	746337	G/T	non-synonymous	P28T	N/A	N/A	N/A
SLC52A3	rs199588390	746357	T/C	non-synonymous	N21S	N/A	0.01254	0.001
SLC52A3	rs148387972	746361	T/G	non-synonymous	I20L	TT=181/TG=1/GG=0	0.0231	N/A
SLC52A3	rs142206705	746371	G/C	synonymous	S16S	N/A	0.0077	N/A
SLC52A3	rs146302587	746382	C/G	non-synonymous	G13R	N/A	0.0077	N/A
SLC52A3	rs201545356	746389	G/A	synonymous	C10C	N/A	N/A	0.001
SLC52A3	rs139486822	746410	G/A	synonymous	F3F	GG=178/GA=2/AA=0	0.8077	0.007

Table VI-3: Transcript references used for primer design, as well as primer sequences and PCR cycling conditions for *SLC52A1*, *SLC52A2* and *SLC52A3* primers. *This primer has a common SNP (rs35655964) therefore primers were redesigned; primer pairs labelled exon 2-1, exon 2-2B and exon 2-3 were subsequently used to cover exon 2 in *SLC52A3*.

Gene	Ensembl transcript	Exon/primer pair	Direction	Primer sequence (5' to 3')	Annealing temperature	PCR protocol	Amplicon length (bp)
SLC52A1	ENST00000254853	primer pair 1	forward	agcatctttggacctacc	65-60°C	Roche	539
SLC52A1	ENST00000254853	primer pair 1	reverse	taggaaggccacagagtg			
SLC52A1	ENST00000254853	primer pair 2	forward	gcctgtggtggtaaaagacc	65-60°C	Roche	485
SLC52A1	ENST00000254853	primer pair 2	reverse	tagggcactgagaccctgac			
SLC52A1	ENST00000254853	primer pair 3	forward	ctgagtgtagtgggcacag	65-60°C	Roche	579
SLC52A1	ENST00000254853	primer pair 3	reverse	accatgggctgagaacag			
SLC52A1	ENST00000254853	primer pair 4	forward	aggaagaagaggctttgc	65-60°C	Roche	610
SLC52A1	ENST00000254853	primer pair 4	reverse	acacagacacagcacccac			
SLC52A1	ENST00000254853	primer pair 5	forward	gagcaagtggagacatgaag	65-60°C	Roche	354
SLC52A1	ENST00000254853	primer pair 5	reverse	agcctcacgatgaagacag			
SLC52A2	ENST00000329994	exon 2	forward	cagttcccctggtctcacc	65-60°C	Roche	410
SLC52A2	ENST00000329994	exon 2	reverse	caccctctggaagctctctg			
SLC52A2	ENST00000329994	exon 3-1	forward	gcaggtgtgcccaagact	65-60°C	Roche	626
SLC52A2	ENST00000329994	exon 3-1	reverse	gaaaacgctcaaggaagtcg			
SLC52A2	ENST00000329994	exon 3-2	forward	atgctgtgcctcgaatgtc	65-60°C	Roche	386
SLC52A2	ENST00000329994	exon 3-2	reverse	gctcttgcagtggtgaggac			
SLC52A2	ENST00000329994	exon 3-3	forward	ccaccaccatctgtacccac	65-60°C	Roche	433
SLC52A2	ENST00000329994	exon 3-3	reverse	gagcgagcagaatgtcagg			
SLC52A2	ENST00000329994	exon 4	forward	gcttttcctgcttaccctacg	65-60°C	Roche	450
SLC52A2	ENST00000329994	exon 4	reverse	gagaacacgccaagacacag			
SLC52A2	ENST00000329994	exon 5	forward	gtggtcctcgtggtgagc	65-60°C	Roche	387
SLC52A2	ENST00000329994	exon 5	reverse	caggcactcaggcatgg			
SLC52A3	ENST00000217254	exon 2-1	forward	tcacaggaaggggagtaataag	65-60°C	Roche	445
SLC52A3	ENST00000217254	exon 2-1	reverse	ccagcacccaggaggtc			
SLC52A3	ENST00000217254	exon 2-2	forward	tccgaagtgcccatcatc*	65-60°C	Roche	454
SLC52A3	ENST00000217254	exon 2-2	reverse	agaaggatggaggtgagcag			
SLC52A3	ENST00000217254	exon 2-2B	forward	ctgcaggctgatctgagaaa	65-60°C	Roche	497
SLC52A3	ENST00000217254	exon 2-2B	reverse	agaggccgctgagtcctt			
SLC52A3	ENST00000217254	exon 2-3	forward	accctgctccatcacttcc	65-60°C	Roche	498
SLC52A3	ENST00000217254	exon 2-3	reverse	ataggccgaccaaagaacct			
SLC52A3	ENST00000217254	exon 3-1	forward	gcagtcattattgccaccttg	65-60°C	Roche	378
SLC52A3	ENST00000217254	exon 3-1	reverse	aggccaccagggtatagat			
SLC52A3	ENST00000217254	exon 3-2	forward	accaggtcaccctccactc	65-60°C	Roche	508
SLC52A3	ENST00000217254	exon 3-2	reverse	taggtgcgtttggaattctg			
SLC52A3	ENST00000217254	exon 4	forward	tatggagacactggccatcc	65-60°C	Roche	292
SLC52A3	ENST00000217254	exon 4	reverse	cccaagctctcccaggc			
SLC52A3	ENST00000217254	exon 5	forward	gccctgtgagagttctttgc	65-60°C	Roche	469
SLC52A3	ENST00000217254	exon 5	reverse	ggcacttgcgttcatgattc			

Table VI-4: Primer sequences and PCR cycling conditions used to determine the genotype of SNPs around the p.Gly306Arg mutation in *SLC52A2* in Lebanese BVVL families.

dbSNP ID	Direction	Primer sequence (5' to 3')	Annealing temperature	PCR protocol	Amplicon length (bp)
rs2272666	forward	atacaagagcacccgtcacc	65-60°C	Roche	577
	reverse	ggttttcacagctccagagg			
rs4993862	forward	gcaactttgtgagcaacgag	65-60°C	Roche	358
	reverse	gctccaggtccttctcactg			
rs3817681	forward	cactcaccctctggaagctc	65-60°C	Roche	595
	reverse	ggatctgacttggctcttgc			
rs7016335	forward	ccttcttgaggctgttcctg	65-60°C	Roche	743
	reverse	ggattgggctggtcagagta			
rs6599528	forward	caccgctatgcccaactaat	65-60°C	Roche	555
	reverse	cgcactgaggagcaaacata			
rs1052951, rs1052952, rs1871532	forward	cacctgtgacctgtgacctg	65-60°C	Roche	678
	reverse	ctgacacctgtgcctgtacg			
rs2280837	forward	cgacacggtctcctcactg	65-60°C	Roche	276
	reverse	tcttggggaagccctactct			
rs2977835, rs2977834	forward	tacctccatggtgccattct	65-60°C	Roche	589
	reverse	ccgacccctatgtggtcat			

Table VI-5: Primer sequences and PCR cycling conditions used for transcriptional analysis of *SLC52A2* cDNA.

Gene	Primer pair	Direction	Primer sequence (5' to 3')	Annealing temperature	PCR protocol	Amplicon length (bp)
SLC52A2	primer pair 1	forward	gccctaggtgggaaaagaac	65-60°C	Roche	522
SLC52A2	primer pair 1	reverse	ccttgacccaggaagaatga			
SLC52A2	primer pair 2	forward	agttgcattctgtggccttc	65-60°C	Roche	586
SLC52A2	primer pair 2	reverse	aagcaggaaaagctctgcac			
SLC52A2	primer pair 3	forward	gagtcctcaccactgcaaga	65-60°C	Roche	427
SLC52A2	primer pair 3	reverse	aggagaacacgccaagacac			
SLC52A2	primer pair 4	forward	ctctgctgggcgtgttct	65-60°C	Roche	357
SLC52A2	primer pair 4	reverse	gagggaaagacaggtgttgg			
Primers used to check for NMD in patient E3:						
SLC52A2	primer pair 5	forward	cagcccccatcaacggcacc	60°C (35 cycles only)	Roche	619
SLC52A2	primer pair 5	reverse	acccacgacagcaccacgag			

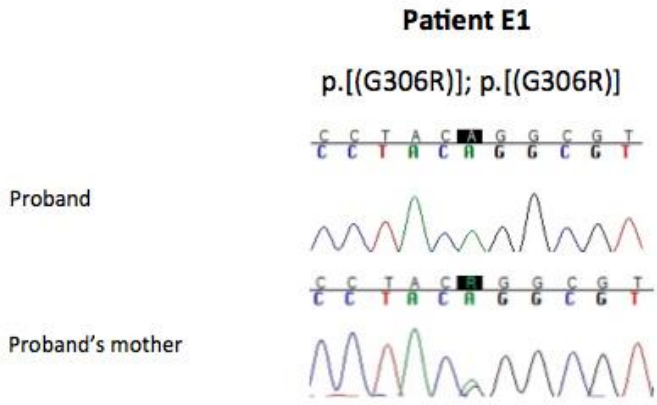
Patient E1
p.[(G306R)]; p.[(G306R)]
Proband
Proband's mother

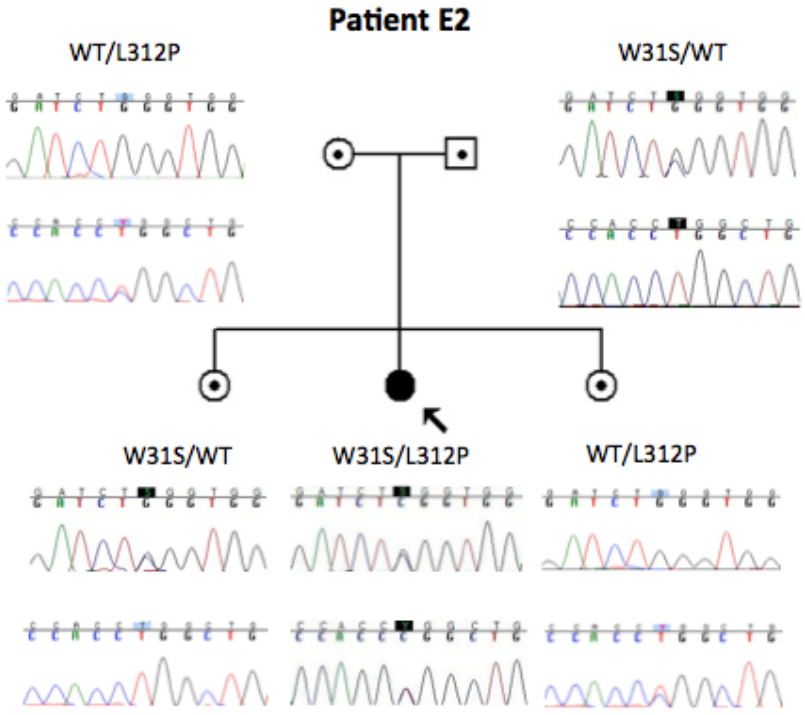
Patient E2
WT/L312P
W31S/WT
W31S/WT
W31S/L312P
WT/L312P

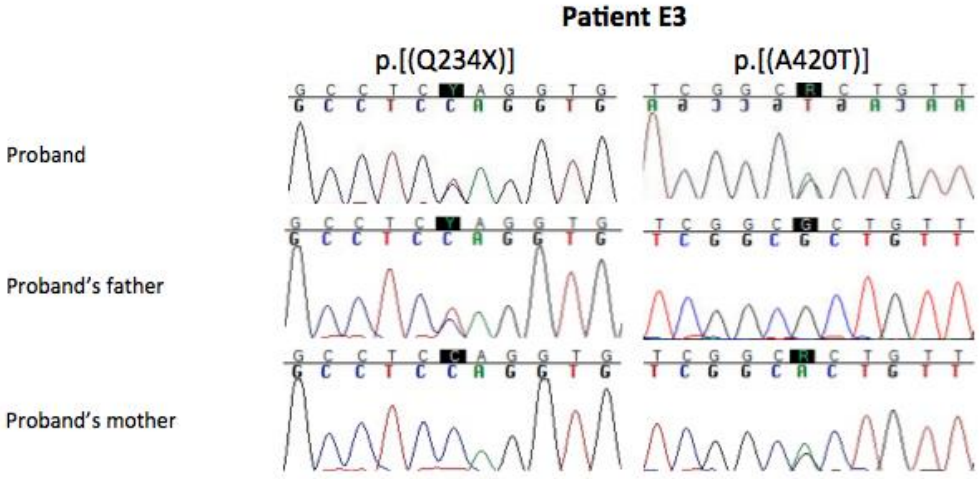
Patient E3
p.[(Q234X)]
p.[(A420T)]
Proband
Proband's father
Proband's mother

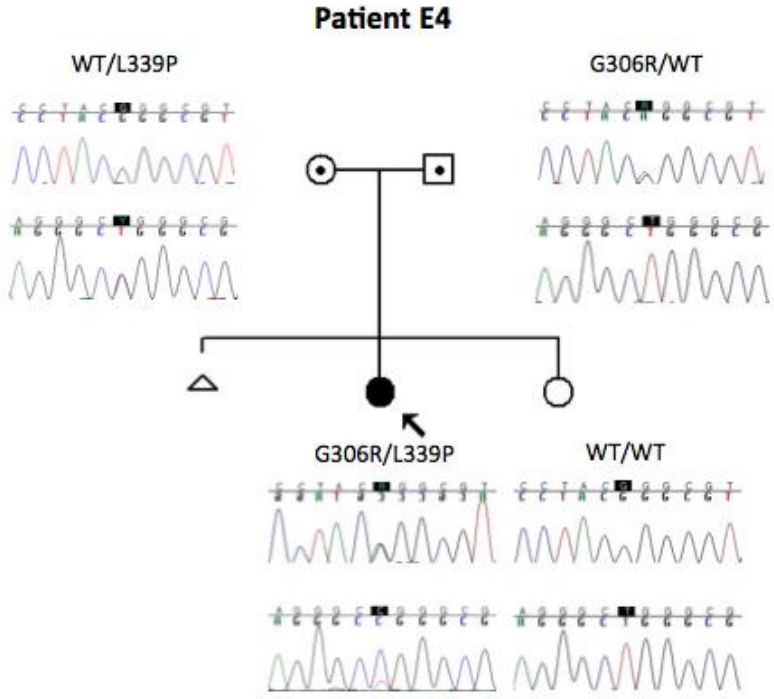
Patient E4
WT/L339P
G306R/WT
G306R/L339P
WT/WT

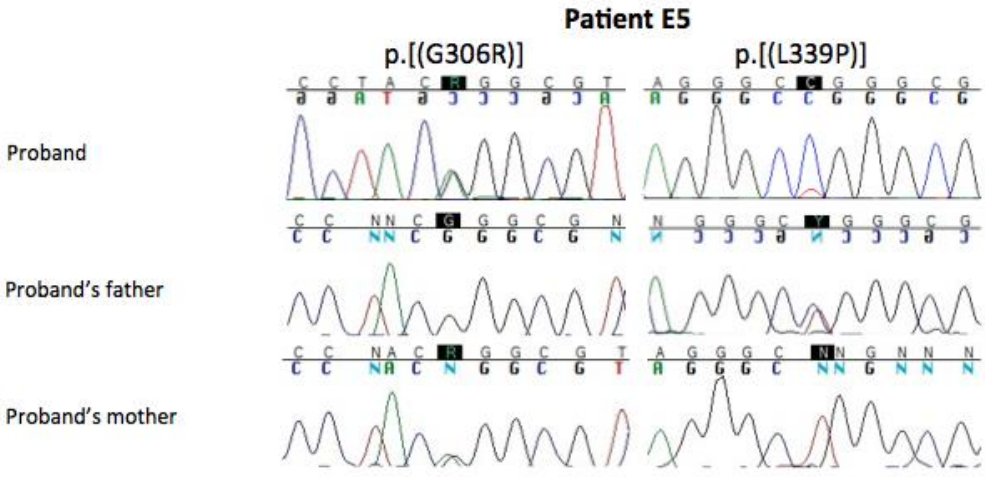
Patient E5
p.[(G306R)]
p.[(L339P)]
Proband
Proband's father
Proband's mother

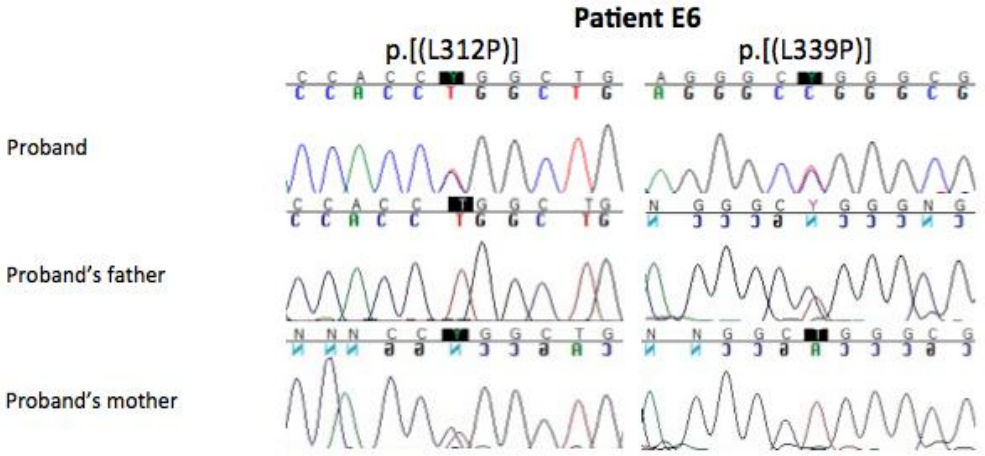
Patient E6
p.[(L312P)]
p.[(L339P)]
Proband
Proband's father
Proband's mother

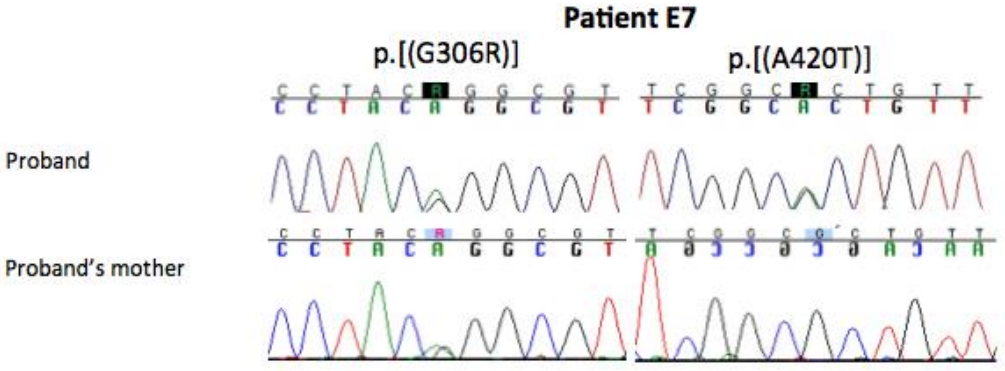
Patient E7
p.[(G306R)]
p.[(A420T)]
Proband
Proband's mother

Patient E8

p.[(L312P)]; p.[(L312P)]

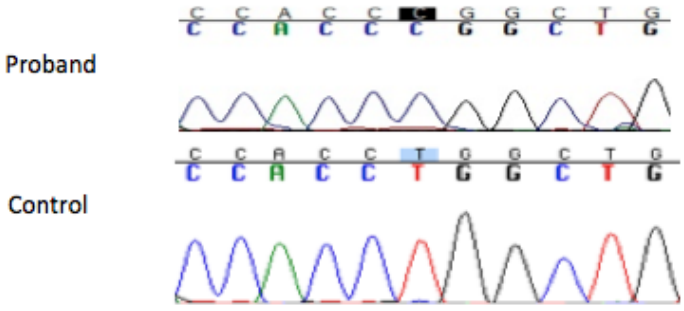

Patients A1 and A2

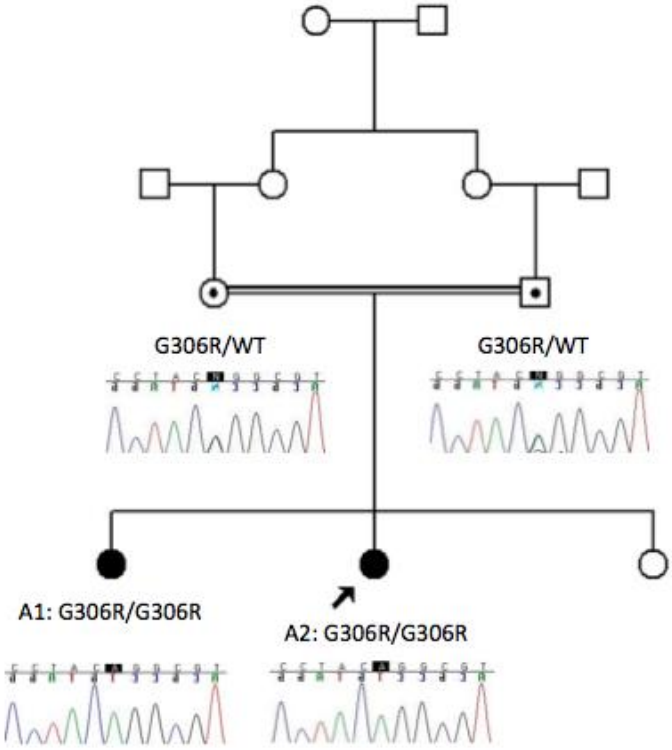

Patients A3 and A4

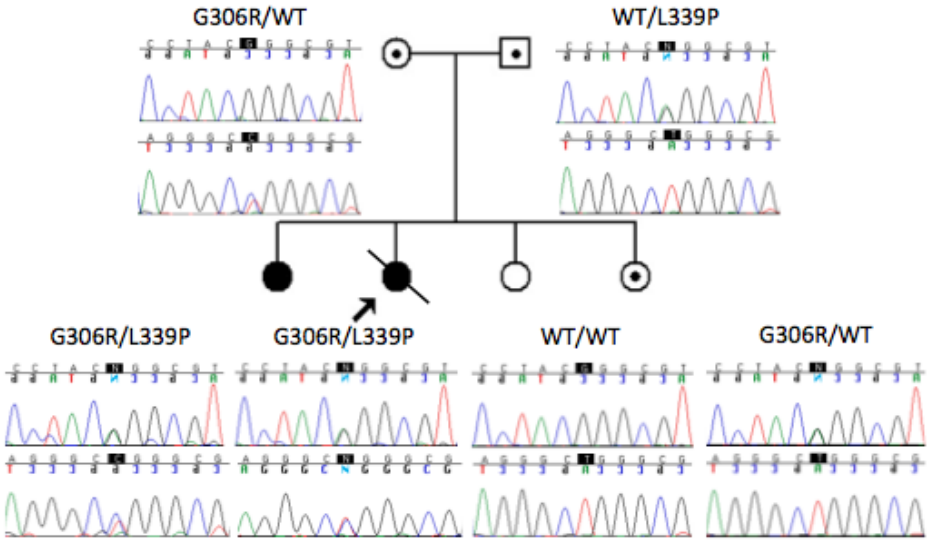

Patients A5, A6, A7

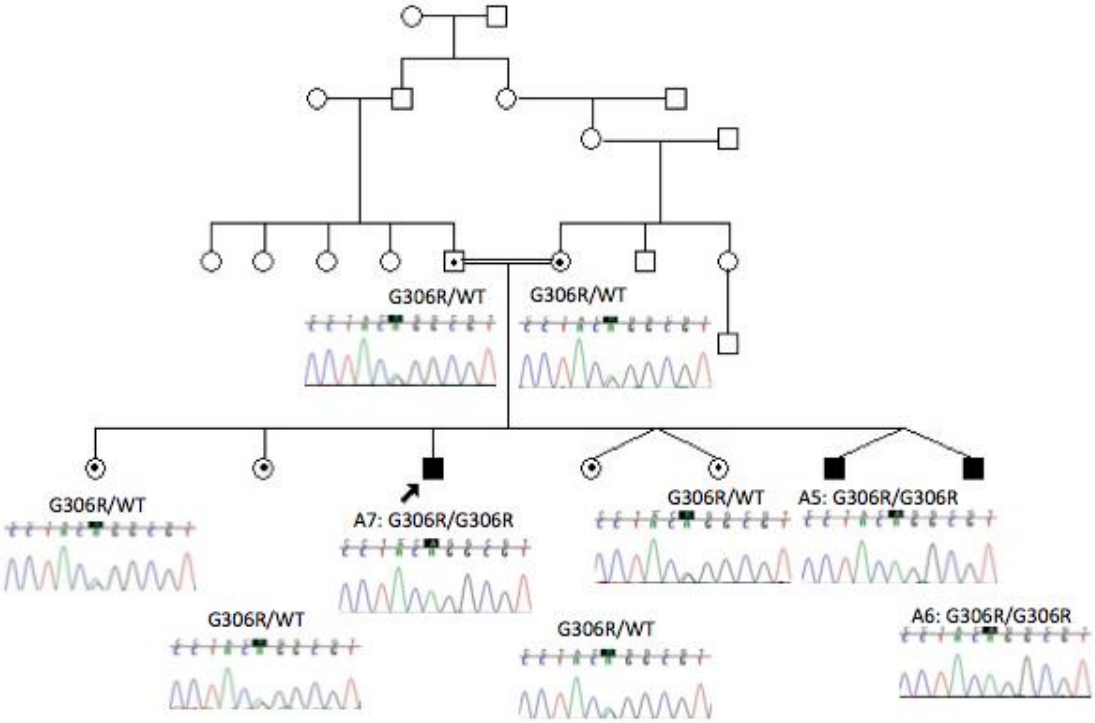

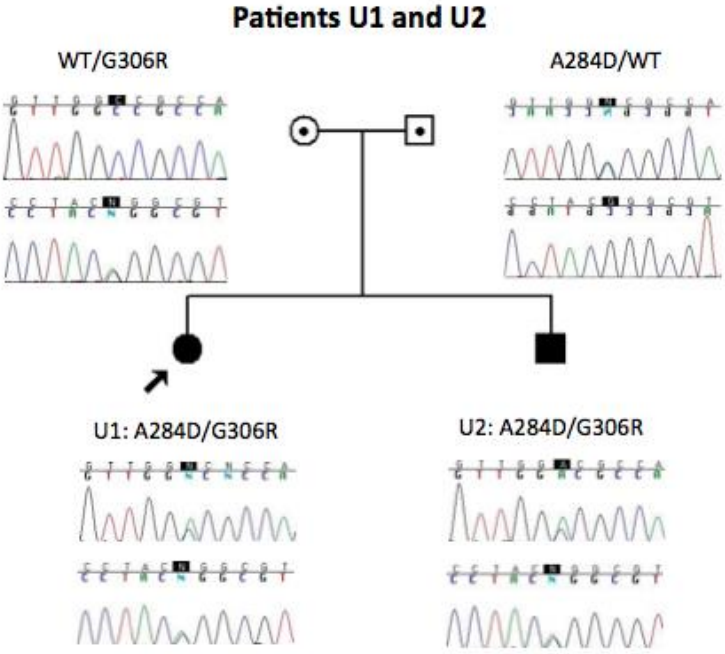
Patients U1 and U2
WT/G306R
A284D/WT
U1: A284D/G306R
U2: A284D/G306R

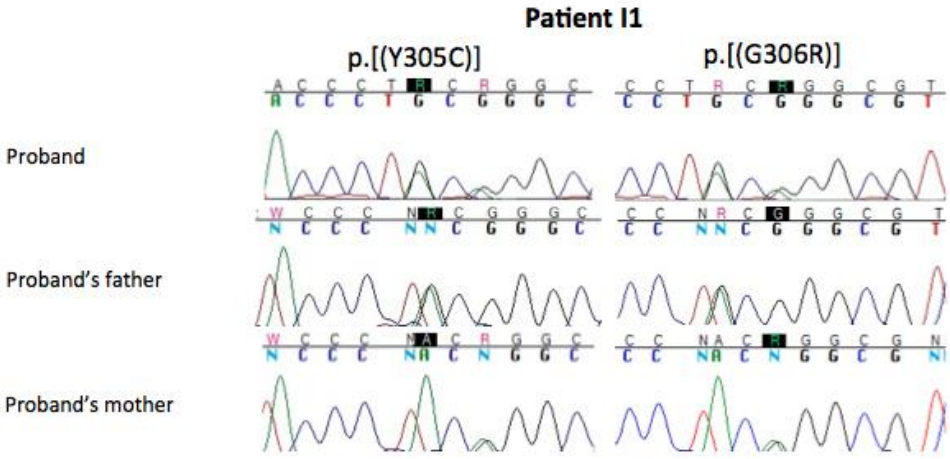
Patient I1
p.[(Y305C)]
p.[(G306R)]
Proband
Proband's father
Proband's mother

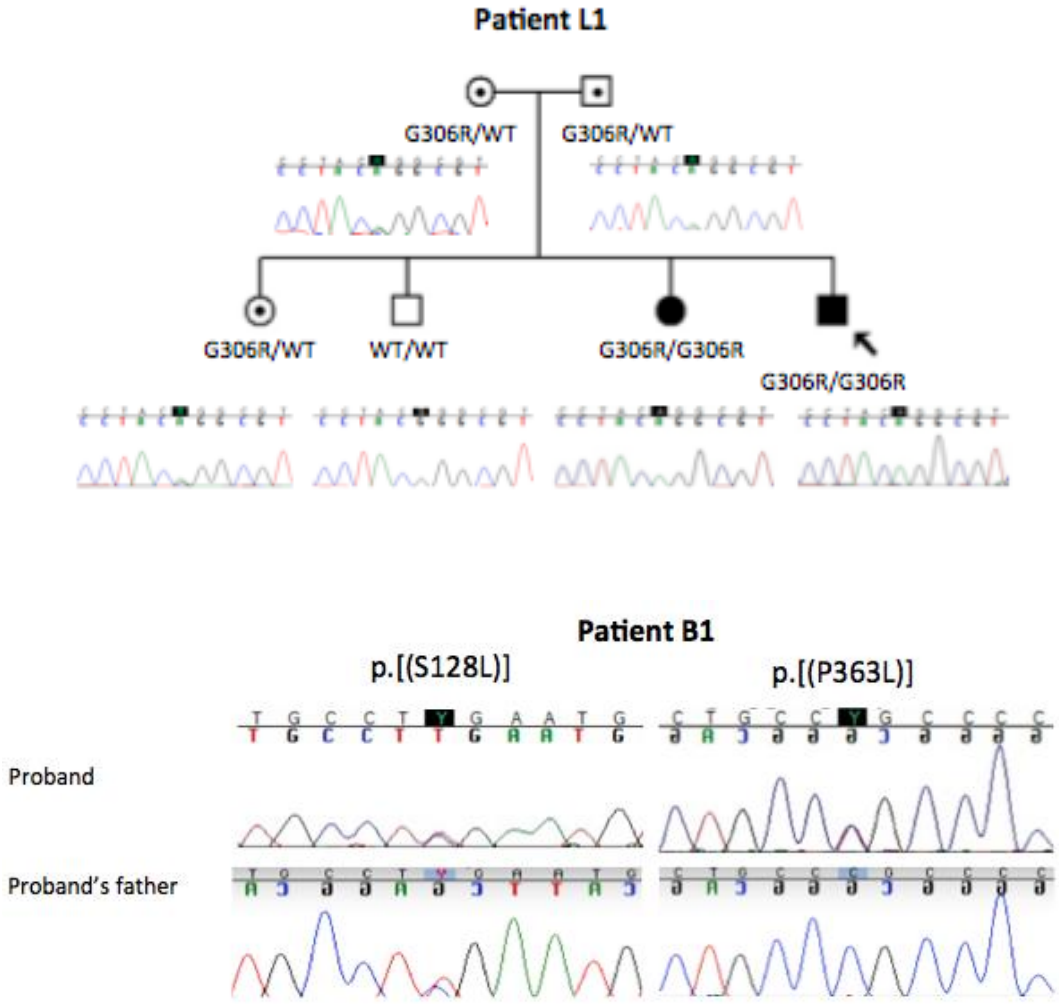

Figure VI-1: Chromatograms and pedigrees (where available) of *SLC52A2* mutations in BVVL cohort. Squares indicate males, circles females, shaded shapes affected individuals, and shapes with dots carriers. Double bars indicate consanguineous unions, and arrows indicate probands (adapted from Foley et al., 2014).

Patients RDB and NDB

SLC52A3 p.[(G13R)]

Patient RDB

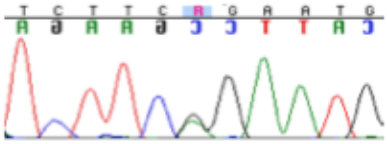

Patient NDB (sibling of RDB)

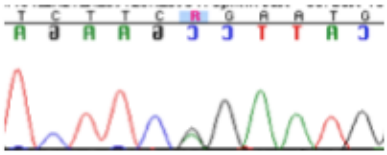

Control

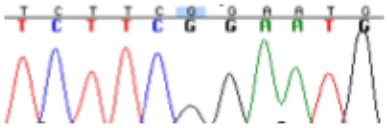

Patient JG

SLC52A3 p.[(I20L)]

Patient JG

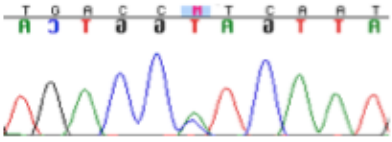

Control

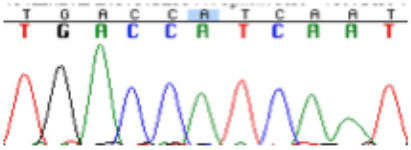

Patient HM

SLC52A3 p.[(E36K)]

Proband

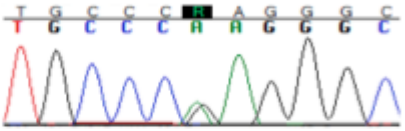

Proband's father

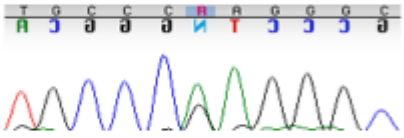

Proband's mother

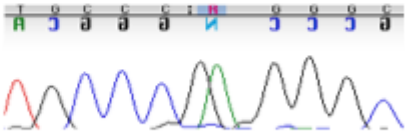

Control

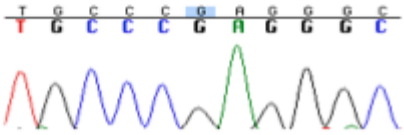

Patient LF

SLC52A3 p.[(T125N)]

Proband

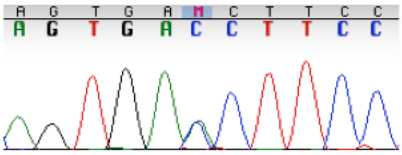

Proband's father

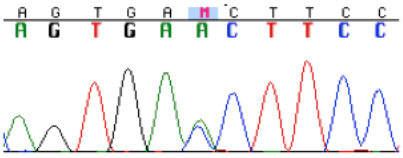

Control

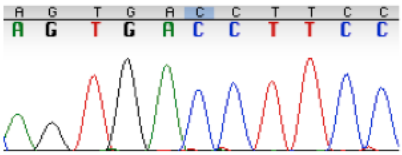

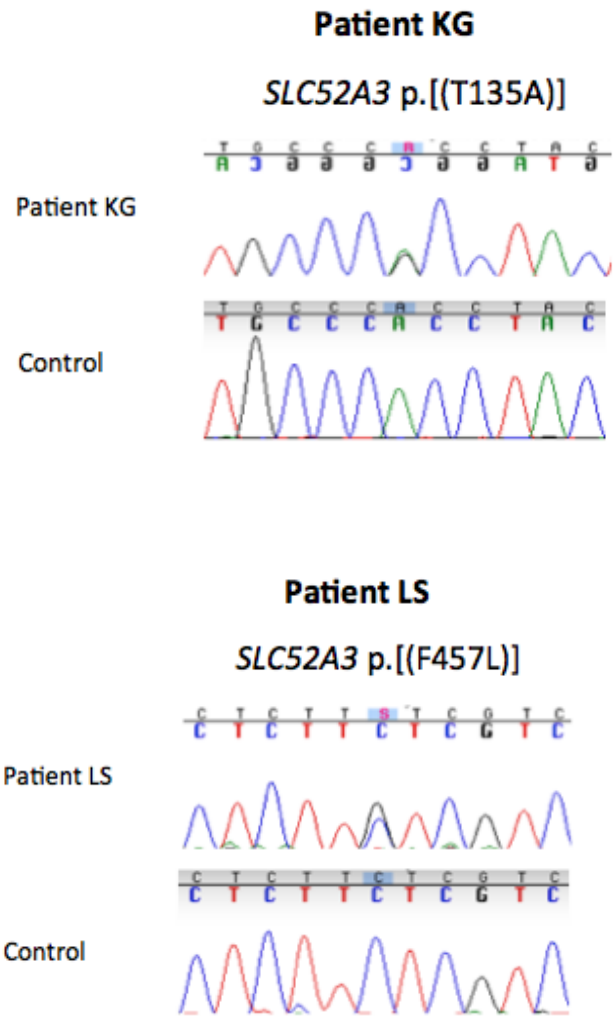

Figure VI-2: Chromatograms of *SLC52A3* mutations in BVVL cohort.

Table VI-6: Results of haplotype analysis around the *SLC52A2* p.Gly306Arg mutation in Lebanese BVVL families. *obligate carriers.

				Family of L1				Family described in Mégarbané et al., 2000					Australian Lebanese Families			
Gene Name	**Chr**	**Position**	**dbSNP ID**	**Unaffected father of L1***	**Unaffected mother of L1***	**Patient L1**	**Affected sister of L1**	**Proband**	**Unaffected father of proband***	**Unaffected sister of proband**	**Unaffected brother of proband**	**Affected cousin of proband**	**Reference allele**	**Observed allele**	**Affected**	**Unaffected**
p.Gly306Arg status				**Het**	**Het**	**Hom**	**Hom**	**Hom**	**Het**	**Het**	**Het**	**Hom**			**Hom**	**Het**
Downstream of *FBXL6*	chr8	145574775	rs7016335	CC	TC	CC	CC	CC	CC	CC	TC	CC	T	C	Hom	Het
FBXL6	chr8	145579953	rs4993862	GG	N/A	GG	GG	GG	N/A	N/A	N/A	GG	**T**	**A**	Hom	Het
FBXL6	chr8	145580984	rs2272666	GG	GA	GG	GG	GG	GG	GA	GA	GG	A	G	Hom	Het
FBXL6	chr8	145582839	rs3817681	N/A	GA	GG	GG	GG	N/A	GA	GA	GG	A	G	Hom	Het
ADCK5	chr8	145603114	rs6599528	CC	CA	CC	CC	CC	CA	CA	CA	CC	A	C	Hom	Het
ADCK5	chr8	145618309	rs1052951	AA	N/A	AA	AA	AA	GA	GA	GA	AA	G	A	Hom	Het
ADCK5	chr8	145618312	rs1052952	AA	N/A	AA	AA	AA	GA	GA	GA	AA	G	A	Hom	Het
Downstream of *ADCK5*	chr8	145618597	rs1871532	AA	N/A	AA	AA	AA	GA	GA	GA	AA	G	A	Hom	Het
Downstream of *ADCK5*	chr8	145620296	rs2280837	GG	GC	GG	GG	GG	GC	GC	GC	GG	C	G	Hom	Het
Downstream of *ADCK5*	chr8	145622923	rs2977835	CC	TC	CC	CC	CC	TC	TC	TC	CC	T	C	Hom	Het
Downstream of *ADCK5*	chr8	145623098	rs2977834	CC	TC	CC	CC	CC	TC	TC	TC	CC	T	C	Hom	Het

Table VI-7: Biochemical profiles before starting riboflavin therapy in *SLC52A2* patients (from Foley et al., 2014). *no reference range (at laboratory where testing performed); values in bold fall outside the reference range. Carnitine species concentrations are in micromoles per litre. Riboflavin, FAD and FMN concentrations are in nanomoles per litre.

Patient	E1	E2	E3	E4	E5	E6	E7	Family 1 A1	Family 1 A2
Age at time of biochemical testing	10 years	6 years	5 years	5 years	3.5	17 years	22 yrs	10 years	9 years
Riboflavin [reference range]	7*	8.5*	14.9*	2.9*	not done	not done	7.2*	not done	not done
FAD [reference range]	201 [174-471]	185 [174-471]	87.2*	253 [174-471]	not done	not done	311 [174-471]	267 [174-471]	253 [174-471]
FMN [reference range]	<4*	7.4*	4.5*	5.8*	not done	not done	9.9*	not done	not done
C0-carnitine [reference range]	18.3 [<52.4]	normal	normal	**14** [17-55]	normal	41 [23-75]	37.0 [<52.4]	16.8 [13-56]	25.6 [13-56]
C2-carnitine [reference range]	**19.3** [<11.5]	normal	normal	10 [10-27.8]	normal	20.8 [10-34.5]	**14.7** [<11.5]	4.1 [2.8-22.5]	3.7 [2.8-22.5]
C4-carnitine [reference range]	**1.72** [<0.60]	normal	normal	**0.5** [0.11-0.49]	normal	1.69 [0.43-2.44]	0.44 [<0.60]	0.35 [0.12-0.67]	0.24 [0.12-0.67]
C5-carnitine [reference range]	**0.34** [<0.24]	normal	normal	**0.56** [0.08-0.35]	normal	0.21 [0.1-0.53]	0.06 [<0.24]	**0.37** [<0.28]	**3.82** [<0.28]
C6-carnitine [reference range]	**0.79** [<0.12]	normal	normal	**0.19** [0.02-0.11]	normal	0.23 [0.06-0.31]	0.06 [<0.12]	**0.58** [<0.13]	**0.31** [<0.13]
C8-carnitine [reference range]	**1.64** [<0.24]	normal	normal	**0.49** [0-0.18]	normal	0.00 [0.04-0.2]	0.17 [<0.24]	**1.31** [<0.24]	**0.29** [<0.24]
C10:1-carnitine [reference range]	0.47 [<0.51]	normal	normal	not done	normal	not done	0.16 [<0.51]	**0.79** [<0.5]	**0.68** [<0.5]
C10-carnitine [reference range]	**2.15** [<0.40]	normal	normal	**0.42** [<0.2]	normal	not done	0.36 [<0.40]	**1.39** [<0.4]	**0.61** [<0.4]
C12-carnitine [reference range]	**1.64** [<0.22]	normal	normal	not done	normal	not done	0.15 [<0.22]	0.12 [<0.62]	**0.79** [<0.62]
C14:1-carnitine [reference range]	**2.19** [<0.25]	normal	normal	not done	normal	not done	**0.33** [<0.25]	0.16 [<0.73]	0.11 [<0.73]
C14-carnitine [reference range]	**0.94** [<0.12]	normal	normal	0.14 [0.09-0.25]	normal	0.12 [0.02-0.21]	0.05 [<0.12]	0.03 [<0.34]	0.12 [<0.34]
C16-carnitine [reference range]	**0.61** [<0.28]	normal	normal	0.8 [0.4-1.7]	normal	0.8 [0.5-2.2]	0.09 [<0.28]	0.07 [<0.64]	0.08 [<0.64]
C18:1-carnitine [reference range]	**1.45** [<0.40]	normal	normal	not done	normal	not done	0.15 [<0.40]	not done	not done
C18:2-carnitine [reference range]	**0.44** [<0.23]	normal	normal	not done	normal	not done	0.04 [<0.23]	not done	not done

Patient	Family 2		Family 3			Family 4		
	A3	**A4**	**A5**	**A6**	**A7**	**U1**	**U2**	**I1**
Age at time of biochemical testing	3.5 years	15 years	16 years	16 years	21 years	52 years	44 years	1.8 years
Riboflavin [reference range]	not done	not done	not done	not done	not done	not done	not done	9.8 [3.9-49.0]
FAD [reference range]	not done	245 [174-471]	369 [174-471]	310 [174-471]	337 [174-471]	256 [137-370]	242 [137-370]	64.4 [46.0-114.0]
FMN [reference range]	not done	not done	not done	not done	not done	not done	not done	**2.5** [2.8-21.4]
C0-carnitine [reference range]	38.8 [13-56]	30.2 [13-56]	21.9 [13-56]	18.3 [13-56]	27.3 [13-56]	not done	not done	24.30 [22.30-54.80]
C2-carnitine [reference range]	9.5 [2.8-22.5]	11.1 [2.8-22.5]	3.1 [2.8-22.5]	3.4 [2.8-22.5]	5.1 [2.8-22.5]	8.69 [3.74-16.56]	5.70 [3.74-16.56]	4.97 [3.40-13.00]
C4-carnitine [reference range]	0.65 [0.12-0.67]	0.6 [0.12-0.67]	0.1 [0.12-0.67]	0.03 [0.12-0.67]	0.28 [0.12-0.67]	0.29 [0.00-0.45]	**0.46** [0.00-0.45]	0.25 [0.07-0.58]
C5-carnitine [reference range]	0 [<0.28]	**0.31** [<0.28]	0.1 [<0.28]	0.08 [<0.28]	0.26 [<0.28]	0.15 [0.00-0.30]	**0.96** [0.00-0.30]	0.13 [0.04-0.22]
C6-carnitine [reference range]	0.12 [<0.13]	**0.27** [<0.13]	0.04 [<0.13]	0.04 [<0.13]	0.07 [<0.13]	**0.21** [0.00-0.12]	0.09 [0.00-0.12]	**0.14** [0.02-0.12]
C8-carnitine [reference range]	**0.34** [<0.24]	**0.7** [<0.24]	0.09 [<0.24]	0.11 [<0.24]	0.16 [<0.24]	**0.40** [0.00-0.23]	**0.24** [0.00-0.23]	**0.25** [0.04-0.22]
C10:1-carnitine [reference range]	0.19 [<0.5]	**0.53** [<0.5]	0.1 [<0.5]	0.13 [<0.5]	0.08 [<0.5]	**0.40** [0.00-0.31]	0.25 [0.00-0.31]	0.15 [0.04-0.22]
C10-carnitine [reference range]	**0.52** [<0.4]	**0.8** [<0.4]	0.13 [<0.4]	0.16 [<0.4]	0.2 [<0.4]	**0.45** [0.00-0.31]	0.29 [0.00-0.31]	**0.36** [0.04-0.30]
C12-carnitine [reference range]	0.16 [<0.62]	0.09 [<0.62]	0.01 [<0.62]	0.03 [<0.62]	0.02 [<0.62]	0.09 [0.00-0.12]	0.06 [0.00-0.12]	0.11 [0.04-0.14]
C14:1-carnitine [reference range]	0.16 [<0.73]	0.18 [<0.73]	0.06 [<0.73]	0.09 [<0.73]	0.05 [<0.73]	**0.17** [0.00-0.16]	0.07 [0.00-0.16]	**0.20** [0.02-0.18]
C14-carnitine [reference range]	0.06 [<0.34]	0 [<0.34]	0 [<0.34]	0.04 [<0.34]	0.01 [<0.34]	**0.06** [0.00-0.05]	0.03 [0.00-0.05]	0.06 [0.00-0.08]
C16-carnitine [reference range]	0.03 [<0.64]	0.11 [<0.64]	0.04 [<0.64]	0.09 [<0.64]	0.05 [<0.64]	0.09 [0.00-0.10]	0.08 [0.00-0.10]	0.11 [0.06-0.24]
C18:1-carnitine [reference range]	not done	not done	not done	not done	not done	0.12 [0.00-0.17]	0.08 [0.00-0.17]	0.22 [0.06-0.28]
C18:2-carnitine [reference range]	not done	not done	not done	not done	not done	0.08 [0.00-0.10]	0.06 [0.00-0.10]	0.08 [0.02-0.18]

Table VI-8: Neurophysiological characteristics of patients with mutations in *SLC52A2* (from Foley et al., 2014).

Patient	E1	E2	E3	E4	E5	E6	E7	Family 1 A1	Family 1 A2
Age at nerve conduction testing	8 years	2 years	4 years	5 years	4 years	2 years	10 years	8 years	3 years
Sensory responses	absent SNAPs in upper limbs and lower limbs	low amplitude or absent SNAPs in upper limbs; absent in lower limbs	low amplitude or absent SNAPs in upper limbs; low amplitude SNAPs in lower limbs	low amplitude SNAPs in upper limbs; low amplitude or absent SNAPs in lower limbs	normal	absent SNAPs in upper limbs; lower amplitude SNAPs in lower limbs	low amplitude or absent SNAPs in upper limbs; absent in lower limbs	absent SNAPs in upper limbs and lower limbs	low amplitude SNAPs in upper limbs; absent in lower limbs
Motor responses	low amplitude CMAPs in upper limbs and low amplitude or absent CMAPs in lower limbs	low amplitude CMAPs in upper limbs and lower limbs	absent CMAPs in upper limbs; normal in lower limbs	low amplitude CMAPs in lower limbs (upper limbs not tested)	low amplitude or absent CMAPs in upper limbs (lower limbs not tested)	Normal in lower limbs (upper limbs not tested)	low amplitude CMAPs in upper limbs; normal in lower limbs	normal	normal
Age at repeat nerve conduction testing	10 years	6 years	not done	not done	10 years	10 years	not done	10 years	9 years
Sensory responses	absent SNAPs in upper limbs and lower limbs	absent SNAPs in upper limbs (lower limbs not tested)	not done	not done	low amplitude SNAPs in upper limbs (lower limbs not tested)	absent SNAPs in upper limbs; (lower limbs not tested)	not done	absent SNAPs in upper limbs and lower limbs	absent SNAPs in upper limbs and lower limbs
Motor responses	low amplitude CMAPs in upper limbs (lower limbs not tested)	absent CMAPs in upper limbs; low amplitude CMAPs in lower limbs	not done	not done	low amplitude CMAPs in upper limbs (lower limbs not tested)	low amplitude CMAPs in upper limbs; (lower limbs not tested)	not done	normal	low amplitude CMAPs in upper limbs; normal in lower limbs

	Family 2		Family 3			Family 4			
Patient	**A3**	**A4**	**A5**	**A6**	**A7**	**U1**	**U2**	**I1**	**L1**
Age at nerve conduction testing	3 years	3 years	16 years	16 years	3 years	51 years	43 years	2 years	6 years
Sensory responses	absent SNAPs in upper limbs and lower limbs	low amplitude SNAPs in upper limbs; absent in lower limbs	absent SNAPs in upper limbs and lower limbs	absent SNAPs in upper limbs and lower limbs	absent SNAPs in upper limbs and lower limbs	low amplitude or absent SNAPs in upper limbs; absent in lower limbs	absent SNAPs in upper limbs; (lower limbs not tested)	low amplitude SNAPs in upper limbs; absent in lower limbs	low amplitude SNAPs in upper limbs and lower limbs
Motor responses	not done	normal	low amplitude or absent CMAPs in upper limbs; normal in lower limbs	low amplitude CMAPs in upper limbs; normal in lower limbs	normal	low amplitude CMAPs in upper limbs and lower limbs	low amplitude or absent CMAPs in upper limbs; (lower limbs not tested)	low amplitude CMAPs in upper limbs and lower limbs	normal
Age at repeat nerve conduction testing	not done	16 years	not done	not done	not done	not done	not done	not done	not done
Sensory responses	not done	low amplitude SNAPs in upper limbs; absent in lower limbs	not done	not done	not done	not done	not done	not done	not done
Motor responses	not done	absent CMAPs in upper limbs; normal in lower limbs	not done	not done	not done	not done	not done	not done	not done

Table VI-9: Sural nerve pathology findings in patients with *SLC52A2* mutations (from Foley et al., 2014). *g ratio=axon diameter/total nerve fibre diameter.

Patient	E2	E3	E5	A3	I1
Sex	Female	Female	Female	Female	Male
Age at nerve biopsy	2 years	4 years	4 years	3 years	2 years
Axonal loss	2+; large myelinated fibres > small myelinated fibres	2+; large myelinated fibres>small myelinated fibres	1+ large myelinated fibres>small myelinated fibres	2+ large myelinated fibres>small myelinated fibres	3+ large myelinated fibres>small myelinated fibres
Fibrosis	2+	1+	1+	1+	3+
Degeneration	Mild	Moderate	Moderate	Mild	Mild
Regeneration	Absent	Absent	Absent	Absent	Absent
Demyelination	Absent	Absent	Absent	Absent	Absent
Endoneurial inflammation	0-1/Field	Absent	Absent	Absent	Absent
Epineurial inflammation	Occasional single cell	Absent	Absent	Absent	Absent
Endoneurial macrophages	Sparse	Sparse	Sparse	Absent	Sparse
Electron microscopy	Confirms chronic axonal neuropathy	Confirms chronic axonal neuropathy	Confirms chronic axonal neuropathy	Not done	Confirms chronic axonal neuropathy
Teased fibres	Not done	Axonal degeneration	Axonal degeneration	Not done	Not done
Morphometry	Not done	g ratio* normal for age; large myelinated fibre loss confirmed	Not done	Not done	Not done

Table VI-10: Biochemical profiles after the initiation of riboflavin therapy in *SLC52A2* patients (from Foley et al., 2014). *no reference range (at laboratory where testing performed); values in bold fall outside the reference range. Carnitine species concentrations are in micromoles per litre. Riboflavin, FAD and FMN concentrations are in nanomoles per litre.

					Family 1		Family 2
Patient	**E1**	**E3**	**E4**	**E7**	**A1**	**A2**	**A4**
Riboflavin [reference range]	71.9*	28.4 [3.9-49.0]	24.3*	14.7*	not done	not done	not done
FAD [reference range]	313 [174-471]	**126.6** [46.0-114.0]	367 [174-471]	359 [174-471]	407 [174-471]	383 [174-471]	324 [174-471]
FMN [reference range]	68.6*	5.6 [2.8-21.4]	73.5*	31.5*	not done	not done	not done
C0-carnitine [reference range]	22 [17-55]	not done	37 [17.0-55.0]	50 [<52.4]	9 [13-56]	17 [13-56]	27 [13-56]
C2-carnitine [reference range]	16.7 [10-27.8]	not done	19.7 [10-27.8]	5.2 [<11.5]	2 [2.8-22.5]	3 [2.8-22.5]	5 [2.8-22.5]
C4-carnitine [reference range]	0.32 [0.11-0.49]	not done	0.22 [0.11-0.49]	0.39 [<0.60]	not done	not done	not done
C5-carnitine [reference range]	0.15 [0.08-0.35]	not done	0.17 [0.08-0.35]	0.05 [<0.24]	not done	not done	not done
C6-carnitine [reference range]	0.03 [0.02-0.11]	not done	0.04 [0.02-0.11]	0.03 [<0.12]	<0.1 [<0.13]	<0.1 [<0.13]	0.1 [<0.13]
C8-carnitine [reference range]	0.14 [0-0.18]	not done	0.16 [0-0.18]	0.06 [<0.24]	<0.1 [<0.24]	<0.1 [<0.24]	0.1 [<0.24]
C10:1-carnitine [reference range]	not done	not done	not done	0.05 [<0.51]	<0.1 [<0.5]	<0.1 [<0.5]	0.1 [<0.5]
C10-carnitine [reference range]	not done	not done	not done	0.09 [<0.40]	0.1 [<0.4]	0.1 [<0.4]	0.2 [<0.4]

Patient	Family 3			Family 4		
	A5	**A6**	**A7**	**U1**	**U2**	**I1**
Riboflavin [reference range]	not done	not done	not done	not done	**219.8** [6.2-39.0]	not done
FAD [reference range]	396 [174-471]	380 [174-471]	337 [174-471]	not done	not done	not done
FMN [reference range]	not done	not done	not done	not done	not done	not done
C0-carnitine [reference range]	21 [13-56]	20 [13-56]	27	not done	not done	normal
C2-carnitine [reference range]	4 [2.8-22.5]	5 [2.8-22.5]	5	7.30 [4.04-12.19]	4.64 [4.04-12.19]	not done
C4-carnitine [reference range]	not done	not done	not done	0.07 [<0.38]	0.19 [<0.38]	not done
C5-carnitine [reference range]	not done	not done	not done	0.04 [<0.30]	**0.35 [<0.30]**	normal
C6-carnitine [reference range]	<0.1 [<0.13]	0 [<0.13]	0.1 [<0.13]	0.02 [<0.09]	0.02 [<0.09]	normal
C8-carnitine [reference range]	<0.1 [<0.24]	0.1 [<0.24]	0.2 [<0.24]	0.12 [<0.65]	0.04 [<0.65]	normal
C10:1-carnitine [reference range]	<0.1 [<0.5]	0.1 [<0.5]	0.1 [<0.5]	0.11 [<0.81]	0.07 [<0.81]	not done
C10-carnitine [reference range]	<0.1 [<0.4]	0.1 [<0.4]	0.2 [<0.4]	0.17 [<0.51]	0.05 [<0.51]	not done

Table VI-11: Observed responses to riboflavin therapy including treatment dose and duration for patients E1-E4, E6, E7, A1-A2, A4-A7, U1-U2, I1 and L1. *had been started on low-dose riboflavin (3 mg/kg/day) at age 15 years by patient's metabolic consultant for evidence of a mitochondrial disorder; riboflavin dose was increased to 300 mg/day (10 mg/kg/day) when *SLC52A2* mutations were found. **unable to tolerate further increase in dose due to reported associated gastrointestinal symptoms. ***had been on a riboflavin dose of 50 mg/kg/day for six months prior to recent increase in dose up to 60 mg/kg/day.

							Family 1	
Patient	**E1**	**E2**	**E3**	**E4**	**E6***	**E7**	**A1**	**A2**
Age at first symptom	1.5 years	1 year	3.5 years	1.5 years	0.6 years	2 years	8 years	3 years
Age at initiation of high-dose riboflavin therapy	10.6 years	6 years	5.4 years	5 years	17.5 years	22.4 years	10 years	9 years
Present dose of riboflavin	50 mg/kg/day	10 mg/kg/day	7 mg/kg/day	40 mg/kg/day	300 mg/day	1,500 mg/day	23 mg/kg/day	26 mg/kg/day
Length of time at <u>present</u> dose	12 months	15 months	15 months	11 months	13 months	2 weeks	7 months	7 months
Observed response(s)	able to go from supine to sitting and then standing independently (skills lost at age 9 years); stronger/louder voice	*lost to follow-up*	stable functioning; no changes noted	can walk independently; can jump (skill lost at age 4 years); hearing grossly better	stable functioning; no changes noted	increased sensation in legs	normalisation of both pure tone audiometry; normalisation of brainstem auditory evoked responses; fewer falls	stable functioning; decreased fatigability reported

Patient	A4	Family 3 A5	A6	A7	Family 4 U1	U2	I1	L1
Age at first symptom	5 years	3 years	3 years	5 years	2 years	4 years	1.3 years	3 years
Age at initiation of high-dose riboflavin therapy	15 years	16 years	16 years	21 years	52 years	44 years	1.8 years	6.5 years
Present dose of riboflavin	21 mg/kg/day	1,000 mg/day	1,000 mg/day	1,000 mg/day	400 mg/day**	800 mg/day**	60 mg/kg/day***	10 mg/kg/day
Length of time at <u>present</u> dose	7 months	7 months	7 months	7 months	6 months	6 months	2 months***	13 months
Observed response(s)	stable functioning; decreased fatigability reported	better at transferring; stronger kick; significant decrease in ventilator pressures	stable functioning; no changes noted	stable functioning; no changes noted	stable functioning; no changes noted	stable functioning; no changes noted	improved upper limb and neck strength: antigravity shoulder abduction, elbow flexion and extension and neck extension; can walk with truncal support; stronger/louder voice; decreased nystagmus	less frequent falls

Table VI-12: Clinical features of patients without mutations in *SLC52A1*, *SLC52A2* and *SLC52A3* in the cohort of patients referred for BVVL testing.

Patient	Phenotype
1	severe bulbar weakness requiring ventilation via tracheostomy; severe truncal hypotonia; no hearing loss; feeding difficulties; on riboflavin treatment; suspected to have MADD; respiratory and limb muscle weakness; bulbar muscle abnormalities on EMG; reduced activities of all respiratory chain complexes; sent for mitochondrial DNA sequencing and previously tested for *POLG* mutations
2	neurogenic weakness with upper motor neuron signs; presented at 2 years of age with a collapse; intermittently noisy breathing; absent hearing; unresponsive and paralysed for first few days after arrest, then distal movement in hands and feet started to reappear; weakness and inexpressive appearance in facial expression; difficulty closing eyes; generalised hypotonia; increased reflexes in upper and lower limbs; underwent tracheostomy; sudden noticeable improvement in physical abilities and responsiveness within hours of starting riboflavin, followed by steading improvement with improved hearing; neuronopathy on electromyography; nocturnal ventilatory support; currently unable to sit unsupported although neck and trunk support is improving; partial antigravity movement in forelimbs; better strength in legs than arms; better distal than proximal power; no muscle wasting; brisk reflexes; full eye movements; BVVL with unusual features (very early onset, very sudden deterioration with weakness)
3	40-year history of progressive distal weakness and wasting; 5-year history of breathing myoclonus; swallowing abnormalities; tongue fasciculations; brisk reflexes in upper limbs; previously diagnosed with axonal recessive CMT2
4	perhaps odd CMT variant; axonal pattern on neurophysiology; onset at 10 years old after flu-like illness; hearing loss; at 12 years old, foot drop and unable to stand on heels; difficulty keeping arms up above his head; wasted, fasiculating tongue; respiratory muscle weakness; orthopnoea; condition has remained static
5	poor swallowing; failed hearing tests; hypotonic (sister of patient below)
6	poor swallowing; failed hearing tests; hypotonic (sister of patient above)
7	born to consanguineous parents; nasogastric tube necessary for feeding; general lethargy and unsteadiness; slow to stand up from sitting position; significant and progressive hearing loss; admitted to intensive care for respiratory failure and put on ventilation; bi-temporal narrowing, high arch to palate and micrognathia; convergent squint; muscle weakness in all four limbs; positive gowers sign; lumbar lordosis; no contractures. MRI scan of the head and muscle biopsy essentially normal; normal blood and CSF lactate; normal sensory and motor NCVs; SMARD1 testing negative and normal very long chain fatty acids; no evidence of cardiomyopathy; normal EMG; no evidence of generalised neuropathy; presently on overnight non-invasive ventilation; patient has shown some improvement in motor ability and has remained stable.
8	bilateral sensorineural hearing loss; bilateral progressive facial weakness; tongue and palatal weakness
9	optic atrophy; ataxia; auditory neuropathy
10	46 year old patient with onset in first few years of life with proximal leg weakness and foot drop; slowly progressive; mild facial weakness; dysarthria; proximal and distal weakness in the limbs; minimal changes on muscle biopsy; neurogenic EMG; son has developed rapid onset unexplained sensorineural hearing loss in late teens
11	clinical diagnosis of BVVL; hearing loss and progressive anterior horn cell disease with spastic hemiparesis; muscle atrophy on left side; poor appetite; normal reflexes; no sensory abnormalities; occasional dysarthria; no visual impairment; no facial weakness; no tongue atrophy or fasciculations; normal acylcarnitine profile; improvement with riboflavin treatment
12	respiratory failure at 6 years old; hearing impairment; progressive weakness; neurogenic features on muscle biopsy, EMG and NCS; normal mitochondrial respiratory chain enzyme activities; two younger siblings with hearing impairment passed away with chest infection
13	dysarthria; dysphagia; restricted lateral gaze

Patient	Phenotype
14	vocal cord palsy
15	atypical CIDP; respiratory muscle weakness
16	4 year old girl with progressive sensorineural hearing loss; slurred speech; ataxia; abducens paresis (6th nerve palsy)
17	respiratory chain enzyme deficiencies; demyelinating neuropathy; predominant upper limb and bulbar involvement; severe fatigue; sweats; episodes of profound collapse; some symptomatic response to CoQ10
18	facial weakness and lack of facial expression; neonatal bilateral hip dislocation; hypotonia with preserved antigravity strength and delayed motor milestones; severe sucking and swallowing difficulty from birth; gastrostomy and fundoplication at six months of age; recurrent chest infections; hospitalised for the first six and a half months of life; hearing difficulties; motor neuronopathy in bulbar nuclei and anterior horn cells on EMG; trend for gradual improvement; normal MRC enzyme activities; normal plasma acylcarnitines; fatty acid beta oxidation studies in fibroblasts normal; negative POLG and APTX testing.
19	progressive ataxia; deafness; normal imaging; normal CSF; normal muscle biopsy and EMG
20	bulbospinal muscular atrophy from 18 months of age; losing ambulation at 3 years old; no hearing loss
21	rapidly progressive and slightly later-onset BVVL; rapidly progressive ataxia; motor involvement; possible autonomic involvement; early-childhood onset; dragging feet
22	profound motor and sensory peripheral neuropathy; early-childhood onset; MRC score of 0; requires non-invasive ventilation; no hearing impairment
23	early-onset; marked hypotonia; feeding problems at birth; severe bulbar weakness; bilateral facial weakness; hemiatrophy and fasciculations of the tongue; hypotrophic shoulder girdle muscles; normal legs; normal brain MRI; mild hearing loss; normal eye movements; static course
24	hypotonia; failure to thrive; paresis of diaphragm; psychomotor retardation; myopathy
25	preexisting mild autistic spectrum disorder; acute onset of severe epilepsy at 10 years old; profound loss of skills from 10 years old with regression and speech loss; currently non-ambulant; jejunostomy; EMG suggestive of motor neuronopathy; cerebellar change and progressive hippocampal change on brain MRI; extensive neurometabolic tests inconclusive; open muscle biopsy showed unusual core-like lesions; normal respiratory chain function; normal genetic investigations include POLG sequencing
26	unilateral cranial neuropathy
27	early-onset BVVL; progressive muscle weakness; head lag; respiratory muscle involvement; axial weakness
28	suspected BVVL; sensory motor neuropathy and denervation on NCS and EMG, with predominant arm involvement; onset at two and a half years after flu-like illness; arm and hand weakness but was initially able to run at the start of her illness; no swallowing problems or ptosis; mild facial weakness; atrophy of the tongue with fasciculations; difficulty with large pieces of food; MRI of brain and spine normal; areflexic throughout; downgoing plantar response; bilateral foot drop; normal acylcarnitine profile; no response to riboflavin or CoQ10
29	familial motor neuron disease; AD inheritance; BVVL-like; 4-year history of bulbar respiratory failure; mother died in her seventies with bulbar respiratory failure; *SOD1* genetic testing is negative
30	severe axonal CMT
31	respiratory distress syndrome; lactic acidosis
32	13 years old; undetectable riboflavin levels; bilateral sensorineural hearing loss; progressive limb weakness; progressive bulbar palsy; scoliosis; on riboflavin treatment
33	failure to thrive with recurrent chest infections, wheezing and vomiting; episodes of choking when eating; legs are thin distally; normal tone and power; EMG revealed widespread denervation of bulbar muscles and tibialis anterior; awaiting a gastrostomy; 2 years old at present; twin brother has drooling episodes and bulbar denervation

Table VI-13: Clinical features of patients without mutations in *SLC52A1*, *SLC52A2* and *SLC52A3* in the BVVL-like cohort designed by a database search.

Patient	Phenotype
1	developmental delay; respiratory problems
2	ataxia with pseudobulbar palsy; patient had a child with respiratory distress who died at 10 years old
3	cataracts; developmental delay; ceberellar atrophy; abnormal muscle respiratory chain enzyme activities
4	myoclonus; respiratory depression; myopathic EMG
5	rapidly progressive brainstem and cerebellar dysfunction leading to respiratory failure; dysphagia; ataxia; nystagmus
6	seizures; developmental delay; respiratory failure
7	5-year history of external ophtalmoplegia; bulbar weakness; respiratory failure
8	sudden-onset weakness; possible mitochondrial respiratory chain disorder
9	died on first day of life; lactic acidosis; respiratory failure
10	daily life-threatening episodes with disordered respiratory pattern; frequently needs resuscitation
11	neurodevelopmental delay; mitochondrial respiratory chain disorder
12	congenital foot deformity; hypotonia; respiration impaired; facial and proximal weakness
13	generalised hypotonia; respiratory insufficiency; normal EMG and MRI of the head
14	muscle respiratory chain enzyme activities indicate reduced complex II/III activity on muscle biopsy
15	weakness and atrophy of neck extensors; onset at about 55 years old; respiratory difficulty
16	twin brother died of respiratory failure
17	respiratory distress syndrome; lactic acidosis
18	acute collapse at 3 hours old; respiratory and metabolic acidosis
19	on ventilation; bilateral sensorineural deafness; developmental delay
20	congenital deafness; cognitive impairment; epilepsy; retinal pigmentation; cortical changes on MRI
21	hypotonia; respiratory infections; feeding difficulties

Patient	Phenotype
22	affected sensory and motor pathways in distal limbs; onset at 9 years old; progressive shortness of breath; weakness of distal extremities; bilateral symmetrical facial weakness; tongue fasciculations; wheelchair-bound
23	generalised weakness; breathlessness on exertion; muscle pain after exertion
24	cardiorespiratory arrest at 24 hours of age; MRI suggestive of global cerebral infarction; possible neurometabolic disorder
25	hypotonia; respiratory failure; gastrostomy-fed; complex III deficiency on biopsy
26	cardiac arrest at 2 hours of age; no respiratory effort; abnormal EEG and EMG
27	signs of motor neurone atrophy on EMG; normal vision; mild hearing loss; mild swallowing difficulties; feet and lower legs most significantly affected; cannot walk on heels or tip toes; distal sensory loss in feet
28	bilateral sensorineural deafness; cerebral symptoms; EMG suggestive of myopathy of facial muscles
29	CMT1A-like but with severe arm involvement; respiratory dysfunction; dominant inheritance
30	breathing problems; seizures
31	progressive myalgia; exercise-induced fatigue; respiratory depression; palatal tremor
32	neuromuscular respiratory failure
33	10-year history of predominant motor neuropathy but with respiratory involvement
34	axonal sensorimotor neuropathy with worsening intercurrent respiratory infections; a mitochondrial-like underlying condition is suspected; normal mitochondrial respiratory chain enzyme activities

Table VI-14: Poorly covered exons in riboflavin transporter genes and *GSTZI* gene in exome sequencing for families SP, MO and TB with BVVL and related neuropathies.

Gene	Family SP- Individual II-3	Family SP- Individual III-1	Family MO- Individual III-3	Family TB- Individual III-3	Family TB- Individual III-8
SLC52A1	None	None	None	None	None
SLC52A2	None	None	Exon 4	None	None
SLC52A3	None	None	Exon 4	None	None
GSTZ1	N/A	N/A	None	N/A	N/A

Table VI-15: Variants identified in known riboflavin transporters in family SP.

Gene	Position	Reference allele	Observed allele	Amino acid change	Type	Functional change	Call	1000 Genomes MAF	EVS MAF	CG69 MAF	dbSNP ID
Individual II-3											
SLC52A1	4937575	T	C	p.Gln70Arg	exonic	nonsynonymous	hom	0.93	0.952965	0.957	rs346822
SLC52A1	4936972	G	A	p.Ala271Val	exonic	nonsynonymous	hom	0.55	0.687674	0.71	rs346821
Individual III-1											
SLC52A1	4937575	T	C	p.Gln70Arg	exonic	nonsynonymous	hom	0.93	0.952965	0.957	rs346822
SLC52A1	4936972	G	A	p.Ala271Val	exonic	nonsynonymous	hom	0.55	0.687674	0.71	rs346821

Table VI-16: Variants identified in known riboflavin transporters and in candidate gene *GSTZ1* in individual III-3 of family MO.

Gene	Position	Reference allele	Observed allele	Amino acid change	Type	Functional change	Call	1000 Genomes MAF	EVS MAF	CG69 MAF	dbSNP ID
SLC52A1	4937575	T	C	p.Gln70Arg	exonic	nonsynonymous	hom	0.93	0.952965	0.957	rs346822
SLC52A1	4936972	G	A	p.Ala271Val	exonic	nonsynonymous	hom	0.55	0.687674	0.71	rs346821
SLC52A3	744415	G	A	p.Pro267Leu	exonic	nonsynonymous	hom	0.21	0.198643	0.167	rs3746804
SLC52A3	744382	G	A	p.Thr278Met	exonic	nonsynonymous	hom	0.09	0.098717	0.051	rs3746803
SLC52A3	744308	T	C	p.Ile303Val	exonic	nonsynonymous	hom	0.1	0.098624	0.058	rs3746802
GSTZ1	77794283	T	C	p.Met27Thr	exonic	nonsynonymous	het	0.87	0.841699	0.906	rs1046428
GSTZ1	77793207	G	A	p.Glu32Lys	exonic	nonsynonymous	het	0.34	0.314464	0.326	rs7975

Table VI-17: Variants identified in known riboflavin transporters in family TB.

Gene	Position	Reference allele	Observed allele	Amino acid change	Type	Functional change	Call	1000 Genomes MAF	EVS MAF	CG69 MAF	dbSNP ID
Individual III-3											
SLC52A1	4937575	T	C	p.Gln70Arg	exonic	nonsynonymous	hom	0.93	0.952965	0.957	rs346822
SLC52A1	4936972	G	A	p.Ala271Val	exonic	nonsynonymous	hom	0.55	0.687674	0.71	rs346821
Individual III-8											
SLC52A1	4937575	T	C	p.Gln70Arg	exonic	nonsynonymous	hom	0.93	0.952965	0.957	rs346822
SLC52A1	4936972	G	A	p.Ala271Val	exonic	nonsynonymous	hom	0.55	0.687674	0.71	rs346821

APPENDIX VII

Table VII-1: MRC complex activities for first optimisation trial of riboflavin concentration in fibroblast cell medium; n=1. All MRC complex activities are expressed as a ratio to CS activity to normalise for mitochondrial enrichment (Hargreaves et al., 1999). *Grown first for four days in medium with 4.7 μg/L (12.6 nM) riboflavin, followed by four days in defined medium.

Control fibroblast line	Riboflavin concentration in cell medium*	MRC Complex I activity	MRC Complex II activity
C1	0.32 μg/l (0.85 nM)	0.065390563	0.084436825
C1	113 μg/l (300.6 nM)	0.282603275	0.332510125
C2	0.32 μg/l (0.85 nM)	0.186116831	0.108491589
C2	113 μg/l (300.6 nM)	0.823152088	0.296516026
C3	0.32 μg/l (0.85 nM)	0.173873657	0.157641114
C3	113 μg/l (300.6 nM)	0.663658178	0.310432895

Table VII-2: MRC complex activities for second optimisation trial of riboflavin concentration in fibroblast cell medium; n=1. All MRC complex activities are expressed as a ratio to CS activity to normalise for mitochondrial enrichment (Hargreaves et al., 1999). *Grown first for four days in medium with 4.7 μg/L (12.6 nM) riboflavin, followed by four days in defined medium.

Control fibroblast line	Riboflavin concentration in cell medium*	MRC Complex I activity	MRC Complex II activity
C1	1.17 μg/l (3.1 nM)	0.477076195	0.170098895
C1	4.7 μg/l (12.6 nM)	0.576471835	0.205537864
C1	113 μg/l (300.6 nM)	0.607107195	0.253486911
C2	1.17 μg/l (3.1 nM)	0.317714591	0.184945944
C2	4.7 μg/l (12.6 nM)	0.430646317	0.104612789
C2	113 μg/l (300.6 nM)	0.674008811	0.161198371
C3	1.17 μg/l (3.1 nM)	0.665687714	0.200517542
C3	4.7 μg/l (12.6 nM)	0.604744473	0.235675835
C3	113 μg/l (300.6 nM)	0.737721086	0.239118543

Table VII-3: Sequences of *SLC52A2* shRNA hairpins and targeted regions.

shRNA clone	Clone ID	Hairpin target region	Hairpin sequence
1	V3LHS_356232	exon 5	cagcatctatcacgtgttcca
2	V3LHS_356235	exon 3	ccaccactgcaagagccaccaa

Table VII-4: Sequence of primer used for sequencing during quality control of the pGIPZ vector.

Primer sequence (5' to 3')
gcattaaagcagcgtatc

Table VII-5: MRC complex activities for optimisation trials of riboflavin concentration in cell medium of shRNA-transfected SH-SY5Y cells. All MRC complex activities are expressed as a ratio to CS activity to normalise for mitochondrial enrichment (Hargreaves et al., 1999). *Riboflavin-free DMEM with regular FBS used (not dialysed FBS).

Experiment Number	Riboflavin concentration in medium	Days in medium	Clone	MRC Complex I activity	MRC Complex II activity
1	10 nM	8	Empty	0.23	0.132
1	10 nM	8	Scrambled	0.204	0.102
1	10 nM	8	*SLC52A2*-shRNA 1	0.198	0.106
1	10 nM	8	*SLC52A2*-shRNA 2	0.15	0.126
1	10 nM	8	*SLC52A2*-shRNA 1+2	0.156	0.128
1	300.6 nM	8	Empty	0.223	0.163
1	300.6 nM	8	Scrambled	0.289	0.131
1	300.6 nM	8	*SLC52A2*-shRNA 1	0.238	0.125
1	300.6 nM	8	*SLC52A2*-shRNA 2	0.193	0.103
1	300.6 nM	8	*SLC52A2*-shRNA 1+2	0.162	0.121
2	3.1 nM	7	Empty	0.088	0.11
2	3.1 nM	7	Scrambled	0.016	0.088
2	3.1 nM	7	*SLC52A2*-shRNA 1	0.037	0.111
2	3.1 nM	7	*SLC52A2*-shRNA 2	0.041	0.077
2	3.1 nM	7	*SLC52A2*-shRNA 1+2	0.051	0.064
2	300.6 nM	7	Empty	0.066	0.18
2	300.6 nM	7	Scrambled	0.07	0.188
2	300.6 nM	7	*SLC52A2*-shRNA 1	0.11	0.211
2	300.6 nM	7	*SLC52A2*-shRNA 2	0.094	0.186
2	300.6 nM	7	*SLC52A2*-shRNA 1+2	0.118	0.175
3	5.89 nM*	8	Scrambled	0.068	0.097
3	5.89 nM*	8	*SLC52A2*-shRNA 1	0.099	0.152
3	5.89 nM*	8	*SLC52A2*-shRNA 1+2	0.155	0.17
3	12.6 nM	4	Scrambled	0.109	0.175
3	12.6 nM	4	*SLC52A2*-shRNA 1	0.094	0.193
3	12.6 nM	4	*SLC52A2*-shRNA 1+2	0.184	0.183
3	8 nM	4	Scrambled	0.116	0.15
3	8 nM	4	*SLC52A2*-shRNA 1	0.144	0.155
3	8 nM	4	*SLC52A2*-shRNA 1+2	0.136	0.166
3	300.6 nM	4	Scrambled	0.123	0.228
3	300.6 nM	4	*SLC52A2*-shRNA 1	0.161	0.188
3	300.6 nM	4	*SLC52A2*-shRNA 1+2	0.094	0.162
4	3.1 nM	1	Empty	0.137	0.14
4	3.1 nM	1	Scrambled	0.125	0.125
4	3.1 nM	1	*SLC52A2*-shRNA 1	0.166	0.141
4	3.1 nM	1	*SLC52A2*-shRNA 2	0.236	0.155
4	3.1 nM	1	*SLC52A2*-shRNA 1+2	0.203	0.119
4	300.6 nM	1	Empty	0.147	0.138
4	300.6 nM	1	Scrambled	0.156	0.133
4	300.6 nM	1	*SLC52A2*-shRNA 1	0.141	0.143
4	300.6 nM	1	*SLC52A2*-shRNA 2	0.142	0.125
4	300.6 nM	1	*SLC52A2*-shRNA 1+2	0.179	0.149

Experiment Number	Riboflavin concentration in medium	Days in medium	Clone	MRC Complex I activity	MRC Complex II activity
5	0.66 nM	1	Empty	0.116	0.136
5	0.66 nM	1	Scrambled	0.095	0.133
5	0.66 nM	1	*SLC52A2*-shRNA 1	0.132	0.129
5	0.66 nM	1	*SLC52A2*-shRNA 2	0.147	0.139
5	0.66 nM	1	*SLC52A2*-shRNA 1+2	0.18	0.106
5	3.1 nM	3	Empty	0.106	0.129
5	3.1 nM	3	Scrambled	0.103	0.114
5	3.1 nM	3	*SLC52A2*-shRNA 1	0.101	0.126
5	3.1 nM	3	*SLC52A2*-shRNA 2	0.166	0.132
5	3.1 nM	3	*SLC52A2*-shRNA 1+2	0.145	0.141

Table VII-6: Sequences of primers used for sequencing during quality control of pCMV6-*SLC52A2*-myc-DDK constructs.

Direction	Primer sequence (5' to 3')
forward	ggactttccaaaatgtcg
reverse	attaggacaaggctggtggg

Table VII-7: Sequences of primers used for site-directed mutagenesis of the pCMV6-*SLC52A2*-myc-DDK plasmid.

Mutation	Direction	Primer sequence (5' to 3')
c.92G>C (p.Trp31Ser)	sense	gctgcggtcaatgggatctcggtggagcta
	antisense	tagctccaccgagatcccattgaccgcagc
c.700C>T (p.Gln234Stop)	sense	ggatcaggcctctaggtgggagccc
	antisense	gggctcccacctagaggcctgatcc
c.916G>A (p.Gly306Arg)	sense	cttttcctgcttaccctacaggcgtctggcctaccacc
	antisense	ggtggtaggccagacgcctgtagggtaagcaggaaaag
c.935T>C (p.Leu312Pro)	sense	ctggcctaccacccggctgtggtgctg
	antisense	cagcaccacagccgggtggtaggccag
c.1016T>C (p.Leu339Pro)	sense	cttggcagggccgggcggcctct
	antisense	agaggccgcccggccctgccaag
c.1258G>A (p.Ala420Thr)	sense	ggctctctgctcggcactgttgctatgttcc
	antisense	ggaacatagcaacagtgccgagcagagagcc

Table VII-8: Sequences of mouse *Slc52a2* and *Slc52a3* shRNA hairpins and targeted regions.

Gene	shRNA clone	Clone ID	Hairpin target region	Hairpin sequence
Slc52a2	Slc52a2-1	V3LMM_485753	exon 3	tgtgggttcagatgtcggg
Slc52a3	Slc52a3-1	V2LMM_17940	5' UTR	aggagaacctgatagatgc
Slc52a3	Slc52a3-2	V3LMM_508722	exon 2	tctccatagtgttcaaggt

Table VII-9: Sequences of DNA primers for the mouse *Slc52a2* used for cDNA quality control.

Gene	Ensembl transcript	Exon	Direction	Primer sequence (5' to 3')	Annealing temperature	PCR protocol	Amplicon length (bp)
Slc52a2	ENSMUST00000023220	5	forward	cgaatctcccctctacgaca	60°C	Roche	247
Slc52a2	ENSMUST00000023220	5	reverse	cacactggtccacacagtcc			

Table VII-10: Sequences of cDNA primers for the mouse *Slc52a2* used for cDNA quality control.

Gene	Direction	Primer sequence (5' to 3')	Annealing temperature	PCR protocol	Amplicon length (bp)
Slc52a2	forward	cggtgcaggctccatgaata	60°C	Roche	207
Slc52a2	reverse	agctctacccagatcccgtt			

APPENDIX VIII

Supplementary study into genetic modifiers of the CMT1A phenotype (Chapter 4)

Introduction

The *PMP22* p.Thr118Met variant in CMT1A: disease modifier, pathogenic mutation, or polymorphism?

Much debate surrounds the potential pathogenicity of the p.Thr118Met variant in *PMP22*. It has been found in both CMT1 and HNPP families, but did not always segregate with the phenotype. While some studies have concluded that it is a non-pathogenic SNP, others have suggested it may act as an AR mutation or a mutation with reduced penetrance; it has also been postulated to either have no influence on the CMT1A phenotype, to cause milder CMT1A phenotypes, or to act as a partial loss of function mutation causing HNPP (Keckarevic-Markovic et al., 2009; Kochañski, 2006; Mersiyanova et al., 2000; Naef & Suter, 1999; Nelis et al., 1997; Niedrist et al., 2009; Roa, Garcia, Pentao, et al., 1993; Russo et al., 2011; Seeman et al., 1999; Shy et al., 2006; Sinkiewicz-Darol et al., 2010; Young et al., 2000). The p.Thr118Met variant has also been proposed to cause a severe form of CMT1 in the compound heterozygous state with the HNPP deletion (Roa, Garcia, Pentao, et al., 1993). Individuals who carried only the p.Thr118Met variant in the heterozygous state in *PMP22* were either phenotypically normal or had CMT1 or HNPP (Nelis et al., 1994; Niedrist et al., 2009; Roa, Garcia, Pentao, et al., 1993; Russo et al., 2011; Seeman et al., 1999; Shy et al., 2006). An individual homozygous for this mutation had an axonal neuropathy, but it remains unclear whether the neuropathy may have been due to another unknown mutation (Shy et al., 2006).

The p.Thr118Met variant causes abnormal PMP22 intracellular trafficking, although less severely so than other *PMP22* point mutations (Naef & Suter, 1999). If this variant indeed decreases trafficking of PMP22, it might decrease the dosage effect of CMT1A and cause milder disease via partial loss of function (Shy et al., 2006), or the two genetic defects may add up to a more severe disease (Marques et al., 2003).

Interestingly, this substitution is found in a CpG dinucleotide, known to be a hypermutable sequence, which may increase the occurrence of this mutation (Marques et al., 2003). Overall, it remains unknown whether the p.Thr118Met variant in *PMP22* may modify the CMT1A phenotype.

The *PMP22* promoter region

Given that changes in *PMP22* copy number cause neuropathy, *PMP22* levels must be tightly controlled (Li et al., 2013). The *PMP22* gene has two alternatively transcribed promoters, promoters 1 and 2, which are developmentally and temporally associated with myelination, providing an additional level of transcriptional control (Maier et al., 2002). Both transcripts produce the same protein and differ only in their 5'UTR region. Promoter 1 is mostly but not exclusively expressed in the PNS, specifically in myelinating Schwann cells (Bosse et al., 1994; Van de Wetering et al., 1999). All the elements needed for Schwann cell-specific expression of a reporter gene are reportedly located 300 bp upstream of the transcription start site in promoter 1 (Saberan-Djoneidi et al., 2000).

The 5' upstream region of the nerve-specific transcript of *PMP22*, including promoter 1 and non-coding exon 1A (Figure VIII-1) contains regulatory elements such as a TATA box (a binding site of transcription factors or histones often found in tissue-specific promoters) as well as an inverted CCAAT box (needed for the initiation of transcription). It also possesses several potential binding sites for transcription factors including steroid receptors, cAMP response element-binding protein and nuclear factor 1 (Hai et al., 2001; Saberan-Djoneidi et al., 2000; Suter et al., 1994). The cAMP response element-binding protein binding sites are located at −1,699 bp and −1,725 bp and are responsible for silencing *PMP22* promoter activity. Nearby these two binding sites is a region polymorphic in terms of the number of CA dinucleotide repeats it contains. Variability in the repeat number could affect the binding of transcription factors at these sites; the number of CA repeats was suggested to be a potential source of phenotypic variability in CMT1A (Saberan-Djoneidi et al., 2000). The 5' upstream region of promoter 1 also includes a "late myelination Schwann cell-specific element" which is responsible for gene regulation

during late phases of myelination during development and in remyelination following injury (Maier et al., 2003).

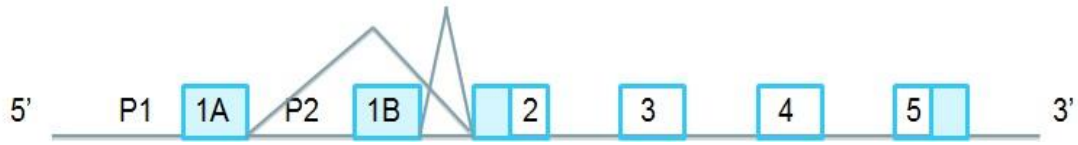

Figure VIII-1: Structure of the *PMP22* gene including location of promoters 1 and 2 (P1 and P2) and non-coding exons 1A and 1B. Adapted from Hai et al. (2001).

Promoter mutations in the *GJB1* nerve-specific 5'UTR region have been associated with CMT1 (Houlden et al., 2004; Kabzinska et al., 2011; Murphy, Polke, et al., 2011). One of these mutations was in a highly conserved binding site for *SRY (sex determining region Y)-box 10* (*SOX10*), a regulator of myelin gene expression, and was found to reduce promoter activity (Houlden et al., 2004). Another *GJB1* promoter variant was located within a domain important for initiation of translation (Kabzinska et al., 2011). Variants in the promoter region found in conjunction with a disease-causing variant in the same gene may modify disease severity. A study of Treacher Collins syndrome, a craniofacial malformation disorder due to null mutations in the *Treacher Collins-Franceschetti syndrome 1* (*TCOF1)* gene, has evaluated the effect on disease severity of promoter mutations in *trans* with the pathogenic mutation. This disease exhibits high intra- and interfamilial clinical variability as is seen in CMT1A. Several variants in the 5'UTR were identified, one of which decreased promoter activity by impairing DNA-binding to a transcription factor. Although the sample size was small, individuals with this functional promoter variant had a milder phenotype (Masotti et al., 2005).

As the *PMP22* promoter region is not traditionally sequenced as part of the CMT1A genetic diagnostic test, variants in this region have rarely been described. A recent study of 45 CMT1A/HNPP patients identified five SNPs in 3.6 Kb of the 5'UTR region of *PMP22*, three of which were also found in controls; the authors concluded that the 5' regulatory sequence of *PMP22* is highly conserved (Sinkiewicz-Darol et al., 2010). Furthermore, a c.-134G>A variant was found in a CMT patient with optic atrophy and a c.-40G>A change was described in a CMT2 patient; both variants were

considered to be benign polymorphisms although an effect on splicing or translational efficiency could not be dismissed (Numakura et al., 2002). The *PMP22* nerve-specific promoter region was also sequenced in 15 CMT1 patients and 16 HNPP patients without Chr17p11.2 rearrangements or *PMP22* point mutations to assess whether variants in this region may be disease-causing. The authors identified one variant in non-coding exon 1A in a CMT1 patient which did not co-segregate with disease in the family, and concluded that variants in this region were not likely to be an important cause of CMT1 or HNPP (Nelis et al., 1998). While variants in the nerve-specific promoter of *PMP22* are not thought to be a common genetic cause of CMT1A, a SNP in the promoter region of *PMP22* may modulate gene dosage by increasing or decreasing the effectiveness of transcription, or by affecting mRNA translation or mRNA stability (Nelis et al., 1998; Sinkiewicz-Darol et al., 2010). Increased *PMP22* dosage causes decreased protein turnover, accumulation of PMP22 and aggregate formation (Fortun et al., 2006; Notterpek et al., 1999); these processes may be relieved or aggravated by the effect of a promoter SNP on transcription or translation of *PMP22* in CMT1A. A mutation in the promoter may also affect exon splicing and the location of the transcription start site (Nelis et al., 1998).

Studies of CMT1A patients found non-uniform *PMP22* mRNA expression in nerve biopsies, with both elevated and nearly normal mRNA levels in heterozygous CMT1A patients (Hanemann et al., 1994; Yoshikawa et al., 1994), as well as highly variable levels of PMP22 protein density in dermal nerve myelin from CMT1A patient skin biopsies (Katona et al., 2009; Li et al., 2005). There was no correlation between the CMTNS and *PMP22* mRNA and protein levels in the dermal nerve myelin of CMT1A patients (Katona et al., 2009). In one of these studies, the most severely affected patient had the lowest *PMP22* mRNA levels, and the most mildly affected patient had the highest *PMP22* mRNA levels (Hanemann et al., 1994). Although this may be an incidental finding, the authors postulated that *PMP22* expression may be down-regulated as the disease progresses (Hanemann et al., 1994). Furthermore, patients with four copies of *PMP22* do not always have a more severe phenotype (Boerkoel et al., 1999; Kaku et al., 1993; LeGuern et al., 1997; Lupski et al., 1991). These studies would suggest that *PMP22* levels do not completely determine the CMT1A phenotype. It may be that genetic modifiers of

CMT1A do not affect *PMP22* levels *per se*, but rather modulate severity by affecting other pathways in which PMP22 is involved. However, studies on this topic are rather scarce and the largest study seeking to correlate *PMP22* levels and CMT1A disease severity in humans used tissue from skin biopsies rather than nerve biopsies to measure *PMP22* levels (Katona et al., 2009).

Inhibiting *PMP22* expression was found to alleviate disease in a CMT1A mouse model, suggesting a link between *PMP22* levels and disease severity (Passage et al., 2004). Admittedly, unlike humans these animals have a defined genetic background, therefore the possibility of genetic modifiers acting as confounding variables is eliminated (Katona et al., 2009). Progesterone, a known stimulator of *Pmp22* expression in cultured rat Schwann cells (Desarnaud et al., 1998) caused upregulation of *Pmp22* mRNA levels and an increase in disease progression in a rat CMT1A model; a progesterone antagonist decreased *Pmp22* mRNA levels and ameliorated the phenotype (Sereda et al., 2003). As progesterone levels increase significantly during pregnancy, it is perhaps not surprising that symptoms worsened during pregnancy in 52% of women with CMT1A (Swan et al., 2007). These studies suggested a relationship between *PMP22* levels and disease severity in CMT1A.

In keeping with the conflicting evidence presented here, it is undoubtedly too early to entirely exclude the role of *PMP22* levels in modulating disease severity in CMT1A. Promoter SNPs in *PMP22* may be a source of further alterations in gene dosage in CMT1A.

The Chr17p11.2 duplication: a source of phenotypic variability?

NAHR, introduced in Section 1.4.3, is responsible for the majority of recurrent rearrangements in the human genome including the CMT1A duplication (Boerkoel et al., 1999; Gu et al., 2008). The CMT1A duplication usually results from NAHR between two highly homologous low-copy repeat sequences located at the extremities of the duplicated region (Chance et al., 1994; Pentao et al., 1992; Reiter et al., 1996). In CMT1A, this event most frequently involves unequal interchromosomal (non-sister chromatid) exchange at meiosis, usually during spermatogenesis (Palau et al., 1993). CMT1A duplications may also result from non-

recurrent mechanisms such as non-homologous end joining (NHEJ), *Alu-Alu* mediated rearrangements, and replication-based Fork Stalling and Template Switching (FosTeS) (Choi et al., 2011; Huang et al., 2010; Zhang et al., 2010). In NAHR, the two duplicated alleles are non-identical except in the rare CMT1A cases with intrachromosomal exchange, where recombination occurs between identical sister chromatids (Lopes et al., 1997). In non-recurrent mechanisms such as FosTeS, alleles are identical as the mechanism is replication-based (Choi et al., 2011). It is possible that meiotic recombination within the duplicated region may lead to differences in the duplicated copies of *PMP22* within a family, which may account for a percentage of the intrafamilial variability in CMT1A (Choi et al., 2011).

Rearrangements occurring via NAHR have fixed breakpoints and result in duplications of identical size in different individuals (Boerkoel et al., 1999; Gu et al., 2008; Zhang et al., 2010). Duplications arising from non-recurrent mechanisms such as NHEJ or FosTeS are variable in size (Gu et al., 2008). The hotspot for recombination within the CMT1A-REP is common to approximately 75%-80% of CMT1A patients and is similar in all populations studied (Boerkoel et al., 1999; Chance et al., 1994; Kiyosawa & chance, 1996, Lopes et al 1996; Marques et al., 2005; Reiter et al., 1996; Yamamoto et al., 1998). CMT1A patients with different breakpoints and smaller duplications which do or do not encompass *PMP22* have been described. These duplications most likely arose from one of the non-recurrent mechanisms described above (Choi et al., 2011; Huang et al., 2010; Ionasescu et al., 1993; Valentijn et al., 1993; Zhang et al., 2010). The phenotypes of the patients with the smaller duplications which included *PMP22* were variable with a large intrafamilial phenotypic spectrum, but were not different from those with the typical duplication (Choi et al., 2011; Kanwal et al., 2011). The subgroup of patients with duplications located upstream of and not including *PMP22* had a somewhat milder phenotype but there were no outstanding clinical features. These alternatively sized duplications would have been missed by traditional diagnostic methods (Weterman et al., 2010; Zhang et al., 2010). It is likely that highly conserved regulatory sequences located in the *PMP22* upstream region are disrupted, thus affecting *PMP22* expression, as the genes located within these smaller duplications are not predicted to be associated with a neuropathy phenotype (Weterman et al., 2010,

Zhang et al., 2010). In fact, three distal enhancers have been found which are approximately 100 Kb upstream of *PMP22* and within the boundaries of two recently identified smaller duplications not containing *PMP22* (Jones et al., 2012). These upstream enhancers contain binding sites for *SOX10* and *EGR2*, two transcription factors known to regulate *PMP22*; duplications at these sites are proposed to cause CMT1A by increasing enhancer activity, and thus *PMP22* expression as well (Jones et al., 2012).

The variable size of the duplication and different haplotypes on the Chr17p11.2 duplicated region observed in these studies highlight the diverse origins of the CMT1A duplication (Lupski et al., 1991; Palau et al. 1993; Raeymaekers et al., 1991). It is possible that variations in the size of the duplication may account for some of the phenotypic heterogeneity in CMT1A.

Methods

Sequencing of *PMP22* gene and upstream promoter region, and detection of p.Thr118Met variant

Patient consent, phenotypes, and DNA samples were obtained as described in Section 4.3.1. Sequencing of the *PMP22* gene and upstream nerve-specific promoter region was performed to identify possible compound forms of CMT1A, to detect the p.Thr118Met variant, and to assess whether *PMP22* SNPs in the promoter region may modulate the CMT1A phenotype. The *PMP22* coding exons and flanking intronic regions, as well as the upstream promoter region and non-coding exon 1A were sequenced in 379 CMT1A patients (186 UK, 83 USA and 110 Brazil patients). PCR amplification, agarose gel electrophoresis, purification of PCR products, Sanger sequencing, dye removal and sequencing analysis were performed using standard conditions as described in Sections 2.1.9-2.1.12. Transcript references used for primer design, as well as primer sequences and PCR cycling conditions can be found in Appendix III Table III-1 and Appendix IV Table IV-2. Primers for the *PMP22* promoter/upstream and exon 1A region were designed to span from 560 bp upstream of the transcription start site to the end of exon 1A, including 15 bp of flanking intronic sequence. Although this would not cover some of the transcription factor

binding sites discussed previously, it encompasses the minimal region necessary for Schwann cell-specific expression. SNP chromosomal locations are based on Genome Build 37.3. In-silico analyses were performed as described in Section 2.6.

Detection of atypical Chr17p11.2 duplications

In the UK CMT1A cohort, atypical Chr17p11.2 duplications were detected as part of the routine diagnostic tests of Chr17p11.2 dosage analysis in the NHNN Neurogenetics Unit. The Neurogenetics laboratory at the NHNN is the main CMT diagnostic centre in South East England. DNA samples were obtained by referrals both external and internal to the Neurogenetics Unit. The P033B-2 CMT1A/HNPP MLPA kit (MRC-Holland, The Netherlands) was used to measure dosage of each *PMP22* exon and other markers within the commonly duplicated 1.5 Mb region (total of eight probes in the duplicated segment) following the manufacturer's instructions. MLPA is a highly sensitive and specific technique to assess sequence dosage in CMT1A (Slater et al., 2004). MLPA data was analysed using GeneMarker software (SoftGenetics, USA). This work was performed entirely by Dr James Polke from the Neurogenetics diagnostic laboratory, NHNN.

Results

Identifying SNPs in the *PMP22* upstream promoter region

The SNPs identified in the *PMP22* promoter region and exon 1A of 379 CMT1A patients are summarized in Table VIII-1. Chromosome locations refer to Genome Build 37.3.

Table VIII-1: *PMP22* promoter and exon 1A SNPs identified in our CMT1A cohort.

Chromosomal Location	PMP22 Region	Base Change	dbSNP ID	Number of CMT1A patients with SNP	CMTNS, if available
17:15168880	UPSTREAM	CC>CT	N/A	1/379	NA
17:15168778	UPSTREAM	TT>TG	N/A	2/379	Patient 1 CMTNS=20; Patient 2 CMTNS=6
17:15168708	UPSTREAM	AA>AG	N/A	1/379	NA
17:15168577; c.-141	5'UTR (non-coding exon 1A)	CC>CG	N/A	1/379	NA
17:15168522; c.-86	5'UTR (non-coding exon 1A)	AA>AC	rs140650630	1/379	CMTNS=13

All SNPs were found in the heterozygous state. Three SNPs were located in the upstream region of *PMP22* and two in the non-coding exon 1A (Figure VIII-2).

Figure VIII-2: Location of regulatory regions and transcription factor binding sites, as well as SNPs within the sequenced region of the *PMP22* promoter and exon 1A identified in this study and in previous studies.

The SNP at 17:15,168,522 (rs140650630) is the only SNP found in online control databases. According to the 1000 Genomes database, it is not found in the European population but has a MAF of 0.039 in the African population. Only the SNP at 17:15,168,708 (SNP closest to the underlined sequence in Figure VIII-2) is located in a known critical region of the promoter; this region is thought to contain a positive regulatory element (Hai et al., 2001). This SNP was found in one patient, but the CMTNS is not available. Also worthy of note is the SNP at 17:15,168,778 in the upstream region, which was found in one severe and one mild patient. The SNP at 17:15,168,577 had been previously identified in a CMT1 patient by Nelis et al. (1998); however, the SNP did not segregate with disease in the family in this study. All SNPs were found in UK patients, except the SNPs at 17:15,168,522 and 17:15,168,880, which were found in Brazilian CMT1A patients. No promoter/exon 1A SNPs were found in the USA cohort. As parental DNA was not available for segregation analysis, phase information is not available for these variants as it is unknown whether the variant was inherited on the duplicated or non-duplicated chromosome in these patients. Whether a variant is in *cis* or *trans* with the duplication may influence its ability to modify *PMP22* expression (Tewhey et al., 2011).

PMP22 sequencing and detection of the p.Thr118Met variant

Sequencing of *PMP22* identified the p.Thr118Met (c.353C>T) variant (dbSNP ID rs104894619) in the heterozygous state in 6 out of 379 CMT1A patients (1.58%; 2 UK patients, 2 USA patients, 2 Brazilian patients). It was found in three mildly affected patients (two of which are from the same family) and one moderately affected patient. Interestingly, in one instance, one sibling with the variant is somewhat more mildly affected than her sibling who does not have this variant. The phenotype is not available for the other two patients carrying this variant. The MAF of this variant is 0.002 in the 1000 Genomes database; it occurs at a frequency of 0.75% in the EVS database. The allele frequency of this variant was 0.019 in a study of 262 Swedish controls (Nelis et al., 1997) and 0.007 in 1,018 German controls (Young et al., 2000). However, in a study of the English population, this variant was not found in 220 individuals including 150 controls, 50 patients with the CMT1A

duplication and 20 patients with the HNPP deletion (Marques et al., 2003); another English study found the variant in 1 out of 176 controls (Russo et al., 2011). A Polish study found the p.Thr118Met variant in 1/45 (2.2%) of CMT1A/HNPP patients (Sinkiewicz-Darol et al., 2010). Notably, this variant was detected in 1/89 *PMP22* sequencing diagnostic tests performed by Dr James Polke in the NHNN Neurogenetics diagnostic laboratory. The cohort included CMT1, CMT2 and HNPP patients; the variant was found in an HNPP patient with recurring episodes of mononeuropathy (Polke et al., 2011). The variant is predicted probably damaging by Polyphen-2 and SIFT, and is highly conserved between species (GERP score=5.16). As is the case for the *PMP22* promoter variants identified in this study, it is unknown whether the p.Thr118Met variant was inherited on the duplicated or non-duplicated chromosome in these patients.

Sequencing of the *PMP22* coding region did not reveal any other potentially pathogenic mutations in the CMT1A cohort; all variants identified other than the p.Thr118Met variant were found at a high frequency in controls in the 1000 Genomes database.

Atypical Chr17p11.2 duplications associated with CMT1A

Between 2008 and 2012, the diagnostic laboratory has detected 200 Chr17p11.2 duplications, 9 of which were of an atypical size; therefore, the frequency for atypical duplications at our diagnostic centre was 4.5% (Polke et al., 2011). All of these atypical duplications included all *PMP22* exons and other MLPA probes within the Chr17p11.2 region except the two probes for the *cytochrome c oxidase assembly homolog 10* (*COX10*) gene, both of which are located in *COX10* exon 7 (Figure VIII-3).

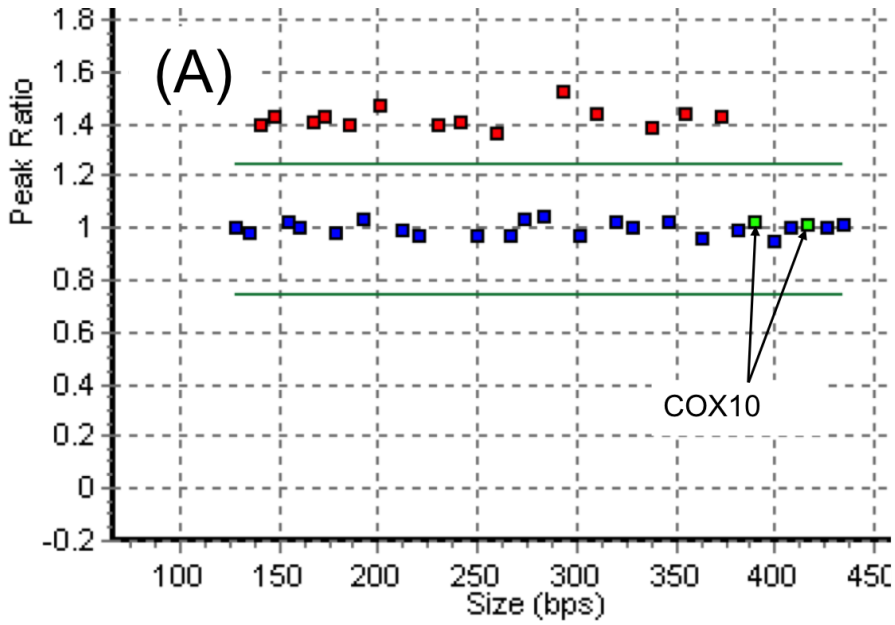

Figure VIII-3: Atypical CMT1A duplication shown on GeneMarker analysis, with dosage of control (blue) and patient (red and green) MLPA probes. A peak ratio of 1 indicates a genomic copy number of 2. Red probes suggest a duplication (peak ratio > 1.25). This example shows one of the atypical Chr17p11.2 duplications found in our study in which all probes except the *COX10* probes are duplicated (reproduced from Polke et al., 2011).

All CMT1A patients with the atypical Chr17p11.2 duplication for which clinical information was available had a mild, typical CMT1A phenotype. The CMTNS had not been determined for these patients. The CMTES was available for one patient (CMTES=14). No data on the frequency of atypical CMT1A duplications was available for the Brazil and USA cohorts.

Discussion

The frequency of the p.Thr118Met variant identified in our CMT1A cohort (1.58%) was similar to the frequency reported in online control databases and studies of English controls. Other than the p.Thr118Met variant, there was no evidence for additional *PMP22* point mutations which may have caused a compound phenotype in the CMT1A patients in this study.

The small number of CMT1A patients with detailed phenotypes who carried promoter/non-coding exon 1A variants and/or the p.Thr118Met variant precludes any conclusion to be drawn about the effects of these variants on disease severity in CMT1A. In retrospect, SNPs identified in the upstream and exon 1A region are not informative because it is not known which allele is duplicated for each SNP. Indeed, due to the nature of the duplication in CMT1A - most frequently unequal crossing-over event between non-sister chromatids - the two duplicated alleles are usually non-identical. Therefore, the haplotype across the duplicated region could not be ascertained without the use of small families with one affected and one unaffected parent and at least one affected child, plus unaffected siblings if available. This part of the study is inconclusive but does not rule out the role of *PMP22* promoter SNPs and the p.Thr118Met variant in modulating the CMT1A phenotype. Larger studies with small families and detailed phenotypes would be necessary in the future. In-vitro functional analysis would be required to determine how the mutations identified in the promoter region and non-coding exon 1A may play a role in modifying the phenotype, if any.

In addition to the *PMP22* upstream enhancer sites, other enhancers outside the promoter region of *PMP22* have been found to regulate *PMP22* expression, including *EGR2* and *SOX10* binding sites within the largest intron of *PMP22* (Jones et al., 2011). *PMP22* is also post-transcriptionally regulated by microRNAs (Verrier et al., 2009). It may be advisable to sequence these binding sites as mutations in these regions may be a cause of CMT or HNPP, or may modify the CMT1A phenotype. Coding polymorphisms within the *PMP22* gene may also alter mRNA stability and modulate the CMT1A phenotype, however again both parents would be needed to determine the genotype of the patients at these SNPs.

The frequency for atypical duplications at our diagnostic centre was 4.5%. The patients with these atypical duplications did not have any outstanding clinical features; the phenotype was that of classic, mild CMT.

COX10 is located approximately 1 Mb from *PMP22*. In typical Chr17p11.2 duplications, only *COX10* exons 6 and 7 are located within the duplicated region therefore one of the *COX10* genes on the duplicated chromosome is missing its first

five exons and promoter region (Figure VIII-4). The *COX10* exon 6 is found on both CMT1A-REPs however the copy on the distal CMT1A-REP is the ancestor copy while the proximal CMT1A-REP has a pseudo copy of *COX10* exon 6 (Boerkoel et al., 1999; Reiter et al., 1997).

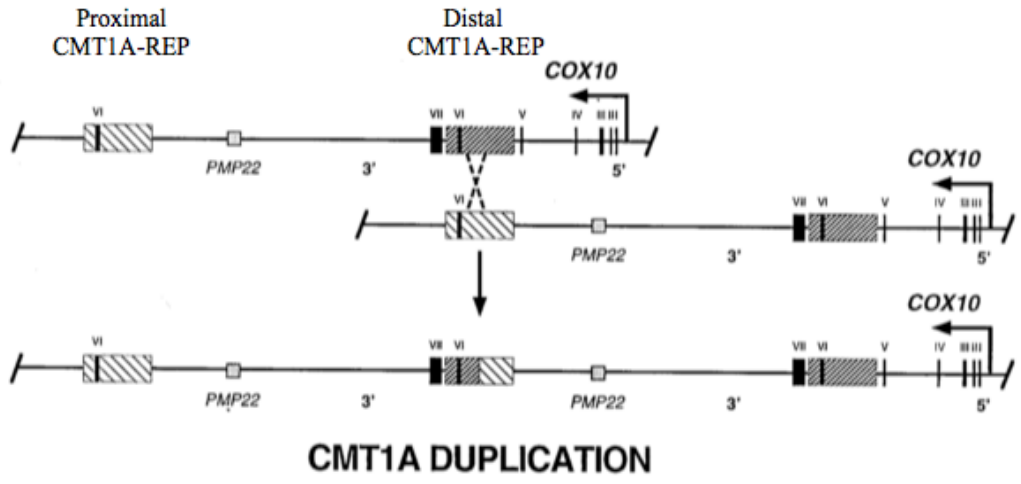

Figure VIII-4: *COX10* and the CMT1A duplication. Roman numerals represent *COX10* exons. Only *COX10* exons 6 and 7 are duplicated in the typical CMT1A duplication (adapted from Reiter et al., 1997).

Although the exact size of the duplication was not determined, all the atypical duplications in our cohort did not include the last (seventh) exon of the *COX10* gene. Patients with the typical duplication have only two normal copies of *COX10* since the rearranged *COX10* gene on the duplicated chromosome is incomplete, and thus it would not be expected to result in a functional COX10 protein (Reiter et al., 1997). Our patients with the atypical duplications not encompassing exon 7 of *COX10* would also be predicted to have two normal copies of *COX10,* which may explain why their phenotype is not dissimilar from CMT1A cases with the typical duplication. Most of the previously described smaller CMT1A duplications also did not encompass *COX10* exon 7 (Choi et al., 2011; Huang et al., 2010; Zhang et al., 2010).

Deletions too small to include *COX10* have been described in HNPP patients. The *COX10* gene on the chromosome of HNPP patients carrying the typical deletion only

contains exons 1 through 6, likely resulting in a null allele of *COX10*. As compound heterozygous mutations in *COX10* lead to severe *COX10* deficiency phenotypes such as Leigh syndrome, an HNPP patient with a mutation in *COX10* on the non-deleted chromosome is predicted to have a much more severe, if not lethal phenotype (Reiter et al., 1997).

The aim of this supplementary study was to assess the potential contribution of selected genetic variants and genomic features in modifying the CMT1A phenotype. The small number of CMT1A patients with duplications of an atypical size had a classic CMT1A phenotype. Screening of the nerve-specific *PMP22* promoter and 5'UTR, a region which is not usually investigated in diagnostic tests, revealed very few rare variants. No concomitant pathogenic variants were identified in the *PMP22* coding region, and the frequency of the *PMP22* p.Thr118Met variant with ambiguous pathogenicity was similar to that reported in control databases. Due to unavailability of DNA for family members, the haplotype across the duplicated region could not be determined for all investigations described above, therefore the SNPs are not informative as the duplicated allele could not be ascertained. Furthermore, the number of patients studied was too small to evaluate the effect of the variants on disease severity in CMT1A. Due to these limitations, data from this study cannot exclude the role of SNPs within the *PMP22* promoter region and the p.Thr118Met variant in modulating CMT1A disease severity.

This supplementary study highlighted some important study design features to be taken into consideration for future research into CMT1A phenotype modifiers. Future studies seeking to identify genetic modifiers of the CMT1A phenotype may wish to determine the haplotype across the entire Chr17p11.2 region in a large cohort of CMT1A patients using small families. Additionally, other CMT genes, neuromuscular genes, or genes encoding components of the myelin sheath may be investigated as potential candidate modifier genes.

APPENDIX IX

The following manuscripts are a result of work presented in this Thesis or undertaken as part of collaborative work during this Thesis. The full text of all published papers are available on the attached disc or specified website.

Foley, R.*, Menezes, M.*, **Pandraud, A.*,** Gonzalez, M. A., Al-Odaib, A., Abrams, A. J., Sugano, K., Yonezawa, A., Manzur, A. Y., Burns, J., Hughes, I., McCullagh, B. G., Jungbluth, H., Lim, M. J., Lin, J. P., Megarbane, A., Urtizberea, J. A., Shah, A. H., Antony, J., Webster, R., Broomfield, A., Ng, J., Mathew, A. A., O'Byrne, J. J., Forman, E., Scoto, M., Prasad, M., O'Brien, K., Olpin, S., Oppenheim, M., Hargreaves, I., Land, J. M., Wang, M. X., Carpenter, K., Horvath, R., Straub, V., Lek, M., Gold, W., Farrell, M. O., Brandner, S., Phadke, R., Matsubara, K., McGarvey, M. L., Scherer, S. S., Baxter, P. S., King, M. D., Clayton, P., Rahman, S., Reilly, M. M., Ouvrier, R. A., Christodoulou, J., Zuchner, S., Muntoni, F., & Houlden, H. (2014). Treatable childhood neuronopathy caused by mutations in riboflavin transporter RFVT2. *Brain, 137*(Pt 1), 44-56. ***These authors contributed equally to this work.**

Johnson, J. O., Gibbs, J. R., Megarbane, A., Urtizberea, J. A., Hernandez, D. G., Foley, A. R., Arepalli, S., **Pandraud, A.**, Simon-Sanchez, J., Clayton, P., Reilly, M. M., Muntoni, F., Abramzon, Y., Houlden, H., & Singleton, A. B. (2012). Exome sequencing reveals riboflavin transporter mutations as a cause of motor neuron disease. *Brain, 135*(Pt 9), 2875–2882.

Koutsis, G., Karadima, G., **Pandraud, A.**, Sweeney, M. G., Paudel, R., Houlden, H., Wood, N.W., & Panas, M. (2012). Genetic screening of Greek patients with Huntington's disease phenocopies identifies an *SCA8* expansion. *Journal of neurology, 259*(9), 1874-1878.

Koutsis, G., **Pandraud, A.**, Karadima, G., Panas, M., Reilly, M. M., Floroskufi, P., Wood, N. W., & Houlden, H. (2013). Mutational analysis of *PMP22*, *EGR2*,

LITAF and *NEFL* in Greek Charcot-Marie-Tooth type 1 patients. *Clinical genetics*, *83*(4), 388–391.

Koutsis, G., **Pandraud, A.**, Polke, J. M., Wood, N. W., Panas, M., Karadima, G., & Houlden, H. (2012). Novel *peripheral myelin protein 22* (*PMP22*) micromutations associated with variable phenotypes in Greek patients with Charcot–Marie–Tooth disease. *Brain*, *135*(Pt 8), e217.

Murphy, S. M., Laura, M., Fawcett, K., **Pandraud, A.**, Liu, Y.-T., Davidson, G. L., Rossor, A. M., Polke, J. M., Castleman, V., Manji, H., Lunn, M. P., Bull, K., Ramdharry, G., David, M., Blake, J. C., Houlden, H., & Reilly, M. M. (2012). Charcot-Marie-Tooth disease: frequency of genetic subtypes and guidelines for genetic testing. *Journal of neurology, neurosurgery, and psychiatry*, *83*(7), 706–710.

Pandraud, A. (in press). Peripheral nerve neuropathies including CMT disease. In A. Schapira, Z. Wszolek, T. Dawson, & N. Wood (Eds.), Neurodegeneration (pp. unknown). Oxford: Wiley-Blackwell.

Pandraud, A., Liu, Y., & Houlden, H. (2012). Advances in the genetics of peripheral nerve disorders. *Advances in clinical neuroscience and rehabilitation*, *12*(2), 8-13.

Urtizberea, J. A., Megarbane, A., & **Pandraud, A**. (2013). Tête tombante, surdité et vitamine B_2: une association non fortuite. *Les cahiers de myologie*, *8*, 9–10. **(available at http://medias.afm-telethon.fr/Media/1855/cdm_08.zip/index.htm).**

Voermans, N. C., Kleefstra, T., Gabreëls-Festen, A. A., Faas, B. H. W., Kamsteeg, E.-J., Houlden, H., Laura, M., Polke, J. M., **Pandraud, A**., van Ruissen, F., van Engelen, B. G., & Reilly, M. M. (2012). Severe Dejerine-Sottas disease with respiratory failure and dysmorphic features in association with a *PMP22* point mutation and a 3q23 microdeletion. *Journal of the peripheral nervous system*, *17*(2), 223–225.

References

Abe, A., Numakura, C., Saito, K., Koide, H., Oka, N., Honma, A., Kishikawa, Y., & Hayasaka, K. (2009). Neurofilament light chain polypeptide gene mutations in Charcot-Marie-Tooth disease: nonsense mutation probably causes a recessive phenotype. *Journal of human genetics*, *54*(2), 94–97.

Abramov, A. Y., Smulders-Srinivasan, T. K., Kirby, D. M., Acin-Perez, R., Enriquez, J. A., Lightowlers, R. N., Duchen, M. R., & Turnbull, D. M. (2010). Mechanism of neurodegeneration of neurons with mitochondrial DNA mutations. *Brain*, *133*(Pt 3), 797–807.

Acsadi, G., Lee, I., Li, X., Khaidakov, M., Pecinova, A., Parker, G. C., & Hüttemann, M. (2009). Mitochondrial dysfunction in a neural cell model of spinal muscular atrophy. *Journal of neuroscience research*, *87*(12), 2748–2756.

Adlkofer, K., Martini, R., Aguzzi, A., Zielasek, J., Toyka, K., & Suter, U. (1995). Hypermyelination and demyelinating peripheral neuropathy in Pmp22-deficient mice. *Nature genetics*, *11*, 274–280.

Adzhubei, I. A., Schmidt, S., Peshkin, L. Ramensky, V. E., Gerasimova, A., Bork, P., Kondrashov, A. S., & Sunyaev, S. R. (2010). A method and server for predicting damaging missense mutations. *Nature methods*, *7*(4), 248-249.

Alhadeff, L., Gualtieri, C. T., & Lipton, M. (1984). Toxic effects of water-soluble vitamins. *Nutrition reviews*, *42*(2), 33–40.

Allgrove, J., Clayden, G. S., Grant, D. B., & Macaulay, J. C. (1978). Familial glucocorticoid deficiency with achalasia of the cardia and deficient tear production. *The Lancet*, *1*(8077), 1284–1286.

Amato, A. A., & Reilly, M. M. (2011). The death panel for Charcot-Marie-Tooth panels. *Annals of neurology*, *69*(1), 1–4.

Anand, G., Hasan, N., Jayapal, S., Huma, Z., Ali, T., Hull, J., Blair, E., McShane, T., & Jayawant, S. (2012). Early use of high-dose riboflavin in a case of Brown-Vialetto-Van Laere syndrome. *Developmental medicine and child neurology*, *54*(2), 187–189.

Anderson, C. A, Pettersson, F. H., Clarke, G. M., Cardon, L. R., Morris, A. P., & Zondervan, K. T. (2010). Data quality control in genetic case-control association studies. *Nature protocols*, *5*(9), 1564–1573.

Asbury, A. K., & Thomas, P. K. (1995). *Peripheral Nerve Disorders 2.* Oxford: Butterworth-Heinemann.

Azzedine, H., Senderek, J., Rivolta, C., & Chrast, R. (2012). Molecular genetics of charcot-marie-tooth disease: from genes to genomes. *Molecular syndromology*, *3*(5), 204–214.

Bafunno, V., Giancaspero, T. A., Brizio, C., Bufano, D., Passarella, S., Boles, E., & Barile, M. (2004). Riboflavin uptake and FAD synthesis in Saccharomyces cerevisiae mitochondria: involvement of the Flx1p carrier in FAD export. *The Journal of biological chemistry*, *279*(1), 95–102.

Baker, S. K., & Tarnopolsky, M. A. (2003). Targeting cellular energy production in neurological disorders. *Expert opinion on investigational drugs*, *12*(10), 1655–1679.

Balding, D. J. (2006). A tutorial on statistical methods for population association studies. *Nature reviews: genetics*, *7*(10), 781–791.

Bamshad, M. J., Ng, S. B., Bigham, A. W., Tabor, H. K., Emond, M. J., Nickerson, D. A., & Shendure, J. (2011). Exome sequencing as a tool for mendelian disease gene discovery. *Nature reviews: genetics*, *12*(11), 745–755.

Bandettini di Poggio, M., Gagliardi, S., Pardini, M., Marchioni, E., Monti Bragadin, M., Reni, L., Doria-Lamba, L., Roccatagliata, L., Ceroni, M., Schenone, A., &

Cereda, C. (2013). A novel compound heterozygous mutation of *C20orf54* gene associated with Brown-Vialetto-Van Laere syndrome in an Italian family. *European journal of neurology*, *20*(7), e94–95.

Bandettini Di Poggio, M., Monti Bragadin, M., Reni, L., Doria-Lamba, L., Cereda, C., Pardini, M., Roccatagliata, M., Rossi, A., & Schenone, A. (2014). Brown-Vialetto-Van Laere syndrome: Clinical and neuroradiological findings of a genetically proven patient. *Amyotrophic lateral sclerosis & frontotemporal degeneration*, *15*(1-2), 141-144.

Banerjee, J., & Wedegaertner, P. B. (2004). Identification of a novel sequence in PDZ-RhoGEF that mediates interaction with the actin cytoskeleton. *Molecular biology of the cell*, *15*, 1760–1775.

Bar-Meir, M., Elpeleg, O. N., & Saada, A. (2001). Effect of various agents on adenosine triphosphate synthesis in mitochondrial complex I deficiency. *The Journal of pediatrics*, *139*(6), 868–870.

Baranowska, I., Jäderlund, K. H., Nennesmo, I., Holmqvist, E., Heidrich, N., Larsson, N.-G., Andersson, G., Wagner, E. G., Hedhammar, A., Wibom, R., & Andersson, L. (2009). Sensory ataxic neuropathy in golden retriever dogs is caused by a deletion in the mitochondrial tRNATyr gene. *PLoS genetics*, *5*(5), e1000499.

Barile, M., Brizio, C., Valenti, D., De Virgilio, C., & Passarella, S. (2000). The riboflavin/FAD cycle in rat liver mitochondria. *European journal of biochemistry*, *267*(15), 4888–4900.

Bartolini, F., Tian, G., Piehl, M., Cassimeris, L., Lewis, S. A, & Cowan, N. J. (2005). Identification of a novel tubulin-destabilizing protein related to the chaperone cofactor E. *Journal of cell science*, *118*(Pt 6), 1197–1207.

Bartolome, F., Wu, H.-C., Burchell, V. S., Preza, E., Wray, S., Mahoney, C. J., Fox, N. C., Calvo, A., Canosa, A., Moglia, C., Mandrioli, J., Chio, A., Orrell, R. W.,

Houlden, H., Hardy, J., Abramov, A. Y., & Plun-Favreau, H. (2013). Pathogenic *VCP* mutations induce mitochondrial uncoupling and reduced ATP levels. *Neuron*, *78*(1), 57-64.

Ben Youssef-Turki, I., Kraoua, I., Gargouri, A., Bouche, P., Leguern, E., & Gouider-Khouja, N. (2011). Un CMT1A genetiquement confirmee mimant une CIDP a rechute. *Revue neurologique*, *167*(12), 955-959.

Bennett, M. J. (2012). Brown-Vialetto-Van Laere and Fazio Londe syndromes: defects of riboflavin transport with biochemical similarities to multiple acyl-CoA dehydrogenation defects (MADD). *Journal of inherited metabolic disease*, *35*(6), 941–942.

Berciano, J., Fernández-Torre, J. L., Ramón, C., Pelayo-Negro, A. L., & Infante, J. (2012). Subclinical Charcot-Marie-Tooth disease type 1A in an ex-professional cyclist. *Clinical neurology and neurosurgery*, *114*(4), 394-395.

Bernsen, P. L., Gabreëls, F. J., Ruitenbeek, W., & Hamburger, H. L. (1993). Treatment of complex I deficiency with riboflavin. *Journal of the neurological sciences*, *118*(2), 181–187.

Biedler, J. L., Helson, L., & Spengler, B. A. (1973). Morphology and growth, tumorigenicity, and cytogenetics of human neuroblastoma cells in continuous culture. *Cancer research*, *33*(11), 2643–2652.

Biedler, J. L., Roffler-tarlov, S., Schachner, M., & Freedman, L. S. (1978). Multiple neurotransmitter synthesis by human neuroblastoma cell lines and clones. *Cancer research*, *38*(11 Pt 1), 3751–3757.

Bilsland, L. G., Nirmalananthan, N., Yip, J., Greensmith, L., & Duchen, M. R. (2008). Expression of mutant $SOD1^{G93A}$ in astrocytes induces functional deficits in motoneuron mitochondria. *Journal of neurochemistry*, *107*, 1271-1283.

Birch-Machin, M. A., Briggs, H. L., Saborido, A. A., Bindoff, L. A., & Turnbull, D. M. (1994). An evaluation of the measurement of the activities of complexes I-IV in the respiratory chain of human skeletal muscle mitochondria. *Biochemical medicine and metabolic biology*, *51*(1), 35-42.

Birouk, N., Gouider, R., Le Guern, E., Gugenheim, M., Tardieu, S., Maisonobe, T., LeForestier, N., Agid, Y., Brice, A., & Bouche, P. (1997). Charcot-Marie-Tooth disease type 1A with 17p11.2 duplication: Clinical and electrophysiological phenotype study and factors influencing disease severity in 119 cases. *Brain*, *120*(Pt 5), 813–823.

Biswas, A., Elmatari, D., Rothman, J., LaMunyon, C. W., & Said, H. M. (2013). Identification and functional characterization of the Caenorhabditis elegans riboflavin transporters rft-1 and rft-2. *PloS one*, *8*(3), e58190.

Blair, I. P., Nash, J., Gordon, M. J., & Nicholson, G. A. (1996). Prevalence and origin of de novo duplications in Charcot-Marie-Tooth disease type 1A: first report of a de novo duplication with a maternal origin. *American journal of human genetics*, *58*(3), 472–476.

Boerkoel, C. F., Inoue, K., Reiter, L., Warner, L., & Lupski, J. (1999). Molecular mechanisms for CMT1A duplication and HNPP deletion. *Annals New York academy of sciences*, *883*, 22–35.

Boerkoel, C. F., Takashima, H., Bacino, C., Daentl, D., & Lupski, J. (2001). EGR2 mutation R359W causes a spectrum of Dejerine-Sottas neuropathy. *Neurogenetics*, *3*(3), 153–157.

Boerkoel, C. F., Takashima, H., Garcia, C. A., Olney, R. K., Johnson, J., Berry, K., Russo, P., Kennedy, S., Teebi, A. S., Scavina, M., Williams, L. L., Mancias, P., Butler, I. J., Krajewski, K., Shy, M., & Lupski, J. R. (2002). Charcot-Marie-Tooth disease and related neuropathies: Mutation distribution and genotype-phenotype correlation. *Annals of neurology*, *51*(2), 190–201.

Boitier, E., Degoul, F., Desguerre, I., Charpentier, C., François, D., Ponsot, G., Diry, M., Rustin, P., & Marsac, C. (1998). A case of mitochondrial encephalomyopathy associated with a muscle coenzyme Q10 deficiency. *Journal of the neurological sciences*, *156*(1), 41-46.

Bommel, H., Xie, G., Rossoll, W., Wiese, S., Jablonka, S., Boehm, T., & Sendtner, M. (2002). Missense mutation in the tubulin-specific chaperone E (Tbce) gene in the mouse mutant progressive motor neuronopathy, a model of human motoneuron disease. *The Journal of cell biology*, *159*(4), 563–569.

Bosch, A. M., Abeling, N. G. G. M., Ijlst, L., Knoester, H., van der Pol, W. L., Stroomer, A. E. M., Wanders, R. J., Visser, G., Wijburg, F. A., Duran, M., & Waterham, H. R. (2011). Brown-Vialetto-Van Laere and Fazio Londe syndrome is associated with a riboflavin transporter defect mimicking mild MADD: a new inborn error of metabolism with potential treatment. *Journal of inherited metabolic disease*, *34*(1), 159–164.

Bosch, A. M., Stroek, K., Abeling, N. G., Waterham, H. R., Ijlst, L., & Wanders, R. J. A. (2012). The Brown-Vialetto-Van Laere and Fazio Londe syndrome revisited: natural history, genetics, treatment and future perspectives. *Orphanet journal of rare diseases*, *7*, 83.

Bosse, F., Zoidl, G., Wilms, S., Gillen, C. P., Kuhn, H. G., & Müller, H. W. (1994). Differential expression of two mRNA species indicates a dual function of peripheral myelin protein PMP22 in cell growth and myelination. *Journal of neuroscience research*, *37*(4), 529–537.

Bouhy, D., & Timmerman, V. (2013). Animal models and therapeutic prospects for Charcot-Marie-Tooth disease. *Annals of neurology*, *74*(3), 391-396.

Braathen, G. J., Sand, J. C., Lobato, A., Høyer, H., & Russell, M. B. (2011). Genetic epidemiology of Charcot-Marie-Tooth in the general population. *European journal of neurology*, *18*(1), 39-48.

Brady, P. S., & Hoppel, C. L. (1985). Hepatic peroxisomal and mitochondrial fatty acid oxidation in the riboflavin-deficient rat. *The Biochemical journal*, *229*(3), 717–721.

Brand, M. D., & Nicholls, D. G. (2011). Assessing mitochondrial dysfunction in cells. *The Biochemical journal*, *435*(2), 297–312.

Briani, C., Taioli, F., Lucchetta, M., Bombardi, R., & Fabrizi, G. (2010). Adult onset Charcot-Marie-Tooth disease type 1D with an Arg381Cys mutation of *EGR2*. *Muscle & nerve*, *41*(6), 888–889.

Brown, C.H. (1894). Infantile amyotrophic lateral sclerosis of the family type. *Journal of nervous and mental disease*, *21*, 707–716.

Bruun, C. S., Jäderlund, K. H., Berendt, M., Jensen, K. B., Spodsberg, E. H., Gredal, H., Shelton, G. D., Mickelson, J. R., Minor, K. M., Lohi, H., Bjerkas, I., Stigen, O., Espenes, A., Rohdin, C., Edlund, R., Ohlsson, J., Cizinauskas, S., Leifsson, P. S., Drogemuller, C., Moe, L., Cirera, S., & Fredholm, M. (2013). A Gly98Val mutation in the N-Myc downstream regulated gene 1 (NDRG1) in Alaskan Malamutes with polyneuropathy. *PloS one*, *8*(2), e54547.

Bugiani, M., Lamantea, E., Invernizzi, F., Moroni, I., Bizzi, A., Zeviani, M., & Uziel, G. (2006). Effects of riboflavin in children with complex II deficiency. *Brain & development*, *28*(9), 576–581.

Burch, H. B., Hunter, F. E., Combs, A. M., & Schutz, B. A. (1960). Oxidative enzymes and phosphorylation in hepatic mitochondria from riboflavin-deficient rats. *The Journal of biological chemistry*, *235*(6), 1540–1544.

Burch, H. B., Lowry, O., Padilla, A., & Combs, A. (1956). Effects of riboflavin deficiency and realimentation on flavin enzymes of tissues. *The Journal of biological chemistry*, *223*, 29–45.

Burchell, V. S., Gandhi, S., Deas, E., Wood, N. W., Abramov, A. Y., & Plun-Favreau, H. (2010). Targeting mitochondrial dysfunction in neurodegenerative disease: Part I. *Expert opinion on therapeutic targets*, *14*(4), 369–385.

Burgess, C. M., Slotboom, D. J., Geertsma, E. R., Duurkens, R. H., Poolman, B., & van Sinderen, D. (2006). The riboflavin transporter RibU in Lactococcus lactis: Molecular characterization of gene expression and the transport mechanism. *Journal of bacteriology*, *188*(8), 2752–2760.

Cai, Z., Blumbergs, P. C., Finnie, J. W., Manavis, J., & Thompson, P. D. (2009). Selective vulnerability of peripheral nerves in avian riboflavin deficiency demyelinating polyneuropathy. *Veterinary pathology*, *46*(1), 88–96.

Camporeale, G., & Zempleni, J. (2003). Oxidative folding of interleukin-2 is impaired in flavin-deficient jurkat cells, causing intracellular accumulation of interleukin-2 and increased expression of stress response genes. *The Journal of nutrition*, *133*, 668–672.

Camu, W., & Henderson, C. E. (1994). Rapid purification of embryonic rat motoneurons: an in vitro model for studying MND/ALS pathogenesis. *Journal of the neurological sciences*, *124*(suppl), 73-74.

Carenini, S., Mäurer, M., Werner, A., Blazyca, H., Toyka, K. V, Schmid, C. D., Raivich, G., & Martini, R. (2001). The role of macrophages in demyelinating peripheral nervous system of mice heterozygously deficient in p0. *The Journal of cell biology*, *152*(2), 301–308.

Cartoni, R., Arnaud, E., Médard, J.-J., Poirot, O., Courvoisier, D. S., Chrast, R., & Martinou, J.-C. (2010). Expression of mitofusin 2(R94Q) in a transgenic mouse leads to Charcot-Marie-Tooth neuropathy type 2A. *Brain*, *133*(Pt 5), 1460–1469.

Carvalho, A. A. S., Vital, A., Ferrer, X., Latour, P., Lagueny, A., Brechenmacher, C., & Vital, C. (2005). Charcot-Marie-Tooth disease type 1A: clinicopathological

correlations in 24 patients. *Journal of the peripheral nervous system, 10*(1), 85–92.

Castro, C., Gómez-Hernandez, J. M., Silander, K., & Barrio, L. C. (1999). Altered formation of hemichannels and gap junction channels caused by C-terminal connexin-32 mutations. *The Journal of neuroscience, 19*(10), 3752–3760.

Cecchini, G. (2003). Function and structure of complex II of the respiratory chain. *Annual review of biochemistry, 72*, 77–109.

Chance, P. F., Abbas, N., Lensch, M. W., Pentao, L., Roa, B. B., Patel, P. I., & Lupski, J. R. (1994). Two autosomal dominant neuropathies result from reciprocal DNA duplication/deletion of a region on chromosome 17. *Human molecular genetics*, *3*(2), 223–228.

Chance, P. F., Alderson, M. K., Leppig, K. A., Lensch, M. W., Matsunami, N., Smith, B., Swanson, P. D., Odelberg, S. J., Disteche, C. M., & Bird, T. D. (1993). DNA deletion associated with hereditary neuropathy with liability to pressure palsies. *Cell*, *72*(1), 143–151.

Chapon, F., Diraison, P., Lechevalier, B., Chazot, G., Viader, F., Bonnebouche, C., Vandenberghe, A., Timmerman, V., & Van Broeckhoven, C. (1996). Hereditary neuropathy with liability to pressure palsies with a partial deletion of the region often duplicated in Charcot-Marie-Tooth disease, type 1A. *Journal of neurology, neurosurgery and psychiatry*, *61*(5), 535–536.

Charcot, J. M., & Marie, P. (1886). Sur une forme particulière d'atrophie musculaire progressive, souvent familiale débutant par les pieds et les jambes et atteignant plus tard les mains. *Revue de medecine, 6,* 97–138.

Chiong, M. A., Sim, K., Carpenter, K., Rhead, W., Ho, G., Olsen, R. K. J., & Christodoulou, J. (2007). Transient multiple acyl-CoA dehydrogenation deficiency in a newborn female caused by maternal riboflavin deficiency. *Molecular genetics and metabolism*, *92*, 109–114.

Choi, B.-O., Kim, N. K., Park, S. W., Hyun, Y. S., Jeon, H. J., Hwang, J. H., & Chung, K. W. (2011). Inheritance of Charcot-Marie-Tooth disease 1A with rare nonrecurrent genomic rearrangement. *Neurogenetics*, *12*(1), 51–58.

Choi, B.-O., Koo, S. K., Park, M.-H., Rhee, H., Yang, S.-J., Choi, K.-G., Jung, S. C., Kim, H. S., Hyun, Y. S., Nakhro, K., Lee, H. J., Woo, H. M., & Chung, K. W. (2012). Exome sequencing is an efficient tool for genetic screening of Charcot-Marie-Tooth disease. *Human mutation*, *33*(11), 1610–1615.

Choi, B., Lee, M. S., Shin, S. H., Hwang, J. H., Choi, K., Kim, W.-K., Sunwoo, I. N., Kim, N. K., & Chung, K. W. (2004). Mutational analysis of *PMP22, MPZ, GJB1, EGR2* and *NEFL* in Korean Charcot-Marie-Tooth neuropathy patients. *Human mutation*, *24*(2), 185-186.

Choi, M., Scholl, U. I., Ji, W., Liu, T., Tikhonova, I. R., Zumbo, P., Nayir, A., Bakkaloglu, A., Ozen, S., Sanjad, S., Nelson-Williams, C., Farhi, A., Mane, S., & Lifton, R. P. (2009). Genetic diagnosis by whole exome capture and massively parallel DNA sequencing. *PNAS*, *106*(45), 19096–19101.

Chung, K. W., Sunwoo, I. N., Kim, S. M., Park, K. D., Kim, W.-K., Kim, T. S., Koo, H., Cho, M., Lee, J., & Choi, B. O. (2005). Two missense mutations of *EGR2* R359W and *GJB1* V136A in a Charcot-Marie-Tooth disease family. *Neurogenetics*, *6*(3), 159–163.

Ciccolella, M., Catteruccia, M., Benedetti, S., Moroni, I., Uziel, G., Pantaleoni, C., Chiapparini, L., Bizzi, A., D'Amico, A., Fattori, F., Salsano, M. L., Pastore, A., Tozzi, G., Piemonte, F., & Bertini, E. (2012). Brown-Vialetto-van Laere and Fazio-Londe overlap syndromes: a clinical, biochemical and genetic study. *Neuromuscular disorders*, *22*(12), 1075–1082.

Ciccolella, M., Corti, S., Catteruccia, M., Petrini, S., Tozzi, G., Rizza, T., Carrozzo, R., Nizzardo, M., Bordoni, A., Ronchi, D., D'Amico, A., Rizzo, C., Comi, G. P., & Bertini, E. (2013). Riboflavin transporter 3 involvement in infantile

Brown-Vialetto-Van Laere disease: two novel mutations. *Journal of medical genetics*, *50*(2), 104–107.

Cirak, S., Foley, A. R., Herrmann, R., Willer, T., Yau, S., Stevens, E., Torelli, S., Brodd, L., Kamynina, A., Vondracek, P., Roper, H., Longman, C., Korinthenberg, R., Marrosu, G., Nürnberg, P., UK10K Consortium, Michele, D., Plagnol, V., Hurles, M., Moore, S. A., Sewry, C. A., Campbell, K. P., Voit, T., & Muntoni, F. (2013). *ISPD* gene mutations are a common cause of congenital and limb girdle muscular dystrophies. *Brain*, *136*(Pt 1), 269-281.

Clarke, G. M., Anderson, C. A., Pettersson, F. H., Cardon, L. R., Morris, A. P., & Zondervan, K. T. (2011). Basic statistical analysis in genetic case-control studies. *Nature protocols*, *6*(2), 121–133.

Coates, J. R., & O'Brien, D. P. (2004). Inherited peripheral neuropathies in dogs and cats. *Veterinary Clinics of North America: Small Animal Practice*, *34*(6), 1361–1401.

Cooper, G. M., & Shendure, J. (2011). Needles in stacks of needles: finding disease-causal variants in a wealth of genomic data. *Nature reviews: Genetics*, *12*(9), 628–640.

Cornelius, N., Byron, C., Hargreaves, I., Guerra, P. F., Furdek, A. K., Land, J., Radford, W. W., Frerman, F., Corydon, T. J., Gregersen, N., & Olsen, R. K. J. (2013). Secondary coenzyme Q10 deficiency and oxidative stress in cultured fibroblasts from patients with riboflavin responsive multiple acyl-CoA dehydrogenation deficiency. *Human molecular genetics*, *22*(19), 3819-3827.

Cornelius, N., Frerman, F. E., Corydon, T. J., Palmfeldt, J., Bross, P., Gregersen, N., & Olsen, R. K. (2012). Molecular mechanisms of riboflavin responsiveness in patients with ETF-QO variations and multiple acyl-CoA dehydrogenation deficiency. *Human molecular genetics*, *21*(15), 3435–3448.

Cortes, A., & Brown, M. A. (2011). Promise and pitfalls of the Immunochip. *Arthritis research & therapy*, *13*(1), 101.

Côté, F., Collard, J. F., & Julien, J. P. (1993). Progressive neuronopathy in transgenic mice expressing the human neurofilament heavy gene: a mouse model of amyotrophic lateral sclerosis. *Cell*, *73*(1), 35–46.

Cozzolino, M., & Carrì, M. T. (2012). Mitochondrial dysfunction in ALS. *Progress in neurobiology*, *97*(2), 54–66.

Crossman, A. R., & Neary, D. (2010). *Neuroanatomy (Fourth edition)*. Edinburgh: Churchill Livingstone, Elsevier.

D'Ydewalle, C., Benoy, V., & Van Den Bosch, L. (2012). Charcot-Marie-Tooth disease: emerging mechanisms and therapies. *The International journal of biochemistry & cell biology*, *44*(8), 1299–1304.

Da Silva-Júnior, F. P., Moura, R. D. D., Rosemberg, S., Marchiori, P. E., & Castro, L. H. M. (2011). Cor pulmonale in a patient with Brown-Vialetto-Van Laere syndrome: a case report. *Journal of the neurological sciences*, *300*(1-2), 155–156.

Dakhil, F. O., Bensreiti, S. M., & Zew, M. H. (2010). Pontobulbar palsy and sensorineural deafness (Brown-Vialetto-van Laere syndrome): the first case from Libya. *Amyotrophic lateral sclerosis*, *11*(4), 397–398.

Dalakas, M. C. (2011). Advances in the diagnosis, pathogenesis and treatment of CIDP. *Nature reviews. Neurology*, *7*(9), 507–517.

Davey, G. P. (1998). Energy thresholds in brain mitochondria: Potential involvement in neurodegeneration. *Journal of biological chemistry*, *273*(21), 12753–12757.

De Grandis, D., Passadore, P., Chinaglia, M., Brazzo, F., Ravenni, R., & Cudia, P. (2005). Clinical features and neurophysiological follow-up in a case of Brown-Vialetto-Van Laere syndrome. *Neuromuscular disorders*, *15*(8), 565–568.

De Jonge, R. R., Vreijling, J. P., Meintjes, A., Kwa, M. S., van Kampen, A. H., van Schaik, I., & Baas, F. (2003). Transcriptional profile of the human peripheral nervous system by serial analysis of gene expression. *Genomics*, *82*(2), 97–108.

Depeint, F., Bruce, W. R., Shangari, N., Mehta, R., & O'Brien, P. J. (2006). Mitochondrial function and toxicity: role of the B vitamin family on mitochondrial energy metabolism. *Chemico-biological interactions*, *163*(1-2), 94–112.

Desarnaud, F., Do Thi, A. N., Brown, A. M., Lemke, G., Suter, U., Baulieu, E. E., & Schnumacher, M. (1998). Progesterone stimulates the activity of the promoters of peripheral myelin protein-22 and protein zero genes in Schwann cells. *Journal of neurochemistry*, *71*(4), 1765–1768.

Descatha, A., Goddet, S., Aboab, J., Allary, J., Gergereau, A., Baer, M., & Fletcher, D. (2006). Cardiac arrest in a patient with Brown-Vialetto-Van Laere syndrome. *Amyotrophic lateral sclerosis*, *7*(3), 187–188.

Desurkar, A., Lin, J.-P., Mills, K., Al-Sarraj, S., Jan, W., Jungbluth, H., & Wraige, E. (2009). Charcot-Marie-Tooth (CMT) disease 1A with superimposed inflammatory polyneuropathy in children. *Neuropediatrics*, *40*(2), 85–88.

Dezfouli, M. A., Yadegari, S., Nafissi, S., & Elahi, E. (2012). Four novel *C20orf54* mutations identified in Brown-Vialetto-Van Laere syndrome patients. *Journal of human genetics*, *57*(9), 613–617.

Dipti, S., Childs, A.-M., Livingston, J. H., Aggarwal, A. K., Miller, M., Williams, C., & Crow, Y. J. (2005). Brown-Vialetto-Van Laere syndrome; variability in

age at onset and disease progression highlighting the phenotypic overlap with Fazio-Londe disease. *Brain & development*, *27*(6), 443–446.

Distelmaier, F., Koopman, W. J. H., van den Heuvel, L. P., Rodenburg, R. J., Mayatepek, E., Willems, P. H., & Smeitink, J. A. (2009). Mitochondrial complex I deficiency: from organelle dysfunction to clinical disease. *Brain*, *132*(Pt 4), 833–842.

Dixit, A., Chow, G., & Sarkar, A. (2011). Neurologic presentation of triple A syndrome. *Pediatric neurology*, *45*(5), 347–349.

Don, R. H., Cox, P. T., Wainwright, B. J., Baker, K., & Mattick, J. S. (1991). "Touchdown" PCR to circumvent spurious priming during gene amplification. *Nucleic acids research*, *19*(14), 4008.

Donaghy, M., Sisodiya, S. M., Kennett, R., McDonald, B. Haites, N., & Bell, C. (2000). Steroid responsive polyneuropathy in a family with a novel myelin protein zero mutation. *Journal of neurology, neurosurgery and psychiatry*, *69*(6), 799–805.

Drögemüller, C., Becker, D., Kessler, B., Kemter, E., Tetens, J., Jurina, K., Jaderlund, K. H., Flagstad, A., Perloski, M., Lindblad-Toh, K., & Matiasek, K. (2010). A deletion in the *N-Myc Downstream Regulated Gene 1* (*NDRG1*) gene in Greyhounds with polyneuropathy. *PLoS ONE*, *5*(6), e11258.

Drögemüller, C., Reichart, U., Seuberlich, T., Oevermann, A., Baumgartner, M., Kühni Boghenbor, K., Stoffel, M. H., Syring, C., Meylan, M., Muller, S., Muller, M., Gredler, B., Solkner, K., & Leeb, T. (2011). An unusual splice defect in the *mitofusin 2* gene (*MFN2*) is associated with degenerative axonopathy in Tyrolean Grey cattle. *PloS one*, *6*(4), e18931.

Duberley, K. E. C., Hargreaves, I. P., Chaiwatanasirikul, K.-A., Heales, S. J. R., Land, J. M., Rahman, S., Mills, K., & Eaton, S. (2013). Coenzyme Q_{10} quantification in muscle, fibroblasts and cerebrospinal fluid by liquid

chromatography/tandem mass spectrometry using a novel deuterated internal standard. *Rapid communications in mass spectrometry*, *27*(9), 924–930.

Duchen, M. R. (2004). Mitochondria in health and disease: perspectives on a new mitochondrial biology. *Molecular aspects of medicine*, *25*(4), 365–451.

Dumić, M., Barišić, N., Rojnić-Putarek, N., Kušec, V., Stanimirović, A., Koehler, K., & Huebner, A. (2011). Two siblings with triple A syndrome and novel mutation presenting as hereditary polyneuropathy. *European journal of pediatrics*, *170*(3), 393–396.

Dyck, P. J., & Lambert, E. H. (1968a). Lower motor and primary sensory neuron diseases with peroneal muscular atrophy. I. Neurologic, genetic, and electrophysiologic findings in hereditary polyneuropathies. *Archives of neurology*, *18*(6), 603-618.

Dyck, P. J., & Lambert, E. H. (1968b). Lower motor and primary sensory neuron diseases with peroneal muscular atrophy. II. Neurologic, genetic, and electrophysiologic findings in various neuronal degenerations. *Archives of neurology*, *18*(6), 619-625.

Dyck, P. J., Swanson, C. J., Low, P.A., Bartleson, J. D., & Lambert, E. H. (1982). Prednisone-responsive hereditary motor and sensory neuropathy. *Mayo Clinic Proceedings*, *57*(4), 239–246.

Ekici, A., Schweitzer, D., Park, O., Lorek, D., Rautenstrauss, B., Kruger, G., Friedl, W., Uhlhaas, S., Bathke, K., Heuss, D., Kayser, C., & Grehl, H. (2000). Charcot-Marie-Tooth disease and related peripheral neuropathies: novel mutations in the peripheral myelin genes *connexin 32* (*Cx32*), *peripheral myelin protein 22* (*PMP22*), and peripheral *myelin protein zero* (*MPZ*). *Neurogenetics*, *3*(1), 49–50.

Eli, M., Li, D.-S., Zhang, W.-W., Kong, B., Du, C.-S., Wumar, M., Mamtimin, B., Sheyhidin, I., & Hasim, A. (2012). Decreased blood riboflavin levels are

correlated with defective expression of RFT2 gene in gastric cancer. *World journal of gastroenterology*, *18*(24), 3112–3118.

Ericsson, T., Takeuchi, Y., Templin, C., Quinn, G., Farhadian, S. F., Wood, J. C., Oldmixon, B. A., Suling, K. M., Ishii, J. K., Kitagawa, Y., Miyazawa, T., Salomon, D. R., Weiss, R. A., & Patience, C. (2003). Identification of receptors for pig endogenous retrovirus. *Proceedings of the national academy of sciences of the United States of America*, *100*(11), 6759–6764.

Fazio, M. (1892). Ereditarieta della paralisi bulbare progressiva. *Reforma Medica*, *8*, 327.

Feder, S., Daniel, H., & Rehner, G. (1991). In vivo kinetics of intestinal absorption of riboflavin in rats. *The Journal of nutrition*, *121*, 72–79.

Federico, A., Cardaioli, E., Da Pozzo, P., Formichi, P., Gallus, G. N., & Radi, E. (2012). Mitochondria, oxidative stress and neurodegeneration. *Journal of the neurological sciences*, *322*(1-2), 254–262.

Figlewicz, D. A., Krizus, A., Martinoli, M. G., Meininger, V., Dib, M., Rouleau, G. A., & Julien, J. (1994). Variants of the heavy neurofilament subunit are associated with the development of amyotrophic lateral sclerosis. *Human Molecular Genetics*, *3*(10), 1757–1761.

Fledrich, R., Schlotter-Weigel, B., Schnizer, T. J., Wichert, S. P., Stassart, R. M., Meyer zu Hörste, G., Klink, A., Weiss, B. G., Haag, U., Walter, M. C., Rautenstrauss, B., Paulus, W., Rossner, M. J., & Sereda, M. W. (2012). A rat model of Charcot-Marie-Tooth disease 1A recapitulates disease variability and supplies biomarkers of axonal loss in patients. *Brain*, *135*(Pt 1), 72–87.

Fledrich, R., Stassart, R. M., & Sereda, M. W. (2012). Murine therapeutic models for Charcot-Marie-Tooth (CMT) disease. *British medical bulletin*, *102*, 89–113.

Foley, R., Menezes, M., Pandraud, A., Gonzalez, M. A., Al-Odaib, A., Abrams, A. J., Sugano, K., Yonezawa, A., Manzur, A. Y., Burns, J., Hughes, I., McCullagh, B. G., Jungbluth, H., Lim, M. J., Lin, J. P., Megarbane, A., Urtizberea, J. A., Shah, A. H., Antony, J., Webster, R., Broomfield, A., Ng, J., Mathew, A. A., O'Byrne, J. J., Forman, E., Scoto, M., Prasad, M., O'Brien, K., Olpin, S., Oppenheim, M., Hargreaves, I., Land, J. M., Wang, M. X., Carpenter, K., Horvath, R., Straub, V., Lek, M., Gold, W., Farrell, M. O., Brandner, S., Phadke, R., Matsubara, K., McGarvey, M. L., Scherer, S. S., Baxter, P. S., King, M. D., Clayton, P., Rahman, S., Reilly, M. M., Ouvrier, R. A., Christodoulou, J., Zuchner, S., Muntoni, F., & Houlden, H. (2014). Treatable childhood neuronopathy caused by mutations in riboflavin transporter RFVT2. *Brain*, *137*(Pt 1), 44-56.

Foley, C., Schofield, I., Eglon, G., Bailey, G., Chinnery, P. F., & Horvath, R. (2012). Charcot-Marie-Tooth disease in Northern England. *Journal of neurology, neurosurgery and psychiatry*, *83*(5), 572-573.

Foraker, A. B., Khantwal, C. M., & Swaan, P. W. (2003). Current perspectives on the cellular uptake and trafficking of riboflavin. *Advanced drug delivery reviews*, *55*(11), 1467–1483.

Fortun, J., Go, J. C., Li, J., Amici, S. A., Dunn, W. A., & Notterpek, L. (2006). Alterations in degradative pathways and protein aggregation in a neuropathy model based on PMP22 overexpression. *Neurobiology of disease*, *22*(1), 153–164.

Fraga, M. F., Ballestar, E., Paz, M. F., Ropero, S., Setien, F., Ballestar, M. L., Heine-Suner, D., Cigudosa, J. C., Urioste, M., Benitez, J., Boix-Chornet, M., Sanchez-Anguilera, A., Ling, C., Carlsson, E., Poulsen, P., Vaag, A., Stephan, Z., Spector, T. D., Wu, Y. Z., Plass, C., & Esteller, M. (2005). Epigenetic differences arise during the lifetime of monozygotic twins. *Proceedings of the national academy of sciences of the United States of America*, *102*(30), 10604–10609.

Francis, D. A., Ponsford, J. R., Wiles, C. M., Thomas, P. K., & Duchen, L. W. (1993). Case report: Brown-Vialetto-Van laere syndrome. *Neuropathology and applied neurobiology*, *19*, 91–94.

Fujimura, M., Yamamoto, S., Murata, T., Yasujima, T., Inoue, K., Ohta, K., & Yuasa, H. (2010). Functional characteristics of the human ortholog of riboflavin transporter 2 and riboflavin-responsive expression of its rat ortholog in the small intestine indicate its involvement in riboflavin absorption. *The Journal of nutrition*, *140*(10), 1722–1727.

Fyfe, J. C., Al-Tamimi, R. A., Liu, J., Schäffer, A. A., Agarwala, R., & Henthorn, P. S. (2011). A novel mitofusin 2 mutation causes canine fetal-onset neuroaxonal dystrophy. *Neurogenetics*, *12*(3), 223-232.

Gabriel, C. M., Gregson, N. A., & Hughes, R. (2000). Anti-PMP22 antibodies in patients with inflammatory neuropathy. *Journal of neuroimmunology*, *104*, 139–146.

Gabriel, C. M., Gregson, N. A., Wood, N. W., & Hughes, R. A. (2002). Immunological study of hereditary motor and sensory neuropathy type 1a (HMSN1a). *Journal of neurology, neurosurgery and psychiatry*, *72*(2), 230-235.

Gabriel, C. M., Hughes, R. A. C., Moore, S. E., Smith, K. J., & Walsh, F. S. (1998). Induction of experimental autoimmune neuritis with peripheral myelin protein-22. *Brain*, *121*, 1895–1902.

Gallai, V., Hockaday, J., Hughes, J., Lane, D., Oppenheimer, D., & Rushworth, G. (1981). Ponto-bulbar palsy with deafness (Brown-Vialetto-Van Laere syndrome): A report on three cases. *Journal of the neurological sciences*, *50*(2), 259–275.

Gandhi, S., Wood-Kaczmar, A., Yao, Z., Plun-Favreau, H., Deas, E., Klupsch, K., Downward, J., Latchman, D. S., Tabrizi, S. J., Wood, N. W., Duchen, M. R., &

Abramov, A. Y. (2009). PINK1-associated Parkinson's disease is caused by neuronal vulnerability to calcium-induced cell death. *Molecular cell*, *33*(5), 627–638.

Gandre-babbe, S., & van der Bliek, A. M. (2008). The novel tail-anchored membrane protein MFF controls mitochondrial and peroxisomal fission in mammalian cells. *Molecular biology of the cell*, *19*, 2402–2412.

Garcia, C. A, Malamut, R. E., England, J. D., Parry, G. S., Liu, P., & Lupski, J. R. (1995). Clinical variability in two pairs of identical twins with the Charcot-Marie-Tooth disease type 1A duplication. *Neurology*, *45*(11), 2090–2093.

Gempel, K., Topaloglu, H., Talim, B., Schneiderat, P., Schoser, B. G. H., Hans, V. H., Palmafy, B., Kale, G., Tokatli, A., Quinzii, C., Hirano, M., Naini, A., DiMauro, S., Prokisch, H., Lochmuller, H., & Horvath, R. (2007). The myopathic form of Coenzyme Q_{10} deficiency is caused by mutations in the *electron-transferring-flavoprotein dehydrogenase* (*ETFDH*) gene. *Brain*, *130*(Pt 8), 2037–2044.

Génin, E., Feingold, J., & Clerget-Darpoux, F. (2008). Identifying modifier genes of monogenic disease: strategies and difficulties. *Human genetics*, *124*(4), 357–368.

Gerards, M., van den Bosch, B. J. C., Danhauser, K., Serre, V., van Weeghel, M., Wanders, R. J., Nicolaes, G. A., Sluiter, W., Schoonderwoerd, K., Scholte, H. R., Prokisch, H., Rotig, A., de Coo, I. F., & Smeets, H. J. (2011). Riboflavin-responsive oxidative phosphorylation complex I deficiency caused by defective ACAD9: new function for an old gene. *Brain*, *134*(Pt 1), 210–219.

Gess, B., Schirmacher, A., Boentert, M., & Young, P. (2013). Charcot-Marie-Tooth disease: Frequency of genetic subtypes in a German neuromuscular center population. *Neuromuscular disorders*, *23*(8), 647-651.

Giambonini-Brugnoli, G., Buchstaller, J., Sommer, L., Suter, U., & Mantei, N. (2005). Distinct disease mechanisms in peripheral neuropathies due to altered *peripheral myelin protein 22* gene dosage or a *Pmp22* point mutation. *Neurobiology of disease*, *18*(3), 656–668.

Gianazza, E., Vergani, L., Wait, R., Brizio, C., Brambilla, D., Begum, S., Giancaspero, T. A., Conserva, F., Eberini, I., Bufano, D., Angelini, C., Pegoraro, E., Tramontano, A., & Barile, M. (2006). Coordinated and reversible reduction of enzymes involved in terminal oxidative metabolism in skeletal muscle mitochondria from a riboflavin-responsive, multiple acyl-CoA dehydrogenase deficiency patient. *Electrophoresis*, *27*(5-6), 1182–1198.

Giancaspero, T. A., Busco, G., Panebianco, C., Carmone, C., Miccolis, A., Liuzzi, G. M., Colella, M., & Barile, M. (2013). FAD synthesis and degradation in the nucleus create a local flavin cofactor pool. *The Journal of biological chemistry*, *288*(40), 29069-29080.

Gilliam, D., Coates, J. R., Johnson, G. S., Hansen, L., Mhlanga-Mutangadura, T., Taylor, J. F., Johnson, G. C., Schnabel, R. D., & O'Brien, D. P. (2013, October 22nd- 26th). *The whole genome sequence of a Jack Russell Terrier with progressive spinocerebellar ataxia and myokymia contains a homozygous disease-associated KCNJ10 missense mutation.* Paper presented at the American Society of Human Genetics Meeting, Boston, MA, USA.

Ginsberg, L., Malik, O., Kenton, A. R., Sharp, D., Muddle, J. R., Davis, M. B., Winer, J. B., Orrell, R. W., & King, R. H. (2004). Coexistent hereditary and inflammatory neuropathy. *Brain*, *127*(Pt 1), 193–202.

Gonzalez, M. A., Lebrigio, R. F., Van Booven, D., Ulloa, R. H., Powell, E., Speziani, F., Tekin, M., Schüle, R., & Züchner, S. (2013). GEnomes Management Application (GEM.app): a new software tool for large-scale collaborative genome analysis. *Human mutation*, *34*(6), 842-846.

González-Pérez, P., Lu, Y., Chian, R.-J., Sapp, P. C., Tanzi, R. E., Bertram, L., McKenna-Yasek, B., Gao, F. B., & Brown, R. H. (2012). Association of *UBQLN1* mutation with Brown-Vialetto-Van Laere syndrome but not typical ALS. *Neurobiology of disease*, *48*(3), 391–398.

Goodman, S. I. (1981). Organic aciduria in the riboflavin-deficient rat. *The American journal of clinical nutrition*, *34*, 2434–2437.

Gough, S. C. L., & Simmonds, M. J. (2007). The HLA region and autoimmune disease: Associations and mechanisms of action. *Current genomics*, *8*(7), 453–465.

Gouvea, S. P., S Borghetti, V. H., Bueno, K. C., Genari, A. B., Lourenço, C. M., Sobreira, C., Barreria, A. A., & Marques, W. (2010). Compound Charcot-Marie-Tooth disease may determine unusual and milder phenotypes. *Neurogenetics*, *11*(1), 135–138.

Grad, L. I., & Lemire, B. D. (2006). Riboflavin enhances the assembly of mitochondrial cytochrome c oxidase in *C. elegans* NADH-ubiquinone oxidoreductase mutants. *Biochimica et biophysica acta*, *1757*(2), 115–122.

Granger, N. (2011). Canine inherited motor and sensory neuropathies : An updated classification in 22 breeds and comparison to Charcot-Marie-Tooth disease. *The Veterinary journal*, *188*, 274–285.

Green, P., Wiseman, M., Crow, Y. J., Houlden, H., Riphagen, S., Lin, J.-P., Raymond, F. L., Childs, A. M., Sheridan, E., Edwards, S., & Josifova, D. J. (2010). Brown-Vialetto-Van Laere syndrome, a ponto-bulbar palsy with deafness, is caused by mutations in *C20orf54*. *American journal of human genetics*, *86*(3), 485–489.

Gregersen, N. (1985). Riboflavin-responsive defects of β-oxidation. *Journal of inherited metabolic disease*, *8*(1), 65–69.

Gregersen, N., Andresen, B. S., Pedersen, C. B., Olsen, R. K. J., Corydon, T. J., & Bross, P. (2008). Mitochondrial fatty acid oxidation defects--remaining challenges. *Journal of inherited metabolic disease*, *31*(5), 643–657.

Gu, W., Zhang, F., & Lupski, J. R. (2008). Mechanisms for human genomic rearrangements. *Pathogenetics*, *1*(1), 4.

Gutman, I., & Wahlefeld, W. W. (1974). L-Lactate determination with lactate dehydrogenase and NAD. In B. Hu (Eds.), *Methods of enzymatic analysis* (pp. 1464–1468). New York: Academic Press.

Haack, T. B., Danhauser, K., Haberberger, B., Hoser, J., Strecker, V., Boehm, D., Uziel, G., Lamantea, E., Invernizzi, F., Poulton, J., Rolinski, B., Iuso, A., Biskup, S., Schmidt, T., Mewes, H. W., Wittig, I., Meitinger, T., Zeviani, M., & Prokisch, H. (2010). Exome sequencing identifies *ACAD9* mutations as a cause of complex I deficiency. *Nature genetics*, *42*(12), 1131–1134.

Haack, T. B., Makowski, C., Yao, Y., Graf, E., Hempel, M., Wieland, T., Tauer, U., Ahting, U., Mayr, J. A., Freisinger, P., Yoshimatsu, H., Inui, K., Strom, T. M., Meitinger, T., Yonezawa, A., & Prokisch, H. (2012). Impaired riboflavin transport due to missense mutations in *SLC52A2* causes Brown-Vialetto-Van Laere syndrome. *Journal of inherited metabolic disease*, *35*(6), 943–948.

Hai, M., Bidichandani, S. I., & Patel, P. I. (2001). Identification of a positive regulatory element in the myelin-specific promoter of the *PMP22* gene. *Journal of neuroscience research*, *65*, 508–519.

Handschug, K., Sperling, S., Yoon, S. J., Hennig, S., Clark, J., & Huebner, A. (2001). Triple A syndrome is caused by mutations in *AAAS*, a new WD-repeat protein gene. *Human molecular genetics*, *10*(3), 283–290.

Hanemann, C. O., Stoll, G., D'Urso, D., Fricke, W., Martin, J. J., Van Broeckhoven, C., Mancardi, G. L., Bartke, I., & Müller, H. W. (1994). Peripheral myelin

protein-22 expression in Charcot-Marie-Tooth disease type 1A sural nerve biopsies. *Journal of neuroscience research, 37*(5), 654–659.

Hardiman, O., van den Berg, L. H., & Kiernan, M. C. (2011). Clinical diagnosis and management of amyotrophic lateral sclerosis. *Nature reviews neurology, 7*(11), 639–649.

Harding, A. E., & Thomas, P. (1980). The clinical features of hereditary motor and sensory neuropathy types I and II. *Brain, 103*, 259–280.

Hargreaves, I. P., Heales, S. J., & Land, J. M. (1999). Mitochondrial respiratory chain defects are not accompanied by an increase in the activities of lactate dehydrogenase or manganese superoxide dismutase in paediatric skeletal muscle biopsies. *Journal of inherited metabolic disease, 22*(8), 925–931.

Harpey, J. P., Charpentier, C., Goodman, S. I., Darbois, Y., Lefbvre, G., & Sebbah, J. (1983). Multiple acyl-CoA dehydrogenase deficiency occurring in pregnancy and caused by a defect in riboflavin metabolism in the mother. Study of a kindred with seven deaths in infancy: Value of riboflavin therapy in preventing this syndrome. *The Journal of pediatrics, 103*(3), 394–398.

Harrison, J., Hodson, A. W., Skillen, A. W., Stappenbeck, R., Agius, L., & Alberti, K. G. (1988) Blood glucose, lactate, pyruvate, glycerol, 3-hydroxybutyrate and acetoacetate measurements in man using a centrifugal analyser with a flourimetric attachment. *Journal of clinical chemistry and clinical biochemistry, 26*(3), 141–146.

Hawkins, S. A., Nevin, N. C., & Harding, A. E. (1990). Pontobulbar palsy and neurosensory deafness (Brown-Vialetto-Van Laere syndrome) with possible autosomal dominant inheritance. *Journal of medical genetics, 27*(3), 176–179.

Heller, S., Salkeld, R. M., & Korner, W. F. (1974). Riboflavin status in pregnancy. *American journal of clinical nutrition, 27*, 1225–1230.

Henriques, B. J., Olsen, R. K., Bross, P., & Gomes, C. M. (2010). Emerging roles for riboflavin in functional rescue of mitochondrial oxidation flavoenzymes. *Current medicinal chemistry*, *17*, 3842–3854.

Henriques, B. J., Rodrigues, J. V, Olsen, R. K., Bross, P., & Gomes, C. M. (2009). Role of flavinylation in a mild variant of multiple acyl-CoA dehydrogenation deficiency: a molecular rationale for the effects of riboflavin supplementation. *The Journal of biological chemistry*, *284*(7), 4222–4229.

Ho, G., Yonezawa, A., Masuda, S., Inui, K.-I., Sim, K.-G., Carpenter, K., Olsen, R. K., Mitchell, J. J., Rhead, W. J., Peters, G., & Christodoulou, J. (2010). Maternal riboflavin deficiency, resulting in transient neonatal-onset glutaric aciduria type 2, is caused by a microdeletion in the riboflavin transporter gene *GPR172B*. *Human mutation*, *32*(1), 1976–1984.

Hodapp, J. A., Carter, G. T., Lipe, H. P., Michelson, S. J., Kraft, G. H., & Bird, T. D. (2006). Double trouble in hereditary neuropathy: concomitant mutations in the *PMP22* gene and another gene produce novel phenotypes. *Archives of neurology*, *63*(1), 112-117.

Hoppel, C., Dimarco, J. P., & Tandler, B. (1979). Riboflavin and rat hepatic cell structure and function. Mitochondrial oxidative metabolism in deficiency states. *The Journal of biological chemistry*, *254*(10), 4164-4170.

Horvath, R. (2012). Update on clinical aspects and treatment of selected vitamin-responsive disorders II (riboflavin and CoQ_{10}). *Journal of inherited metabolic disease*, *35*(4), 679–687.

Houlden, H. (2012). A commentary on "Four novel *C20orf54* mutations identified in Brown-Vialetto-Van Laere syndrome patients." *Journal of human genetics*, *57*(9), 555.

Houlden, H., Girard, M., Cockerell, C., Ingram, D., Wood, N. W., Goossens, M., Walker, R. W., & Reilly, M. M. (2004). *Connexin 32* promoter P2 mutations: a

mechanism of peripheral nerve dysfunction. *Annals of neurology*, *56*(5), 730–734.

Houlden, H., Laura, M., Ginsberg, L., Jungbluth, H., Robb, S. A., Blake, J., Robinson, S., King, R. H., & Reilly, M. M. (2009). The phenotype of Charcot-Marie-Tooth disease type 4C due to *SH3TC2* mutations and possible predisposition to an inflammatory neuropathy. *Neuromuscular disorders*, *19*(4), 264–269.

Houlden, H., Smith, S., De Carvalho, M., Blake, J., Mathias, C., Wood, N. W., & Reilly, M. M. (2002). Clinical and genetic characterization of families with triple A (Allgrove) syndrome. *Brain*, *125*(Pt 12), 2681–2690.

Huang, Y., Sirkowski, E. E., Stickney, J. T., & Scherer, S. S. (2005). Prenylation-defective human *connexin 32* mutants are normally localized and function equivalently to wild-type *connexin 32* in myelinating Schwann cells. *The Journal of neuroscience*, *25*(31), 7111–7120.

Huang, S. N., & Swaan, P. W. (2001). Riboflavin uptake in human trophoblast-derived BeWo cell monolayers: cellular translocation and regulatory mechanisms. *The Journal of pharmacology and experimental therapeutics*, *298*(1), 264–271.

Huang, J., Wu, X., Montenegro, G., Price, J., Wang, G., Vance, J. M., Shy, M. E., & Zuchner, S. (2010). Copy number variations are a rare cause of non-CMT1A Charcot-Marie-Tooth disease. *Journal of neurology*, *257*(5), 735–741.

Hughes, R. A. (2008). Peripheral nerve diseases: the bare essentials. *Practical neurology*, *8*(6), 396–405.

Hustad, S., McKinley, M. C., McNulty, H., Schneede, J., Strain, J. J., Scott, J. M., & Ueland, P. M. (2002). Riboflavin, flavin mononucleotide, and flavin adenine dinucleotide in human plasma and erythrocytes at baseline and after low-dose riboflavin supplementation. *Clinical chemistry*, *48*(9), 1571–1577.

Inoue, K., Dewar, K., Katsanis, N., Reiter, L. T., Lander, E. S., Devon, K. L., Wyman, D. W., Lupski, J. R., & Birren, B. (2001). The 1.4-Mb CMT1A duplication/HNPP deletion genomic region reveals unique genome architectural features and provides insights into the recent evolution of new genes. *Genome research*, *11*(6), 1018–1033.

Ionasescu, V. V., Ionasescu, R., Searby, C., & Barker, D. F. (1993). Charcot-Marie-Tooth neuropathy type 1A with both duplication and non-duplication. *Human molecular genetics*, *2*(4), 405–410.

Ionasescu, V. V., Searby, C. C., Ionasescu, R., Chatkupt, S., Patel, N., & Koenigsberger, R. (1997). Dejerine-Sottas neuropathy in mother and son with same point mutation of *PMP22* gene. *Muscle & nerve*, *20*(1), 97–99.

Ionasescu, V. V., Searby, C., Ionasescu, R., Reisin, R., Ruggieri, V., & Arberas, C. (1997). Severe Charcot-Marie-Tooth neuropathy type 1A with 1-base pair deletion and frameshift mutation in the *peripheral myelin protein 22* gene. *Muscle & nerve*, *20*, 1308–1310.

Ip, C. W., Kroner, A., Fischer, S., Berghoff, M., Kobsar, I., Mäurer, M., & Martini, R. (2006). Role of immune cells in animal models for inherited peripheral neuropathies. *Neuromolecular medicine*, *8*(1-2), 175–189.

Jain-Ghai, S., Cameron, J. M., Al Maawali, A., Blaser, S., MacKay, N., Robinson, B., & Raiman, J. (2013). Complex II deficiency--a case report and review of the literature. *American journal of medical genetics, 161A*(2), 285–294.

Jessen, K. R., & Mirsky, R. (1998). Origin and early development of Schwann cells. *Microscopy research and technique*, *41*(5), 393–402.

Johnson, J. O., Gibbs, J. R., Megarbane, A., Urtizberea, J. A., Hernandez, D. G., Foley, A. R., Arepalli, S., Pandraud, A., Simon-Sanchez, J., Clayton, P., Reilly, M. M., Muntoni, F., Abramzon, Y., Houlden, H., & Singleton, A. B. (2012).

Exome sequencing reveals riboflavin transporter mutations as a cause of motor neuron disease. *Brain*, *135*(Pt 9), 2875–2882.

Johnson, J. O., Gibbs, J. R., Van Maldergem, L., Houlden, H., & Singleton, A. B. (2010). Exome sequencing in Brown-Vialetto-van Laere syndrome. *American journal of human genetics*, *87*(4), 567–569.

Johnson, J. O., Mandrioli, J., Benatar, M., Abramzon, Y., Van Deerlin, V. M., Trojanowski, J. Q., Gibbs, J. R., Brunetti, M., Gronka, S., Wuu, J., Ding, J., McCluskey, L., Martinez-Lage, M., Falcone, D., Hernandez, D. G., Arepalli, S., Chong, S., Schymick, J. C., Rothstein, J., Landi, F., Wang, Y. D., Calvo, A., Mora, G., Sabatelli, M., Monsurro, M. R., Battistini, S., Salvi, F., Spataro, R., Sola, P., Borghero, G., ITALSGEN Consortium, Galassi, G., Scholz, S. W., Taylor, J. P., Restagno, G., Chio, A., & Traynor, B. J. (2010). Exome sequencing reveals VCP mutations as a cause of familial ALS. *Neuron*, *68*(5), 857–864.

Jones, E. A., Brewer, M. H., Srinivasan, R., Krueger, C., Sun, G., Charney, K. N., Keles, S., Antonellis, A., & Svaren, J. (2012). Distal enhancers upstream of the Charcot-Marie-Tooth type 1A disease gene *PMP22*. *Human molecular genetics*, *21*(7), 1581–1591.

Jones, E. A., Lopez-Anido, C., Srinivasan, R., Krueger, C., Chang, L.-W., Nagarajan, R., & Svaren, J. (2011). Regulation of the *PMP22* gene through an intronic enhancer. *Journal of neuroscience*, *31*(11), 4242–4250.

Jordanova, A., De Jonghe, P., Boerkoel, C. F., Takashima, H., De Vriendt, E., Ceuterick, C., Martin, J. J., Butler, I. J., Mancias, P., Papasozomenos, S., Terespolsky, D., Potocki, L., Brown, C. W., Shy, M., Rita, D. A., Tournev, I., Kremensky, I., Lupski, J. R., & Timmerman, V. (2003). Mutations in the *neurofilament light chain* gene (*NEFL*) cause early onset severe Charcot-Marie-Tooth disease. *Brain*, *126*(3), 590–597.

Jung, C., Higgins, C. M. J., & Xu, Z. (2002). Mitochondrial electron transport chain complex dysfunction in a transgenic mouse model for amyotrophic lateral sclerosis. *Journal of neurochemistry*, *83*(3), 535–545.

Kabzinska, D., Kotruchow, K., Ryniewicz, B., & Kochanski, A. (2011). Two pathogenic mutations located within the 5'-regulatory sequence of the *GJB1* gene affecting initiation of transcription and translation. *Acta biochimica Polonica*, *58*(3), 359–363.

Kaku, D. A., Parry, G. J., Malamut, R., Lupski, J. R., & Garcia, C. A. (1993). Nerve conduction studies in Charcot-Marie-Tooth polyneuropathy associated with a segmental duplication of chromosome 17. *Neurology*, *43*(9), 1806-1808.

Kanekura, K., Suzuki, H., Aiso, S., & Matsuoka, M. (2009). ER stress and unfolded protein response in amyotrophic lateral sclerosis. *Molecular neurobiology*, *39*(2), 81–89.

Kansara, V., Pal, D., Jain, R., & Mitra, A. K. (2005). Identification and functional characterization of riboflavin transporter in human-derived retinoblastoma cell line (Y-79): mechanisms of cellular uptake and translocation. *Journal of ocular pharmacology and therapeutics*, *21*(4), 275–287.

Kanwal, S., Choi, B.-O., Kim, S.-B., Koo, H., Kim, J. Y., Hyun, Y. S., Lee, H. J., & Chung, K. W. (2011). Wide phenotypic variations in Charcot-Marie-Tooth 1A neuropathy with rare copy number variations on 17p12. *Animal cells and systems*, *15*(4), 301–309.

Karadima, G., Floroskufi, P., Koutsis, G., Vassilopoulos, D., & Panas, M. (2011). Mutational analysis of *PMP22, GJB1* and *MPZ* in Greek Charcot-Marie-Tooth type 1 neuropathy patients. *Clinical genetics*, *80*, 497–499.

Karlsson, E. K., Baranowska, I., Wade, C. M., Salmon Hillbertz, N. H. C., Zody, M. C., Anderson, N., Biagi, T. M., Patterson, N., Pielberg, G. R., Kulbokas, E. J., Comstock, K. E., Keller, E. T., Mesirov, J. P., von Euler, H., Kampe, O.,

Hedhammar, A., Lander, E. S., Andersson, L., & Lindblad-Toh, K. (2007). Efficient mapping of mendelian traits in dogs through genome-wide association. *Nature genetics*, *39*(11), 1321–1328.

Katona, I., Wu, X., Feely, S. M. E., Sottile, S., Siskind, C. E., Miller, L. J., Shy, M. E., & Li, J. (2009). PMP22 expression in dermal nerve myelin from patients with CMT1A. *Brain*, *132*(Pt 7), 1734–1740.

Keckarevic-Markovic, M., Milic-Rasic, V., Mladenovic, J., Dackovic, J., Kecmanovic, M., Keckarevic, D., Savic-Pavicevic, D., & Romac, S. (2009). Mutational analysis of *GJB1*, *MPZ*, *PMP22*, *EGR2*, and *LITAF/SIMPLE* in Serbian Charcot-Marie-Tooth patients. *Journal of the peripheral nervous system*, *14*(2), 125–136.

Kerr, D. S. (2013). Review of clinical trials for mitochondrial disorders: 1997-2012. *Neurotherapeutics*, *10*(2), 307–319.

Kim, Y. H., Chung, H. K., Park, K. D., Choi, K.-G., Kim, S.-M., Sunwoo, I.-N., Choi, Y. C., Lim, J. G., Lee, K. W., Kim, K. K., Lee, D. K., Joo, I. S., Kwon, K. H., Gwon, S. B., Park, J. H., Kim, D. S., Kim, S. H., Kim, W. K., Suh, B. C., Kim, S. B., Kim, N. H., Sohn, E. H., Kim, O. J., Kim, H. S., Cho, J. H., Kang, S. Y., Park, C. I., Oh, J., Shin, J. H., Chung, K. W., & Choi, B.-O. (2012). Comparison between clinical disabilities and electrophysiological values in Charcot-Marie-Tooth 1A patients with *PMP22* duplication. *Journal of clinical neurology (Seoul, Korea)*, *8*(2), 139–145.

Kim, S. W., Lee, K. S., Jin, H. S., Lee, T. M., Koo, S. K., Lee, Y. J., & Jung, S. C. (2003). Rapid detection of duplication/deletion of the *PMP22* gene in patients with Charcot-Marie-Tooth disease type 1A and hereditary neuropathy with liability to pressure palsy by real-time quantitative PCR using SYBR green I dye. *Journal of Korean medical science*, *18*(5), 727–732.

Kiyosawa, H., & Chance, P. F. (1996). Primate origin of the CMT1A-REP repeat and analysis of a putative transposon-associated recombinational hotspot. *Human molecular genetics*, *5*(6), 745–753.

Kleopa, K. A, Abrams, C. K., & Scherer, S. S. (2012). How do mutations in *GJB1* cause X-linked Charcot-Marie-Tooth disease? *Brain research*, *1487*, 198–205.

Kloeckener-Gruissem, B., Vandekerckhove, K., Nurnberg, G., Neidhardt, J., Zeitz, C., Nurnberg, P., Schipper, I., & Berger, W. (2008). Mutation of solute carrier *SLC16A12* associates with a syndrome combining juvenile cataract with microcornea and renal glucosuria. *American journal of human genetics*, *82*, 772–779.

Kobsar, I., Hasenpusch-Theil, K., Wessig, C., Müller, H. W., & Martini, R. (2005). Evidence for macrophage-mediated myelin disruption in an animal model for Charcot-Marie-Tooth neuropathy type 1A. *Journal of neuroscience research*, *81*(6), 857–864.

Kochañski, A. (2006). How to assess the pathogenicity of mutations in Charcot-Marie-Tooth disease and other diseases? *Journal of applied genetics*, *47*(3), 255–260.

Koehler, K., End, K., Kind, B., Landgraf, D., Mitzscherling, P., & Huebner, A. (2013). Changes in differential gene expression in fibroblast cells from patients with triple A syndrome under oxidative stress. *Hormone and metabolic research*, *45*(2), 102–108.

Kohl, B., Groh, J., Wessig, C., Wiendl, H., Kroner, A., & Martini, R. (2010). Lack of evidence for a pathogenic role of T-lymphocytes in an animal model for Charcot-Marie-Tooth disease 1A. *Neurobiology of disease*, *38*(1), 78–84.

Koul, R., Jain, R., Chacko, A., Alfutaisi, A., Hashim, J., & Chacko, J. (2006). Pontobulbar palsy and neurosensory deafness (Brown-Vialetto-Van Laere Syndrome) with hyperintense brainstem nuclei on magnetic resonance

imaging: new findings in three siblings. *Journal of child neurology*, *21*, 523–525.

Koutsis, G., Pandraud, A., Karadima, G., Panas, M., Reilly, M. M., Floroskufi, P., Wood, N. W., & Houlden, H. (2013). Mutational analysis of *PMP22, EGR2, LITAF* and *NEFL* in Greek Charcot-Marie-Tooth type 1 patients. *Clinical genetics*, *83*(4), 388–391.

Koutsis, G., Pandraud, A., Polke, J. M., Wood, N. W., Panas, M., Karadima, G., & Houlden, H. (2012). Novel *peripheral myelin protein 22* (*PMP22*) micromutations associated with variable phenotypes in Greek patients with Charcot–Marie–Tooth disease. *Brain*, *135*(Pt 8), e217.

Koy, A., Pillekamp, F., Hoehn, T., Waterham, H., Klee, D., Mayatepek, E., & Assmann, B. (2012). Brown-Vialetto-Van Laere syndrome: a riboflavin-unresponsive patient with a novel mutation in the *C20orf54* gene. *Pediatric neurology*, *46*(6), 407–409.

Krogh, A., Larsson, B., von Heijne, G., & Sonnhammer, E. L. (2001). Predicting transmembrane protein topology with a hidden Markov model: application to complete genomes. *Journal of molecular biology*, *305*(3), 567-580.

Kumar, C. K., Yanagawa, N., Ortiz, A., & Said, H. M. (1998). Mechanism and regulation of riboflavin uptake by human renal proximal tubule epithelial cell line HK-2 mechanism and regulation of riboflavin uptake by human renal proximal tubule epithelial cell line HK-2. *The American journal of physiology*, *274*(1 Pt 2), F104-110.

Lariviere, R. C., & Julien, J.-P. (2004). Functions of intermediate filaments in neuronal development and disease. *Journal of neurobiology*, *58*(1), 131–148.

Latour, P., Gonnaud, P., Ollagnon, E., Chan, V., Perelman, S., Stojkovic, T., Stoll, C., Vial, C., Ziegler, F., Vandenberghe, A., & Maire, I. (2006). *SIMPLE* mutation analysis in dominant demyelinating Charcot-Marie-Tooth disease:

three novel mutations. *Journal of the peripheral nervous system*, *11*(2), 148–155.

Latov, N. (2011). Biomarkers of CIDP in patients with diabetes or CMT1. *Journal of the peripheral nervous system*, *16*(Suppl 1), 14–17.

Lee, E.-S., Corfe, B. M., & Powers, H. J. (2013). Riboflavin depletion of intestinal cells in vitro leads to impaired energy generation and enhanced oxidative stress. *European journal of nutrition*, *52*(5), 1513–1521.

Lee, I., Lehner, B., Vavouri, T., Shin, J., Fraser, A. G., & Marcotte, E. M. (2010). Predicting genetic modifier loci using functional gene networks. *Genome research*, *20*(8), 1143–1153.

Lees, J. F., Shneidman, P. S., Skuntz, S. F., Carden, M. J., & Lazzarini, R. A. (1988). The structure and organization of the human heavy neurofilament subunit (NF-H) and the gene encoding it. *The EMBO journal*, *7*(7), 1947–1955.

LeGuern, E., Gouider, R., Mabin, D., Tardieu, S., Birouk, N., Parent, P., Bouche, P., & Brice, A. (1997). Patients homozygous for the 17p11.2 duplication in Charcot-Marie-Tooth type 1A disease. *Annals of neurology*, *41*(1), 104–108.

Lenssen, P. P., Gabreëls-Festen, A. A., Valentijn, L. J., Jongen, P. J., van Beersum, S. E., van Engelen, B. G., van Wensen, P. J., Bolhuis, P. A., Gabreels, F. J., & Mariman, E. C. (1998). Hereditary neuropathy with liability to pressure palsies. Phenotypic differences between patients with the common deletion and a *PMP22* frame shift mutation. *Brain*, *121*(17), 1451–1458.

Leshner, R. T., Hartlage, P. L., & Hahn, D. (1981). Riboflavin deficiency- A reversible “neurodegenerative disease.” *Annals of neurology*, *10*(3), 294–295.

Levy, G., & Jusko, W. J. (1966). Factors affecting the absorption of riboflavin in man. *Journal of pharmaceutical sciences*, *55*(3), 285–289.

Li, J., Bai, Y., Ghandour, K., Qin, P., Grandis, M., Trostinskaia, A., Ianakova, E., Wu, X., Schenone, A., Vallat, J. M., Kupsky, W. J., Hatfield, J., & Shy, M. E. (2005). Skin biopsies in myelin-related neuropathies: bringing molecular pathology to the bedside. *Brain*, *128*(Pt 5), 1168–1177.

Li, J., Parker, B., Martyn, C., Natarajan, C., & Guo, J. (2013). The *PMP22* gene and its related diseases. *Molecular neurobiology*, *47*(2), 673–698.

Lienhart, W.-D., Gudipati, V., & Macheroux, P. (2013). The human flavoproteome. *Archives of biochemistry and biophysics*, *535*(2), 150–162.

Lin, J., Diamanduros, A., Chowdhury, S. A., Scelsa, S., Latov, N., & Sadiq, S. A. (2009). Specific electron transport chain abnormalities in amyotrophic lateral sclerosis. *Journal of neurology*, *256*(5), 774–782.

Lipson, M. H., Kraus, J. A. N., & Rosenberg, L. E. (1980). Affinity of cystathionine beta-synthase for pyridoxal 5'-phosphate in cultured cells. *Journal of clinical investigation*, *66*, 188–193.

Livak, K. J., & Schmittgen, T. D. (2001). Analysis of relative gene expression data using real-time quantitative PCR and the 2(-Delta Delta C(T)) method. *Methods*, *25*(4), 402–408.

Lombaert, A., Dom, R., Carton, H., & Brucher, J. M. (1976). Progressive pontobulbar palsy with deafness: A clinico-pathological study. *Acta Neurologica Belgica*, *76*, 309-314.

Londe, P. (1893). Paralysie bulbaire progressive, infantile et familiale. *Revue de medecine*, *13*, 1020-1030.

Londe, P. (1894). Paralysie bulbaire progressive, infantile et familiale (suite et fin). *Revue de medecine*, *14*, 212-254.

Lopes, J., LeGuern, E., Gouider, R., Tardieu, S., Abbas, N., Birouk, N., Gugenheim, M., Bouche, P., & Brice, A. (1996). Recombination hot spot in a 3.2-kb region of the Charcot-Marie-Tooth type 1A repeat sequences: new tools for molecular diagnosis of hereditary neuropathy with liability to pressure palsies and of Charcot-Marie-Tooth type 1A. French CMT Collaborative Research Group. *American journal of human genetics*, *58*(6), 1223–1230.

Lopes, J., Vandenberghe, A., Tardieu, S., Ionasescu, V., Levy, N., Wood, N., Tachi, N., Bouche, P., Latour, P., Brice, A., & LeGuern, E. (1997). Sex-dependent rearrangements resulting in CMT1A and HNPP. *Nature genetics*, *17*(2), 136–137.

Lupski, J. R., de Oca-Luna, R. M., Slaugenhaupt, S., Pentao, L., Guzzetta, V., Trask, B. J., Saucedo-Cardenas, O., Barker, D. F., Killian, J. M., Garcia, C. A., Chakravarti, A., & Patel, P. I. (1991). DNA duplication associated with Charcot-Marie-Tooth disease type 1A. *Cell*, *66*(2), 219–232.

Lupski, J. R., Reid, J., Gonzaga-Jauregui, C., Rio Deiros, D., Chen, D. C. Y., Nazareth, L., Bainbridge, M., Dinh, H., Jing, C., Wheeler, D. A., McGuire, A. L., Zhang, F., Stankiewicz, P., Halperin, J. J., Yang, C., Gehman, C., Guo, D., Irikat, R. K., Tom, W., Fantin, N. J., Muzny, D. M., & Gibbs, R. A. (2010). Whole-genome sequencing in a patient with Charcot–Marie–Tooth neuropathy. *The New England journal of medicine*, *362*(13), 1181–1191.

Lupski, J. R., Wise, C. A., Kuwano, A., Pentao, L., Parke, J. T., Glaze, D. G., Ledbetter, D. H., Greenberg, F., & Patel, P. I. (1992). Gene dosage is a mechanism of Charcot-Marie-Tooth disease type 1A. *Nature genetics*, *1*(1), 29–33.

McCormick, D. B. (1989). Two interconnected B vitamins: riboflavin and pyridoxine. *Physiological reviews*, *69*(4), 1170–1198.

McInnes, J. (2013). Insights on altered mitochondrial function and dynamics in the pathogenesis of neurodegeneration. *Translational neurodegeneration*, *2*(1), 12.

Mackay, N., & Robinson, B. H. (2007). Measurement of the ratio of lactate to pyruvate in skin fibroblast cultures. *Methods in cell biology*, *80*(6), 173–178.

McShane, M. A., Boyd, S., Harding, B., Brett, E. M., & Wilson, J. (1992). Progressive bulbar paralysis of childhood: a reappraisal of Fazio-Londe disease. *Brain*, *115*(6), 1889–1900.

Maier, M., Berger, P., Nave, K.-A., & Suter, U. (2002). Identification of the regulatory region of the *peripheral myelin protein 22* (*PMP22*) gene that directs temporal and spatial expression in development and regeneration of peripheral nerves. *Molecular and cellular neurosciences*, *20*(1), 93–109.

Maier, M., Castagner, F., Berger, P., & Suter, U. (2003). Distinct elements of the *peripheral myelin protein 22* (*PMP22*) promoter regulate expression in Schwann cells and sensory neurons. *Molecular and cellular neuroscience*, *24*(3), 803-817.

Malandrini, A., Villanova, M., Dotti, M. T. & Federico, A. (1999). Acute inflammatory neuropathy in Charcot-Marie-Tooth disease. *Neurology*, *52*(4), 859-861.

Male, D., Brostoff, J., Roth, D., & Roitt, I. (2006). *Immunology (Seventh edition)*. Edinburgh: Mosby Elsevier.

Malheiros, J. A., Camargos, S. T., Oliveira, J. T., & Cardoso, F. E. C. (2007). A Brazilian family with Brown-Vialetto-van Laere syndrome with autosomal recessive inheritance. *Arquivos de neuro-psiquiatria*, *65*(1), 32–35.

Mancuso, M., Orsucci, D., Volpi, L., Calsolaro, V., & Siciliano, G. (2010). Coenzyme Q_{10} in neuromuscular and neurodegenerative disorders. *Current drug targets*, *11*(1), 111–121.

Manthey, K. C., Chew, Y. C., & Zempleni, J. (2005). Riboflavin deficiency impairs oxidative folding and secretion of apolipoprotein B-100 in HepG2 cells, triggering stress response systems. *The Journal of nutrition*, *135*, 978–982.

Marques, W., Freitas, M. R., Nascimento, O. J. M., Oliveira, A. B., Calia, L., Melo, A., Lucena, R., Rocha, V., & Barreira, A. A. (2005). 17p duplicated Charcot-Marie-Tooth 1A: characteristics of a new population. *Journal of neurology*, *252*(8), 972–979.

Marques, W, Sweeney, M., & Wood, N. (2003). Thr(118)Met amino acid substitution in the peripheral myelin protein 22 does not influence the clinical phenotype of Charcot-Marie-Tooth disease type 1A due to the 17p11.2-p12 duplication. *Brazilian journal of medical and biological research*, *36*, 1403–1407.

Marriage, B., Clandinin, M. T., & Glerum, D. M. (2003). Nutritional cofactor treatment in mitochondrial disorders. *Journal of the American dietetic association*, *103*(8), 1029–1038.

Martin, L. J. (2011). Mitochondrial pathobiology in ALS. *Journal of bioenergetics and biomembranes*, *43*(6), 569–579.

Martin, J.-E., Assassi, S., Diaz-Gallo, L.-M., Broen, J. C., Simeon, C. P., Castellvi, I., Vicente-Rabaneda, E., Fonollosa, V., Ortego-Centeno, N., Gonzalez-Gay, M. A., Espinosa, G., Carreira, P., Spanish Scleroderma Group, SLEGEN consortium, U.S. Scleroderma GWAS group, BIOLUPUS, Camps, M., Sabio, J. M., D'alfonso, S., Vonk, M. C., Voskuyl, A. E., Schuerwegh, A. J., Kreuter, A., Witte, T., Riemekasten, G., Hunzelmann, N., Airo, P., Beretta, L., Scorza, R., Lunardi, C., Van Laar, K., Chee, M. M., Worthington, J., Herrick, A., Denton, C., Fonseca, C., Tan, F. K., Arnett, F., ZHou, X., Reveille, J. D., Gorlova, O., Koeleman, B. P., Radstake, T. R., Vyse, T., Mayes, M. D., Alarcon-Riquelme, M. E., & Martin, J. (2013). A systemic sclerosis and systemic lupus erythematosus pan-meta-GWAS reveals new shared susceptibility loci. *Human molecular genetics*, *22*(19), 4021–4029.

Martini, R., & Toyka, K. V. (2004). Immune-mediated components of hereditary demyelinating neuropathies: lessons from animal models and patients. *Lancet neurology*, *3*(8), 457–465.

Martyn, C. N., & Hughes, R. A. (1997). Epidemiology of peripheral neuropathy. *Journal of neurology, neurosurgery, and psychiatry*, *62*(4), 310–318.

Masotti, C., Armelin-Correa, L. M., Splendore, A., Lin, C. J., Barbosa, A., Sogayar, M. C., & Passos-Bueno, M. R. (2005). A functional SNP in the promoter region of *TCOF1* is associated with reduced gene expression and YY1 DNA-protein interaction. *Gene, 359*, 44–52.

Massey, V. (2000). The chemical and biological versatility of riboflavin. *Biochemical Society transactions*, *28*(4), 283–296.

Matiasek, K., & Drögemüller, C. (2011). Charcot-Marie-Tooth disease: inherited neuropathies revisited. *Veterinary journal*, *188*(3), 254–255.

Matsunami, N., Smith, B., Ballard, L., Lensch, M. W., Robertson, M., Albertsen, H., Hanemann, C. O., Muller, H. W., Bird, T. D., White, R., & Chance, P. F. (1992). *Peripheral myelin protein-22* gene maps in the duplication in chromosome 17p11.2 associated with Charcot-Marie-Tooth 1A. *Nature genetics*, *1*, 176-179.

Mäurer, M., Kobsar, I., Berghoff, M., Schmid, C. D., Carenini, S., & Martini, R. (2002). Role of immune cells in animal models for inherited neuropathies: facts and visions. *Journal of anatomy*, *200*(4), 405–414.

Mazur-Bialy, A. I., Buchala, B., & Plytycz, B. (2013). Riboflavin deprivation inhibits macrophage viability and activity - a study on the RAW 264.7 cell line. *The British journal of nutrition*, *110*(3), 509-514.

Mazzeo, A., Stancanelli, C., Russo, M., Granata, F., Gentille, L., Di Leo, R., Vita, G., Nobile-Orazio, E., & Toscano, A. (2012). Subacute inflammatory

demyelinating polyneuropathy disclosed by massive nerve root enhancement in CMT1A. *Muscle & nerve*, *45*(3), 449–450.

Mégarbané, A., Desguerres, I., Rizkallah, E., Delague, V., Nabbout, R., Barois, A., & Urtizberea, A. (2000). Brown-Vialetto-Van Laere syndrome in a large inbred Lebanese family: confirmation of autosomal recessive inheritance? *American journal of medical genetics*, *92*(2), 117–121.

Meggouh, F., de Visser, M., Arts, W. F. M., De Coo, R. I. F. M., van Schaik, I. N., & Baas, F. (2005). Early onset neuropathy in a compound form of Charcot-Marie-Tooth disease. *Annals of neurology*, *57*(4), 589–491.

Mersiyanova, I., Ismailov, S. M., Alexandr, V., Dadali, E. L., Fedotov, V., Nelis, E., Lofgren, A., Timmerman, V., van Broeckhoven, C., & Evgrafov, O. V. (2000). Screening for mutations in the peripheral myelin genes *PMP22*, *MPZ* and *Cx32* (*GJB1*) in Russian Charcot-Marie-Tooth neuropathy patients. *Human mutation*, *15*(4), 340–347.

Metzker, M. L. (2010). Sequencing technologies - the next generation. *Nature reviews: Genetics*, *11*(1), 31–46.

Meyer Zu Hörste, G., & Nave, K.-A. (2006). Animal models of inherited neuropathies. *Current opinion in neurology*, *19*(5), 464–473.

MHC Sequencing Consortium (1999). Complete sequence and gene map of a human major histocompatibility complex. *Nature*, *401*(6756), 921–923.

Miao, J., Li, H., Lin, H., Su, C., Liu, Y., Lei, G., Yang, T., & Li, Z. (2007). Severe sleep-disordered breathing in a patient with Brown-Vialetto-Van Laere syndrome: polysomnographic findings. *Journal of the neurological sciences*, *263*(1-2), 214–217.

Miki, Y., Tomiyama, M., Haga, R., Nishijima, H., Suzuki, C., Kurihara, A., Sugimoto, K., Hashiguchi, A., Takashima, H., & Baba, M. (2013). A family

with IVIg-responsive Charcot-Marie-Tooth disease. *Journal of neurology*, *260*(4), 1147–1151.

Moges, H., Vasconcelos, O. M., Campbell, W. W., Borke, R. C., McCoy, J. A., Kaczmarczyk, L., Feng, J., & Anders, J. J. (2009). Light therapy and supplementary riboflavin in the SOD1 transgenic mouse model of familial amyotrophic lateral sclerosis (FALS). *Lasers in surgery and medicine*, *41*(1), 52-59.

Montenegro, G., Powell, E., Huang, J., Speziani, F., Edwards, Y. J. K., Beecham, G., Hulme, W., Siskind, C., Vance, J., Shy, M., & Züchner, S. (2011). Exome sequencing allows for rapid gene identification in a Charcot-Marie-Tooth family. *Annals of neurology*, *69*(3), 464-470.

Moriyama, Y. (2011). Riboflavin transporter is finally identified. *Journal of biochemistry*, *150*(4), 341–343.

Mostacciuolo, M. L., Righetti, E., Zortea, M., Bosello, V., Schiavon, F., Vallo, L., Merlini, L., Siciliano, G., Fabrizi, G. M., Rizzuto, N., Milani, M., Baratta, S., & Taroni, F. (2001). Charcot-Marie-Tooth disease type I and related demyelinating neuropathies: Mutation analysis in a large cohort of Italian families. *Human mutation*, *18*(1), 32–41.

Mullis, K., Faloona, F., Scharf, S., Saiki, R., Horn, G., & Erlich, H. (1986). Specific enzymatic amplification of DNA in vitro: the polymerase chain reaction. *Cold Spring Harbor Symposia on Quantitative Biology*, *51*(Pt 1), 263-273.

Murakami, T., Sun, Z. S., Lee, C. C., & Lupski, J. R. (1997). Isolation of novel genes from the CMT1A duplication/HNPP deletion critical region in 17p11.2-p12. *Genomics*, *39*(1), 99–103.

Murphy, M. P. (2009). How mitochondria produce reactive oxygen species. *The Biochemical journal*, *417*(1), 1–13.

Murphy, S. M., Herrmann, D. N., McDermott, M. P., Scherer, S. S., Shy, M. E., Reilly, M. M., & Pareyson, D. (2011). Reliability of the CMT neuropathy score (second version) in Charcot-Marie-Tooth disease. *Journal of the peripheral nervous system*, *16*(3), 191–198.

Murphy, S. M., Laura, M., Fawcett, K., Pandraud, A., Liu, Y.-T., Davidson, G. L., Rossor, A. M., Polke, J. M., Castleman, V., Manji, H., Lunn, M. P., Bull, K., Ramdharry, G., David, M., Blake, J. C., Houlden, H., & Reilly, M. M. (2012). Charcot-Marie-Tooth disease: frequency of genetic subtypes and guidelines for genetic testing. *Journal of neurology, neurosurgery, and psychiatry*, *83*(7), 706–710.

Murphy, S. M., Ovens, R., Polke, J., Siskind, C. E., Laura, M., Bull, K., Ramdharry, G., Houlden, H., Murphy, R. P., Shy, M. E., & Reilly, M. M. (2012). X inactivation in females with X-linked Charcot-Marie-Tooth disease. *Neuromuscular disorders*, *22*(7), 617-621.

Murphy, S. M., Polke, J., Manji, H., Blake, J., Reiniger, L., Sweeney, M., Houlden, H., Brandner, S., & Reilly, M. M. (2011). A novel mutation in the nerve-specific 5'UTR of the *GJB1* gene causes X-linked Charcot-Marie-Tooth disease. *Journal of the peripheral nervous system*, *16*(1), 65–70.

Nabokina, S. M., Subramanian, V. S., & Said, H. M. (2012). Effect of clinical mutations on functionality of the human riboflavin transporter-2 (hRFT-2). *Molecular genetics and metabolism*, *105*(4), 652-657.

Naef, R., & Suter, U. (1999). Impaired intracellular trafficking is a common disease mechanism of *PMP22* point mutations in peripheral neuropathies. *Neurobiology of disease*, *6*(1), 1–14.

Nagao, M., & Tanakas, K. (1992). FAD-dependent regulation of transcription, translation, post-translational processing, and post-processing stability of various mitochondrial acyl-CoA dehydrogenases and of electron transfer

flavoprotein and the site of holoenzyme formation. *The Journal of biological chemistry*, *267*(25), 17925–17932.

Nagatsu, T., Nagatsu-Ishibashi, I., Okuda, J., & Yagi, K. (1967). Incorporation of peripherally administered riboflavine into flavine nucleotides in the brain. *Journal of neurochemistry*, *14*(2), 207–210.

Nagy, E., & Maquat, L. E. (1998). A rule for termination-codon position within intron-containing genes: when nonsense affects RNA abundance. *Trends in biochemical sciences*, *23*(6), 198–199.

Nakano, E., Mushtaq, S., Heath, P. R., Lee, E.-S., Bury, J. P., Riley, S. A. Powers, H. J., & Corfe, B. M. (2011). Riboflavin depletion impairs cell proliferation in adult human duodenum: identification of potential effectors. *Digestive diseases and sciences*, *56*(4), 1007–1019.

National Research Council. (1998). *Dietary Reference Intakes for Thiamin, Riboflavin, Niacin, vitamin B6, Folate, Vitamin B12, Pantothenic Acid, Biotin, and Choline.* Washington, DC: The National Academies Press.

Nelis, E., De Jonghe, P., De Vriendt, E., Patel, P. I., Martin, J. J., & Van Broeckhoven, C. (1998). Mutation analysis of the nerve specific promoter of the *peripheral myelin protein 22* gene in CMT1 disease and HNPP. *Journal of medical genetics*, *35*(7), 590–593.

Nelis, E., Holmberg, B., Adolfsson, R., Holmgren, G., & van Broeckhoven, C. (1997). *PMP22* Thr(118)Met: recessive CMT1 mutation of polymorphism? *Nature genetics*, *15*, 13–14.

Nelis, E., Timmerman, V., De Jonghe, P., & Van Broeckhoven, C. (1994). Identification of a 5' splice site mutation in the *PMP-22* gene in autosomal dominant Charcot-Marie-Tooth disease type 1. *Human molecular genetics*, *3*(3), 515-516.

Nelis, E., Van Broeckhoven, C., De Jonghe, P., Lofgren, A., Vandenberghe, A., Latour, P., Le Guern, E., Brice, A., Mostacciuolo, M. L., Schiavon, F., Palau, F., Bort, S., Upadhyaya, M., Rocchi, M., Archidiacono, N., Mandich, P., Bellone, E., Silander, K., Savontaus, M. L., Navon, R., Goldberg-Stern, H., Estivill, X., Volpini, V., Friedl, W., Zerres, K., Tyson, J., Malcolm, S., Holmberg, B., Holmgren, G., Mariman, E. C. M., Gabreels-Festern, A. A. W. M., Yapijakis, C., Vassilopoulos, D., Clark, C., Haites, N., Hilbert, P., van Maldergem, L., Rautenstrauss, B., Grehl, H., Mountford, R., Mann, K., Bettecken, T., Burgunder, J. M., Hanemann, C. O., Muller, H. W., Hertz, J. M., Schorderet, D. F., Kuntzer, T., Wolf, C., Kunert, E., Muntoni, F., Emmerick-Bock, P., Orth, U., & Gal, A. (1996). Estimation of the mutation frequencies in Charcot-Marie-Tooth disease type 1 and hereditary neuropathy with liability to pressure palsies: a European collaborative study. *European journal of human genetics*, *4*(1), 25–33.

Ng, S. B., Buckingham, K. J., Lee, C., Bigham, A. W., Tabor, H. K., Dent, K. M., Huff, C. D., Shannon, P. T., Jabs, E. W., Nickerson, D. A., Shendure, J., & Bamshad, M. J. (2010). Exome sequencing identifies the cause of a Mendelian disorder. *Nature genetics*, *42*(1), 30–35.

Ng, P. C., & Henikoff, S. (2001). Predicting deleterious amino acid substitutions. *Genome research*, *11*(5), 863-874.

Nicholls, D. G. (2002). Mitochondrial function and dysfunction in the cell: its relevance to aging and aging-related disease. *The International journal of biochemistry & cell biology*, *34*, 1372–1381.

Nicolaou, P., Zamba-Papanicolaou, E., Koutsou, P., Kleopa, K. A, Georghiou, A., Hadjigeorgiou, G., Papadimitriou, A., Kyriakides, T., & Christodoulou, K. (2010). Charcot-Marie-Tooth disease in Cyprus: epidemiological, clinical and genetic characteristics. *Neuroepidemiology*, *35*(3), 171–177.

Niedrist, D., Joncourt, F., Mátyás, G., & Müller, A. (2009). Severe phenotype with cis-acting heterozygous *PMP22* mutations. *Clinical genetics*, *75*(3), 286–289.

Northrop-Clewes, C. A., & Thurnham, D. I. (2012). The discovery and characterization of riboflavin. *Annals of nutrition & metabolism*, *61*(3), 224–230.

Notterpek, L., Ryan, M. C., Tobler, A. R., & Shooter, E. M. (1999). PMP22 accumulation in aggresomes: implications for CMT1A pathology. *Neurobiology of disease*, *6*(5), 450–460.

Numakura, C., Lin, C., Ikegami, T., Guldberg, P., & Hayasaka, K. (2002). Molecular analysis in Japanese patients with Charcot-Marie-Tooth disease: DGGE analysis for *PMP22*, *MPZ*, and *Cx32*/*GJB1* mutations. *Human mutation*, *20*(5), 392–398.

Nuwal, T., Kropp, M., Wegener, S., Racic, S., Montalban, I., & Buchner, E. (2012). The Drosophila homologue of tubulin-specific chaperone E-like protein is required for synchronous sperm individualization and normal male fertility. *Journal of neurogenetics*, *26*(3-4), 374–381.

Ogle, R. F., Christodoulou, J., Fagan, E., Blok, R. B., Kirby, D. M., Seller, K. L., & Dahl, H. M. (1997). Mitochondrial myopathy with tRNA(Leu(UUR)) mutation and complex I deficiency responsive to riboflavin. *The Journal of pediatrics*, *130*(1), 138-145.

Olpin, S. E., & Bates, C. J. (1982). Lipid metabolism in riboflavin-deficient rats. *British journal of nutrition*, *47*, 589-596.

Olsen, R. K. J., Olpin, S. E., Andresen, B. S., Miedzybrodzka, Z. H., Pourfarzam, M., Merinero, B., Frerman, F. E., Beresford, M. W., Dean, J. C., Cornelius, N., Andersen, O., Oldfors, A., Holme, E., Gregersen, N., Turnbull, D. M., & Morris, A. M. (2007). *ETFDH* mutations as a major cause of riboflavin-responsive multiple acyl-CoA dehydrogenation deficiency. *Brain*, *130*(Pt 8), 2045–2054.

Padidela, R., Kelberman, D., Press, M., Al-Khawari, M., Hindmarsh, P. C., & Dattani, M. T. (2009). Mutation in the *TBCE* gene is associated with hypoparathyroidism-retardation-dysmorphism syndrome featuring pituitary hormone deficiencies and hypoplasia of the anterior pituitary and the corpus callosum. *The Journal of clinical endocrinology and metabolism*, *94*(8), 2686–2691.

Pál, Z., Kiss, E., Gál, A., Csépány, T., Lengyel, A., & Molnar, M. J. (2009). Genetically determined neuropathy (CMT1A) accompanied by immune dysfunction: a case report. *Inflammation research*, *58*(7), 359–361.

Palau, F., Lofgren, A., De Jonghe, P. D., Bort, S., Nelis, E., Sevilla, T., Martin, J. J., Vilchez, J., Prieto, F., & Van Broeckhoven, C. (1993). Origin of the de novo duplication in Charcot-Marie-Tooth disease type 1A: unequal nonsister chromatid exchange during spermatogenesis. *Human molecular genetics*, *2*(12), 2031–2035.

Pandraud, A. (in press). Peripheral nerve neuropathies including CMT disease. In A. Schapira, Z. Wszolek, T. Dawson, & N. Wood (Eds.), *Neurodegeneration* (pp. unknown). Oxford: Wiley-Blackwell.

Pandraud, A., Liu, Y., & Houlden, H. (2012). Advances in the genetics of peripheral nerve disorders. *Advances in clinical neuroscience and rehabilitation*, *12*(2), 8-13.

Papp, E., Nardai, G., Mandl, J., Bánhegyi, G., & Csermely, P. (2005). FAD oxidizes the ERO1-PDI electron transfer chain: the role of membrane integrity. *Biochemical and biophysical research communications*, *338*(2), 938–945.

Pareyson, D., & Marchesi, C. (2009). Diagnosis, natural history, and management of Charcot–Marie–Tooth disease. *The Lancet neurology*, *8*, 654–667.

Pareyson, D., Taroni, F., Botti, S., Morbin, M., Baratta, S., Lauria, G., Ciano, C., & Sghirlanzoni, A. (2000). Cranial nerve involvement in CMT disease type 1 due to *early growth response 2* gene mutation. *Neurology*, *54*(8), 1696–1698.

Park, H.-K., Kim, B. J., Sung, D. H., Ki, C.-S., & Kim, J.-W. (2006). Mutation analysis of the *PMP22*, *MPZ*, *EGR2*, *LITAF*, and *GJB1* genes in Korean patients with Charcot-Marie-Tooth neuropathy type 1. *Clinical genetics*, *70*(3), 253–256.

Parmley, J. L., & Hurst, L. D. (2007). How do synonymous mutations affect fitness? *BioEssays : news and reviews in molecular, cellular and developmental biology*, *29*(6), 515–519.

Passage, E., Norreel, J. C., Noack-Fraissignes, P., Sanguedolce, V., Pizant, J., Thirion, X., Robaglia-Schlupp, A., Pellissier, J. F., & Fontes, M. (2004). Ascorbic acid treatment corrects the phenotype of a mouse model of Charcot-Marie-Tooth disease. *Nature medicine*, *10*(4), 396-401.

Patel, P. I., Roa, B., Welcher, A. A., Schoener-Scott, R., Trask, B. J., Pentao, L., Snipes, G. J., Garcia, C. A., Francke, U., Shooter, E. M., Lupski, J. R., & Suter, U. (1992). The gene for the peripheral myelin protein PMP-22 is a candidate for Charcot-Marie-Tooth disease type 1A. *Nature genetics*, *1*(3), 159–165.

Patel, M., Vadlapatla, R. K., Pal, D., & Mitra, A. K. (2012). Molecular and functional characterization of riboflavin specific transport system in rat brain capillary endothelial cells. *Brain research*, *1468*, 1–10.

Pathak, R. U., & Davey, G. P. (2008). Complex I and energy thresholds in the brain. *Biochimica et biophysica acta*, *1777*(7-8), 777–782.

Patzkó, A., & Shy, M. E. (2011). Update on Charcot-Marie-Tooth disease. *Current neurology and neuroscience reports*, *11*(1), 78–88.

Peluchetti, D., Antozzi, C., Roi, S., DiDonato, S., & Cornelio, F. (1991). Riboflavin responsive multiple acyl-CoA dehydrogenase deficiency: functional evaluation of recovery after high dose vitamin supplementation. *Journal of the neurological sciences*, *105*, 93–98.

Pentao, L., Wise, C. A., Chinault, A. C., Patel, P., & Luspki, J. R. (1992). Charcot-Marie-Tooth type 1A duplication appears to arise from recombination at repeat sequences flanking the 1.5Mb monomer unit. *Nature genetics*, *2*, 292–300.

Piscosquito, G., Salsano, E., Ciano, C., Palamara, L., Morbin, M., & Pareyson, D. (2013). Coexistence of Charcot-Marie-Tooth disease type 1A and anti-MAG neuropathy. *Journal of the peripheral nervous system*, *18*, 185–188.

Polke, J. M., Laura, M., Murphy, S. M., Sweeney, M. G., Davis, M. B., & Reilly, M. M. (2011, June 29th- July 1st). *17p11.2 dosage and PMP22 sequencing analysis in a cohort of patients in the UK.* Poster presented at the 4th International CMT Consortium Meeting, Potomac, MD, USA.

Pollard, J. D., & Armati, P. J. (2011). CIDP – the relevance of recent advances in Schwann cell/axonal neurobiology. *Journal of the peripheral nervous system*, *16*, 15–23.

Powers, H. J. (2003). Riboflavin (vitamin B-2) and health. *The American journal of clinical nutrition*, *77*(6), 1352–1360.

Prasad, P. A., Lakshmi, A. V., Suresh, P. & Bamji, M. S. (1991). Effect of respiratory infection on tissue riboflavin and flavin enzymes in mice. *Annals of nutrition and metabolism*, 35, 19-24.

Prentice, A. M., & Bates, C. J. (1981a). A biochemical evaluation of the erythrocyte glutathione reductase test for riboflavin status. 1. Rates and specificity of response in acute deficiency. *The British journal of nutrition*, *45*, 37-52.

Prentice, A. M., & Bates, C. J. (1981b). A biochemical evaluation of the erythrocyte glutathione reductase test for riboflavin status. 2. Dose-response relationships in chronic marginal deficiency. *The British journal of nutrition*, *45*, 53-65.

Purcell, S., Neale, B., Todd-Brown, K., Thomas, L., Ferreira, M. A., Bender, D., Maller, J., Sklar, P., de Bakker, P. I., Daly, M. J., & Sham, P. C. (2007). PLINK: a tool set for whole-genome association and population-based linkage analyses. *American journal of human genetics*, *81*(3), 559–575.

Quinzii, C. M., López, L. C., Gilkerson, R. W., Dorado, B., Coku, J., Naini, A. B., Lagler-Tourenne, C., Schuelke, M., Salviati, L., Carrozzo, R., Santorelli, F., Rahman, S., Tazir, M., Koenig, M., DiMauro, S., & Hirano, M. (2010). Reactive oxygen species, oxidative stress, and cell death correlate with level of CoQ_{10} deficiency. *FASEB journal*, *24*(10), 3733–3743.

Quinzii, C. M., López, L. C., Naini, A., DiMauro, S., & Hirano, M. (2008). Human CoQ_{10} deficiencies. *BioFactors*, *32*(1-4), 113–118.

R Development Core Team (2008). R: A language and environment for statistical computing. R Foundation for Statistical Computing, Vienna, Austria.

Raeymaekers, P., Timmerman, V., De Jonghe, P., Swerts, L., Gheuens, J., Martin, J. J., Muylle, L., De Winter, G., Vandenberghe, A., & Van Broeckhoven, C. (1989). Localization of the mutation in an extended family with Charcot-Marie-Tooth neuropathy (HMSN I). *American journal of human genetics*, *45*(6), 953–958.

Raeymaekers, P., Timmerman, V., Nelis, E., De Jonghe, P., Hoogenduk, J., Baas, F., Barker, D. F., Martin, J. J., De Visser, M., Bolhuis, P., Van Broeckhoven, C., & the HMSN Collaborative Research Group (1991). Duplication in chromosome 17p11.2 in Charcot-Marie-Tooth neuropathy type 1A (CMT1A). *Neuromuscular disorders*, *1*(2), 93–97.

Reed, J. S., & Ragan, C. I.. (1987). The effect of rate limitation by cytochrome c on the redox state of the ubiquinone pool in reconstituted NADH: cytochrome c reductase. *The Biochemical journal*, *247*(3), 657–662.

Reihl, P., & Stolz, J. (2005). The monocarboxylate transporter homolog Mch5p catalyzes riboflavin (vitamin B2) uptake in Saccharomyces cerevisiae. *The Journal of biological chemistry*, *280*(48), 39809–39817.

Reilly, M. M., Murphy, M., & Laura, M. (2011). Charcot-Marie-Tooth disease. *Journal of the peripheral nervous system*, *16*, 1–14.

Reilly, M. M. & Shy, M. E. (2009). Diagnosis and new treatments in genetic neuropathies. *Journal of neurology, neurosurgery, and psychiatry*, *80*(12), 1304–1314.

Reiter, L. T., Murakami, T., Koeuth, T., Gibbs, R. A., & Lupski, J. R. (1997). The human *COX10* gene is disrupted during homologous recombination between the 24 Kb proximal and distal CMT1A-REPs. *Human molecular genetics*, *6*(9), 1595–1603.

Reiter, L. T., Murakami, T., Koeuth, T., Pentao, L., Muzny, D. M., Gibbs, R. A., & Lupski, J. R. (1996). A recombination hotspot responsible for two inherited peripheral neuropathies is located near a mariner transposon-like element. *Nature genetics*, *12*, 288–297.

Ren, J., Wen, L., Gao, X., Jin, C., Xue, Y., & Yao, X. (2009). DOG 1.0: Illustrator of protein domain structures. *Cell research*, *19*(2), 271–273.

Rhead, W., Roettger, V., Marshall, T., & Amendt, B. (1993). Multiple acyl-coenzyme A dehydrogenation disorder responsive to riboflavin: Substrate oxidation, flavin metabolism, and flavoenzyme activities in fibroblasts. *Pediatric Research*, *33*(2), 129-135.

Ritz, M. F., Lechner-Scott, J., Scott, R. J., Fuhr, P., Malik, N., Erne, B., Taylor, V., Suter, U., Schaeren-Wiemers, N., & Steck, A. J. (2000). Characterisation of autoantibodies to peripheral myelin protein 22 in patients with hereditary and acquired neuropathies. *Journal of neuroimmunology*, *104*(2), 155–163.

Roa, B., Garcia, C., Pentao, L., Killian, J., Trask, B., Suter, U., Snipes, G. J., Ortiz-Lopez, R., Shooter, E. M., Patel, P. I., & Lupski, J. R. (1993). Evidence for a recessive *PMP22* point mutation in Charcot-Marie-Tooth disease Type 1A. *Nature genetics*, *5*(2), 189–194.

Roa, B., Garcia, C., Suter, U., Kulpa, D., Wise, C., Mueller, J., Welcher, A. A., Snipes, G. J., Shooter, E. M., Patel, P. I., & Lupski, J. R. (1993). Charcot-Marie-Tooth Disease Type 1A- Association with a spontaneous point mutation in the *PMP22* gene. *The New England journal of medicine*, *329*(2), 96-101.

Roa, B. B., Greenberg, F., Gunaratne, P., Sauer, C. M., Lubsinky, M. S., Kozma, C., Meck, J. M., Magenis, R. E., Shaffer, L. G., & Lupski, J. R. (1996). Duplication of the *PMP22* gene in 17p partial trisomy patients with Charcot-Marie-Tooth type-lA neuropathy. *Human genetics*, *97*(5), 642–649.

Roberts, R. C. (2012). The Charcot-Marie-Tooth diseases: how can we identify and develop novel therapeutic targets? *Brain*, *135*(Pt 12), 3527–3528.

Roeleveld-Versteegh, A. B. C., Braun, K. P. J., Smeitink, J. A. M., Dorland, L., & de Koning, T. J. (2004). Case report: Mitochondrial respiratory chain disease presenting as progressive bulbar paralysis of childhood. *Journal of inherited metabolic disease*, *27*, 281–283.

Rogozin, I. B., & Milanesi, L. (1997). Analysis of donor splice signals in different eukaryotic organisms. *Journal of molecular evolution*, *45*(1), 50-59.

Ross, N. S., & Hansen, T. P. (1992). Riboflavin deficiency is associated with selective preservation of critical flavoenzyme-dependent metabolic pathways. *Biofactors*, *3*(3), 185–190.

Rossor, A. M., Polke, J. M., Houlden, H., & Reilly, M. M. (2013). Clinical implications of genetic advances in Charcot-Marie-Tooth disease. *Nature reviews: neurology*, *9*(10), 562–571.

Rozen, S., & Skaletsky, H. (2000). Primer3 on the WWW for general users and for biologist programmers. *Methods in molecular biology*, *132*, 365-386.

Russo, M., Laurá, M., Polke, J. M., Davis, M. B., Blake, J., Brandner, S., Hughes, R. A., Houlden, H., Bennett, D. L., Lunn, M. P., & Reilly, M. M. (2011). Variable phenotypes are associated with *PMP22* missense mutations. *Neuromuscular disorders*, *21*(2), 106–114.

Saberan-Djoneidi, D., Sanguedolce, V., Assouline, Z., Levy, N., Passage, E., & Fontes, M. (2000). Molecular dissection of the Schwann cell specific promoter of the *PMP22* gene. *Gene*, *248*(1-2), 223-231.

Said, H. M., & Ma, T. Y. (1994). Mechanism of riboflavine uptake by Caco-2 human intestinal epithelial cells. *The American journal of physiology. Gastrointestinal and liver physiology*, *266*(1), G15–21.

Said, H. M., Ma, T. Y., & Grant, K. (1994). Regulation of riboflavin intestinal uptake by protein kinase A: studies with Caco-2 cells. *The American journal of physiology*, *267*(6 Pt 1), G955-959.

Said, H. M., & Mohammed, Z. M. (2006). Intestinal absorption of water-soluble vitamins: an update. *Current opinion in gastroenterology*, *22*(2), 140–146.

Said, H. M., Ortiz, A., Ma, T. Y., & McCloud, E. (1998). Riboflavin uptake by the human-derived liver cells Hep G2: mechanism and regulation. *Journal of cellular physiology*, *176*(3), 588–594.

Saijo, T., & Tanaka, K. (1995). Isoalloxazine ring of FAD is required for the formation of the core in the Hsp60-assisted folding of medium chain acyl-coA

dehydrogenase subunit into the assembly competent conformation in mitochondria. *The Journal of biological chemistry*, *270*(4), 1899–1907.

Sakurai, T., Miyazawa, S., Furuta, S., & Hashimoto, T. (1982). Riboflavin deficiency and beta-oxidation systems in rat liver. *Lipids*, *17*(9), 598–604.

Sambuughin, N., de Bantel, A., McWilliams, S., & Sivakumar, K. (2003). Deafness and CMT disease associated with a novel four amino acid deletion in the *PMP22* gene. *Neurology*, *60*(3), 506–508.

Sandrini, F., Farmakidis, C., Kirschner, L. S., Wu, S. M., Tullio-Pelet, A., Lyonnet, S., Metzger, D. L., Bourdony, C. J., Tiosano, D., Chan, W. Y., & Stratakis, C. A. (2001). Spectrum of mutations of the *AAAS* gene in Allgrove syndrome: lack of mutations in six kindreds with isolated resistance to corticotropin. *The Journal of clinical endocrinology and metabolism*, *86*(11), 5433–5437.

Sanger, F., & Coulson, A. R. (1975). A rapid method for determining sequences in DNA by primed synthesis with DNA polymerase. *Journal of molecular biology*, *94*(3), 441–448.

Sanvito, L., Makowska, A., Mahdi-Rogers, M., Hadden, R. D. M., Peakman, M., Gregson, N., Nemni, R., & Hughes, R. A. C. (2009). Humoral and cellular immune responses to myelin protein peptides in chronic inflammatory demyelinating polyradiculoneuropathy. *Journal of neurology, neurosurgery, and psychiatry*, *80*(3), 333–338.

Saporta, A. S. D., Sottile, S. L., Miller, L. J., Feely, S. M. E., Siskind, C. E., & Shy, M. E. (2011). Charcot-marie-tooth disease subtypes and genetic testing strategies. *Annals of neurology*, *69*(1), 22–33.

Sathasivam, S. (2008). Brown-Vialetto-Van Laere syndrome. *Orphanet journal of rare diseases*, *3*(1), 9.

Sathasivam, S, O'Sullivan, S., Nicolson, A., Tilley, P. J., & Shaw, P. J. (2000). Brown-Vialetto-Van Laere syndrome: case report and literature review. *Amyotrophic lateral sclerosis and other motor neuron disorders*, *1*(4), 277–281.

Scherer, S. S., & Wrabetz, L. (2008). Molecular mechanisms of inherited demyelinating neuropathies. *Glia*, *56*(14), 1578–1589.

Schmid, C. D., Stienekemeier, M., Oehen, S., Bootz, F., Zielasek, J., Gold, R., Toyka, K. V., Schachner, M., & Martini, R. (2000). Immune deficiency in mouse models for inherited peripheral neuropathies leads to improved myelin maintenance. *The Journal of neuroscience*, *20*(2), 729–735.

Scholte, H. R., Busch, H., Bakker, H., Bogaard, J., Luyt-Houwen, I., & Kuyt, L. (1995). Riboflavin-responsive complex I deficiency. *Biochimica et biophysica acta*, *1271*, 75–83.

Schulz, J. B., Lindenau, J., Seyfried, J., & Dichgans, J. (2000). Glutathione, oxidative stress and neurodegeneration. *European journal of biochemistry*, *267*(16), 4904–4911.

Schuman Jorns, M., Wang, B., & Jordan, S. P. (1987). DNA repair catalyzed by Escherichia coli DNA photolyase containing only reduced flavin: Elimination of the enzyme's second chromophore by reduction with sodium borohydride. *Biochemistry*, *26*(21), 6810–6816.

Schwarz, J. M., Rödelsperger, C., Schuelke, M., & Seelow, D. (2010). MutationTaster evaluates disease-causing potential of sequence alterations. *Nature methods*, *7*(8), 575-576.

Seeman, P., Mazanec, R., Marikova, T., & Rautenstrauss, B. (1999). Charcot-Marie-Tooth 1A: Heterozygous T118M mutation over a CMT1A duplication has no influence on the phenotype. *Annals New York Academy of Sciences*, *883*, 485–489.

Seo, A. J., Shin, Y. H., Lee, S. J., Kim, D., Park, B. S., Kim, S., Choi, K. H., Jeong, N. Y., Park, C., Jang, J. Y., Huh, Y., & Jung, J. (2014). A novel adenoviral vector-mediated mouse model of Charcot-Marie-Tooth type 2D (CMT2D). *Journal of molecular histology*, *45*(2), 121-128.

Sereda, M. W., Meyer zu Horste, G., Suter, U., Uzma, N., & Nave, K. (2003). Therapeutic administration of progesterone antagonist in a model of Charcot-Marie-Tooth disease (CMT-1A). *Nature medicine*, *9*(12), 1533–1537.

Sevier, C. S., & Kaiser, C. A. (2008). Ero1 and redox homeostasis in the endoplasmic reticulum. *Biochimica et biophysica acta*, *1783*(4), 549–556.

Shakher, J., & Stevens, M. J. (2011). Update on the management of diabetic polyneuropathies. *Diabetes, metabolic syndrome and obesity: targets and therapy*, *4*, 289–305.

Shaw, P. J. (2005). Molecular and cellular pathways of neurodegeneration in motor neurone disease. *Journal of neurology, neurosurgery, and psychiatry*, *76*(8), 1046–1057.

Shelton, G. D., Podell, M., Poncelet, L., Schatzberg, S., Patterson, E., Powell, H. C., & Mizisin, A. P. (2003). Inherited polyneuropathy in Leonberger dogs: a mixed or intermediate form of Charcot-Marie-Tooth disease? *Muscle & nerve*, *27*, 471-477.

Shepherd, J. A., & Garland, P. B. (1969) Citrate synthase activity from rat liver. *Methods in enzymology*, *13*, 11-19.

Sheth, S., Francies, K., Siskind, C. E., Feely, S. M. E., Lewis, R. A., & Shy, M. E. (2008). Diabetes mellitus exacerbates motor and sensory impairment in CMT1A. *Journal of the peripheral nervous system*, *13*(4), 299–304.

Shy, M. E., Blake, J., Krajewski, K., Fuerst, D. R., Laura, M., Hahn, A. F., Li, J., Lewis, R. A., & Reilly, M. M. (2005). Reliability and validity of the CMT neuropathy score as a measure of disability. *Neurology*, *64*(7), 1209–1214.

Shy, M. E., Chen, L., Swan, E. R., Taube, R., Krajewski, K. M., Herrmann, D., Lewis, R. A., & McDermott, M. P. (2008). Neuropathy progression in Charcot-Marie-Tooth disease type 1A. *Neurology*, *70*(5), 378–383.

Shy, M. E., & Patzkó, A. (2011). Axonal Charcot-Marie-Tooth disease. *Current opinion in neurology*, *24*(5), 475-483.

Shy, M. E., Scavina, M. T., Clark, A., Krajewski, K. M., Li, J., Kamholz, J., Kolodny, E., Szigeti, K., Fischer, R. A., Saifi, G. M., Scherer, S. S., & Lupski, J. R. (2006). T118M *PMP22* mutation causes partial loss of function and HNPP-like neuropathy. *Annals of neurology*, *59*(2), 358–364.

Silander, K., Meretoja, P., Juvonen, V., Ignatius, J., Pihko, H., Saarinen, A., Wallden, T., Herrgard, E., Aula, P., & Savontaus, M. L. (1998). Spectrum of mutations in Finnish patients with Charcot-Marie-Tooth disease and related neuropathies. *Human mutation*, *12*(1), 59–68.

Singleton, A. B. (2011). Exome sequencing : a transformative technology. *The Lancet neurology*, *10*(10), 942–946.

Sinkiewicz-Darol, E., Kabzińska, D., Moszyńska, I., & Kochanski, A. (2010). The 5' regulatory sequence of the *PMP22* in the patients with Charcot-Marie-Tooth disease. *Acta biochimica Polonica*, *57*(3), 373–377.

Siskind, C. E., & Shy, M. E. (2011). Genetics of neuropathies. *Seminars in neurology*, *31*(5), 494-405.

Skre, H. (1974). Genetic and clinical aspects of Charcot-Marie-Tooth's disease. *Clinical genetics*, *6*(2), 98–118.

Slater, H., Bruno, D., Ren, H., La, P., Burgess, T., Hills, L., Nouri, S., Schouten, J., & Choo, K. H. (2004). Improved testing for CMT1A and HNPP using multiplex ligation-dependent probe amplification (MLPA) with rapid DNA preparations: comparison with the interphase FISH method. *Human mutation*, *24*(2), 164–171.

International Consortium for Systemic Lupus Erythematosus Genetics (SLEGEN), Harley, J. B., Alarcón-Riquelme, M. E., Criswell, L. A., Jacob, C. O., Kimberly, R. P., Moser, K. L., Tsao, B. P., Vyse, T. J., Langefeld, C. D., Nath, S. K., Guthridge, J. M., Cobb, B. L., Mirel, D. B., Marion, M. C., Williams, A. H., Divers, J., Wang, W., Frank, S. G., Namjou, B., Gabriel, S. B., Lee, A. T., Gregersen, P. K., Behrens, T. W., Taylor, K. E., Fernando, M., Zidovetzki, R., Gaffney, P. M., Edberg, J. C., Rioux, J. D., Ojwang, J. O., James, J. A., Merrill, J. T., Gilkeson, G. S., Seldin, M. F., Yin, H., Baechler, E. C., Li, Q. Z., Wakeland, E. K., Bruner, G. R., Kaufman, K. M., & Kelly J. A. (2008). Genome-wide association scan in women with systemic lupus erythematosus identifies susceptibility variants in *ITGAM*, *PXK*, *KIAA1542* and other loci. *Nature genetics*, *40*(2), 204–210.

Sorour, E., Thompson, P., MacMillan, J., & Upadhyaya, M. (1995). Inheritance of CMT1A duplication from a mosaic father. *Journal of medical genetics*, *32*(6), 483–485.

Spaan, A. N., Ijlst, L., van Roermund, C. W. T., Wijburg, F. A., Wanders, R. J. A., & Waterham, H. R. (2005). Identification of the human mitochondrial FAD transporter and its potential role in multiple acyl-CoA dehydrogenase deficiency. *Molecular genetics and metabolism*, *86*(4), 441–447.

Spagnoli, C., & De Sousa, C. (2011). Brown-Vialetto-Van Laere syndrome and Fazio-Londe disease - treatable motor neuron diseases of childhood. *Developmental medicine and child neurology*, *54*(4), 292–293.

Spagnoli, C., Pitt, M. C., Rahman, S., & de Sousa, C. (2014). Brown-Vialetto-Van Laere syndrome: A riboflavin responsive neuronopathy of infancy with singular features. *European journal of paediatric neurology*, *18*(2), 231-234.

Spector, R. (1980a). Riboflavin accumulation by rabbit brain slices in vitro. *Journal of neurochemistry*, *34*(6), 1768–1771.

Spector, R. (1980b). Riboflavin homeostasis in the central nervous system. *Journal of neurochemistry*, *35*(1), 202–209.

Spector, R. (1980c). Riboflavin transport in the central nervous system. Characterization and effects of drugs. *The Journal of clinical investigation*, *66*(4), 821–831.

Spector, R., & Johanson, C. (2006). Micronutrient and urate transport in choroid plexus and kidney: implications for drug therapy. *Pharmaceutical research*, *23*(11), 2515–2524.

Spindler, M., Beal, M. F., & Henchcliffe, C. (2009). Coenzyme Q_{10} effects in neurodegenerative disease. *Neuropsychiatric disease and treatment*, *5*, 597–610.

Stahl, E. A., Raychaudhuri, S., Remmers, E. F., Xie, G., Eyre, S., Thomson, B. P., Li, Y., Kurreeman, F. A., Zhernakova, A., Hinks, A., Guiducci, C., Chen, R., Alfredsson, L., Amos, C. I., Ardlie, K. G., BIRAC Consortium, Barton, A., Bowes, J., Brouwer, E., Burtt, N. P., Catanese, J. J., Coblyn, J., Coenen, M. J., Costenbader, K. H., Criswell, L. A., Crusius, J. B., Cui, J., de Bakker, P. I., De Jager, P. L., Ding, B., Emery, P., Flynn, E., Harrison, P., Hocking, L. J., Huizinga, T. W., Kastner, D. L., Ke, X., Lee, A. T., Liu, X., Martin, P., Morgan, A. W., Padyukov, L., Radstake, T. R., Reid, D. M., Seielstad, M., Seldin, M. F., Shadick, N. A., Steer, S., Tak, P. P., Thomson, W., van der Helm-van Mil, A. H., van der Horst-Bruinsma, I. E., van der Schoot, C. E., van Riel, P. L., Weinblatt, M. E., Wilson, A. G., Wolbink, G. J., Wordsworth, B. P., YEAR Consortium, Wijmenga, C., Karlson, E. W., Toes, R. E., de Vries,

N., Begovich, A. B., Worthington, J., Siminovitch, K. A., Gregersen, P. K., Klareskog, L., Plenge, R. M. (2010). Genome-wide association study meta-analysis identifies seven new rheumatoid arthritis risk loci. *Nature genetics, 42*(6), 508–514.

Steiner, I., Gotkine, M., Steiner-Birmanns, B., Biran, I., Silverstein, S., Abeliovich, D., Argov, Z., & Wirguin, I. (2008). Increased severity over generations of Charcot-Marie-Tooth disease type 1A. *Journal of neurology*, *255*(6), 813–819.

Stendel, C., Roos, A., Deconinck, T., Pereira, J., Castagner, F., Niemann, A., Kirschner, J., Korinthenberg, R., Ketelsen, U. P., Battaloglu, E., Parman, Y., Nicholson, G., Ouvrier, R., Seeger, J., De Jonghe, P., Weis, J., Kruttgen, A., Rudnik-Schnoneborn, S., Bergmann, C., Suter, U., Zerres, K., Timmerman, V., Relvas, J. B. & Senderek, J. (2007). Peripheral nerve demyelination caused by a mutant Rho GTPase guanine nucleotide exchange factor, frabin/FGD4. *American journal of human genetics*, *81*(1), 158-164.

Stoll, G., Gabreëls-Festen, A. A., Jander, S., Müller, H. W., & Hanemann, C. O. (1998). Major histocompatibility complex class II expression and macrophage responses in genetically proven Charcot-Marie-Tooth type 1 and hereditary neuropathy with liability to pressure palsies. *Muscle & nerve*, *21*(11), 1419–1427.

Stripp, B. (1965). Intestinal absorption of riboflavin by man. *Acta pharmacologica et toxicologica*, *22*(4), 353–362.

Subramanian, V. S., Rapp, L., Marchant, J. S., & Said, H. M. (2011). Role of cysteine residues in cell surface expression of the human riboflavin transporter-2 (hRFT2) in intestinal epithelial cells. *American journal of physiology. Gastrointestinal and liver physiology*, *301*(1), G100–109.

Subramanian, V. S., Subramanya, S. B., Ghosal, A., & Said, H. M. (2013). Chronic alcohol feeding inhibits physiological and molecular parameters of intestinal

and renal riboflavin transport. *American journal of physiology. Cell physiology*, *305*(5), C539-546.

Subramanian, V. S., Subramanya, S. B., Rapp, L., Marchant, J. S., Ma, T. Y., & Said, H. M. (2011). Differential expression of human riboflavin transporters -1, -2, and -3 in polarized epithelia: A key role for hRFT-2 in intestinal riboflavin uptake. *Biochimica et biophysica acta*, *1808*(12), 3016-3021.

Susin, S. A., Lorenzo, H. K., Zamzami, N., Marzo, I., Snow, B., Brothers, G. M., Mangion, J., Jacotot, E., Costantini, P., Loeffier, M., Larochette, N., Goodlett, D. R., Aebersold, R., Siderovski, D. P., Penninger, J. M., & Kroemer, G. (1999). Molecular characterization of mitochondrial apoptosis-inducing factor. *Nature*, *397*(6718), 441–446.

Suter, U., Moskow, J. J., Welcher, A. A., Snipes, G. J., Kosaras, B., Sidman, R. L., Buchberg, A. M., & Shooter, E. (1992). A leucine-to-proline mutation in the putative first transmembrane domain of the 22-kDa peripheral myelin protein in the trembler-J mouse. *Proceedings of the national academy of sciences USA*, *89*(10), 4382–4386.

Suter, U., Snipes, G. J., Schoener-Scott, R., Welcher, A. A., Pareek, S., Lupski, J. R., Murphy, R. A., Shooter, E. M., & Patel, P. I. (1994). Regulation of tissue-specific expression of alternative *peripheral myelin protein-22* (*PMP22*) gene transcripts by two promoters. *The Journal of biological chemistry*, *269*(41), 25795–25808.

Suter, U., Welcher, A., Ozcelik, T., Snipes, G., Kosaras, B., Francke, U., Billings-Gagliardi, S., Sidman, R. L., & Shooter, E. M. (1992). Trembler mouse carries a point mutation in a myelin gene. *Nature*, *356*(6366), 241–244.

Swan, E. R., Fuerst, D. R., & Shy, M. E. (2007). Women and men are equally disabled by Charcot-Marie-Tooth disease type 1A. *Neurology*, *68*, 873–876.

Szigeti, K., Wiszniewski, W., Saifi, G. M., Sherman, D. L., Sule, N., Adesina, A. M., Mancias, P., Papsozomenos, SCh., Miller, G., Keppen, L., Daenti, D., Brophy, P. J., & Lupski, J. R. (2007). Functional, histopathologic and natural history study of neuropathy associated with *EGR2* mutations. *Neurogenetics*, *8*(4), 257–262.

Taioli, F., Cabrini, I., Cavallaro, T., Acler, M., & Fabrizi, G. M. (2011). Inherited demyelinating neuropathies with micromutations of *peripheral myelin protein 22* gene. *Brain*, *134*(Pt 2), 608–617.

Taioli, F., Cabrini, I., Cavallaro, T., Simonati, A., Testi, S., & Fabrizi, G. M. (2011). Déjerine-Sottas syndrome with a silent nucleotide change of *myelin protein zero* gene. *Journal of the peripheral nervous system*, *16*(1), 59–64.

Takashima, H., Boerkoel, C. F., & Lupski, J. R. (2001). Screening for mutations in a genetically heterogeneous disorder: DHPLC versus DNA sequence for mutation detection in multiple genes causing Charcot-Marie-Tooth neuropathy. *Genetics in medicine*, *3*(5), 335–342.

Taroni, F., Pareyson, D., Botti, S., Sghirlanzoni, A., Nemni, R., & Riva, D. (1999). Mutations in the Schwann cell transcription factor *EGR2*/*Krox-20* in patients with severe hereditary demyelinating neuropathies. *Neurology*, *52*(6), A258–A259.

Tazir, M., Bellatache, M., Nouioua, S., & Vallat, J.-M. (2013). Autosomal recessive Charcot-Marie-Tooth disease: from genes to phenotypes. *Journal of the peripheral nervous system*, *18*, 113-129.

Tewhey, R., Bansal, V., Torkamani, A., Topol, E. J., & Schork, N. J. (2011). The importance of phase information for human genomics. *Nature reviews genetics*, *12*(3), 215–223.

Thomas, P. K., Marques, W., Davis, M. B., Sweeney, M. G., King, R. H., Bradley, J. L., Muddle, J. R., Tyson, J., Malcolm, S., & Harding, A. E. (1997). The

phenotypic manifestations of chromosome 17p11.2 duplication. *Brain*, *120*, 465–478.

Thompson, J. D., Higgins, D. G., & Gibson, T. J. (1994). CLUSTAL W: improving the sensitivity of progressive multiple sequence alignment through sequence weighting, position-specific gap penalties and weight matrix choice. *Nucleic acids research*, *22*(22), 4673-4680.

Timmerman, V., De Jonghe, P., Ceuterick, C., De Vriendt, E., Lofgren, A., Nelis, E., Warner, L. E., Lupski, J. R., Martin, J. J., & van Broeckhoven, C. (1999). Novel missense mutation in the *early growth response 2* gene associated with Dejerine-Sottas syndrome phenotype. *Neurology*, *52*(9), 1827–1832.

Timmerman, V., Nelis, E., Van Hul, W., Nieuwenhuijsen, B., Chen, K., Wang, S., Ben Othman, K., Cullen, B., Leach, R. J., Hanemann, C. O., De Jonghe, P., Raeymaekers, P., van Ommen, G-J.B., Martin, J. J., Muller, H. W., Vance, J. M., Fischbeck, K. H., & Van Broeckhoven, C. (1992). The peripheral myelin protein gene *PMP-22* is contained within the Charcot-Marie-Tooth disease type 1A duplication. *Nature genetics*, *1*, 171–175.

Tobler, A. R., Notterpek, L., Naef, R., Taylor, V., Suter, U., & Shooter, E. M. (1999). Transport of trembler-J mutant peripheral myelin protein 22 is blocked in the intermediate compartment and affects the transport of the wild-type protein by direct interaction. *The Journal of neuroscience*, *19*(6), 2027–2036.

Togashi, H., Nagata, K., Takagishi, M., Saitoh, N., & Inagaki, M. (2000). Functions of a rho-specific guanine nucleotide exchange factor in neurite retraction. Possible role of a proline-rich motif of KIAA0380 in localization. *The Journal of biological chemistry*, *275*(38), 29570–29578.

Tomkins, J., Usher, P., Slade, J. Y., Ince, P. G., Curtis, A., Bushby, K., & Shaw, P. J. (1998). Novel insertion in the KSP region of the neurofilament heavy gene in amyotrophic lateral sclerosis (ALS). *Neuroreport*, *9*(17), 3967–3970.

Tooth, H. (1886). *The Peroneal Type of Progressive Muscular Atrophy*. London: H.K. Lewis and Co.

Tu, B. P., Ho-Schleyer, S. C., Travers, K. J., & Weissman, J. S. (2000). Biochemical basis of oxidative protein folding in the endoplasmic reticulum. *Science, 290*(5496), 1571–1574.

Tu, B. P., & Weissman, J. S. (2002). The FAD- and O(2)-dependent reaction cycle of Ero1-mediated oxidative protein folding in the endoplasmic reticulum. *Molecular cell, 10*(5), 983–994.

Tullio-Pelet, A., Salomon, R., Hadj-Rabia, S., Mugnier, C., de Laet, M. H., Chaouachi, B., Bakiri, F., Brottier, P., Cattolico, L., Penet, C., Begeot, M., Naville, D., Nicolino, M., Chaussain, J. L., Weissenback, J., Munnich, A., & Lyonnet, S. (2000). Mutant WD-repeat protein in triple-A syndrome. *Nature genetics*, *26*(3), 332–335.

Tzagoloff, A., Jang, J., Glerum, D., & Wu, M. (1996). *FLX1* codes for a carrier protein involved in maintaining a proper balance of flavin nucleotides in yeast mitochondria. *The Journal of biological chemistry*, *271*(13), 7392–7397.

Ursino, G., Alberti, M. A., Grandis, M., Reni, L., Pareyson, D., Bellone, E., Gemelli, C., Sabatelli, M., Pisciotta, C., Luigetti, M., Santoro, L., Massollo, L., & Schenone, A. (2013). Influence of comorbidities on the phenotype of patients affected by Charcot-Marie-Tooth neuropathy type 1A. *Neuromuscular disorders*, *23*(11), 902-906.

Urtizberea, J. A., Megarbane, A., & Pandraud, A. (2013). Tête tombante, surdité et vitamine B2: une association non fortuite. *Les cahiers de myologie*, *8*, 9–10.

Valentijn, L., Baas, F., Wolterman, R., Hoogendijk, J., van den Bosch, N., Zorn, I., Gabreels-Festen, A. W., de Visser, M., & Bolhuis, P. A. (1992). Identical point mutations of *PMP22* in trembler-J mouse and Charcot-Marie-Tooth disease type 1A. *Nature genetics*, *2*(4), 288–291.

Valentijn, L. J., Baas, F., Zorn, I., Hensels, G. W., de Visser, M., & Bolhuis, P. A. (1993). Alternatively sized duplication in Charcot-Marie-Tooth disease type 1A. *Human molecular genetics*, *2*(12), 2143–2146.

Valentijn, L., Bolhuis, P., Zorn, I., Hoogendijk, J., van den Bosch, N., Hensels, G., Stanton, V. P. Jr, Housman, D. E., Fischbeck, K. H., Ross, D. A., Nicholson, G. A., Meershoek, E. J., Dauwerse, H. G., van Ommen, G.-J. B., & Baas, F. (1992). The peripheral myelin gene *PMP-22*/*GAS-3* is duplicated in Charcot-Marie-Tooth disease type 1A. *Nature genetics*, *1*(1), 166–170.

Vallet, A.-E., Verschueren, A., Petiot, P., Vandenberghe, N., Nicolino, M., Roman, S., Pouget, J., & Vial, C. (2012). Neurological features in adult Triple-A (Allgrove) syndrome. *Journal of neurology*, *259*(1), 39–46.

Van de Wetering, R. A., Gabreëls-Festen, A. A., Kremer, H., Kalscheuer, V. M., Gabreëls, F. J., & Mariman, E. C. (1999). Regulation and expression of the murine *PMP22* gene. *Mammalian genome*, *10*(4), 419–422.

Van Laere, M. J. (1966). Paralysie bulbo-pontine chronique progressive familiale avec surdité. Un cas de syndrome de Klippel-Trenaunay dans la même fratrie – problèmes diagnostiques et génétiques. *Revue Neurologique*, *115*(2), 289-295.

Van Spronsen, M., Mikhaylova, M., Lipka, J., Schlager, M. A., van den Heuvel, D. J., Kuijpers, M., Wulf, P. S., Keijzer, N., Demmers, J., Kapitein, L. C., Jaarsma, D., Gerritsen, H. C., Akhmanova, A. & Hoogenraad, C. C. (2013). TRAK/Milton motor-adaptor proteins steer mitochondrial trafficking to axons and dendrites. *Neuron*, *77*(3), 485-502.

Vance, J., Nicholson, G., Yamaoka, L. H., Stajich, J., Stewart, C. S., Speer, M. C., Hung, W. Y., Roses, A. D., Barker, D., & Pericak-Vance, M. A. (1989). Linkage of Charcot-Marie-Tooth neuropathy type 1A to chromosome 17. *Experimental neurology*, *104*(2), 186–189.

Vandenberghe, A., Upadhyaya, M., Gatignol, A., Boutrand, L., Boucherat, M., Chazot, G., Vandenberghe, A., & Latour, P. (2002). Frequency of mutations in the *early growth response 2* gene associated with peripheral demyelinating neuropathies. *Journal of medical genetics*, *39*(12), e81.

Vanhaesebrouck, A. E., Couturier, J., Cauzinille, L., Mizisin, A. P., Shelton, G. D., & Granger, N. (2008). Demyelinating polyneuropathy with focally folded myelin sheaths in a family of Miniature Schnauzer dogs. *Journal of the neurological sciences*, *275*, 100–105.

Varsányi, M., Szarka, A., Papp, E., Makai, D., Nardai, G., Fulceri, R., Csermely, P., Mandl, J., Benedetti, A., & Bánhegyi, G. (2004). FAD transport and FAD-dependent protein thiol oxidation in rat liver microsomes. *The Journal of biological chemistry*, *279*(5), 3370–3374.

Vergani, L., Barile, M., Angelini, C., Burlina, A. B., Nijtmans, L., Freda, M. P., Brizio, C., Zerbetto, E., & Dabbeni-Sala, F. (1999). Riboflavin therapy. Biochemical heterogeneity in two adult lipid storage myopathies. *Brain*, *122*(Pt 12), 2401–2411.

Verhoeven, K., De Jonghe, P., Van de Putte, T., Nelis, E., Zwijsen, A., Verpoorten, N., De Vriendt, E., Jacobs, A., Van Gerwen, V., Francis, A., Ceuterick, C., Huylebroeck, D., & Timmerman, V. (2003). Slowed conduction and thin myelination of peripheral nerves associated with mutant rho Guanine-nucleotide exchange factor 10. *American journal of human genetics*, *73*(4), 926–932.

Verrier, J. D., Lau, P., Hudson, L., Murashov, A. K., Renne, R., & Notterpek, L. (2009). Peripheral myelin protein 22 is regulated post-transcriptionally by miRNA-29a. *Glia*, *57*(12), 1265–1279.

Vialetto, E. (1936). Contributo alla forma ereditaria della paralisi bulbare progressiva. *Rivista sperimentale di freniatria*, *40*, 1–24.

Vital, A, Vital, C., Julien, J., & Fontan, D. (1992). Occurrence of active demyelinating lesions in children with hereditary motor and sensory neuropathy (HMSN) type I. *Acta neuropathologica*, *84*, 433–436.

Vital, A., Vital, C., Lagueny, A., Ferrer, X., Ribière-Bachelier, C., Latour, P., & Petry, K. G. (2003). Inflammatory demyelination in a patient with CMT1A. *Muscle & nerve*, *28*(3), 373–376.

Voermans, N. C., Kleefstra, T., Gabreëls-Festen, A. A., Faas, B. H. W., Kamsteeg, E.-J., Houlden, H., Laura, M., Polke, J. M., Pandraud, A., van Ruissen, F., van Engelen, B. G., & Reilly, M. M. (2012). Severe Dejerine-Sottas disease with respiratory failure and dysmorphic features in association with a *PMP22* point mutation and a 3q23 microdeletion. *Journal of the peripheral nervous system*, *17*(2), 223–225.

Voudris, K., Skardoutsou, A., & Vagiakou, E. (2002). Infantile progressive bulbar palsy with deafness. *Brain and development*, *24*(7), 732–735.

Warner, L. E., Svaren, J., Milbrandt, J., & Lupski, J. R. (1999). Functional consequences of mutations in the *early growth response 2* gene (*EGR2*) correlate with severity of human myelinopathies. *Human molecular genetics*, *8*(7), 1245–1251.

Weedon, M. N., Hastings, R., Caswell, R., Xie, W., Paszkiewicz, K., Antoniadi, T., Williams, M., King, C., Greenhaigh, L., Newbury-Ecob, R., & Ellard, S. (2011). Exome sequencing identifies a *DYNC1H1* mutation in a large pedigree with dominant axonal Charcot-Marie-Tooth disease. *American journal of human genetics*, *89*(2), 308-312.

Wei, W., Ji, A., Wang, J., Wei, Z., Lian, C., Yang, J., Ma, L., Ma, L., Qin, X., & Wang, L. D. (2013). Functional single nucleotide polymorphism in *C20orf54* modifies susceptibility to esophageal squamous cell carcinoma. *Diseases of the esophagus*, *26*(1), 97–103.

Werner, R., Manthey, K., Griffin, J., & Zempleni, J. (2005). HepG2 cells develop signs of riboflavin deficiency within four days of culture in riboflavin-deficient medium. *The Journal of nutritional biochemistry*, *16*(10), 617–624.

Weterman, M. A., van Ruissen, F., de Wissel, M., Bordewijk, L., Samijn, J. P., van der Pol, W. L., Meggouh, F., & Baas, F. (2010). Copy number variation upstream of *PMP22* in Charcot-Marie-Tooth disease. *European journal of human genetics*, *18*(4), 421–428.

Williams, L. L., & Penn, G. M. (1979). Selective IgA deficiency in Charcot-Marie-Tooth disease. *American journal of clinical pathology*, *72*(5), 800-806.

Williams, L. L., Shannon, B. T., & Wright, F. S. (1993). Circulating cytotoxic immune components in dominant Charcot-Marie-Tooth syndrome. *Journal of clinical immunology*, *13*(6), 389–396.

Yamamoto, S., Inoue, K., Ohta, K., Fukatsu, R., Maeda, J., Yoshida, Y., & Yuasa, H. (2009). Identification and functional characterization of rat riboflavin transporter 2. *Journal of biochemistry*, *145*(4), 437–443.

Yamamoto, M., Keller, M., Yasuda, T., Hayasaka, K., Ohnishi, A., Yoshikawa, H., Yanagihara, T., Mitsuma, T., Chance, P. F., & Sobue, G. (1998). Clustering of CMT1A duplication breakpoints in a 700 bp interval of the CMT1A-REP repeat. *Human mutation*, *11*(2), 109–113.

Yamamoto, M., Yoshihara, T., Hattori, N., & Sobue, G. (2004). Glu528del in *NEFL* is a polymorphic variant rather than a disease-causing mutation for Charcot-Marie-Tooth disease in Japan. *Neurogenetics*, *5*(1), 75–77.

Yao, Z., Gandhi, S., Burchell, V. S., Plun-Favreau, H., Wood, N. W., & Abramov, A. Y. (2011). Cell metabolism affects selective vulnerability in PINK1-associated Parkinson's disease. *Journal of cell science*, *124*(Pt 24), 4194–4202.

Yao, Y., Yonezawa, A., Yoshimatsu, H., Masuda, S., Katsura, T., & Inui, K.-I. (2010). Identification and comparative functional characterization of a new human riboflavin transporter hRFT3 expressed in the brain. *The Journal of nutrition*, *140*(7), 1220–1226.

Yao, Y., Yonezawa, A., Yoshimatsu, H., Omura, T., Masuda, S., & Matsubara, K. (2013). Involvement of riboflavin transporter RFVT2/Slc52a2 in hepatic homeostasis of riboflavin in mice. *European journal of pharmacology*, *714*(1-3), 281-287.

Yiu, E. M., & Ryan, M. M. (2012). Genetic axonal neuropathies and neuronopathies of pre-natal and infantile onset. *Journal of the peripheral nervous system*, *17*(3), 285–300.

Yonezawa, A., & Inui, K. (2013). Novel riboflavin transporter family RFVT/SLC52: identification, nomenclature, functional characterization and genetic diseases of RFVT/SLC52. *Molecular aspects of medicine*, *34*(2-3), 693–701.

Yonezawa, A., Masuda, S., Katsura, T., & Inui, K. (2008). Identification and functional characterization of a novel human and rat riboflavin transporter, RFT1. *American journal of physiology. Cell physiology*, *295*(3), C632–641.

Yoshihara, T., Kanda, F., Yamamoto, M., Ishihara, H., Misu, K., Hattori, N., Chihara, N., & Sobue, G. (2001). A novel missense mutation in the *early growth response 2* gene associated with late-onset Charcot-Marie-Tooth disease type 1. *Journal of the neurological sciences*, *184*(2), 149–153.

Yoshihara, T., Yamamoto, M., Hattori, N., Misu, K.-I., Mori, K., Koike, H., & Sobue, G. (2002). Identification of novel sequence variants in the neurofilament-light gene in a Japanese population: analysis of Charcot-Marie-Tooth disease patients and normal individuals. *Journal of the peripheral nervous system*, *7*(4), 221-224.

Yoshikawa, H., Nishimura, T., Nakatsuji, Y., Fujimura, H., Himoro, M., Hayasaka, K., Sakoda, S., & Yanagihara, T. (1994). Elevated expression of messenger RNA for *peripheral myelin protein 22* in biopsied peripheral nerves of patients with Charcot-Marie-Tooth disease type 1A. *Annals of neurology*, *35*(4), 445–450.

Yoshimatsu, H., Yonezawa, A., Yao, Y., Sugano, K., Nakagawa, S., Omura, T., & Matsubara, K. (2014). Functional involvement of RFVT3/SLC52A3 in intestinal riboflavin absorption. *American journal of physiology. Gastrointestinal and liver physiology*, *306*(2), G102-110.

Young, T., Shuey, N., Partridge, J., Bremner, F. D., & Nicholl, D. J. (2013). Compound Charcot-Marie-Tooth disease: a kindred with severe hereditary neuropathy, pupil abnormalities and a novel *MPZ* mutation. *Journal of neurology, neurosurgery, and psychiatry*, *84*(2), 234–236.

Young, P., Stögbauer, F., Eller, B., Jonghe, P. De, Löfgren, A., Timmerman, V., Rautenstrauss, B., Oexle, K., Grehl, H., Kuhlenbaumer, G., Van Broeckhoven, C., Ringelstein, E. B., & Funke, H. (2000). *PMP22* Thr118Met is not a clinically relevant CMT1 marker. *Journal of neurology*, *247*(9), 696–700.

Zaman, Z., & Verwilghen, R. (1975). Effects of riboflavin deficiency on oxidative phosphorylation, flavin enzymes and coenzymes in rat liver. *Biochemical and biophysical research communications*, *67*(3), 1192–1198.

Zempleni, J., Galloway, J. R., & McCormick, D. B. (1996). Pharmacokinetics of orally and intravenously administered riboflavin in healthy humans. *The American journal of clinical nutrition*, *63*(1), 54–66.

Zhang, F., Seeman, P., Liu, P., Weterman, M. A. J., Gonzaga-Jauregui, C., Towne, C. F., Batish, S. D., De Vriendt, E., De Jonghe, P., Rautenstrauss, B., Kruase, K. H., Khajavi, M., Posadka, J., Vandenberghe, A., Palau, F., Van Maldergem, L., Baas, F., Timmerman, V., & Lupski, J. R. (2010). Mechanisms for nonrecurrent genomic rearrangements associated with CMT1A or HNPP: Rare

CNVs as a cause for missing heritability. *American journal of human genetics*, *86*(6), 892–903.